

**THE TECTONIC EVOLUTION OF THE HATAY OPHIOLITE OF SOUTHEAST
TURKEY**

by

JENNIFER INWOOD

A thesis submitted to the University of Plymouth in partial fulfilment for the degree of

DOCTOR OF PHILOSOPHY

School of Earth, Ocean and Environmental Science

August 2005

University of Plymouth Library
Item No. 9007193825
Shelfmark THESIS 551-81NW

**THE TECTONIC EVOLUTION OF THE HATAY OPHIOLITE OF SOUTHEAST
TURKEY**

ABSTRACT

A combination of palaeomagnetic and structural analyses have been used to constrain rotations in the Hatay (Kizildağ) ophiolite of southeast Turkey in the eastern Mediterranean region and to produce a tectonic model for its evolution. The ophiolite comprises part of a prominent chain of southern Neotethyan ophiolites that stretches from the Troodos ophiolite of Cyprus eastwards to the Semail ophiolite of Oman. The Hatay ophiolite and the related Baër-Bassit ophiolite of Syria comprise the most westerly ophiolites emplaced onto the Arabian platform in the Maastrichtian.

The palaeomagnetic analyses demonstrate that a large coherent anticlockwise rotation was experienced by the Hatay ophiolite, with minor variability resulting from differential rotations of adjacent tectonic blocks. Positive inclination-only tilt tests indicate that the Hatay ophiolite preserves a pre-deformational magnetisation. This is supported by rock magnetic analyses, consistent with a seafloor origin of magnetisation acquisition, soon after genesis at a spreading ridge. Magnetic carriers capable of preserving a remanence stable over geological time are identified. Palaeomagnetic analyses of the sedimentary cover sequences of the Hatay and Baër-Bassit ophiolites have been performed to provide timing constraints on the rotations in the underlying ophiolites. These illustrate that a large component of the rotations occurred pre-emplacment of the Hatay/Baër-Bassit sheet. Structural analyses performed on all levels of the Hatay ophiolite and its sedimentary cover add insight into the phases of deformation that have affected the ophiolite and enable rotations to be constrained in relation to the structural development of the ophiolite. The structural events recognised can be linked to the regional tectonic evolution of the ophiolite and used to critically evaluate previous tectonic interpretations of the Hatay ophiolite.

Comparison between the large coherent anticlockwise rotations observed in the Troodos, Hatay and Baër-Bassit ophiolites imply that a significant component is likely to be linked to a common cause, inferred to be of intraoceanic origin as part of a coherent microplate. Thus, existing models for the rotation of the Troodos microplate have been revised to incorporate a larger area and also account for the rotations of the Hatay and Baër-Bassit ophiolites. Restoration of sheeted dykes to their original orientations implies that a primary variation in dyke strike existed within the southern Neotethyan ocean. In combination with the implications of the palaeomagnetic results for microplate rotation, these characteristics suggest formation of the ophiolites within a complex Neotethyan spreading system, analogous in many respects to fast-spreading marginal basin systems of the modern oceans.

LIST OF CONTENTS

CHAPTER ONE

1. INTRODUCTION	1
1.1 <u>Introduction</u>	1
1.2 <u>The Hatay ophiolite</u>	3
1.3 <u>Oceanic tectonics</u>	6
1.3.1 Ophiolites and comparison with oceanic crust	6
1.3.2 Geophysical investigations of seafloor fabrics and their interpretation	6
1.4 <u>Structural development of ophiolites</u>	11
1.5 <u>Regional tectonics of eastern Mediterranean Neotethyan orogenic belt</u>	12
1.6 <u>Significance of new palaeomagnetic and structural work in the Hatay ophiolite</u>	13
1.7 <u>Aims and objectives</u>	14
1.8 <u>Layout of thesis</u>	15

CHAPTER TWO

2. TECTONIC AND REGIONAL GEOLOGICAL FRAMEWORK	16
2.1 <u>Introduction to chapter</u>	16
2.2 <u>Present-day plate tectonic framework and regional structural history</u>	16
2.2.1 Present plate tectonic framework	18
2.2.2 Nature and locations of fault intersections in SE Turkey	22
2.2.3 Fault kinematics and stress evolution in the Hatay region	26
2.3 <u>Relative motion history of major plates</u>	28
2.4 <u>Ophiolites of the eastern Mediterranean</u>	31
2.4.1 Origin and distribution	31
2.4.2 Ophiolite emplacement mechanisms	35
2.5 <u>Implications of ophiolites for the evolution of the eastern Mediterranean</u>	38
2.5.1 The palaeogeography of the Tethys ocean in the eastern Mediterranean	38
2.5.2 Ophiolite root zones in the eastern Mediterranean	42
2.6 <u>Ophiolites of the peri-Arabian chain</u>	46
2.7 <u>Geology of the Hatay ophiolite</u>	49
2.7.1 General description	49
2.7.2 Overview of geological research	53
2.7.3 Description of lithologies	53
2.7.4 Sedimentary cover of the ophiolite	57
2.7.5 Emplacement of the ophiolite	58
2.7.6 Post-emplacement structures	60
2.7.7 Petrogenesis	62
2.8 <u>Previous suggestions on the tectonic evolution of the Hatay ophiolite</u>	63
2.9 <u>Overview of the geology of related ophiolites</u>	68
2.9.1 Troodos ophiolite	68
2.9.2 Baër-Bassit ophiolite	74
2.10 <u>Synthesis</u>	80

CHAPTER THREE

3. THE EARTH'S MAGNETIC FIELD AND PALAEOMAGNETIC METHODS	81
3.1 <u>Introduction to chapter</u>	81
3.2 <u>The Earth's magnetic field</u>	81
3.3 <u>Magnetisation theory and acquisition of magnetisation</u>	82

3.3.1	Fundamentals of magnetism and magnetic terms and parameters	84
3.3.2	Acquisition of magnetisation	89
3.4	<u>Measurement, demagnetisation and rock magnetic techniques</u>	91
3.4.1	Alternating field (AF) demagnetisation	93
3.4.2	Thermal demagnetisation	94
3.4.3	Measurement of magnetisation	95
3.4.4	Magnetic fabric	95
3.4.5	Rock magnetic experiments	96
3.5	<u>Analysis of magnetisation data</u>	98
3.5.1	Plotting and analysis of results	98
3.5.2	Components of magnetisation	100
3.5.3	Secular variation and virtual geomagnetic poles (VGPs) in sampling	101
3.5.4	Standard structural corrections	102
3.5.5	Net tectonic rotation analysis method	103
3.5.6	Statistical tests for the timing of magnetisation acquisition	106
3.6	<u>Apparent polar wander paths (APWPs)</u>	109
3.6.1	African and Eurasian apparent polar wander paths	109
3.6.2	Determination of tectonic rotations	111
3.7	<u>Synthesis</u>	112

CHAPTER FOUR

4.	PREVIOUS PALAEOMAGNETIC RESEARCH IN TETHYAN OPHIOLITES	113
4.1	<u>Introduction to chapter</u>	113
4.2	<u>Palaeomagnetic insights into the regional structural history</u>	113
4.3	<u>Palaeomagnetic insights into the evolution of Tethys</u>	115
4.4	<u>Review of palaeomagnetic results from the Troodos ophiolite and its sedimentary cover</u>	118
4.4.1	Palaeomagnetic results from the ophiolite	118
4.4.2	Palaeomagnetic results from the sedimentary cover	126
4.4.3	Rotation of the Troodos microplate	129
4.5	<u>Review of palaeomagnetic results from the Baër-Bassit ophiolite</u>	132
4.5.1	Palaeomagnetic results from the ophiolite	132
4.5.2	Palaeomagnetic results from the sedimentary cover	133
4.5.3	Tilt about dyke-normal axes	135
4.6	<u>Review of palaeomagnetic results from the Semail ophiolite</u>	137
4.7	<u>Tectonic rotation models</u>	138
4.8	<u>Synthesis</u>	142

CHAPTER FIVE

5.	PALAEOMAGNETIC RESULTS FROM THE HATAY OPHIOLITE	143
5.1	<u>Introduction to chapter</u>	143
5.2	<u>Sampling and measurement procedures</u>	143
5.2.1	Sampling and measurement methods	143
5.2.2	Structural controls on the choice of sampling sites	145
5.3	<u>Sampling localities</u>	146
5.3.1	Antakya (4 sites)	147
5.3.2	Coast (15 sites)	147
5.3.3	Isikli (4 sites)	148
5.3.4	Karaçay (20 sites)	148
5.3.5	Kisecik (8 sites)	148
5.3.6	Kömürçukuru (5 sites)	149

5.3.7	Tahtaköprü (5 sites)	149
5.4	<u>Rock magnetic summary</u>	150
5.5	<u>Magnetic fabric analyses</u>	150
5.6	<u>Palaeomagnetic results overview</u>	155
5.7	<u>Palaeomagnetic results by locality</u>	163
5.7.1	Antakya (4 sites; extrusive rocks)	163
5.7.2	Coast (15 sites; cumulate rocks, gabbros and SDC)	164
5.7.3	Isikli (4 sites; SDC)	165
5.7.4	Karaçay (20 sites; cumulate rocks, gabbros and SDC)	166
5.7.5	Kisecik (8 sites; cumulate rocks and SDC)	169
5.7.6	Kömürçukuru (5 sites; extrusive rocks)	170
5.7.7	Tahtaköprü (5 sites; extrusive rocks)	171
5.8	<u>Grouping of sites</u>	172
5.9	<u>Summary of results</u>	177
5.9.1	Results from sites with palaeohorizontal control	177
5.9.2	Results from sites with palaeovertical control	180
5.9.3	Reversely magnetised sites	182
5.9.4	Low coercivity (LC) components	183
5.9.5	Magnetisation of different dyke populations and gabbro screens	185
5.10	<u>Timing of magnetisation acquisition (tilt tests)</u>	185
5.11	<u>Analysis of the sheeted dyke complex</u>	187
5.11.1	Net tectonic rotation analysis method	188
5.11.2	'Inclination restoration to a reference' method	192
5.12	<u>Analysis of the extrusive sequence</u>	193
5.13	<u>Discussion</u>	195
5.13.1	Implications of westerly directed remanences	195
5.13.2	Age implications of reverse/normal magnetisation components	197
5.13.3	Implications of restoration of dyke strike to original orientations	201
5.13.4	Rotations about dyke-normal axes	202
5.14	<u>Synthesis</u>	203

CHAPTER SIX

6.	PALAEOMAGNETIC RESULTS FROM THE SEDIMENTARY COVER SEQUENCES OF THE HATAY AND BAËR-BASSIT OPHIOLITES	204
6.1	<u>Introduction to chapter</u>	204
6.2	<u>Sampling and measurement procedures</u>	204
6.3	<u>Hatay sedimentary cover</u>	206
6.3.1	Sampling localities	206
6.3.2	Rock magnetic summary	208
6.3.3	Magnetic fabric analyses	210
6.3.4	Palaeomagnetic results	212
6.3.5	Timing of magnetisation acquisition (tilt tests)	216
6.4	<u>Baër-Bassit sedimentary cover</u>	217
6.4.1	Sampling localities	217
6.4.2	Rock magnetic summary	217
6.4.3	Magnetic fabric analyses	219
6.4.4	Palaeomagnetic results	222
6.4.5	Timing of magnetisation acquisition (tilt tests)	227
6.5	<u>Summary of results from Hatay and Baër-Bassit sedimentary covers</u>	229
6.6	<u>Discussion</u>	229
6.7	<u>Synthesis</u>	231

CHAPTER SEVEN

7. ROCK MAGNETIC RESULTS AND SCANNING ELECTRON MICROSCOPE ANALYSES FROM THE HATAY OPHIOLITE	232
7.1 <u>Introduction to chapter</u>	232
7.2 <u>Magnetic minerals in ocean floor rocks</u>	233
7.2.1 Magnetic minerals	233
7.2.2 Formation processes of the magnetic minerals in oceanic crust	235
7.3 <u>Rock magnetic experiments</u>	239
7.3.1 Overview of experiments	239
7.3.2 Hysteresis of magnetic minerals	241
7.3.3 Acquisition of isothermal remanent magnetisation (IRM) analyses	243
7.3.4 Curie point determinations	244
7.3.5 Low temperature experiments: the Verwey transition	246
7.3.6 Alternating current (AC) susceptibility experiments	251
7.3.7 Sample preparation	252
7.4 <u>Rock magnetic results and discussion</u>	253
7.4.1 Preliminary results from the University of Plymouth	253
7.4.2 Cumulate gabbros and isotropic gabbros	258
7.4.3 Sheeted dykes	260
7.4.4 Extrusive rocks	262
7.4.5 Summary of rock magnetic results	263
7.4.6 Discussion of rock magnetic results	265
7.5 <u>Thin section analyses under the polarising microscope</u>	266
7.6 <u>Scanning electron microscope (SEM) analyses</u>	267
7.6.1 Sample preparation	269
7.7 <u>Scanning electron microscope (SEM) results and discussion</u>	269
7.7.1 Cumulate rocks and gabbros	270
7.7.2 Sheeted dykes	272
7.7.3 Extrusive rocks	272
7.7.4 Discussion of scanning electron microscope analyses	275
7.8 <u>Discussion of results from rock magnetic and supplementary analyses</u>	279
7.9 <u>Comparison with the magnetisation of modern oceanic crust and ophiolites</u>	279
7.9.1 Comparison with oceanic crustal rocks of the modern day oceans	280
7.9.2 Comparison with other ophiolites	282
7.9.3 Timing of magnetisation acquisition	283
7.10 <u>Synthesis</u>	284

CHAPTER EIGHT

8. STRUCTURAL ANALYSES AND SYNTHESIS OF STRUCTURAL AND PALAEOMAGNETIC DATA	285
8.1 <u>Introduction to chapter</u>	285
8.2 <u>Structural sampling localities and nature of data</u>	287
8.3 <u>Regional structure</u>	288
8.3.1 Outcrop patterns and topographic expression	288
8.3.2 Inherited structure of the ophiolitic basement	290
8.3.3 Structural indicators of tectonic rotation	286
8.3.4 Faults and shear zones	297
8.3.5 Summary and discussion of regional structure	307
8.4 <u>Palaeostress analysis</u>	308
8.4.1 Methodology of palaeostress analysis	309
8.4.2 Assumptions and limitations	310

8.5	<u>Description of data and results of palaeostress analysis</u>	312
8.5.1	Overview of data	312
8.5.2	Palaeostress maps	317
8.5.3	Separation into categories: cover framework	320
8.5.4	Separation into categories: ophiolitic basement	321
8.5.5	Identified structural events	323
8.5.6	Description of identified structural events: cover framework	328
8.5.7	Description of identified structural events: ophiolitic basement	331
8.5.8	Stress ratios and conjugate angles	336
8.5.9	Analysis of faults with non-vertical palaeostress axes	337
8.6	<u>Reactivation</u>	339
8.6.1	Reactivation in the ophiolitic basement	339
8.6.2	Propagation of reactivated basement structures into the cover	342
8.7	<u>Structural synthesis</u>	343
8.8	<u>Discussion</u>	345
8.8.1	Faults not accounted for by the palaeostress analysis	345
8.8.2	Relative timing of the identified events	346
8.9	<u>Comparison with previous tectonic interpretations and regional structural history</u>	347
8.9.1	Critical appraisal of previous tectonic interpretations for the Hatay ophiolite	347
8.9.2	Comparison with regional structural history	349
8.10	<u>Combining palaeomagnetic and structural results</u>	350
8.10.1	Main results and timing of rotations	350
8.10.2	Spatial distribution of rotations	354
8.10.3	Successive rotations and implications for microplate rotation	356
8.11	<u>Synthesis</u>	362
CHAPTER NINE		
9.	DISCUSSION AND MODEL FOR TECTONIC EVOLUTION OF THE HATAY OPHIOLITE	363
9.1	<u>Introduction to chapter</u>	363
9.2	<u>Can existing models for the rotation of the 'Troodos' microplate account for the rotations of the Hatay and Baër-Bassit ophiolites?</u>	364
9.3	<u>Modern analogues of microplate rotation</u>	366
9.4	<u>Complex spreading systems</u>	369
9.5	<u>Synthesis of rotations in Neotethyan ophiolite belt</u>	374
9.6	<u>Regional and major plate movements</u>	375
9.7	<u>Model for the tectonic evolution of the Hatay ophiolite</u>	377
CHAPTER TEN		
10.	SUGGESTIONS FOR FUTURE WORK AND CONCLUSIONS	380
10.1	<u>Rotations and timing constraints</u>	380
10.2	<u>Synthesis of structural and palaeomagnetic observations</u>	382
10.3	<u>Implications for the evolution of the eastern Mediterranean Neotethys</u>	383
LIST OF REFERENCES		
385		
PUBLISHED CONFERENCE ABSTRACTS AND PAPERS		
427		

LIST OF TABLES

2.1	Summary of kinematics in the Hatay region	27
3.1	The expected declination and inclination for the Hatay, Troodos and Baër-Bassit ophiolites between 50 to 110 Ma using the African APWP of Besse and Courtillot (2002)	111
5.1	Average NRM intensities for the various ophiolitic lithologies	155
5.2	Site palaeomagnetic data for sites with palaeohorizontal structural indicators	157
5.3	Site palaeomagnetic data for sites with palaeovertical structural indicators	158
5.4	Palaeomagnetic, location and structural data for the eleven identified groups of sites	174
5.5	Results of the inclination-only tilt test formulation of Enkin and Watson (1996) for the Hatay ophiolite	185
6.1	Site palaeomagnetic data for the sedimentary cover of the Hatay ophiolite	214
6.2	Results of the inclination-only tilt test formulation of Enkin and Watson (1996) for the sedimentary cover of the Hatay ophiolite	216
6.3	Site palaeomagnetic data for the neoautochthonous sedimentary cover of the Baër-Bassit ophiolite	223
6.4	Results of the inclination-only tilt test formulation of Enkin and Watson (1996) for the sedimentary cover of the Baër-Bassit ophiolite	227
7.1	The rock magnetic experiments carried out in the University of Plymouth and the Institute for Rock Magnetism (IRM)	240
7.2	The division of magnetic minerals into domain state using H_{cr}/H_c and M_r/M_s ratios to aid diagnosis	242
7.3	The Curie temperatures for the main magnetic minerals and the effect of the addition of titanium and of maghemitisation processes	244
7.4	The temperature and nature of the Verwey transition for various magnetic mineral compositions	247
7.5	The magnetic properties of modern oceanic oceanic crust for comparison With those of the Hatay ophiolite	274
8.1	Orientations of palaeostress axes for all faults and for the initial breakdown of data into basement and cover and fault types	314
8.2	Orientations of palaeostress axes and other parameters for the five identified structural events	324
9.1	Comparison of microplate rotation in the modern oceans and those inferred to have occurred within Neotethys in the eastern Mediterranean	367

LIST OF ILLUSTRATIONS

1.1	The eastern Mediterranean 'peri-Arabian ophiolite crescent' of Ricou (1971)	3
1.2	The location of the Hatay ophiolite in the eastern Mediterranean	4
1.3	The present plate tectonic setting of the eastern Mediterranean region and the location of the Hatay ophiolite in relation to the major fault zones in Turkey	5
1.4	The depth of DSDP/ODP/IODP Holes in modern-day oceanic crust	8
2.1	Major structural features of the Turkish area	17
2.2	Two different reconstructions of the relative motion between the African and Eurasian continents from 190 Ma to the present-day	29
2.3	The relative positions of Africa and Eurasia at three selected times	30
2.4	The location of major ophiolites of the eastern Mediterranean	32
2.5	Tectonic models of various methods of ophiolite genesis	33
2.6	Various models of ophiolite emplacement	36
2.7	Suture zones in the eastern Mediterranean	39
2.8	Alternative tectonic reconstructions of the of the eastern Mediterranean Neotethys for Early-Mid Cretaceous time	40
2.9	Root zones for the Late Cretaceous ophiolites of the eastern Mediterranean	44
2.10	The relationship between the Hatay, Baër-Bassit and Troodos ophiolites	47
2.11	Various models for seafloor processes that may sometimes become preserved in ophiolites	48
2.12	The geology of the Hatay ophiolite	50
2.13	The lithologies within the Hatay ophiolite	51
2.14	The geology of the Troodos ophiolite	69
2.15	The geology of the Baër-Bassit ophiolite and sedimentary cover	75
2.16	Baër-Bassit ophiolite cross-section and emplacement	79
3.1	The Earth's magnetic field	83
3.2	Fundamental types of magnetic behaviour	84
3.3	Types of spin alignment in ferromagnetism	85
3.4	Types of magnetic domain structure	86
3.5	Examples of orthogonal demagnetisation plots	100
3.6	Net tectonic rotation method of Allerton and Vine (1987) demonstrated using sheeted dyke site CD01	105
3.7	Field tests for palaeomagnetic stability	108
4.1	End-member tectonic cross-sections (i.e. the widest and narrowest solution for the Neotethyan ocean) across a N-S transect constrained using palaeomagnetic data	116
4.2	Inclination-only tilt test for the Troodos ophiolite	119
4.3	Outline geological map of Cyprus showing the location of areas that have been investigated palaeomagnetically. Lower hemisphere stereonet show tilt-corrected site-level palaeomagnetic directions and associated α_{95} cones of confidence from each area	121
4.4	Various palaeomagnetic results from the Troodos ophiolite	124
4.5	Timing of the rotation of the Troodos ophiolite	128
4.6	Various models proposed for the rotation of the Troodos microplate	130
4.7	Summary of the palaeomagnetic data obtained from the Baër-Bassit ophiolite	134
4.8	Possible mechanisms by which rotation occurs in a deforming area within a continental region	141

5.1	Localities within the Hatay ophiolite sampled for palaeomagnetic analysis	144
5.2	Anisotropy of magnetic susceptibility for rocks from the Hatay ophiolite	152
5.3	Anisotropy of magnetic susceptibility for cumulate gabbros and ultramafics	154
5.4	Sample demagnetisation plots for sites with palaeohorizontal control	159
5.5	Sample demagnetisation plots from sites with palaeovertical control	160
5.6	Stereographic projections of magnetic remanence directions for each locality, displaying only those sites with palaeohorizontal control on the structural orientation	161
5.7	Stereographic projections of magnetic remanence directions for each locality, displaying only those sites with palaeohorizontal control on the structural orientation	162
5.8	Demagnetisation data from a reversely magnetised sample from the Isikli locality	167
5.9	Spatial distribution of the eleven groups of palaeomagnetic sites identified	173
5.10	Groups identified and basis for grouping for sites within the coastal exposures	176
5.11	Stereonets illustrating the mean remanence magnetisation directions for the eleven groups identified	178
5.12	Summary of magnetic remanence directions for sites with palaeohorizontal control on the structural corrections applied	179
5.13	Low-coercivity components of magnetisation	184
5.14	Sample level characteristic remanent magnetisation direction in geographic coordinates for all coastal sites	186
5.15	Results of an inclination-only tilt test performed on all palaeohorizontal sites within the ophiolite	187
5.16	Results of net tectonic rotation analysis performed on site level directions with the results displayed in localities	190
5.17	Illustration of the effect of potential errors in measurement of pillow lavas propagating through analysis procedures, using the K�m�r�ukuru pillow lavas as an example	196
5.18	Timing of events in the peri-Arabian ophiolites from various dating methods	198
6.1	Localities within the sedimentary cover of the Hatay ophiolite sampled for palaeomagnetic analysis	207
6.2	Selected rock magnetic data from sites within the sedimentary cover of the Hatay ophiolite	209
6.3	Anisotropy of magnetic susceptibility for the sedimentary cover of Hatay	211
6.4	Sample demagnetisation plots for samples from the sedimentary cover of the Hatay ophiolite	213
6.5	Stereonets displaying site mean magnetic remanences for sites from the sedimentary cover of the Hatay ophiolite	215
6.6	Results of an inclination-only tilt test performed on sites from the sedimentary cover of the Hatay ophiolite	216
6.7	Geological map of the Ba�r-Bassit area, showing the distribution of Palaeogene and Neogene sequences of the neoautochthonous sedimentary cover and the location of palaeomagnetic sampling sites	218
6.8	Rock magnetic results from the Ba�r-Bassit sedimentary cover	219
6.9	Summary of the magnetic fabrics of the neoautochthonous sedimentary cover of the Ba�r-Bassit ophiolite	220
6.10	Examples of orthogonal demagnetisation plots from the sedimentary cover of the Ba�r-Bassit ophiolite	224
6.11	Stereographic projections showing the distribution of site mean directions of magnetisation within the sampled Neogene and Palaeogene sedimentary sequences of the Ba�r-Bassit ophiolite	226

6.12	Results of inclination-only tilt tests performed on site mean directions of magnetisation from the sedimentary cover of the Baër-Bassit ophiolite	228
6.13	Tertiary palaeolatitudes for the Baër-Bassit area predicted from the African apparent polar wander path (of Besse and Courtillot 1991)	230
7.1	The composition of the magnetic minerals common in oceanic crust and their methods of formation	234
7.2	LT SIRM curves for synthetic titanomagnetites with varying titanium concentrations that can be used for comparison with natural samples	250
7.3	High temperature curves showing T_c points for a representative sample of each ophiolitic lithology	254
7.4	Representative low temperature curves for each lithology, showing the Verwey transition (where present)	255
7.5	A Day plot of the samples measured from all lithologies of the Hatay ophiolite	256
7.6	Alternating current susceptibility curves for a sample from the SDC and a reference curve	257
7.7	Examples of typical iron oxide grains in isotropic gabbros and cumulate gabbros and ultramafics as observed under the SEM	271
7.8	Examples of typical iron oxide grains in the sheeted dyke complex as observed under the SEM	273
7.9	Examples of typical iron oxide grains in the pillowed lavas and lava flows as observed under the SEM	274
7.10	SEM images of exsolution textures, observed in all lithologies of the ophiolite	276
8.1	Distribution of structural sampling localities and palaeomagnetic sampling sites	286
8.2	Various possible models for the outcrop patterns observed within the Hatay ophiolite	289
8.3	The nature and orientation of major contacts within the Hatay ophiolite	292
8.4	Geology map and stereonet showing the orientation of dykes within the SDC and discrete dykes within gabbros and ultramafic cumulates by locality in order to recognise any spatial variation	293
8.5	Geology map and stereonet showing the orientation of cumulate layering and pillowed and sheet lava flows (extrusive palaeohorizontals) by locality in order to recognise any spatial variation	294
8.6	Geology map and stereonet showing the orientation of bedding planes by locality in order to recognise any spatial variation	295
8.7	Synoptic diagram of structures expected to form within a shear zone, and as were measured within the basal shear zone of the Hatay ophiolite	299
8.8	Photos of the kinematic indicators measured within the basal shear zone of the Hatay ophiolite, with the stereonet and rose plots illustrating the orientation of these structures	301
8.9	Kinematic indicators and their spatial distribution within the basal shear zone (Komürçukuru) area	302
8.10	Comparison between published map fault strikes and those measured during structural sampling for this thesis	303
8.11	Geology map and rose diagrams illustrating fault strikes separated into localities in order to recognise any spatial variations in orientation	304
8.12	Comparison between the fault strikes of all faults measured compared to the strikes of faults limited to those used in the palaeostress analysis	315
8.13	Stereographic projections illustrating the necessity of categorising data prior to a palaeostress analysis	316

8.14	The orientation of the horizontal palaeostress axis identified from the palaeostress analysis for each individual fault analysed	319
8.15	The five final events identified within the ophiolitic basement and cover framework of the Hatay ophiolite	325
8.16	Examples of faults from each pre-cover structural event identified within the ophiolitic basement	326
8.17	Photos of faults of the Neotectonic events identified within the ophiolitic basement and cover framework	327
8.18	Faults of Neotectonic post-emplacement events and cross-cutting relationships within the cover framework and ophiolitic basement	329
8.19	Cross-cutting relationships and faults of pre-cover events within the basement	332
8.20	Nature of fault dip amounts along the coast and of the ophiolite-sedimentary cover boundary	334
8.21	Reactivation in the Hatay ophiolite	340
8.22	Lower hemisphere stereographic projections of tilt-corrected site-level palaeomagnetic data summarising palaeomagnetic data obtained from the Hatay and Baër-Bassit ophiolites and their sedimentary covers	351
8.23	Synthesis of palaeomagnetic and structural data along the coast including rotations identified from analysis of the SDC	353
8.24	Transects along the coast illustrating the orientations of various features of the faults and lithologies. illustrating various properties	355
8.25	The method of modelling the effect of successive rotations illustrating the effect of these successive rotations on the magnetisation	358
8.26	An illustration of the effect of successive rotations, firstly on a palaeovertical case, for both a pole to the average present-day strike of dykes in the SDC and dykes restored using NTR analysis, and secondly for a palaeohorizontal case	359
8.27	Effect of incorporating a coherent vertical axis rotation in its postulated place in the sequence of tectonic events to have affected the ophiolite	360
8.28	Summary of effect of successive rotations illustrating the possible end scenarios obtained from preceding three diagrams, both with and without a coherent microplate rotation	361
9.1	Existing models for the palaeorotation of Troodos	365
9.2	An example of an existing model for the framework of the Neotethyan ocean	370
9.3	Models illustrating causes and mechanisms by which the orientation of dykes may change within a spreading system	371
9.4	Model for the potential affect of large-scale plate movements on Neotethyan ophiolites	376
9.5	Revised model for the evolution of the Neotethyan ophiolites	378

ACKNOWLEDGMENTS

This research was financed by a University of Plymouth PhD studentship. I received additional financial support for fieldwork from the Geological Society of London (Fund for Fieldwork, 2002-3 and 2003-4) and for laboratory research from the Institute of Rock Magnetism (Visiting Fellowship 2004) and the British Federation for Women Graduates (Johnstone and Florence Stoney Studentship, 2003-4).

I would like to thank my supervisors from Plymouth, Tony Morris and Mark Anderson for all their considerable help, advice and encouragement throughout the duration of the research. Also, I appreciate their ability to always find the necessary time to discuss the research, and for training both in the field, the laboratory and help with analytical techniques. I would also like to thank my third supervisor, Ulvi Can Ünlügenç (Çukurova University, Turkey) for his encouragement, especially for his considerable logistical support during the two Turkish fieldseasons. I would like to thank several other scientists for helpful discussions and advice, most particularly Alastair Robertson (Edinburgh), not only for these but for visiting me in the field and encouragement and valuable discussions throughout the duration of the PhD. I would like to thank Conall MacNiocaill from the University of Oxford for the training and help given whilst using equipment at the Oxford Palaeomagnetic Laboratory. I would also like to acknowledge the University of Oxford Palaeomagnetic Laboratory for providing use of their palaeomagnetic equipment on two separate occasions. I would like to thank everyone at the Institute of Rock Magnetism in Minneapolis, especially Mike Jackson, for their friendliness and for sharing their expertise whilst using the facilities at the Institute. I would like to acknowledge both the funding from the Institute to carry out this additional research, and also the generous financial aid received from the British Federation for Women Graduates, without which this visit may not have been possible.

I would like to thank all of my Turkish field assistants, particularly Alican Kop and Selahattin Üyüdücü, not only for their help in the field, but also for the considerable time they spent away from their own work and for making my time in Turkey more enjoyable. Çok Teşekkürler!

I would also like to thank everyone in the University of Leicester Borehole Research Group for their encouragement and for the very generous amount of time given to me to complete my PhD over the last few months.

I would like to thank all of my family, my boyfriend Paul, and my friends and housemates for everything they have done to help me throughout my PhD. The ways in which they have helped me are far too numerous to list. I am particularly appreciative of their encouragement over the last year, which ensured that I reached the stage of writing acknowledgments, and also for ensuring that the time I spent doing my PhD was so enjoyable!

AUTHOR'S DECLARATION

At no time during the registration for the degree of Doctor of Philosophy has the author been registered for any other University award without prior agreement of the Graduate Committee.

This study was financed with the aid of a studentship from the University of Plymouth. Relevant scientific seminars and conferences were regularly attended at which work was often presented and external institutions were visited for consultation purposes and for use of specialised equipment.

Presentations and conferences attended:

- Geological Society of London Tectonic Studies Group: University of Plymouth 2005; University of Durham 2004; University of Liverpool 2003.
- British Geophysical Association Postgraduate Research in Progress Geophysics: University of Liverpool 2004; University of Leeds 2003.
- European Geophysical Society-American Geophysical Union-European Union of Geosciences Joint Assembly 2003, Nice, France.
- European Geophysical Society General Assembly 2002, Nice, France.
- British Sedimentology Research Group 2001, University of Plymouth.
- Fourth International Turkish Geology Symposium 2001, Adana, Turkey.

Published papers and conference abstracts:

- Inwood, J., Morris, A., Anderson, M. W., Robertson, A. H. F., Unlugenc, U. 2003. First Palaeomagnetic Results from the Hatay (Kizil Dağ) Ophiolite of Turkey and their Implication for the Tectonic Evolution of the Eastern Mediterranean Neotethys. Geophysical Research Abstracts, 5, EGS-AGU-EUG Joint Assembly.
- Inwood, J. 2004. Rock Magnetic Evidence for a Sea-floor Origin for Magnetic Remanences in a Late Cretaceous Tethyan Ophiolite. The IRM Quarterly, Volume 14, No 2, p3-4.
- Morris, A., Inwood, J. and Anderson, M. W. 2005. Palaeomagnetic Insights into the Tectonic Evolution of the Eastern Mediterranean Neotethys. In: Robertson, A. H. F. et al., Tectonic Evolution of the Eastern Mediterranean, Geological Society of London Special Publication. *In press*.

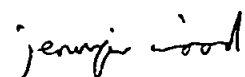
Additional Sources of Funding:

- Institute of Rock Magnetism Visiting Fellowship, University of Minnesota, 2004
- British Federation for Women Graduates Johnstone and Florence Stoney Studentship, 2003-4
- The Geological Society of London Fund for Fieldwork, 2002-3 and 2003-4

External Contacts:

- Institute of Rock Magnetism, University of Minnesota, U.S.A.
- University of Oxford Palaeomagnetic Laboratory

Word count of main body of thesis: 79712

Signed: 

Date: 7/4/06

CHAPTER ONE

1. INTRODUCTION

1.1 Introduction

Following the early identification of the Troodos ophiolite of Cyprus as a fragment of oceanic crust and upper mantle exposed above sea level (Gass 1968; Moores and Vine 1971), geological, geochemical and geophysical investigations of ophiolites have provided key insights into plate tectonic processes operating at constructive plate margins. Although it is now recognised that the majority of ophiolites (including Troodos) were generated by spreading above subduction zones (Pearce 2003), there is a general consensus that the processes of crustal accretion in this setting are in most respects similar to those operating at true mid-ocean ridges. Hence, detailed studies of structures and lithological relationships exposed in three dimensions within well-preserved ophiolites can provide insights into the nature of spreading systems in modern oceans, or conversely can act as a test ground for concepts arising from investigations in the modern oceans. Relatively undeformed and unaltered ophiolites like Troodos allow investigation of the rock magnetic properties of oceanic crustal lithologies, and hence insights into the sources of the magnetic anomalies that lie at the heart of plate tectonic theory. The information provided by ancient magnetic remanences preserved in such terranes allow quantification of the role of tectonic rotations in the development of seafloor structural architectures and post-spreading tectonic disruption of oceanic crust (e.g. Moores and Vine 1971; MacLeod et al. 1990; Allerton and Vine 1991; Morris et al. 1990, 1998).

In addition to their utility as natural laboratories for the study of crustal accretion processes, the interpretation of ophiolites as oceanic lithospheric fragments provides invaluable constraints on the palaeogeography and tectonic development of orogenic belts. For example, the eastern Mediterranean and Middle Eastern orogenic belt is marked by

several discontinuous lines of ophiolites that are believed to have been generated in several, relatively narrow (Neotethyan) strands of the Tethys ocean (e.g. Robertson 2004). Of these ophiolites, two have been foci of international research campaigns for the last 30 years: the Semail ophiolite of Oman (interpreted to have formed at a fast-spreading axis) and the Troodos ophiolite (interpreted to have formed at a slow-spreading axis). These lie at the eastern and western ends of the ‘peri-Arabian ophiolite crescent’ of Ricou (1971) (Figure 1.1). Other ophiolites of this lineament have received relatively little attention but are critical to understanding the regional tectonic evolution.

This thesis, therefore, describes a new palaeomagnetic and structural investigation of the Hatay ophiolite of SE Turkey that lies to the immediate east of Troodos. It occupies a key position in the regional context since, in contrast to the well-known Troodos ophiolite, the Hatay terrane was tectonically emplaced onto the Arabian margin in the Late Cretaceous during regional convergence. Although the consensus is that both ophiolites formed along strike in the same Neotethyan basin, the relationship between the two (and the more highly deformed Baër-Bassit ophiolite of NW Syria located immediately south of Hatay) in terms of rotational deformation remains unclear. Hence, this investigation represents an ideal opportunity to contribute to understanding of the regional development of the eastern Mediterranean Neotethyan orogenic belt, and to potentially relate processes involved in this development to those inferred in modern orogenic belts.

There remain many unknowns and debates surrounding the processes of both ophiolite evolution and elements of the evolution of the eastern Mediterranean. This thesis enables several of these key research questions to be addressed (section 1.6).

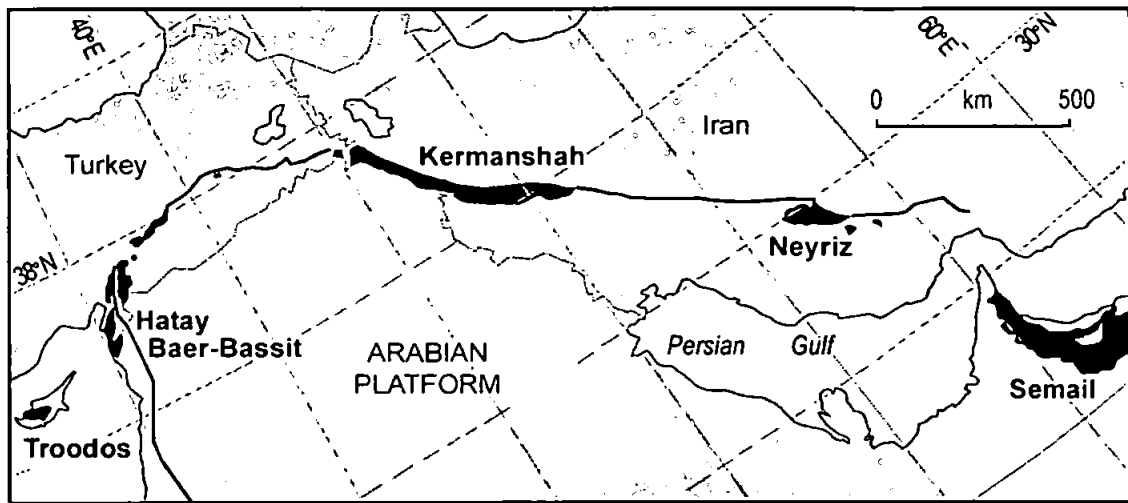


Figure 1.1: The eastern Mediterranean 'peri-Arabian ophiolite crescent' of Ricou (1971) extending eastwards from the Troodos ophiolite of Cyprus to the Semail ophiolite of Oman.

1.2 The Hatay ophiolite

The Hatay ophiolite of SE Turkey (Figure 1.2A) covers 950 square kilometres and is alternatively known as the Kizildağ ophiolite, named after the highest mountain within the ophiolite massif, Kizildağ (1750m). The major part of the ophiolite outcrops between the cities of Iskenderun in the NW and Antakya (formerly Antioch) in the SE (Figure 1.2B), and forms part of the NNE-SSW trending Amanos mountains. The Gulf of Iskenderun and plains of Arsuz and Iskenderun to the NW and the Karasu Valley, the Amik plain and the valley of the river Asi (Oronte) to the SE form the boundaries to the mountain range (Pişkin et al. 1986). The Belen pass cuts this range in two with the relief more pronounced to the south. In the wider context, the Hatay ophiolite comprises part of a prominent chain of ophiolites in the eastern Mediterranean believed to have been generated by suprasubduction zone spreading in the southernmost basin of the Mesozoic Neotethys. The Hatay and Baër-Bassit ophiolites are believed to comprise part of the same ophiolitic sheet, with Baër-Bassit comprising the more dismembered leading edge of the sheet and Hatay displaying greater coherency. This ophiolitic sheet was emplaced onto the Arabian margin in the Maastrichtian.

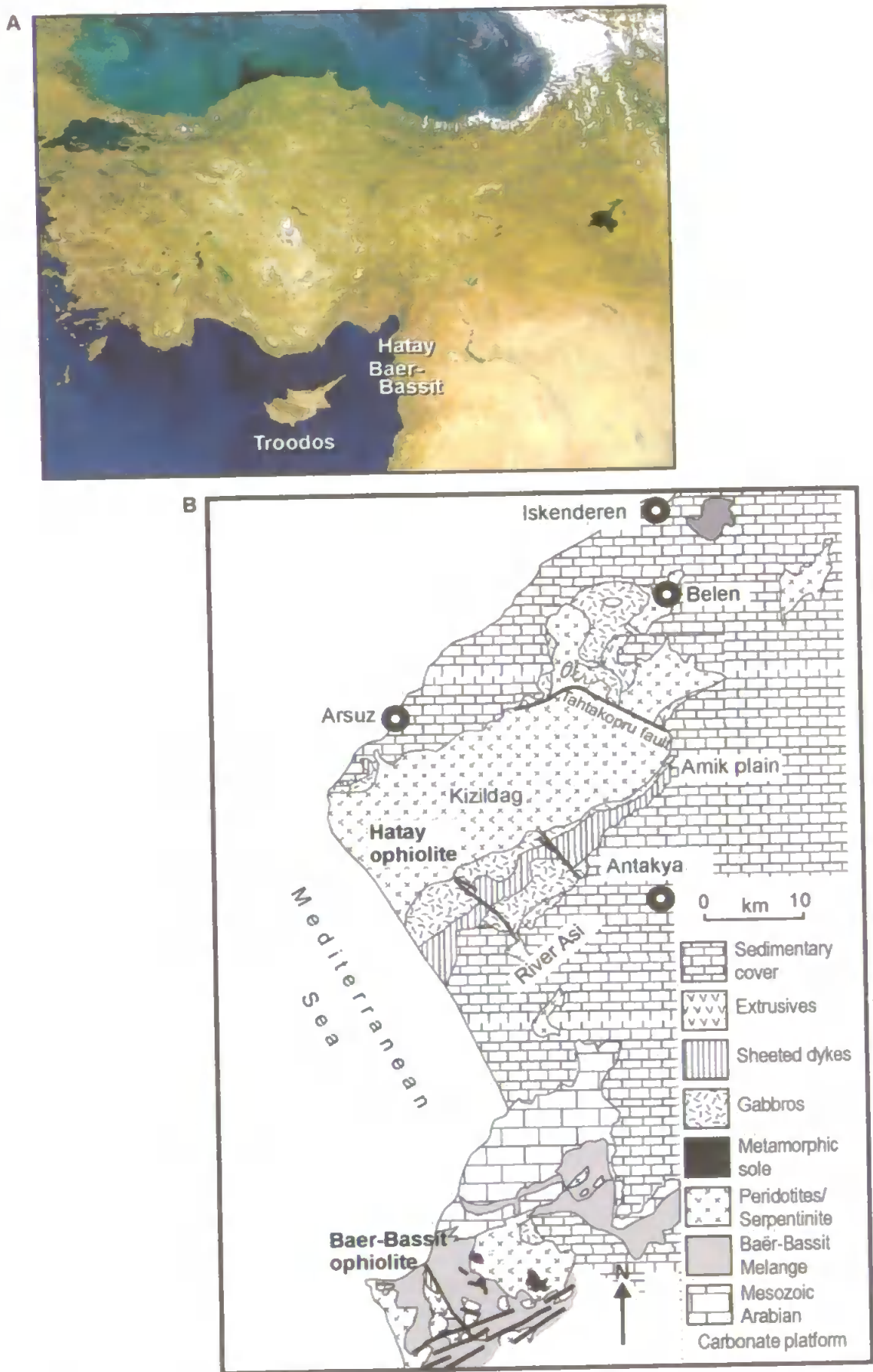


Figure 1.2: The location of the Hatay ophiolite in the eastern Mediterranean.
 A. Satellite image showing the location of the Hatay, Troodos and Baer-Bassit ophiolites.
 B. The geology of the Hatay ophiolite and surrounding region.

The Hatay region is located at the NW edge of the Arabian plate within the Arabia-Eurasia collision zone but has been dominated for large parts of its evolution by extensional/transensional structures (Kempler and Garfunkel 1994; Robertson 2000). The region lies in an area of active neotectonics in the intersection domain between the northern termination of the Dead Sea Fault, the western end of the East Anatolian Fault and the Cyprus arc (Perinçek and Çemen 1990; Robertson 1998; Figure 1.3) and is affected both by the complex interaction between the African, Eurasian and Arabian plates and potentially by rollback of the Aegean and Cyprus arcs producing extensional stresses in the overlying plate. The exact nature and location of the intersection between major structural features in this region is debated, with some authors suggesting a location in the Amanos mountains in the Hatay region and some suggesting a more northerly location.

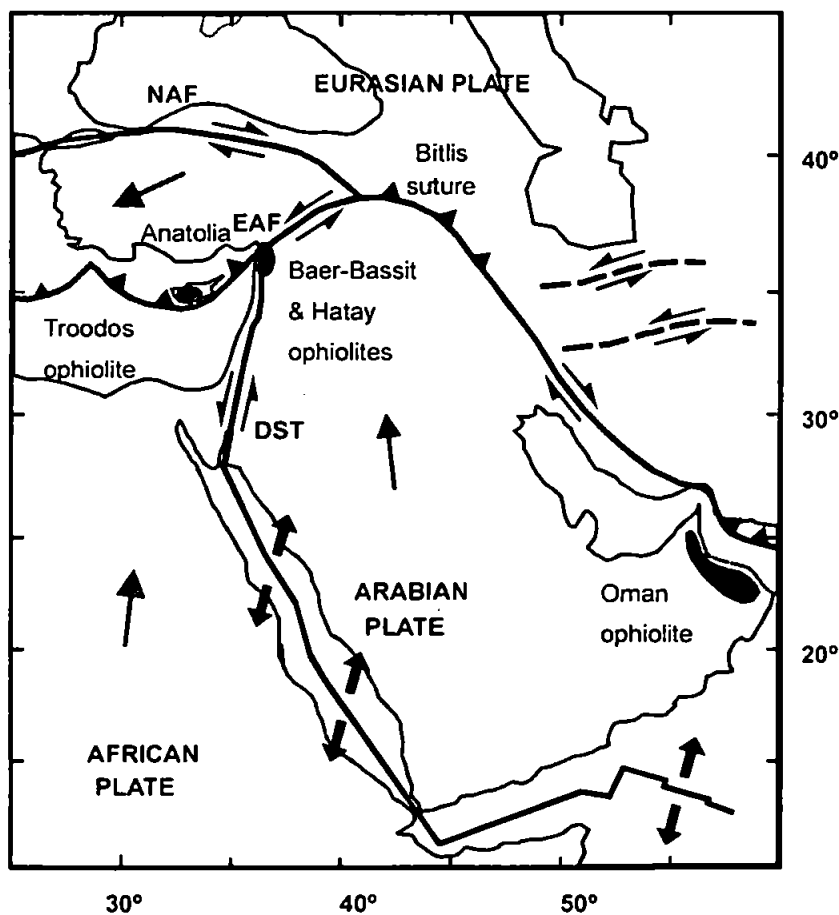


Figure 1.3: The present plate tectonic setting of the eastern Mediterranean region and the location of the Hatay ophiolite in relation to the major fault zones in Turkey. Grey arrows illustrate the direction of movement of tectonic plates (as determined from GPS measurements); thinner black arrows indicate the direction of movement on the major faults, and thicker black arrows show the direction of opening of spreading ridges. NAF = North Anatolian Fault; EAF = East Anatolian Fault; DSF = Dead Sea Fault.

1.3 Oceanic tectonics

1.3.1 Ophiolites and comparison with oceanic crust

Ophiolitic terranes are recognised as fragments of oceanic crust which have been tectonically emplaced onto land during orogenic activity. The Troodos ophiolite of Cyprus was the first ophiolite where the link with oceanic crust was recognised (Gass 1968), with research by Moores and Vine (1971) establishing the relationship. As the majority of oceanic crust is subducted, ophiolites provide an invaluable opportunity to investigate processes operating on the ocean floor and to study the structural architecture of oceanic crust in three dimensions. However, the fact that ophiolites are only emplaced onto land in unusual circumstances indicates that they are not 'typical' of oceanic crust. One of the ophiolites generated at a true mid-oceanic ridge is the Macquarie Island ophiolite, 1100 km SW of New Zealand, which is on a rise linking New Zealand with the actively spreading Indian-Antarctic ridge, and as such represents an anomalously raised segment of oceanic crust. The majority of ophiolites are now recognised as having formed by spreading above subduction zones (i.e. in suprasubduction zone settings). The most widely studied of such ophiolites are the slow-spreading rate Troodos ophiolite and the fast-spreading rate Semail ophiolite. Both have been influential in the development of concepts of seafloor spreading, providing the impetus for renewed investigations of spreading structures in the modern oceans.

1.3.2 Geophysical investigations of seafloor fabrics and their interpretation

Geophysical studies of the oceanic crust include ocean drilling, seismological and gravity studies and collection of samples and investigation of the seafloor by submersibles. Results from these have provided information on oceanic structure and tectonics with a

significant increase in the knowledge of the oceanic crust and processes operating within it in the last few decades.

Seismological studies provide information on the layering, structure and porosity of the crust and the extent and existence of subaxial magma bodies. The oceanic crust has been divided by seismologists into three layers: a surface layer of oceanic sediments on average 0.4 km thick, and two lower layers, both comprised of igneous units. The middle layer is on average 2.1 km thick and is mostly basaltic and the lower level is on average 4.9 km thick and is mostly gabbroic (Hall 1996). Gravity studies allow examination of lateral crustal thickness variations and density variations within the mantle, and association of these with underlying accretionary processes. Submersibles such as Alvin allow observations (both visual and instrumental) and samples to be collected from the ocean floor.

Drilling of oceanic crust has provided many insights into its structure, with the establishment of the Deep Sea Drilling Program (DSDP), succeeded by the Ocean Drilling Program (ODP) and now the Integrated Ocean Drilling Program (IODP) providing much of the data. Figure 1.4A shows the depth of DSDP/ODP/IODP holes drilled into in-situ basement and Figure 1.4B shows those holes that sample deeper crustal levels. The deepest hole drilled into oceanic basement is Hole 504B from the eastern Pacific, 200 km south of the Costa Rica Rift, in which 0.3 km of sediments are followed by 0.8 km of lavas and 1.1 km of dykes (Alt 1996; Figure 1.3A), consistent with thicknesses of the same layers observed in ophiolites. The dykes vary from steeply inclined (50° to 60° dip) to vertical and generally display only one chilled margin (Hall 1996). Other holes have penetrated deeper into the basement into gabbros or serpentinites where they are exposed in tectonic windows (e.g. Hess Deep), in oceanic core complexes by major crustal detachment faulting.

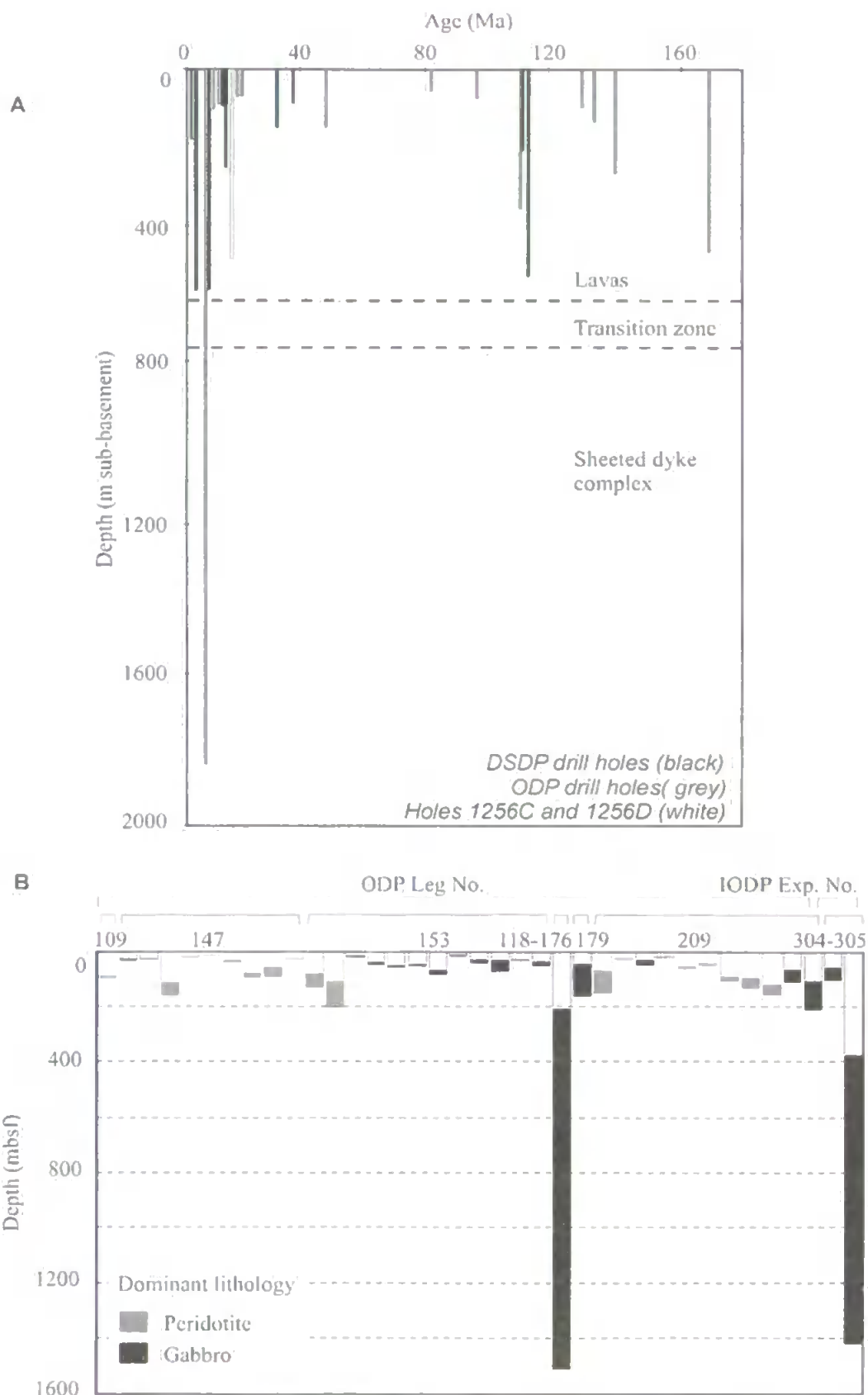


Figure 1.4: The depth of DSDP/OPD/IODP holes in modern-day oceanic crust.

A. Holes drilled >50 m into in situ oceanic crust formed at mid-oceanic ridges (Proc. ODP, Init. Repts. 206 2003 Fig. F2.) Lithological boundaries are placed at arbitrary depths based loosely on Hole 504B stratigraphy. Predictions based on marine seismic reflection studies indicate that the combined thickness of the lava-dyke sequences should decrease with spreading rate.

B. All Holes (recovery > 5%) in upper mantle and lower crustal rocks drilled to date at or near mid-ocean ridges during nine different ODP legs and IODP expeditions (IODP, Prel. Rept. 305 2005 Fig. F5.) ODP Leg 147 is the only one which took place in crust created at a fast-spreading ridge (Hess Deep, East Pacific Rise).

For example, gabbroic oceanic crust comprising part of a layered sequence and serpentinitised peridotites was drilled during ODP Leg 153 at the Mid-Atlantic ridge near the Kane fracture zone (Karson et al. 1997). The upper plutonic sequence in Hess Deep closely resembles that of the Semail ophiolite of Oman (Macleod et al. 1996; Dilek 1998).

Geophysical studies have identified variations in the spreading rate of different spreading systems within modern oceans, with rates of over 100 mm/yr at fast-spreading ridges to less than 50 mm/yr at slow-spreading ridges. Rates below 25 mm/yr are found for super-slow-spreading ridges (Dick et al. 2003). The Hatay ophiolite has been suggested to have formed at a slow-spreading ridge (section 2.8) and so the findings of geophysical investigations on slow-spreading ridges are relevant to this project. The details of spreading in marginal basins and overlapping spreading systems along fast-spreading ridges are also important due to their significance for later discussions on microplate rotation mechanisms as fast-spreading systems are the only places in the modern ocean where oceanic microplates are known to be forming and rotating.

Morphological features vary dependent on spreading rate. Ridges spreading at intermediate rates display transitional features between slow and fast spreading systems. Slow-spreading systems are characterised by spatial and temporal variations in magma supply which leads to periods of amagmatic extension. The Mid-Atlantic Ridge (MAR) is an example of a slow-spreading system in the modern-day oceans and the Hatay ophiolite has been suggested as an analogue to segments of the MAR. Slow-spreading ridges lead to the development of more deformed oceanic lithosphere due to lack of continuous magma supply resulting in episodes of extension by brittle faulting and crustal denudation. Some normal faults, referred to as detachment faults, appear to rupture to depths of 8 to 10 km across the entire thickness of the crust (e.g. Mutter and Karson 1992). Detachment faults allow extension to occur during these amagmatic periods and have been recognised in

ophiolites e.g. the Troodos ophiolite of Cyprus and the Josephine ophiolite of California, and have also been suggested as an explanation for structures within the Hatay ophiolite (Dilek and Thy 1998). Indeed, Dilek and Thy (1998) interpret various features of the Hatay ophiolite, not just a potential detachment surface, in terms of structures associated with slow-spreading ridges, for instance suggesting that evidence exists for block faulting.

Fast-spreading systems are characterised by near-continuous supply of magma and as such generally produce relatively undeformed sequences and lack significant block faulting. The East Pacific Rise (EPR) is an example of a fast-spreading ridge in the modern-day oceans. Fast-spreading systems frequently occur in backarc basins where the active subduction is located near enough to the ridge to be exerting a potential 'pull' force on the oceanic crust. Fast-spreading ridges can display complex spreading features due to the effect of rapidly propagating ridges resulting in overlaps between ridges. Complexities in these spreading systems may result in areas of oceanic crust rotating as small microplates, such as the Easter microplate of the Pacific. These complexities are discussed further in Chapter Nine. To date, the majority of seismic investigations and other studies have concentrated on faster spreading ridges where seafloor conditions are more favourable for seismic imaging.

All of the above methods of investigation provide a restricted view of the oceanic crust and processes operating within it. Remote geophysical surveying techniques can lack resolution and there may be difficulties in interpreting observations in the appropriate geological context. Recovery of drill cores and isolated samples by submersibles only sample very limited sections of the oceanic crust and the lack of three dimensional geological observations limits interpretation. Drill cores recovered from the ocean basement are restricted by limitations of modern drilling equipment and processes. Although this technology is continuously improving, the maximum depth currently

penetrated into in-situ oceanic basement is less than two kilometres and does not reach beyond the sheeted dyke complex into the deeper levels of undeformed oceanic crust. Palaeomagnetic studies often suffer from difficulties in constraining the orientation of recovered cores, although this can be aided by correlation with formation microresistivity (FMS) images. Therefore, although studies on crustal structure and development in the modern-day oceans have provided extremely valuable insights, these difficulties in analysis result in significant limitations in the information obtained. Ophiolites are the only place where oceanic crust can be observed on land and thus have a far higher accessibility in comparison with the ocean floor itself, providing an ideal opportunity to study crustal processes in three dimensions.

1.4 Structural development of ophiolites

Ophiolites allow seafloor structures to be observed in three dimensions, although this is complicated in the majority of ophiolites due to the overprinting of these primary spreading relationships during subsequent structural development. Ophiolites have a complex structural history resulting from seafloor tectonics, emplacement and post-emplacement phases of deformation. The Troodos ophiolite is an exception as it has not been thrust emplaced and so primary seafloor spreading relationships may still be observed. In order to determine the nature of each process, and so gain valuable insight into the many stages in the evolution of an ophiolite, it is necessary to separate out the structures resulting from each successive phase.

Post-emplacement deformation is assessed by the observation and analysis of structures in post-emplacement sedimentary cover sequences. Emplacement-related deformation can be studied by observation of the kinematic compatibility of structures with the emplacement direction inferred from regional considerations, and by studying the signature of

emplacement on the basal thrust planes of the ophiolite. This back-stripping has not previously been done in Hatay, despite some workers interpreting structures in the context of spreading fabrics (e.g. Dilek and Thy 1998).

1.5 Regional tectonics of eastern Mediterranean Neotethyan orogenic belt

The eastern Mediterranean (and Middle East) is a critical region for understanding the processes of progressive orogenesis and ophiolites play a key role in improving understanding of the regional evolution. The common occurrence of ophiolites and their organised distribution throughout the region suggests a complex palaeogeographic evolution. The origin of some of these ophiolites remains contentious (Pearce 2003), with, for instance, some authors proposing formation of the Semail ophiolite in a mid-ocean ridge setting (e.g. Boudier et al. 1985; Nicolas et al. 2000) and others suggesting formation in a suprasubduction zone setting (e.g. Pearce et al. 1981; Searle and Cox 1999). The establishment of likely tectonic settings for genesis and emplacement of the eastern Mediterranean ophiolites places constraints on the development and destruction of Neotethyan ocean basins through time. Fundamental to this tectonic evolution is the palaeorotation of the Troodos ophiolite- a major event within the southernmost Neotethyan ocean. It is essential to understand the relationship between the Troodos ophiolite and the more easterly emplaced ophiolites in the chain if this rotation is to be understood in the regional context.

1.6 Significance of new palaeomagnetic and structural work in the Hatay ophiolite

Key research questions remain regarding both the evolution and structural development of ophiolites as well as elements of the evolution of the eastern Mediterranean. The precise tectonic setting of genesis and mode of emplacement of many ophiolites, including those of the eastern Mediterranean are debated. The palaeorotation of the Troodos microplate was a significant event in the evolution of the eastern Mediterranean but the precise nature and causes of the rotation are not known. Diverse opinions exist on the structural framework and on the origin of structures within the Hatay ophiolite, as well as their relationship to events in the regional tectonic history. This thesis will add significantly to current knowledge in these areas.

The Troodos, Baër-Bassit and Hatay ophiolites are intimately linked with the general acceptance that all three formed within the same small Neotethyan oceanic basin above a subduction zone. The Troodos ophiolite experienced a large anticlockwise rotation, the timing of which is well-constrained from palaeomagnetic analysis of the in-situ sedimentary cover. The Baër-Bassit ophiolite also experienced large anticlockwise rotations (Morris et al. 2002), the origin of which cannot be determined precisely without further knowledge of the timing of the rotations. These constraints can be provided by comparison with palaeomagnetic results from the Hatay ophiolite and identification of rotations recorded by the post-emplacement sedimentary sequences. No previous palaeomagnetic research had been done on either the Hatay ophiolite or the sedimentary cover of the Hatay/Baër-Bassit sheet prior to this thesis, so the results of this investigation add insight into the rotational and tectonic history of these key eastern Mediterranean ophiolites.

No previous research has attempted to separate out the phases of the structural development of the Hatay ophiolite in relation to its seafloor, emplacement and post-emplacement history. This will add to knowledge on the processes operating on ophiolites, from the time of their formation, emplacement and post-emplacement, through recognition of the signature of these processes from structural analyses. The analysis of structural data in conjunction with new palaeomagnetic data will enable a more complete tectonic synthesis of the ophiolite to be constructed and will also have important implications for the evolution of the eastern Mediterranean. The combination of analyses obtained by this thesis enables robust interpretations to be made of the significance of the results.

1.7 Aims and objectives

The overall aim of this thesis is to use a combination of palaeomagnetic and structural analyses of the Hatay ophiolite to provide insights into the tectonic history of the ophiolite and the evolution of the eastern Mediterranean. This will be achieved by meeting the following objectives:

- (1) To use palaeomagnetic analyses on the main body of the Hatay ophiolite massif to establish the age of magnetic remanences in relation to the deformation of the ophiolite and the nature and magnitude of rotations to have affected the ophiolite.
- (2) To constrain the timing of these rotations through additional palaeomagnetic analyses of the sedimentary cover sequences of both the Hatay and the related Baër-Bassit ophiolites.
- (3) To establish the carriers of magnetisation in the ophiolitic units through rock magnetic experiments and their relationship to the seafloor history of the ophiolite.
- (4) To compare structures observed in the ophiolite and autochthonous sedimentary cover in order to distinguish phases of pre- and post-emplacement structural development.

(5) To integrate the rock magnetic, palaeomagnetic and structural results to constrain the tectonic history of the Hatay ophiolite.

(6) To interpret the new results in the context of the tectonic history of the eastern Mediterranean region, assessing the applicability of existing models, and if necessary producing a revised model.

1.8 Layout of thesis

The thesis is divided into ten chapters, with this introduction providing an overview of the research carried out and the reasons to do this research and its implications. Chapters Two to Four provide essential background on the evolution of the eastern Mediterranean, the geology of the Neotethyan ophiolites, palaeomagnetic methodologies and a review of palaeomagnetic research carried out in the eastern Mediterranean of relevance to this thesis. The new palaeomagnetic and rock magnetic results are discussed in Chapters Five to Seven. Chapter Eight presents a new structural synthesis of the development of the Hatay ophiolite and links this to the rotations identified from the palaeomagnetic results. Chapter Nine discusses the implications of the results and Chapter Ten presents the major conclusions of this thesis and suggestions for future work.

CHAPTER TWO

2. TECTONIC AND REGIONAL GEOLOGICAL FRAMEWORK

2.1 Introduction to chapter

This chapter reviews the geological history of the eastern Mediterranean, with particular emphasis on the history of the numerous ophiolites preserved in this region. The geology of the Hatay ophiolite and its regional tectonic setting are reviewed, as well as a brief overview of the geology of the Troodos and Baër-Bassit ophiolites since their tectonic evolution is intimately linked to that of the Hatay ophiolite. The regional structural history is significant for interpretations of the structural data and the timing of the rotations identified by the palaeomagnetic analysis. These reviews identify areas where current views contrast or where the existing literature is lacking in relation to the aims of the thesis.

2.2 Present-day plate tectonic framework and regional structural history

The Neogene-Recent tectonic evolution of the Mediterranean is the conclusion of a long geological history dominated by the opening of the Neotethys ocean in early Mesozoic time and its subsequent progressive closure (Robertson and Comas 1998). The major present-day tectonic features of the eastern Mediterranean and the Turkey area are discussed initially prior to a focussed review of the tectonic framework of the Hatay region. Figure 2.1 shows the structures mentioned within the text, including a detailed diagram of the structural framework of southeastern Turkey, centred on the Hatay region.

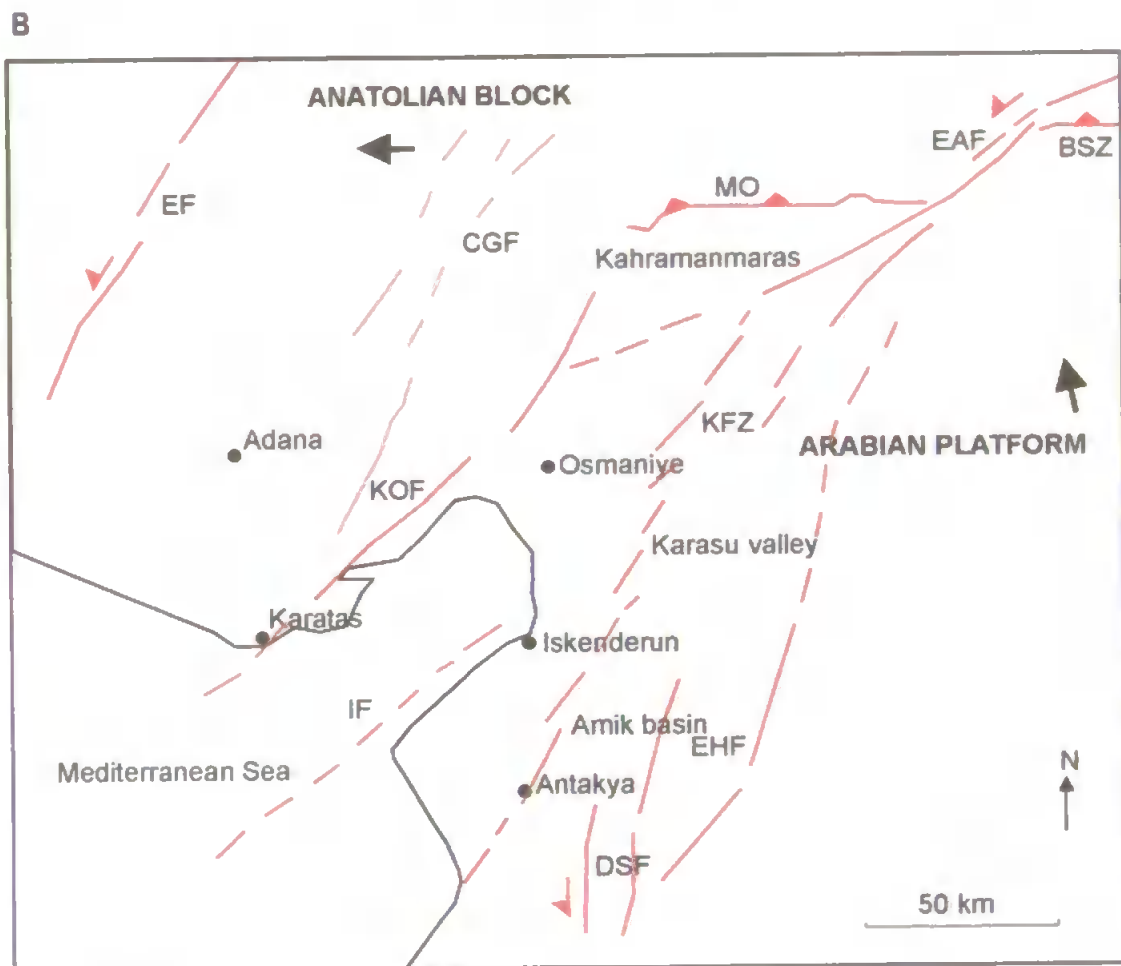
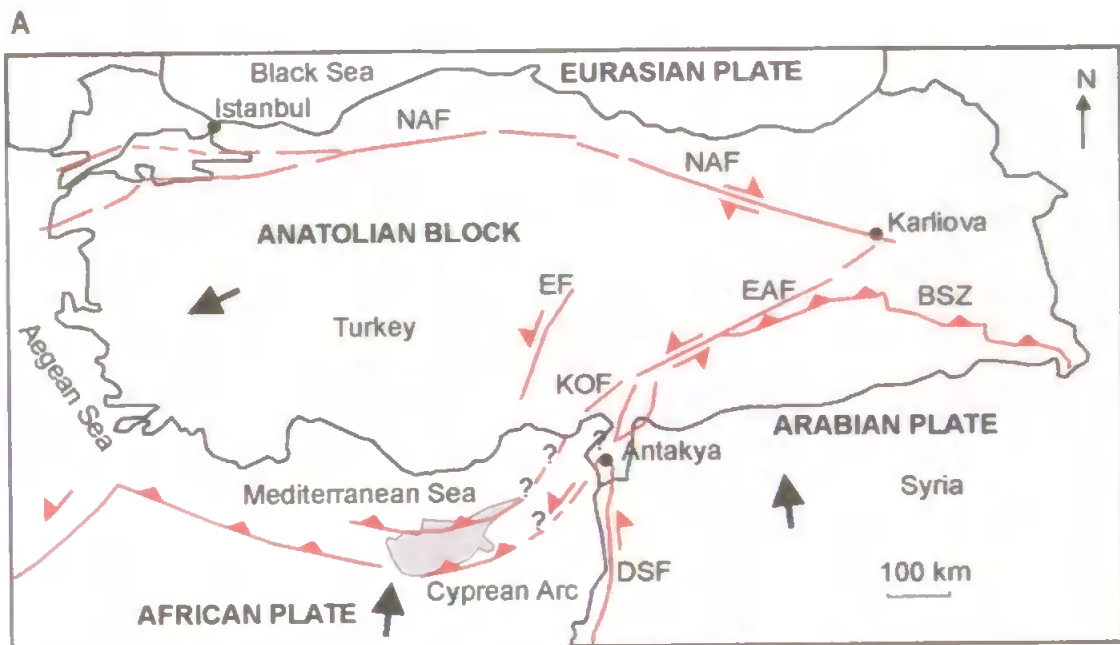


Figure 2.1: Major structural features of the Turkish area. Major faults are displayed in red and plate motions are shown by black arrows in both diagrams.

A. The main faults in Turkey (adapted from various authors).

B. A more detailed view of southeastern Turkey (adapted from Gursoy et al 2003). Abbreviations: NAF= North Anatolian fault, EAF= East Anatolian fault, DSF= Dead Sea fault, BSZ= Bitlis suture zone, KOF= Karatas-Osmaniye fault, EF= Ecemis fault, MO= Maras overthrust, CGF= Cicek-Goksun fault zone, EHF= East Hatay fault, KFZ= Karasu fault zone.

2.2.1 Present plate tectonic framework

The deformation in the eastern Mediterranean area is primarily influenced by the interaction between the major African and Eurasian plates, but also by smaller lithospheric plates such as the Anatolian plate, and the Adriatic and Arabian promontories (Tapponier 1977). The major features of the present-day tectonics comprise the northwards convergence of the African plate, the differential movement between Africa and Arabia facilitated by the Dead Sea fault (DSF), and the westwards extrusion of Anatolia between the dextral North Anatolian fault (NAF) and sinistral East Anatolian fault (EAF) away from the compressional deformation to the east (Figure 2.1A). Although the deformation as a whole is related to large-scale compressional movements, due to the complexity of the plate-tectonic situation and the influence of rollback processes operating in the trench, the Aegean region and much of Turkey is dominated by strike-slip and extensional motions (Jackson 1994). Thus, the westward motion of Turkey, the pull from the subducting slabs in the Hellenic and Cyprus trenches, resistance to shortening in the northwest and the strength of the pre-existing anisotropy of the crust all contribute to the dynamics of the region (Jackson 1994).

The Eurasian and African plates have been converging since the Mesozoic, since around 90 Ma (Şengör et al. 1985; Robertson et al. 1991) with initial collision occurring at 16 to 23 Ma (Allen 2004). The present-day Africa-Eurasia plate boundary is postulated to have been in place in the eastern Mediterranean since the Miocene (Şengör et al. 1985; Robertson et al. 1991). To the east of Turkey, the convergence is taken up by crustal thickening with compressional deformation along the Zagros fold and thrust zone, marked by the Bitlis suture, which closed in the Eocene (Bozkurt 2001).

Northward movement of the African plate is taken up in the eastern Mediterranean by a subduction zone along both the Hellenic and Cyprus arcs (McKenzie 1972), with the African plate being subducted beneath Anatolia in a N-NE direction (McKenzie 1978). Progressive subduction along this zone is thought to have resulted in the destruction of several hundred kilometres of Neotethyan oceanic crust (Le Pichon and Angelier 1979). Seismicity to the east of Cyprus shows the existence of a Benioff zone dipping roughly northwards beneath Anatolia (Rotsein and Kafka 1982). The crust to the south of Cyprus may be either oceanic crust with a thick deposition of sediments or attenuated continental crust of the African continental margin (Makris et al. 1983). The Cyprean arc is considered to be the presently active plate boundary (McKenzie 1970, 1972) and in detail is characterised by NE subduction to the west of Cyprus (e.g. Oral et al. 1995), collision-influenced subduction due to the Eratosthenes seamount to the south of Cyprus (Robertson et al. 1995; Robertson 1998) and strike-slip deformation to the east of Cyprus with no subduction (e.g. McKenzie 1972). Rollback processes are accepted to be occurring along the Aegean arc, producing slab-pull forces in the overriding plate (Robertson et al. 1991) resulting in the extensional regime observed in western Turkey (Le Pichon and Angelier 1979). Slab retreat is also thought to be occurring above the subduction zone along the Cyprus arc (Robertson 1990).

The Anatolian block is undergoing westwards extrusion, away from the Zagros fold and thrust zone of crustal thickening. The timing of initiation of this extrusion is coincident with the commencement of seafloor spreading in the southern Red Sea and eastern Gulf of Aden (Hempton 1987). The present-day rate of westwards tectonic escape in the region of the Marmara Sea is around 20 mm/yr (e.g. Reilinger et al. 1997). GPS measurements (e.g. McClusky 2000) and some palaeomagnetic studies (e.g. Kissel et al. 2003) indicate that Anatolia is rotating anticlockwise. Detailed palaeomagnetic studies (e.g. Gürsoy et al. 2003; section 4.2) show that this rotation is distributed across Anatolia and occurring in

small blocks. The extent to which the westwards extrusion of the Anatolian plate is driven by the energy difference between the thick crust in eastern Turkey and the Caucasus and the low elevations of the Aegean and western Mediterranean (push forces) and the extent to which the subduction zone is exerting a southwards force (pull force) is uncertain (Jackson 1994). The thickened crust in the continent-continent collision belt between Greece and the Apulian platform in the west acts to resist the westwards motion of Turkey (Jackson 1994).

The left-lateral EAF and right-lateral NAF facilitate the westwards extrusion of Anatolia (McKenzie 1972) and meet in the region of Karliova in eastern Turkey (Şengör et al. 1985). The NAF is an approximately 1500 km long strike-slip fault that extends from eastern Turkey westwards to Greece, predominantly as a single zone of a few hundred metres to 40 km wide, running sub-parallel to the Black Sea coast (Bozkurt 2001). The character of the NAF is not in doubt as it has ruptured along virtually its entire length in a series of large earthquakes over the last hundred years (Jackson 1994). The EAF is a roughly NE trending sinistral strike-slip zone around 550 km long that comprises a series of faults that lie parallel or sub-parallel to the main trend (Şengör et al. 1985; Hempton 1987; Lyberis et al. 1992). It runs from Karliova in eastern Turkey to the Kahramanmaraş area in southwest Turkey (Şengör et al. 1985; McKenzie 1970; Lyberis 1992). The magnitude of displacement along both the EAF and NAF is significant, with for example a minimum estimate of around 25 km of dextral movement postulated to have taken place on the NAF since the Late Miocene by Barka and Hancock (1984), ranging up to estimates of around 85 km (Sengör 1979). The EAF and NAF are both generally considered to have initiated more recently than the DSF (e.g. less than 6 Ma; Allen et al. 2004) with slip rates in the region of 26 ± 3 mm/yr and 11 ± 2 mm/yr respectively (Reilinger 1997), varying on the EAF from below 10 mm/yr (Westaway and Arger 1996; Yürür and Chorowicz 1998) to 29 mm/yr (Taymaz et al. 1991). However, there is considerable debate over the precise

ages of initiation of these faults and their slip rates. Estimates of the age of initiation of the NAF vary from Middle Miocene (McKenzie 1970; Sengör 1979) to the latest Miocene/early Pliocene (e.g. Arpat and Şaroğlu 1972; Barka et al. 2000) and estimates for the age of initiation of the EAF vary from Late Miocene/Early Pliocene (Arpat and Şaroğlu 1972; Sengör 1985; Hempton 1987; Perinçek and Çemen 1990; Lyberis et al. 1992) to Late Pliocene (Şaroğlu et al. 1992) to younger (e.g. 1.8 Ma; Yürür and Çhorowicz 1998).

GPS rates are invaluable for giving an 'instant image' of the contemporary tectonics of the eastern Mediterranean. These indicate that the Arabian plate is currently moving northwards faster than the African plate, with rates of 25 and 10 mm/yr respectively (Oral et al. 1995; Barka and Reilinger 1997). GPS rates can conflict with the longer term image of distributed crustal deformation derived from palaeomagnetism and other Neotectonic parameters; for instance geologically determined rates of movement on the DSF are lower (e.g. Westaway 1994) than GPS derived rates (e.g. 18 ± 2 mm/yr; Garfunkel 1981). The DSF system takes up the differential motion between the African and Arabian plates, and consists of several overlapping en echelon left-lateral strike-slip fault segments that run roughly N-S connecting the active oceanic spreading centres in the Red Sea to the collisional zones in southeast Anatolia and the Zagros (Garfunkel 1981). The total length of the zone is around 1000 km with around 105 km of total displacement (Allen 2004), decreasing in the north to around 20 km (Freund 1970; Garfunkel 1981) and with a present-day slip of between 2-8 mm/yr (Allen et al. 2004). Several authors suggest that the DSF fault zone has been active since the Middle Miocene, possibly coincident with the breakaway of Arabia from Africa at around 18 Ma (Hempton 1987; Garfunkel and Ben-Avraham 1996). An older age is suggested by Tinkler et al. (1981) who attribute pre-Cenomanian age faults from a locality in Syria to the DSF, but this age is not supported by most authors and would suggest that by the time of emplacement of the Hatay ophiolite, faulting had already occurred along at least some segments of the DSF. It has also been

suggested that displacement along the zone occurred in two stages, with a 60-65 km offset occurring in the Miocene and 40-45 km in the last 4.5 Ma (Freund et al. 1968). The DSF zone is accompanied in places by regional uplift (up to 1 km) and widespread igneous activity from the Gulf of Aquaba in the south to the Amik Basin in the north (e.g. Çapan et al. 1987; Parlak et al. 1998), and remains active today as evidenced by the displacement of Upper Quaternary sediments (Zack and Freund 1981) and seismic activity (Mart and Rabiowitz 1986).

2.2.2 Nature and location of fault intersections in SE Turkey

The precise location where the subduction zone to the east of Cyprus, the EAF and the DSF meet each other in SE Turkey is much debated and little consensus has been reached. The fault network in the intersection region is complex (Figure 2.1B), with the Hatay region interpreted by various authors to form the intersection domain between some or all of these major structural lineaments.

The EAF is commonly believed to meet the DSF in a triple junction between the African/Arabian, Eurasian and Anatolian plates in the region of Kahramanmaraş (e.g. McKenzie 1972; Arpat and Şaroğlu 1972; Şengor et al. 1985; Lyberis et al. 1992; Westaway 1994). Another suggestion is that the EAF and DSF zones are not connected and that the EAF continues in a southwest direction through Osmaniye, Yumurtalik and the Gulf of Iskenderen to Cyprus (e.g. Hempton 1987; Taymaz et al. 1991; Westaway 1994; Yurtmen 2000). Other authors claim that although faulting runs through these places that it is not part of the EAF zone, merely the boundary between the African and Eurasian plates, which meet the EAF further east at the triple junction (see review by Bozkurt 2001). The faults to the SW of Kahramanmaraş are represented by left-lateral strike-slip faults and constitute the Karataş-Osmaniye and Yumurtalik fault zones that bound the northwest

margin of the Gulf of Iskenderun (Bozkurt 2001). Triple junctions are inherently unstable (McKenzie and Morgan 1969) and evolve and change location over time. This may explain a large degree of the diverse opinions on the precise location triple junctions. For instance, Perinçek and Çemen (1990) note triple junction points in Antakya, Kahramanmaraş and near Hazar Lake, further to the NE, with the Antakya triple junction defined by the DSF and the Amanos fault (as part of the EAF). Saroğlu et al. (1992) define a triple junction in the region of Antakya between the DSF, the EAF and a third smaller local NNW-SSE trending non-plate-bounding Reyhanli fault and Yürür and Chorowicz (1998) suggest the triple junction jumped from the Kahramanmaraş region to the vicinity of Antakya around 2 Ma. Over et al. (2004b) suggest the Amik basin as the most obvious tectonic feature for the location of a triple junction in the Antakya region.

The Hatay region contains a graben that runs from the Mediterranean coast NE to Antakya, then northwards through the Amik plain, potentially linking the DSF to the EAF and as such provides a key area in which to collect data to aid the determination of fault intersection locations. The terminology of this graben is variously defined in the literature as the Hatay graben (Perinçek and Çemen 1990), the Amanos fault zone (Lyberis et al. 1992) or the Karasu rift (Westaway 1994; Rojay et al. 2001; Over et al. 2004c). The graben developed subsequently to the emplacement of the Hatay and Baër-Bassit ophiolites onto the Arabian platform (Delaloye 1980; Tinkler et al. 1981; Parlak et al. 1998). There are different interpretations for the link between this graben and the major EAF and DSF zones. For example, the graben is sometimes considered to be the northward continuation of the DSF zone (Tinkler et al. 1981; Parlak et al. 1998), the southward continuation of the EAF zone (Şengör et al. 1985; Lyberis et al. 1992), or that the graben is separate from both the EAF and the DSF (Yürür and Çhorowicz 1998). Within this thesis, the Hatay graben will be used to refer to the section between the Mediterranean coast to the SW and Antakya. The displacement in this SW section is

believed to comprise several hundred metres of vertical displacement (Tinkler et al. 1981; Lyberis et al. 1992).

The northern end of the DSF appears to splay into separate faults (e.g. Nur and Ben-Avraham 1978; Walley 1988), with the Amanos (Perinçek and Çemen 1990) or Karasu fault (Chorowicz et al. 1994) to the west and the East Hatay fault and the Afrin fault to the east suggested to be the continuation of the DSF (Tatar 2004). The Amanos fault is around 145 km long and runs NNE-SSW from the Kahramanmaraş region to Antakya with a present-day slip rate 10-20% of that on the EAF (Over et al. 2004b). The combined slip rate on the Amanos-Afrin-East Hatay fault array is estimated to be a minimum of 4.6 mm/yr (Tatar et al. 2004) and on the Karasu fault zone itself varies from lower estimates (1.3 mm/yr; Yurtmen et al. 2002) to considerably larger slip rates (4.1 mm/yr; Rojay et al. 2001). The cumulative slip across the Amanos and East Hatay fault is around 70-80 km from offset of the Hatay ophiolite (Freund et al. 1970; Dewey et al. 1986; Lyberis et al. 1992). The Amanos fault zone is believed to have comprised the main strand of the African-Arabian plate boundary from mid-Miocene to late Pliocene times (Westaway and Arger 1996; Yurtmen et al. 2002). The Amanos fault bounds the western edge of the 30 km wide Amik basin which contains Plio-Quaternary sediments (Lyberis et al. 1992). Quaternary age basalts have been erupted along the central parts of the Karasu valley (Çapan et al. 1987; Yürür and Chorowicz 1998; Rojay et al. 2001). Clockwise rotations ($< 10^\circ$) are observed in the Karasu valley, facilitated by NW-SE cross-faults between the NNE-SSW trending major faults as the Arabian plate has moved NW (Tatar et al. 2004). Many of the studies focussed within the Karasu valley have concentrated on dating young basaltic lava flows by K-Ar methods to determine slip on the Amanos fault and establish its importance in the EAF-DSF system (Parlak et al. 1998; Rojay et al. 2001; Yurtmen et al. 2002). Palaeomagnetic studies can provide additional timing constraints as well as add

insight into block rotations resulting from the strike-slip deformation (e.g. Tartar et al. 2004; section 4.2).

Over et al. (2004b) interpret the eastwards extension of the Cyprus arc as linking to Antakya and describe it as the Cyprus-Antakya transform (CAT). The Kizildağ mountain is interpreted to comprise the northern block of the CAT and indicates an active tectonic regime due to the top of the mountain being 1750 m and located only 30 km from the sea (Over et al. 2004). From SPOT image analysis a general pattern of NE-SW trending lineaments is observed, dying out in the Amik basin to the east and interpreted to continue southwestwards, linking with the Cyprus arc in the west (Over et al. 2004b). Lineament analysis of three areas- located (from north to south) south of Iskenderun, around the central part of the Hatay ophiolite, and to the SE of Antakya- show in all cases numerous NE-SW oriented lineaments, with an ENE-WSW trend also picked out in the central area and interpreted to relate to the CAT. The triple junction located in the Amik basin by Over et al. (2004b) is interpreted to result in NE-SW transtension within the surrounding region in the Quaternary. An alternative view of the location of the plate boundary between Africa and Eurasia is that the Gulf of Iskenderun is a flexural basin developed on African crust ahead of the Anatolian thrust front, linking the Kyrenia range on Cyprus, and the Misis and Amanos ranges, and representing the African-Eurasian plate boundary (Lyberis et al. 1992).

Further south strike-slip faults trending ENE-WSW and dominantly sinistral are observed in the Baër-Bassit region of Syria and have been interpreted to represent part of the present-day plate boundary zone between the African plate and Turkish microplate, running eastwards from Cyprus as a zone of distributed deformation (Kempler and Garfunkel 1994; Ben-Avraham et al. 1995) and continuing onshore, linking with the DSF to the east (Robertson 1998; Al-Riyami et al. 2000).

2.2.3 Fault kinematics and stress evolution in the Hatay region

Most palaeostress studies carried out in the Turkish area have concentrated on western Anatolia or the NAF (e.g. Angelier et al. 1987; Hancock and Barka 1987; Zanchi and Angelier 1993; Bellier et al. 1997) but a few studies have focussed on southeastern Anatolia, including some studies to the south of Hatay on the DSF (e.g. Hatzor and Reches 1990; Zanchi et al. 2002; Diabat et al. 2004) and further to the north (Over et al. 2004a, 2004c-d). Palaeostress analysis focussed on the Hatay region (e.g. Over et al. 2002) is limited and restricted to fault kinematic analysis of faults within localised areas; Table 2.1 summarises the results from analyses of relevance for the Hatay region. As a general rule, a change from an earlier compressive/transpressive regime to a younger extensional/transensional regime that continues to the present-day is recognised. The timing of this switch is poorly constrained, although most studies suggest it is recent (within the Neogene or Quaternary). Many studies highlight rapid changes from one regime to another spatially, either away from the vicinity of the major faults or due to along-strike variations (e.g. Kempler and Garfunkel 1994; Over et al. 2004a). For instance, a difference in palaeostress orientation is apparent between the Amanos and Misis ranges (Over et al. 2004a). The younger NE-SW extensional/transensional regime widely recognised produces a sinistral component of movement on major faults, with variations in the slab-pull force caused by rollback along the Cyprus arc suggested as a major influence on the change from transpression to transtension (Over et al. 2004a). An additional extensional event is recognised in the Hatay regime by Over et al. (2002), suggested to be later than the regionally significant transtensional regime and only of local significance, although GPS results may support the existence of this direction (Barka and Reilinger 1997).

Reference	Area covered/Age	Older regime	Younger regime (s)
Over et al. 2004a (Synthesis of Over et al. 2002; Over et al. 2004 b-d.)	NE corner of Mediterranean. (area extends S of Antakya, to W of Adana), N to Kahramanmaraş / Late Cenozoic	Transpression; Stress ratio 0.25 ^D	Transtension; Stress ratio 0.81
Over et al. 2002	Hatay/ Quaternary	Strike-slip regime; Stress ratio 0.7; NE-trending σ_3 axis	(i) NE-SW Extension; Stress ratio 0.37 ; NE-trending σ_3 axis (ii) E-W Extension; ESE- trending σ_3 axis
Over et al. 2004c	Karasu valley/ Mio-Pliocene	Transpression; NW-trending σ_1 axis	Transtension; NW-trending σ_3 axis
Over et al. 2004d	Misis range	NNW- trending σ_1 axis	NNW- trending σ_3 axis
Yürür and Çhorowicz 1998	Karasu graben	Transpression; Analysis of striations indicates NW-SE compression	Karasu Rift volcanism resulted from switch to transtension; NW-SE trending coastline is normal fault
Westaway 1994	Karasu graben	N-S compression	E-W extension
Karig and Kozlu 1990; Chorowicz et al. 1994	Misis and Amanos ranges	Transpression; Reverse faults and folds	
Çoskun and Çoskun 2000	EAF to DSF	Transpression; Positive flower structures on seismic profiles	
Reference	Area covered/Age	Older regime	Younger regime (s)
Çapan et al. 1987	South of Iskenderun	Transpression indicated from reverse faulting in Miocene formations	
Lyberis et al. 1992	Amik Basin (north of Antakya)	Strike-slip ^A	NE-SW Extensional regime (including NW- SW trending coastline) ^A
Rojay et al. 2001	Western border of Karasu rift		NNE-SSW/NE-SW normal faults; parallel to rift margins; Normal component increases N to S.
Rojay et al. 2001	Hatay graben (Antakya to Çevlik)	Strike-slip faults; dextral striking 10- 20°N ^B	Normal faults striking 30- 60° NE rake 34-76° sinistral slip component ^B
Perinçek and Çemen 1990	Antakya to Kirikhan		NE-SW extension; NW trending normal faults; well-developed graben under Iskenderun Bay; Formation of Amik graben
Zanchi et al. 2002	Extensive area focussed around DSF; W region closest to Hatay concentrated on in this table	Transpression NW-SE compression; folds and thrusts; related to rotation of the Arabian plate ^C	NE-SW extension; Large N-S sinistral and WNW- ESE dextral strike-slip faults, accompanied by NW-SE normal faults ^C

Table 2.1: Summary of kinematics in the Hatay region.

^A These two regimes are suggested to be coeval but spatially discrete.

^B The normal faults are dominant but relative timing of the normal and strike-slip faults is not given.

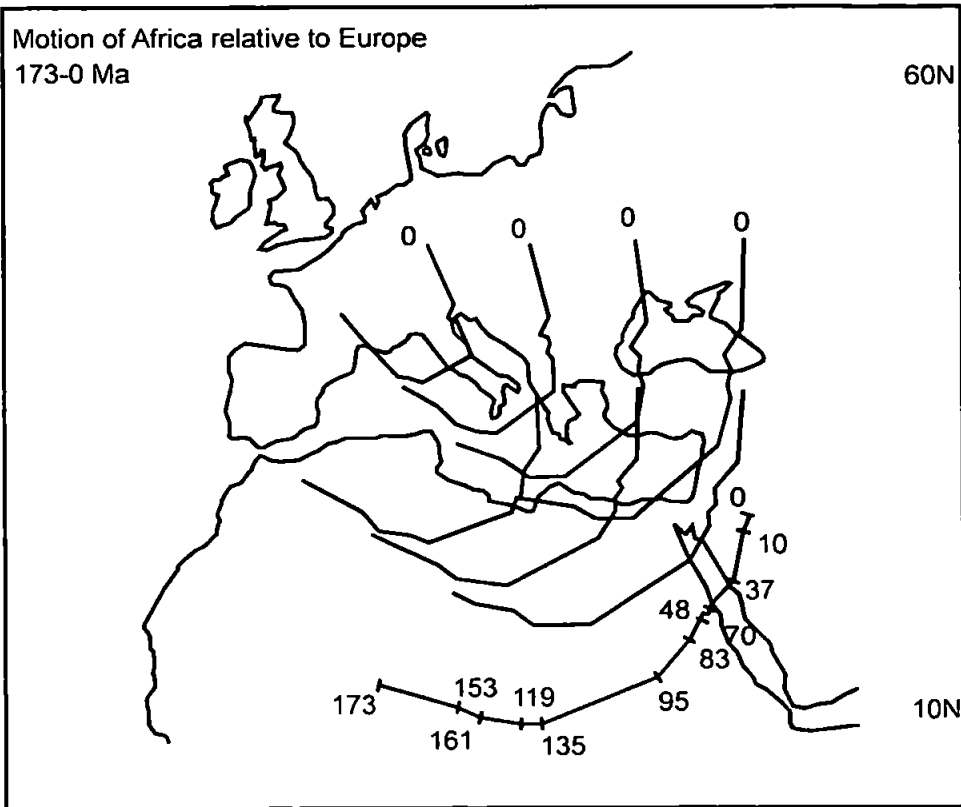
^C At least four major tectonic regimes are recognised with the NE-SW extension the most recent. Generally older palaeostress regimes are transpressive around the DSF succeeded by younger extensional/transtensional regimes.

^D Stress ratio = $(\sigma_2 - \sigma_3) / (\sigma_1 - \sigma_3)$, after Angelier (1994).

2.3 Relative motion history of major plates

The relative motion history of the African and Eurasian plates provides the first-order control on the tectonic history of the Hatay ophiolite and wider eastern Mediterranean region. Figure 2.2 shows relative motion paths with for the African continent fixed with respect to Eurasia. The opening of the North Atlantic ocean gave rise in the eastern Mediterranean to complex relative movements that can be partly resolved into a west to the east shear between the Triassic and middle Cretaceous and a subsequent SW-NE contraction (Delaloye and Wagner 1984), with the change in motion occurring in the Late Cretaceous (Livermore and Smith 1983; Savostin et al. 1986; Dewey et al. 1989). A smooth sinistral strike-slip motion from the Late Triassic to the Cretaceous was thus succeeded by convergence from the Cretaceous to the Recent. Figure 2.3 shows the position of Africa and Eurasia at three selected times in the history of the eastern Mediterranean, clearly illustrating the strike-slip and closure phases of the relative motion path and the progressive destruction of the Tethyan ocean. Major events in the geodynamic evolution of the Mediterranean Tethys can be linked to this kinematic framework. For instance, the shear is responsible for rifting and volcanism in Syria as well as the formation of a basin capable of producing the Hatay and Baër-Bassit ophiolites (Delaloye and Wagner 1984). Compression and ophiolite emplacement in the Late Cretaceous in Turkey (Delaloye and Wagner 1984) and Early to Mid-Tertiary in the central Mediterranean are linked to the Late Cretaceous and Tertiary convergent phase (Robertson and Grasso 1995).

A



B

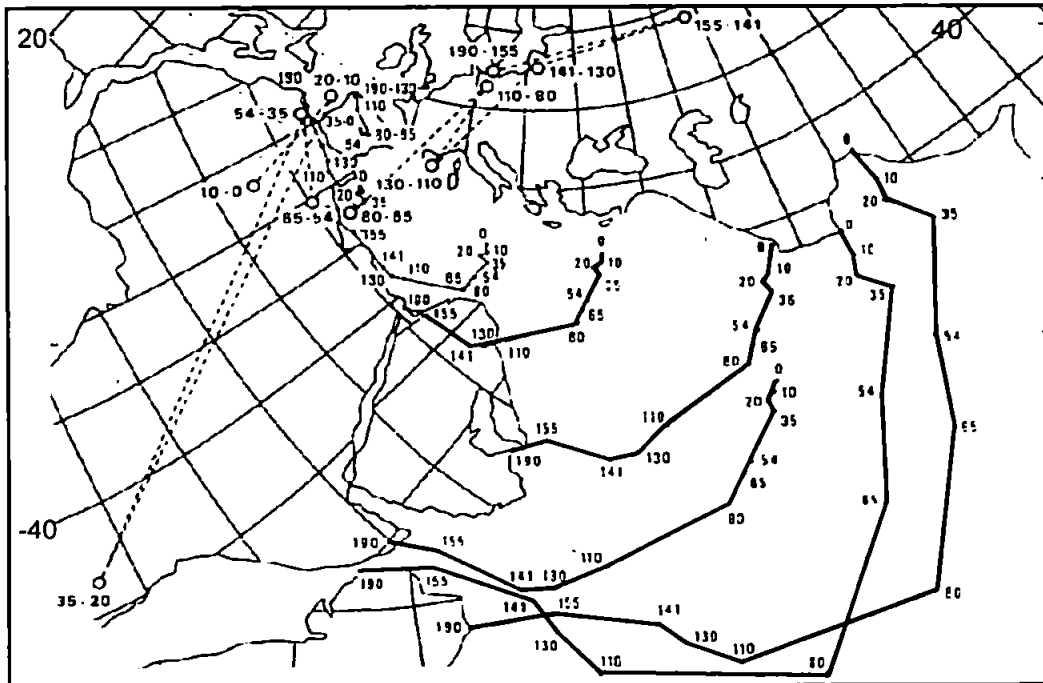


Figure 2.2: Two different reconstructions of the relative motion between the African and Eurasian plates from 190 Ma to the present-day:

A. After Livermore and Smith (1984); B. After Savostin et al. (1986).

The continuous black lines on both diagrams illustrate the position over time of various points of the African continent with respect to Eurasia with the time in Ma shown alongside (the top diagram only displays the time on the lower curve). The lower diagram also displays the position of the pole (open circles connected by dashed lines) showing the motion of Africa with respect to Eurasia over time. In both reconstructions a change from sinistral shear to north-south convergence is apparent around 80 to 90 Ma, although the nature of this change (smooth or rapid) varies slightly depending on both the reconstruction and the geographical position of the point of interest.

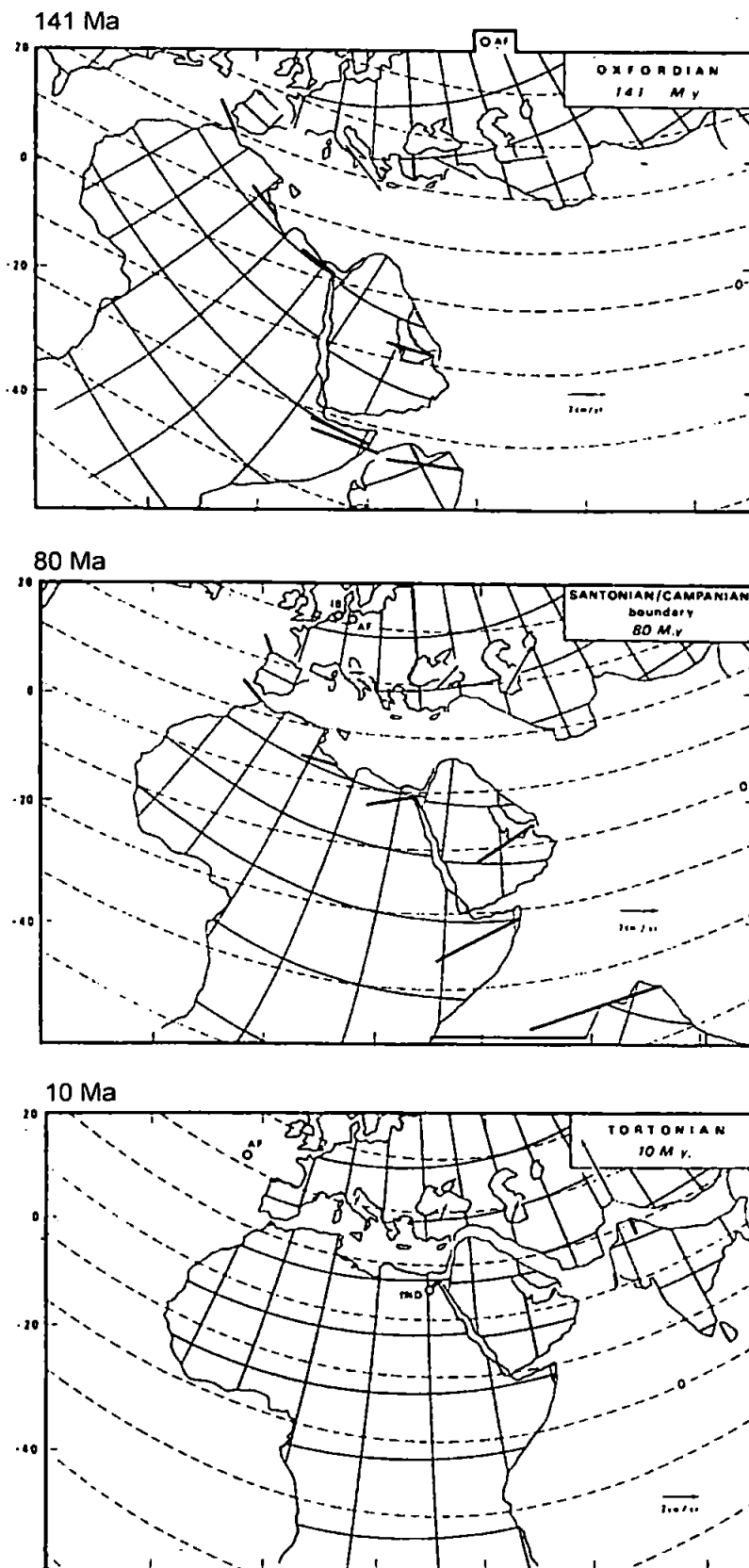


Figure 2.3: The relative positions of Africa and Eurasia at three selected times: firstly prior to the formation of the ophiolites, secondly around the time of their formation and lastly significantly post-emplacement and not dissimilar to the present-day setting (reconstructions from Savostin et al. 1986 with superimposed palaeolatitudes calculated from APWPs of Westphal et al. 1986 by Morris and Taring 1996).

2.4 Ophiolites of the eastern Mediterranean

2.4.1 Origin and distribution

Ophiolites represent fragments of oceanic crust and lithospheric mantle exposed on land by tectonic processes (Anonymous 1972). There is a greater density of ophiolites by area in the Mediterranean and Middle East than perhaps anywhere else in the world (Robertson 2004). The region is marked by numerous ophiolite chains that occur mostly along linear belts (Figure 2.4) and represent the remnants of Mesozoic oceanic crust from basins that have since been consumed by subduction processes. Eastern Mediterranean ophiolites occur in variable states of preservation and can be divided into three main ages (Triassic, Mid-Late Jurassic and Late Cretaceous), each group being restricted to well-defined and relatively brief time intervals (Robertson 2004). The Cretaceous ophiolites of Turkey and adjacent regions occur in three main belts, with one belt comprising the Pontide ophiolites, one comprising the ophiolites of the Anatolides and Taurides and a southern belt comprising the Troodos ophiolite of Cyprus and ophiolites of SE Turkey and Syria. Petrologic and geochemical evidence (e.g. Bağcı et al. 2005) shows a subduction-influence in these ophiolites and therefore formation in a suprasubduction zone (SSZ) setting (Figure 2.5). This is now recognised as the most common petrogenetic setting for the genesis of ophiolites, although the interpretation of the geochemical evidence is not universally accepted (see Pearce 2003 for a full account). The Tauride ophiolites are thought to have formed in a northern Neotethyan ocean around 78-110 Ma, based on a compilation of radiometric dates from the metamorphic soles (and assuming that these do not significantly post-date ophiolite genesis), and were emplaced southwards over the Anatolide margin onto the Tauride/Bolkar carbonate platforms in Campanian-Maastrichtian time (Robertson 2002).

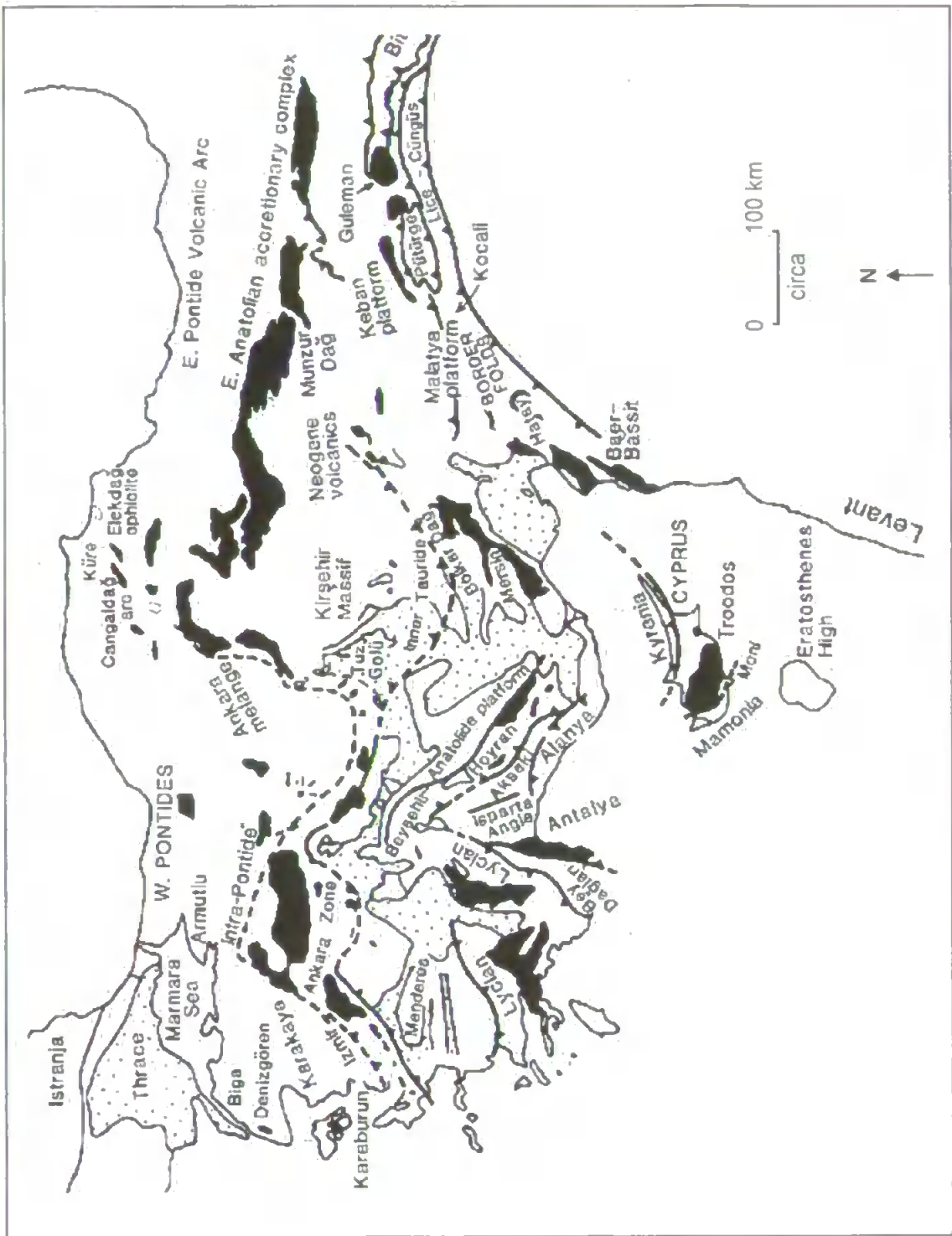
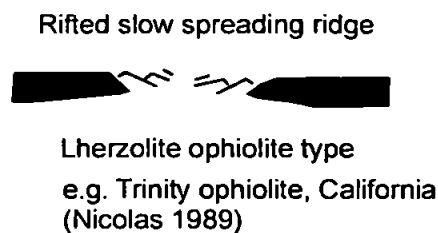
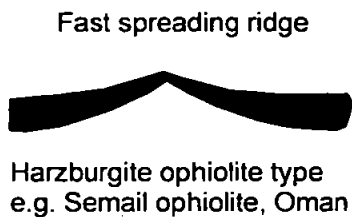
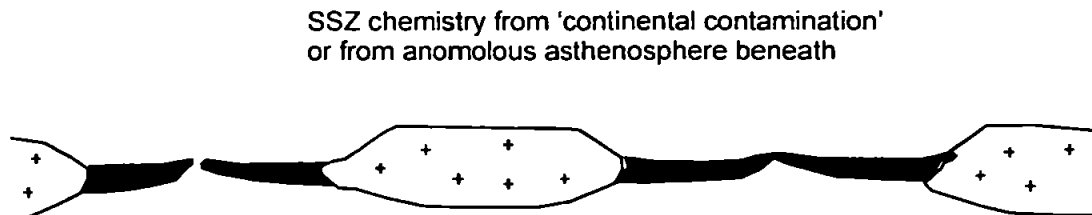


Figure 2.4: The location of major ophiolites of the eastern Mediterranean. The southerly belt including the Hatay ophiolite can be seen to comprise a prominent belt within the eastern Mediterranean (Robertson et al. 1996).

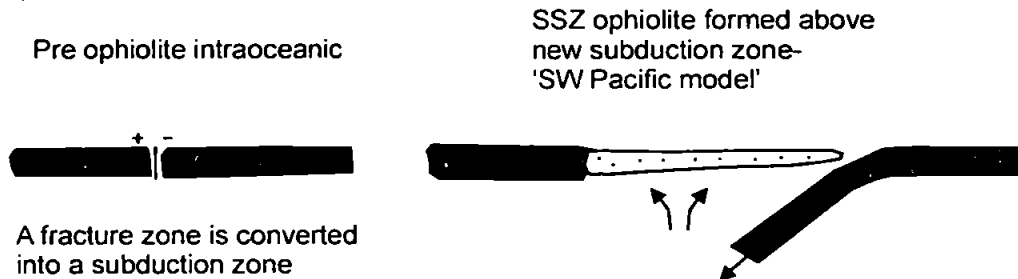
A Fast and slow spreading ridges



B Spreading ridges between microcontinents (very narrow basins)



C Rollback



D Asymmetrical spreading ridge collapse

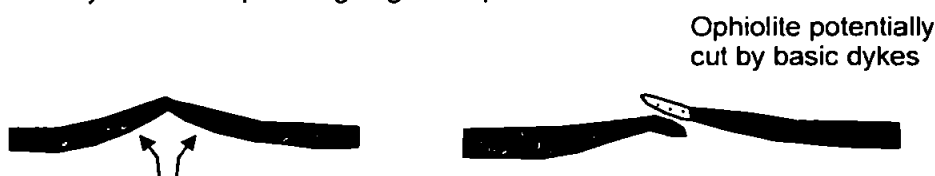


Figure 2.5: Tectonic models of various methods of ophiolite genesis (Robertson 2004; Fig. 2). Model A shows 'normal' ophiolite genesis at mid ocean ridges. There are both compositional and structural differences between ophiolites that form at spreading ridges with different spreading rates, with genesis at fast and slow-spreading ridges schematically illustrated above. Models invoke different degrees of partial melting of a homogenous lherzolitic source and a heterogenous deep mantle source. Fast-spreading results in a more continuous ophiolite sequence than rifted slow-spreading ridges. Model B shows genesis by spreading between continental fragments. Model C illustrates a fracture zone that converts to a subduction zone and is followed by suprasubduction zone spreading above. Model C is believed to be applicable to many of the Jurassic Balkan ophiolites, the eastern Mediterranean Late Cretaceous ophiolites and the Oman ophiolite (although initiation of spreading along a fracture is difficult to prove). Model D may also be relevant if a buoyant spreading axis could collapse, initiating subduction despite the buoyancy constraints

The southerly chain of ophiolites of which the Hatay ophiolite comprises part is one of the most prominent ophiolite belts in the eastern Mediterranean area. The ophiolites in this chain are generally accepted to be Late Cretaceous in age and are believed to have formed by SSZ spreading in a small southerly Neotethyan ocean basin. Emplacement occurred as a vast laterally continuous sheet, with the Kocali, Amanos and Hatay ophiolites of Turkey and Baër-Bassit ophiolite of Syria (Figure 2.4) remaining subsequent to tectonic disruption and differential erosion in the Tertiary (e.g. Şengör and Yilmaz 1981; Yilmaz 1993).

Although many ophiolites are now believed to have formed by SSZ spreading, modern analogues (e.g. SW Pacific region) displaying both ridge geology and subduction geochemistry are not common and do not provide exact analogues. The vast scale of the inferred Late Cretaceous SSZ spreading stretching for thousands of kilometres from Greece to Oman appears to have no modern analogue (Robertson 2004). If a multi basin palaeogeography is accepted (section 2.5), SSZ spreading must have taken place more or less synchronously in several adjacent ocean basins, and again there is no known modern analogue. SSZ ophiolites are thought to typically form during short-lived periods (< 5 Ma) of regional plate re-organisation (Robertson 2002) but there is no general consensus on their origin. Drastic reorganisation of plate boundaries may provide the specific conditions necessary for ophiolite genesis and later emplacement, which may include convergence along former transform faults or the collapse of a small spreading ridge related to a pulse of regional convergence (Robertson 2004). The times of major SSZ-type genesis include the Early Ordovician (Iapetus ocean), Mid-Jurassic (Tethys and beyond), Late Cretaceous (Tethys) and the Eocene (SW Pacific).

The SSZ model allows a mechanism of both formation and emplacement of ophiolites, with both backarc and forearc settings as possible settings for genesis. Examples from both oceanic and intra-continental backarc are basins known. Ophiolitic metamorphic

soles commonly overlap in age with the overlying lithologies which is consistent with simultaneous underplating of subducted material with SSZ-spreading above.

2.4.2 Ophiolite emplacement mechanisms

The precise mode of ophiolite emplacement is debated, although almost all workers suggest some sort of thrust emplacement. A series of alternative tectonic scenarios for the emplacement of ophiolites was initially suggested by Dewey (1976) and Casey and Dewey (1984). Various tectonic scenarios are shown in Figure 2.6, after Robertson (2004). Evidence for thrusting is present in most of the major ophiolite complexes, and in several, such as in the Oman ophiolite, individual outcrops can be interpreted as thrust slices (references within Hall 1996). It is very common for regions showing metamorphism of the high pressure type (glaucophane-schist facies) to also contain ophiolites. These facies require a low geothermal gradient i.e. a combination of high pressure and low temperature; conditions characteristic of subduction zones (Hall 1996). In subduction zones, convergence of continental and oceanic crust (or oceanic crust only) is continually occurring. Robust explanations for the observation that only small areas of oceanic crust are obducted whilst the majority is subducted are yet to be agreed upon. Most MOR-type oceanic crust is subducted, or is preserved as dismembered thrust sheets, or as blocks in an ophiolitic melange, and is commonly metamorphosed under high-pressure/low-temperature (HP/LT) conditions (Robertson 2002). Generally, seamounts, oceanic plateaus, transform faults, forearc and rift-related units appear to have a higher chance of preservation on land than MOR-type crust (Robertson 2002).

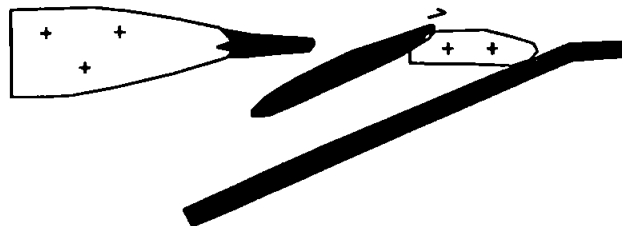
A Trench-margin collision



B Ridge collapse



C Micro-continent (or seamount) collision



D Transpression (reactivated transform)

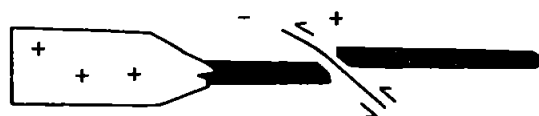


Figure 2.6: Various models of ophiolite emplacement (Robertson 2004; Fig. 19). Model A invokes trench-collision with the oceanic lithosphere and mantle detached and emplaced as several intact thrust sheets. The same subduction zone is responsible for both creating the ophiolites and for emplacement several Ma later. Model A is applicable to Oman and many of the Cretaceous and Jurassic ophiolites of the eastern Mediterranean. Model B involves collapse of an active oceanic ridge, with thrusting initiated at/near the spreading ridge which remains active during emplacement. This model is problematic due to ridge buoyancy. It has also been suggested as applicable for the Oman ophiolite. C involves emplacement/docking along an active continental margin and D involves emplacement along strike-slip (transpressional) margins. Model D occurs where the continental margin edge is oriented at an oblique angle to the direction of ophiolite emplacement e.g. in the case of the Tekirova ophiolite. Models A, C and D are generally accepted whereas B is more controversial.

The normal thickness of mature oceanic plates is 60 to 100 km whereas the largest exposed ophiolite complexes are significantly less than this, around 10 km thick (Hall 1996). This suggests that either only a small part of the oceanic plate has been obducted, that the obducted crust was anomalously thin, or alternatively, that the obducted material is derived from the region of a spreading ridge, where the oceanic crust is thin and mechanically weak (Christensen and Salisbury 1975). This theory is generally accepted at the present time and explains the existence of contact metamorphic aureoles beneath a number of ophiolites (e.g. Karamata 1980).

Ophiolite emplacement, particularly in the eastern Mediterranean, appears to commonly be the result of trench-margin collision. It tends to correlate to discrete periods of regional to global plate re-organisation with emplacement of the large ophiolites occurring when the leading edges of SSZ slabs collided with Tethyan continental margins (Robertson 2002). Strike-slip (due to transpression) and large-scale accretion along subducting margins played a role in certain cases in eastern Mediterranean ophiolites (Robertson, 2004). For example, the Tekirova ophiolite of the Antalya area of Turkey is believed to have been emplaced by strike-slip (transform) mechanisms which appear to have influenced both its genesis and emplacement (Robertson 2002).

There are few modern analogues of ophiolite emplacement with possible examples including the Bismarck arc, located to the north of the Papuan ultramafic belt and the Ocussi ophiolite in Timor (Robertson 2004). The Plio-Quaternary uplift and relative southward displacement of the Troodos ophiolite may also be considered as a current example of ongoing ophiolite emplacement, although significantly post-dating initial Late Cretaceous genesis at a spreading centre (Robertson 2002).

2.5 Implications of ophiolites for the evolution of the eastern Mediterranean

2.5.1 The palaeogeography of the Tethys ocean in the eastern Mediterranean

The existence of an ocean between Africa and Eurasia was first proposed early in the last century. Geological evidence favours the existence of a long-lived Tethyan ocean in the Mediterranean region, between the African (Gondwanan) and Eurasian plates and extending at least as far as the Oman region (Robertson 2004). There have been various different terminologies used to describe this ocean with the precise meanings of terms varying from worker to worker. Palaeotethys is generally used to describe the wide ocean that existed between the two continental masses, although the timing of its closure and the location of the suture vary (Robertson, 2004). More specifically, Ustaomer and Robertson (1994) use the term Palaeotethys to refer to oceanic crust of Late-Palaeozoic to early Mesozoic age in the eastern Mediterranean region regardless of its exact location. Neotethys generally refers to oceanic crust located adjacent to Gondwana in the south, although again there are variations in the interpretation of the timing of rifting and width of the ocean. Palaeotethys is generally accepted to be an older ocean than Neotethys, although may not be either entirely temporally or spatially discrete. Tethys in the eastern Mediterranean as a whole was generally closed by the Early Tertiary (Eocene-Oligocene) although oceanic remnants in the eastern Mediterranean Sea and Black Sea still survive (Robertson 2002). Figure 2.7 illustrates the major suture zones in Turkey.

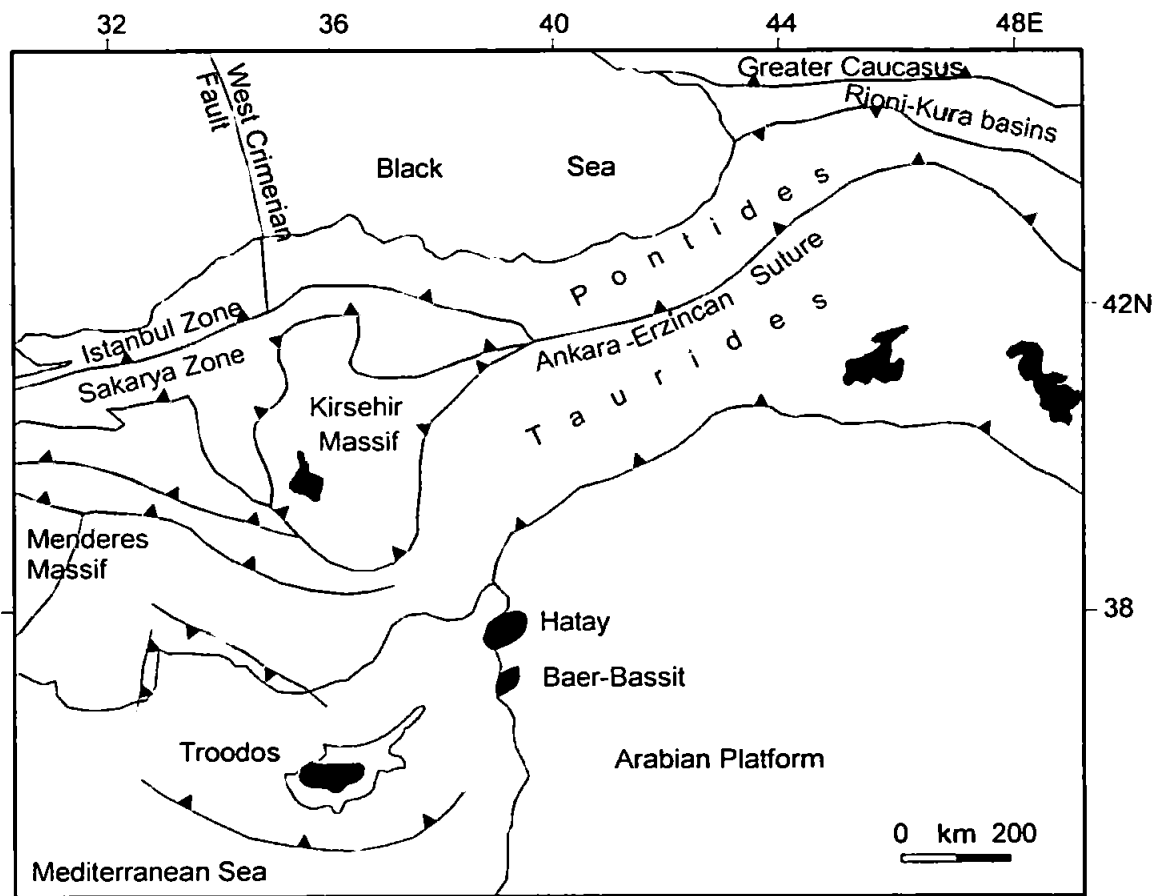


Figure 2.7: Suture zones in the eastern Mediterranean.

Some Tethyan reconstructions assumed a single Tethyan ocean was located between the Gondwanan passive margin to the south and the active Eurasian margin to the north (e.g. Dercourt et al. 1986), whereas others used the increasing body of evidence for the existence of multiple ophiolite root zones (section 2.5.3) to incorporate the concept of a flexible collage of microplates rifted from the Gondwanan margin. In this type of model, the ophiolites were generated in convergent settings rather than at normal mid-ocean ridges (e.g. Şengör and Yilmaz 1981; Robertson and Dixon 1984). A comprehensive review of the various models can be found in Robertson et al. (1996) and Robertson (2004). The three main types of model were proposed by Robertson and Dixon (1984), Dercourt et al. (1986; 1992) and Şengör et al. (1984). Figure 2.8 illustrates significant features of the Robertson and Dixon (1984) and Dercourt et al. (1986; 1992) models.

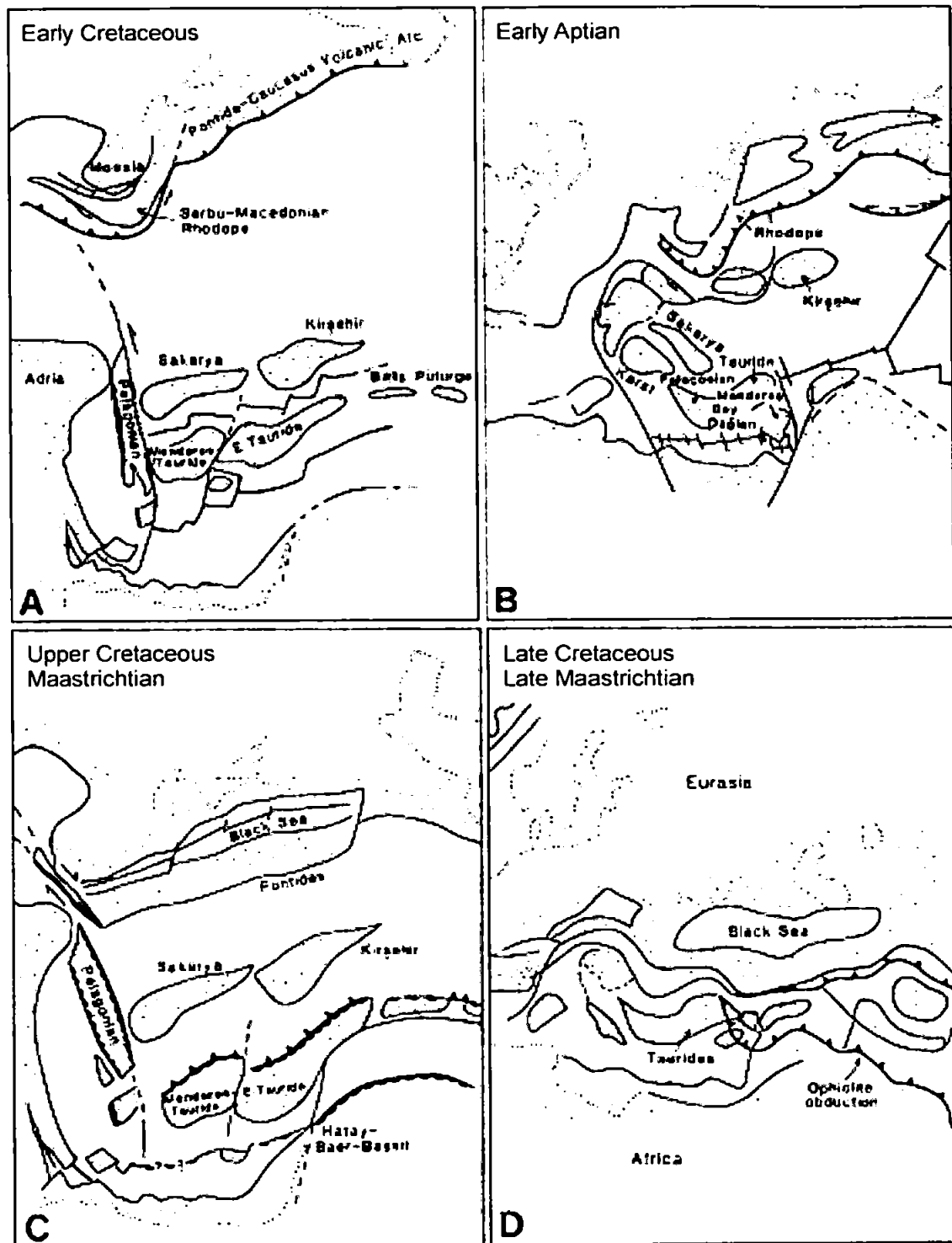


Figure 2.8: Alternative tectonic reconstructions of the eastern Mediterranean Neotethys for Early-Mid Cretaceous time (from Robertson et al. 1996).

The LHS diagrams (A and C) show two reconstructions at different times from the Robertson and Dixon (1984) model, and the RHS diagrams (B and D) show two reconstructions from the Dercourt et al. (1992) model. In both cases, the upper diagrams (A and B) show the tectonic setting at an earlier time with the lower diagrams illustrating the tectonic setting closer to the time of ophiolite emplacement. The main difference between these is that the LHS model suggests ophiolite emplacement from multiple smaller oceanic basins within Neotethys whereas the RHS model suggests emplacement from a single northerly Neotethys.

A. Early Cretaceous: Pindos ocean in west is partly closed while opening continues in the east. C. Upper Cretaceous: Suprasubduction zone ophiolite emplacement from several strands of the Neotethys in the Turkish area.

B. Early Aptian: With a new rifted Cretaceous oceanic basin. D. Late Cretaceous: Ophiolite obduction from a single northerly Neotethys.

In the first model (Robertson and Dixon 1984; Figure 2.8A and C) a continuous Tethyan ocean continuously existed in the eastern Mediterranean region, at least from the Late Palaeozoic onwards, with episodic northward subduction of Tethyan oceanic crust beneath Eurasia and the northwards drift of Gondwanan continental fragments towards Eurasia. In the Mesozoic, the south Tethyan area was interspersed with rifted continental fragments and small ocean basins with ophiolites mainly forming by SSZ spreading during times of regional plate convergence and emplaced as a result of trench-passive margin collisions. In a related model, Stampfli et al. (1991) argued for spreading along the North African margin in the Late Permian. In the second model (Dercourt et al. 1986) only one evolving Tethys existed. Triassic-Jurassic crust (Neotethys) formed in a single Tethyan ocean basin located north of the Gondwana related units. Spreading subsequently formed a small ocean basin in the eastern Mediterranean sea during the Cretaceous with Jurassic and Cretaceous ophiolites forming during times of regional divergence and Mesozoic ophiolites are viewed as being far-travelled. The last model (Şengör et al. 1984; Figure 2.8B and D) invokes southward subduction beneath the northern margin of Gondwana, leading to the opening of Triassic backarc basins and a rifted continental fragment drifting across a pre-existing Tethys to collide with the passive Eurasian margin. Mesozoic ophiolites mainly formed above subduction zones and were seen as far-travelled in the Greek area and more locally rooted in the Turkish region. Robertson et al. (1996) describe difficulties with all of these models, although suggest that the first meets four key lines of evidence: northward subduction in the north; multiple ocean basins from the Triassic onwards in the south; SSZ spreading of the major ophiolites; and emplacement from both northerly and southerly Mesozoic ocean basins.

Most models have certain features in common, such as a widening from the Late Palaeozoic onwards of the Tethys ocean eastwards from an oceanic gulf into a wider ocean (Robertson 2002). The Izmir-Ankara-Erzincan suture may be viewed as the 'main'

Tethyan suture and the site of formation and consumption of oceanic crust of both Late Palaeozoic-Early Tertiary (Palaeotethys) and Mesozoic (Neotethys) age (Robertson 2004).

Although various later reconstructions have been produced (e.g. Garfunkel 1998; Robertson et al. 1999; Dercourt et al. 2000; Ziegler et al. 2001; Stampfl et al. 2001; Stampfli and Borel 2002), a near consensus has now emerged in favour of a Tethyan palaeogeography involving microcontinents and oceanic strands, akin to the SW Pacific area of today (Robertson 2004). The palaeogeographic model adopted in this thesis is that of Robertson (2002), which is based on that proposed by Robertson et al. (1996) and Robertson and Dixon (1984).

2.5.2 Ophiolite root zones in the eastern Mediterranean

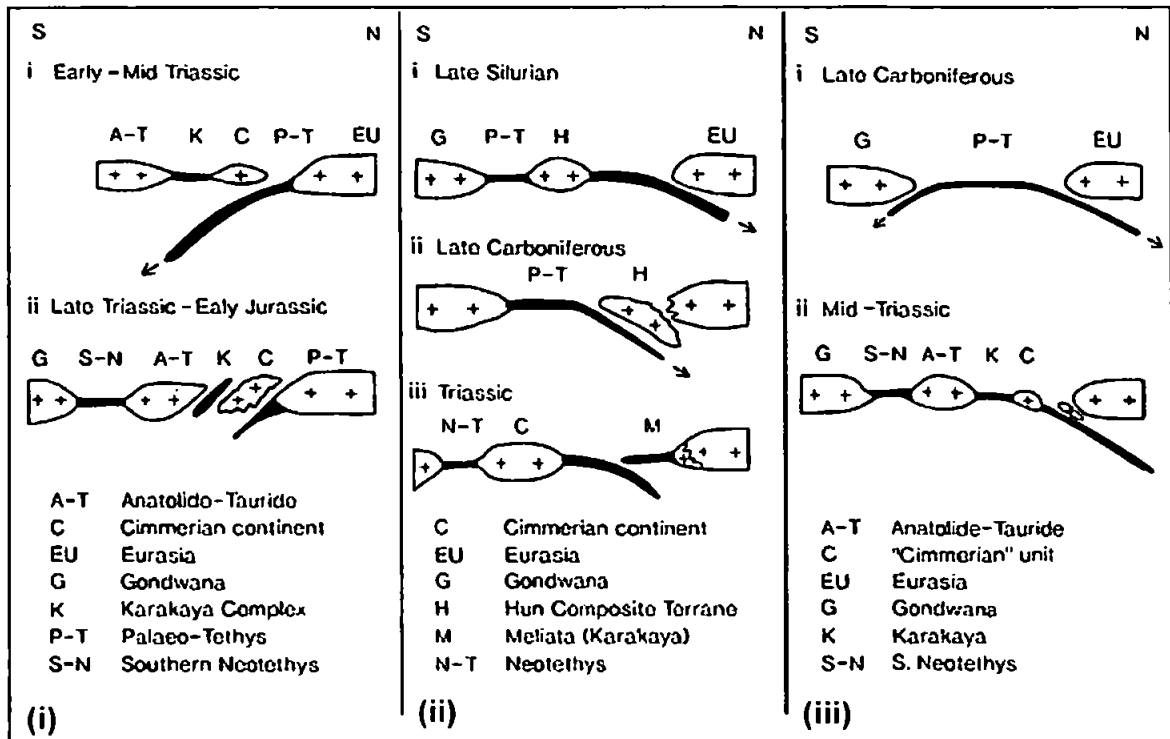
A controversial question in Tethyan geology has concerned the nature and number of the root zones for the eastern Mediterranean ophiolites. For instance, Ricou et al. (1984) and Stampfli et al. (1991) suggest formation of all eastern Mediterranean ophiolites (including Troodos, Hatay and Baër-Bassit) within a single basin in north Anatolia whereas Şengör et al. (1984) and Robertson and Dixon (1984) suggest instead that almost every ophiolite could have been rooted in a separate basin with little movement during emplacement into their present day position. As a variation, Dilek and Thy (1999) suggest that the Troodos ophiolite is unique in being southerly derived.

The Ricou et al. (1984) model contradicts reconstructions of the eastern Mediterranean that involve the existence of at least a separate southern strand of the Neotethys (e.g. Robertson and Woodcock 1980) and those that involve a complex palaeogeography involving a braided pattern of oceanic strands and microcontinental slivers (Şengör and Yilmaz 1981). The basis of this model is the idea that the similarity between marginal sedimentary

successions preserved within separate ophiolite massifs indicates that all of the allochthonous ophiolite units were derived from a single root zone in north Anatolia. This model involves progressive northwards subduction beneath the Pontides (the Eurasian margin in this model) from the Middle Cretaceous onwards, followed by emplacement in successive southwards stages over the Tauride and Arabian platforms from the Late Cretaceous to reach present positions by the Late Eocene/Late Miocene.

The alternative Şengör et al. (1984) model (section 2.5.1; Figure 2.9A) suggests genesis of the ophiolites in numerous smaller basins, involving the southwards subduction of Palaeotethyan oceanic crust resulting in the rifting of a small E-W trending continental sliver and the Neotethys ocean opening to the south. Continued southwards subduction results in the separation of further continental slivers (Şengör et al. 1984). The Robertson and Dixon (1984) model adapts this idea but has a northwards subducting Palaeotethys. A model by Dercourt et al. (1986), similarly to the Ricou et al. (1984) model, involves a single root zone for all of the ophiolites in the southerly belt, of which Troodos, Hatay and Baër-Bassit comprise part, the emplacement of which onto the Arabian margin would involve a 1000 km long plus zone of young oceanic crust stretching eastwards to Oman.

A



B

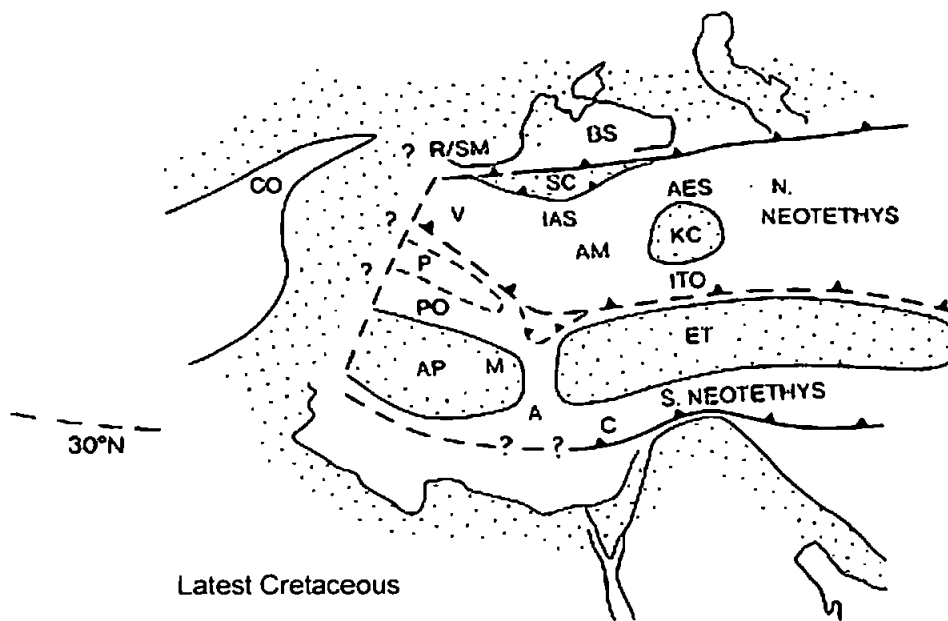


Figure 2.9: Root zones for the Late Cretaceous ophiolites of the eastern Mediterranean.

A. Alternative plate tectonic models for the genesis of ophiolitic suture zones in Turkey in Late Palaeozoic to Early Mesozoic (Robertson 2004; Fig. 24). Model (i) is the southward subduction model of Sengor et al. (1984); model (ii) is the northward subduction model of Stampfli et al. (2001) and model (iii) is a variable subduction polarity model of Robertson et al. (1999).

B. Simplified palaeogeographic sketch map (from Robertson 2002) concentrating on the origin of Cretaceous ophiolites where some ophiolites originate in a northern Neotethyan ocean and some are derived from a separate southerly Neotethyan ocean basin. Key to letters: A Antalya, AES Ankara-Erzincan suture zone, AM Ankara melange, AP Apulia, BS Black Sea marginal basin, C Cyprus, CO Carpathian ocean (Western Tethys), IAS Izmir-Ankara suture zone, ITO Inner Tauride ocean, K Kisehir/Nigde metamorphic massif, M Menderes metamorphic massif, P Pelagonian, PO Pindos ocean, R/SM Rhodope/Serbo-Macedonian, SC Sakarya metamorphic massif, ET East Tauride (Bolkar), V Vardar.

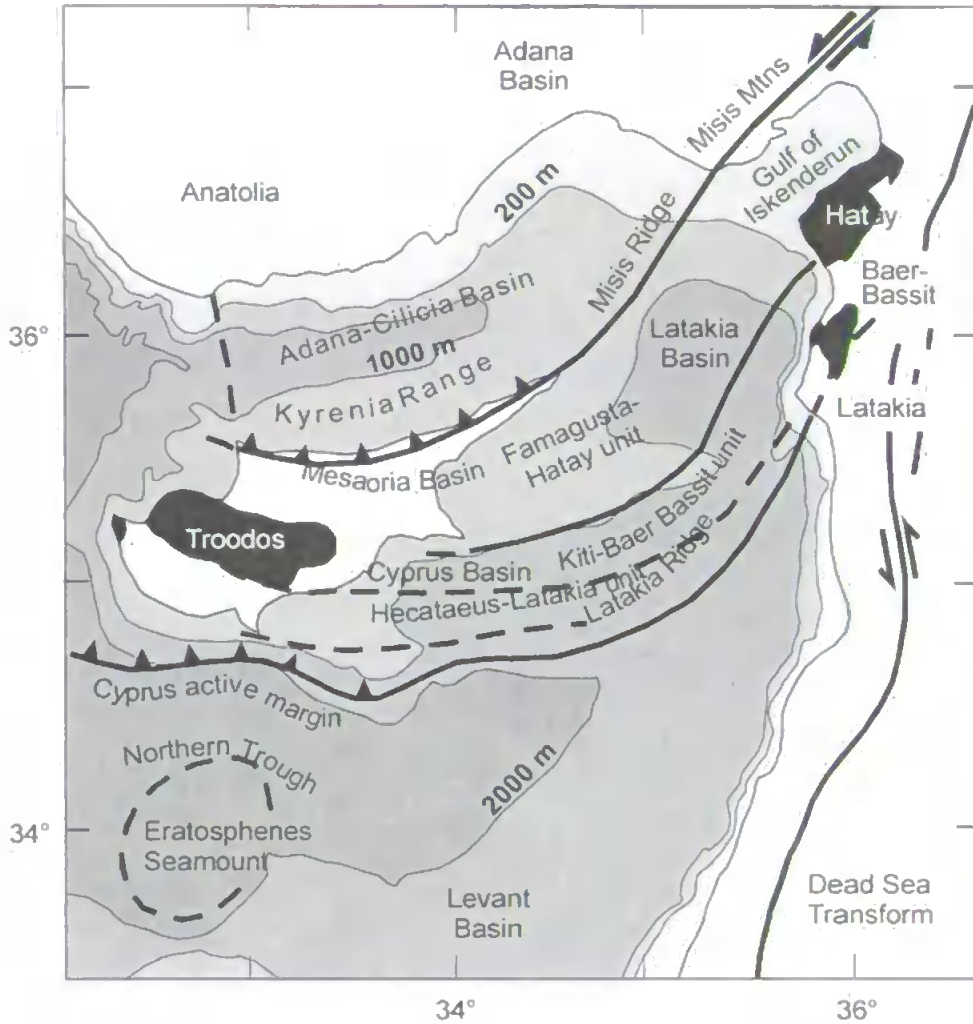
The models involving more than one root zone for the southern ophiolites appear to be more likely (Figure 2.9B) as various lines of geological evidence provide difficulties for models where ophiolites are rooted in a northerly basin and travelled for hundreds of kilometres to their present positions. For example, the presence of the Campanian (Perapedhi Formation) to Lower Tertiary (Lefkara Formation) sedimentary sequence overlying the Troodos ophiolite, that is essentially continuous between these times, is difficult to explain if complex multi-stage southerly emplacement had been occurring over this time period as suggested in the Ricou et al. (1984) model, suggesting instead that the ophiolites cannot have been thrust far over a platform in the Late Cretaceous (Robertson et al. 1996). Also coeval carbonate platform successions exposed between outcrops of supposedly once continuous ophiolitic nappes include sedimentary successions extend in age beyond the time of emplacement (Şengör and Yilmaz 1981). This is difficult to explain if the ophiolites have travelled far over the platform. A complex mode of emplacement of the ophiolites first onto the Mesozoic platform in the north (i.e. Bey Dağlari) followed by thrusting of the complete platform southwards is suggested by Ricou et al. (1984) to account for the lack of disruption to the coeval sediments exposed between the ophiolites, but this is not supported by field studies that find no evidence for a major thrust discontinuity within the Bey Dağlari carbonate platform (Robertson 1993). Evidence of emplacement directions also supports generation in smaller ocean basins. The ophiolites and related marginal units in the Isparta angle area along the SW margin of the Bey Dağlari platform were emplaced westwards and so cannot be correlated with the regionally extensive Lycian nappes exposed further northwest, which were emplaced southwards (Robertson 2004)

Generally, the increasing acceptance of a varied Mesozoic Tethyan palaeogeography of oceanic strands separating microcontinents increases the likelihood that ophiolites were derived from several oceanic basins by various tectonic processes (Robertson 2004).

2.6 Ophiolites of the peri-Arabian chain

The southerly ophiolite belt in the eastern Mediterranean stretches for over 1000 km from Troodos in the west to the Semail ophiolite of Oman in the east (Figure 1.1). There is strong evidence for genesis of the largest eastern Mediterranean ophiolites (including Troodos and Semail) above subduction zones during times of regional plate convergence. The sedimentary covers indicate that large contemporaneous volcanic arcs were not present (Robertson 2004). The Hatay, Baër-Bassit and Troodos ophiolites are intimately linked, both in the fact that they are believed to have formed within the same southerly Mesozoic Neotethyan basin, and in the preservation of both Hatay and Baër-Bassit adjacent to each other on the Arabian platform. Figure 2.10A shows the relationship of these ophiolites in the present-day eastern Mediterranean area and the cross-section of Figure 2.10B illustrates the inferred relationship between the Hatay and Baër-Bassit massifs (after Delaloye and Wagner 1984). These ophiolites are interpreted to have formed in the Late Cretaceous within the Neotethys ocean to the north of the Arabian passive margin, although the absolute ages of formation may differ. Convergence, subduction/accretion and ophiolite emplacement all occurred in the Late Cretaceous. During emplacement of the Hatay and Baër-Bassit ophiolites onto the Arabian platform, the Arabian passive margin subsided to form a foredeep which was infilled with debris shed from the advancing nappes and including continental margin units similar to those preserved in the Baër-Bassit melange (Al-Riyami et al. 2000). In contrast to Baër-Bassit, a metamorphic sole is absent from the Hatay ophiolite, although a serpentinite melange is developed (Al-Riyami et al. 2000; section 2.9.2) and a thick melange of continental margin and oceanic units is also absent. Both ophiolites were emergent following emplacement, followed by latest-Cretaceous shallow-marine transgression, deepening upwards into the early Tertiary (Al-Riyami et al. 2000).

A



B

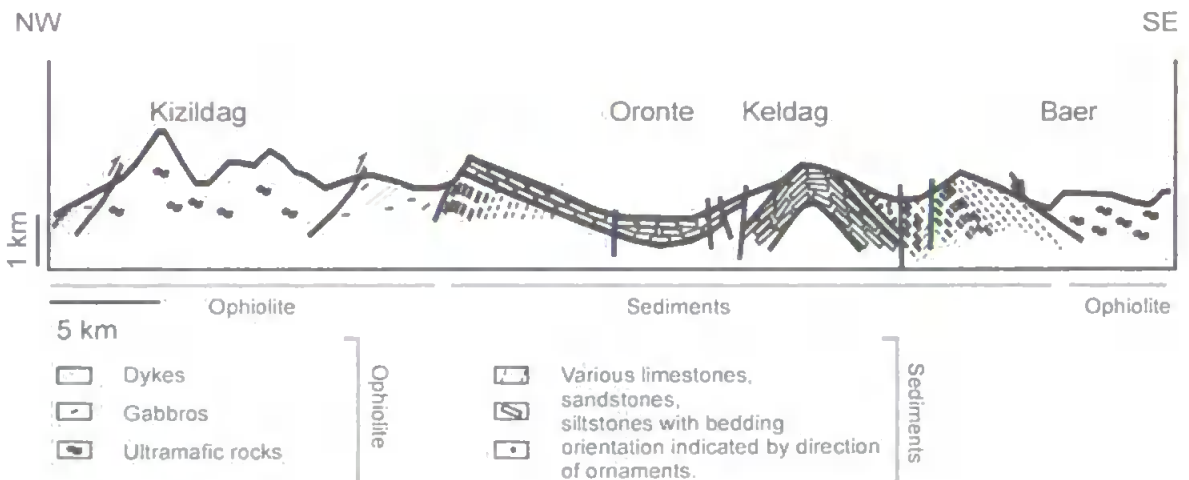


Figure 2.10: The relationship between the Hatay, Baer-Bassit and Troodos ophiolites.

A. Map showing the three ophiolites and the major structural features and present-day basins of the eastern Mediterranean.

B. Cross-section showing the inferred relationship between the Hatay and Baer-Bassit ophiolites (after Delaloye and Wagner 1984). Both ophiolites are believed to be part of the same ophiolite thrust sheet with the sediments of the Arabian platform between separating the present-day outcrops.

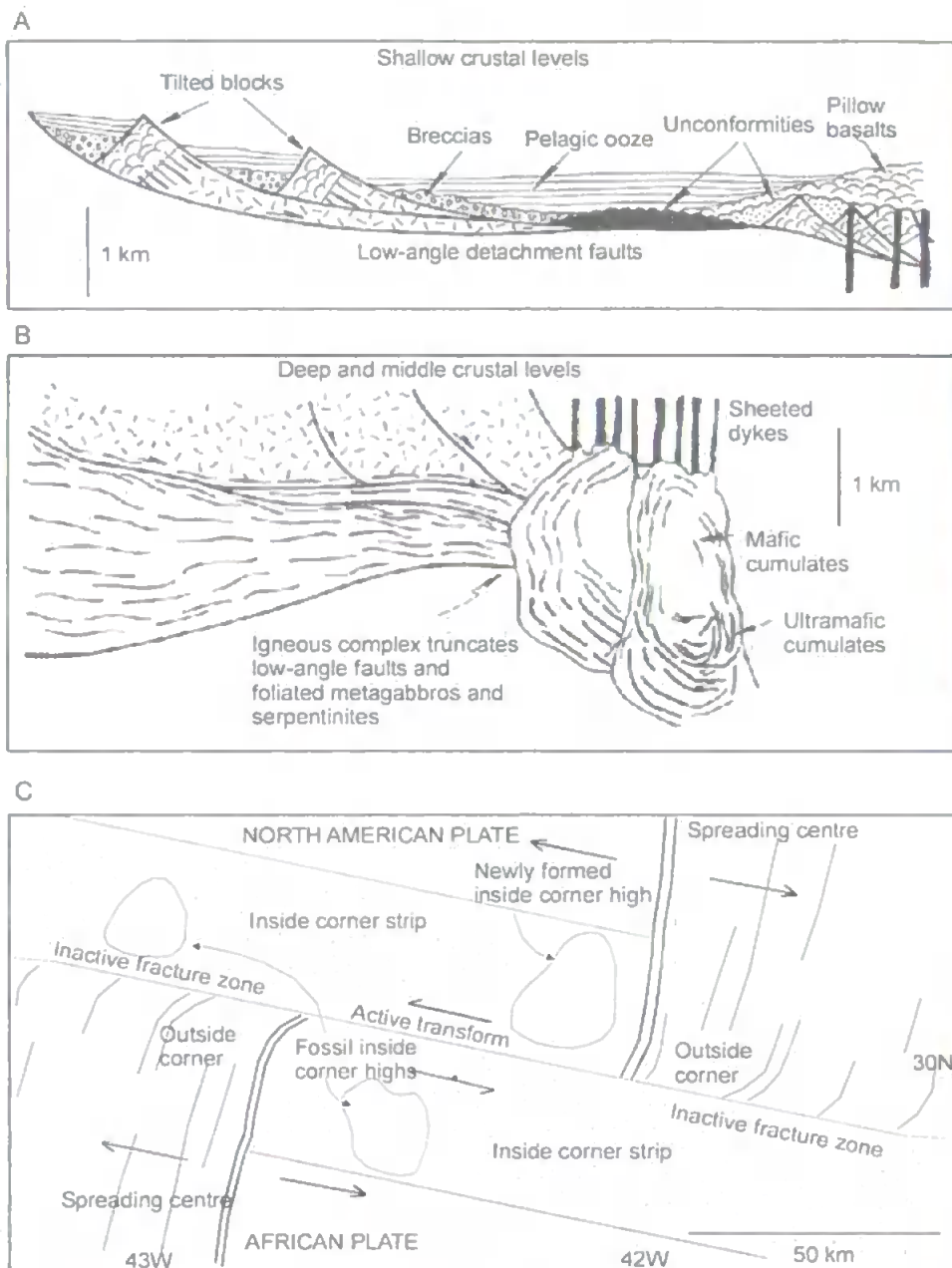


Figure 2.11: Schematic diagrams illustrating seafloor processes that may sometimes become preserved in ophiolites.

A and B. Schematic cross-sections illustrating the geological relationships that might be expected in ophiolites or oceanic lithosphere from slow-spreading ridges with non-steady state magma supply, that have been deformed and intruded, such as in the northern spreading cell of the MARK area of the MAR (Karson 1990). A. Upper crustal exposures with various types of unconformities: lavas, breccias and/or pelagic ooze over tilted volcanics and dykes, variably deformed and metamorphosed gabbroic rocks, and/or serpentinites. Dykes feeding lavas may cut tilted and attenuated upper units and low-angle detachment faults. B. Lower crustal and upper mantle structures with intrusive relationships: dykes, trondhjemitic, gabbroic and ultramafic cumulates cut low-angle faults and shear zones in metagabbros and serpentinites and more pervasively deformed lower crustal/upper mantle rocks. The geological relationships shown in B would be found at deeper levels than those illustrated in A, where the lower crustal units are only present at higher crustal levels due to exposure along low-angle detachment faults.

C. Summary geological overview in plan section of the Atlantis transform fault at 30°N on the MAR (after Cann et al. 2001). The active transform lies between the two spreading axes. Crust formed at one of the inside corners moves first along the transform fault, shearing against inside corner crust formed at the other spreading centre, until it reaches that centre. There, magmatic activity constructs new outside corner crust which is welded onto the inside corner crust as it passes from transform fault to the fracture zone. The dashed lines show the orientation of topographic ridges, mostly, oriented parallel to the spreading axes, representing periods of increased magmatic activity at the spreading centres. This tectonic scenario has been suggested as a possibility for part of the Troodos ophiolite (section 2.9.1).

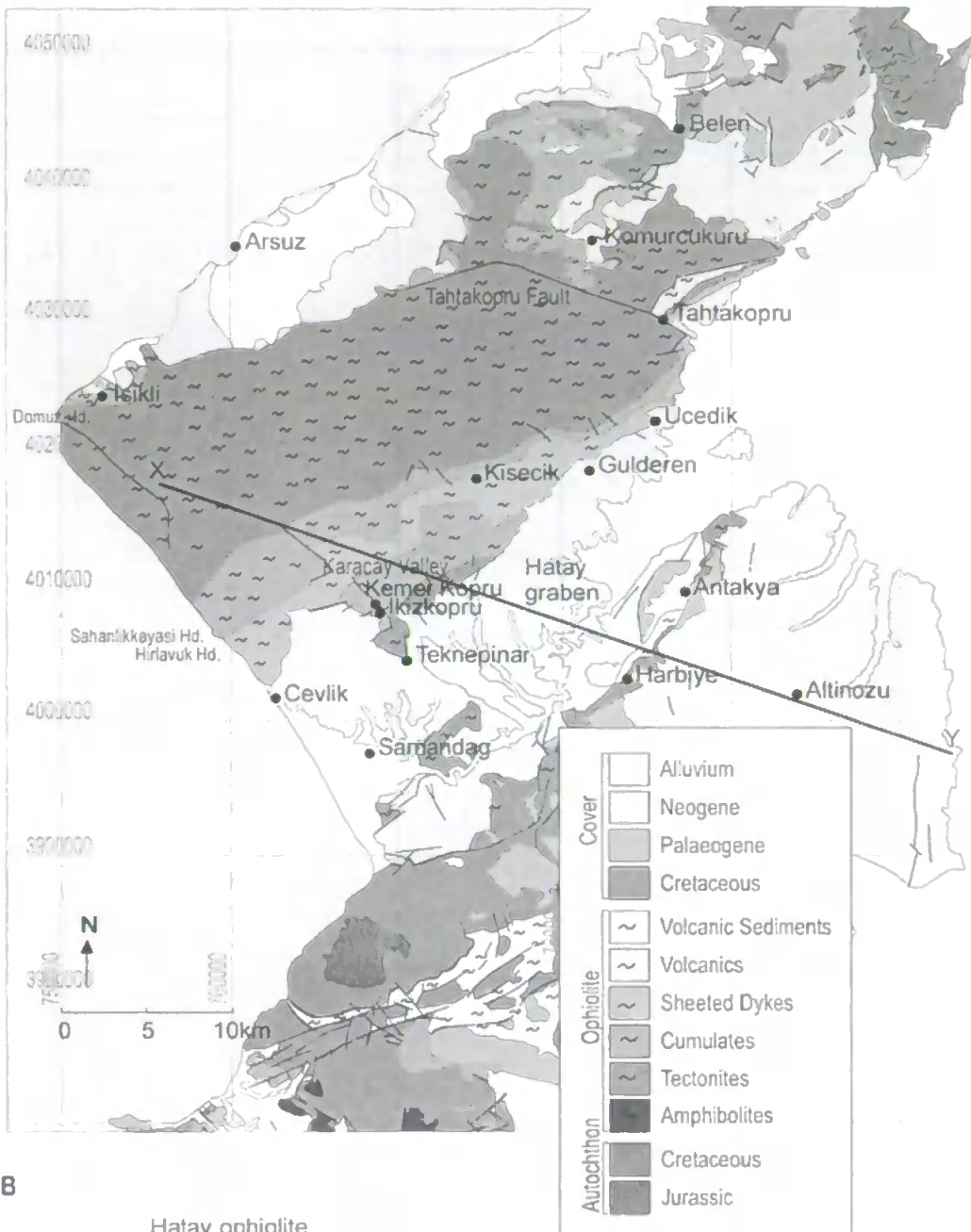
The Troodos, Hatay and Baër-Bassit ophiolites are all believed to have been formed within slow-spreading systems, as indicated by tectonic and morphological features within these ophiolites. For instance, a seafloor detachment surface has been recognised in the Troodos ophiolite (section 2.9.1). This ophiolite preserves various original seafloor structures, including as a fossil transform fault zone and three inferred axial spreading grabens (section 2.9.1). The Hatay ophiolite has also been interpreted to preserve original seafloor spreading relationships, such as a seafloor spreading graben formed by detachment faulting (Dilek and Thy 1998; section 2.8). Figure 2.11A shows the formation of detachment faults at slow-spreading ridges and Figure 2.11B shows the processes occurring at transform fault-ridge intersections.

2.7 Geology of the Hatay ophiolite

2.7.1 General description

The Hatay massif covers 950 square kilometres (25 by 45 km) and is composed of an ophiolite sequence that is up to 7 km thick, including serpentinitised peridotites and harzburgites, layered gabbros, a sheeted dyke complex and pillow lavas. The geology of the ophiolite is shown in Figure 2.12, along with an inferred cross-section (Pişkin et al. 1986). The ophiolite consists of two structurally distinct massifs that are separated by the NW-SE striking, steeply dipping Tahtaköprü fault (Figure 2.12A) with the main massif lying to the west of this fault. Ophiolite units to the north have complex relationships with outcrops ranging from the lowest exposed levels of the ophiolite (the basal shear zone) to the highest levels (pillow lavas and associated metalliferous sediments). The Hatay ophiolite contains almost a complete Penrose sequence, lacking only a metamorphic sole and deep-sea radiolarite cover (Figure 2.13).

A



B



Figure 2.12: The geology of the Hatay ophiolite.

A. The map shows the major outcrops of the ophiolite and locations discussed in the text.

B. A representative cross-section of the ophiolite (Pişkin et al. 1986) with the rough line of section illustrated on the map of 2.12A. The Tahtakopru fault lies off the line of this section but displaces the ophiolite sequence to the NE, containing the extrusive series at the top, above the main ophiolite sequences to the SE. The ultramafics of the ophiolite can be seen from the cross section to comprise a topographic high, flanked by the shallower levels. The sedimentary cover sequences are generally gently to moderately dipping, with the Hatay graben representing several kilometres of vertical displacement.

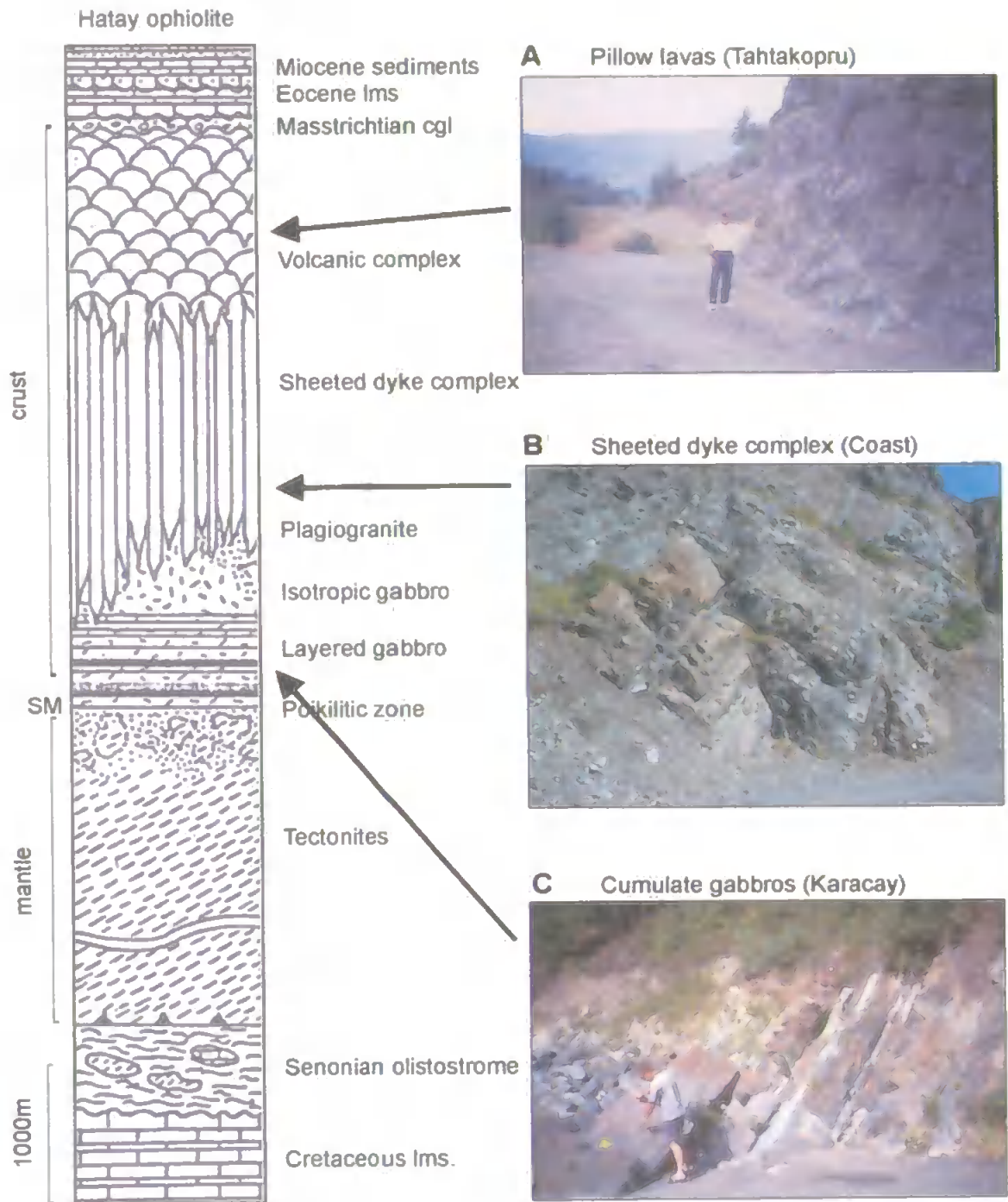


Figure 2.13: The lithologies within the Hatay ophiolite, with photos illustrating the major ophiolitic units (see Figure 2.12 for location). A. Pillow lavas exposed along a road section near Tahtakopru. B. Sheeted dykes exposed along the coastal road (note size in comparison to person in bottom right corner). C. Cumulate gabbros exposed at river level along the Karacay river valley.

The ultramafic complex of the massif outcrops in the centre of the area and comprises the core of an antiformal structure which trends NE-SW (e.g. Tinkler et al. 1981). The shallower levels of the ophiolite are exposed on the limbs of the antiform, and the gabbros and sheeted dyke complex exposed to the south form a smaller synform (Tinkler et al. 1981). The contacts between the different units of the ophiolite are generally interpreted to be tectonic in the north. In the south contacts have been differently interpreted to be tectonic (e.g. Delaloye et al. 1980; Tinkler et al. 1981) or in some cases as primary magmatic transitions (e.g. Parrot 1973; Çoğulu 1975). The ophiolite has been subjected to a zeolite facies metamorphism which is believed to be an oceanic phenomenon because the continental sediments lying stratigraphically above and below the ophiolites are not metamorphosed (Tinkler et al. 1981). The Hatay ophiolite shows little sign of internal deformation (foliation and associated microstructures) in all lithologies except for some moderately deformed 20-30 m thick zones in the ultramafics and the lower part of the gabbro sequence (Tinkler et al. 1981). The ophiolite occurs as a thick thrust sheet that lies tectonically over Lower Cretaceous limestones of the Arabian platform, from which it is separated by a thin melange (Robertson 2002). These limestones are of Albian to Aptian age. The contact is only exposed in two small areas and so many of the details of emplacement are uncertain (Aslaner 1973). The oldest sediments covering the ophiolite are Upper Cretaceous limestones of Maastrichtian age, which rest discordantly on top of the ophiolite. The base of this sedimentary sequence is an extensive conglomerate, 2-5 m thick, which contains abundant ophiolitic detritus. Dubertret (1955) suggested that ophiolite emplacement occurred in the Maastrichtian or pre-Maastrichtian from the age constraints provided by this conglomerate and the emplacement onto Upper Cretaceous limestones of the Arabian platform.

2.7.2 Overview of geological research

Dubertret (1955) provided the first complete geological description of the Hatay area, laying the foundation for various subsequent descriptions (e.g. Vuagnat and Çoğulu 1967; Çoğulu 1975; Aslaner 1973; Parrot 1973; Delaloye et al. 1980; Tinkler et al. 1981; Pişkin et al. 1986). Tinkler et al. (1981) constructed two detailed structural sections across the ophiolite: one along the coastal section and one through the Karaçay valley, both oriented roughly NE-SW. Delaloye et al. (1980) constructed a geological section through the ophiolite along the coast between Arsuz in the north and Çevlik in the south, as did Parrot (1973). Tekeli (1985) prepared a detailed field guide for the Ophiolites and Lithosphere of Marginal Seas project field meeting held in Hatay, with a report on this field excursion and a discussion of the metalliferous and volcanoclastic rocks subsequently produced by Robertson (1986). Pişkin et al. (1986) produced a field guide to the geology of Hatay that included a geological map of the ophiolite. Dilek and Thy (1998) discuss the structure, petrology and seafloor spreading tectonics of the Hatay ophiolite. The petrogenesis of the ophiolite is discussed in detail by Lytwyn and Casey (1993) and by Bağcı et al. (2005).

2.7.3 Description of lithologies

The following ophiolitic units occur in the Hatay ophiolite (from the deepest levels to the shallowest):

- (i) Ultramafic rocks
- (ii) Gabbros
- (iii) Sheeted dyke complex (SDC)
- (iv) Extrusive sequences

(i) Ultramafic rocks: tectonites and cumulate sequences

The ultramafic sequences of the Hatay ophiolite are comprised largely of serpentinised harzburgite tectonite with intercalations of dunite, wehrlite and feldspathic peridotites. The ultramafic rocks are generally highly serpentinised and massive but occasionally display layering and as such can be separated into the tectonites comprising the majority of the rocks and the ultramafic cumulate sequences. Due to the lack of unequivocal exposure of the contact between the platform limestones and the base of the ophiolite thrust sheet, it is impossible to ascertain the thickness of the ultramafic rocks of the ophiolite. However, their maximum thickness is in excess of 3 km (Tinkler et al. 1981). The ultramafic rocks form the most dominant sequence of the ophiolite, and outcrop over the largest area and form the highest peaks of the massif. In some zones, a layer-parallel foliation can be observed. The ultramafic rocks are cut by dykes of gabbro and dolerite, and rodingitised gabbro dykes can also be observed within the ultramafic rocks (Tinkler et al. 1981). The dolerite dykes have good chilled margins whereas the gabbro dykes do not. A general northerly dip of the dykes in the north and a southerly dip in the south has been suggested by Pişkin et al. (1986), which Tinkler et al. (1981) explain by late folding on a large scale. There are some moderately deformed 20-30 m thick zones in the ultramafic sequence and the lower part of the gabbro sequence with the foliation in these zones most easily picked out by the olivine rich layers. These zones may represent regions of differential flow in the upper parts of the mantle (Tinkler et al. 1981). The foliation is always parallel or sub-parallel to the igneous stratification. There are some areas (such as near Kemer Köprü in the Karaçay Valley) where tight isoclinal folds and termination of magmatic layering are observed within the ultramafic cumulates and these are interpreted as syn-magmatic slump structures (Tinkler et al. 1981).

(ii) Gabbros

The gabbros reach a maximum thickness of 2.5 km and vary from cumulate ultramafic rocks and olivine gabbros at the base, to anorthositic gabbros at the top (Tinkler et al. 1981). In general, these cumulate rocks flank the tectonites forming the core of the massif with the transitions from one layer to another caused by a change of phase, concentration or mineralogy (Pişkin et al. 1986). Magmatic layering occurs on many scales. In the upper part of the ultramafic cumulate series an alternation between ultramafics and cumulate gabbros is seen and described as a hybrid zone (Vuagnat and Cogulu 1967) or a transition zone (Delaloye et al. 1980). Towards the upper parts of the series the ultramafic levels become less frequent and the series becomes gabbroic (Pişkin et al. 1986). The lower part of the cumulate gabbros often display flow structures, cross bedding, graded bedding, isoclinal folds and magmatic slump structures which may indicate fractional crystallisation and layering produced in a disturbed environment, possibly in one or more magma chambers of moderate size (Pişkin et al. 1986).

Towards the top of the gabbros the layering disappears and the gabbros become isotropic. The gabbros change mineralogically with the olivine and orthopyroxene disappearing whilst the clinopyroxenes, amphiboles and plagioclase become the major minerals (Pişkin et al. 1986). The gabbros are cut by dykes of both gabbro and dolerite and in some localities are net-veined by plagiogranite. In the ultramafic parts of the gabbro there is occasionally a foliation parallel to the layering.

Plagiogranite is locally developed and outcrops in places at the top of the gabbros near the sheeted dyke complex. It occurs either as small veinlets and dykes or as irregular masses of variable size. The contacts between the gabbros and the plagiogranite are generally

irregular and ill-defined whilst within the sheeted dyke complex the contacts with the plagiogranites are sharp.

(iii) Sheeted dyke complex (SDC)

The sheeted dyke complex is very well developed with a minimum thickness of 1 km. Due to the lack of exposure of extrusives in stratigraphic continuity with the dykes, it is not possible to give a maximum thickness for the sheeted dykes. There are numerous examples of gabbro screens outcropping between the dykes and two generations of dykes can be observed: a grey dolerite and a more weathered green-brown dolerite. The majority of dykes in the complex are grey dolerites (up to 90%) and these are older than the brown dykes, as demonstrated by observations of chilled margins and cross-cutting relationships (Tinkler et al. 1981). The grey dolerites pre-date the plagiogranite and the brown dykes post-date it (Tinkler et al. 1981). Dilek and Thy (1998) suggest that the older dykes display NE-SW strikes whereas the younger generation of dykes display NNE-SSW strikes, but this is not supported by the E-W average strike measured by most other workers (e.g. Tinkler et al. 1981; Pişkin et al. 1986) or by work presented within this thesis. The individual dykes are generally of a few metres in width and no asymmetry is observed in the orientation of the chilled margins (Delaloye et al. 1980). A third generation of dykes is also evident consisting of younger finer-grained, darker, basaltic dykes, usually only a few centimetres thick and cross-cutting the other dyke populations (Dilek and Thy 1998).

(iv) Extrusive sequences

The uppermost levels of the ophiolite massif outcrop in the north of the area and are tectonically separated from the lower levels. The extrusives outcrop in the eastern massif

of the Hatay ophiolite i.e. on the other side of the Tahtaköprü fault from the main massif. Pillow lavas outcrop in two main localities in the eastern massif and are generally steeply dipping. The volcanic outcrop near the village of Tahtaköprü is around 400 m thick and includes both massive and pillow lavas intercalated with metalliferous sedimentary rocks (Erendil 1984; Robertson 1986). The second locality of extrusive rocks occurs around Kömürçukuru village and is nearly 600 m thick, including pillow and massive flows intercalated with metalliferous umbers (Dilek and Thy 1998). The existence in places of pillow-disintegration breccias, hyaloclastite and rapidly quenched micro-pillows ('eggs') indicates eruption onto a tectonically active seafloor of marked relief (Robertson 1986).

There is a further locality to the south of Antakya where mafic extrusive rocks are exposed (Figure 2.12), up to 300m thick (Robertson 1986). According to Erendil (1984), these extrusive rocks overlie gabbros or serpentinites, separated by low-angle fault contacts but clear preserved primary contacts with the intrusive units of the main body of the ophiolite are not apparent and the contact relationship is thus uncertain. These extrusives include highly magnesian boninite-type lavas, referred to as 'sakalavites' by Delaloye and Wagner (1984) within both sheet and pillow lava flows.

2.7.4 Sedimentary cover of the ophiolite

The ophiolite is covered transgressively by sedimentary sequences ranging from Upper Cretaceous to Miocene in age with a total thickness of around 3 km (Pişkin et al. 1986).

In the NE the sheeted dykes are overlain unconformably by the oldest sediments represented by Maastrichtian non-marine to shallow-marine sediments, presumably deposited after the erosion of ophiolitic extrusives (Erendil 1984; Pişkin et al. 1986). The lowest part of the Maastrichtian is an extensive conglomerate horizon 2-5 m thick and

containing 70-80% ophiolitic detritus (Tinkler et al. 1981). The provenance of most clasts is the pillow lava and sheeted dyke sequences and the clasts are angular and poorly-sorted implying a local source. The Upper Maastrichtian is overlain concordantly by a series of clays, sandstones, limestones and marls whose age is between Palaeocene to Upper Eocene (Pişkin et al. 1986) with a thickness of around 600 m. The Miocene is always transgressive on the older sedimentary sequences and the ophiolite (Pişkin et al. 1986) with a total thickness of around 1.6 km. The Miocene, like the Maastrichtian, contains an extensive conglomerate horizon with abundant ophiolitic detritus and poorly sorted, angular cobble-sized clasts. The depositional environment of the Miocene sediments is shallow to very shallow, but occasionally passes laterally into pelagic sediments that are often very rich in both macro and micro faunas (Pişkin et al. 1986). The Pliocene consists of sandstones, marly limestones, clays and slaty clays with a thickness between 100 to 400 m and the Quaternary sediments are conglomerates with angular or rounded fragments that are poorly cemented, travertines, alluvium and beach sand (Pişkin et al. 1986).

2.7.5 Emplacement of the ophiolite

The lowest tectonic level of the ophiolites is exposed in an erosional window near the village of Kömürçukuru, 24 km north of Antakya (Figure 2.12). At this locality, the ultramafic rocks rest tectonically above the Lower Cretaceous limestones of the Arabian platform and the contact is interpreted as a basal thrust along which the ophiolites were emplaced (Dubertret 1955; Aslaner 1973). The ultramafic rocks contain large 'slices' and blocks of limestone 10-20 m thick and 20-40 m long. These blocks are believed to have originally been part of the carbonate sequences on the Arabian platform that were detached and incorporated into the ultramafic sequences as the ophiolite was thrust over the platform limestones (Aslaner 1973; Delaloye and Wagner 1984). The blocks vary in age: most are Lower or Upper Cretaceous in age and the lithologies are similar to carbonate sequences

observed in nearby parts of the region. The abundance of these limestone wedges casts doubt on the interpretation that the lowest limestone unit observed is the true tectonic basement of the ophiolite; it may represent another allochthonous tectonic slice underlain by more ophiolitic rocks.

The ultramafic rocks and enclosed limestone wedges are cut in places by narrow highly deformed shear zones, thought to be linked to the emplacement of the ophiolite with the precise deformation history within the zone varying locally. Tinkler et al. (1981) observe, in some places, a four-phase history consisting of: (1) an early foliation which is cut by; (2) an echelon tension gashes; (3) a later foliation that refolds (1) and (2) and is itself cut by; (4) conjugate sets of an echelon tension gashes.

Emplacement of the ophiolite is thought to be from the north from a consideration of the regional geology in adjacent areas of Turkey and Syria (Delaune-Mayere et al. 1976; Parrot 1973; Ricou 1971); this is consistent with the SE directed emplacement direction of the Baër-Bassit ophiolite (Al-Riyami et al. 2002) to the south of Hatay. The lower timing constraint on the emplacement of the ophiolite is that wedges of Campanian limestone are observed in the serpentinites in the tectonic window near Kömürçukuru and the youngest platform sediments under the thrust plane of the ophiolite have been palaeotologically dated as Cenomanian to Santonian (95-83 Ma; Selçuk 1981). The upper limit is that the Maastrichtian sediments overlying the ophiolite are the earliest to incorporate ophiolitic detritus and they are associated with other Upper Cretaceous sediments that show continental affinities (Dubertret 1955), dated as Middle-Upper Maastrichtian (69-75 Ma; Selçuk 1981). This implies a gap of 26-8 Ma between the youngest sediments of the Arabian platform and the oldest sediments overlying the ophiolite.

2.7.6 Post-emplacment structures

Interpretations of which structures observed in the ophiolite are post-emplacment vary. The autochthonous sedimentary cover is affected by faulting and so it is known that the ophiolite is also likely to have experienced post-emplacment deformation under these same events. Within the ophiolite massif, it has been suggested that many of the contacts between different members of the ophiolite sequence are normal faults of post-emplacment origin.

The NE-SW trending antiformal structure of the ophiolite may either pre- or post-date emplacment (Tinkler et al. 1981). Where the tectonic contact between the serpentinites and Arabian platform limestones is approached near K m r ukuru, the ultramafic rocks and enclosed limestone wedges are interpreted by Tinkler et al. (1981) to be folded around an open antiform with the same orientation and attitude as the main folds in the rest of the massif which would imply that folding occurred after the emplacment of the ophiolite. Tinkler et al. (1981) also suggest that the Maastrichtian sediments that lie unconformably above the pillow lavas may themselves be folded, but they do not outcrop extensively enough to determine this, preventing further timing constraints on the age of the folding.

Tinkler et al. (1981) observe pre-Miocene age faults cutting the folds which must thus have formed between Maastrichtian and pre-Miocene times. Tinkler et al. (1981) suggest that the faults forming the boundaries between the ophiolitic units trend NE-SSW and cross-cut the NE-SW trending axis of the synform, with an estimate for movement on these of potentially 1-2 km from reconstructing the folds to produce a continuous ophiolite sequence, and an upper age limit of faulting in the Miocene from observation of overlying undisturbed Miocene limestones near  evlik. According to Tinkler et al. (1981), there is also evidence for post-Maastrichtian-pre-Lutetian normal faulting from recognition of a

normal fault in the main body of Cretaceous sediments 5 km south of Harbiye that cuts Middle and Upper Cretaceous sediments but is overlain by undisturbed Middle Eocene (Lutetian) limestones, proving that normal faulting was active during pre-Lutetian times and not restricted solely to the ophiolite body.

The sedimentary sequences contain two conglomerate horizons, one at the base of the Maastrichtian and one at the base of the Miocene. The Maastrichtian conglomerate is never observed to be overthrust by the ophiolite and so cannot have originated by erosion at the toe of the advancing ophiolite sheet (Tinkler et al. 1981). Instead, Tinkler et al. (1981) suggest that it could be generated by erosion along a fault scarp that had exposed the highest members of the ophiolite sequence. The Miocene conglomerate could also be derived from erosion along a fault scarp. The Miocene sequences are described by Tinkler et al. (1981) as flanking the edges of the ophiolite and forming a broad NW-SE trending anticline.

The dip of the ophiolite and sedimentary cover can be used as an indication of the post-emplacement deformation that has occurred. For instance, 7 km to the south of Belen (near Üç Oluk; Figure 2.12), pillow lavas dip at 60° SE and are overlain unconformably by Maastrichtian and Palaeocene sediments (with the Maastrichtian conglomerate at the base), dipping at 40° SE, and finally by the Miocene conglomerate and limestones dipping at 20° SE. This sequence of events requires at least one and possibly two periods of pre-Miocene block tilting to have occurred (Tinkler et al. 1981). The 20° dip of the Miocene rocks implies that at least one episode of post-Miocene tilting must also have occurred and this appears to be a regional phenomenon. The ophiolite is observed by Lyberis et al. (1992) to be thrust over Neogene sediments in the north of the massif, indicating compressional deformation, at least in the north of the area.

Recent raised beach deposits can be observed along the coast to the north of Şahanlıkkayasi Headland (Figure 2.12), with uplifts of 50 and 75 m observed for two terraces (Pişkin et al. 1986).

2.7.7 Petrogenesis

Various workers have analysed the petrogenesis of the Hatay ophiolite (e.g. Dilek and Thy 1998; Pişkin et al. 1990; Lytwyn and Casey 1993; Bağcı et al. 2005). The basaltic dykes of the Hatay ophiolite have higher SiO_2 and Al_2O_3 and lower FeO and TiO_2 contents compared to typical oceanic basalt suites and are also less evolved than typical oceanic island suites (Dilek and Thy 1998). However, the analysed Hatay dykes compare very closely with the compositional characteristics of the volcanic suites of the Troodos ophiolite (e.g. Robinson et al. 1983; Thy and Xenophontos 1991). Both the major and trace element concentrations in the Hatay ophiolite display strong similarities with those of the extrusive sequences of the Troodos ophiolite (Cameron 1985; Rautenschlein et al. 1985; Taylor and Nesbit 1988), with both ophiolites having low incompatible trace element concentrations and strong depletion in LRE elements. Dilek and Thy (1998) conclude that in general, the observed compositional variations within the dykes can be explained by a relatively high degree of melting (20%) and a small enrichment (1%) of a slightly depleted source. This is consistent with the formation of the Hatay ophiolite in a tectonic setting where enriched fluid or liquid was derived from a deeper and more fertile source (e.g. a subducting slab) and added to the overlying mantle. The presence of a high Mg composition in the olivine, clinopyroxene, orthopyroxene and the absence of a Ca-rich plagioclase as an early fractionating phase co-precipitating with forsteritic olivine suggest that the Hatay plutonic suite is not likely to have originated in a mid-ocean ridge environment. Instead the whole-rock and mineral chemistry of the cumulates indicates derivation from an island arc tholeiitic magma (Bağcı et al. 2005). Bağcı et al. (2005)

conclude that all the whole-rock and mineral chemistry evidence suggests that the Hatay ophiolite formed along a slow-spreading centre in a forearc region of an SSZ tectonic setting, in line with the large body of data supporting a similar petrogenetic setting for the Troodos ophiolite. The lower lavas of the Troodos ophiolite are typically of differentiated island arc character whereas the upper lavas are commonly of high-Mg type (Robinson et al. 1983). In Baër-Bassit, the extrusives appear to all be of high-Mg type and the overlying umbers are more terrigenous than in Troodos, which might be indicative of deposition closer to a continental margin (Al-Riyami et al. 2000). The high-Mg lavas of the Hatay ophiolite, 'sakalavites' of Delaloye and Wagner (1984) are similar in composition to those of the Baër-Bassit massif.

2.8 Previous suggestions on the tectonic evolution of the Hatay ophiolite

There are contrasting views regarding the tectonic evolution of the Hatay ophiolite. Most of the earlier workers interpret the majority of the faults and folds observed within the ophiolite as post-emplacment in origin, although at least part of the outcrop pattern is interpreted to be emplacements-related. An alternative view is that certain of these same structures preserve original seafloor relationships. The main views are discussed below.

(i) Structures formed during emplacements

The majority of earlier work interprets at least some of the structures and outcrop pattern of the Hatay ophiolite to have formed during emplacements. For example, the contact between the ultramafic rocks and the gabbros is widely interpreted to be a reverse fault(s) (e.g. Tinkler et al. 1981; Pişkin et al. 1986; Delaloye et al. 1980; see cross-section of Figure 2.12). Reverse faults are also shown in the Karaçay valley on the cross-section of Tinkler et al. (1981).

(ii) Structures formed post-emplacement

Tinkler et al. (1981) have produced a synthesis of the structural events to have affected the ophiolite based on sedimentological and field evidence. Tectonic interpretations from other authors are often primarily based on the Tinkler et al. (1981) interpretation (e.g. Pişkin et al. 1986). Tinkler et al. (1981) suggest that the post-emplacement history of the Hatay ophiolite is characterised by several episodes of normal faulting and gentle folding with structures trending approximately NE-SW and running parallel to the Karasu rift valley. Tinkler et al. (1981) suggest that this zone represents a slight bend in the generally N-S trending Dead Sea rift zone and that the sinistral movement along the fault zone may have produced the compressional and extensional stresses observed in the region of Hatay. Seven structural events are defined with upper and lower age limits assigned to these:

- (1) post-Campanian-pre-Maastrichtian/Maastrichtian emplacement;
- (2) Maastrichtian/post-Maastrichtian-pre-Miocene folding (and faulting?);
- (3) post-Maastrichtian-Pre-Lutetian normal faulting;
- (4) Post-Maastrichtian-Pre-Miocene normal faulting;
- (5) post-Miocene gentle folding;
- (6) post-Pliocene normal faulting;
- (7) Recent raised beaches.

Tinkler et al. (1981) suggest that due to age uncertainties, (3) and (4) may be the same event and it is possible that all of the faulting events represent local expressions of the same larger pre-Lutetian, pre-Miocene and post-Pliocene event. The post-Maastrichtian-pre-Miocene faults have produced a graben with a vertical displacement of 1-2 km and so comprise a significant event in the history of the region. Pişkin et al. (1986) attribute the 1 to 2 km uplift of the central part of the ophiolite to the pre-Miocene NNW-SSE normal

faults forming the boundaries between lithologies. Delaloye et al. (1980) interpret the contact between the gabbros and SDC along the coast as tectonic, marked by a normal fault, and suggest it is transitional in the north.

(ii) Primary seafloor spreading structures

Dilek and Thy (1998) interpret many of the relationships observed in the Hatay ophiolite as primary seafloor spreading structures. They argue that the internal structure of the ophiolite, the areal distribution between ophiolite subunits and the temporal and spatial relations between magmatic and tectonic features can all be attributed to extensional tectonics that the ophiolite underwent in intraoceanic conditions (Erendil 1984; Tekeli and Erendil 1986; Dilek and Delaloye 1992). All faults within the ophiolite are interpreted in terms of seafloor processes. They recognise two major sets of faults along the coast- a dyke parallel set and a dyke normal set, with the dyke parallel set displaying a listric geometry and forming horst and graben structures, analogous to those documented in the Troodos ophiolite and interpreted to represent a fossil spreading axis. Dilek and Thy (1998) suggest that the Hatay ophiolite underwent crustal denudation and unroofing of the upper mantle as a result of tectonic extension at a spreading centre. The boundary between the dykes and gabbros is interpreted as a low-angle detachment surface of seafloor origin, locally marked by mutually intrusive relationships between the sheeted dykes, gabbros and plagiogranites. The Tahtaköprü fault separating the two massifs is interpreted as an accommodation zone that allowed differential movements between adjacent ridge segments with variable extensional strain during generation of the oceanic lithosphere. Dilek and Thy (1998) describe the massif to the east of the Tahtaköprü fault as consisting of serpentinites directly overlain by pillow lavas, rotated dyke blocks and gabbros and interpret sulphide mineralisation along some fault planes in the extrusive rocks as

indicative of the operation of hydrothermal systems acting synchronously with magmatic and extensional tectonic processes.

They describe the contact between the mantle rocks and the gabbros as characterised by a 50-100 m thick zone composed of highly altered, fine-grained, sheared rocks, with the gabbros displaying cumulate textures commonly cut by low-angle shear zones and boudinage structures. They suggest that the boundary between the gabbros and SDC is gradational and that the original seafloor relationship is preserved. Dilek and Thy (1998) describe the main outcrop of the SDC as comprising a synform oriented NE-SW, bounded by inward-dipping faults overlying the plutonic sequence and containing mineralised oceanic faults. One subset of these is parallel to the dykes with shallower dip angles causing the dykes to form horst and graben structures. These faults are interpreted as syn-magmatic and believed to die out in the upper part of the gabbros below. The second set of faults in the SDC are described by Dilek and Thy (1998) as NW-SE striking tear faults that cut and offset the generally NE-SW striking contacts between the ophiolite subunits, dying out towards the NW and overlain by the sedimentary sequence. Other faults described by Dilek and Thy (1998) are local high-angle normal faults within the extrusive sequence that die out downwards. The contact between the extrusive rocks and serpentinites is described as a gently SE dipping normal fault and several NW-SE striking faults that are parallel with the Tahtaköprü fault are described.

Other structures within the ophiolite are recognised by Dilek and Thy (1998) as similar to those developed on the seafloor, for instance, the mineralisation of the faults and cross-cutting of basaltic dykes. According to Dilek and Thy (1998), faults/shear zones and associated deformed rocks between the ultramafic rocks and gabbros and between the gabbros and the SDC show shear sense indicators compatible with an extensional origin. These authors say that the formation of the structural graben containing the ultramafic

rocks, gabbros and sheeted dykes and the high angle normal faults forming local horst and graben structures within the SDC suggest a spreading-related origin for the faults and that they are inconsistent with the contractional style that would have developed during convergence and ophiolite emplacement. The oblique-slip faults that are perpendicular to the contacts between the ophiolitic lithologies are interpreted to be zones that facilitate differential extension and rotation between adjacent blocks along the spreading axis, analogous to ones documented from the MAR (Karson and Rona 1990; Figure 2.11A-B).

The boundary between the serpentinitised mantle units and crustal units is mostly tectonic and juxtaposes the uppermost levels of the ophiolite with the mantle units along low-angle tectonic contacts, which Dilek and Thy (1998) suggest points to high levels of tectonic extension, driven by an asymmetric extension along a low-angle detachment surface (e.g. Wernicke 1985). In Dilek and Thy's (1998) tectonic model, the Cretaceous oceanic lithosphere preserved in the Hatay ophiolite is interpreted to have developed along a NE-SW trending (in present coordinate system) spreading centre and to have undergone simple shear deformation associated with asymmetric tectonic extension along a SE dipping low-angle fault. The present day surfaces either side of the peridotite core are interpreted by Dilek and Thy (1998) as representing remnants of the master fault. The doming of the peridotite core is believed by these authors to have resulted from the uplifting of the unloaded footwall and isostatic rebound and warping of the low-angle normal fault. Uplifting of upper mantle rocks and development of a mantle antiform is inferred to have been further facilitated by extensive serpentinitisation and diapiric activity during and subsequent to displacement of the oceanic lithosphere from its original spreading environment (Dilek et al. 1991). If this scenario is correct, it is similar to the tectonics of the western median valley along the wall of the MAR in an area south of the Kane fracture zone (Cannat et al. 1988; Karson et al. 1990). Dilek and Thy's (1998) tectonic model infers a slow-spreading origin for the Neotethyan oceanic lithosphere, with the oceanic

lithosphere being tectonised and deformed within the plate boundary zone i.e. the deformation fabric seen in some ophiolites may represent ocean floor rather than obduction tectonics.

2.9 Overview of the geology of related ophiolites

The Hatay, Baër-Bassit and Troodos ophiolites are believed to have formed within the same ocean basin, with emplacement of Hatay and Baër-Bassit occurring whilst they comprised part of the same ophiolite sheet. A review of the geology of the Troodos and Baër-Bassit ophiolites thus provides valuable background information for interpretations in later chapters of the new palaeomagnetic and structural data from the Hatay ophiolite. A brief geological overview is relevant prior to discussions of previous palaeomagnetic results from these ophiolites (see review in Chapter Four), and particularly important in relation to the new palaeomagnetic results obtained from the sedimentary cover of the Baër-Bassit ophiolite.

2.9.1 Troodos ophiolite

The Troodos ophiolite of Cyprus is one of the most studied ophiolite complexes in the world and as such it would be impossible here to provide an extensive review of all previous research. A comprehensive synthesis of the history of geological research in Cyprus is given by Robertson and Xenophontos (1993) and a geological review of research in Cyprus is given by Robertson (1990). The Troodos massif has previously been used as a proto-type for all ophiolites. The ophiolite consists of a complete Penrose pseudostratigraphy forming a domal structure as a result of Late-Pliocene to Recent uplift, which results in a broadly concentric outcrop pattern with the mantle and lower crustal sections outcropping around the central topographic high (Figure 2.14).

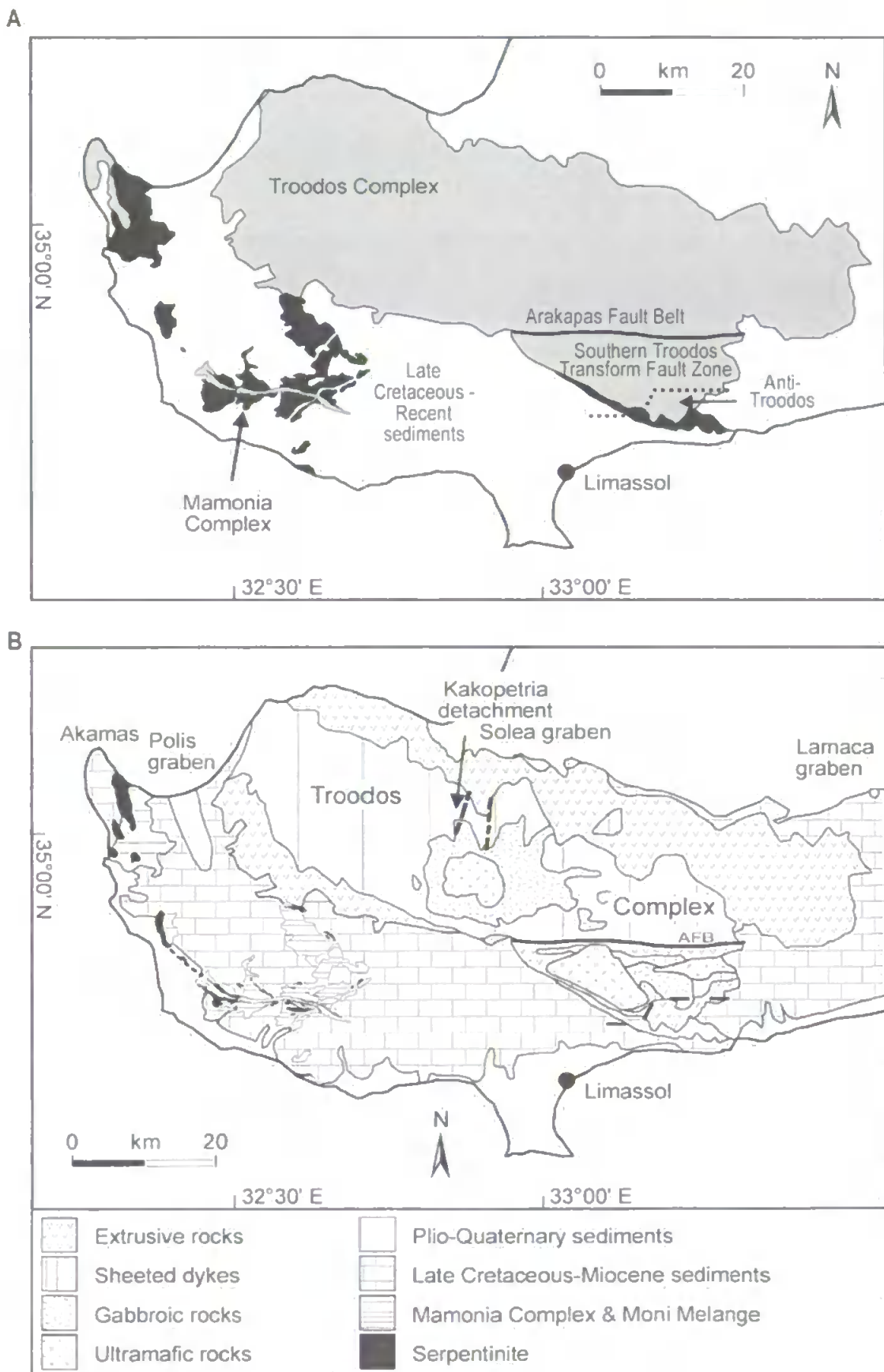


Figure 2.14: Geology of the Troodos ophiolite.

A. Location of the Troodos massif in Cyprus with major areas discussed in the text illustrated and the Troodos ophiolite complex units shaded in grey and the Mamonia complex and Moni melange shaded in black.

B. Outline geological map of Cyprus showing the ophiolite units in more detail and also the location of major structural features.

The Troodos ophiolite was not subaerially exposed and deeply eroded until the Plio-Quaternary time (Robertson and Xenophontos 1993). The ophiolite is extremely well preserved due to a lack of large-scale thrust tectonics during emplacement, allowing unique exposures of many original seafloor relationships to be observed.

A metamorphic sole is absent, and seismic reflection evidence indicates that the ophiolite is underlain at depth by crust of average continental thickness (Makris 1983). The deepest levels of the Troodos ophiolite are tectonised harzburgites which are interpreted as refractory mantle, together with intrusions of dunite and lherzolite (Robertson 2002). The plutonic section includes layered cumulates that are cut by gabbroic intrusions, providing clear evidence for the existence of multiple small magma chambers beneath the Troodos spreading axis (Robinson and Malpas 1990). The upper massive gabbros are locally overlain by small plagiogranite bodies that intrude in places into the SDC (Robertson 2002).

The SDC of the Troodos ophiolite is exposed over an 80 km wide area with a consistent N-S mean strike of the dykes (present-day coordinates). The complex is 1 to 1.5 km thick and dykes are in places rotated to low angles and cut by later dykes (Dietrich and Spencer 1993). In the western and central regions of the complex dykes trend predominantly N-S, with deviations observed in the vicinity of the Southern Troodos Transform Fault Zone (STTFZ) and in the north (Simonian and Gass 1978).

The extrusive sequence is best exposed along the northern and southwestern margins of the ophiolite and there are classic sections where the interplay between magmatic, tectonic and hydrothermal processes during construction of the oceanic crust can be established (Schmincke et al. 1983; Schmincke and Rautenschlein 1987). The extrusive sequence is around 1 to 1.5 km thick and is split into three divisions, although there is no strong

evidence for structural or metamorphic discontinuities between the layers (Gass and Smewing 1973). Variable hydrothermal alteration occurs throughout the lavas, which also contain massive sulphides in places (Robertson 2002). The extrusives are overlain by metalliferous umbers within small seafloor half grabens (Robertson 2002).

The contact between the sheeted dykes and gabbros in places is a low-angle extensional detachment fault zone (Varga and Moores 1985), providing evidence for amagmatic stretching during crustal formation, indicative of spreading in a slow-spreading system. Dietrich and Spencer (1993) have demonstrated that tectonic extension was accommodated in the upper levels of the Troodos ophiolite by the combination of large dyke-parallel faults, sub-horizontal shear zones and a network of small-scale normal faults. The presence of cross-cutting dykes and epidote mineralisation within the fault gauges indicates that the observed extensional faults and shear zones formed within the plate accretion zone. Spreading took place either by steady state processes (Allerton and Vine 1987) or by the formation of discrete, ephemeral seafloor grabens (Varga and Moores 1985). The best-documented graben is the Solea graben which is interpreted to be a fossil spreading axis.

The southern margin of the main ophiolite massif is marked by the east-west trending Arakapas fault belt (Figure 2.14) which is a strike-slip system interpreted to be a fossil oceanic transform fault (Moores and Vine 1971; Simonian and Gass 1978). An anomalous ophiolitic sequence is exposed to the south of the Arakapas fault belt within the Limassol Forest Complex (Figure 2.14) where mantle sequences and lower crustal rocks are exposed at a high structural level and are cut by numerous east-west trending shear zones (Murton 1986; MacLeod 1990). This is interpreted to have formed within a leaky (transtensional) transform fault zone: the South Troodos Transform Fault Zone (STTFZ) with the principal displacement zone represented by the Arakapas fault belt (MacLeod and Murton 1993). A

progressive change in dyke orientation within the SDC occurs as the STTFZ is approached from the north, suggestive either of primary variation in the Late Cretaceous stress field adjacent to a sinistrally slipping transform, or post-emplacement tectonic rotations of dykes due to dextral shear along the transform (Simonian and Gass 1978); palaeomagnetic data support the second possibility (e.g. Morris et al. 1990). A small area of normal Troodos-type crust exposed in the SE of the Limassol Forest Complex is believed to represent a fragment of crust formed at an Anti-Troodos spreading axis located to the south of the transform domain (MacLeod 1990).

An alternative model has recently been proposed by Cann et al. (2001), who reinterpret the Limassol Forest area as an oceanic core complex. The Arakapas fault zone is interpreted by these authors to represent the evolution of a transform fault into a fracture zone with mantle peridotites within the Limassol Forest area recognised as core complexes exposed either at seafloor or covered by overlapping crustal blocks, separated by low-angle detachment faults. The extension is inferred to have occurred shortly after crustal construction in crust formed in an inside corner area, extended by detachment faulting and deformed further during slip along the transform, then intruded by new magma as it passes the second spreading centre (Figure 2.11B). In this model, the Troodos ophiolite formed to the east of a ridge-transform-ridge intersection, with the Limassol Forest area produced at the western inside corner, spreading eastwards past a second ridge, with the ophiolite to the north of the Arakapas fault created and welded to it at this time. The Cann et al. (2001) model indicates a sinistral sense of displacement along the transform model and is thus essentially incompatible with the numerous palaeomagnetic data from the ophiolite that support dextral displacement along the STTFZ.

In the Late Cretaceous, shortly after genesis at the Neotethyan spreading axis, the Troodos oceanic crust became tectonically juxtaposed along its SW margin (present-day

coordinates) with an allochthonous, highly deformed sequence of Upper Triassic to mid-Cretaceous rocks, known as the Mamonia Complex, and interpreted to represent remnants of a passive continental margin and marginal oceanic crust (Robertson and Woodcock 1979; Swarbrick 1993). The mode of juxtaposition of the two complexes is under debate. To the north of the Troodos ophiolite lies another allochthonous terrane- the Kyrenia terrane (Robertson and Xenophontos 1993).

The Troodos ophiolite is overlain by a continuous in situ Late Cretaceous to Recent pelagic sedimentary cover, consisting of the Perapedhi, Kannaviou, Lefkara and Pakhna formations (Robertson and Xenophontos 1993). The Perapedhi members are of Turonian-Campanian age and overlie the stratigraphically highest pillow lavas located within hollows in the pillowed surface. Conformably overlying these sediments is the Lefkara Formation, consisting of pelagic chalks with subordinate cherts (Robertson and Hudson 1974), divided into Lower (Maastrichtian), Middle (Palaeocene to Eocene) and Upper (Oligocene) units on the basis of both lithological and micropalaeontological criteria (Mantis 1970).

The Troodos ophiolite has not been emplaced by overthrusting onto a continental platform and so there is a lack of large-scale thrust tectonics. It provides a rare example of an ophiolite that could be considered to be undergoing active emplacement today in that uplift of the massif is still occurring (Robertson et al. 1995). The Eratoshenes seamount is an inferred crustal fragment located to the south of Cyprus which is interpreted to be in the process of incipient collision with the active margin of the Eurasian plate to the north and as such represents an opportunity to study processes that occur as an ophiolite is obducted and emplaced (Robertson 1998). Cyprus has been undergoing progressive uplift from the Pliocene to Quaternary, with a marked acceleration during and subsequent to the Late Pliocene (Robertson 1990). The rate then slowed following the mid-Pleistocene (Poole

and Robertson 1992). The rapid uplift of southern Cyprus is coincident in time with increased subsidence of the Eratoshenes seamount and these two events are likely to result from the same cause (Robertson 1998). The driving force of the uplift is probably not limited solely to the underthrusting of the seamount as uplift was associated with diapiric protusion of serpentinite that now forms the core of Mount Olympos (Robertson 1990). This is inferred to represent ultramafic oceanic mantle beneath Cyprus that became hydrated, increased in volume and rose diapirically (Robertson 1998). Due to the simultaneous uplift of the Kyrenia range of Cyprus, serpentinite diapirism also cannot solely account for the uplift which is hypothesised to be the result of a combination of underthrusting of the Eratoshenes seamount and the onset of diapiric serpentinitisation (Robertson 1998).

2.9.2 Baër-Bassit ophiolite

The dismembered Baër-Bassit ophiolite is located 20 km to the south of the Hatay ophiolite in NW Syria and is interpreted to represent the more dismembered thrustal front of the same ophiolite sheet of which Hatay comprises part. The ophiolite thrust sheets are underlain by the “Baër-Bassit Mélange” (Al-Riyami et al. 2000; Al-Riyami and Robertson 2002), which consists of deformed Mesozoic rocks of continental margin and oceanic affinities. The ophiolitic outcrop is dominated by two massifs: Baër in the NE (inland) and Bassit in the NW (near the coast), with smaller dismembered outcrops to the south (Figure 2.15), separated into thin thrust slices less than 200 m thick (Al-Riyami et al. 2000). The Baër massif is relatively structurally intact and consists principally of harzburgites, overlain by cumulate ultramafics, layered gabbros and dolerite dykes (Parrot 1977). The Bassit massif comprises a lower sequence of peridotites and gabbros, which are overthrust by a slice of melange and then by thin (<100 m thick) imbricate thrust sheets of gabbro, sheeted dykes and pillow lavas.

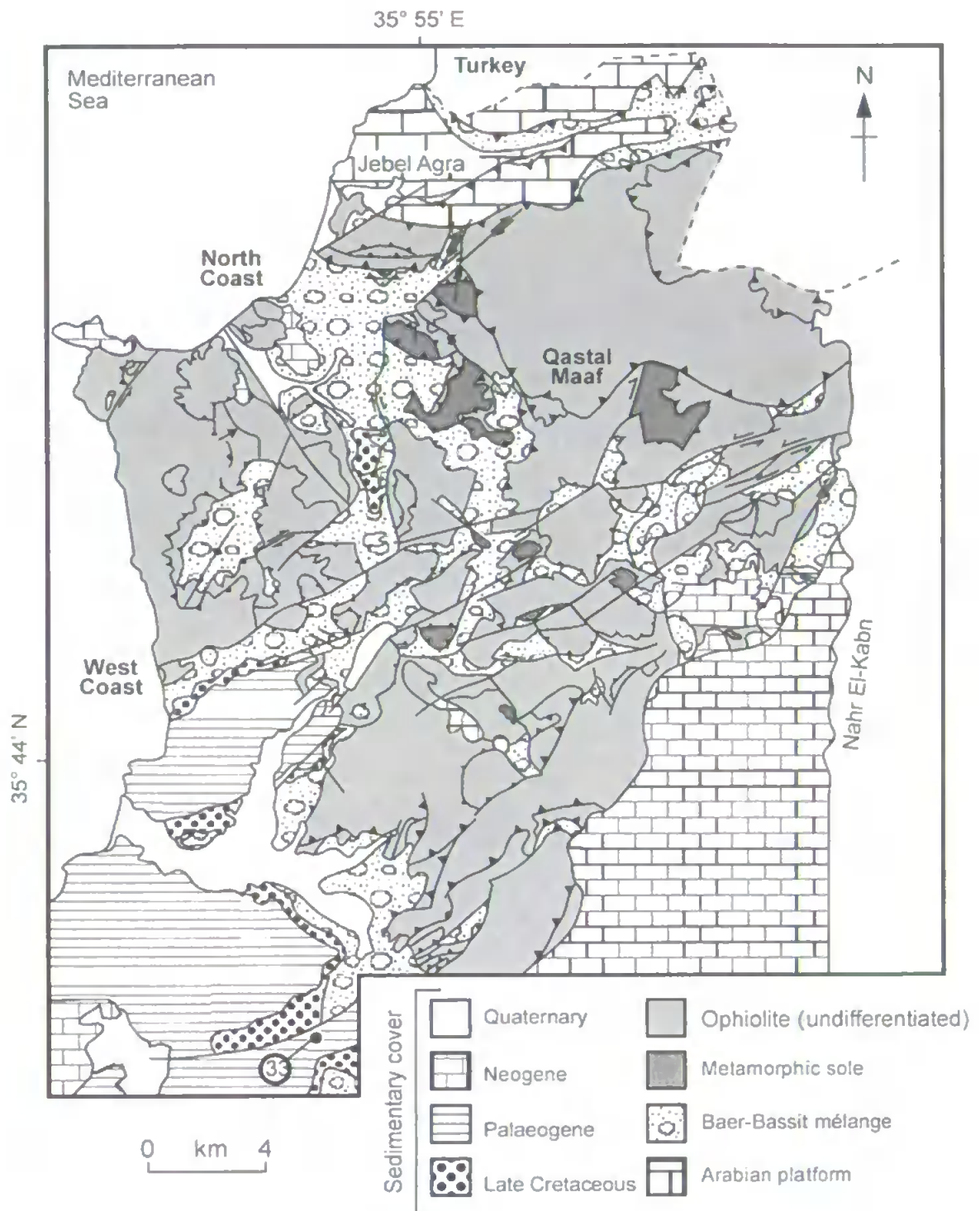


Figure 2.15: The geology of the Baër-Bassit ophiolite and sedimentary cover.

Baër-Bassit was originally described by Dubertret (1955) and mapped by Russian geologists (Kazmin and Kulakov 1968). Recent work on the tectonic evolution of the ophiolite and its metamorphic sole and the emplacement of the ophiolite has been carried out by Al-Riyami et al. (2000) and Al-Riyami and Robertson (2002).

A well-developed metamorphic sole forms the base of the ophiolite sequence and can be divided into high-grade amphibolite facies assemblages in the north and lower-grade greenschist facies in the centre of the region, although no inverted metamorphic gradient is preserved within any one area (Al-Riyami et al. 2002). The protoliths of both the high-grade and lower-grade assemblages are interpreted to be alkali basalts and pelagic sediments, similar to the volcanic rocks in an underlying unmetamorphosed melange (Al-Riyami et al. 2002). The metamorphic sole progressively evolved from ductile to brittle fabrics during tectonic transport, with most fabrics evolving during intense shearing, although some of the metamorphic alkaline metabasites were apparently metamorphosed under relatively static strain conditions. The lack of metamorphic sole preserved in the related Hatay ophiolite is possibly due to it being cut out during the emplacement process (Al-Riyami et al. 2000).

Layered gabbros in the Baër and Bassit massifs are around 1 km thick and are locally cut by doleritic dykes, with an average strike of 130° and a shallow $20-34^{\circ}$ dip in the Baër massif (Al-Riyami et al. 2000). The central area contains small masses of layered gabbro, locally cut by dykes, pegmatitic gabbro, serpentinite and lava. This area is considerably affected by Neotectonic strike-slip faults (Al-Riyami et al. 2000). The SDC in the Bassit massif is composed of sub-vertical dykes with chilled margins and strikes on average NW-SE with the largest known outcrop (dominant strike 330° , dip $70-90^{\circ}$) extending for 3 km along-strike (Al-Riyami et al. 2000). The extrusives are magnesian and strongly depleted,

comparable to primitive island arc tholeiites and some boninitic lavas. The top layer of the ophiolite is unmetamorphosed, lying within, or just above, the upper lavas (Al-Riyami et al. 2000).

The ophiolite is overlain by Late Maastrichtian to Palaeogene marine calcareous sediments. It was transgressed by shallow-water carbonates during Late Maastrichtian time. In Palaeocene-Eocene time, deeper water carbonate deposition over the allochthon resumed and was followed by shallower water carbonate deposition in Early Oligocene time. These Palaeogene sequences are now exposed to the south and SE of the ophiolitic Bassit massif. A subsequent regional cessation of deposition persisted until Early Miocene time (Krasheninnikov 1994). Shallow-water carbonate deposition resumed in the Early Miocene, and Aquitanian sequences occur unconformably above various stratigraphic levels in the Palaeogene sequence. This Neogene sequence is mainly exposed to the west of the Nahr-el-Kabir river.

In middle Maastrichtian time, the ophiolite and the underlying Baër-Bassit Melange were thrust onto the Arabian margin, which then formed part of a regionally submerged carbonate platform (e.g. Kazmin and Kulakov 1968). Radiometric ages of 85-95 Ma (Thuziat et al. 1981) from the metamorphic sole, thought to represent the first detached part of the lithosphere at the ridge axis, thus represent the youngest possible formation age of the ophiolite. This implies a gap of 20-25 Ma between initial detachment and emplacement (Delaloye and Wagner 1984). Structures in the metamorphic sole and in the underlying Baër-Bassit Mélange suggest that ophiolitic thrust sheets were emplaced towards the SE (Al-Riyami et al. 2002; Figure 2.16A). For example, foliation in the greenschists and amphibolites is mainly oriented NW-SE with the lineation parallel to the foliation and mainly plunging to the NW and fold facing directions (Figure 2.16B), although variable, also indicating displacement towards the SE (Al-Riyami et al. 2000). During emplacement the front of the ophiolite was tectonically imbricated and overthrust

by the main ultramafic slab, the Bassit massif. The thrust slices in the southern part of the ophiolite strike NE-SW and dip NW (Al-Riyami et al. 2000).

The emplaced allochthonous units (Baër-Bassit ophiolite, metamorphic sole and Baër-Bassit Mélange) were briefly exposed, then transgressed by shallow and deeper water carbonate sequences during Late Maastrichtian-Early Oligocene time (Figure 2.16C). A subsequent regional cessation of deposition persisted until the Early Miocene (Krasheninnikov 1994) and may relate to closure of the southern Neotethys basin in this region. Related contraction resulted in open folding and faulting of the ophiolite and the Palaeogene neoautochthonous sedimentary cover. This probably led to the updoming of the Jebel Agra carbonate platform in the north. No further regional-scale thrusting took place after latest Cretaceous time. Shallow-water carbonate deposition resumed in the Early Miocene. These sediments lie unconformably on the Palaeogene sequence.

In the Late Miocene the region was dissected by mainly ENE-WSW-trending, dominantly sinistral strike-slip faults. This fault system (the Latakia-Killis lineament) extends offshore, and may represent part of the extension of the present day plate boundary zone between the African plate and the Turkish microplate. This runs eastwards from south of Cyprus as a zone of distributed deformation (Kempner and Garfunkel 1994; Ben-Avraham et al. 1995) and then comes onshore, passing through the Baër-Bassit region to link with the DSF system to the east (Robertson 1998; Al-Riyami et al. 2000). The Neogene-Quaternary deformation produced strike-slip faulting in the south and centre of the massif and normal faulting in the north, which formed large grabens (Al Riyami et al. 2000). The strike-slip faults in the central area are mostly sinistral and strike ENE-WSW with variably oriented dextral strike-slip faults also observed.

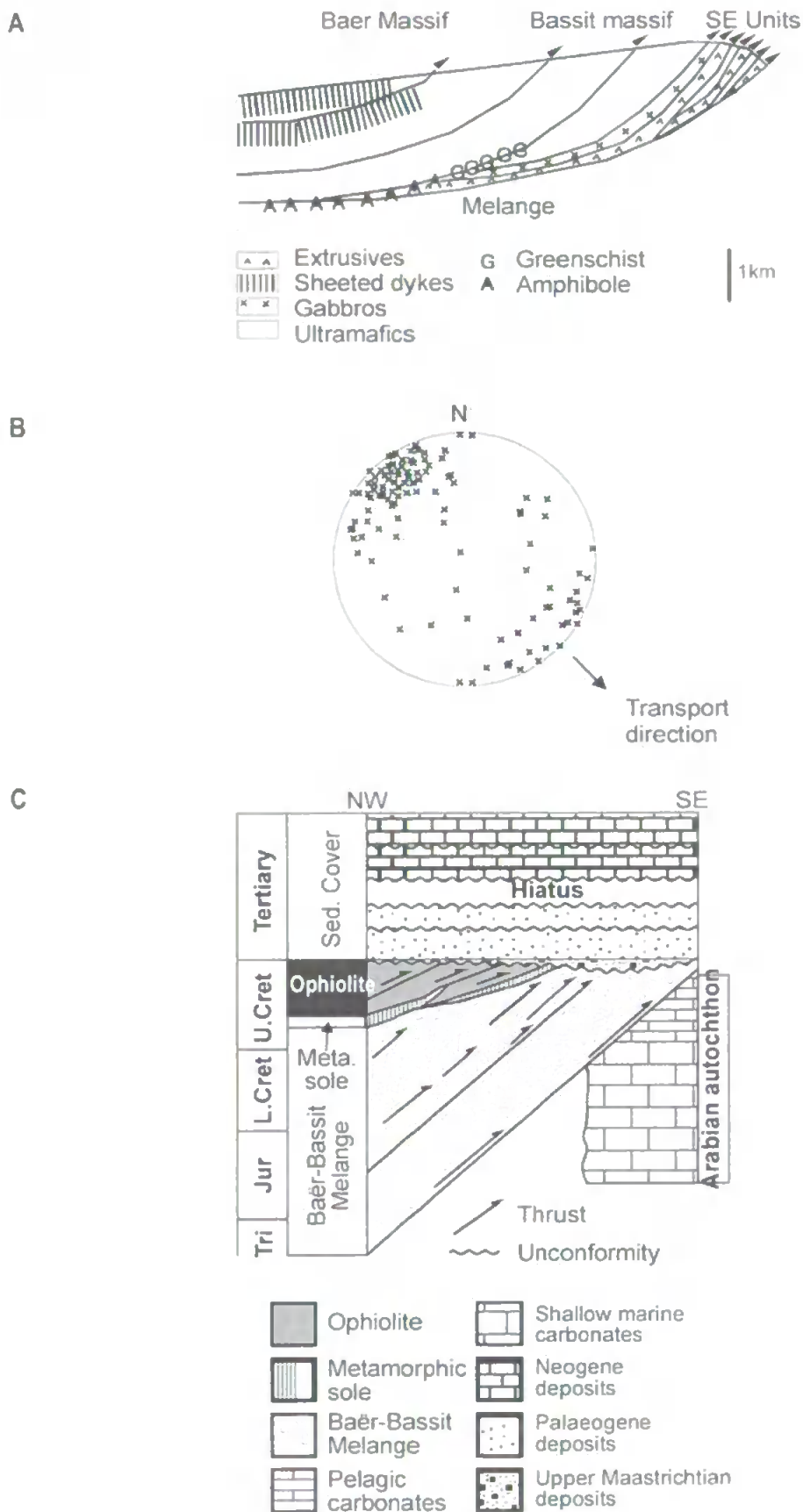


Figure 2.16: Baër-Bassit ophiolite cross-section and emplacement (after K. AL-Riyami et al 2002).

- A. Schematic cross-section showing the emplacement direction towards the SE.
 B. Fold plunge lineations.
 C. Relationship between ophiolite and sedimentary cover units.

2.10 Synthesis

The reviews of the evolution of the eastern Mediterranean, the structural history of the Hatay region and the geology of the surrounding ophiolites provide valuable background information. This is essential in order to produce a robust interpretation of the new palaeomagnetic and structural results from the Hatay ophiolite. The review of existing structural data from the Hatay ophiolite highlights the existence of diverse interpretations of the origins of the structures within the ophiolite as well as a general lack of detailed palaeostress studies in the region. The structural data presented in Chapter Eight significantly extends previous knowledge of the structural development of the Hatay ophiolite and enables some of these contrasting views to be addressed. The geological overview of the Hatay, Troodos and Baër-Bassit ophiolites provides an important overview of features such as the mean strike of their SDCs, which are used in later interpretations. The information provided on the sedimentary cover units and the Neotectonic history is valuable for interpreting the new palaeomagnetic results obtained from the sedimentary covers of the Hatay and Baër-Bassit covers.

CHAPTER THREE

3. THE EARTH'S MAGNETIC FIELD AND PALAEOMAGNETIC METHODS

3.1 Introduction to chapter

The Earth's magnetic field through time can be recorded by rocks and its ancient direction provides a useful reference when applied to many tectonic problems. By recovering the direction of the geomagnetic field at known points in the history of a rock, information can be gained about the degree of rotation experienced by that unit as well as its latitudinal displacement since the magnetisation was acquired. Two key assumptions made are firstly that the rock is able to accurately record and retain a record of the Earth's field over geological periods of time, and secondly that the orientation of the geomagnetic field through time is known with sufficient confidence to infer the ancient position of the sampled rock.

In this chapter, descriptions of the Earth's field and methods by which rocks acquire magnetisation are provided as well as a summary of the palaeomagnetic sampling and analysis methods used within this study. The apparent polar wander paths for Africa and Eurasia will also be described.

3.2 The Earth's magnetic field

The geomagnetic field at the Earth's surface can be described in terms of its horizontal (declination) and vertical (inclination) components (Figure 3.1A). For most palaeomagnetic studies, it is assumed that the Earth's magnetic field can be modelled by a geocentric axial dipole (GAD), which is on average located along the spin axis of the Earth

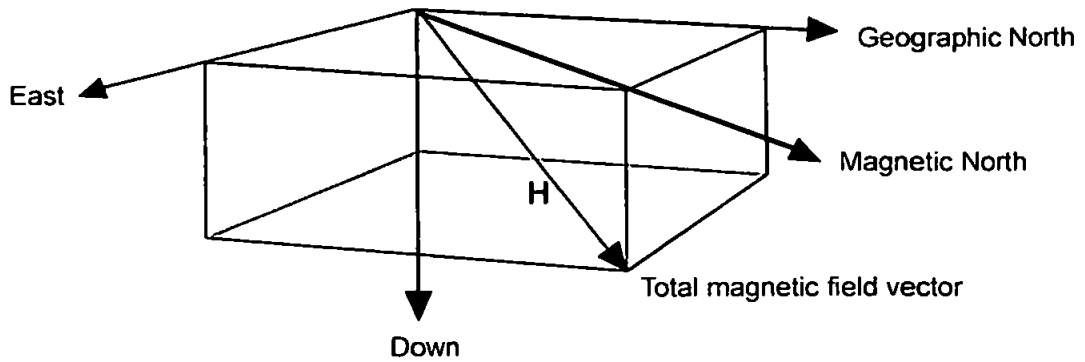
and close to the centre (Figure 3.1B). At present, around 90 % of the Earth's field can be ascribed to such a model, with the dipole currently aligned around 11.5° away from the rotation axis. The assumption that the Earth's field is dipolar is a simplification as there are also non-dipole elements of the Earth's magnetic field. However, the most important component of the field in terms of having the largest effect on magnetisation is the dipolar field, and so it is reasonable to use this assumption in most palaeomagnetic studies.

The Earth's magnetic field is constantly changing direction, oscillating about the GAD with maximum amplitude of around 30° . This is referred to as secular variation. At certain times the Earth's field exhibits variations that cannot be accounted for by secular variation. These are referred to as excursions. The Earth's field also undergoes complete (180°) polarity inversions; these have occurred at a rate on average of two to three per million years on average through the Cenozoic period (Gubbins 1999).

3.3 Magnetisation theory and acquisition of magnetisation

A detailed discussion of magnetic theory is beyond the scope of this thesis, although brief descriptions of some fundamental aspects of magnetic theory are given to provide the necessary background for later results and discussions for the benefit of the non-palaeomagnetist. Further details on magnetic mineralogies within oceanic crustal rocks and rock magnetic parameters are provided in conjunction with the rock magnetic results presented in Chapter Seven.

A



B

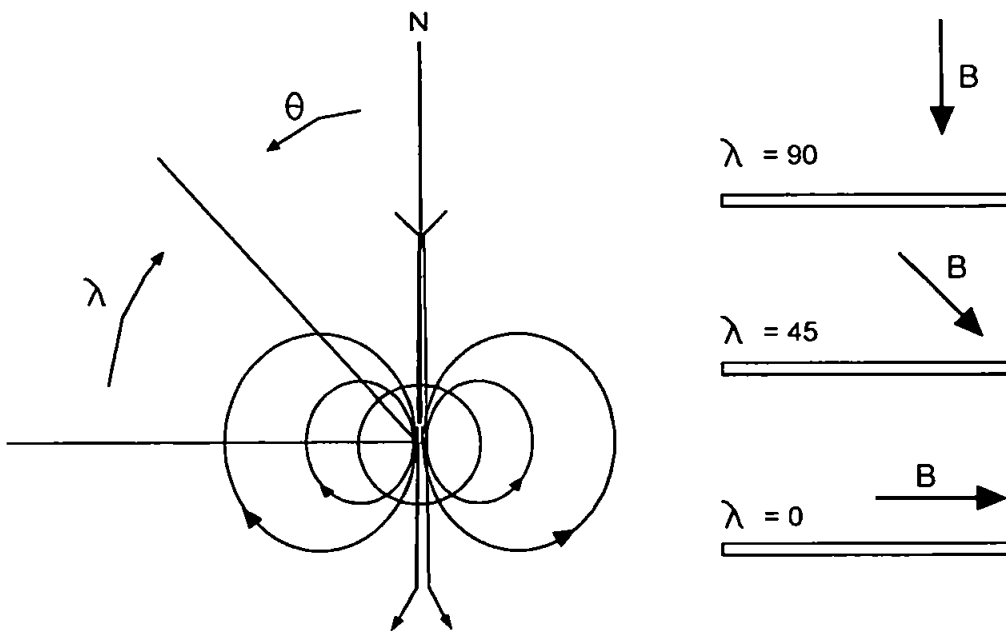


Figure 3.1: The Earth's magnetic field.

A. The total magnetic field vector H can be described in terms of a vertical component and a horizontal component. Declination is the angle between geographic north and the field direction measured in the horizontal plane and inclination is the angle between the field direction and the horizontal measured in the vertical plane.

B. Geocentric dipole field (after Tauxe 1998). A cross-section of the Earth with a dipolar magnetic field superimposed. λ and θ are latitude and colatitude respectively. The illustrations on the right show the inclinations of the magnetic field, B , relative to the Earth's surface at various latitudes. For the GAD model, the inclination (I) can be related to latitude (λ) by the relationship: $\tan I = 2 \tan \lambda$.

3.3.1 Fundamentals of magnetism and magnetic terms and parameters

Figure 3.2 illustrates the three fundamental types of magnetic properties: diamagnetism; paramagnetism, and ferromagnetism. The first two (Figure 3.2A-B) magnetisations are weaker and caused by the properties of electron orbits and atomic spins. Diamagnetism is a weak property of all substances and is results from the interaction of electron spins with external magnetic fields. In the presence of an applied field there is a torque on the electron and the diamagnetic response is the acquisition of a small induced magnetisation opposite to the direction of an applied field. Paramagnetic behaviour is caused by unpaired electronic spins, which also behave as magnetic dipoles. These are essentially randomised unless under the influence of an applied magnetic field, or influenced by neighbouring atomic spins (known as *exchange interactions*). An applied field acts to align the spins and creates a net magnetisation proportional to the strength of the applied field. The elements with most unpaired electron spins are the transition elements and these are responsible for most of the paramagnetic behaviour observed in rocks.

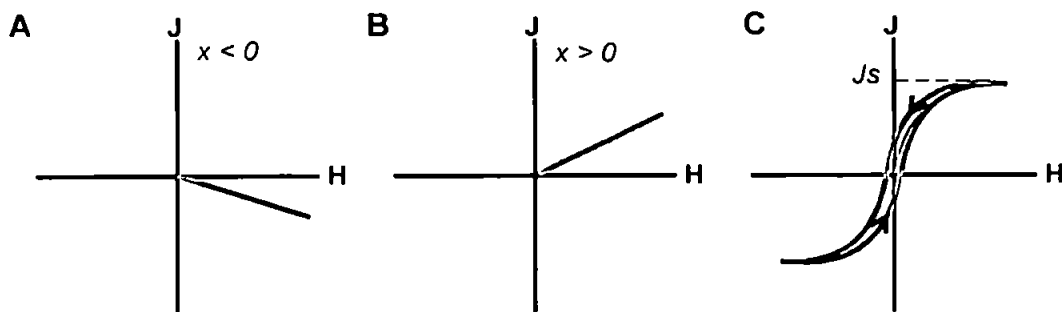


Figure 3.2: Fundamental types of magnetic behaviour.

All plots show the magnetisation, J , versus the magnetising field, H , for:

A. a diamagnetic substance (e.g. quartz); B. a paramagnetic substance (e.g. biotite); and C. a ferromagnetic substance (e.g. magnetite). Magnetic susceptibility, χ , is a negative constant for diamagnetic substances and a positive constant for paramagnetic substances. The path of magnetisation for ferromagnetic substances exhibits hysteresis (irreversible) and magnetic susceptibility is not a simple constant.

Ferromagnetic substances retain a permanent magnetisation in the absence of an applied field, known as *remanent* or *spontaneous* magnetisation caused by strong interactions between neighbouring spins within a crystal lattice. The spin alignment (Figure 3.3) acts to minimise *exchange energy*, which is a consequence of the quantum mechanical principle stating that no two electrons can have the same set of quantum numbers. The 3d orbital of the transition elements is particularly susceptible to exchange interactions due to its shape and the prevalence of unpaired electron spins (Tauxe 1998), so remanence is characteristic of certain crystals containing transition elements with unfilled 3d orbitals. In nature, only certain oxides of iron and iron sulphides display significant magnetism. Magnetic substances that are ferromagnetic at room temperature behave only as paramagnetic minerals above a specific temperature, referred to as the Curie temperature (T_C).

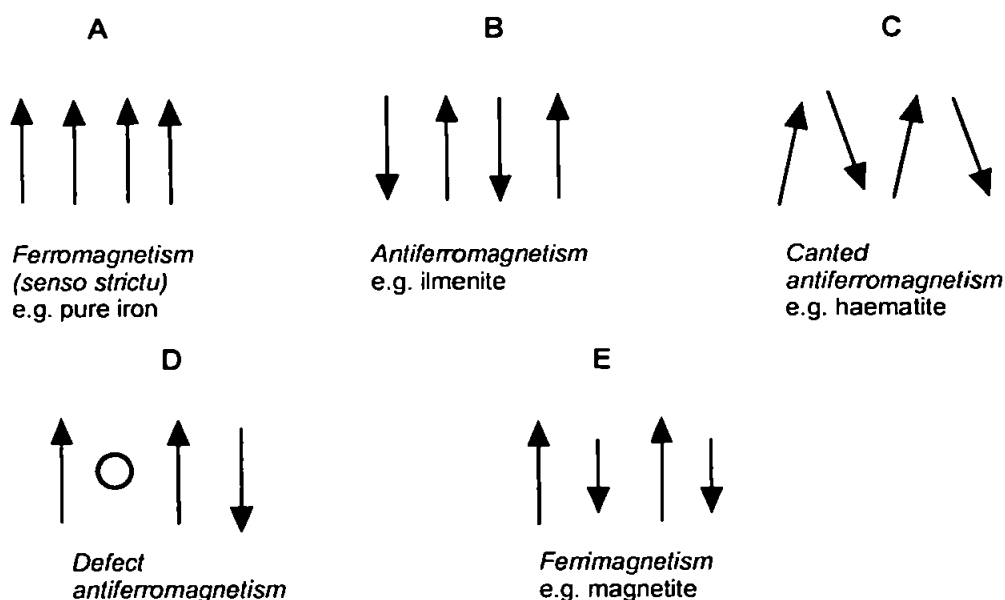


Figure 3.3: Types of spin alignment in ferromagnetism (Tauxe 1998). The strength of the resultant magnetisation is dependent on the spin alignment within the crystal lattice.

A. ferromagnetism (*senso strictu*)- all spins are parallel;

B. antiferromagnetism- spins are perfectly antiparallel and there is no net magnetic moment. In ilmenite Ti^{4+} cations alternate with layers of Fe^{2+} cations. Alternating Fe^{2+} layers are parallel and antiparallel coupled;

C. spin-canted antiferromagnetism- spins are not perfectly aligned in an antiparallel direction but are canted by a few degrees giving rise to a weak net magnetic moment. In haematite atomic magnetic moments of Fe^{3+} cations are parallel coupled within (0001) planes but approximately antiparallel coupled between adjacent layers of cations, with the angle between them departing slightly from 180° ;

D. defect antiferromagnetism- a net magnetic moment can arise if spins are not perfectly compensated owing to defects in the crystal structure, as occurs in fine-grained haematite.

E. ferrimagnetism- spins are aligned antiparallel, but the magnitudes of the moments in each direction are unequal, resulting in a net moment. In magnetite, alternating sublattices contain Fe^{2+} and Fe^{3+} cations with parallel coupled spins alternating with the next sublattice containing an Fe^{3+} arranged antiparallel. The moments of the Fe^{3+} cations effectively cancel, leaving a net magnetic moment due to Fe^{2+} cations, giving rise to a large permanent magnetisation.

Magnetic grains act to minimise the magnetic energy within them, with several different competing energies affecting the grain. There is an *interaction energy* between the magnetisation of individual ferromagnetic particles and an applied magnetic field. This energy increases with grain volume at the surface of grains and at some point it becomes energetically more favourable for the magnetisation to break down into magnetic domains, within which magnetisation is uniformly aligned. A magnetic crystal behaving as a single magnetic dipole is referred to as single domain (SD; Figure 3.4A). Larger grains divided into more than one domain are referred to as multidomain (MD; Figure 3.4C). The domain structure affects the magnetic behaviour of grains. *Exchange energy* refers to the interaction between the magnetic properties of an atom with its neighbouring atoms. *Magnetostatic energy* arises due to repulsion between adjacent magnetic charges and for a uniformly magnetised ellipsoid is the interaction energy between the internal demagnetising field with the magnetisation in the grain. Resistance towards rotating the internal magnetisation of a grain to align with an external field is referred to as magnetic anisotropy with the most significant anisotropies being magnetocrystalline anisotropy and shape anisotropy (Butler 1992). Magnetocrystalline anisotropy is a measure of the magnetic anisotropy within a grain and arises due to preferences for the direction of magnetisation to lie along certain orientations within the crystallographic lattice. Shape anisotropy refers to the difference in magnetic energy depending on the magnetisation direction within a grain in relation to its shape; for instance, a highly elongate ferromagnetic grain has much lower magnetic energy if it is magnetised along its length.

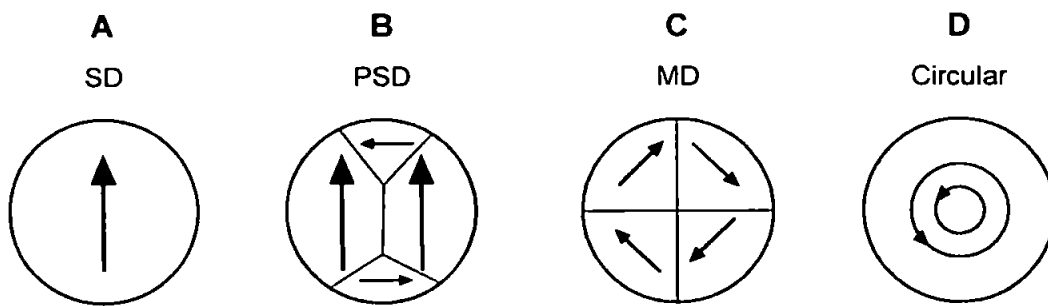


Figure 3.4: Types of magnetic domain structure. A. single domain (SD); B. pseudo-single domain (PSD). C. multi-domain (MD), and D. circular spin arrangement. Smaller grains will usually only have one magnetic domain whereas the magnetisation of larger grains is split between several domains separated by domain walls. It requires energy for magnetic grains to nucleate domain walls, with exchange energy increased for narrow walls and magnetocrystalline energy increased for wider walls. The domain structure that exists in a mineral is also affected by the shape of the magnetic grain. The finest grains tend to behave in a magnetically similar manner to paramagnetic substances and are referred to as superparamagnetic (SP). Pseudo-single-domain (PSD) grains lie in-between SD and MD sizes. The origin of PSD behaviour is likely to be the fixing of domain wall movement by grain shape or lattice imperfections. Other possibilities including domain structures not observed in SD or MD grains, or alternatively PSD behaviour could result from a distribution of grain sizes within the same sample. The circular spin arrangement of D eliminates the associated magnetic field but dramatically increases exchange energy. Hysteresis parameters can be used to infer magnetic grain size (section 7.3.2).

Magnetisation is of two kinds: induced magnetisation, produced when an external magnetic field is applied and remanent magnetisation which is the magnetisation remaining after the external field has been removed. The relationship between the external magnetic field and the induced magnetisation is known as magnetic susceptibility. All magnetisations are time dependent. This is due to the effect of thermal energy within a grain which causes the magnetisation within a grain to relax away from the acquired field direction and effectively randomise over time. Initial magnetisation decays according to the equation: $M(t) = M_0 \exp(-t / \tau)$, where M_0 is the initial magnetisation, t is time and τ is the time for remanence to decay to $1/e$ of its initial value. The value of τ is a function of the balance between magnetic anisotropic and thermal energies: $\tau = 1 / C \exp \frac{[Kv]}{[kT]}$, where C is a frequency factor, the anisotropy energy is given by the dominant anisotropy constant K multiplied by the grain volume v and thermal energy is given by kT . Thus, relaxation time is proportional to coercivity and volume and inversely proportional to temperature.

Coercivity is the ease with which a magnetic grain is magnetised and depends on both mineralogy and grain size as well as shape anisotropy. Smaller grains of the same domain structure (e.g. SD) have lower coercivities because activation energy is lower and a small applied field or lower temperatures are sufficient to allow the grain to reorient itself. Coercivity can increase with increasing titanium content. Coercivities are also lower for magnetite and maghemite and higher for haematite and pyrrhotite. Coercivity is non-unique, for instance a coercivity of 200 mT could be due to elongate SD magnetite grains, equant TM60 grains or intermediate MD haematite grains. Relaxation time refers to the time period over which a magnetisation will decay and is shorter for grains of lower coercivity.

Curie temperature (T_C) depends on magnetic mineralogy only and is the temperature at which thermal vibration destroys exchange couplings so that the spontaneous magnetisation falls to zero. Above this temperature, the grains behave in a superparamagnetic manner. T_C for stoichiometric magnetite is around 580°C and for haematite T_C is 680°C. Addition of titanium reduces T_C in both titanomagnetites and titanohematites. Measurement of T_C can be achieved by monitoring the change in susceptibility or saturation magnetisation with temperature. However, T_C is non-unique, for instance a T_C of 580°C may either indicate magnetite or alternatively haematite with 10% titanium. The T_C of end-member magnetite decreases with increasing ulvospinel content and increases with increasing oxidation parameter (Moskowitz 1987).

Blocking temperature (T_B) is the temperature below which the permanent magnetisation becomes imparted to the mineral. T_B can be considered as analogous to H_C in that, once this value is exceeded, a magnetic grain loses its ability to retain a stable magnetisation. In rocks, a spectrum of blocking temperatures is observed due to the diversity of grain properties. Above T_C the magnetic grains behave in a paramagnetic manner:

magnetisation can be acquired in a magnetic field but has a short relaxation time and decays to zero once the field is removed. As the temperature falls, relaxation time dramatically increases so that randomisation of the magnetisation by thermal vibrations can only occur over enormous time periods. The key result for geological purposes is that the relaxation time rapidly exceeds the age of the Earth for many magnetic grains (particularly SD grains).

Some magnetic minerals display structural transitions at low temperatures. For example, the Verwey transition in magnetite occurs at 120 K (-140°C) for stoichiometric magnetite with the transition temperature decreasing with increasing Ti content. Recovery of the original remanence is almost complete in SD grains but poor in MD grains. The Morin transition occurs at -15°C in haematite with the transition temperature decreasing with increasing titanium content, with recovery of remanence in haematite not being grain size dependent. In pyrrhotite, a low-temperature transition occurs at -240°C and recovery of the original remanence is almost complete in SD grains and poor in MD grains. There is no low-temperature transition in maghemite. Again, low-temperature transitions are non-unique; for example a lack of transition on cooling to 50 K could be due to the presence of maghemite, a high-Ti titanomagnetite or pyrrhotite.

3.3.2 Acquisition of magnetisation

Major assumptions in using palaeomagnetism as an interpretive technique in tectonics are that magnetic minerals within rocks are capable of retaining the direction of the past field over geological time and that the oldest magnetic direction measured in a rock can be assigned to a geologically relevant time. For example, it would be useless to know the oldest direction in a rock but have no knowledge of its history. To satisfy the validity of

these two assumptions, it becomes important to know something about how a rock acquires its magnetisation.

For most palaeomagnetic studies, it is preferable for magnetisation acquisition to occur at the time of formation of the rock and record the same direction as the prevailing geomagnetic field with this satisfying the GAD hypothesis. The magnetisation acquired at the time of rock formation is known as the *primary magnetisation*. For a primary magnetisation to be stable over geological time, the relaxation time must be greater than the age of the rock. This primary component of magnetisation can be acquired in rocks in different ways. For example, some igneous rocks acquire a thermal remanent magnetisation (TRM) with the magnetisation 'fixed' as the rock cools through the blocking temperature spectrum (T_B) of the ferromagnetic grains. In sedimentary rocks, the remanence is usually acquired either as the grains become aligned with the prevailing magnetic field upon deposition- a detrital remanent magnetisation (DRM), or subsequently due to compaction and dewatering processes rearranging the grains (pDRM). Primary magnetisations can be altered by a chemical remanent magnetisation (CRM), where an existing magnetic grain is altered at low temperatures by a chemical reaction, or as a new diagenetic ferromagnetic mineral is precipitated. CRMs are most common in sediments. The primary magnetisation can also be altered, or added to, by lightning strikes as an intense isothermal remanent magnetisation (IRM) remagnetises the grains within a rock. A tectonic event may reheat some magnetic minerals above their blocking temperatures resulting in partial remagnetisation of grains within the rock. Over time the lowest coercive magnetic grains lose their original magnetisation and realign with a later magnetic field direction; this is viscous remanent magnetisation (VRM). These processes result in acquisition of secondary components of magnetisation by the rock, which can be isolated by demagnetisation techniques and allow the primary direction to be recovered in most cases.

There are several reasons why the magnetisation acquired by a rock may not represent the dipolar field at the time of formation. For instance, the GAD hypothesis may not be valid at the time/location where the rock formed; for example if it was acquired during an excursion or during a polarity reversal, the direction of magnetisation will not record a dominant dipolar field. Also, a direction from a single sample is unlikely to record a long-time average of the geomagnetic field and therefore to have averaged out secular variation; it is only when an average direction is determined from samples within a site and several sites are averaged, that secular variation will be accounted for. These sites should be from rock sequences covering time periods sufficiently long to average out secular variation. Another problem is that rocks may be anisotropic and therefore magnetisation will not be acquired parallel to the geomagnetic field direction. All magnetic minerals are anisotropic and can usually be assumed to have a random arrangement in igneous and sedimentary rocks resulting in overall isotropic behaviour of the rock. Anisotropy only becomes significant for palaeomagnetic measurements if the rock itself is strongly anisotropic. The magnetic anisotropy of the rock, in terms of both anisotropy of induced magnetisation (susceptibility; AMS) and anisotropy of remanence (AMR) can be measured; the former was measured for this study since its measurement is a quick straightforward process that gives a good general indication of rock fabric. As strong anisotropy in rocks tends to be confined to relatively small areas, sampling over a wide area will in general minimise this problem, especially as the effect is usually insufficient to substantially deflect remanence. It is important in order to be sure that the magnetisation is primary and determine whether the rock has acquired any secondary components of magnetisation such as CRM or IRM. Also, magnetisation decays over time and the more easily remagnetised grains within a rock (lower coercivity grains) will reorient themselves in the direction of later geomagnetic fields to produce VRM.

3.4 Measurement, demagnetisation and rock magnetic techniques

The sum of all the magnetic components within a rock is referred to as the natural remanent magnetisation (NRM). The individual components are isolated by demagnetisation techniques that work by progressively removing the contribution of the magnetic directions carried by the grains with the lowest coercivity/unblocking temperature and randomising or removing these magnetisations. For most magnetic studies, the objective is identification of the oldest magnetic direction carried by the rock, referred to as the characteristic remanent magnetisation (ChRM). This will represent the primary magnetisation if it was acquired at the time of rock formation and successive events have not completely remagnetised the rock. It can be supported (but not generally conclusively defined) by various field tests, such as fold, conglomerate, reversal and contact tests (section 3.5.7). In this study, alternating field (AF) and thermal magnetic cleaning techniques have been used, with the general application of these techniques being AF demagnetisation for rocks containing magnetite and titanomagnetites and thermal demagnetisation used for rocks containing haematite. The most appropriate demagnetisation technique depends on the mineralogy and magnetic history of a sample. Subjection of a trial sample from a site to both techniques can determine the most appropriate procedure to use for the majority of samples, although checks by measuring a few samples from each site using the other technique allows confidence in results and a better understanding of the magnetisation within the samples. The maximum theoretical coercivity for single domain magnetite is 300mT (for acicular SD grains). Most AF demagnetisers have the capacity to demagnetise grains with coercivities ranging up to 100 mT. Hematite coercivity is considerably greater and AF demagnetisers are usually incapable of producing the fields required. AF demagnetisation is therefore more appropriate for rocks containing magnetite whereas thermal demagnetisation is more suitable for hematite-bearing rocks. AF demagnetisation can be less suitable for multi

domain grains as grain boundaries within these have a tendency to realign with the field prior to reaching H_c and becoming randomised. There may be more than one population of grains within a sample with the populations having different coercivity/unblocking temperature spectra but potentially overlapping with one another. On an orthogonal demagnetisation plot (section 3.5.1) this results in a curve of the magnetisation projection due to the overlap of the spectra and on a stereonet a continuous directional migration is observed.

3.4.1 Alternating field (AF) demagnetisation

AF demagnetisation works by subjecting samples to an alternating field with peak value H . All domains with a coercive force below $H\cos\theta$ (where θ is the angle between H and the domain magnetisation) will align themselves with the alternating field. If this field is applied to all possible domain orientations, then domains with progressively lower coercive force will become stranded as the field is slowly decreased to zero. The combined result will be the randomising of the orientations of all grains with coercive force below that of the applied field. If this process is then repeated at progressively higher fields, at each step the magnetisation can be projected and plotted. The end result is a vector plot of the magnetic field, allowing recognition of all the component contributions to the magnetisation within a sample. This can then be analysed to determine ChRM.

The demagnetisers used for samples in this study were the AGICO LDA3 AF demagnetiser and the Molspin AF tumbling demagnetiser. The Molspin AF tumbling demagnetiser was used for both the majority of the standard palaeomagnetic cores and the hand sampled pillow lavas (section 5.2.1) which required a sample holder capable of holding larger non-standard specimens. The maximum applied field intensity is 100 mT and was increased from 5 mT to 100 mT in 5 mT steps followed by 10 mT steps

subsequent to the loss of most of the magnetisation, at which point little detail becomes lost from using larger steps.

3.4.2 Thermal demagnetisation

Thermal demagnetisation procedures remove the lower unblocking temperature components by heating to progressively higher temperatures and cooling in zero field whereby all grains with unblocking temperatures (T_B) less than the furnace temperature will become randomised. As many natural viscous overprints are caused by an increase in temperature exceeding the blocking temperature of the lowest-stability grains causing resetting of their magnetisation, a laboratory imitation of this process is generally very effective in removing such overprints. Thermal demagnetisation can result in alteration of certain magnetic minerals during treatment, usually due to oxidation. A measurement of sample susceptibility prior to and following each step of a measurement sequence should identify any such mineralogical changes.

Specimens were demagnetised using a Magnetic Measurements MMTD1 furnace, which can achieve a maximum temperature of 800°C. Typically, between 12 and 15 samples were demagnetised at one time, with samples of similar lithology selected and a gap between samples in the holder to minimise any magnetic interference between specimens. Heating was stopped once temperatures were sufficiently high to be greater than the maximum T_{BS} of the samples. In between each step, the susceptibility of the sample was measured using the AGICO KLY3 Kappabridge in order for any mineralogical changes caused by oxidation during the heating process to be identified.

3.4.3 Measurement of magnetisation

For all standard palaeomagnetic samples demagnetised in the University of Plymouth Palaeomagnetic laboratory, the magnetisation between each demagnetisation step was measured using a Molspin spinner magnetometer. A large aperture Digico spinner magnetometer was used to measure the hand sampled pillow lava samples as it is suitable for non-standard specimens. For the sedimentary samples measured in the University of Oxford Palaeomagnetic laboratory, magnetisations were measured using a 2-G superconducting magnetometer system. The operating principles of both spinner and cryogenic magnetometers are fully described by Collinson (1983).

3.4.4 Magnetic fabric

The existence of a magnetic fabric can be caused by sedimentary or magmatic layering. The anisotropy of the magnetic susceptibility (AMS) was measured for all samples using an AGICO KLY3 Kappabridge, prior to AF demagnetisation to avoid field-imposed effects (Tarling and Hrouda 1993).

AMS reflects the preferred orientation of grains, grain distributions, and/or the crystal lattices of minerals which contribute to the magnetic susceptibility of a rock. It corresponds to a second order tensor and can be represented by an ellipsoid specified by the orientation and magnitude of its principal axes (K_1 , K_2 and K_3 , being the maximum, intermediate and minimum susceptibility axes respectively). The AMS of a rock may result from contributions from diamagnetic, paramagnetic, antiferromagnetic and ferrimagnetic minerals (see Tarling and Hrouda 1993 for a review), but where magnetite is present this usually dominates the AMS signal. K_1 axes are aligned along the long axes of non-equant magnetite grains or along the axes of linear chains of interacting equant grains,

usually resulting in correlation of specimen AMS lineations with petrofabric x-axes (e.g. flow lineations). K_3 axes generally lie normal to petrofabric foliations (e.g. sedimentary bedding). These relationships between principal susceptibility axes and petrofabric elements are, however, dependent on magnetic grain size (domain state). Presence of significant non-equant single domain grains of magnetite may result in inverse magnetic fabrics (Stephenson et al. 1986; Rochette 1988), resulting in K_1 axes lying normal to bedding in sedimentary fabrics.

The oblateness or prolateness of individual specimen AMS ellipsoids is described by the shape parameter T , with $0 < T \leq 1.0$ for oblate ellipsoids and $-1.0 \leq T < 0$ for prolate ellipsoids. Strength of anisotropy is described by the corrected anisotropy degree, P_j (Jelinek 1981). If no preferred relationship between P_j and T is observed, and no correlation between P_j and mean susceptibility, the indication is that the degree of anisotropy is not dependent on ferrimagnetic concentration.

At a site level, clustering of K_1 and K_3 axes defines the magnetic lineation and the pole to the magnetic foliation respectively. Oblate fabrics are characterized by clusters of K_3 axes orthogonal to great circle girdle distributions of K_1 and K_2 axes, whereas prolate fabrics are characterized by clusters of K_1 axes orthogonal to girdle distributions of K_2 and K_3 axes. In triaxial fabrics, the three principal susceptibility axes form distinct groups.

3.4.5 Rock magnetic experiments

In order to have greater confidence in the interpretation of the magnetisation directions, it is preferable to have some knowledge of the magnetic minerals carrying the magnetisation. Knowledge of the rock magnetic characteristics of a sample can give insight into the timing of the acquisition of magnetisation as well as the potential for the magnetisation to

remain stable over geological time. There are many rock magnetic tests that can be performed in order to find parameters such as Curie points, low temperature transitions and coercivities. Standard demagnetisation procedures give some indication of the rock magnetic characteristics of a sample, although detailed analysis requires specific rock magnetic testing. The rock magnetic experiments carried out for this thesis and their results are described in detail in Chapter Seven and so will only be summarised below.

Both alternating field demagnetisation and thermal demagnetisation techniques give some indication of the rock magnetic carriers of the NRM. Alternating field demagnetisation enables insight to be gained into the coercivity of a sample. This is done by identifying the median destructive field (MDF) of a sample, which is the field at which the magnetisation of a sample falls to 50% of its initial value. Lower coercivity minerals will have lower MDFs than higher coercivity minerals. Thermal demagnetisation gives an indication of the unblocking temperature (T_{UB}) of the magnetic minerals within a sample. The unblocking temperature can be recognised during demagnetisation as the temperature when a significant decrease in magnetisation is observed.

Basic rock magnetic analyses using simple equipment available in most laboratories enable further characterisation of rock magnetic characteristics. Analyses of the acquisition of isothermal remanent magnetisation use a pulse magnetiser and Molspin spinner magnetometer. Stepwise increasing magnetic pulses are imparted into a sample using the pulse magnetiser, followed by measurement of the remanent magnetisation (out of field) using the Molspin, which is then plotted against the applied field to produce an acquisition of isothermal remanent magnetisation (IRM) curve. The shape of the curve and the maximum remanent magnetisation produced (SIRM) gives an indication of sample coercivity and hence grain size and mineralogy. From a saturated sample, the magnetisation required to return the magnetisation to zero can be found- the coercivity of

remanence or backfield coercivity (section 7.3.3). These experiments can be followed by hysteresis measurements where the magnetisation of the sample is measured in field, with diagnostic points including the saturation magnetisation (M_s) and coercivity.

High temperature experiments enable the mineralogy of a sample to be identified from the temperature at which the spontaneous magnetisation falls to zero- the Curie point (T_C). These can be done either measuring magnetisation as the temperature is increased (e.g. using a Curie balance or a Vibrating Sample Magnetometer with a furnace attachment; section 7.3.4) or by measuring the susceptibility of a sample against temperature (e.g. using a Kappabridge enabling susceptibility to be measured over temperatures between 77 and 970 K).

Low temperature experiments look for low temperature transitions, such as the Verwey transition in magnetite and the Morin transition in haematite. The temperatures at which these transitions occur can be affected by the amount of titanium and oxidation and the transitions are identified by a change in remanence across the transition (section 7.3.5).

3.5 Analysis of magnetisation data

3.5.1 Plotting and analysis of results

Various analysis methods are used in palaeomagnetism to plot and extract the components of magnetisation. Display of the magnetisation involves projection onto orthogonal axes, plotting on stereonet and step versus intensity plots, allowing maximum detail to be gained on all components of magnetisation. Line-fit analysis packages are used to fit the various observed components of magnetisation.

Plots commonly known as either Zijderfeld diagrams (z-plots), after Zijderfeld (1967), or orthogonal plots, project the magnetic vector onto orthogonal axes, with distance from the origin corresponding to magnetic intensity. This enables NRM components to be clearly seen and analysed. The principal components of magnetisation are delineated by calculation of the best-fitting vector through the appropriate points on the z-plot, with the highest stability direction of magnetisation being the last straight line segment that decays to the origin.

Orthogonal projections commonly display at least two-components of magnetisation; the first often corresponding to a viscous magnetisation acquired in the present-day field and the second to that of an ancient field (Figure 3.5). Plots with few components that decay cleanly to the origin are easy to interpret. Samples with a magnetisation that does not decay to the origin following a complete demagnetisation procedure indicates incomplete demagnetisation, and can be caused by the presence of grains of high coercivity/unblocking temperatures. If the direction of the highest temperature/field component bypasses the origin, this may represent failure to remove all of the overprinting direction(s). On a stereonet, this can be recognised as a smear and continuous migration of points along a great circle from the initial component towards that of the ancient field. If great circles are plotted using the results from a number of samples which have been influenced to different degrees by the overprinting field, these circles should converge to an intersection at the true direction of the past field.

Freeware programs developed by Randy Enkin¹ were used to plot the magnetisation as z-plots, stereonets and intensity plots, with least squares and principal component analysis after Kirschvink (1980) used to calculate sample directions. Contained within these

¹ http://www.pgc.nrcan.gc.ca/people/renkin_e.php

programs are various tools such as fold and reversal tests, some of which were also used in this study. Site mean directions were calculated using Fisher (1953) statistics.

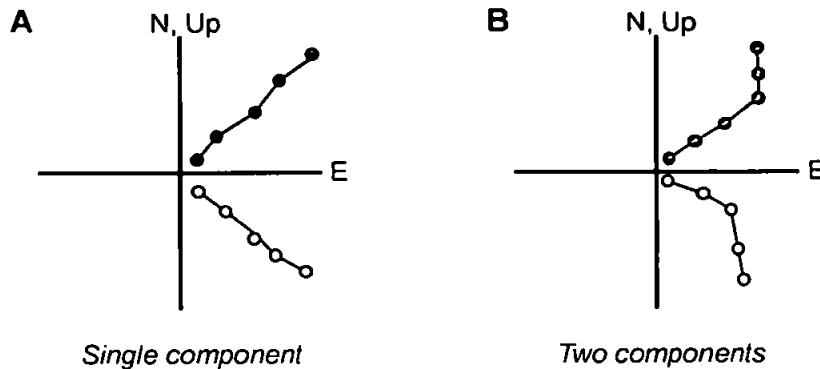


Figure 3.5: Examples simple orthogonal demagnetisation plots. The black and white circles show the projection of the magnetic vector onto the horizontal and vertical planes respectively. Magnetisation (in A/m) is plotted along the axes. For projection onto the horizontal plane, north, east, south and west orientations are shown on the axes. For the projection onto the vertical plane, up and down directions are displayed on the axes. A. a single component of magnetisation decays linearly to the origin. B. two components of magnetisation are removed by the demagnetisation process.

3.5.2 Components of magnetisation

For most samples a stable component of magnetisation can be isolated by principal component analysis (as for almost all samples for this thesis; Chapters Five and Six). Sample directions were averaged to obtain a site level ChRM. Ideally, at least six samples should be used to obtain a site ChRM in order to average out secular variation, which was the case for this study in all except two sites. Some of these site level ChRMs were then grouped further in order for a locality ChRM to be obtained, which would then be expected to have completely averaged out secular variation. This was checked by examining the dispersion in virtual geomagnetic poles (VGPs; see later section) between sites in the same group.

Those samples where a stable component of magnetisation was not identified were sufficiently few to be excluded from the analysis with no effect on the results. For sites

with more than one component of magnetisation, where it was possible to isolate a direction from lower or middle coercivity/unblocking temperature components, these directions were also plotted.

3.5.3 Secular variation and virtual geomagnetic poles (VGPs) in sampling

The effect of secular variation is important both for interpretations of the degree of angular dispersion between sites and for tectonic interpretations. Secular variation may not be averaged out on a site level, in which case a tight distribution of ChRM directions is expected, representing a spot reading of the Earth's magnetic field. The orientation of a pole calculated from the site mean declination and inclination will also represent a spot reading of the field, a virtual geomagnetic pole (VGP), rather than the palaeopole. A consideration of the degree to which both sample ChRM directions within a site and average directions from a group of sites average out secular variation is important in order to interpret whether dispersion is that expected from secular variation or due to true tectonic rotations. Ideally samples within an individual site should have ChRM directions that cluster tightly within site in order to be confident that the site direction and resultant VGP for that site are known precisely. To either determine an accurate palaeopole from a collection of site VGPs or (as more important for this study) to correctly analyse tectonic rotations requires a certain degree of dispersion between sites in order to average out the effects of secular variation.

From studies of lavas over the last 5 Ma, the secular variation over this period is known and so the expected variation in VGPs due to secular variation at different localities is known (Merrill and McElhinny 1983). The degree of secular variation increases by a factor of about two with latitude from the equator to the poles. The dispersion of VGPs for any latitude is well-constrained to the range 10-20°. The latitude of the Hatay sampling

sites was around 20° N at the time of magnetisation acquisition (see Chapter Five), for which the degree of dispersion in VGPs over the last 5 Ma would be expected to be around 13° . For the interval 45 to 100 Ma (in which the age of the Hatay sampling sites falls), the variation differs slightly and around 13.5° VGP dispersion is expected.

If VGP dispersion between sites is much less than that predicted the implication is that either sampling sites do not span a sufficiently long time interval to afford adequate sampling of the variation, or that possibly, some degree of within site averaging may have occurred. To average out secular variation necessitates sampling over timescales greater than the dominant periodicities of the variation. From analyses of the geomagnetic field over the last 5 Ma it is known that the dominant periodicities of secular variation are less than 10^5 years, so a number of sites that randomly sample the geomagnetic field over 10^5 or 10^6 years should average out secular variation. Within-site averaging may occur where the magnetisation has been acquired over long periods of time, such as in deep-level igneous rocks or sediments where a DRM has been acquired over a long period or acquisition of a CRM has been a lengthy process, but will not occur in lavas where a single flow cools rapidly in relation to the time-scales of secular variation. If the VGP dispersion is significantly greater than expected, the implication is that either there has been difficulty in determining the ChRM directions accurately, or that there is a source of VGP dispersion in addition to secular variation, such as tectonic disturbance between sampling sites.

3.5.4 Standard structural corrections

Standard palaeomagnetic practise involves the application of a structural correction to the in situ (geographic coordinates) remanence data by a simple tilt around a strike-parallel axis to restore the palaeohorizontal/palaeovertical surface to the present-day horizontal/vertical. Tilt corrected vectors (stratigraphic coordinates) may then be compared to an appropriate coeval reference vector with the difference in declination

(azimuth) and the corrected magnetisation being interpreted in terms of vertical axis rotations and differences in inclination (dip) being attributed to either palaeolatitudinal movements or to inclination shallowing due to compaction (for sedimentary rocks). This tilt correction approach decomposes the total deformation at a site into components of rotation about horizontal and vertical axes. Declination errors may result if deformation involved tilting around inclined axes or if more than one phase of tilting was involved or if fold axes were plunging (MacDonald 1980). However, declination errors are less than 10° for fold plunges less than 50° provided that the palaeohorizontal dips are less than 40° . Errors are less than 10° even for vertical beds provided as the fold plunge is less than 10° . For sites where there are palaeohorizontal controls on the structural restoration process, standard techniques are generally sufficient to elucidate rotations. The largest error in applying standard structural corrections in ophiolitic terranes arises when restoring sheeted dykes. This is due to the impossibility of resolving components of tilt about dyke-normal axes in the absence of palaeohorizontal markers (Borradaile 2001; Morris and Anderson 2002). If unresolved tilts are present, both declination and inclination anomalies may be produced, and an alternative net tectonic method of analysis may be more appropriate (section 3.5.5). Standard structural corrections were used for the majority of sites in this study with the net tectonic method used in appropriate cases.

3.5.5 Net tectonic rotation analysis method

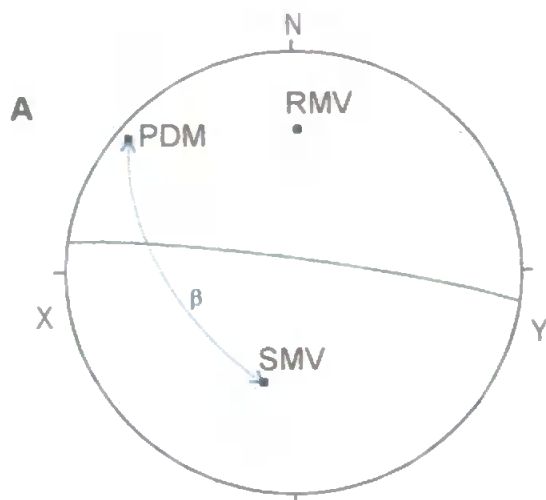
For sites with palaeovertical controls, such as within the sheeted dyke complex, if there has been a significant degree of rotation about a dyke-normal axis, merely restoring the dykes to vertical will not take account of this rotation. The net tectonic method of analysis may be adopted in ophiolitic terranes as an alternative approach to standard structural correction techniques. The deformation at a site is described in terms of a single rotation about an inclined axis that restores both the palaeohorizontal/palaeovertical to its initial orientation

and the site mean magnetisation vector to the appropriate reference direction (Allerton and Vine 1987; Allerton 1989; Morris et al. 1990; Hurst et al. 1992; Morris et al. 1998, 2002). This single rotation may then be decomposed into any number of component rotations on the basis of additional structural data and/or net tectonic rotation axes may be interpreted directly in terms of structural history. In most cases, two solutions are obtained for the original dyke orientations and the pole and angle of net rotation for each dyke sampled. To distinguish between these two solutions, it is necessary to compare to other data in order to choose the most suitable solution. The reference vector used is usually either a previously derived structurally corrected direction (e.g. from sites with palaeohorizontal controls) or to the appropriate palaeomagnetic field direction.

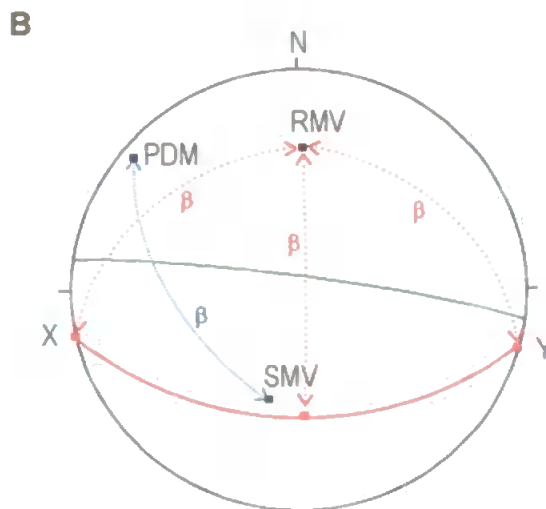
There are several assumptions inherent in using this method (Allerton and Vine 1987):-

- 1) There has been little internal deformation during the rotation history and so the angle between the dyke margin and the remanent magnetic vector remains constant.
- 2) The observed stable remanent magnetisation was acquired prior to any structural deformation.
- 3) An average representative magnetisation vector for the local area can be found that represents the geomagnetic field direction at the time the magnetisation was acquired.
- 4) The dykes are intruded vertically.

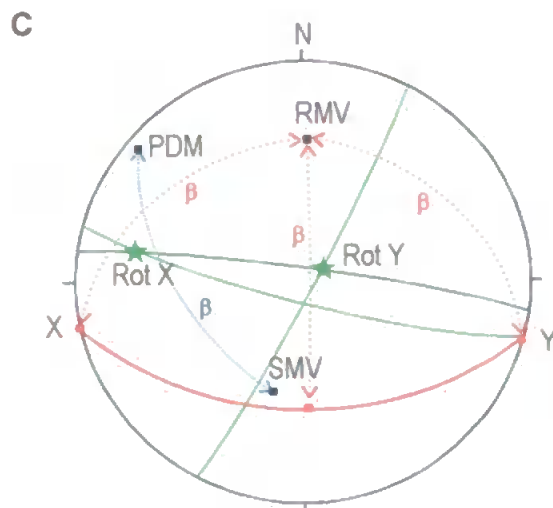
Net tectonic analysis was originally developed by Allerton and Vine (1987) with a Visual Basic Program developed by Morris et al. (1998) used in this project that incorporates an allowance for errors on both the palaeomagnetic and structural directions. An illustration of the net tectonic rotation method using a dyke site from this study is shown in Figure 3.6.



Plot RMV, SMV and PDM on a Wulff Stereonet. Draw the great circle bisectrix between RMV and SMV (278/85). This gives the locus of possible points of the pole that rotates SMV to RMV. Find the angle β between PDM and SMV by aligning both points on the same great circle.



Draw a circle centred on RMV of radius β (by counting β along great circles from RMV and joining up the points in a small circle). The original PDMs X and Y are located on the primitive circle i.e. Vertical dykes.



Find the great circles bisecting solution A (105/82) and solution B (028/86) with the present-day PDM. The points where these cross the great circle between RMV and SMV give the two possible poles of rotation.

Figure 3.6: Net tectonic rotation analysis method of Allerton and Vine (1987) demonstrated using sheeted dyke site CD01.

RMV: Reference Magnetisation Vector e.g. Palaeo-geomagnetic pole (36/002)

SMV: Sample Magnetisation Vector (47/195)

PDM: Pole to dyke margin (07/310)

X: Solution A for original pole to dyke margin (00/258)

Y: Solution B for original pole to dyke margin (00/106)

Rot X: Solution A for the rotation pole (26/281)

Rot Y: Solution B for the rotation pole (82/054)

B: Angular distance between SMV and PDM (101°)

3.5.6 Statistical tests for the timing of magnetisation acquisition

Statistical field tests can be useful for determining the timing of magnetisation acquisition and include such field tests comprising fold, contact, conglomerate and reversal tests (Figure 3.7). The most common field test for palaeomagnetic stability is the palaeomagnetic fold test (McElhinny 1964; McFadden and Jones 1981). This conventional fold test uses both the declination and inclination of the palaeomagnetic vector to find the degree of untilting that results in maximum clustering of the directions (Figure 3.7A-B).

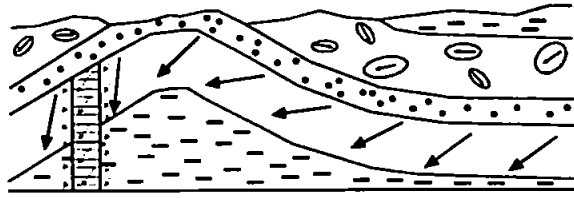
Differential vertical axis rotations between sampling sites, however, invalidate use of area-wide fold tests based on full remanence vectors (declination and inclination). An alternative approach which is independent of the structural history is to determine the effect of untilting on the distribution of inclinations only. The angle between the inclination and the palaeohorizontal (bedding) at a site is assumed to remain constant during rigid body rotation, regardless of the axis of rotation. Therefore, whatever the real rotations were that occurred, a simple restoration about the strike of the section will return the inclinations to their correct value without introducing error. Significant increases/decreases in clustering of inclinations upon tilt correction of mean directions from sites with different structural orientations therefore suggest that pre-tilt/post-tilt magnetisations have been identified, respectively (Enkin and Watson 1996). For shallow inclinations, the arithmetic mean from the distribution does not result in acceptable estimates, but for steeper inclinations, numerical methods are required (Enkin and Watson 1996). If maximum clustering is observed at some intermediate degree of untilting this indicates that a syn-tilting magnetisation is present. The greater the Fisher precision parameter \hat{k} value returned by the analysis the greater the confidence in the result. Strongly peaked distributions with maximum \hat{k} values at 100% untilting demonstrate unequivocally that pre-deformational remanences are identified. If sites are appropriate to

group into localities located on several rigid blocks, the block-rotation Fisher analysis can be applied to the inclination-only tilt tests (Enkin and Watson 1996). For this study, an inclination-only tilt test eliminates the effects of potential movement between blocks that may invalidate a standard tilt test.

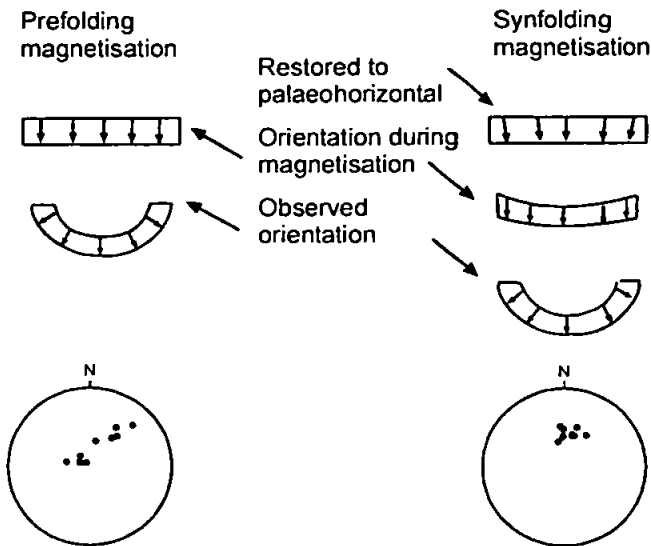
The conglomerate test (Figure 3.7A) uses the fact that, if magnetisation has been stable since the conglomerate was deposited, a random distribution of ChRM directions should be observed. Thus, a non-random distribution of ChRMs indicates acquisition of magnetisation after deposition of the conglomerate. The baked contact test compares the directions of magnetisation in the baked zone surrounding an intrusion to those within the intrusion. If the directions of the baked country rock are parallel to those of the intrusion, but differ from those of the unbaked country rock, it can be inferred that the magnetisation of the intrusion has been stable since formation (Merrill and McElhinny 1983). At all locations, the time-averaged geomagnetic field directions during a normal-polarity interval and during a reversed-polarity interval differ by 180° and this forms the basis for the reversals test (Figure 3.7C).

The reversals test (section 6.3.5) and inclination-only tilt test (sections 5.10; 6.3.5; 6.4.5) and are used in this thesis, with the inclination-only tilt test selected due to potential rotations about adjacent tectonic blocks. The conglomerate and baked contact test are not appropriate as the units sampled for palaeomagnetic analysis did not include either conglomerates or suitable baked contacts.

A Fold, conglomerate and baked contact test



B



C Reversals test

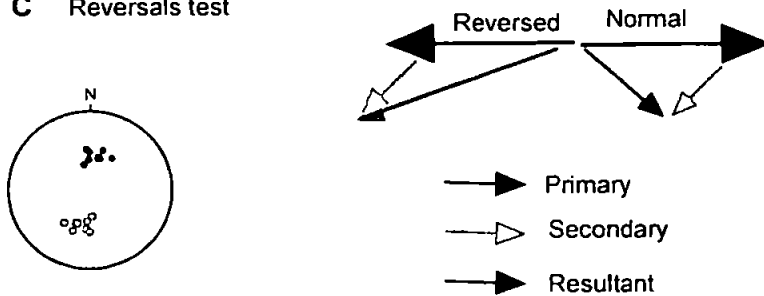


Figure 3.7: Field tests for palaeomagnetic stability.

A. the fold, conglomerate and baked contact test (redrawn from Merrill and McElhinny 1983). Arrows indicate the direction of magnetisation. If the directions of magnetisation of samples collected from different limbs of a fold converge after unfolding the beds, the magnetisation pre-dates the folding and has remained stable since. If directions of magnetisation in conglomerate pebbles derived from the beds under investigation are randomly oriented, the magnetisation of the parent beds has been stable since formation. If directions of magnetisation in the baked zone surrounding an intrusion are parallel to those observed in the intrusion, but differ from that of the unbaked country rock, the magnetisation of the intrusion has been stable since formation.

B. Pre and synfolding magnetisation (Butler 1992). The arrows display ChRM directions. A pre-tilting magnetisation (LHS) will result in inclinations and declinations becoming clustered subsequent to restoration to the palaeohorizontal, whereas directions will become more dispersed in the case of a post-tilting magnetisation. The scenario for a synfolding magnetisation is shown on the RHS. The simplest fold test is where magnetic vectors around both limbs of the same fold and the same layer can be measured. However, this is not normally the case. The fold test can equally be used to establish the timing of magnetisation in rocks, relative to the age of folding, within the same unit where the magnetic vectors do not necessarily lie on opposing limbs of the same fold or where the precise relationship between the areas is not known.

C. A schematic illustration is shown (RHS) of the reversals test (Butler 1992), with an example of normal and reversed directions that pass the test shown on the stereonet (LHS). Solid arrows indicate the expected antiparallel configuration of primary NRM vectors resulting from normal and reversed polarity intervals of the geomagnetic field; an unremoved secondary component is shown by the light grey arrows and the resultant NRM directions by the dark grey arrows.

3.6 Apparent polar wander paths (APWPs)

In order for the ChRM directions obtained from sites to be useful, knowledge of past positions of palaeopoles is required. These are plotted by combining and averaging magnetic measurements from continental divisions that have remained tectonically stable using formations with known ages in order to obtain the positions of the continents over time. Variation in pole position due to secular variation is averaged out by using a sufficiently large number of measurements. The continents move with respect to the poles, but as the magnetic poles are plotted using the present day position of the continent as a reference frame, it is the poles that appear to move and the paths are referred to as apparent polar wander paths (APWPs). Paths can be smoothed by using time windows and running averages. There have been many attempts at plotting accurate APWPs with much discussion over assumptions made and appropriate selection criteria. It is important to know the appropriate APWP for a region in order to be able to determine tectonic rotations that have affected the region from palaeomagnetic data. From knowing the appropriate palaeopole, it is possible to calculate the remanence directions expected at a locality, assuming a geocentric axial dipole source.

3.6.1 African and Eurasian apparent polar wander paths

Various apparent polar wander paths have been plotted for Africa and Eurasia. The movements of Africa and Eurasia partly deduced from these APWPs are discussed in section 2.3. Recent work on APWPs has tended to add data to the original curves or re-evaluated the selection criteria used in choosing appropriate palaeomagnetic data. Programs now exist that can take palaeomagnetic data from any continent and use Euler poles to rotate onto the same reference path (e.g. Schettino and Scotese 2001). However,

the early curves, although improved, are not fundamentally altered for the time period and locality being studied.

Early APWPs for Africa include constructions by Van der Voo and French (1974), Irving and Irving (1982); VandenBerg and Zijdeveld (1982) and Westphal (1986); early APWPs for Eurasia include constructions by Irving (1977) and Westphal et al. (1986). Reliable APWPs from the African continent initially suffered from weak palaeomagnetic data coverage, with the Late Palaeozoic part of the curve being particularly poorly constrained. Real African poles displayed some discrepancies with synthetic curves for the Palaeozoic, but Late Mesozoic and Early Tertiary poles coincide well, which is the period important to this study. The Westphal et al. (1986) construction selected the most reliable data for stable Eurasia (i.e. north of the Alpine belt) and used kinematic data for the major plates around the Atlantic given by Savostin et al. (1986) in order to transfer the polar wander curve to Eurasia. The resultant curve can be divided into four segments with changes in the movement of the pole between each. The first section is from the Permian to lower Jurassic and the pole moves roughly northwards. In the second segment, from Lower Jurassic to Cretaceous, it moves to the east, before moving in a loop in the Middle Cretaceous and finally moving westwards in the fourth segment to approach its present-day position.

Recent studies containing revised APWPs have been published by Besse and Courtillot (1991), Van der Voo (1993) and Besse and Courtillot (2002), although the differences in poles using various published datasets with respect to the times and areas relevant to this thesis are small. The Besse and Courtillot (1991) APWPs have been widely used by recent studies in the eastern Mediterranean region, including many of those referred to within this thesis (e.g. Kissel et al. 2003; Morris 2003). The most recent Besse and Courtillot (2002) APWPs will be used for this study, except where comparison with data referred to earlier

curves makes the use of these more appropriate. The expected directions calculated from Besse and Courtillot (2002) for the Hatay, Troodos and Baër-Bassit areas are shown in Table 3.1.

AGE (Ma)	Troodos (35.00°N; 33.00°E) ^A			Hatay (36.35°N; 36.02°E)			Baër-Bassit (35.75°N; 35.9°E)		
	Dec°	Inc°	Pal Lat. ^B	Dec°	Inc°	Pal Lat.	Dec°	Inc°	Pal Lat.
50	0.7	38.8	21.9	1.4	40.6	23.2	1.4	39.9	23.2
60	356.4	35.5	19.6	357.2	37.1	20.7	357.2	36.4	20.2
70	353.4	32.8	17.9	354.3	34.3	18.9	354.3	33.6	18.4
80	350.3	31.9	17.3	351.2	33.2	18.1	351.2	32.5	17.7
90	346.2	28.7	15.3	347.2	29.7	15.9	347.2	29	15.5
100	345.8	26.5	14	346.8	27.6	14.6	346.8	26.8	14.2
110	337.1	20.5	10.6	338.4	20.9	10.8	338.3	20.1	10.4

Table 3.1: The expected declination and inclination for the Hatay, Troodos and Baër-Bassit ophiolites between 50 to 110 Ma using the African APWP of Besse and Courtillot (2002). Data were calculated using software programmes developed by Randy Enkin.

^A The present-day average latitude and longitude of each ophiolite is given in brackets as (lat; lon).

^B Pal Lat. Is the palaeolatitude of the region calculated using the African APWP of Besse and Courtillot (2002).

3.6.2 Determination of tectonic rotations

Tectonic rotations are specified by comparing site mean remanences with a reference vector derived from the APWP of an appropriate undeformed region or major plate. During formation the ophiolites were situated just north of the African continent and the Hatay and Baër-Bassit areas have formed part of the Arabian margin throughout the Tertiary, following emplacement of the Baër-Bassit and Hatay ophiolites on to the continental margin in the Late Cretaceous. Remanences may therefore be compared with reference directions calculated from the African APWP (following correction for Pliocene-Recent opening of the Red Sea by applying an Euler rotation of -3.2° around a pole at 36.5° N/ 18.0° E; McKenzie et al. 1972; Le Pichon and Francheteau 1978; Savostin et al. 1986). Use of alternative APWPs results in little difference in inferred rotation angles. For instance, reference directions calculated from the Westphal et al. (1986) and Besse and Courtillot (1991) for the Hatay area from the 50 Ma onwards African mean poles vary by

only 2° in expected declination and by 10° in expected inclination. Rotation angles are not therefore sensitive to the choice of mean reference pole. Confidence limits on rotation angles are calculated using the methodology of Butler (1992).

3.7 Synthesis

The information within this chapter provides a basic introduction to magnetic principles for the non-palaeomagnetist as well as an explanation of the techniques used to analyse the palaeomagnetic and rock magnetic results presented in Chapters Five to Seven. This chapter also provides the necessary background in palaeomagnetism prior to the review of previous palaeomagnetic research in the eastern Mediterranean presented in the following chapter.

CHAPTER FOUR

4. PREVIOUS PALAEOMAGNETIC RESEARCH IN TETHYAN OPHIOLITES

4.1 Introduction to chapter

This chapter reviews previous palaeomagnetic research in the eastern Mediterranean and highlights the contributions made from this to knowledge of eastern Mediterranean geological history. Particular consideration is given to palaeomagnetic research from the Troodos and Baër-Bassit ophiolites due to their key locations within the southern Neotethyan ophiolite belt of which Hatay comprises part. Results from the Semail ophiolite are also briefly described. Palaeomagnetic results from these ophiolites are significant for knowledge of the regional evolution but are also important for later interpretations and discussions of the implications of the new (and first) palaeomagnetic data obtained from the Hatay ophiolite. In particular, through comparison of the rotations experienced by all these ophiolites, a far greater insight into their timing and mechanisms is achieved than is possible by restricting analysis to a single ophiolite. Finally, a brief overview of the mechanisms of fault block rotation in deforming orogens is provided.

4.2 Palaeomagnetic insights into the regional structural history

Palaeomagnetic data can be valuable in providing both time constraints and information on the rotations that have occurred in the tectonic evolution of the eastern Mediterranean. Numerous palaeomagnetic studies have been carried out within the Turkish area, and knowledge of the magnitude of rotations has provided insight into how the present-day deformation is being taken up and how this has changed through time. Previously, the database of palaeomagnetic data from the eastern Mediterranean was limited, in particular

from Anatolia, but more recent palaeomagnetic studies on Eocene and Miocene rocks from southern and western Turkey (e.g. Kissel et al. 1993), across the major fault zones (e.g. Platzman et al. 1994; Piper et al. 1996) and on Pliocene to Quaternary volcanics (e.g. Gürsoy et al. 1998) have significantly contributed to knowledge of the deformation. Detail on the nature of the westwards extrusion of Anatolia (section 2.2) is one area where palaeomagnetic data have been significant and another important contribution has been to add to knowledge of the mechanisms and rates of deformation by studying rotations and slip rates to aid determination of major fault continuations or intersections (e.g. as for the Karasu graben; Tatar et al. 2004).

Anatolia appears to be rotating anticlockwise as the result of the westwards extrusion. However, there is debate over whether Anatolia is rotating as a coherent block (e.g. Kissel 2003) or as a series of smaller blocks (e.g. Gürsoy et al. 2003) and the degree to which the rotation is progressive or episodic. Some authors report smaller rotations from Pliocene-Quaternary sites than for older sites (e.g. Platzman 1998), implying a more progressive rotation and some suggesting equivalently large rotations (e.g. Gürsoy et al. 1997), implying a large amount of rotation confined to more recent time. An average magnitude of $\sim 25^\circ$ rotation since the Miocene is suggested by Kissel et al. (2003) which results in a westwards displacement of ~ 500 km at the average latitude of 40° , using the location of the Anatolian rotation pole given by McClusky et al. (2000). Detailed palaeomagnetic studies in various areas of the Anatolian block indicate differential amounts and rates of regional rotation, suggesting that deformation may be occurring as distributed internal deformation as a series of smaller blocks (Gürsoy et al. 2003). Rotations in the south appear to be younger than those to the north and the magnitude of rotation decreases westwards (Gürsoy 2003). Alternatively, Kissel et al. (2003) suggest that the consistency of rotations in Eocene and Miocene samples identified from their palaeomagnetic research indicates that Anatolia was welded into a coherent block at least by the Miocene. However, this

observation is based on samples confined to a single N-S transect through Anatolia. Rotation does not appear to be limited to areas between the EAF and NAF, but also to have affected the Pontides and northern part of the Arabian plate, and rotation on both sides of the NAF in certain areas may be of equivalent magnitude (Platzman 1994). This would imply that the geographical extent of the region undergoing rotation is larger than the area between the fault zones, which themselves may have rotated (Kissel et al. 2003). The EAF and NAF may thus comprise narrow zones of deformation accommodating only part of the rotation, with the zone of decoupling between the Turkish unit and Europe previously situated to the north of the NAF (Kissel et al. 2003). A difference may therefore exist between the present-day deformation known from GPS data where the areas to the north of the NAF appear to be fixed (McClusky 2000) and the Neogene rotations determined from palaeomagnetic data which affect a wider geographical region (Kissel et al. 2003).

4.3 Palaeomagnetic insights into the evolution of Tethys

Palaeolatitudes of around 21-24° N derived from inclination-only statistical analysis of the palaeomagnetic database from Troodos and Baër-Bassit ophiolites are consistent with a Late Cretaceous position for the Neotethyan spreading axis between the Arabian and Eurasian margins (Morris 2003). Average inclinations for Troodos and Baër-Bassit are 37.0° ±2.6° and 41.1° ±3.4° respectively, indicating respective palaeolatitudes of 20.6° ±1.8° N and 23.6° ±2.5° N (Morris 2003). These data, together with a well-defined Late Cretaceous palaeolatitude of 26° N for the eastern Pontides (Channell et al. 1996) and palaeolatitudes of the Arabian and Eurasian margins (Figure 2.2) derived from APWPs (e.g. Besse and Courtillot 1991) provide constraints on potential tectonic reconstructions of the eastern Mediterranean Tethys. Two end-member model reconstructions are shown in Figure 4.1 that involve genesis of the ophiolites in a southerly basin (e.g. Robertson and Dixon 1984; Robertson 1998) and which satisfy the palaeolatitudinal data.

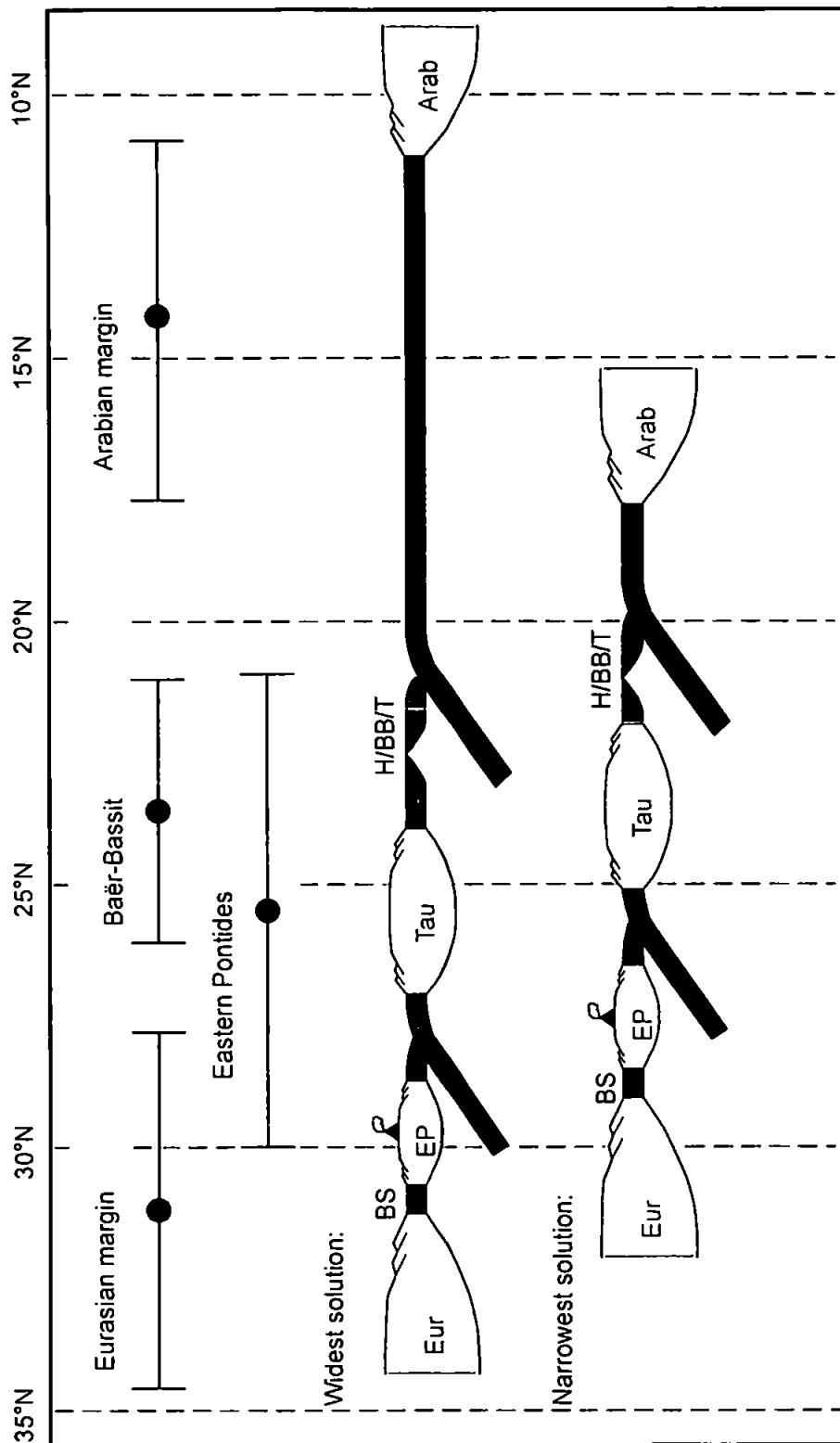


Figure 4.1: End-member tectonic cross-sections (i.e. the widest and narrowest solution for the Neotethyan ocean) across a N-S transect (from the Arabian margin through the Hatay and Baër-Bassit spreading axis and eastern Pontides to the Eurasian margin) constrained using palaeomagnetic data that satisfy palaeolatitudinal constraints on the Eurasian and Arabian continental margins, the spreading axis and the eastern Pontide volcanic arc from Morris et al. (2005; Fig. 8). Key: Eur = Eurasian margin; EP = Eastern Pontides; Tau = Taurides; BB/H/T = Baër-Bassit/Hatay/Troodos segment of Neotethyan spreading axis; BS = Black Sea; Arab = Arabian margin.

The solution giving the widest southerly Neotethys is obtained by placing the Arabian continental margin at its southernmost limit, producing a 1000 km wide Neotethyan strand to the south of the subduction zone associated with the Baër-Bassit/Hatay spreading axis. Major arc magmatism would result from subduction of the lithosphere during continued plate convergence. However, arc-related products are rare in SE Turkey, although the Late Cretaceous Başkil arc (Aktaş and Robertson 1984; Yazgan and Chessex 1991) 200 km to the NE of Baër-Bassit provides evidence for Late Cretaceous Andean-type magmatism along the southern Tauride margin (Robertson 2002). If a narrower solution is used, with a smaller oceanic strand ~300 km wide to the south of the subduction zone, the problem of the scarcity of arc products is avoided. In both solutions, the northern Neotethyan strand has essentially been consumed by subduction beneath the Pontides, consistent with geological evidence suggesting that northwards subduction beneath the Pontides was active from the Late Jurassic onwards (Ustaomer and Robertson 1993, 1994), providing sufficient time for the northern Neotethys to have subducted by the Late Cretaceous. The narrowest solution implies a restricted width of the southern Neotethyan strand following emplacement. Geological evidence is more consistent with an intermediate solution with the Eurasian margin placed further to the north. This allows the southern Neotethyan basin to persist to the north of the Arabian margin into the Tertiary (Aktaş and Robertson 1984; Yilmaz 1993; Robertson et al. 1996), after partial basin closure resulted in ophiolite emplacement. Alternative tectonic models (e.g. Ricou 1971; Ricou et al. 1984; Dercourt et al. 1993) involve formation of the ophiolites in a northerly Neotethyan basin by spreading at a normal oceanic ridge, with subsequent Late Cretaceous large-scale southwards thrusting over hundreds of kilometres over microcontinental fragments prior to reaching their current positions (section 2.5.1). These models cannot be discounted on a purely palaeomagnetic basis due to the absence of reliable data from the eastern Taurides (Morris 2003) but are not supported by a number of key geological observations, including both sedimentological and structural indicators. For example the presence of the essentially

continuous Campanian to Lower Tertiary sedimentary sequence overlying the Troodos ophiolite is difficult to explain if southerly emplacement had been occurring over this time period (Robertson et al. 1996).

4.4 Review of palaeomagnetic results from the Troodos ophiolite and its sedimentary cover

4.4.1 Palaeomagnetic results from the ophiolite

The palaeomagnetic data obtained from the Troodos ophiolite are numerous, and can be broadly divided into contributions that relate to microplate tectonics and those that relate to tectonism and deformation during crustal genesis. A significant finding with respect to this thesis concerns the rotation of the Troodos microplate (section 4.4.3). A review of the palaeomagnetic data from Troodos was provided by Morris (1996) and the results from a number of published palaeomagnetic studies of the Troodos ophiolite were also compiled by Morris (2003) for the purpose of assessing the palaeolatitude of the Neotethyan spreading axis. This compilation consisted of results from 100 palaeomagnetic sampling sites- 41 from the extrusive series and 59 from the SDC- drawn from studies by Clube (1985), Bonhommet et al. (1988), Allerton (1989), Morris et al. (1990), Hurst et al. (1992) and Morris et al. (1998), with additional sites from the Mandria area of Troodos from Macleod et al. (1990) also discussed by Morris et al. (2005).

The extensive database available for the Troodos ophiolite has enabled the age of the magnetisation of the extrusive sequences and SDC to be considered separately. Positive tilt tests are obtained from both structural levels of the ophiolite (Figure 4.2) and a close similarity between the tilt-corrected mean inclinations suggests that the SDC dataset is sufficiently extensive to ensure averaging out of any components of tilting about dyke-

normal axes at individual sites with no resultant bias in the overall mean inclination (Borradaile 2001; Morris and Anderson 2002). Palaeomagnetic data from the Troodos ophiolite may thus be discussed in tilt-corrected coordinates since the tilt tests demonstrate that the magnetisation is pre-deformational in origin. However, Borradaile and Lucas (2003) argued that the magnetisation in the Troodos ophiolite and sedimentary cover should be considered in un-tilt-corrected coordinates due to the gentle tilts of the sedimentary cover and structural simplicity of both the cover and the Troodos complex itself. These authors believe the complicated assumptions necessary for tilt corrections significantly increase errors and stress that tilt tests are inappropriate if magnetisation postdates penetrative deformation and metamorphism. Although Borradaile and Lucas (2003) extensively discuss all the errors that may result from the assumptions of the method, they do not account for the clear improvement in the clustering of inclinations subsequent to tilt corrections (e.g. see comment by Morris et al. 2005).

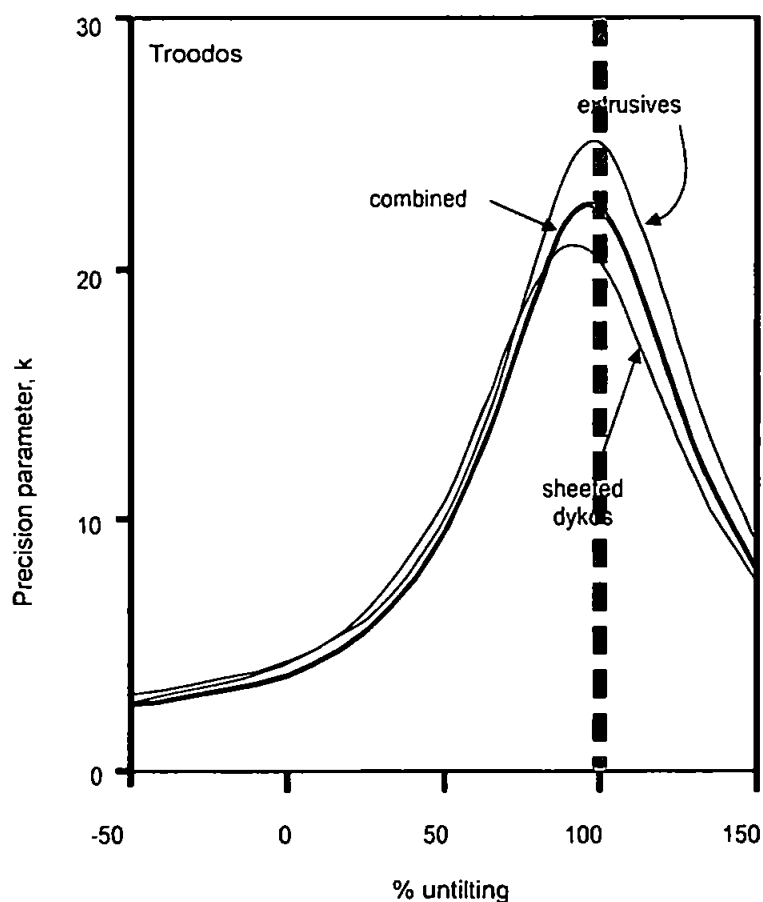


Figure 4.2: Inclination-only tilt test for the Troodos ophiolite (Enkin and Watson 1996), including analysis of separate units (extrusive rocks and sheeted dyke complex), demonstrating unequivocally that the magnetisation is pre-deformational.

Borradaile and Lucas (2003) use the existing database combined with their own new data to produce an APWP for the Troodos and Mamonia terranes that places the Troodos ophiolite at equatorial latitudes between 88 and ~50 Ma. They suggest that Troodos first rotated about an internal vertical axis by 60° whilst at the equator and then rotated more slowly about a distant axis located to the west. In the comment to this paper, Morris et al. (2005) suggest that due to the large number of serious errors and misinterpretations Borradaile and Lucas (2003) introduce into their compiled database, that this APWP should be discounted. An equatorial latitude for Troodos in the Late Cretaceous is not supported by Late Cretaceous palaeopoles (e.g. Besse and Courtillot 1991) which place the Africa/Arabian margin north of the equator and geological reconstructions of the eastern Mediterranean Neotethys (e.g. Robertson 1998a) place Troodos north of this margin between Africa and Eurasia. The $20.6^{\circ \pm 2.6^{\circ}}\text{N}$ latitude obtained from the Troodos ophiolitic rocks by Morris et al. (2003) from inclination-only tilt corrections is consistent with both the geological positioning of the ophiolite and the well-defined 26° palaeolatitude for the eastern Pontides (Channell et al. 1996) as well as the African and Eurasian palaeopoles (e.g. Besse and Courtillot 1991).

There is a clear distinction in the Troodos massif between regions with magnetisation vectors that cluster around a westerly declination and regions where declinations are widely variable from WSW through northerly to easterly declinations (Figure 4.3).

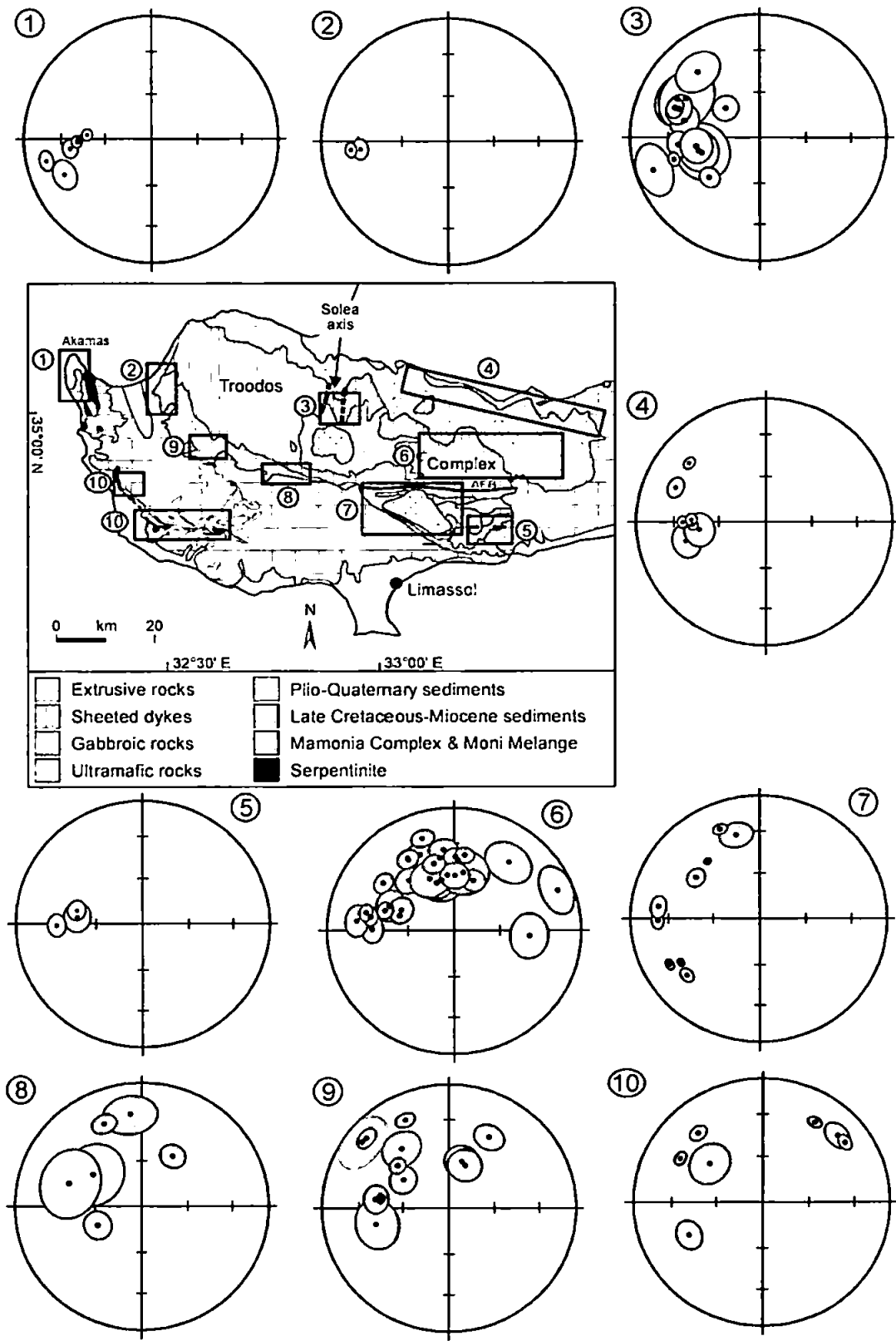


Figure 4.3: Outline geological map of Cyprus showing the location of areas that have been investigated palaeomagnetically (from Morris et al. 2005; Fig. 4). Lower hemisphere stereonet show tilt-corrected site-level palaeomagnetic directions and associated α_{95} cones of confidence from each area. Shaded ellipses indicate data obtained from ophiolitic crust that is inferred to have experienced significant transform tectonism. Data sources: Clube (1985); Bonhommet et al. (1988); Allerton (1989); Morris et al. (1990); Hurst et al. (1992); Morris et al. (1998).

The former regions form the northern margin of the main ophiolite (Clube 1985), the Solea region (Allerton and Vine 1987; Allerton 1989; Hurst et al. 1992), the Akamas peninsula (Clube 1985; Morris et al. 1998) and the western margin of the ophiolite (Morris et al. 1998). These regions are remote from the STTFZ and its inferred westerly along-strike extension and provide the evidence for the coherent ophiolite-wide 90° anticlockwise rotation of a Troodos microplate, first identified from NRM data by Vine and Moores (1969) and Moores and Vine (1971). A westerly-directed magnetisation is also observed at sites within the SE part of the Eastern Limassol Forest Complex to the immediate south of the STTFZ (Morris et al. 1990). The timing of this regionally significant microplate rotation is discussed more fully in section 4.4.3. Clube et al. (1985) suggested that there was little rotation of the Troodos complex during formation.

The Solea graben (Figure 2.14B) is a 15-20 km wide asymmetrical structure defined principally by variations in dyke attitude in the SDC (Varga and Moores 1985), separated from the underlying plutonic complex by the low-angle Kakopetria detachment fault zone (Figure 2.14B). An oceanic environment for graben formation is demonstrated by the horizontal disposition of the overlying sedimentary sequences (MacLeod et al. 1990). To the east of the inferred spreading axis, dykes generally have steep to sub-vertical dips and trend NNW except for several small areas where dykes dip more gently (Hurst et al. 1992). The wider western flank is distinctly different. N-S trending dykes dip at low angles (25-45°) to the east, attributed by Verosub and Moores (1981) to listric normal faulting associated with the Kakopetria detachment, above the active spreading axis with plate separation at least partly accommodated by tectonic thinning of the upper crust during periods of amagmatic stretching. Palaeomagnetic analysis (Allerton and Vine 1987; Allerton 1989; Hurst et al. 1992) confirms that these dykes were originally intruded in (sub-)vertical orientations. Tilt-corrected vectors generally cluster around the mean inclination observed at localities far from the STTFZ, in contrast to wide variation of in situ inclinations (-25-75°). The net tectonic rotation approach (Allerton and Vine 1987)

reveals rotation axes for the western dykes that are sub-horizontal and sub-parallel to the original dyke strikes (Allerton and Vine 1987; Allerton 1989; Hurst et al. 1992), consistent with tilting of dykes by faults above the detachment surface. For the eastern Solea graben, marked by steeper and more variable dyke orientations, structural evidence does not support the existence of a through-going detachment fault. Analysis here indicates that some dykes were tilted towards the Solea axis, but the majority show minor to significant rotation about vertical axes, attributed by Hurst et al. (1992) to local variations in the amount of extension, related to late stage episodic intrusions.

Extensive palaeomagnetic data (Clube 1985; Bonhommet et al. 1988; Allerton 1989; Morris et al. 1990; MacLeod et al. 1990) from the southern half of the main Troodos ophiolite and the Limassol Forest Complex have been used to address a debate on the sense of displacement along the STTFZ and its relationship with the Solea axis. A progressive change in dyke trend is observed within the SDC as the transform zone is approached from the north, from a predominant N-S orientation into eventual alignment with the transform lineament (Figure 4.4A). This has been interpreted as the result of either dyke injection into a sigmoidal stress field, implying that dykes are in their original orientations relative to the sinistrally slipping transform, or clockwise vertical axis fault block rotations in response to dextral slip (Simonian and Gass 1978). Discrimination between these alternative models can be achieved palaeomagnetically since systematic tectonic rotations would result in systematic variations in magnetisation vectors away from the westerly directed vectors observed outside the transform-influenced zone (Figure 4.4B-C). Data from the region to the north and NE of the Arakapas Fault Belt (Bonhommet et al. 1988; Allerton 1989a) show a broad spread of directions that are clearly rotated in a clockwise sense relative to this westerly vector, supporting a dextral shear sense along the transform between sinistrally offset spreading axes.

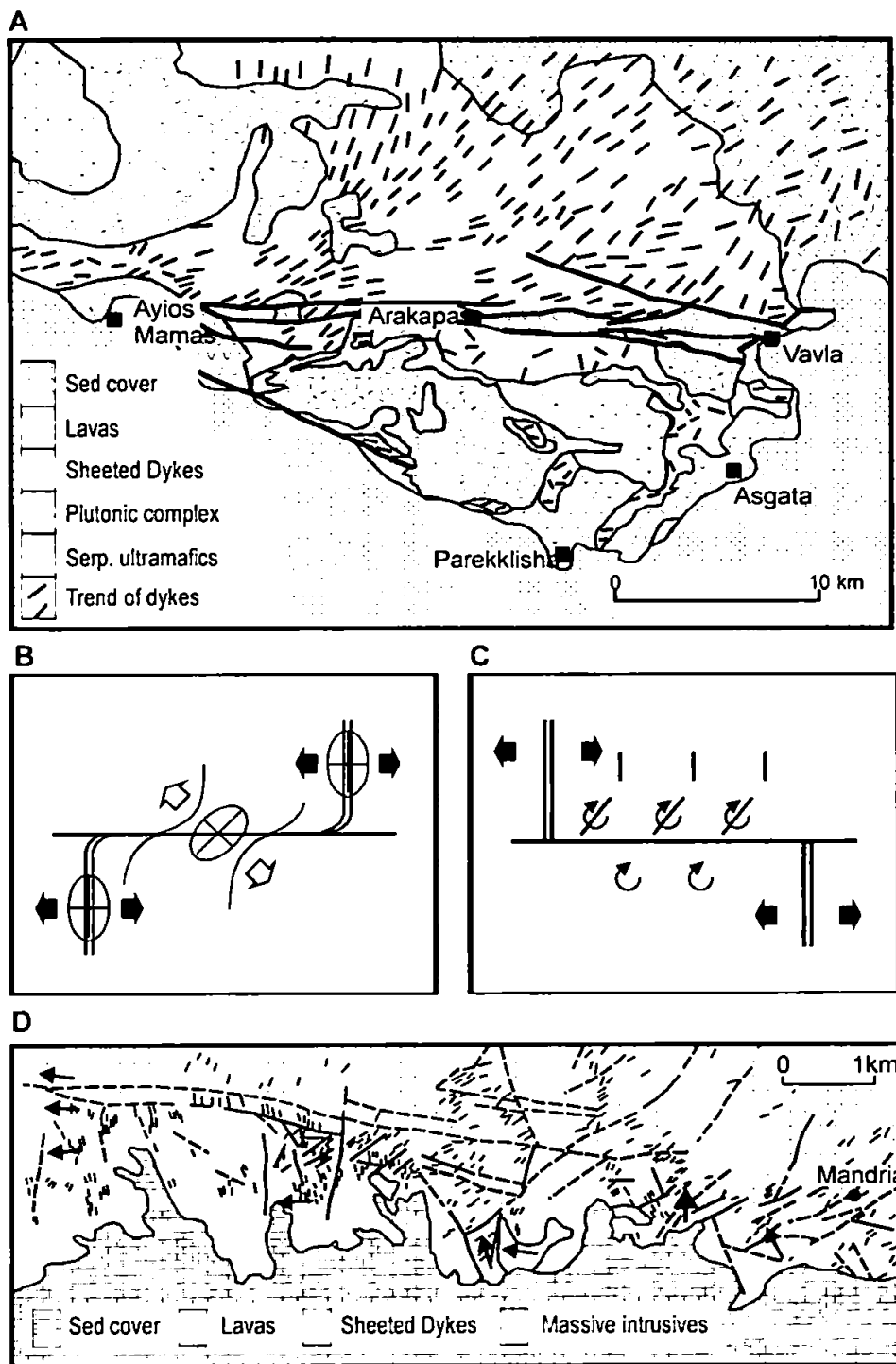


Figure 4.4: Various palaeomagnetic results from the Troodos ophiolite.

A. Simplified geological map of the southern margin of the main Troodos ophiolite and the Limassol forest complex (after Simonian and Gass 1978), showing the progressive change in dyke trend into near parallelism with the STTFZ (from Morris et al. 1990). B-C. Possible alternative settings in which deviations in dyke trend could occur close to the STTFZ (from Morris et al. 1990).

B. Dyke injection into a sigmoidal stress field operating across a sinistrally slipping transform between dextrally offset spreading centres. C. Rotation of fault blocks related to dextral slip along the active transform domain between sinistrally offset spreading axes. D. Geological map of the Mandria area (modified from MacLeod et al. 1990 by Morris et al. 2005) with in situ declinations of palaeomagnetic directions shown by arrows. Dykes in the west have an average N-S trend in contrast to highly rotated dykes to the east, with the boundary between these domains representing a fossil ridge-transform intersection.

The most unequivocal analysis was presented by Bonhommet et al. (1988) who showed that magnetisations in sampled dykes cluster tightly with westerly declinations after correction of dykes back to the predominant N-S trend, thereby ruling out initial NE-SW trends. Further palaeomagnetic support for dextral shear along the transform zone is provided by dykes from the SSTFZ itself (Morris et al. 1990), the majority of which are also rotated clockwise away from the general Troodos vector. Net tectonic rotation analysis from sets of cross-cutting dykes (Morris et al. 1990; Allerton and Vine 1990) demonstrates that clockwise block rotations were actively occurring during crustal genesis, rather than resulting from later reactivation of the fault zone.

Analysis of upper crustal rocks of Troodos-type exposed in fault-bounded slivers along the suture zone with the Mamonia Complex in SW Cyprus (Figure 2.14) reveals significant rotations in a generally clockwise sense away from the Troodos vector (Morris et al. 1998). In particular, differences in remanence directions between cross-cutting units are observed at several localities, interpreted elsewhere as a characteristic of syn-magmatic rotation during transform tectonism. Net tectonic rotation analyses allow decomposition of the total rotation at these sites into early and late components. Early rotations are consistently clockwise, in agreement with studies of rotations associated with the STTFZ further to the east. These data, therefore, suggest that transform-tectonised crust is preserved in SW Cyprus, an interpretation supported by stratigraphic and geochemical similarities between these units and the main Troodos ophiolite and its transform fault-related southern margin.

The overwhelming palaeomagnetic evidence for clockwise fault block rotations associated with dextral slip along the STTFZ contrasts with sinistral kinematic data reported by Murton (1986) within the western Limassol Forest Complex (i.e. within the transform zone). This apparent conflict was addressed by MacLeod and Murton (1995), who proposed a model in which sinistral shear developed locally at block boundaries within an

overall dextral shear zone. As discussed in section 2.9, an alternative interpretation of the Limassol Forest area is that it represents an oceanic core complex (Cann et al. 2001) formed at the inside corner of an oceanic transform-ridge intersection, but this is incompatible with the palaeomagnetic evidence and alternative structural interpretations (MacLeod 1990) remain valid.

Detailed palaeomagnetic and structural analyses (MacLeod et al. 1990) have identified a limit to the zone of transform-related rotations along the STTFZ. The changeover from rotated to unrotated dykes occurs across a complex zone between 2 and 5 km wide. This zone is interpreted by MacLeod et al. (1990) as a fossilised intersection between the Solea axis and the SSTFZ. They note that the radius of curvature of dyke swing remains approximately constant across the entire exposed width of the Troodos massif to the east of the ridge-transform intersection. MacLeod et al. (1990) conclude that transform-related rotations occurred within the active corner of the intersection itself rather than being accommodated progressively with increasing strike-slip displacement along the transform. This supports a theoretical model (Allerton 1989) for distortions within weak crust at ridge-transform intersections. Distributed rotational deformation is therefore considered to be largely confined to the inside corner of the intersection itself (MacLeod et al. 1990), and subsequent strain is taken up by strike-slip faulting concentrated almost exclusively in the principal transform displacement zone within the transform valley (Arakapas Fault Belt).

4.4.2 Palaeomagnetic results from the sedimentary cover

The large anticlockwise rotation of the “Troodos microplate” is a regionally significant event within the Neotethys ocean. Initial estimates of the size of the rotated unit (Clube 1985; Clube and Robertson 1986) suggested that rotation was restricted to an oceanic microplate of approximately the same area as the Troodos ophiolite itself, although this is

re-evaluated in this thesis. The timing of the rotation may be determined by palaeomagnetic analysis of the continuous Late Cretaceous to Recent in situ sedimentary cover to the ophiolite, on the basis that magnetic declinations within the sediments record rotation of the underlying ophiolitic basement (Figure 4.5). Although the sedimentary formations have NRM intensities which are approximately two orders of magnitude lower than those of the dykes and extrusive rocks, remanences are easily measurable using cryogenic magnetometers and stable, primary components of magnetisation can be isolated. Investigations by Clube (1985) and Abrahamsen and Schönharting (1987) yielded a number of data distributed throughout the sedimentary succession, and further constraints on the early rotation history were provided by Morris et al. (1990). Hydrothermal sediments (umbers) of the Perapedhi Formation share a common direction with the underlying extrusive sequence. The overlying Campanian radiolarian mudstones (Perapedhi Fm) and Maastrichtian-Oligocene chalks (Lefkara Fm) show a general progression from WNW to northerly declinations upwards through the stratigraphy. Data from some time intervals show significant scatter, most notably in the inclination of the Maastrichtian sites and in both inclination and declination of the Palaeocene sites. This may reflect the influence of compaction-related inclination shallowing and/or potential contamination of site-level remanence vectors by residual normal polarity overprints. This latter effect is the most likely explanation of the inclination difference between the two Maastrichtian sites with the shallowest inclinations (representing inverted reversed polarity sites) and the remaining three (normal polarity) sites of this age. Late Oligocene to Miocene sites exhibit exclusively northerly declinations (within error). Overall, these data clearly indicate the progressive and prolonged nature of the rotation of the Troodos microplate during the Campanian-Eocene interval (Figure 4.5).

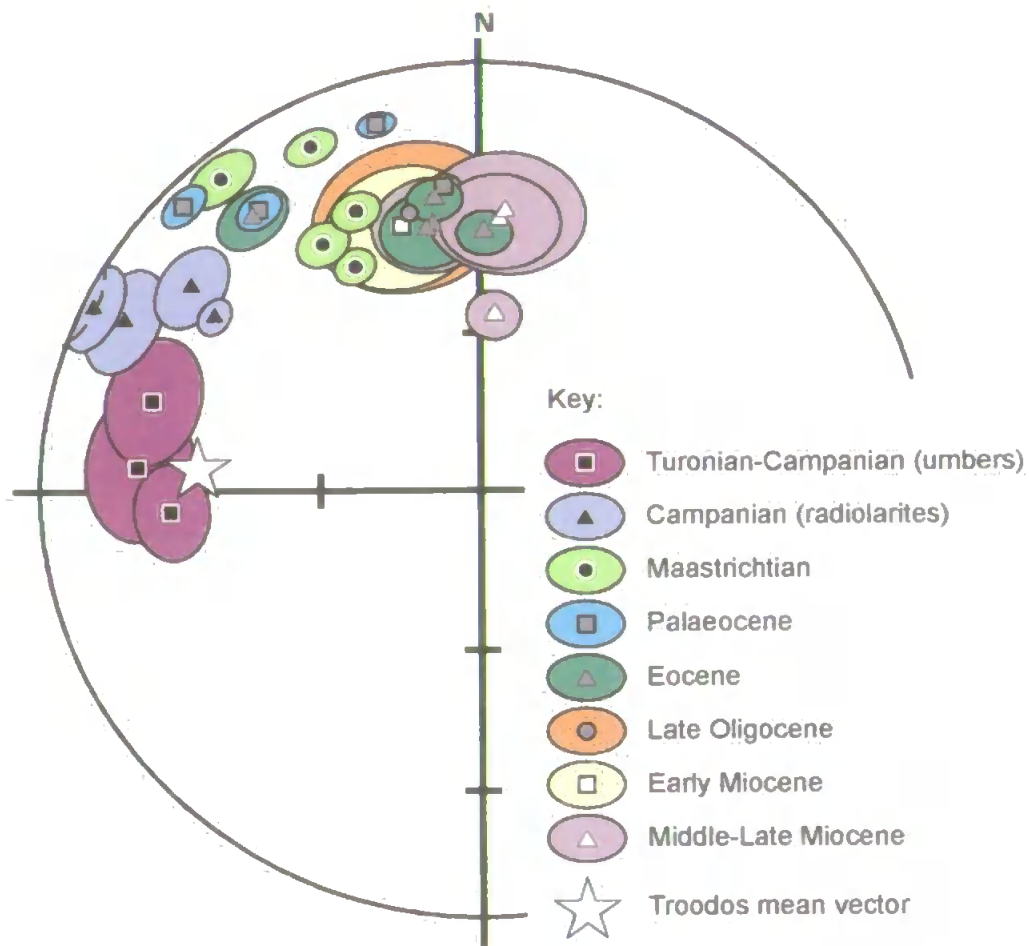


Figure 4.5: The palaeomagnetic results from the sedimentary cover of the Troodos ophiolite. Lower hemisphere stereographic projection of tilt-corrected site-level palaeomagnetic data obtained from the in situ sedimentary cover of the Troodos ophiolite, demonstrating the progressive anticlockwise rotation of the underlying ophiolite during the Palaeogene as indicated by the latest compilation of available data (Morris et al. 2005). Data from Campanian radiolarites and Maastrichtian and Palaeocene carbonates include both normal and reversely magnetised sites, with the latter inverted to the lower hemisphere in this plot. Eocene to Miocene data are of normal polarity. Data sources: Clube (1985); Abrahamsen and Schonharting (1987); Morris et al. (1990).

4.4.3 Rotation of the Troodos microplate

Palaeorotation of an oceanic microplate within a narrow Neotethyan ocean basin undergoing regional compression can be accommodated in several potential tectonic settings. No consensus is presently reached on the most likely. The most popular models invoke either collision or oblique subduction as driving mechanisms for the rotation (Figure 4.6). Several authors have related rotation to inferred collision between a seamount or microcontinent and a subduction zone (Moores et al. 1984; Murton 1990; Robinson and Malpas 1990; Malpas et al. 1992; Figure 4.6A). However, the Troodos terrane shows little evidence of regional compression or fault disruption that would be anticipated from forceful collision and underthrusting with partial or complete subduction of a seamount or microcontinent. Also, this would have been a shorter-lived collisional event than the observed steady $\sim 2^\circ \text{ Ma}^{-1}$ rotation of the Troodos microplate from the Late Cretaceous to Early Eocene (Robertson 1990). Another mechanism suggested is tectonic expulsion from the Isparta angle (Robertson and Woodcock 1986), where the Troodos microplate becomes detached and rotates as it is forced away from the Isparta angle due to the action of strike-slip faults bounding the corner to the north and west of the oceanic crust (Figure 4.6B). Alternatively, oblique subduction beneath the Troodos ophiolite may produce the driving force (Figure 4.6C), as suggested by Clube et al. (1985), although from this alone it is difficult to produce the required torque. Clube and Robertson (1986) developed this idea further with collision outside Cyprus in combination with northward subduction producing the necessary torque (Figure 4.6D). Clube and Robertson (1986) originally suggested that the near coincidence of the timing of initiation of palaeorotation and the emplacement of the Hatay and Baër-Bassit ophiolites could be linked but it was later established from more precise timing of rotations in the sedimentary cover that a significant component of rotation may have occurred prior to emplacement (see Morris et al. 2005).

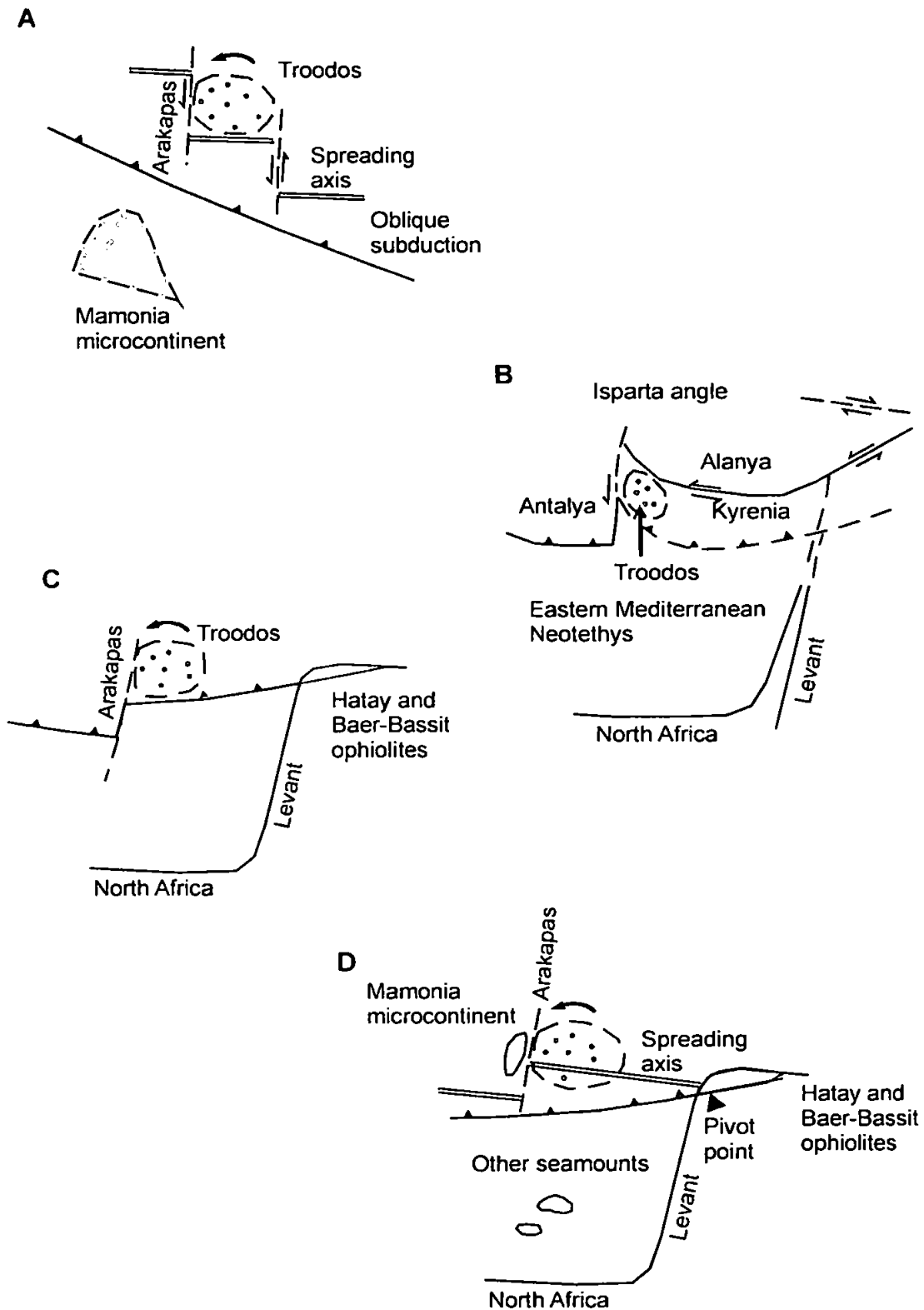


Figure 4.6: Various models proposed for the rotation of the Troodos microplate (from Robertson 1990). Models A, C and D are generally more accepted than model B, where the reason for rotation is less easy to account for. Model D is the most widely accepted as this provides the most credible explanation for both rotation initiation and the anticlockwise direction of the rotation. A. Collision, subduction and underthrusting of a Mamonia microcontinent (Moores 1984; Murton 1990; Robinson and Malpas 1990; Malpas et al 1992);(modified after Robertson and Woodcock 1980); B. Expulsion from the Isparta angle; C. Rotation due to collision with a trench to the east (Clube and Robertson 1986). D. Model C as modified by Robertson (1990).

The collision of these more easterly fragments of Neotethyan oceanic crust with the offset Levant continental margin could have pinned one segment of the subduction zone while the Troodos ophiolite remained above a down-going slab. Continued northwards movement of the African plate resulted in the trench pivoting about the intersection of the transform passive margin with the subduction front (Robertson 1990). Southwards roll-back of the trench to the west of the pivot point exerted a pull on the overriding plate and as a consequence an anticlockwise torque developed in the forearc region. The Troodos microplate could then detach and rotate about a series of dextral strike-slip faults and associated relay faults (Clube and Robertson 1986; Robertson 1990). In this model, fragments of the northern continental margin (Mamonia Complex, Moni Melange) became attached to the rotating microplate along strike-slip lineaments and were carried southwards to their current position. The nature of the boundaries of the microplate are often drawn as a ring of strike-slip faults, although the reason for their precise location and why the zone of weakness along the transform fault or spreading axis was not utilised is unknown. The inferred microplate boundary faults probably followed existing zones of crustal weakness, such as the westwards extension of the STTFZ. The postulated curved microplate boundary would have cut across the pre-existing more-linear oceanic fracture zone (Robertson 1990). In southern Cyprus, microplate boundary faults were inferred to lie south of the fossil transform zone and close to the present-day coastline (Clube and Robertson 1986). This model involving impingement of a subduction zone on the Arabian margin is more consistent with the regional tectonic setting than models that invoke push mechanisms involving microcontinental collision.

The lines of evidence that were used to constrain the size of the rotated microplate were palaeomagnetic data from mainland Turkey to the north and the African margin to the south, showing that these were unrotated. Closer to Troodos (and more applicable), the E-W trending structures in Kyrenia (immediately to the north) and main dyke strike in Hatay

and Baër-Bassit (to the east) were used to infer they were unrotated, as previously no palaeomagnetic data existed for these regions, with the E-W trending dykes of Hatay used as the strongest line of evidence for this area being unrotated. However, in light of the new palaeomagnetic data obtained both from this thesis from the Hatay ophiolite, and recent data from the Baër-Bassit ophiolite by Morris et al. (2002; see below), the models used to explain the Troodos microplate rotation need to be re-evaluated (Chapter Nine).

4.5 Review of palaeomagnetic results from the Baër-Bassit ophiolite

4.5.1 Palaeomagnetic results from the ophiolite

Morris and Anderson (2002) and Morris et al. (2002) discuss the first palaeomagnetic results from 27 sites in the Baër-Bassit ophiolite. Morris et al. (2002) presented palaeomagnetic results from 19 sampling sites distributed between four localities in Baër-Bassit ophiolite, predominantly within the western Bassit massif where extrusive rocks, sheeted dykes and layered gabbros were sampled. The eastern massif is dominated by mantle sequence rocks and only one locality could be sampled, which was within the SDC. Sites from a fifth locality are discussed in Morris and Anderson (2002) and below (section 4.5.3). Results show that large anticlockwise rotations have been observed for the Baër-Bassit ophiolite, varying on a kilometric scale, generally increasing in magnitude southwards, exceeding 200° in the lowest structural levels in the imbricate thrust sheets in the south. Rotations in the north are of similar magnitude to those observed in the Troodos massif. Unequivocal evidence that the ophiolite records pre-deformational magnetisations was provided by an inclination-only tilt test (“block-rotation Fisher” method of Enkin and Watson 1996) applied to the site-mean magnetisation directions grouped according to locality, together with a positive standard palaeomagnetic tilt test (McFadden and Jones 1981) and a positive reversal test (McFadden and McElhinny 1990) at one locality. The

magnetic mineralogy was shown to be consistent with an ocean-floor origin of magnetisation, and the data are interpreted as primary remanences acquired during or shortly after crustal genesis (Morris et al. 2002). Directions of magnetisation are consistent within each locality, but vary widely between localities indicating large relative rotations across the ophiolite (Morris et al. 2002). Rotations were further assessed by net tectonic rotation analysis (Allerton and Vine 1987; extended by Morris et al. 1998), which provided estimates of rotation axes and angles and their associated uncertainties. The rotation in the north of the area, nearest to Hatay, is lowest. Within the Bassit massif, anticlockwise net tectonic rotations increase from $\sim 90^\circ$ in the north ("North Coast" locality) to in excess of 200° in the south ("West Coast" locality) and rotation axes are steeply plunging to sub-vertical (Morris et al. 2002). The possibility that the largest rotations occurred in a clockwise sense can not be excluded, but anticlockwise solutions were preferred by Morris et al. (2002) since this results in a more systematic pattern of rotations. Within the eastern Baër massif, net anticlockwise rotations of $\sim 80^\circ$ are observed but these occurred around shallowly plunging axes, indicating a dominance of tilting over vertical axis rotation at this sampling locality. This net rotation may be decomposed into a pure tilt and a 30° anticlockwise vertical axis rotation (Morris et al. 2002). This ophiolite is interpreted as the more dismembered thrustal front of the Hatay/Baër-Bassit sheet and is affected by large-scale Neotectonic strike-slip faulting. The rotations are interpreted to be of a composite origin and are summarised in Figure 4.7.

4.5.2 Palaeomagnetic results from the sedimentary cover

No previous palaeomagnetic data exist for the sedimentary cover of the Baër-Bassit ophiolite. Samples from the Baër-Bassit sedimentary cover were collected recently by A. Morris and M. W. Anderson and were measured and analysed as part of this thesis. These results are discussed in Chapter Six.

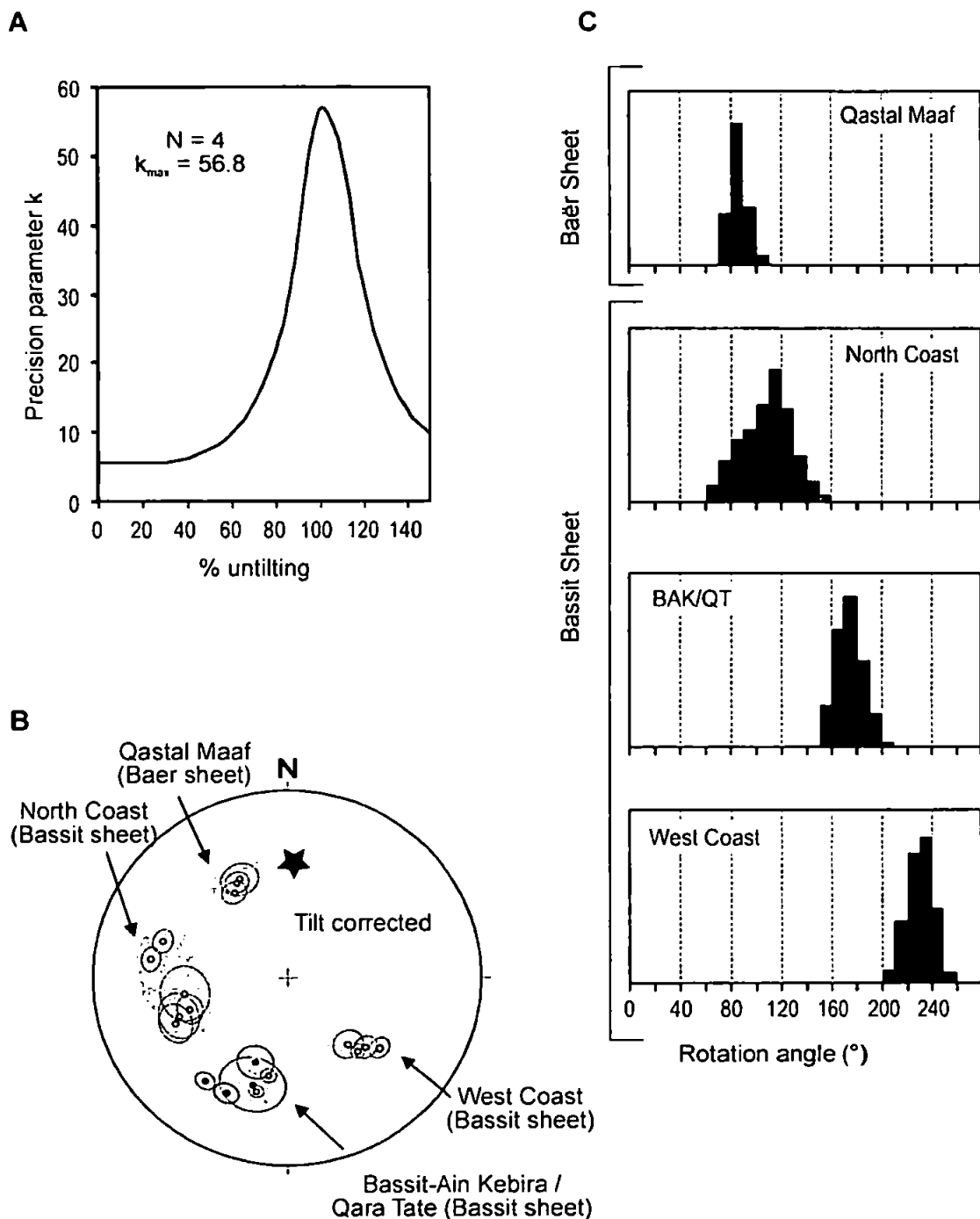


Figure 4.7: Summary of the palaeomagnetic results obtained by Morris et al. (2002) from the Baër-Bassit ophiolite.

A. Variation in the Fisher precision parameter with progressive untilting of palaeomagnetic data indicating a positive inclination-only tilt test (Enkin and Watson 1996), with peaked distribution centred on 100% untilting unequivocally indicates that pre-deformation remanences are carried by the ophiolite.

B. Stereographic projections showing the distribution of site mean directions of magnetisation in tilt-corrected coordinates from the four main sampling localities. The large differences in declination between localities indicate extreme relative rotations within the ophiolite (reversed magnetisations have been inverted to the lower hemisphere; ellipses = projection of α_{95} cones of confidence around site mean remanences; black star = Late Cretaceous normal polarity reference direction).

C. Results of a net tectonic rotation analysis, which confirms extreme relative rotations within the ophiolite, with an apparent increase in net rotation angle southwards across the Bassit massif.

4.5.3 Tilt about dyke-normal axes

Data from eight sites within an exposure of doleritic dykes at a fifth locality (in the Bassit massif) display sub-vertical upwards remanence directions that may result from rotation around shallow- to moderately-plunging dyke-normal axes (Morris and Anderson 2002).

This rotation would produce no visible change in dyke orientation but would rotate magnetic remanences around small circles centred on the tilt axis. If a simple strike-parallel tilt is assumed and this site is included in the inclination-only analysis of the other Baër-Bassit localities (section 4.5.1) it introduces a large degree of error and invalidates the test. These results are clearly anomalous with respect to those observed at other Baër-Bassit localities and the expected reference direction. The magnetic properties of samples from this fifth locality are indistinguishable from those observed in the remaining four localities, and there is no geological reason to suppose that these rocks have been selectively remagnetised, and so remanences are assumed to similarly represent pre-deformational remanences (Morris and Anderson 2002). However, these data should be analysed differently in order to take into consideration potentially more complex rotations. Two methods of analysis have been used; firstly the net tectonic rotations method, as described in section 3.5.6 and secondly a method that allows less constraints to be placed on the restoration of the magnetic remanence to a reference. This second method is described in section 5.10.3 in relation to its applicability to data from this thesis and is referred to as the 'inclination restoration to a reference method'.

The net tectonic rotation analysis method returns a net rotation pole that is sub-normal to the observed mean dyke strike. The rotation axis is shallowly-plunging towards the ENE about which 60-70° of anticlockwise rotation has occurred and estimates of pre-rotational deformational dyke strikes are NNE-NE. The second method restores the dykes to the

vertical and the inclination to the expected inclination of 41° (from the pre-deformational average of the other sites analysed in the Baër-Bassit ophiolite). Two potential solutions are obtained, both of which yield tilt axes that are sub-normal to the mean dyke strike at that locality. After propagation of confidence limits on remanences and structural orientations through the analysis, the tilt corrected magnetisations for the two solutions indicate either a $4-63^\circ$ or a $170-228^\circ$ anticlockwise rotation (or a $132-190^\circ$ clockwise rotation). Both solutions therefore indicate rotations about a dyke-normal axis that would be undetectable in the field (Morris and Anderson 2002).

In order for such rotations to occur, structures that facilitate tilts about a NE-SW near-horizontal axis are required. The Baër-Bassit ophiolite is interpreted to have been emplaced towards the SE (Al-Riyami et al. 2002), and so tilts towards either a SE or NW direction may be expected to result. This emplacement direction is parallel to the average strike of the sheeted dykes (Morris and Anderson 2002) and so rotations during emplacement would be about a roughly dyke-normal axis. Therefore rotations about a dyke-normal axis are attributed to be the cause of rotations during the emplacement of the ophiolite.

The absence of dyke-normal rotations observed from the remaining localities within the SDC of the Baër-Bassit ophiolite indicates that not all sites experienced coherent rotations during emplacement of the ophiolite.

4.6 Review of palaeomagnetic results from the Semail ophiolite

The Semail ophiolite in the Oman mountains is one of the most complete and best exposed ophiolite sequences in the world, covering 10000 square km and is composed of 8-12 km of upper mantle peridotites and 4-7 km of oceanic crustal rocks (e.g. Nicolas 1989; Searle and Cox 2002). Palaeomagnetic results obtained from the ophiolite, located at the eastern end of the Neotethyan ophiolite belt, may provide insight into rotations affecting the Hatay ophiolite. The Semail ophiolite was obducted onto the southeastern part of the Arabian platform subsequent to intraplate subduction initiating at around 100 Ma with emplacement at least 250 km west and southwest onto the Arabian passive margin during the Late Cretaceous period. The ophiolite contains separate submarine volcanic series erupted at different times: One series (Geotimes V1) is interpreted as ridge-axis volcanism and a second series (Lasail V2) is possibly linked to the initiation of thrusting (Perrin et al. 2000). Hornblende $^{40}\text{Ar}/^{39}\text{Ar}$ ages from the amphibolites of the metamorphic sole range from 95-93 Ma, synchronous with the 95 Ma age of formation of plagiogranites in the ophiolite crustal sequence and the eruption of the second (V2) volcanic series (Searle and Cox 2002). The ophiolite experienced large-scale thrusting during emplacement but no significant post-emplacement deformation. The Semail ophiolite has experienced large, differential internal rotations, with clockwise rotation of the northern part of the massif of around 120° (Weiler 2000).

Palaeomagnetic studies in the Semail ophiolite have been carried out on the gabbros by Luyendyk and Day (1982) and on the SDC by Luyendyk et al. (1982). Large rotations identified by these studies are attributed by Thomas et al. (1988) to intraoceanic thrusting. Two studies were carried out on the extrusive sequences by Perrin et al. (1994) and Perrin et al. (2000). The first palaeomagnetic study of volcanics by Perrin (1994) concluded that the rotation of the Semail ophiolite nappe could be modelled as a clockwise rotation in the

order of 145-150° as a coherent block about a single Euler pole located less than 200 km from the northern extent of the nappe and occurring between the detachment of the nappe and the end of the obduction. The later study by Perrin et al. (2000) sampled lava flows from both volcanic units and indicated that relative rotations of the order of 90° occurred between the northerly and southerly parts of the ophiolite after eruption of the Lasail V2 volcanic series. They also suggest that, by the time the second unit of lavas was emplaced, the northern domain was acting as a tectonically coherent unit although at the time of emplacement of the earlier lavas, this area may have been experiencing differential rotations. More recently, Weiler (2000) suggests that the southern part of the ophiolite is relatively unrotated and that the rotation affecting the northern part of the ophiolite is internal to the ophiolite. They suggest that this rotation can be attributed to rapid, active microplate rotation of a portion of the ophiolite resulting from spreading at an EPR-type propagating ridge at a high angle to the previous spreading direction. The palaeospreading direction of the Semail ophiolite is believed to have been ENE-WSW, with a tectonic regime to E-W compression around 100 Ma initiating the transition from spreading to subduction (Umino et al. 1990).

4.7 Tectonic rotation models

As this thesis involves the application of palaeomagnetic and structural techniques in order to establish the tectonic evolution of the Hatay ophiolite, with particular reference to potential rotations, it is important to briefly discuss the causes of rotations in deforming zones. Rotation can be about any axis- horizontal, vertical or inclined- with a discussion of the causes of vertical axis rotation especially relevant to this study. An important point when discussing proposed mechanisms for vertical axis rotations is that coherent rotation of the Troodos ophiolite affected an area of oceanic crust whereas many of the current theories explain vertical axis rotation relate to continental crust.

The nature of the way in which deformation acting in brittle crust is taken up is important, as well as the regional causes of the stresses acting on an area. Stresses acting at a regional scale may be taken up on smaller scales by rigid blocks. The bounding faults on these blocks produce a series of stresses within a localised domain that may differ to those acting on a regional scale. There have been various models proposed to account for the way in which a region will take up deformation. These variations relate to whether deformation is assumed to be homogenous across an area or whether it is taken up by spatially discrete blocks. The nature of the structures involved in deformation will affect the resultant palaeomagnetic direction, as well as the size of the rotating blocks, and the mechanism by which they rotate.

The deformation may be the result of ongoing transtension or transpression, or be due to temporally discrete events. Transpression or transtension are strike slip deformations that deviate from simple shear because of, respectively, a component of shortening or extension orthogonal to the deformation zone (Dewey et al. 1998). They occur on a wide variety of scales from the plate tectonic scale involving movement of plates on a spherical surface, down to much smaller scales. If transtension is occurring on the scale of the Hatay region, so that there is strike slip faulting along the boundaries with a component of orthogonal extension, it will likely result in strain partitioning within the Hatay area into normal and strike slip faults.

The kinematics of in situ vertical axis rotation in the upper crust is debated. Models range from continuum to discrete with the former case involving distributed deformation over a wide area and the second case involving the rotation of integral blocks which deform at the boundaries (e.g. Ron et al. 1984; Nelson and Jones 1987; King et al. 1994; Piper et al. 1997). Continuum models generally consider the rotation involves crustal areas considerably smaller than the size of the deforming zone and that it occurs in response to

motion of the ductile lower crust. Shear is distributed across the zone and creep and diffusive mass transfer accommodates the rotation so that palaeomagnetic directions show diminishing rotation away from the main fault. Discrete models take up deformation on rigid crustal blocks with lengths roughly equivalent to the width of the deforming zone, and the deformation uses systems of strike-slip faults (Freund 1970) about which fault blocks progressively rotate on vertical axes. This type of deformation conserves area and so is a plane strain. Rotation and deformation occur in response to shear applied along the edge of the blocks by strike-slip faults. All blocks and block-bounding faults within the same domain will rotate by the same amount and in the same direction, except in cases where the strike-slip faults form two domains and produce an opposite sense of rotation within each domain (Ron et al. 1984). The rotation is predicted to be clockwise in regions of net dextral shear and anticlockwise in regions of net sinistral shear (Sonder et al. 1986). The sense of motion on the smaller block-bounding faults can be the same or opposite to the system bounding faults (Figure 4.8) depending on the initial orientation of the block bounding faults and whether the blocks are pinned to the outside of the deforming zone (i.e. a wide zone of shear) or to the inside (i.e. the system bounding faults exist as discrete faults either side of the rotating blocks). An example of an area where the deformation is occurring on blocks between discrete system bounding faults is the central part of the Karasu rift valley where the Amanos fault and East Hatay fault are acting as the system bounding faults (Tatar et al. 2004).

An early proposal by Beck (1976) for zones of distributed deformation suggested that strike-slip deformation could result in the rotation of circular blocks of crust in a manner similar to ball bearings. This situation is not supported by geological field studies or fault plane solutions as a combination of strike-slip faulting and extension or thrust faulting is more common (McKenzie and Jackson 1988).

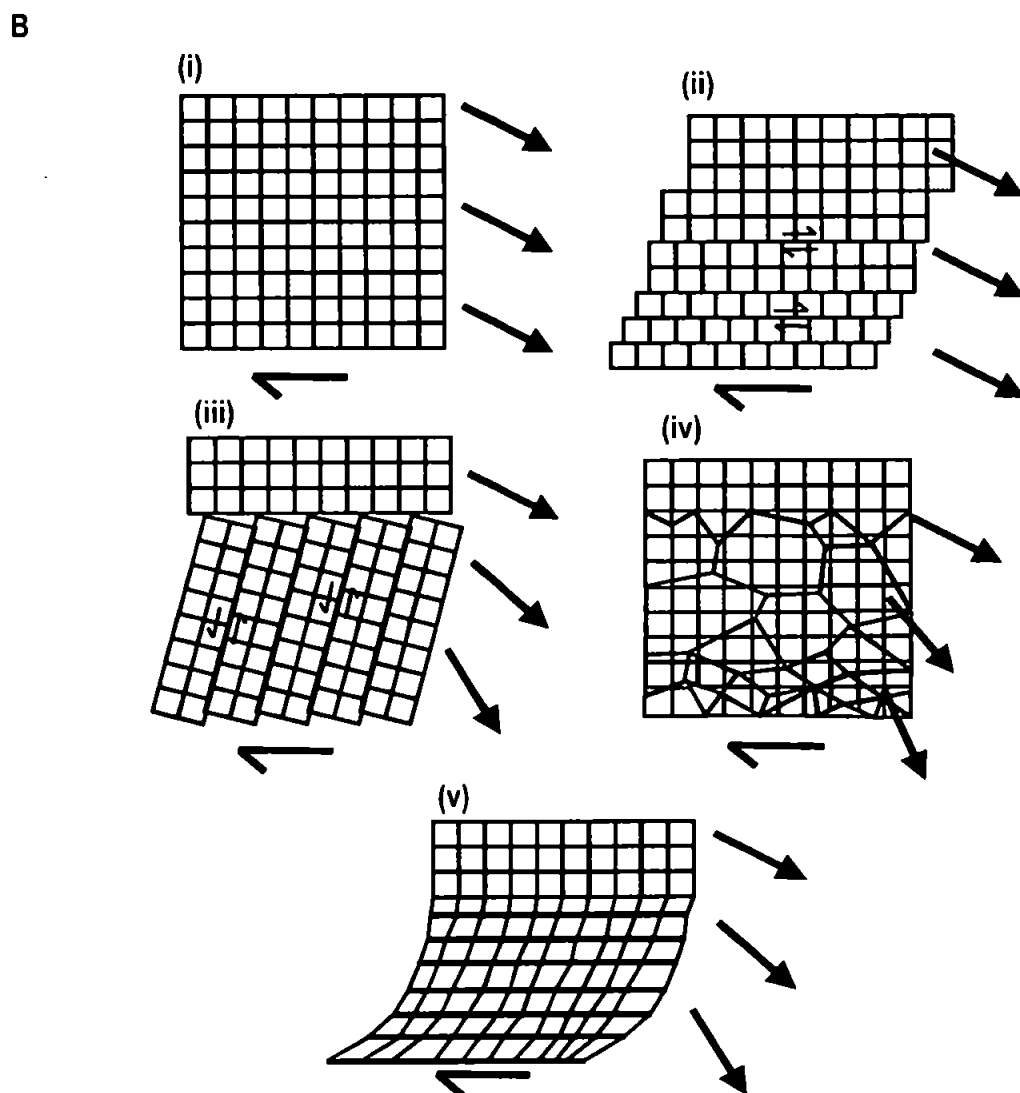
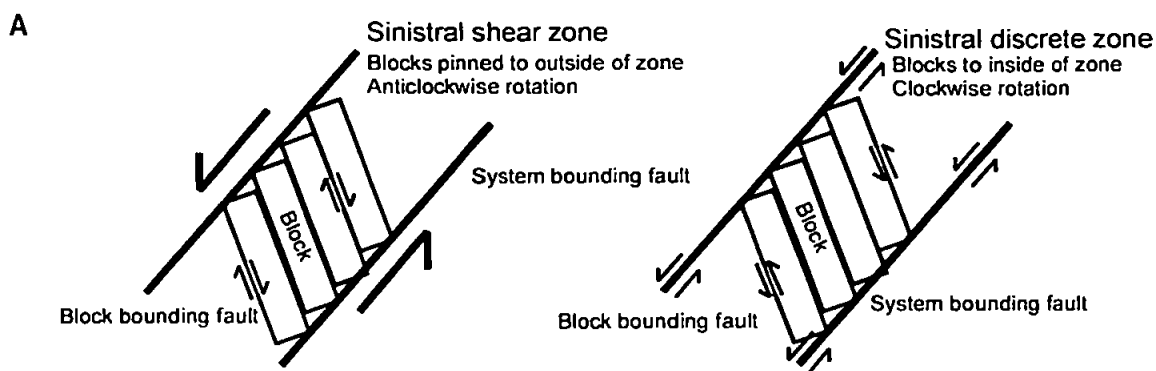


Figure 4.8: Possible mechanisms by which rotation occurs in a deforming area within a continental region.

A. Rotation due to plane strain on systems of strike-slip faults producing rotations of blocks between the system-bounding faults.

B. Various ways in which strike-slip deformation may affect an area (from Nelson and Jones 1987). Arrows show the declination of palaeomagnetic directions subsequent to rotation. (i) undeformed block (ii) deformation accommodated on parallel faults (iii) in situ rigid block model (iv) small random-sized block model (v) pervasive continuum deformation.

These mechanisms do not accommodate rotations about inclined axes. McKenzie and Jackson (1983, 1986) propose that blocks floating on a deforming lithosphere will rotate with the angular velocity of the underlying 'fluid' and explain the declination differences observed from palaeomagnetic studies. Rotation axes of faults are inclined to the vertical and so can result in changes in dip of strata. These authors also note that the scale of the deformation is also important. Small rotating blocks are confined to the seismogenic upper crust whereas larger blocks will be rooted in the lower crust and microplates represent discrete plates. Processes with wavelengths much greater than the thickness of the crust are more likely to be influenced by the motion of the underlying mantle. This would be particularly true for segments of oceanic crust, such as the 'Troodos' microplate, where the thickness of the crust is much thinner than in areas of continental deformation.

4.8 Synthesis

Palaeomagnetic results have been invaluable in providing information on the current and past deformation of the eastern Mediterranean region and palaeolatitudinal constraints on Neotethys. The background provided from these early sections of this review chapter enable the new palaeomagnetic results obtained from this thesis to be interpreted in context. Significant comparisons are made between the palaeomagnetic results from Troodos and Baër-Bassit with the new results from Hatay in the subsequent results chapters, particularly in relation to the sense and magnitude of rotations and in establishing the timing of these. The information provided here on rotations identified in these ophiolites, of both western and eastern ends of the southern Neotethyan belt, is essential in order to interpret the new results from Hatay (Chapter Five and Six) and discuss their significance for the evolution of the eastern Mediterranean (Chapter Nine).

CHAPTER FIVE

5. PALAEOMAGNETIC RESULTS FROM THE HATAY OPHIOLITE

5.1 Introduction to chapter

The Hatay ophiolite was sampled for palaeomagnetic analysis at various crustal levels, from the cumulate gabbros up to the extrusive rocks, excluding only the serpentinitised ultramafic rocks (Figure 5.1). Sixty three sites from seven localities were analysed in total, with the sampling, measurement and analysis of the data from each locality described and discussed below.

5.2 Sampling and measurement procedures

5.2.1 Sampling and measurement methods

The majority of sites were sampled using a standard portable petrol-driven rock drill, using water-cooled 25 mm diameter diamond-tipped drill bits. Each sample was orientated with both a standard magnetic compass and a sun compass. Each drilled core was cut to a 22 mm length in the laboratory, ensuring that weathered surfaces were removed. Remanence measurements were carried out using a Molspin fluxgate spinner magnetometer. Four of the pillow lava sites (AL01; AL03; ML01; ML05) were unsuitable for drilling due to their tendency to fracture. For these sites, a 'cork method' was used, consisting of attaching cork discs to pillows with glue, marking the strike line on the cork and recording the orientation of the flat surface to allow the magnetisation measured in the laboratory to be corrected into geographic coordinates. In the laboratory, these samples were cut to as near a cube shape as possible and measured in a large aperture fluxgate spinner magnetometer, designed to measure the remanence of irregularly shaped archaeomagnetic samples.

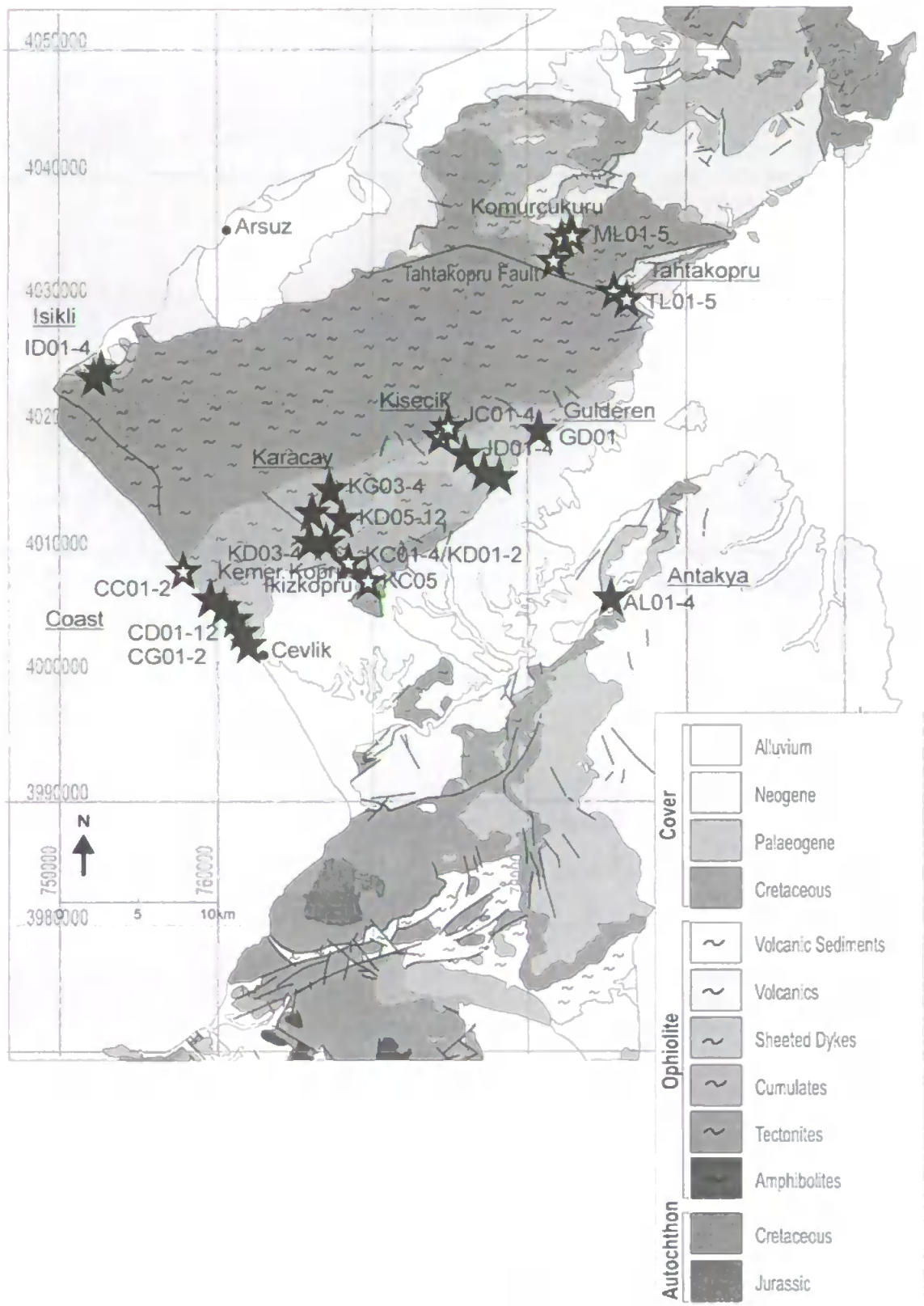


Figure 5.1: Localities within the Hatay ophiolite sampled for palaeomagnetic analysis. Only the major localities where samples were taken from are illustrated on this map for clarity. Other places mentioned in the text are shown in the map of Figure 2.12. The sites where palaeohorizontal indicators were measured in the field (cumulate layering or average flattening direction of pillow lavas) are shown by the grey stars and those sites where palaeovertical indicators were used to apply a structural correction (SDC and gabbro screens at base of SDC) are shown by the black stars. Individual localities are not always displayed due to the scale of the map with the labels sometimes referring to a number of sites represented by the same star.

The system used to label samples was two letters followed by the site number, with the first letter referring to the locality and the second letter referring to the ophiolite unit sampled: cumulate rocks (C); gabbros (G); dykes (D) and sheet and pillowed lava flows (L).

5.2.2 Structural controls on the choice of sampling sites

Drilling sites were limited to those areas where either a palaeohorizontal or a palaeovertical surface could be identified. Where layering was observed in the gabbros or ultramafic rocks, this was assumed to be originally horizontal, and sites where this layering was consistent and extensive were favoured. The improvement of clustering of magnetic inclinations subsequent to a structural correction (section 5.7) supports the choice of palaeohorizontal. The pillow lavas and lava flows were assumed to have been extruded in an originally near horizontal orientation. The average flattening direction of the pillow lavas was used as the palaeohorizontal; the shape of individual pillows cannot be used as each pillow gives a slightly different palaeohorizontal. The assumption is made that the sheeted dykes were originally intruded in near vertical orientations, particularly in those areas where the SDC is extensive, with large areas of dykes in almost identical orientations. These assumptions allow structural corrections to be applied to the palaeomagnetic data. The accuracy of these assumptions depends on the consistency and extensiveness of the palaeovertical and palaeohorizontal indicators observed in the field and the accuracy with which these can be measured. The geological likelihood of the chosen surfaces representing a true palaeohorizontal or palaeovertical is also a factor. For instance, pillow lavas are known to have the potential to be extruded down steep slopes with quite variable orientations. However, in most cases, the assumption that the average flattening direction in the majority of pillow lavas is a palaeohorizontal remains a good approximation, and more accurate than applying no structural correction. Errors up to 15°

in measurement of pillow lava palaeohizontals may be expected due to the difficulty of measuring the average flattening direction accurately. Where discrete dykes were observed, both their orientation and that of any adjacent layering were measured because the assumption that discrete dykes are intruded vertically is less likely in these cases. The assumption becomes more valid as the proportion of dykes relative to the host rock increases. In the Hatay SDC, the coastal and Karaçay valley exposures contain over 90% sheeted dykes.

5.3 Sampling localities

Sampling localities were situated throughout all structural levels of the ophiolite (Figure 5.1), with the exclusion of the deeper part of the ultramafic sequence (outcropping over an extensive area in the core of the massif) due to lack of palaeohorizontal or palaeovertical controls and extensive serpentinisation. The quality of outcrops of the Hatay ophiolite is generally good allowing selectivity in choosing the most appropriate sections to sample. The most intensively sampled localities were along the coastal road between Çevlik and Şahanlıkkayasi Headland and also along the Karaçay valley (Figure 5.1). In these localities the outcrops were particularly well exposed, especially the SDC along the coast and the cumulate gabbros in the Karaçay valley. Many small rivers cut deeply into the massif, such as the Karaçay River, although in places the exposures are hard to access. Other sampling localities were dispersed through adjacent valleys and in the north of the ophiolite massif. The two main localities where lavas were sampled were located in the north of the area with an additional locality to the SE of Antakya, separate from the main massif. There follows a brief description of each locality in alphabetical order; their locations can be seen on Figure 5.1. For one valley section (Gulderen) it was only possible to sample one section of sheeted dykes. This valley was located immediately to the north

of the Kisecik valley and so the results from this single site have been discussed within the Kisecik section.

5.3.1 Antakya (4 sites)

Four sites were located around 12 km to the SW of Antakya within an outcrop of extrusives that are separated from the main body of the ophiolite massif, and with their relationship to the latter uncertain (Figure 5.1). The extrusives include highly magnesian boninites and are the 'sakalavites' of Delaloye and Wagner (1984). Two of these sites were sampled within lava flows using the petrol drill (AL02 and AL04) and two were located within pillowed lava flows and were sampled using the cork method (AL01 and AL03).

5.3.2 Coast (15 sites)

The 25 km long exposure along the coast between Çevlik in the south and Arsuz in the north (Figure 5.1) can be split from south to north into 5 km of SDC and gabbro screens, 3 km of gabbros and 15 km of ultramafic rocks (Delaloye 1980). The coastal section thus progresses from south to north down through successively deeper levels of the ophiolite. The boundaries between the major lithology changes are generally picked out by gullies interpreted to result from movement on large faults and often accompanied by considerable areas of landslip. Fifteen sampling sites were located along the coast mainly within the steeply dipping- vertical SDC. Sampling sites were located in two different generations of dykes, referred to as 'brown' and 'grey' in this thesis, with the brown dykes commonly displaying chilled margins and clearly younger than the grey dykes. These two dyke populations can be correlated to those described by several authors (e.g. Tinkler et al. 1981; Dilek and Thy 1998) and were discussed in section 2.7.3. Two of the fifteen sites

were located in cumulate gabbros, although the layering in these was not entirely convincing, but has been supported by both later structural work (section 8.3.2) and the improvement in clustering of inclinations following application of a structural correction.

5.3.3 Isikli (4 sites)

Isikli is located close near the coast in the NW of the ophiolite massif (Figure 5.1). Serpentinised peridotites are tectonically overlain by gabbro, rotated dykes and lavas (Dilek and Thy 1998). Four dyke sites were sampled in the Isikli area. Dykes in this locality are more shallowly dipping than the majority of dykes from the SDC elsewhere.

5.3.4 Karaçay (20 sites)

The Karaçay valley runs NW-SE and is a major river valley in the Hatay area. Sampling sites were located in outcrops of sheeted dykes, gabbros and cumulate gabbros (Figure 5.1). The cumulate gabbros in this locality were the best exposed and most continuous of any locality. Five sampling sites were located in ultramafic cumulates, with two sampling sites in discrete dykes in these rocks. Four of these cumulate sites were located at river level in the Karaçay valley at Kemer Köprü (Figure 5.1) in a very good exposure displaying both clear and consistent magmatic layering (see photo of Figure 2.13). Four sites were located at İkizköprü in an area of dykes and gabbro screens (Figure 5.1). The remaining ten dyke sites and one gabbro site were dispersed throughout the Karaçay valley area.

5.3.5 Kisecik (8 sites)

The Kisecik valley is located to the NE of the Karaçay valley, running roughly parallel with it (Figure 5.1). Four sites within ultramafic cumulates were located to the north of the

river at a level topographically higher level than the river itself. Shallower structural levels of the ophiolite (the SDC) are exposed at river level further down the valley and four sites were located in these outcrops. These dyke sites generally display a higher degree of weathering than either the coastal or Karaçay dykes and due to less extensive exposure, the consistency of the orientation of the dykes is less apparent. This should be considered when assuming the dykes were intruded vertically and provide an accurate palaeovertical. The confidence of the assumption is decreased in one site where only four dykes could be observed.

5.3.6 Kömürçukuru (5 sites)

The Kömürçukuru sampling sites are located in an outcrop of extrusives in the north of the Hatay ophiolite (Figure 5.1). This area lies to the NE of the Tahtaköprü Fault. The extrusives in this locality lie tectonically above ultramafic rocks along a shallowly dipping contact and are massive and pillowed lavas that are rarely interbedded with, or overlain by, metalliferous sediments (Erendil 1984; Robertson 1986). There are five sites, one located in a lava flow and four located in pillowed flows, with one of these flows also interbedded with metalliferous sediments/umber. Two of the sites in the pillowed lava flows were sampled using the cork method.

5.3.7 Tahtaköprü (5 sites)

Tahtaköprü is located to the north of the ophiolite massif and not far to the east of Kömürçukuru and similarly is located to the NE of the Tahtaköprü Fault (Figure 5.1). Five sites were located in pillowed lava flows and massive flows near Tahtaköprü and were sampled by field drilling. These sites may be spatially divided into two groups; three sites

within one area exposed along a small stream and two sites sampled from a second area several kilometres distant.

5.4 Rock magnetic summary

Chapter Seven deals in detail with the rock magnetic properties of the sampled lithologies. However, in order for the palaeomagnetic results to be discussed more easily, a summary of these results will be given here.

The rock magnetic mineralogy of the samples is compatible with the presence of fine magnetic grain sizes with PSD properties capable of retaining a stable magnetisation throughout the complex history of the ophiolite. Magnetic mineralogy is found to be dependent on the crustal level. Clear Verwey transitions and high Curie temperatures (T_C s) in the deeper levels of the crust (ultramafic cumulates, cumulate gabbros and SDC) indicate that Ti-poor titanomagnetite/magnetite is the major carrier of the magnetic signal, whilst the absence of the Verwey transition and lower T_C s of the higher crustal levels (extrusive rocks) indicate the presence of a more Ti-rich titanomagnetite here. These mineralogies are compatible with acquisition of stable remanences within the crustal/upper mantle section soon after genesis of the ophiolitic crust at an oceanic spreading centre.

5.5 Magnetic fabric analyses

Anisotropy of magnetic susceptibility (AMS) was measured for all samples on the AGICO KLY3 Kappabridge in the University of Plymouth laboratory prior to demagnetisation procedures (with the exception of the non-standard 'cork method' samples which were too large for the KLY3). Results at sample-level were variable and specimens display a mixture of oblate and prolate fabrics. Site-level data also vary between those sites with

oblate (Figure 5.2A) or prolate fabric and those with all three axes well clustered (triaxial fabric) (Figure 5.2B) to sites where either the minimum or maximum principal axes of anisotropy are clustered with the remainder of principal axes arranged in a girdle along the orthogonal plane, to sites where there is no clear fabric observed (Figure 5.2C) and a complete lack of coherency between principal axes. There is no correlation in fabric type between either sites from the same locality or of the same lithology. For example, of the twelve sheeted dyke sites along the coast, three showed clear examples of an oblate fabric, two showed a clear prolate fabric and for seven sites the relationships were less clear or there was a complete lack of clustering of any principal axes. Across all localities, the majority of fabrics were indeterminate. Generally, those sites with oblate fabrics had clearer fabrics than those with prolate, with almost twice as many clearly recognised. Fewer sites displayed triaxial fabrics. A plot of corrected anisotropy degree against shape parameters (Figure 5.2D) illustrates the spread between oblate and prolate fabrics, with roughly 50% in each category. Only a few sites had more than a 5% degree of anisotropy indicating generally weak fabrics and the only site with a significantly higher degree was site KC05 which is believed to have been hit by lightning (section 5.7.4). Those sites where a clear fabric could be identified were almost invariably related to the structure observed in the field, which indicates both that these were accurately measured and that the macroscopic structures are matched in orientation by the microscopic fabrics. Only two sites (JC01 and KD12) displayed a clear fabric unrelated to the structure. For site JC01 (Figure 5.2D), the fabric orientation was used to predict a plausible macroscopic structure. This was used to apply a tilt correction to the palaeomagnetic data, which produces a stratigraphic declination that lies away from the spread observed for the palaeohorizontal sites, suggesting that this should not be used in analysis.

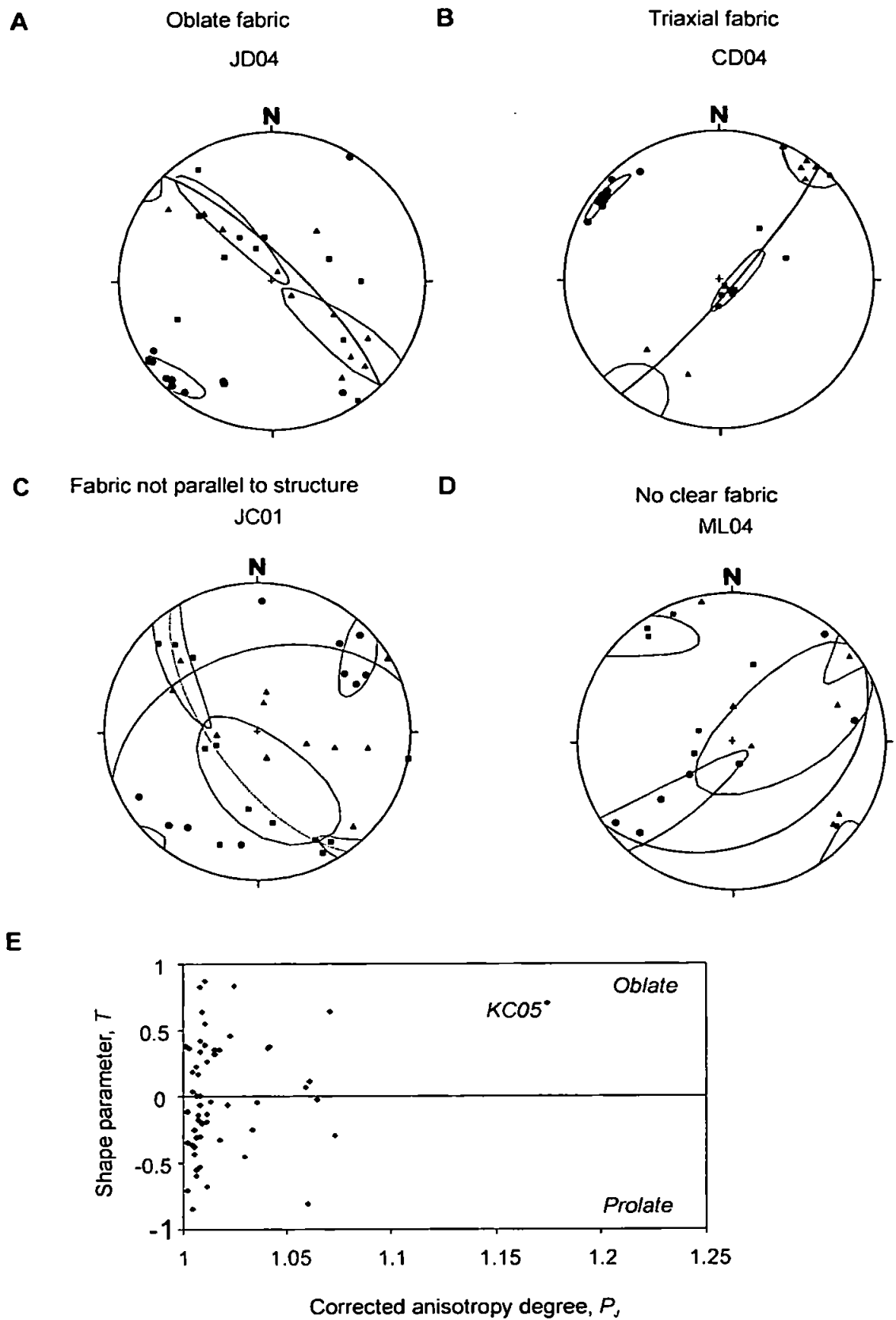


Figure 5.2: Anisotropy of magnetic susceptibility for rocks from the Hatay ophiolite.
 A. Representative fabric relationships at site level within selected samples.
 B. Shape parameter versus corrected anisotropy degree for all sites.

Of all the lithologies, the site-level anisotropy of magnetic susceptibility was slightly more consistent within the cumulate series. The fabrics from the Karaçay valley cumulate sites show a mixture of prolate and oblate fabrics at sample-level and no relationship between the shape parameter, T , and the corrected anisotropy degree, P_J , which varies from around 1.0 to 1.25 (Figure 5.3A). At site-level, three of the five sites have oblate fabrics with k_{\min} axes orthogonal or near-orthogonal to the structure (magmatic layering in this case) and k_{int} and k_{\max} arranged in a girdle distribution along the layering. Site KC04 has a triaxial fabric, with k_{\min} perpendicular to the layering. Site KC01 shows no coherent relationships between the principal axes of anisotropy and the layering. The generally oblate fabric suggests some fabric development associated with the magmatic layering within the rock.

The fabrics from cumulate sites within other localities are not as consistent. The fabric data at sample-level from the coastal cumulates again shows a mixture of prolate and oblate fabrics. These prolate fabrics could be explained by the presence of SD magnetite producing an inverse fabric (Figure 5.3B). At site level, CC01 and CC02 from the coastal cumulates have roughly oblate fabrics, with k_{\min} roughly orthogonal to the layering (which was less clear than the layering in the Karaçay cumulates). In the case of CC01, the distribution is nearly triaxial. The fabrics of the remaining two sites display no relationship to the cumulate layering.

Within the Karaçay valley, the discrete dykes of site KD02 were sampled both within the centre of the dyke and on each dyke margin to recognise any variations in fabric due to flow. This site has a weak oblate fabric and there is an overlap in the distribution of principal anisotropy axes from the opposing dyke margins and with the samples from the centre of the dyke suggesting that in this site there is no flow-alignment in the fabric (although the weak nature of the fabric does not make this certain).

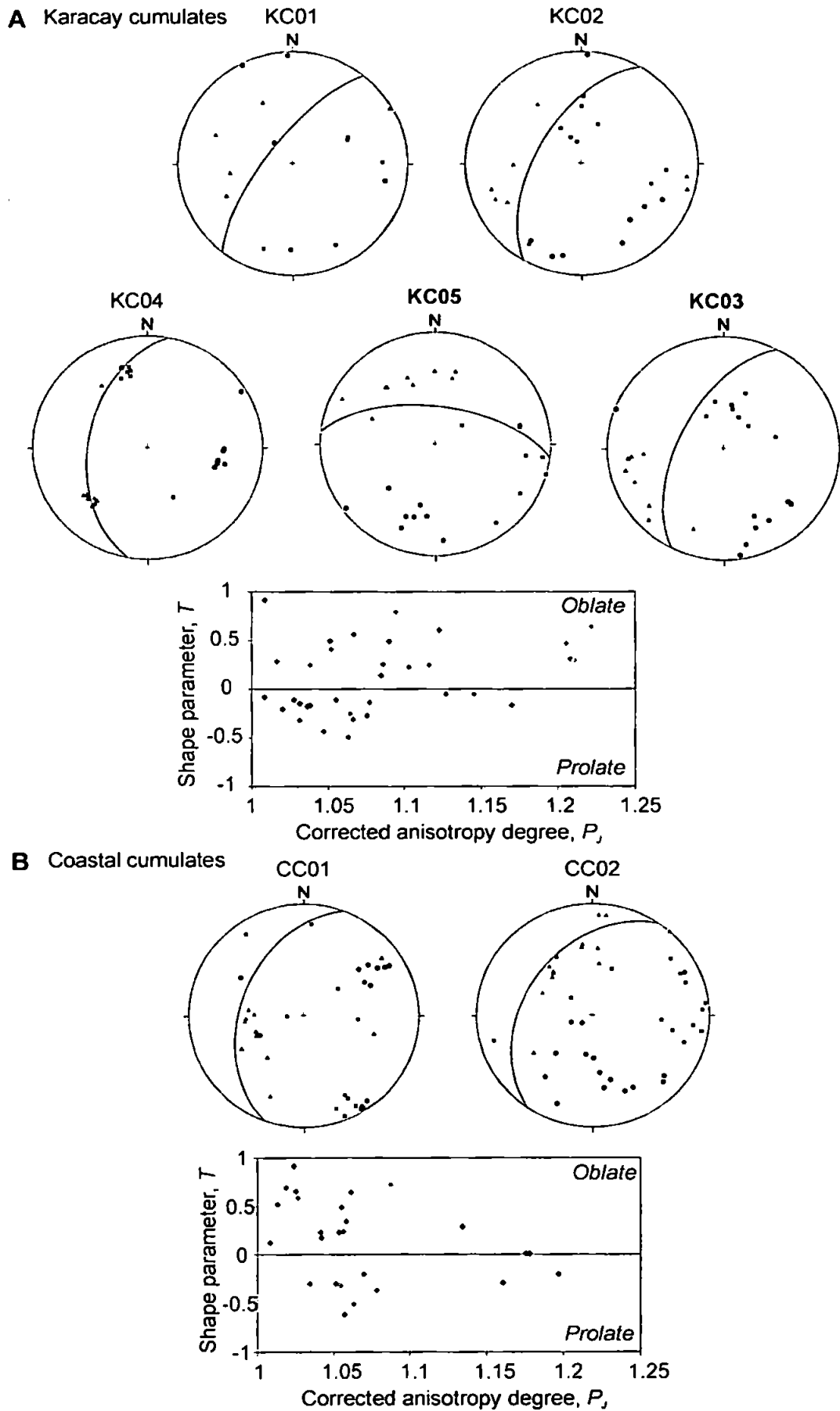


Figure 5.3: Anisotropy of magnetic susceptibility data for cumulate gabbros and ultramafics. A. In the Karacay river section [KC01-5]. B. Along the coast [CC01-2].

5.6 Palaeomagnetic results overview

Prior to demagnetisation, NRM intensities were measured for all samples. NRM intensities in the ophiolite range from less than 0.01 A/m to 27.9 A/m. However, only ten samples have NRMs of less than 0.01 A/m. The NRM intensities vary with lithology with a factor of ten between the weakest and strongest samples. The mean NRM intensities for all of the lithologies palaeomagnetically analysed are given in Table 5.1.

<i>Description</i>	<i>Number of samples</i>	<i>Mean (geometric) Intensity (A/m)</i>
Extrusive rocks ^A	72	2.58
Extrusive rocks ^B	53	2.19
SDC	207	0.31
Discrete dykes ^C	16	0.004
Gabbros	21	0.41
Cumulate rocks ^D	69	0.62
KC05 ^E	9	8.81

Table 5.1. Average NRM intensities for the various ophiolitic lithologies.

^A Including all lava samples.

^B Excluding non-standard-sized lava samples. The intensities of non-standard size lava samples cannot be compared since sample volumes are unknown.

^C Sites KD01 and KD02 in the Karaçay valley.

^D Including both ultramafic cumulates and cumulate gabbros but excluding site KC05.

^E Believed to have anomalously high intensities due to a lightning strike. NRM intensities of the site range from 6.7 to 15.1 A/m; higher than for cumulate samples from any other site.

It is clear that the lava samples on the whole have significantly higher intensities than the deeper lithologies of the ophiolite. The cumulate rocks on average have slightly higher NRM intensities than the SDC and gabbros. Site KC05 has anomalously high intensities, which when combined with information from the demagnetisation procedure suggests that this could be the result of an IRM induced by a lightning strike (section 5.7.4). The samples from the SDC have the lowest average NRM intensities, although the lowest intensities measured from any of the ophiolitic rocks were from the discrete dykes sampled from within the ultramafic sequence exposed in the Karaçay valley. The average NRM intensity for these samples are a factor of 1000 smaller than that of the lavas and 100 times less than the other dykes sampled within the SDC. However, even so, these values are

above the noise level of the Molspin and are significantly higher than the average NRM intensities for the sedimentary cover samples (sections 6.3.4 and 6.4.4).

The palaeomagnetic results from both thermal and AF demagnetisation techniques for each lithology are generally good with consistently clean, often single component decay to the origin. Figures 5.4 and 5.5 show examples of sample demagnetisation plots from various lithologies from both palaeohorizontal and palaeovertical sites and for both thermal and AF demagnetisation techniques, and site-level data are included in Table 5.2 and 5.3. Demagnetisation paths for the lavas and cumulate gabbros in particular, were consistently of high quality, with slightly more variability in quality observed in the SDC. Thermal demagnetisation data are occasionally noisier than the AF data, although there are no cases where the results from the two methods are in major disagreement. Stable components of magnetisation were identified from individual samples using least squares analysis (Kirschvink 1980), which were subsequently combined to give a mean ChRM for the site using Fisher (1953) statistics. Within localities, some of these sites were also grouped where site mean directions were similar and it was appropriate geologically (i.e. no major faults between sites- see section 5.7.8). Dispersions of VGPs obtained from site mean directions within a group were then compared with the expected dispersion for a latitude of 20° N (Merrill and McElhinny 1983).

Of 63 palaeomagnetic sampling sites from the ophiolite, 43 sites have an α_{95} of 10° or lower, with all but three sites having α_{95} below 20° (average α_{95} = 8.8°). The precision parameter (κ) values for all sites except one (KD07) are greater than 10, and all sites except seven have values over 20. More than a third of sites have a κ value over 100 (average of 100.35). The preferred number of samples (n) included in a site ChRM is six to eight, with $n = 8$ being the average number of cores demagnetised per site and $n > 5$ for all sites except three (JC01, GD01 and ML04), which is taken into consideration in the

analysis of their results. These statistics illustrate that the quality of the demagnetisation data from the ophiolitic sites is highly reliable.

Geographic magnetic remanences are almost without exception towards the west and unrelated to the present-day field. Stratigraphic remanences are also towards the west. The details of the palaeomagnetic results from each locality are discussed below in alphabetical order. Figures 5.6 and 5.7 show lower hemisphere stereographic projections illustrating geographic and stratigraphic remanences for each locality, displaying data from sites with palaeohorizontal control (cumulate and extrusive rocks) on Figure 5.6 and those with palaeovertical control (SDC) on structure on Figure 5.7.

Site ^A	Lat.	Lon.	Str.	N	Dg	Ig	kg	α_{95g}	Ds	Is	ks	α_{95S}
AL01	36.16	36.17	70/44	11	203.5	-7.8	99.4	4.6	199.1	22.1	99.4	4.6
AL02	36.16	36.16	175/21	8	261.6	-33.1	20.3	12.6	275.1	-31.8	20.3	12.6
AL03	36.16	36.17	90/30	7	227	-1.1	141	5.1	224.1	18	125.9	5.4
AL04	36.16	36.16	228/29	6	238.1	-47.3	534.4	2.9	255.5	-75.1	534.4	2.9
CC01	36.19	35.87	290/44	7	191.2	80.5	207.4	4.2	276.3	46.6	207.4	4.2
CC02	36.17	35.89	304/40	9	287.5	67.7	601.5	2.1	297	28.4	601.5	2.1
JC01	36.28	36.05	090/00	4	305.7	46.3	55.2	12.5	317.7	6.7	55.2	12.5
JC02	36.28	36.05	355/45	9	271.6	56.2	56.6	6.9	313.8	32.8	56.6	6.9
JC03	36.28	36.05	342/45	6	274	47.3	50.7	9.5	300.1	19.9	50.7	9.5
JC04	36.29	36.06	351/41	8	268.2	38.9	57	7.4	293.2	24.1	57	7.4
KC01	36.19	35.99	308/72	7	185.7	65.5	82.1	6.7	284.3	29.5	82.1	6.7
KC02	36.19	35.99	300/58	10	198.8	66.3	146.7	4	271.8	33.5	146.7	4
KC03	36.19	35.99	297/58	10	199.3	67	260.1	3	269.7	32.2	260.1	3
KC04	36.19	35.99	280/47	10	217.9	79.1	320.9	2.7	267.9	37.2	320.9	2.7
KC05	36.18	36	007/62	11	266.6	73.1	26.1	9.1	347.7	29.7	26.1	9.1
KD01 _{hoz}	36.19	35.99	300/58	8	211.1	64.4	56.5	7.4	270.7	28.1	56.4	7.4
KD02 _{hoz}	36.19	35.99	297/58	7	192.8	63	173.6	4.6	264.8	34.5	172.9	4.6
ML01	36.43	36.14	118/33	7	226.1	27	109.9	5.8	207	32.1	109.9	5.8
ML02	36.43	36.14	174/22	8	292.7	17.6	75.8	6.4	284.4	26.9	75.8	6.4
ML03	36.43	36.14	185/55	6	278.9	13.9	37.4	11.1	265.7	11.1	37.4	11.1
ML04	36.43	36.14	148/35	4	262.3	22	63.7	11.6	244.6	31.8	63.7	11.6
TL01	36.39	36.2	155/85	6	278.4	15	12.2	20	230.3	33.5	12.2	20
TL02	36.39	36.2	155/85	6	281.1	21.7	40.9	10.6	221.9	35.3	40.9	10.6
TL03	36.38	36.18	145/55	6	268.3	5.1	26.7	13.2	251.2	29.9	26.7	13.2
TL04	36.38	36.18	150/42	6	280.9	23	33.7	11.7	255	43.9	33.7	11.7
TL05	36.38	36.18	150/42	5	289.6	21.5	117.1	7.1	265.1	48.3	117.1	7.1

Table 5.2: Site palaeomagnetic data for sites with palaeohorizontal structural indicators.

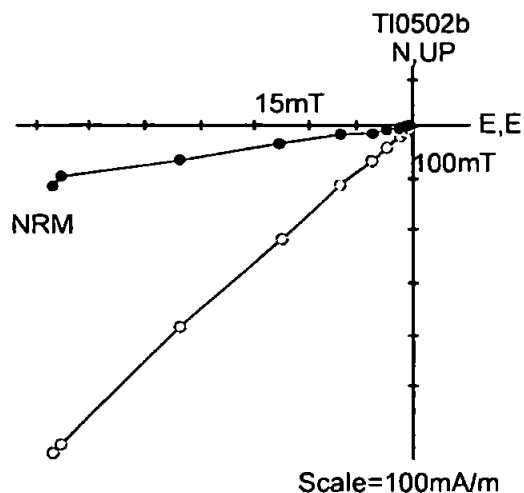
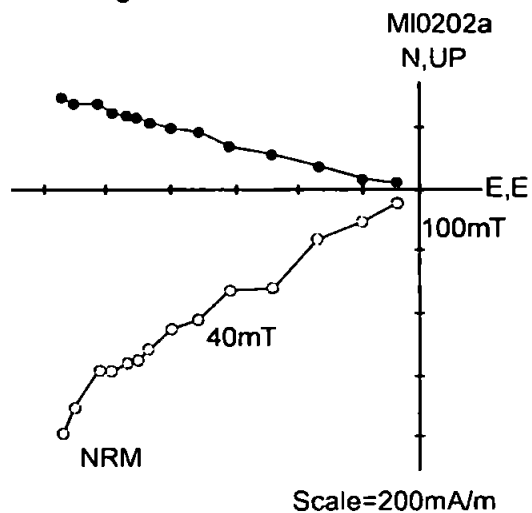
^A The locality of the site is apparent from the 1st letter of the site label: A = Antakya; C = Coast; J = Kiseçik; K = Karacay; M = Komurçukuru; T = Tahtakopru. The lithology of the samples within the site is apparent from the 2nd letter of the label: L = lava; C = cumulate rock; Dhoz = discrete dyke where the layering of the cumulate rocks cut is used in preference to the orientation of the dyke to apply a structural correction.

Site ^A	Lat.	Lon.	Str.	N	Dg	Ig	kg	α_{95g}	Ds	Is	ks	α_{95S}
CD01	36.13	35.91	130/83	11	196.1	46.2	35.2	7.8	203.3	48.6	35.2	7.8
CD02	36.13	35.91	317/80	11	201	61.3	124.9	4.1	187.2	55.8	124.9	4.1
CD03	36.13	35.91	116/80	9	208.3	64.6	72.2	6.1	228.2	62.5	72.2	6.1
CD04	36.14	35.91	160/66	6	243.6	66.7	36.1	11.3	290.3	59	36.1	11.3
CD05	36.15	35.9	190/74	8	262.1	51.4	26.3	11	283	53.6	26.3	11
CD06	36.16	35.9	010/72	7	342.1	69.8	228.6	4	280.2	80.7	228.6	4
CD07	36.16	35.9	010/72	6	300.4	81.3	42.1	10.4	219	73	42.2	10.4
CD08	36.16	35.9	016/68	10	341.3	72.7	133.2	4.2	248.5	77.6	133.2	4.2
CD09	36.17	35.89	000/78	9	328.4	76.3	53.5	7.1	267.4	82.9	53.5	7.1
CD10	36.17	35.89	003/69	7	336.9	62.6	55.1	8.2	291.5	77.7	55.1	8.2
CD11	36.16	35.89	006/74	14	322.9	73.4	104.8	3.9	257.8	78.1	104.8	3.9
CD12	36.14	35.91	162/56	10	231.9	46.9	23.8	10.1	270.4	47.4	23.8	10.1
CG01	36.13	35.91	116/80	6	194.6	59.6	166.9	5.2	211.9	60.1	166.9	5.2
GD01	36.29	36.12	337/46	4	285.6	58	19.2	21.5	206.7	57.1	19.2	21.5
ID01	36.33	35.82	040/45	6	131.8	-11.7	76.7	7.7	122.9	-9.5	76.7	7.7
ID02	36.33	35.81	026/48	8	153.9	-35.9	225	3.7	114	-50.2	225	3.7
ID03	36.33	35.82	040/43	7	139.8	-18.8	207.4	4.2	122.3	-19.7	207.4	4.2
ID04	36.33	35.82	030/38	9	142.6	-11.9	175.2	3.9	124.4	-25	175.2	3.9
JD01	36.26	36.08	251/65	5	321.2	20.8	16.7	19.3	332.1	27.1	16.7	19.3
JD02	36.26	36.08	236/80	7	313.9	26.6	36	10.2	319	28.3	36	10.2
JD03	36.27	36.07	024/80	8	278.3	-33.8	92.1	5.8	285.1	-35.9	92.1	5.8
JD04	36.25	36.09	045/77	6	29.2	50.9	18.5	16	22.6	63.2	18.5	16
KD01	36.19	35.99	153/63	9	210.5	64.8	56.6	6.9	272.9	65.5	56.6	6.9
KD02	36.19	35.99	142/71	8	196.7	62.3	83.4	6.1	217.5	71.5	92.1	5.8
KD03	36.19	35.98	195/72	6	237.8	41.7	42.4	10.4	253.2	53.3	42.4	10.4
KD04	36.19	35.98	195/58	6	243.2	35.8	14.7	18.1	271.1	51.5	14.7	18.1
KD05	36.21	35.97	190/79	7	60.5	60.4	55.1	8.2	48.8	52.5	55.1	8.2
KD06	36.22	35.98	182/75	6	268.7	42.6	12.5	19.7	282.4	41.7	12.5	19.7
KD07	36.22	35.98	182/75	6	296.8	41.7	7.6	25.9	307	34.1	7.6	25.9
KD08	36.25	35.97	350/88	7	243.9	51.1	141	5.1	241.5	50.5	141	5.1
KD09	36.23	35.96	001/82	10	269.6	58.8	111.2	4.6	256.7	57.7	111.2	4.6
KD10	36.21	35.96	174/72	10	228.6	32.4	133.2	4.2	240.4	41.4	133.2	4.2
KD11	36.21	35.96	173/79	7	237.5	45.5	64	7.6	248.8	49.3	64	7.6
KD12	36.21	35.96	168/70	5	201.6	30.1	45.2	11.5	211.4	45.9	45.2	11.5
KG01	36.19	35.98	195/72	5	243.7	50.1	12.6	22.4	266.1	59.3	12.6	22.4
KG02	36.19	35.98	195/58	7	238	38.3	43.1	9.3	268.6	56.1	43.1	9.3
KG03	36.23	35.96	001/82	6	272.5	58.5	129.9	5.9	259.7	57.8	129.9	5.9

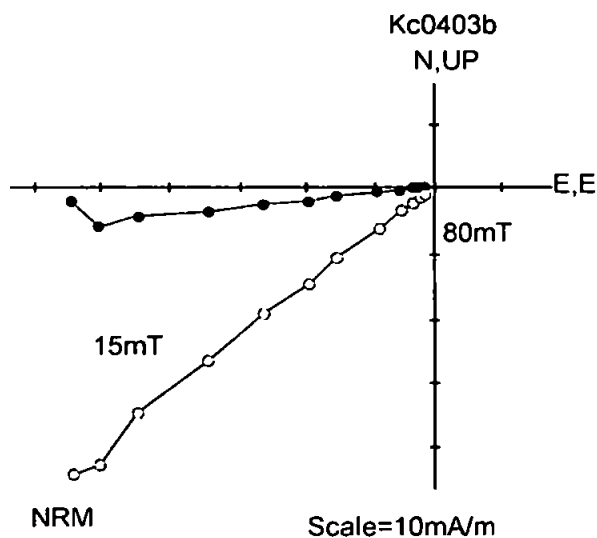
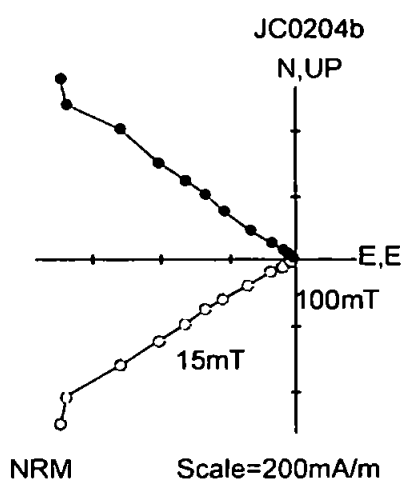
Table 5.3: Site palaeomagnetic data for sites with palaeostructural indicators.

^A The locality of the site is apparent from the 1st letter of the site label: C = Coast; I = Isikli; G = Gulderun; J = Kisecek; K = Karacay. The lithology of the samples within the site is apparent from the 2nd letter of the label: D = dyke; G = gabbros screen where the orientation of the adjacent dykes is used to apply a structural correction.

AF demagnetisation: lava flows



AF demagnetisation: cumulate gabbros



AF and thermal demagnetisation: cumulate gabbros

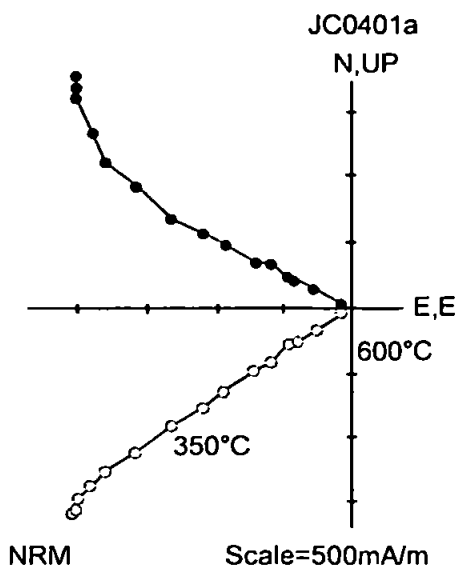
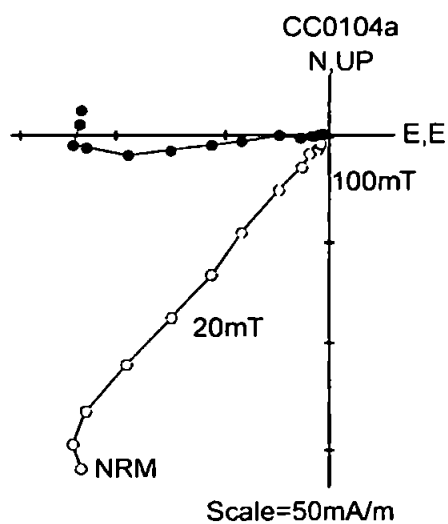
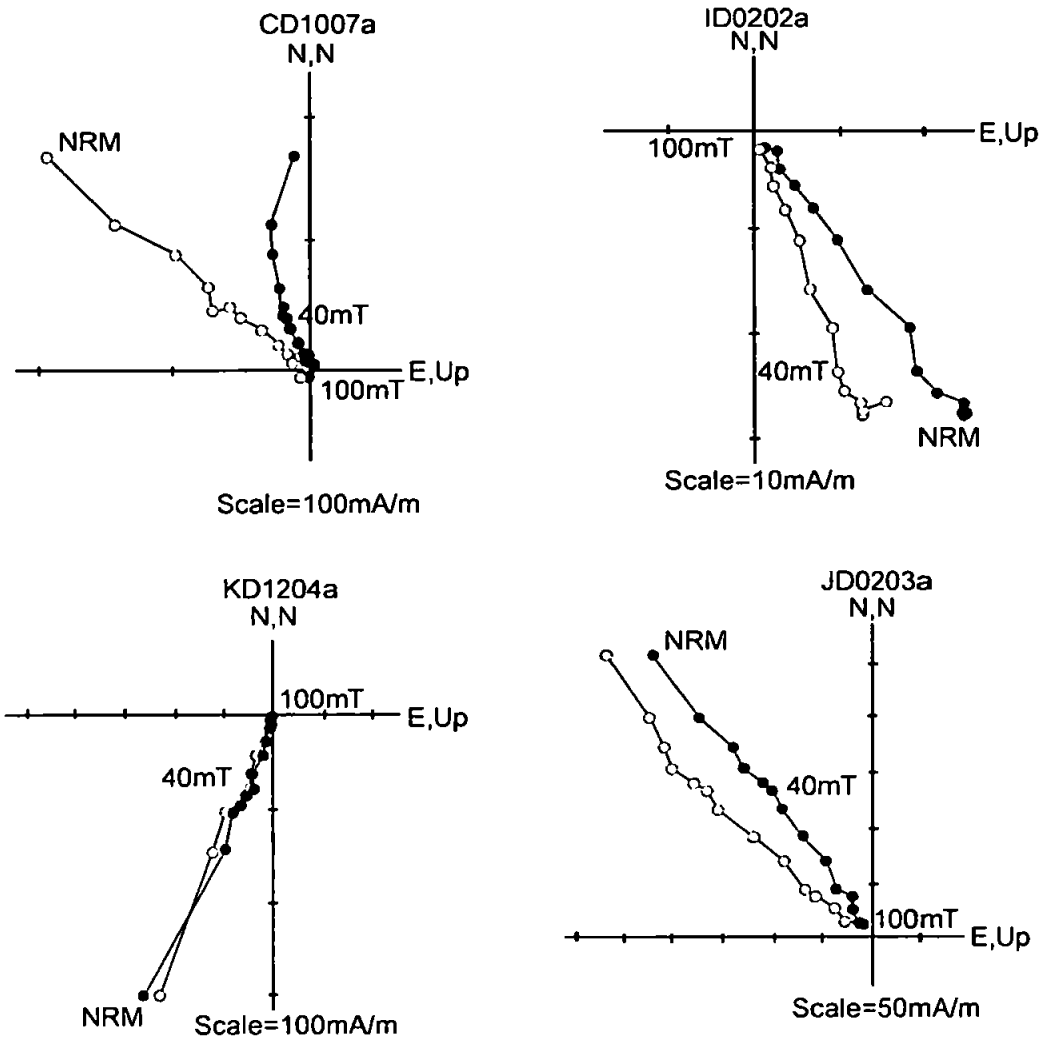


Figure 5.4: Sample demagnetisation plots for sites with palaeohorizontal control in stratigraphic coordinates: open circles show the vertical projection of the demagnetisation vector and closed circles show the horizontal projection of the demagnetisation vector.

AF demagnetisation: sheeted dyke complex



Thermal demagnetisation: sheeted dyke complex

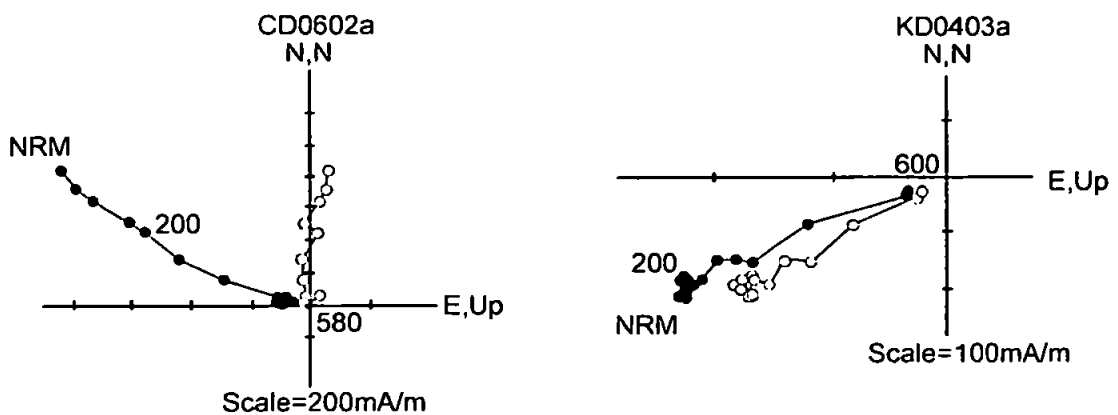


Figure 5.5: Sample demagnetisation plots for sites with palaeovertical control in geographic coordinates: open circles show the vertical projection of the demagnetisation vector and closed circles show the horizontal projection of the demagnetisation vector.

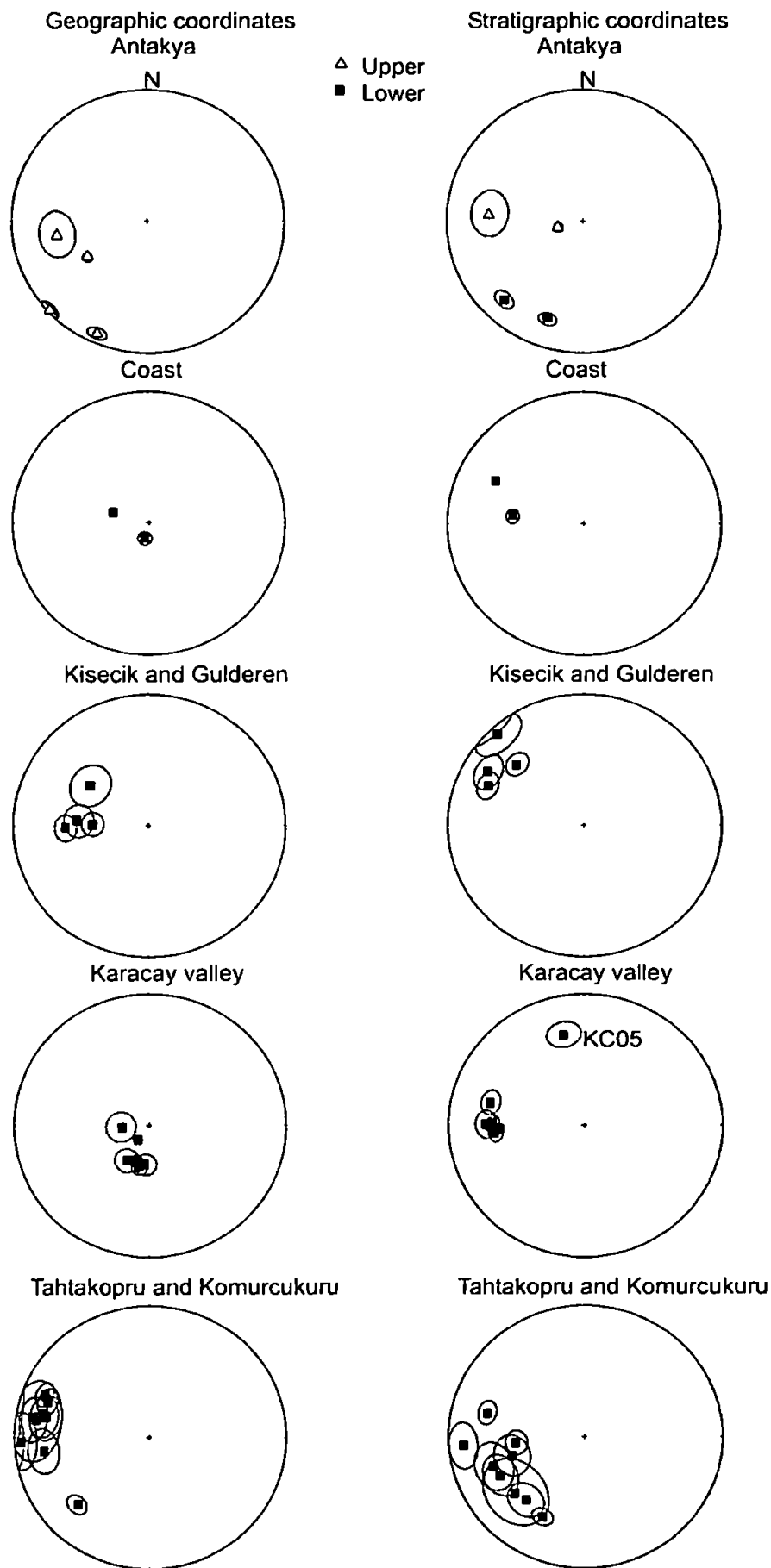


Figure 5.6: Stereographic projections of magnetic remanence directions for each locality, displaying only those sites with palaeohorizontal control on the structural orientation.

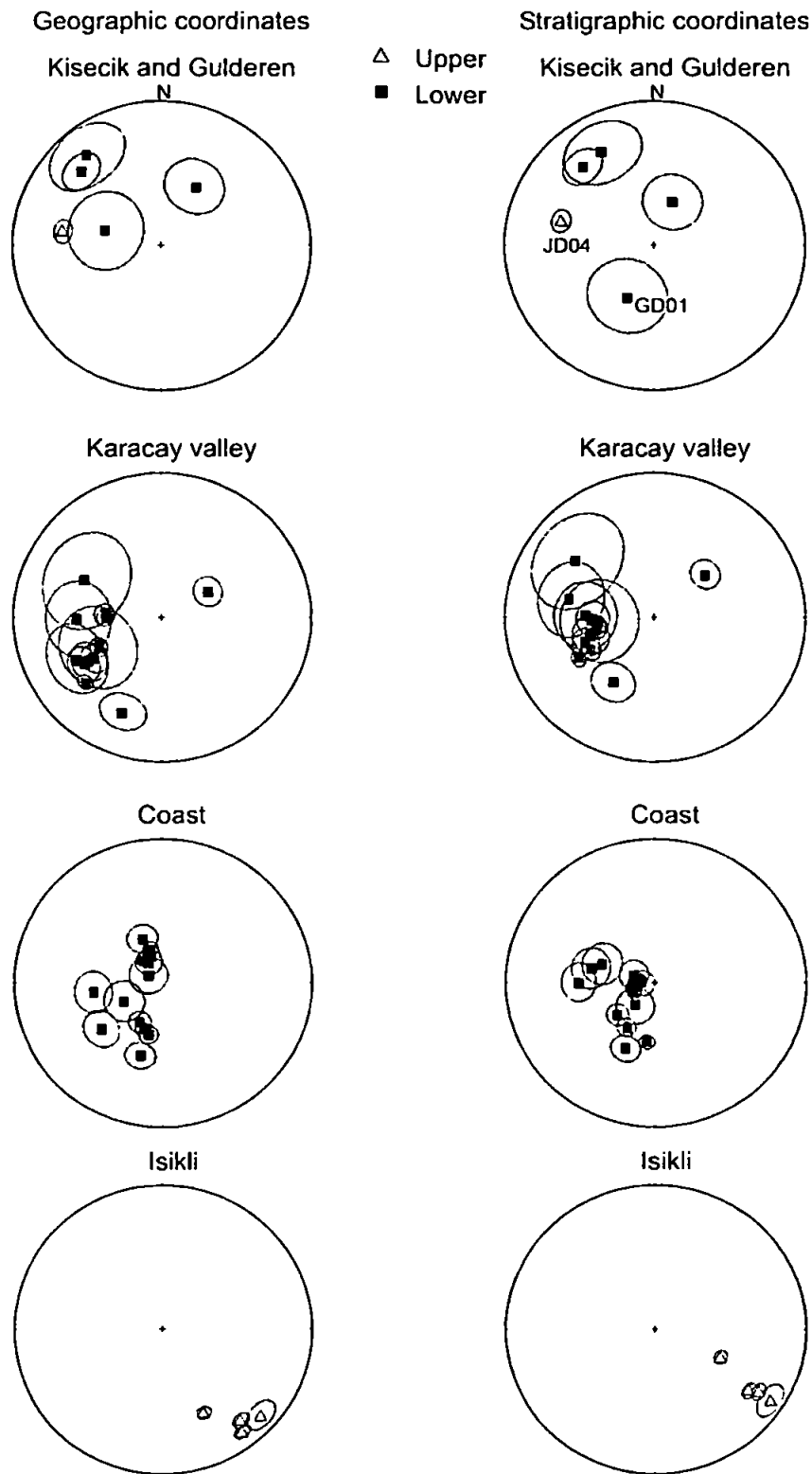


Figure 5.7: Stereographic projections of magnetic remanence directions for each locality, displaying only those sites with palaeovertical control on the structural orientation.

5.7 Palaeomagnetic results by locality

5.7.1 Antakya (4 sites; extrusive rocks)

The Antakya lava sites include samples from both standard and non-standard-sized samples, with an average NRM intensity for the standard-sized samples of 2.80 A/m (Table 5.1). Remanences are generally single component and demagnetise with linear decay to the origin. A few samples from AL02 and AL04 are slightly noisier and a significant proportion of the samples, particularly from AL03, do not completely demagnetise to the origin, suggesting the presence of a high coercivity component, although all approach the origin closely. Demagnetisation plots from all samples from site AL03 display single components of magnetisation that drop to less than a fifth of the original magnetisation, but do not reach the origin. Samples display median destructive fields of generally less than 30mT indicating the dominance of low coercivity minerals, consistent with remanences being carried by titanomagnetite (Chapter Seven).

Geographic magnetisation directions for all the Antakya samples are reversely magnetised but site ChRMs display a large difference in direction from each other, with Kappa and α_{95} values of 7.0 and 37.4° respectively for geographic directions and 2.3 and 79.9° for stratigraphic directions if all four sites are grouped; a clear demonstration that these sites experienced differential deformation between sites and that these sites should be considered at site rather than locality level. The directions of the Antakya sites fall into two groups, with one comprising the two pillow lava sites and one group comprising the two lava flows. The sites from pillow lavas (AL01 and AL03) show some similarity, with geographic directions negative with shallow inclinations towards the SW and stratigraphic directions positive with shallow inclinations towards the SW. The two sites from lava flows also display some similarity, more so for geographic directions which are reversely

magnetised with moderate-steep inclinations towards the WSW. The lava flows have similar dips and 20° difference in strikes, which contrast to the strikes and dips of the two pillow lava sites which strike almost perpendicularly to the lava flows and have very shallow dips.

5.7.2 Coast (15 sites; cumulate rocks, gabbros and SDC)

The average NRM intensity for the cumulate samples is 0.49 A/m, slightly higher than the average for all cumulate sites. Demagnetisation plots from the cumulate samples are single component and without exception demagnetise cleanly to the origin, with median destructive fields of less than 20mT. Occasional low-coercivity components are removed by 10mT and display spurious directions representing a probable laboratory-induced overprint. The average NRM intensity for the coastal gabbro samples (site CG01) is 0.21 A/m and demagnetisation plots from these samples are particularly clean and median destructive fields are slightly above that of the cumulate gabbros. Again, occasional low-coercivity components are removed by 10mT in the demagnetisation procedure.

Average NRM intensities from the samples within the coastal exposures of the SDC are 0.43 A/m. Although samples from the SDC along the coast generally display good demagnetisation data, as a general rule these data are slightly noisier than for the extrusive rocks (section 5.6) which may be attributed to NRMs of around a factor ten less than that of the extrusives, although remaining significantly above the noise level of the magnetometer. Coastal dyke demagnetisation plots commonly show a significant initial decrease in magnetisation followed by a single component decaying cleanly to the origin, with MDFs on average of around 15mT. The overprint direction occasionally appears to be a present-day field overprint but most sites display spurious directions and probably relate to a laboratory induced overprint. Around a third of samples do not completely

demagnetise to the origin indicating the influence of a high-coercivity component, although all except one of these samples decays to less than a few percent of the original magnetisation. If the ChRM data from all samples across all sites within the SDC are included on the same stereonet, three main distinct clusters can be seen in both geographic and stratigraphic coordinates, with a small number of points lying separate from these clusters. The remanences are (with two exceptions from over 100 samples) westerly directed. All of the coastal dyke sites display steep remanences in both geographic and stratigraphic coordinates. The clusters correspond to a southerly group of sites, a central section of dykes and a northerly section of dykes. The remanence directions of the gabbros samples that were located in gabbros screens adjacent to sites CD01-3 display directions that are, within error, indistinguishable from samples from the dyke sites. At a site level, ChRM directions again can be observed to fall into the three clusters mentioned above. These data are discussed further in section 5.7.8.

The cumulate samples display steep remanences (mean inclination of 78.3°) that become shallower following tilt correction (37.9°) and correct to around the mean inclination for all palaeohorizontal sites, with a slight improvement in both K and α_{95} values.

5.7.3 Isikli (4 sites; SDC)

The samples from Isikli are all located within the SDC in moderately-dipping dykes and have an average NRM intensity of 0.21 A/m. Demagnetisation plots from Isikli sites ID01 and ID02-3 display evidence for a low-coercivity overprint that is either removed during demagnetisation by between 10 and 20 mT or overlaps with the ChRM direction resulting in a curved demagnetisation path. The removal of the low-coercivity component is usually accompanied by a slight increase in magnetisation. Sample ID0105a provides a good illustration of this behaviour (Figure 5.8). Samples from site ID02 are less-affected by the

overprint carried by the low-coercivity minerals, which is either removed by 5 mT (and accompanied by only a very slight increase in magnetisation) or single component behaviour is observed. During demagnetisation, the remanence of the majority of the Isikli dyke samples either decays to the origin or almost to the origin and the data are less noisy than from samples from the coastal SDC.

ChRM directions are towards the SE with shallow inclinations, and samples are invariably reversely magnetised. In geographic coordinates, the average declination and inclination for the Isikli dykes are 141.7° and -19.7° respectively, and are 121.3° and 26° in stratigraphic coordinates. If the site average directions are antipoded, they plot in the NW quadrant of the stereonet, with similar declinations and inclinations to many of the sites from other localities, with inclinations becoming more similar subsequent to structural correction.

5.7.4 Karaçay (20 sites; cumulate rocks, gabbros and SDC)

The average NRM intensity for the samples from the Karaçay valley SDC (0.30 A/m) is equivalent to the average for all SDC samples whereas the averages for the gabbros (0.73 A/m) and cumulate rocks (0.29 A/m) are slightly higher and lower respectively than for all samples of these lithologies. The four cumulate sites from river-level in the Karaçay valley display good demagnetisation data and demagnetise cleanly to the origin, almost always with single component decay. Cumulate site KC05 is located high on the valley side, away from the four river-level cumulate sites. The magnetisation of site KC05 samples decays extremely quickly; half of the measured samples have MDFs of ~ 5 mT. Combined with the anomalously high intensities (section 5.6) the implication is that a lightning strike imparted an isothermal remanent magnetisation into these samples.

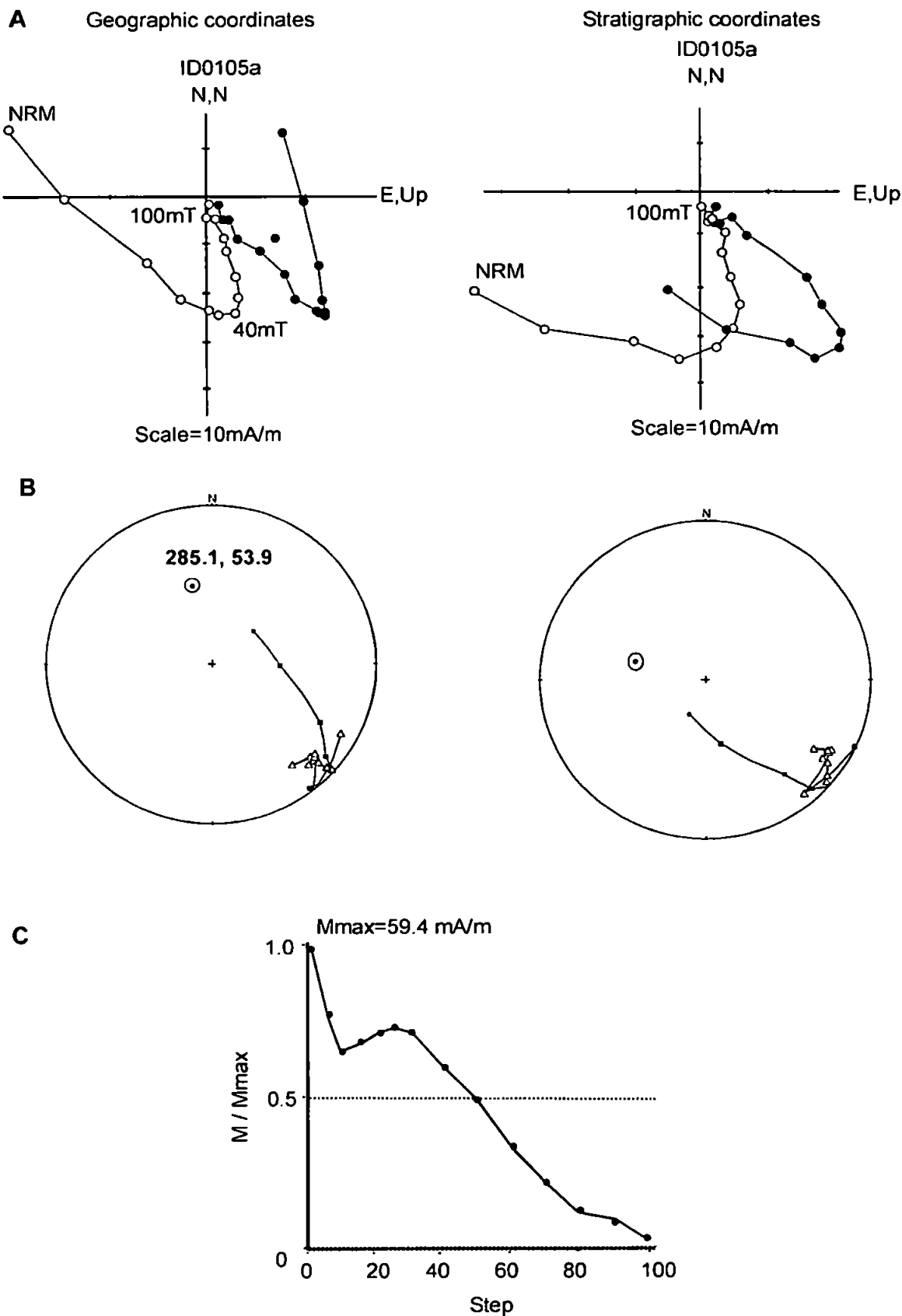


Figure 5.8: Demagnetisation data from a reversely magnetised sample from the Isikli locality. A-B. Demagnetisation plots and stereonets showing sample demagnetisation characteristics (displayed in geographic coordinates on the LHS and stratigraphic coordinates on the RHS). C. Intensity-decay plot.

All except a few of the Karaçay gabbros samples display an initial decrease in magnetisation related to a low-coercivity component carrying a magnetisation directed more towards the present-day field direction than the sample ChRM and removed usually by 10mT.

Demagnetisation plots from the SDC on the whole consistently show either single component decay to the origin or a simple decay subsequent to removal of a low-coercivity overprint, with MDFs on average of around 25mT (to nearest 5mT). The demagnetisation plots are sometimes slightly noisy, although this rarely prevents a stable component of magnetisation being identified. The quality of demagnetisation varies even between samples within the same site, with a general correlation between noisier data and lower NRM intensities.

The sites from both cumulates and sheeted dykes within the Karaçay valley all display westerly directed remanences both in geographic and stratigraphic coordinates, with the exception of site KD05 which has an easterly directed remanence. Of the ten sites located within the SDC in the Karaçay valley only this site has a remanence towards the east suggesting that this direction may be anomalous. This is supported by field observations that this site was located in weathered crumbly dykes, whereas the majority of sites were located in fresher exposures. Similarly to the SDC along the coast, remanences from dykes in the Karaçay valley SDC are steep both before and after tilt correction. The mean directions from the cumulate sites are well clustered both before and after tilt correction and have an α_{95} of less than 6.0° in both cases. The mean declination following tilt correction is almost due west.

Two sites within the Karaçay river (the same location as KC01-4) were sampled in discrete dykes with geographic remanences that are indistinguishable from those of the host cumulate rocks. This implies that the same tilt correction should be used for both

lithologies. If the orientation of the discrete dykes is used to apply a correction to the magnetisation, the resulting directions of magnetisation are significantly different to those of cumulate rocks from the other sites within the Karaçay stream section. The cumulate layering in this locality is consistent and appears more likely to give a true palaeosurface. Accordingly the structural data from the cumulate sequence was applied to the dykes, with resulting restored directions of magnetisation that are similar to the other Karaçay sites. If these assumptions are accurate, restoring the orientation of the discrete dykes by using the orientation of the cumulate layering indicates that the dykes were not intruded vertically.

5.7.5 Kisecik (8 sites; cumulate rocks and SDC)

The average NRM intensity for the Kisecik dykes (0.16 A/m) is lower than the average for all SDC samples and the average for the Kisecik cumulate samples (1.76 A/m) is considerably above the average value for all cumulate samples. This may reflect the fact that all of the Kisecik cumulate sites were located in ultramafic cumulates. Demagnetisation data from the cumulate rocks are consistently good, particularly from sites JC01 and JC02. Samples generally display single component behaviours with a smooth decay to the origin. Samples from site JC03 are noisier with large spurious overprint directions removed during the early steps. The majority of samples from within the Kisecik SDC (sites JD01-3) show good quality demagnetisation data with paths that display simple decay to the origin. Occasional low-coercivity components show only slight differences in direction to the ChRM direction and are always removed by 20mT, generally by between 5 and 10mT. Samples from site JD04 are considerably noisier with large spurious overprint directions carried by the low-coercivity fraction. Site JD04 has an easterly remanence (JD04). There is no obvious field observation that would explain this, although this site was taken from a limited exposure of the SDC and so the consistency and orientation of the sheeted dykes were harder to determine.

Sites within the Kisecik valley (except for JD04) again display westerly directed remanences. Directions from three of the four cumulate sites are well clustered. Site JC01 displays a different stratigraphic declination but the structural data collected in the field were unreliable due to the absence of clear cumulate layering. Due to its spatial nearness to the other cumulate sites, the structural correction used was that of the closest neighbouring cumulate site, which would result in some inaccuracy in correction although the structures are similar. Site JC01 did show clear fabric, but when the orientation of this was used to apply a structural correction (section 5.5) the resultant direction was still significantly different from other Kisecik cumulate sites.

The average NRM intensity for the Gulderen samples (1.98 A/m) is above the average for SDC samples. MDFs are around 25mT on average. The demagnetisation data for the Gulderen samples is variable, with samples displaying both a simple decay following removal of a low-coercivity overprint or evidence of an overlap in directions as well as two samples where no direction could be obtained due to noisy data. The site ChRM direction is towards the west in geographic coordinates and towards the SSW in stratigraphic coordinates, with a steeper remanence in both coordinate systems than the average for the palaeohorizontal sites.

5.7.6 Kömürçukuru (5 sites; extrusive rocks)

The average NRM intensity for the Kömürçukuru sites is 0.65 A/m, which is considerably below the average for all lava samples, by a factor of ten, although remains above that for the deeper units of the ophiolite. Demagnetisation data are of consistently high quality, with the exception of a small number of very slightly noisier samples, mostly from site ML02. Most samples show single component decay to the origin; occasional different initial directions carried by low-coercivity minerals are only slightly different in direction

and are removed around 5mT. MDFs are generally around 20mT. The directions for these lava sites are again westerly directed with no exceptions. Inclinations are shallow and become steeper subsequent to tilt correction, although they remain slightly shallower than the average for other palaeohorizontal sites. Declinations show considerable spread within this locality, with the declinations from sites ML01 and ML04 more southerly than those from other localities.

Four out of the five sites were demagnetised from this area. The fifth site sampled was not demagnetised due to a large amount of rain interfering with the accuracy of the 'cork method' (with superglue slippage potentially influencing the orientation data).

5.7.7 Tahtaköprü (5 sites; extrusive rocks)

The average NRM intensity for the Tahtaköprü sites (6.18 A/m) is higher than the average for all lava samples. Most samples demagnetise with single component decay to the origin and MDFs are on average around 15mT (to the nearest 5mT). The low-coercivity components observed in a small number of samples are removed by around 5mT and are similar in direction to the sample ChRMs. Site mean directions are well clustered both before and after tilt correction with generally shallow inclinations (mean of 17.4°) in geographic coordinates towards the west and inclinations slightly higher than the average (mean of 39.3°) for palaeohorizontal sites and towards the SW subsequent to tilt correction. Site TL01 has an α_{95} of 20° and Kappa value of only 12.2, which are less than desirable; however, the remanence direction lies within the cluster of the Tahtaköprü sites and close to that of site TL02, located nearby, and so the results can be used with confidence.

5.8 Grouping of sites

Sites from similar locations within the ophiolite may be put into groups that are logical on the basis of both field evidence and similarities between site ChRMs. No area (e.g. Karaçay valley, Antakya) could be grouped as an entity, indicating that sites were located on smaller tectonic blocks; for example the coastal dykes were separated into three groups. Eleven potential groups of sites were recognised (Table 5.4), and their location is shown on a map with accompanying stereonet displaying the structure and palaeomagnetic directions (Figure 5.9). Most groups contain only a few sites located nearby each other rather than dispersed over a more extensive area. The remaining sites were left ungrouped and generally, the indication is that tectonic rotations between adjacent sites are common and they are thus more appropriately analysed at site level rather than locality level.

Only four of the grouped sites contain sites that have been structurally corrected using palaeohorizontal indicators. When sites are grouped, three sites display a slight statistical worsening in α_{95S} following structural correction: groups JA (13.6° to 17.5°), CA (9.9° to 12.4°) and IA (10.4° to 12.1°). Kappa values improve for structurally corrected groups and are never below 20 for *in situ* data or 30 for structurally-corrected data (except for three groups). The degree of angular dispersion varies from 4.4-17.6° with an average of 9.8°. The expected secular variation for these sites is around 13° and most sites are slightly lower than this. Lower values for the groups containing cumulate sites may indicate some within site averaging of the palaeomagnetic field, and for groups containing extrusive sites lower values may represent a spot reading of the palaeomagnetic field, indicating that sites within the group may be too close in age to adequately average out secular variation. However, the angular dispersion for all groups is sufficiently similar to the 13° expected to be reasonably confident that most variation has been averaged.

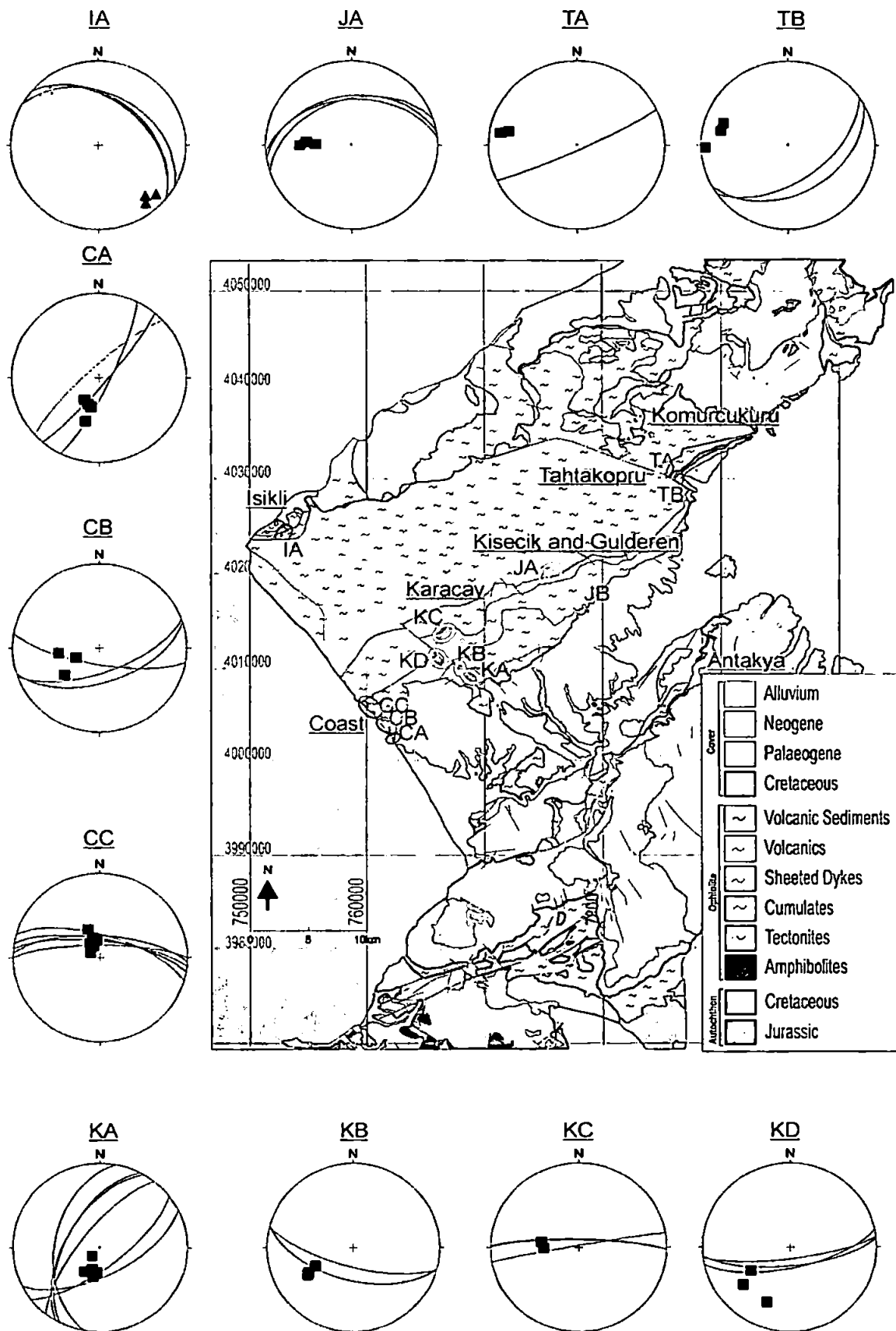


Figure 5.9: Spatial distribution of the eleven groups of palaeomagnetic sites identified. These are grouped according to similar magnetisation directions and lack of structures observed between sites from field observations. The majority of sites cannot be grouped due to the prevalence of differential rotations between sites and are excluded from this diagram. The group names are as described in the text.

<i>Group^A</i>	<i>D_g</i>	<i>I_g</i>	<i>k_g</i>	α_{95g}	<i>D_s</i>	<i>I_s</i>	<i>k_s</i>	α_{95s}	<i>s^D</i>
CA	199.3	58	87.1	9.9	206.4	57.6	56	12.4	14.55
CB	245.7	55.7	34.2	21.4	280.3	53.6	93.9	12.8	10
CC	332.3	73	121.7	6.1	256.9	79.4	161	5.3	11.73
IA	318	14.2	141.5	10.4	303.2	18.1	104.8	12.1	4.36
JA	271.1	47.5	83.2	13.6	302	25.8	50.9	17.5	10.83
KA	199.2	67.8	129.6	5.9	271.6	32.7	150.7	5.5	6.72
KB	240.6	41.5	147.4	7.6	264.7	55.3	197.4	6.6	7.38
KC	260.9	56.8	66.4	15.3	252	55.6	132.3	10.8	8.97
KD	221.6	37	22.3	26.7	233.5	46.6	33.3	21.7	17.59
TA	279.7	18.4	255.3	15.7	226.1	34.5	256.3	15.7	5.64
TB	279.3	16.7	32.2	22.1	256.5	40.9	54.5	16.9	9.45

5.4 A

<i>Group^A</i>	<i>No. Sites</i>	<i>Sites in Group^B</i>	<i>Location^C</i>	<i>Str.</i>	<i>Lat.</i>	<i>Lon.</i>
CA	4	CD01-3; CG01	S	125/81	36.13	35.91
CB	3	CD04-5; CD12	Mid	171/65	36.14	35.91
CC	6	CD06-11	N	008/72	36.16	35.89
IA	3	ID01; ID03-4	E	037/42	36.33	35.82
JA	3	JC02-4	N	349/44	36.29	36.05
KA	6	KC01-4; KD01-2	E	296/59	36.19	35.99
KB	4	KD03-4; KG01-2	W	195/65	36.19	35.98
KC	3	KD08-9; KG03	N	357/84	36.23	35.97
KD	3	KD10-12	W	172/74	36.21	35.96
TA	2	TL01-2	N	155/85	36.39	36.2
TB	3	TL03-5	S	148/46	36.38	36.18

5.4 B

Table 5.4: Palaeomagnetic (5.4A), location and structural data (5.4B) for the eleven identified groups of sites.

^A The locality within which the group is located is clear from the 1st letter of the group name: C = coast; I = Isikli; J = Kisecik; K = Karacy; T = Tahtakopru

^B The lithologies within the group are apparent from the 2nd letter of the site names: D = dykes; G = gabbros; C = cumulate rocks; L = lavas

^C Refers to the location of the smaller group in relation to the other sites within that locality.

^D The angular variation between sites within the group ($s = 81/k$); gives an indication of the degree to which secular variation is averaged out within the group.

The sites along the coast have been divided into three groups, from CA in the south to CC in the north, (Figure 5.10) according to similarities in magnetisation between sites within a group with corresponding changes in either dyke strike (between groups CA and CB) or dyke dip direction (between groups CB and CC). The boundaries between these groups were noted in the field to comprise areas of gullies and/or landslip indicating the presence of large faults and so supporting the inference that the three groups in the dykes are located within different tectonic blocks. The coastal cumulates do not fall into a group as their magnetisation is not sufficiently similar in either geographic or stratigraphic coordinates to justify inclusion in the northerly dyke group or to comprise a separate group. The coastal groups have angular dispersions close to the 13° value expected from secular variation.

Only three of the cumulate sites from the eight sampling sites within the Kisecik valley comprise a valid group, with the remaining Kisecik sites inappropriate to group. The three cumulate sites located on the same side of the valley have similar directions of magnetisation with no obvious major structures separating them in the field. Sites from within the Karaçay locality can be grouped into four different groups, with the largest group comprising six sites (four cumulate sites and two sites in discrete dykes). This group is located along the Karaçay river near Kemer Köprü and no large-scale structures were observed to separate the structures in the field. A second group comprises two sites from the SDC and two sites from gabbros screens located between dykes of the SDC sites. The remaining groups both contain two and three sites from within the SDC from towards the north of the Karaçay locality. The four groups (Figure 5.9) are distributed throughout the length of the Karaçay valley. Three of the four Isikli dyke sites comprise a group, with the remaining dyke site located on the opposite side of Isikli village to the other sites and with a high likelihood of differential rotations between these areas.

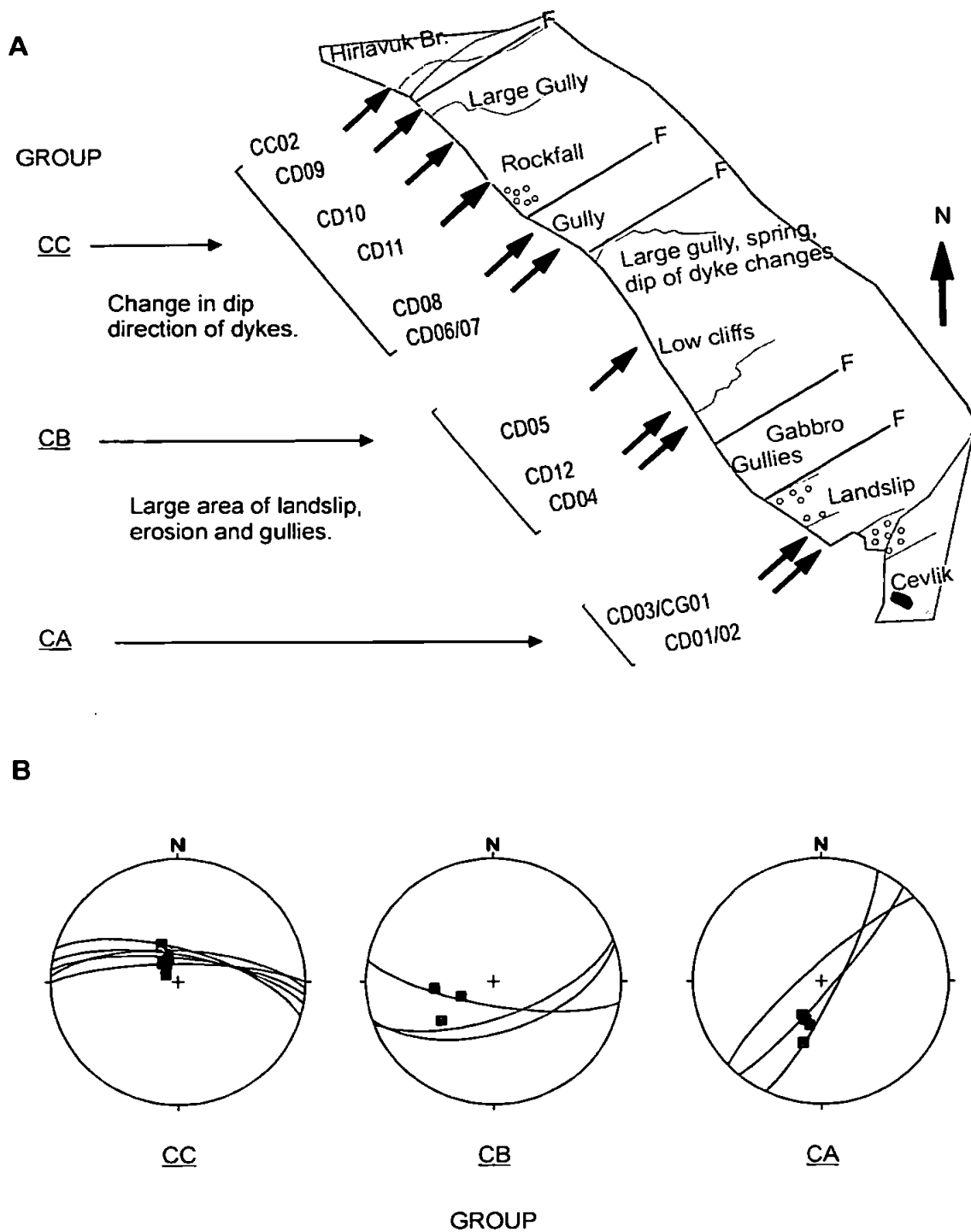


Figure 5.10: Groups identified and basis for grouping of sites within the coastal exposures. Field observations and structural data, such as measurements of dykes margins and fault orientations, were used in combination with remanence data to divide sites into groups where appropriate with the SDC along the coast illustrated below as an example.

A. A map to show the field basis of the division into three groups within the coastal SDC.

B. The geographic magnetic remanence (grey squares) and structural data displayed on stereonet for the three groups identified, showing the basis for division on similarities between remanences.

The only lava sites from the ophiolite that were grouped come from the Tahtaköprü locality (two groups). The sites within both groups are located close to each other and both groups have a low angular dispersion implying that secular variation has not been averaged out. Grouping all lava sites from any locality is necessary in order for the angular dispersion to be in the region of 13° , but this results in such large errors in α_{95} and Kappa values that these groupings would be inappropriate.

Figure 5.11 summarises the results from all groups, with the directions restricted to those groups where sites have palaeohorizontal indicators shown separately. It is generally more appropriate to analyse the data at site-level rather than locality level due to the clear prevalence of differential rotations between sites making it impossible to group a large proportion of sites within the ophiolite.

5.9 Summary of results

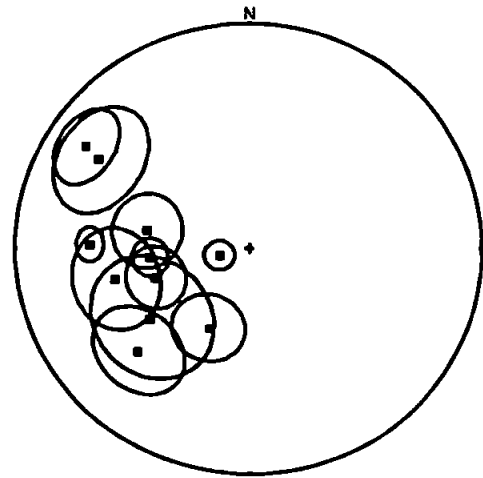
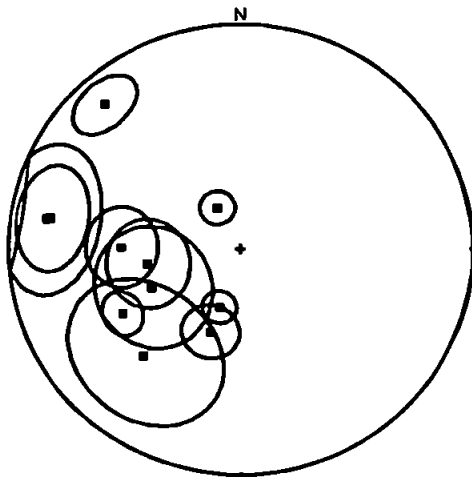
5.9.1 Results from sites with palaeohorizontal control

There are 26 sites with palaeohorizontal control and remanences are without exception towards the west, both in geographic and stratigraphic coordinates (Figure 5.12). Following tilt correction, the directions become spread (between around 250° to 315°) around a small circle centred on an inclination of 32° , with an increase in clustering of the inclinations. Subsequent to tilt correction, the average remanence is almost due west. Thirteen of the sites with palaeohorizontal control are from the extrusives; however four of these sites were located to the southeast of Antakya and are believed to be separated from the main massif. The other 13 sites are either cumulate gabbros or discrete dykes located within the cumulate gabbros and so the structure from the adjacent cumulate sequence has been used as the correction.

Geographic coordinates

Stratigraphic coordinates

A



B

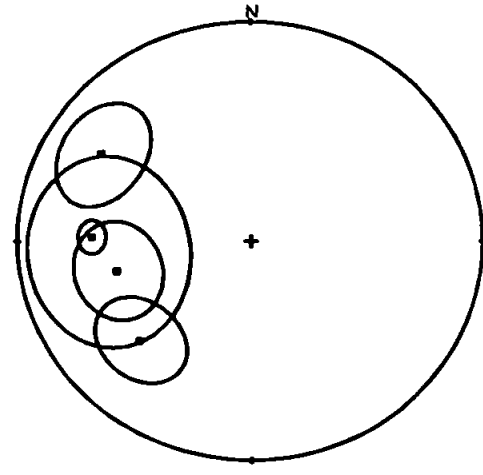
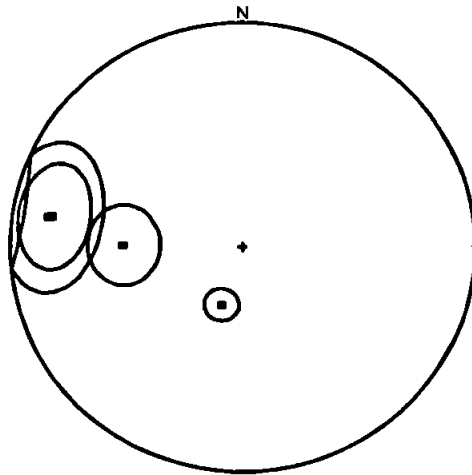


Figure 5.11: Stereonets illustrating the mean remanence magnetisation directions for the eleven groups identified. Error circles are displayed and all directions are in the lower hemisphere. A. Directions for all groups. The mean direction for one group (IA) containing the reversely magnetised Isikli dykes has been antipoded. B. Directions for the four groups where the sites included had palaeohorizontal indicators on structural data.

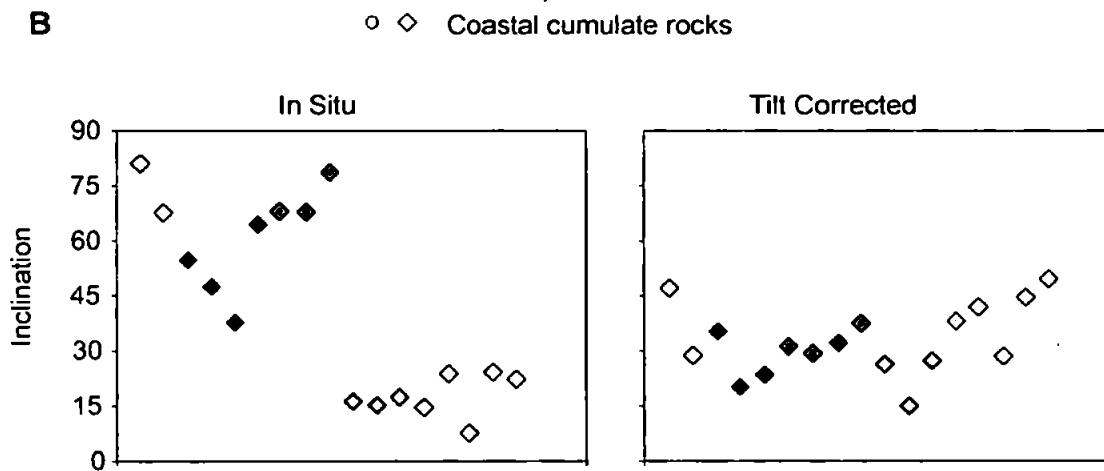
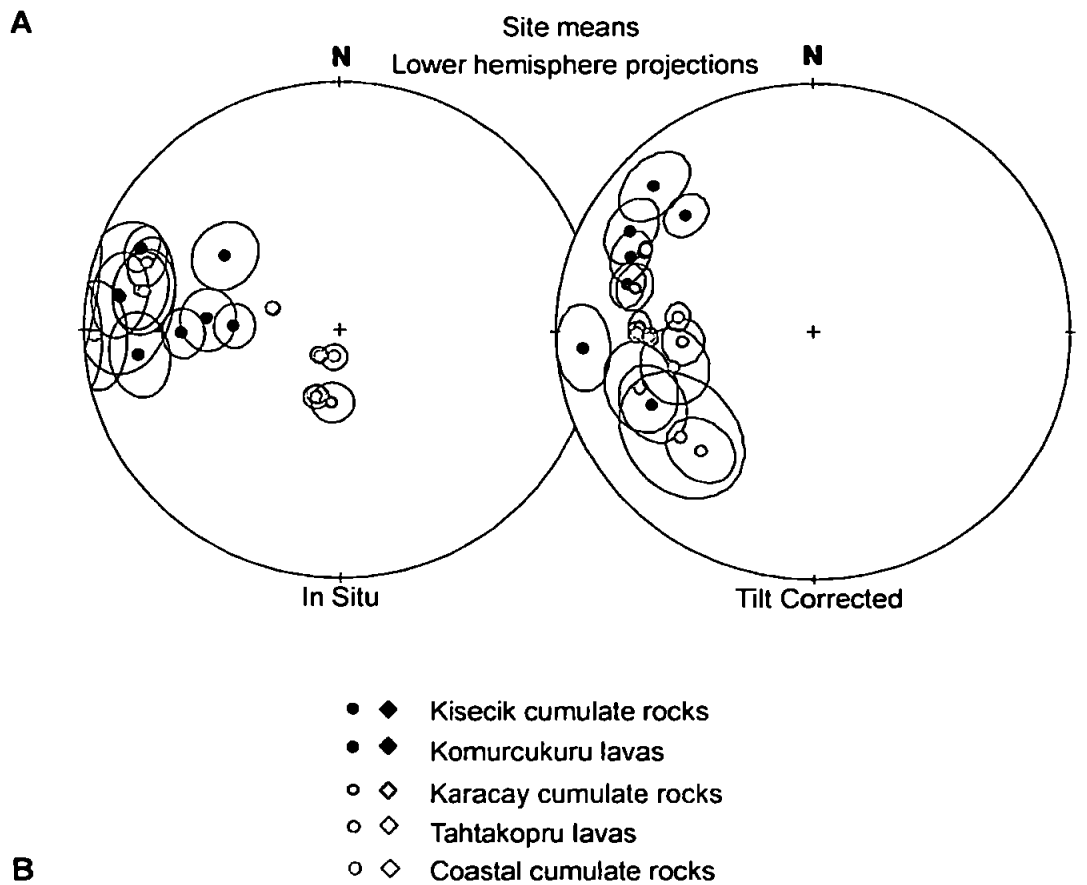


Figure 5.12: Summary of magnetic remanence directions from sites with palaeohorizontal control on the structural corrections applied, excluding those from Antakya (lavas with unknown relationship to main massif) and the one cumulate site with a large error.

A. Stereonets displaying the site means for all sites with palaeohorizontal controls on orientation. Different shades of colour are used for sites within the same area.

B. Improvement of clustering in inclinations upon application of a structural correction.

Of the 26 sites, six have been excluded from the final directional analyses, four due to a location separate from the main ophiolitic massif and two due to the dubious quality of the palaeomagnetic data. Of the cumulate and discrete dyke sites, one site (KC05) has anomalously high intensities that decay rapidly upon demagnetisation, suggesting the possibility of isothermal remanence imparted during a lightning strike. Another site (JC01) has an α_{95} value greater than 20° , and is excluded from the final analysis. If these two sites are excluded from the analysis of the sites with palaeohorizontal control, the results are not significantly affected, although the clustering is slightly improved, especially for the declinations.

The mean remanence for the ophiolite is worked out from the palaeohorizontal sites in order to eliminate the effect of dyke-normal rotations. However, the reversely magnetised Isikli dyke sites (section 5.7.3) fall within the palaeohorizontal grouping and it is appropriate to include these in the determination of the mean direction for the ophiolite. The mean direction for the Hatay ophiolite calculated from 20 sites with palaeohorizontal control and four Isikli dyke sites has a declination of 274° and an inclination of 34° .

5.9.2 Results from sites with palaeovertical control

The sites with palaeovertical control required a different approach to the analysis. Sites with palaeovertical control were located within five different areas of the SDC (Coast, Isikli, Gulderen, Kisecik and Karaçay) and were either dykes or gabbro screens. The necessity for a more sophisticated analytical technique is due to the inability of the standard method of analysis to pick up rotations about dyke normal axes.

From standard analyses, it is clear that these sites with palaeovertical control in geographic coordinates have westerly directed remanences that are not related to the present day field

or to the direction expected for rocks from this locality in the Cretaceous, similar to those measured for sites with palaeohorizontal control. However, following tilt correction, many of these sites with palaeovertical control display steep inclinations that do not correct to the average $\sim 32^\circ$ inclination expected for rocks from this locality (from comparison with the average inclinations from the Troodos ophiolite and the similar values predicted from APWPs), whereas the inclinations for sites with palaeohorizontal control are observed to correct to an average of 32° . Differences in the rock magnetic characteristics between the SDC (palaeovertical control) and deeper levels and extrusives (palaeohorizontal control) cannot explain these differences i.e. there is no basis for magnetisation at contrasting times. The geographic magnetisation direction of the sheeted dykes and the gabbro screens at the base of the SDC within the same site is indistinguishable even though there are slight differences in the magnetic mineralogy identified from rock magnetic experiments. From the rock magnetic analysis (Chapter Seven) the mineralogy of the gabbros at the base of the SDC and that of the deeper cumulate gabbros was found to be similar implying that there is no magnetic mineralogical basis for the observed difference in inclinations between these units. The similarity between the consistent westerly directed declinations in both geographic and stratigraphic coordinates also suggests that there is no palaeomagnetic reason for the inclination differences. Both the shallower extrusives and the deeper cumulate levels display indistinguishable average stratigraphic inclinations and it is geologically difficult to construct a model whereby the SDC could act as an entirely separate entity to both upper and lower crustal lithologies (i.e. selective remagnetisation or a rotation affecting only the SDC). Rotations about a dyke-normal axis however, may account for the steepening of the inclinations.

Not all of the SDC localities displayed steep remanences when standard tilt corrections were applied. The Kisecik dykes are an exception, with tilt corrected magnetisation of dykes from this region, within error, the same as that for the ultramafic cumulates from this

locality (section 5.7.5); the corrected remanence directions lie roughly along a small circle centred on 27°. The reversely magnetised dykes from the Isikli area are another exception as these dykes have shallow stratigraphic inclinations that are similar to those observed for sites with palaeohorizontal control (section 5.7.3). The average orientation of dyke strikes in these two localities is around NW-SE, which contrasts to the average E-W strike of the more extensive SDC outcrops along the coast and in the Karaçay valley. Restoring the westerly directed declinations back to the expected northerly direction of magnetisation would result in restoration of the present-day dyke strikes to a more N-S orientation. These points are discussed further in section 5.10 where the results and implications of more extensive analysis of the SDC are discussed.

5.9.3 Reversely magnetised sites

The majority of ophiolitic sites were normally magnetised with only sites from the Antakya lavas (AL01-4), Isikli Dykes (ID01-4) and one dyke site from Kisecik (JD03) having negative inclinations in geographic coordinates. The Antakya lavas have negative inclinations in geographic coordinates, but display normal components of magnetisation upon structural correction. However, the directions for these lavas do not display much similarity with the palaeohorizontal sites. As the relationship between these lavas and the rest of the ophiolite is uncertain, this adds support to the suggestion that they are geologically distinct. The directions from the two pillow lava sites display most similarity with the palaeohorizontal sites from the main body of the ophiolite, although fall at the southern end of the spread of data with structurally corrected inclinations that are shallower than average (α_{95} of 18° and 22.1°).

Antipoding the Isikli dykes (section 5.7.3) results in directions displaying similarity with those of the palaeohorizontal sites. These sites comprise part of the ophiolite that has

experienced less anticlockwise rotation than the average. The Isikli dykes have shallower dips than dykes in other areas of the SDC, such as along the coast, but their strikes are not dissimilar and they are geologically indistinguishable. The rock magnetic results (Chapter Seven) did not highlight any rock magnetic explanation for the differences in polarity between different areas of the ophiolite (e.g. between the reversely magnetised Isikli SDC and normally magnetised coastal SDC) and the negative inclinations are thus likely to represent magnetisation acquisition in a time of reversed-polarity for this part of the ophiolite. The direction for the single Kisecik dyke locality that displays a negative inclination is quite different to the mean direction for the Kisecik cumulates and two of the Kisecik dyke sites. There is a second dyke site (spurious) that also displays an anomalous direction. The different directions for these sites may result from noisier data (most likely) or a systematic sampling error (section 5.7.5).

5.9.4 Low coercivity (LC) components

Many samples were single component and demagnetised cleanly to the origin. For those samples where more than one component was observed, the lower coercive components as well as the ChRM in the sample were identified from directional analysis and labelled as low coercivity (LC), medium coercivity (MC) or high coercivity (HC). The LC and MC components could then be analysed separately. On a stereonet, LC components are widely distributed and the likelihood is that many of these components are displaying spurious laboratory induced remanences rather than geologically relevant remanences (Figure 5.13A). However, there is a clustering of LC components for certain sites towards the direction of the present-day magnetic field and it seems likely that for these sites, the LC components have been remagnetised in the direction of a recent geomagnetic field, as illustrated by site CD02 from the coastal SDC (Figure 5.13B). MC components are rare and display spurious directions.

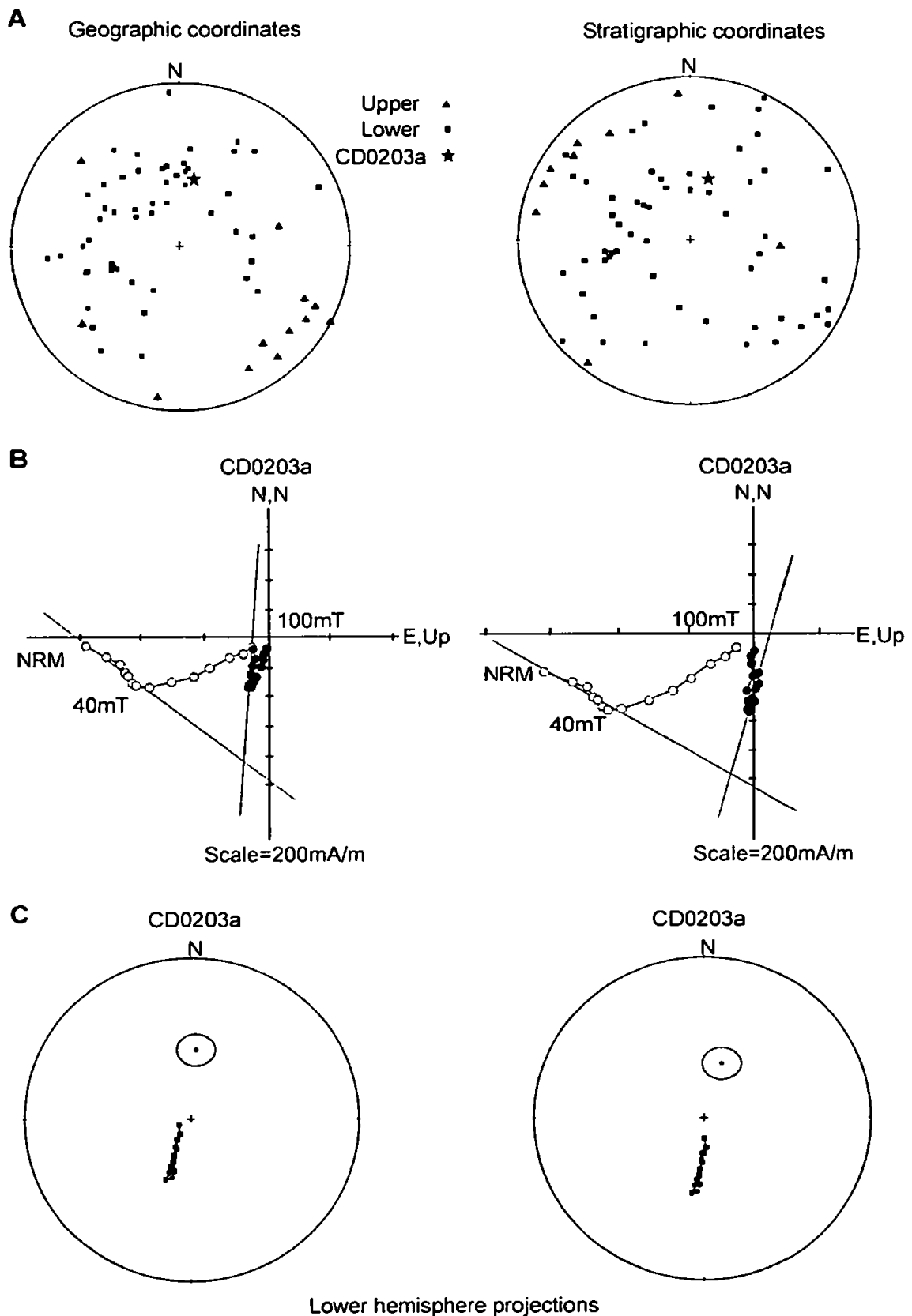


Figure 5.13: Low coercivity components of magnetisation (geographic coordinates on the LHS and stratigraphic coordinates on the RHS).

A. Stereonets displaying the low coercivity components of all sites measured, illustrating the large dispersion in directions.

B-C. Demagnetisation plots and stereonet from sample CD0203a illustrate a low coercivity component representing an overprint by the present-day magnetic field. The best fitting line has been drawn through the low coercivity component on the demagnetisation plots and this direction is also displayed on the stereonet.

5.9.5 Magnetisation of different dyke populations and gabbro screens

The sites along the coast were sampled within the SDC from both brown (later) and grey (earlier) dyke populations; these age relationships were established by analysis of chilled margins. Sites KD06 and KD07 in the Karaçay valley were also drilled in grey and brown dykes respectively. The magnetisations within these two sequences of dykes are indistinguishable (Figure 5.14). Therefore, the results from these dykes do not require separate treatment during analysis. Sites were also drilled in a combination of gabbro screens and sheeted dykes near the base of the SDC, both along the coast (sites CD01-3 and CG01) and within the Karaçay valley (Ikiz Köprü sites). Again, the directions of magnetisation obtained for these different lithologies are indistinguishable (Figure 5.14).

5.10 Timing of magnetisation acquisition (tilt tests)

An inclination-only tilt test was performed on 18 sites, with the results shown in Table 5.5 and Figure 5.15. The tilt test was confined to palaeohorizontal sites due to the possibility of rotations about dyke-normal axes in the SDC resulting in inclination anomalies (as discussed in section 5.8.2 and the analysis presented below). The 95% confidence limits straddle 100% of untilting which is a positive result implying that the sediments have not been remagnetised and indicates acquisition of remanence prior to deformation, with the precision parameter sufficiently high to be confident of a positive result (Enkin and Watson 1996).

	<i>Number of sites included</i>	<i>Inclination \hat{I}^A</i>	<i>Precision parameter $\hat{\kappa}^B$</i>	<i>95% confidence limits</i>
<i>In situ</i>	18	50.1° ^{+29.4°/-15.9°}	4	
Tilt-corrected	18	31.6° ^{±4.6°}	33.2	91-101.2%

Table 5.5: Results of the inclination-only tilt test formulation of Enkin and Watson (1996).

^A The maximum likelihood estimate of the true mean inclination in degrees.

^B The Fisher precision parameter.

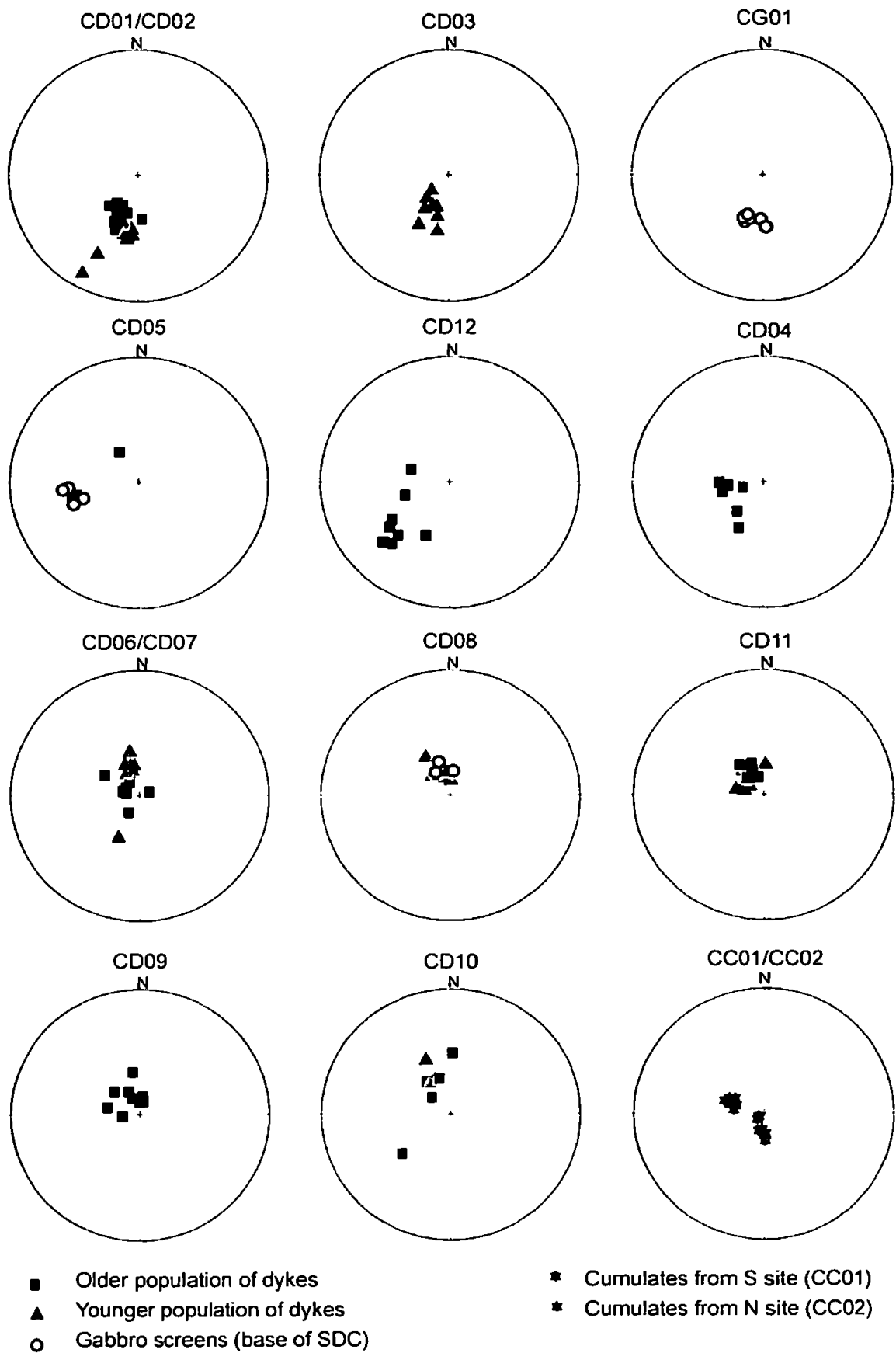


Figure 5.14: Sample level characteristic remanent magnetisation directions in geographic coordinates for all coastal sites. It can be seen that the directions in the two populations of dykes (older in squares and younger as triangles) and also the gabbro screens (circles) are indistinguishable, implying that the magnetisation of all lithologies was acquired at a similar time. The in-situ directions for the two coastal cumulate sites are also shown (stars).

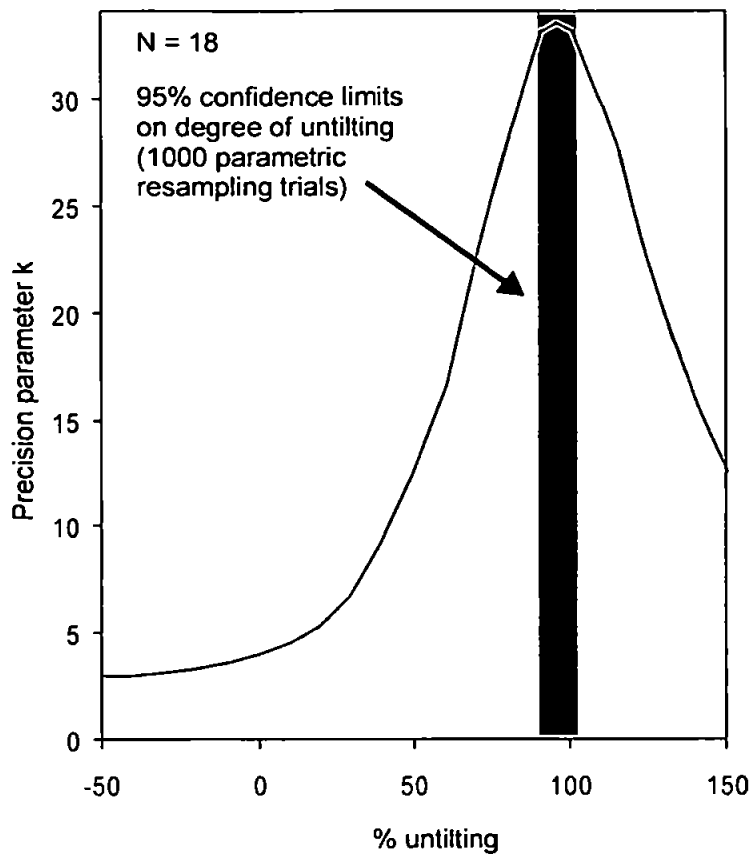


Figure 5.15: Results of an inclination-only tilt test performed on all palaeohorizontal sites within the ophiolite (after Enkin and Watson 1996).

5.11 Analysis of the sheeted dyke complex

Due to potential rotations about a non-vertical axis, it is possible that standard palaeomagnetic analytical techniques do not fully constrain the rotations experienced by the SDC (section 3.5.6 and 4.5.3), and analysis of the SDC can be aided by more sophisticated analytical techniques such as the net tectonic rotation method (section 5.10.1) or by restoring inclinations to a reference value (section 5.10.2). The timing of the rotations identified from these methods and their relation to the results of the structural analyses of this thesis will be discussed in section 8.10.

5.11.1 Net tectonic rotation analysis method

There are several assumptions inherent in using the net tectonic analysis method (Allerton and Vine 1987; section 3.5.6):-

- 1) There has been little internal deformation during the rotation history and so the angle between the dyke margin and the remanent magnetic vector remains constant.
- 2) The observed stable remanent magnetisation was acquired prior to any structural deformation.
- 3) An average representative magnetisation vector for the local area can be found that represents the geomagnetic field direction at the time the magnetisation was acquired.
- 4) The dykes are intruded vertically.

The Hatay ophiolite displays little internal deformation within individual dykes and so the first assumption appears reasonable. Rock magnetic results from this thesis (Chapter Seven) and the positive tilt test from the palaeohorizontal sites are compatible with acquisition of remanences whilst on the seafloor soon after genesis at a spreading ridge, providing a reasonable basis for the second assumption. An appropriate geomagnetic reference direction may be found from the Late Cretaceous part of the APWP for Africa (third assumption). The SDC in Hatay contains a high percentage of dykes over an extensive section and so it is appropriate to assume that the dykes were originally near-vertical, so satisfying the last assumption.

The results from the net tectonic analysis method were analysed at site level. Net rotation angles and poles and the initial dyke strikes shown are grouped into localities on Figure 5.16. The results for the potential anticlockwise rotations rather than the potential clockwise rotations have been displayed as these are geologically more realistic because they require smaller rotations on average.

For the sites located along the coast, the net tectonic analysis method shows that the original orientation of dykes would have been N-S striking on average and rotation poles are near-vertical and located in the NE quadrant of a stereonet, with a good clustering of poles. There is a significant variation in the initial strike of the dykes from NW to NE and the rotation angles vary from 60° to 180°. The results from the one gabbro site from the coast plot in the centre of the sheeted dyke site results.

The rotation angles from both sheeted dyke and gabbro sites in the Karaçay valley peak between 110° to 130°. The rotation poles are steep and dip to the SE. The restored strike of the dykes is extremely diverse, from WNW through north to ENE. One Karaçay dyke site had a large error in α_{95} and this single site therefore accounts for much of the resulting variability in the net tectonic rotation pole axes and dyke strikes. The average restored dyke strike for the Karaçay SDC is again N-S and the two sites from the discrete dykes within the cumulate ultramafics also have dyke strikes clustering around N-S.

The Isikli dykes were reversely magnetised and the remanences for the net tectonic analysis were antipoded prior to the analysis. If the reverse magnetisation of the site is assumed to indicate a reverse polarity, it is appropriate to antipode the magnetic remanence prior to performing a net tectonic rotation analysis. However, if the reverse direction is due to rotation, antipoding the site would be inaccurate and the direction should not be antipoded in order for the rotations that resulted in the negative inclination to be established. The rotation poles from the antipoded Isikli dykes are shallower than for other localities and located in the NW quadrant of the stereonet, with rotation angles varying between 80° and 120°. The mean restored dyke strike is N-S. Only one site was analysed from the Gulderen valley with a similar rotation pole to the Isikli dykes but considerably larger rotation angles and a more NNE strike of the restored dykes.

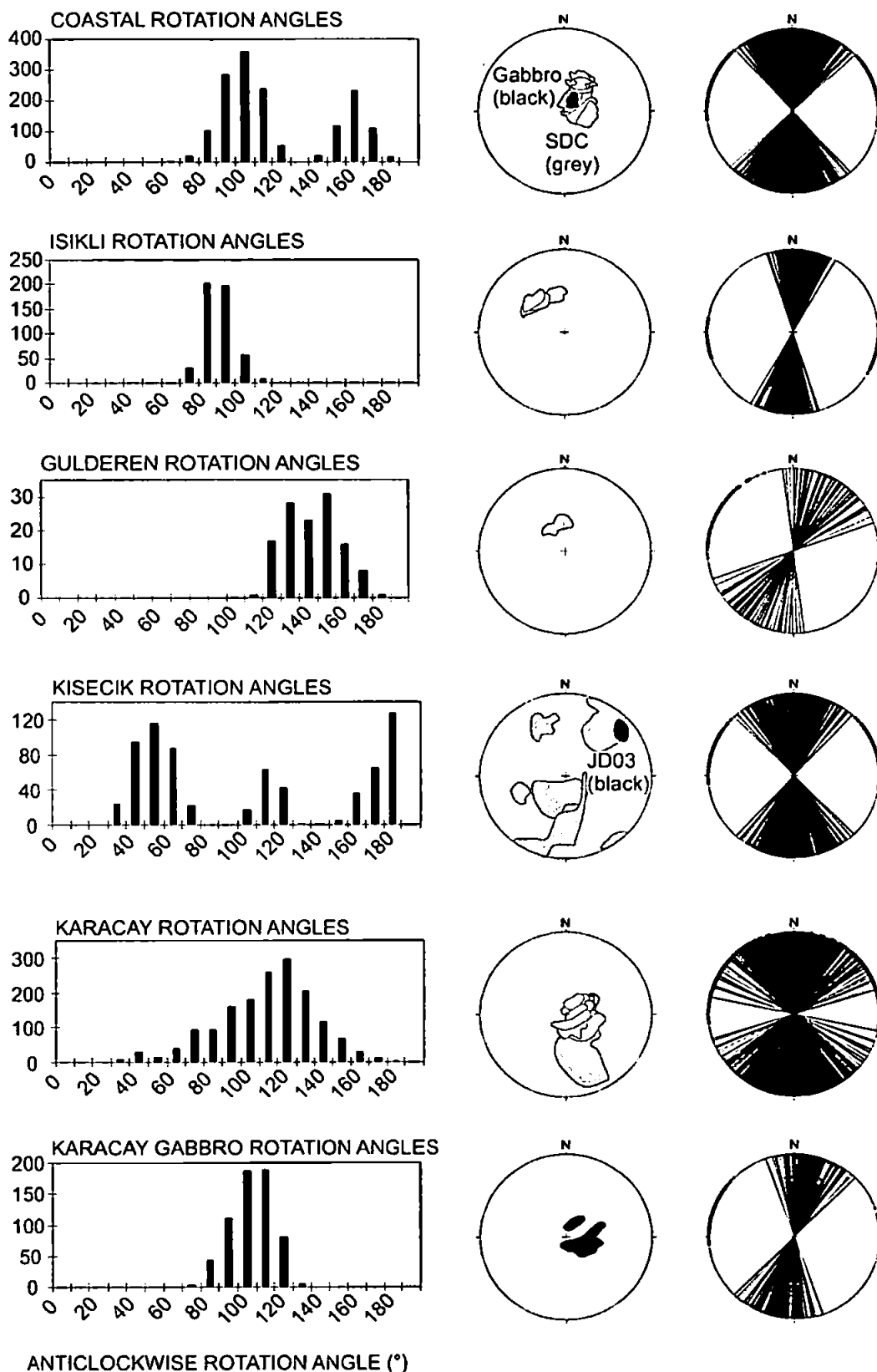


Figure 5.16: Results of net tectonic rotation analysis performed on site-level directions and with an allowance for error in both magnetic remanences and structural measurements incorporated (see section 3.5.5 for description of method) with the results displayed in localities. The sites from Isikli and site JD03 from the Kisecik valley were assumed to be of reverse polarity with magnetic directions antipoded prior to analysis. The histograms on the left illustrate the magnitude of rotation (x-axis) against frequency. The shaded regions on the central stereonets enclose the orientations of the net tectonic rotation poles for each site (dykes in grey and gabbros in black). The larger shaded regions are from those sites where the magnetic remanences are more poorly constrained. The stereonets to the right indicate the restored orientations of the dykes for each locality (the dots represent the poles to the dyke margins).

The results from the four dyke sites from the Kisecik valley are variable, both in rotation pole and rotation angle, although the restored dyke strikes are again on average N-S. As discussed previously, one of the Kisecik dyke sites had a different remanence direction to the rest of the locality, so this may explain some of the degree of variability in the net tectonic analysis results. Another Kisecik site was reversely magnetised and the remanence direction was antipoded prior to the analysis.

In general, all of the net tectonic rotation poles are steep, as expected from the results from the westerly directed remanences and the results from the palaeohorizontal sites indicating the possibility of large anticlockwise vertical axis rotations. The results can be discussed in two groups; firstly the data from the coastal sites and the Karaçay and Gulderen valleys where the remanences are steep in both geographic and stratigraphic coordinates, and secondly the sites where steep remanences are not observed. Although there are differences in rotation pole and angles between these groups, analysis of all dyke sites consistently returns an on-average N-S orientation for the original dyke strike.

The rotation poles from the coastal and Karaçay localities are mostly sub-vertical. Poles for the coastal sites lie within the NE quadrant of the stereonet and poles for the Karaçay sites lie just to the east of vertical. The present-day strike of dykes in both of these localities is E-W, and neither the dyke strike nor the orientation of the rotation poles appear to have a link with the SE directed emplacement direction of the ophiolite (as was observed for dyke-normal rotations in the Baër-Bassit ophiolite; section 4.5.3). A structural event producing tilt about a N-S horizontal axis would account for dyke-normal rotations, or alternatively the rotations may be composite in origin.

The rotation poles for the Isikli dykes are shallower towards the NW, and roughly parallel with the present-day trend of the dykes in this locality, as are the results from one of the two Kisecik dyke sites where the quality of data is good (section 5.7.5), with the other

lying in the same orientation but dipping to the SE. The SDC in both the Kisecik and Isikli localities strikes roughly NW-SE (rather than E-W as along the coast and in the Karaçay valley). These dykes have remanences that are similar to those obtained from the sites with palaeohorizontal control and have not necessarily therefore experienced rotation about a dyke normal axis that was not picked up by the standard palaeomagnetic analyses. Therefore, the outcome that net rotation has occurred about a dyke-parallel rather than a dyke-normal axis and could thus be identified by standard analyses ties in with the observation that dykes in this area do not display ambiguous magnetic inclinations. It is also consistent with a tectonic history that does not involve significant rotations about dyke-normal axes.

The key point in terms of dyke-normal rotations is that the amounts of rotation around dyke-normal axes required to explain the palaeomagnetic data are small compared to the large bulk rotation of the ophiolite demonstrated by results from the palaeohorizontal sites. Therefore, this analysis effectively hides these dyke normal components within the very large net rotations found. The deviations of the net tectonic rotation poles from the vertical result from the components of non-vertical axis rotations. Thus, although this method is useful it can also be helpful to break down the net rotations into components.

5.11.2 'Inclination restoration to a reference' method

The net tectonic analysis finds the net rotation about a single axis for a dyke site. In a region where complex deformations may be expected, it can be more useful to consider both net tectonic rotations and to break the rotation down into rotations about a vertical axis and rotations about a horizontal axis (i.e. similar to a standard tilt correction). The net tectonic analysis method forces the remanence magnetisation back to a reference direction (for example the Cretaceous palaeofield direction or the mean direction of all the sites). It

may be more insightful in certain circumstances to have less constraint on the expected magnetisation and simply find a rotation that will return the observed magnetisation to the inclination expected from averaging all the sites but not force the declination to a reference value. A method of doing this using a stereographic projection is described by Morris and Anderson (2002). Here the assumption is made that the initial inclination vector of the dykes is the same as the pre-deformational stratigraphic inclination, which in the case of Hatay would be 32° as observed for the sites with palaeohorizontal control. The pole to the dyke orientation is plotted as well as the *in situ* remanence magnetisation of the site. Solutions are found that take the dyke pole to the horizontal as well as the remanence to a small circle centred on a vertical axis and connecting points at a 32° inclination. This method returns the horizontal axis rotations that can account for the deviation of remanence inclination from the expected value and the non-verticality of the dykes.

This method was used to evaluate the coastal groups CA, CB and CC, using mean remanences and dyke poles. The results are that CA would need to experience 29° of clockwise rotation about a horizontal axis trending 318° , CB would require a 34° clockwise rotation about a horizontal axis trending 034° and CC would require 50° of clockwise rotation about a horizontal axis trending 353° . These rotations may or may not have occurred during a single event, but it is more likely that they represent composite tilts accommodated during a number of faulting events, particularly when considering the large magnitude of the 50° rotation suggested for group C.

5.12 Analysis of the extrusive sequence

In measuring structural data for the pillow lava sites, the assumption was made that the lavas are extruded on a horizontal surface, and the 'palaeohorizontal' measured is used to correct the lavas to the horizontal. However, it is known that it is possible for lavas to be

extruded onto steeper slopes and indeed this is common. Lavas on the seafloor may also be extruded into hollows or accommodation space created by faults operating syn-emplacement which also may give rise to false palaeohizontals. However, these palaeoslopes are unlikely to be steeper than 30° and are most likely to be significantly shallower than this. Some measurement error is also anticipated due to the difficulty of determining precisely the mean orientation of a section of pillow lavas.

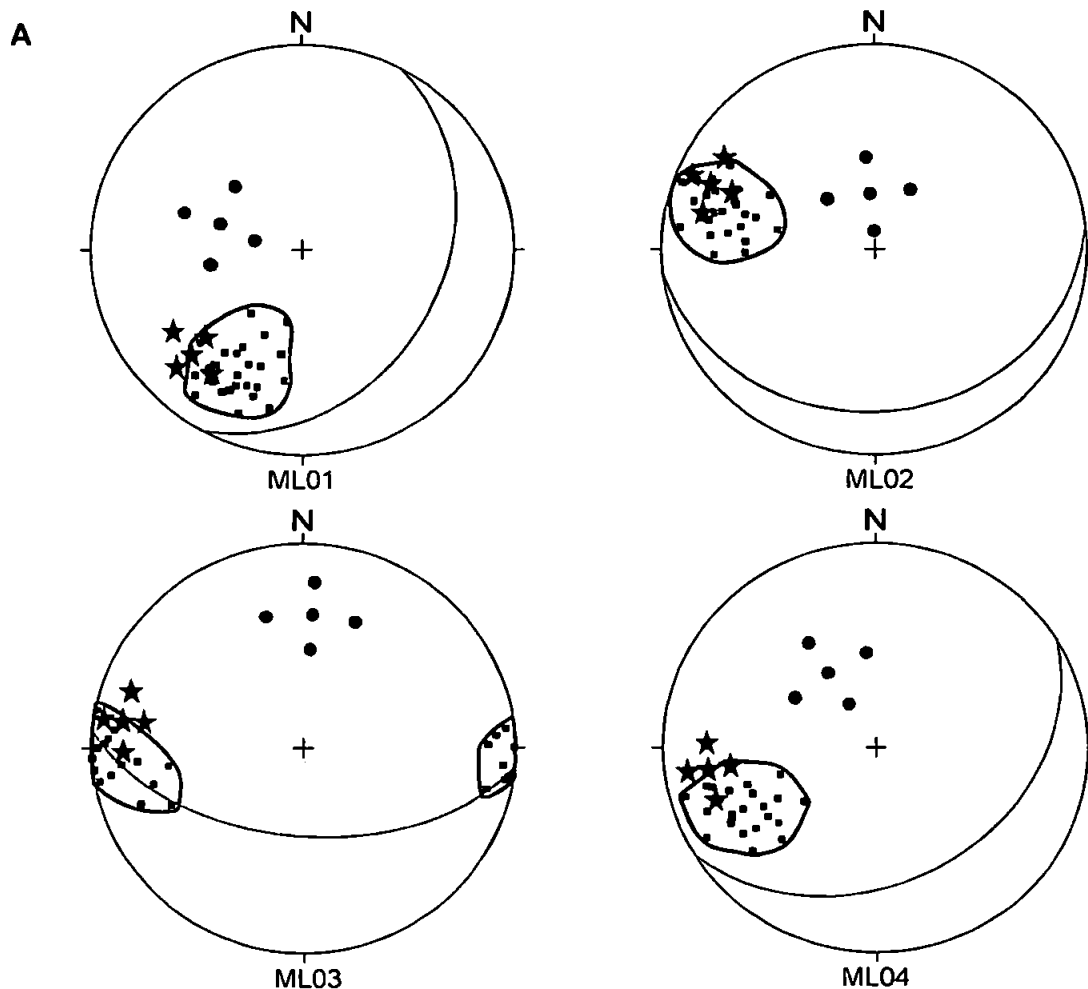
To investigate the effects of these errors, a method of building in cones of error around the structural data and mean site remanence before applying a correction was applied. A 15° error for the structural data and a 10° error around the site mean remanence data were chosen as appropriate. The site mean remanence and pole to the structure (in this case the palaeohorizontal obtained from the average flattening direction of pillow lavas) were plotted on a stereonet. Four points were plotted at 10° distance from the mean remanence point on the stereonet, defining the 'corners' of the cone of confidence around the mean remanence. Similarly, four points were plotted at 15° distance from the pole to the structure on the stereonet, defining the 'corners' of the slightly larger cone of confidence around the structural data. The orientation of each 'corner' point around the structural pole was recorded, as well as the orientation of the horizontal axis of rotation that would take the mean pole and each 'corner' pole back to the vertical. The orientation of the mean remanence and each 'corner' to the cone of confidence around the remanence direction was also recorded. This results in five possible poles to the structure, each with a corresponding (horizontal axis) rotation pole and five possible remanence directions. These data were then input into an excel spreadsheet with formulae allowing rotation of each remanence point about each rotation pole, with 25 possible solutions produced for the original remanences. These could then be plotted on a stereonet with the boundary of the points defining the envelope of confidence around the original remanence direction.

To illustrate the method, the four sites from the K m r kuru pillow lavas were chosen (Figure 5.17A). The result is a larger possible distribution for the tilt-corrected remanence directions. The palaeohorizontals measured for these sites vary from a present-day dip of 22° to 55°, with strikes varying from NNW-SSE to E-W. Remanences prior to structural correction are all westerly directed and shallow. By using the inclination restoration method the initial bounds to the potential magnetisation direction defined by the four ‘corners’ become considerably more spread out. From Figure 5.17B, it can be seen that, within error, differences in the magnetisation of sites ML02-3 following structural corrections are insignificant, particularly when incorporating into this the effect of secular variation. The circle defining the potential corrected magnetic remanence for site ML01 only overlaps with that of site ML04, and thus may represent a real tectonic rotation between this site and ML02-3 (\pm ML04). This is supported by the fact that site ML01 was located in the centre of K m kuru village (in the school yard), at a distance from the remaining three K m kuru lava sites, which were spread out along the road to the north of the village and comparatively spatially near to each other.

5.13 Discussion

5.13.1 Implications of westerly remanences

The westerly directed remanences are similar to those previously documented in the coeval Troodos and Ba r-Bassit ophiolites (Moores and Vine 1971; Clube and Robertson 1986; Morris et al. 2002). The magnitudes of rotations in the Ba r-Bassit ophiolite are similar in the north and increase towards the south, probably due to the effect of later post-emplacement Neotectonic strike-slip faulting (Morris et al. 2002). The inclinations observed in all three ophiolite massifs would be expected to be similar assuming that the ophiolites had formed at similar times and in a similar palaeogeographic location.



- Pole to palaeohorizontal (centre circle) and 15 degree errors (4 'corner' circles)
- ★ In-situ remanence (centre star) and 10 degree error (4 'corner' stars)
- Structurally corrected solutions with and error band around distribution

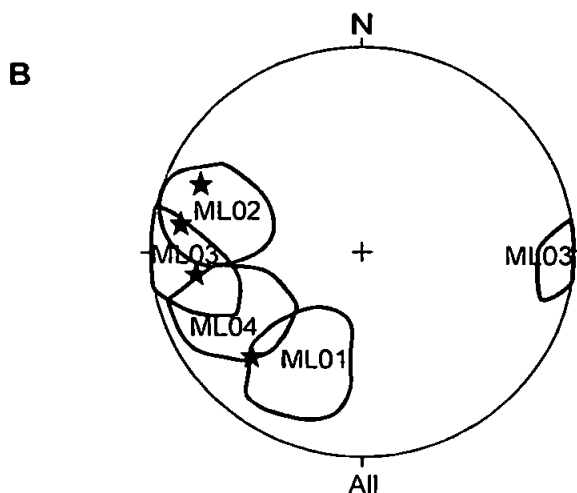


Figure 5.17: Illustration of the effect of potential errors in measurement of pillow lavas propagating through analysis procedures, using the Komurcukuru pillow lavas as an example.

A. Illustration of the method, as described in the text. 15 degree error on the measurement of the palaeohorizontal (pole to palaeohorizontal shown by grey circles) and 10 degree error on the determination of the ChRM (black stars) are assumed, with a band drawn around the possible directions when incorporating these errors (black squares and line).

B. Geographic remanence (without corner errors for clarity) shown for each lava site with bands drawn around the possible directions for the structurally-corrected remanence that would result from the discussed allowance for errors and using the method illustrated above.

However, declinations would only be expected to be similar if the ophiolites had all undergone a similar rotation history. The well documented rotation of the Troodos microplate (section 4.4.3) was previously believed to be constrained to a small area not much more aerially extensive than the massif. This idea was supported by the similarity between the average *original* dyke orientation in Troodos (~E-W) and the similar *present-day* average strike of the Hatay and Baër-Bassit SDCs (~E-W and more NW-SE respectively) which was believed to imply that these more easterly massifs are unrotated.

The new palaeomagnetic results from the Hatay ophiolite show that layered gabbros, massive and pillowed lava flows of the main ophiolite share a common tilt corrected inclination with declinations strung out along a partial small circle through this inclination. The mean direction of Dec = 274°, Inc = 34° is indistinguishable from that commonly reported for non-transform tectonised parts of the Troodos ophiolite, with Dec = 276°, Inc = 32° reported by Vine and Moores (1969) and Dec = 274°, Inc = 36° by Clube and Robertson (1986) and from the northern part of the Baër-Bassit ophiolite (Morris et al. 2002). The identification of westerly directed remanences in the Troodos, Hatay and Baër-Bassit ophiolites suggests a common origin for some of this rotation is likely. This may be better established subsequent to analyses of the sedimentary cover sequences of the Hatay and Baër-Bassit ophiolites (Chapter Six). If a common origin is the case, the implication is that the Troodos 'microplate' extends over a larger area than previously believed.

5.13.2 Age implications of reverse/normal magnetisation components

Figure 5.18 summarises the available age data for the Hatay, Troodos and Baër-Bassit ophiolites. Very few of the eastern Mediterranean ophiolites are dated directly by radiometric means (Robertson 2002), with the Troodos ophiolite being an exception (Mukasa and Ludden 1987).

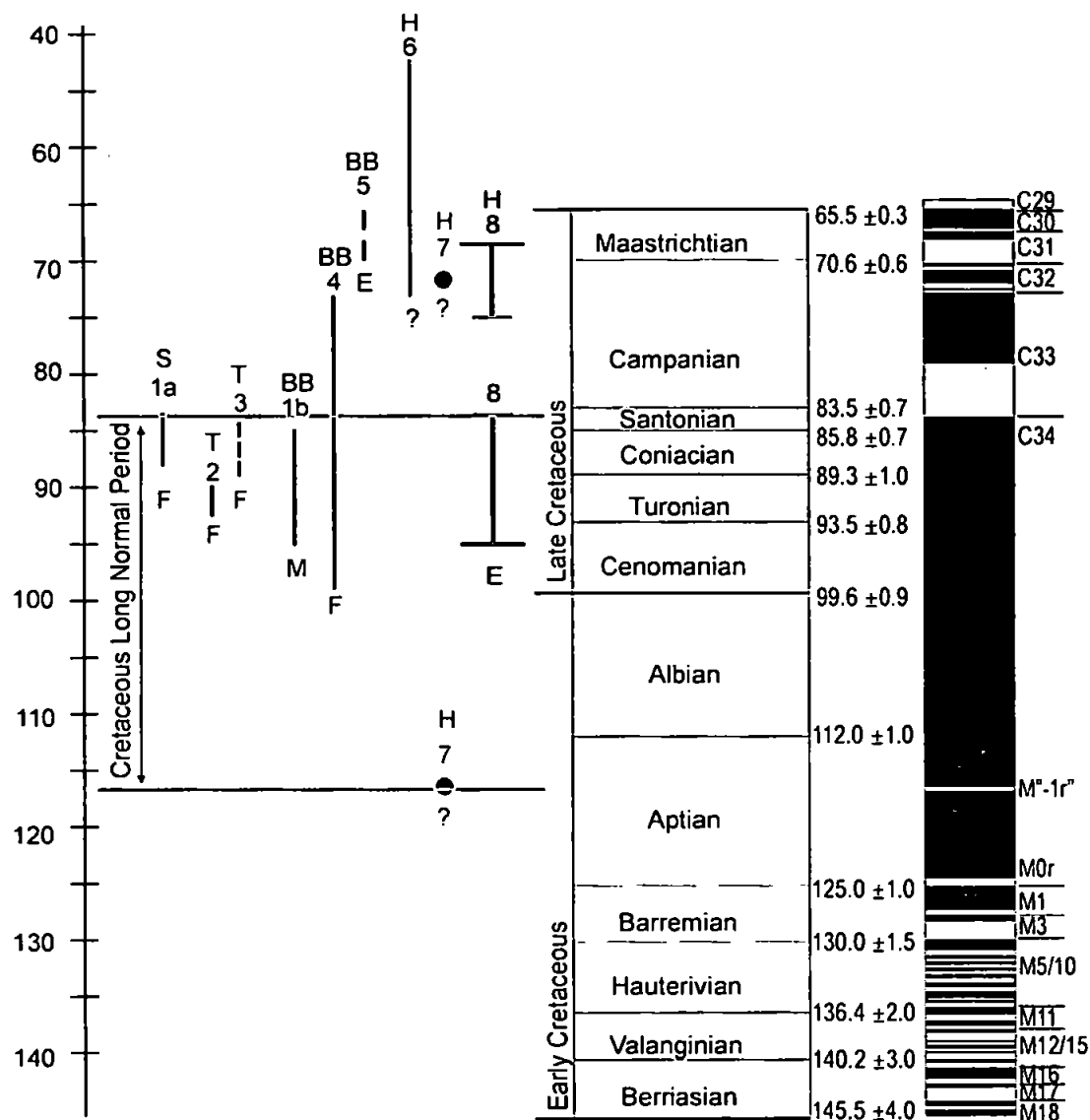


Figure 5.18: Timing of events in the peri-Arabian ophiolites from various dating methods shown against the 2004 timescale for the Cretaceous period (Gradstein et al. 2004) and magnetic polarity reversal sequence (Cande and Kent 1992). Key to symbols: H = Hatay; T = Troodos; BB = Baër-Bassit; S = Semail; F = age interpreted to represent ophiolite formation of ophiolite; E = age interpreted to represent ophiolite emplacement; M = dates from the metamorphic sole; ? = unreliable ages.

1. Thuziat et al. (1981). 1a (S): Radiometric age for formation (97-94 Ma). 1b (BB): Radiometric age for metamorphic sole (85-95 Ma) generally accepted as latest age of ophiolite formation assuming sole formed during initial detachment of oceanic crust near spreading axis (Whitechurch 1977; Coleman 1981; Boudier et al. 1985).

2 (T). Mukasa and Ludden (1987). U/Pb analyses on plagiogranites. There is some scattering in available radiometric dates (not shown), especially from pillows and dykes with some considerably younger than the 88-92 Ma age.

3 (T). Blome and Irwin (1985). The upper constraint on the age of formation provided by Turonian radiolarian assemblages in the overlying Perapedhi Formation.

4 (BB). Delaloye and Wagner (1984). Radiometric ages from SDC from K-Ar dating (73-99 Ma), either representing cooling age or possibly a metamorphic event during emplacement.

5 (BB). The emplacement age bracketed by well-defined ages for youngest carbonates in underlying autochthon and oldest post-emplacement sediments.

6 (H). Delaloye et al. (1980b). Broad span of unreliable radiometric ages from lavas (44-74 Ma); younger age interpreted as tectonic and older as more likely to be true formation age.

7 (H). Cöglü et al. (1975). Radiometric ages from gabbros, but not believed to be reliable.

8 (H). Selcuk (1981). Dating of the youngest underlying platform sediments (95-83 Ma) and oldest overlying sediments (69-75) give constraints on the time of emplacement of the ophiolite. Longest period between emplacement and deposition of the overlying sediments is shown by the longer dark grey bars and youngest emplacement age and shortest period before deposition of the overlying sediments is shown by the shorter light grey bars.

Most ophiolites are indirectly dated using one or another of the following (Robertson 2002): (1) radiometric ages for metamorphic soles that are assumed to have formed near the spreading axis where the crust was sufficiently hot to metamorphose underplated units up to amphibolite facies conditions (e.g. Searle and Cox 1999); (2) dating of pelagic sedimentary covers where preserved, commonly using radiolarians; (3) cross-cutting dykes or other intrusive rocks that can provide a minimum age constraint on ophiolite genesis, and (4) the regional geological setting e.g. timing of emplacement and dating of post-emplacement cover sequences. Comparison of magnetisation polarity directions with the established magnetic polarity timescale (e.g. Hailwood 1989) can be invaluable in providing age constraints on the formation, detachment and emplacement ages, providing that the times of acquisition of magnetisation and remagnetisation episodes within the ophiolite are constrained.

There are no reliable radiometric dates for the Hatay ophiolite and those that exist for Troodos and Baër-Bassit are useful but complications due to errors in these and to the lack of constraints of timing of magnetisation acquisition do not allow straightforward age assignments. The ~90 Ma mid-late Cretaceous age of formation of the Troodos ophiolite is well-constrained and formation ages for Hatay and Baër-Bassit are expected to be similar on the basis of poorly defined K-Ar ages. Thus, all three ophiolites are believed to have formed during the Cretaceous Long Normal Period (LNP) and sites would be expected to be normally magnetised. Pre-deformational characteristic remanences in the Hatay ophiolite are almost all normally magnetised and are ubiquitously of normal polarity in the Troodos ophiolite, consistent with formation during the Cretaceous LNP. In Hatay, only the Antakya lavas (relationship to the main massif uncertain), the Isikli dykes and site JD03 from the Kisecik valley have negative inclinations implying a reverse polarity. This is in contrast to the Baër-Bassit ophiolite where samples with negative inclinations dominate the site-level data, with only four pillow lava sites displaying normal polarities

and 23 sites in the SDC having reversed polarity (Morris et al. 2002). Reverse polarity overprints are observed in the Troodos SDC (Gee et al. 1993), but are not ubiquitous and where they are present, normal polarity ChRMs are also isolated (Gee et al. 1993). The age of the Semail ophiolite also falls within the Cretaceous LNP (Cande and Kent 1992) and so remanences would be expected to be normal but both normal and reverse components are found in the SDC (Luyendyk et al. 1982). In contrast to Troodos, in Hatay where reverse polarity components were identified these appeared to be the oldest direction of magnetisation in the rock rather than a later overprint.

The reverse polarity directions observed in the ophiolites represent either acquisition of the magnetisation off-ridge in the first reverse polarity chron subsequent to formation of the ophiolite (i.e. chron C33R; Figure 5.18), or during a poorly-documented reverse polarity interval in chron C34N, or alternatively indicate an error in the age determination of the ophiolites. Some reversed-polarity components in Troodos are of pre-tilting origin which contradicts either the ~90 Ma age or the presumed near-ridge crustal extension of the ophiolite (Gee et al. 1993) indicated from field relationships (e.g. Varga and Moores 1985). If the age of the ophiolite is applicable, then the reversed polarity overprint may be attributed to early stage, low temperature alteration acquired significantly off-axis (> 5-8 Ma after crustal formation) and would have been restricted to a short period in chron C33R (Gee et al. 1993). A mixed polarity interval in chron C34N relies upon ill-defined short field reversal intervals and would not entirely explain the observations of reverse polarity in the Semail ophiolite (Feinberg et al. 1999) because the formation age is well-constrained. Remagnetisation at a time younger than the Cretaceous LNP could explain the observations and reverse components are observed in the overlying sediments (Thomas et al. 1988) and in the 88-81 Ma volcanics, where they are attributed to hydrothermal alteration (Perrin et al. 1994), but this may not explain the reverse components of magnetisation observed in the deeper levels. From comparisons of the magnetisations of

the lower level of the ophiolite with that of the underlying metamorphosed sediments, Feinberg et al. (1999) postulate a similar time of magnetisation, linked to the hydrothermal wave generated by the emplacement of the ophiolite nappe onto the continental platform. The poorly-defined ages for the Baër-Bassit dykes span chron C33R (Delaloye and Wagner 1984). However, if the 85-95 Ma age (within chron C34N) from the metamorphic sole is taken to represent the latest age of formation of the ophiolite (Whitechurch 1977; Coleman 1981; Boudier et al. 1985) then the observed reversed polarity would require a substantial (possibly > 30 Ma) age difference between Baër-Bassit and Troodos ophiolites, with the magnetisation of the former being acquired during the Early Cretaceous or within a poorly documented reverse polarity event within chron C34N (Hailwood 1989). Alternatively, the sole may have formed during the initiation of subduction, before SSZ spreading began (e.g. Casey and Dewey 1984). This would reconcile the available radiometric age constraints and allow genesis of the Baër-Bassit crust and acquisition of pre-deformational magnetisations during chron C33R, with Neotethyan spreading therefore potentially occurring over a c. 10 Ma period prior to the start of microplate rotation in the Campanian (Morris et al. 2005).

On balance, the reverse polarity ChRMs observed in both Hatay and Baër-Bassit imply that these may have formed later than the Troodos ophiolite to allow acquisition of some components of magnetisation during chron C33R, although without improved age constraints, this must remain uncertain.

5.13.3 Implications of restoration of dyke strike to original orientations

The present-day mean E-W orientation of the SDC restores back to a roughly N-S original strike when the large anticlockwise rotations are backstripped, either by using standard analysis procedures (section 5.8.2) or by using net tectonic analysis (section 5.11.1). This

has important implications for the history of the southern Neotethyan basin in which the ophiolites were forming as it suggests a primary variation in the orientation of dyke strikes between Troodos, Hatay and Baër-Bassit, with an average NE-SW and N-S trend respectively for the continuous and extensive SDCs of Troodos and Hatay. This indicates that the marginal basin setting where the ophiolites formed had a higher degree of complexity than previously believed, with the variation in dyke strike due either to temporal or spatial changes in spreading direction within the basin (see Chapter Nine for further discussion).

5.13.4 Rotations about dyke-normal axes

In the Hatay ophiolite, the large number of sheeted dykes both along the coast and in the Karaçay valley that display steeper inclinations than expected indicates that rotations about a dyke-normal axis are not necessarily a minor localised occurrence. Any dyke-normal rotation would also have affected the palaeohorizontal sites but would have been accounted for in the standard tilt correction. Rotations about dyke-normal axes have been observed in the Baër-Bassit ophiolite (Morris and Anderson 2002; Morris et al. 2002; section 4.5.3) but do not affect the entire SDC. In Baër-Bassit these rotations affected only one locality with net tectonic rotation analysis indicating a shallow dyke-normal rotation axis potentially occurring during emplacement-related deformation (Morris and Anderson 2002). In the Hatay ophiolite, dyke-normal rotations appear more widespread, with the significant exposures both along the coast and in the Karaçay valley all displaying steeper remanences than expected. However, as in Baër-Bassit, these rotations similarly do not affect the entire ophiolite. For instance, dykes from the Kisecik locality have stratigraphic magnetisation inclinations indistinguishable from those of the cumulate sites within the same area (with declinations also similar) and sites from the Isikli locality have inclinations that correct to expected values after a standard tilt correction. A dyke-normal

rotation for E-W striking dykes would require horizontal axis of rotation oriented N-S. Alternatively, a component of dyke-normal rotation may have occurred at an earlier phase in the deformation history about a dyke-normal axis that is not necessarily the same as the one suggested by using the present-day orientation of the dykes. These possibilities are discussed further in section 8.10 subsequent to identification of the major structural events to have affected the ophiolite. An important implication from these results from both Hatay and Baër-Bassit is that dyke-normal rotations do not affect a region ubiquitously, but can affect small areas of dykes that in all other respects are similar to those of adjacent areas.

5.14 Synthesis

Specimens from 63 sites (557 cores) were demagnetised in the University of Plymouth laboratory. Demagnetisation diagrams show mostly simple rectilinear decay to the origin and site mean directions of magnetisation are unrelated to the local present day magnetic field. Westerly-directed remanences indicate that the ophiolite has experienced large anticlockwise rotations during its history. An inclination-only tilt test (Enkin and Watson 1996) demonstrates that magnetisations are pre-deformational in origin, despite a complex history of low temperature seafloor alteration, intra-oceanic detachment, thrust emplacement and subsequent Neotectonic faulting. The new results from this thesis and Morris (2002) show that both Hatay and Baër-Bassit have experienced similarly large anticlockwise rotations to Troodos and previous conceptions of the size of the rotated area need to be revised. The implication from analysis of the SDC that the mean trend was originally N-S indicates that a primary variation in dyke orientation existed in the Neotethyan spreading system, which suggests a higher level of complication than previously assumed. A revised model will be discussed and presented in Chapter Nine.

CHAPTER SIX

6. PALAEOMAGNETIC RESULTS FROM THE SEDIMENTARY COVER SEQUENCES OF THE HATAY AND BAËR-BASSIT OPHIOLITES

6.1 Introduction to chapter

Palaeomagnetic analysis of the sedimentary cover sequences of both the Hatay and Baër-Bassit ophiolites can provide important constraints on the timing of rotations within the underlying ophiolitic basement. As described in section 4.4.2, palaeomagnetic analysis of the *in situ* sedimentary cover of the Troodos ophiolite has documented the timing of rotation of the Troodos microplate. In contrast to this situation, however, the sedimentary covers of the Hatay and Baër-Bassit ophiolites post-date their emplacement and cannot therefore provide information on pre-emplacement rotations. However, if large rotations are recorded by the sediments, this would indicate that a substantial component of the rotations seen in the ophiolite was post-emplacement in age. This chapter therefore describes the results of a palaeomagnetic investigation of the cover sequences and their interpretation, and the implication of these data for the timing of the large rotation described in the Hatay ophiolite in Chapter Five and for the Baër-Bassit ophiolite by Morris et al. (2002).

6.2 Sampling and measurement procedures

All sites from the sedimentary cover of the Hatay ophiolite were sampled using a standard portable petrol-driven rock drill, using water-cooled 25 mm diameter diamond-tipped drill bits. Each sample was orientated with both a standard magnetic compass and a sun compass. Each drilled core was cut into 22 mm lengths in the laboratory, ensuring that weathered surfaces were removed.

Samples from the sedimentary cover of the Baër-Bassit ophiolite were collected previously by hand sampling by A. Morris and M. W. Anderson. The orientation of the strike line of the top surfaces of the hand samples were drawn on in the field. Lines perpendicular to this were drawn on in the laboratory at around 10 mm spacing to give the direction of maximum dip of the surface. Up-dip Arrows were marked onto these lines and the samples were then set in concrete with the top surfaces flush with the top of the concrete. The cores were drilled perpendicular to this surface in the laboratory which gives a simple result for the 'field' orientation of the drill core: the direction of the core is the strike of the hand sample's top surface minus 90° and the hade of the core is identical to the dip of the top surface. Finally, samples were cut to 22 mm length to produce standard palaeomagnetic specimens.

The bedding of the sedimentary sequences sampled was measured in order for a stratigraphic correction to be applied to the palaeomagnetic data. In most cases bedding was not steeply dipping for either the Hatay or Baër-Bassit sedimentary sequences.

Natural remanences were measured for all samples from the sedimentary covers of Hatay and Baër-Bassit at the University of Oxford palaeomagnetic laboratory using a 2-G Enterprises DC SQUID cryogenic magnetometer (noise level = 0.005×10^{-3} A/m) housed in a magnetically-shielded room (ambient field < 200 nT). 159 samples were subjected to alternating field (AF) stepwise demagnetisation using in-line coil systems and 44 samples were demagnetised using step-wise thermal demagnetisation. Characteristic components of magnetisation were found using orthogonal vector plots and principal component analysis (Kirschvink 1980) and site and locality mean remanence directions computed using Fisherian statistics (Fisher 1953).

6.3 Hatay sedimentary cover

The results from palaeomagnetic analysis of the Hatay sedimentary cover are discussed below. The data from the sedimentary cover obtained for this thesis can be usefully compared with palaeomagnetic data from Kissel et al. (2003). This recent study by Kissel et al. (2003) sampled Palaeocene to Miocene rocks along a transect from the Arabian platform to the eastern Pontides in order to provide palaeomagnetic constraints on the Cenozoic evolution of the eastern Mediterranean. Thirt eight of their sites were sampled in the Hatay region, of which 13 were found to be interpretable. These provide an additional database of results to add to the sites sampled specifically for the purposes of this thesis, and so the data from Kissel et al. (2003) are also discussed in this section where relevant.

6.3.1 Sampling localities

Seven sites were sampled in the sedimentary cover within Neogene and Palaeocene sequences (Figure 6.1). Neogene site SN01 was located in sandstones and marls in the Karaçay valley, SN02 in coarse-grained shelly sandstones on the road between Samandağ and Antakya and SN03 in soft sandstones and siltstones in a quarry in the Uçedik valley. The Palaeocene sequences are from pink-coloured limestone sequences, the base of which are possibly Eocene in age. Sites SP01 and SP02 are located on the road between Kömürçukuru and Tahtaköprü, where the sedimentary sequences unconformably outcrop above the ultramafics of the ophiolite massif. Sites SP03 and SP04 are located to the NE of the ophiolite massif, in well-exposed extensive sequences of limestones along the road to the south of Belen. The 38 sites sampled by Kissel et al. (2003) were from Eocene fine-grained limestones and Miocene blue-grey marls (Figure 6.1), located on both sides of the Amanos fault with three of the Miocene sites located on the northern side of the ophiolite massif.

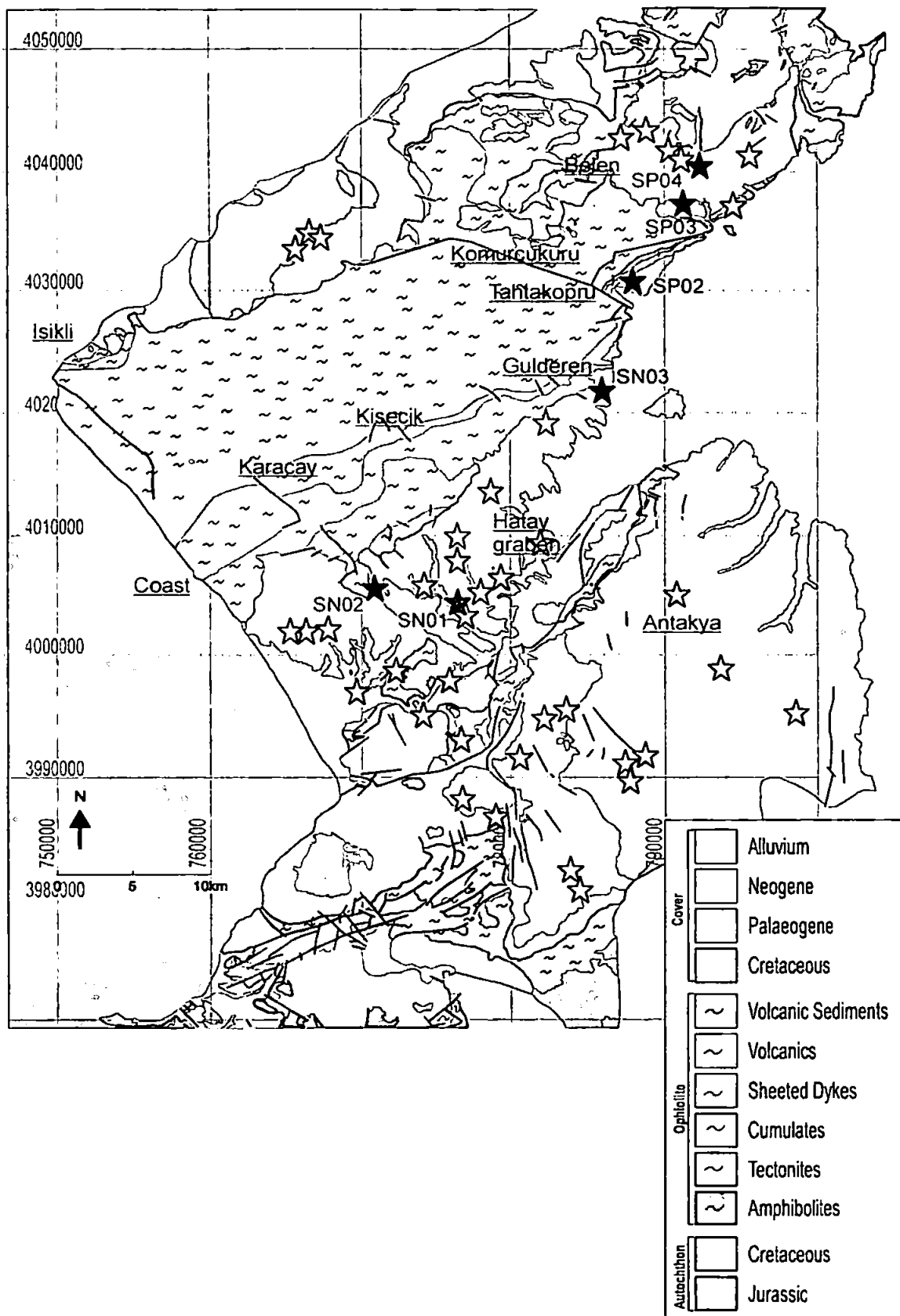


Figure 6.1: Localities within the sedimentary cover of the Hatay ophiolite sampled for palaeomagnetic analysis. The labelled black stars show the 7 sites sampled within the sedimentary cover for this thesis and the white stars show the location of the 38 sites sampled from the sedimentary cover by Kissel et al. (2003), of which 13 were interpretable. Place names as on Figure 2.12.

6.3.2 Rock magnetic summary

The seven sites from the sedimentary cover sampled for this thesis were not subjected to the exhaustive rock magnetic testing that the ophiolitic samples were subjected to at the Institute for Rock Magnetism (Chapter Seven), although tests were carried out on selected samples and standard demagnetisation data also provide a good indication of the rock magnetic mineralogy. Hysteresis loops were measured for 13 cores at the IRM. The hysteresis measurements for nine samples (four samples could not be measured as their magnetisations were too close to the noise level of the 2G cryogenic magnetometer used) show that the samples have a higher coercivity component than observed from the ophiolitic samples, probably due to haematite. Several samples from both Neogene and Palaeocene sites did not demagnetise to the origin following demagnetisation, again indicating the presence of a higher coercivity phase. The average ratio of M_{rs}/M_s is 0.2 and H_{cr}/H_c is 2.3 (with limits $1 < M_{rs}/M_s < 9$) which plot in the pseudo-single-domain field on a Day plot (Figure 6.2A). Backfield coercivities are variable (37- 83 mT) with an average of 64 mT: 74 mT for the Palaeocene sites and 53 mT for the Neogene sites. A low temperature sweep (cooling of a room temperature SIRM followed by warming of a low temperature SIRM) was carried out for sample SP0303 at the IRM (see section 7.3.2 for description of experimental procedure), with no evidence for either the Verwey or Morin transition apparent on warming or cooling curves of an SIRM (Figure 6.2B).

The sites from Kissel et al. (2003) from the Hatay area are not discussed individually, although the results of selected samples from this area are shown in figures within Kissel et al. (2003) (Figure 6.2C). Acquisition of IRM and subsequent demagnetisation of the IRM (SIRM) were studied for all samples, with the majority described as acquiring 90% of IRM in fields less than 300 mT, indicating that the main magnetic carrier is a low-coercivity mineral (Kissel et al. 2003), almost certainly magnetite.

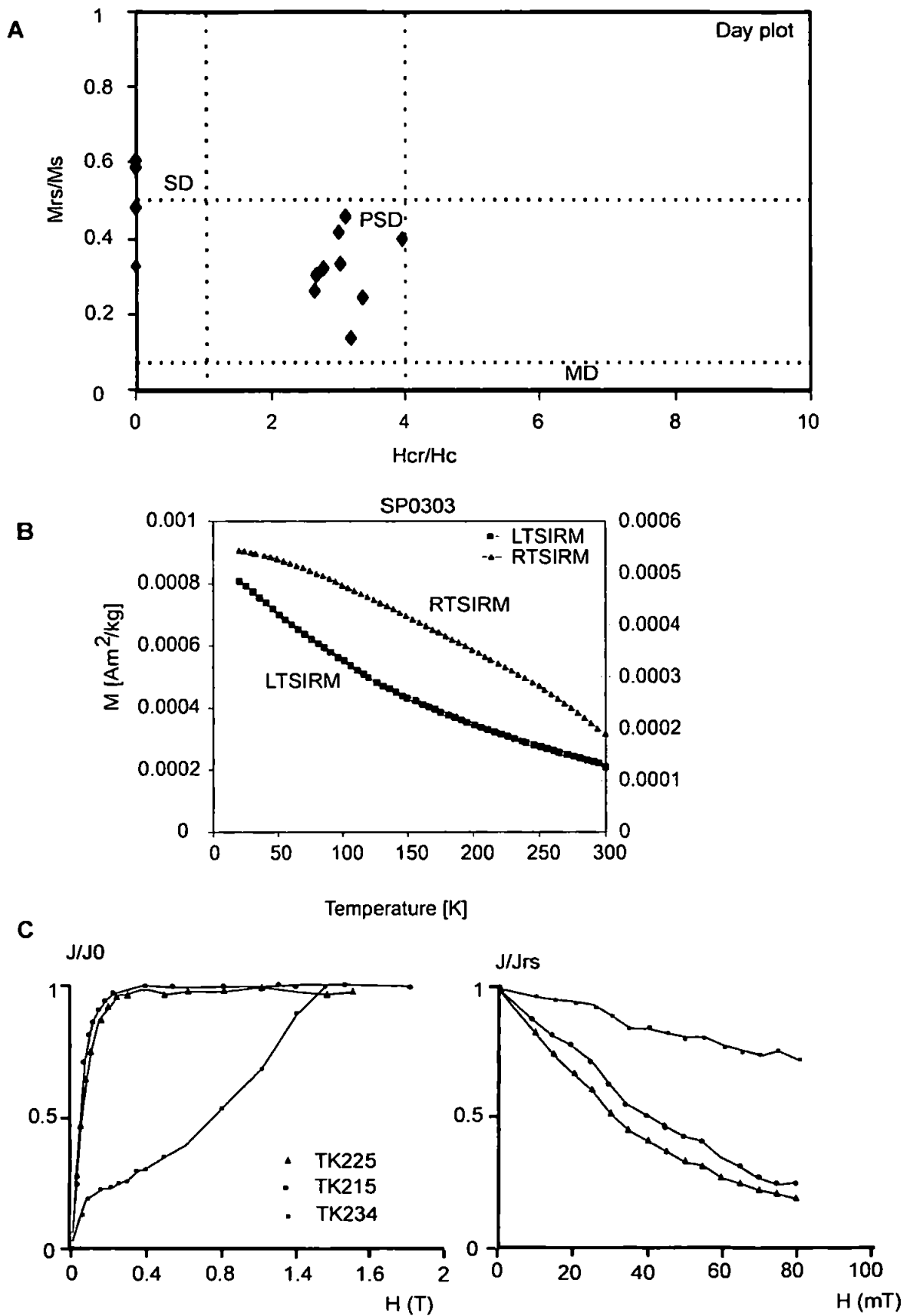


Figure 6.2: Selected rock magnetic data from sites within the sedimentary cover of the Hatay ophiolite.

A. Day plot for all sedimentary samples where hysteresis loops were measured at the IRM.

B. Low temperature RTSIRM-LTSIRM sweep: no evidence for Verwey point.

C. Rock magnetic data from Kissel et al (2003; Fig. 6b) showing typical SIRM acquisition and demagnetisation curves with most samples saturating by 0.2-0.3 mT and a few (illustrated by TK234) showing a mixture of magnetic minerals.

As this result is not restricted to samples from Hatay it is not possible to determine whether these were consistent with the higher coercivity of minerals found from the sedimentary sites sampled for this thesis.

6.3.3 Magnetic fabric analyses

The fabrics of the sedimentary samples were measured prior to demagnetisation on the KLY3 Kappabridge at the University of Plymouth and analysed using the Anisoft programs. At sample-level there is a mixture between oblate and prolate fabrics for both Palaeogene and Neogene rocks (Figure 6.3B) with a generally weak anisotropy. At site level, a mixture of fabrics was also observed. Of the seven sampling sites, two showed clear relationships between the bedding measured and the fabric (Figure 6.3A) with the minimum axes of anisotropy of the fabric perpendicular to the plane containing K_{\max} and K_{int} , with one of these sites Neogene in age (SN02) and one Palaeocene in age (SP02). This oblate fabric is common in sediments where clear sedimentary layering is developed. A further two sites showed a similar relationship although with greater scatter in data. Site SP04 shows k_{\max} aligned with the plane of the bedding with k_{\min} and k_{int} approximately orthogonal i.e. basically a triaxial fabric. The remaining two sites had too great a scatter to determine the fabric relationship.

Again, the paper by Kissel et al. (2003) does not describe the fabrics from the Hatay area individually, but anisotropy of magnetic susceptibility from all of the studied areas is described as characterised by an oblate magnetic fabric with a minimum axis of anisotropy, K_{\min} , perpendicular to the bedding plane. This indicates deposition in a low-energy environment. Stereonets of K_{\max} and K_{\min} fabric data from two samples from the Antakya area are shown by Kissel et al. (2003) with near-vertical K_{\min} and K_{\max} near-horizontal in both cases (Figure 6.3C).

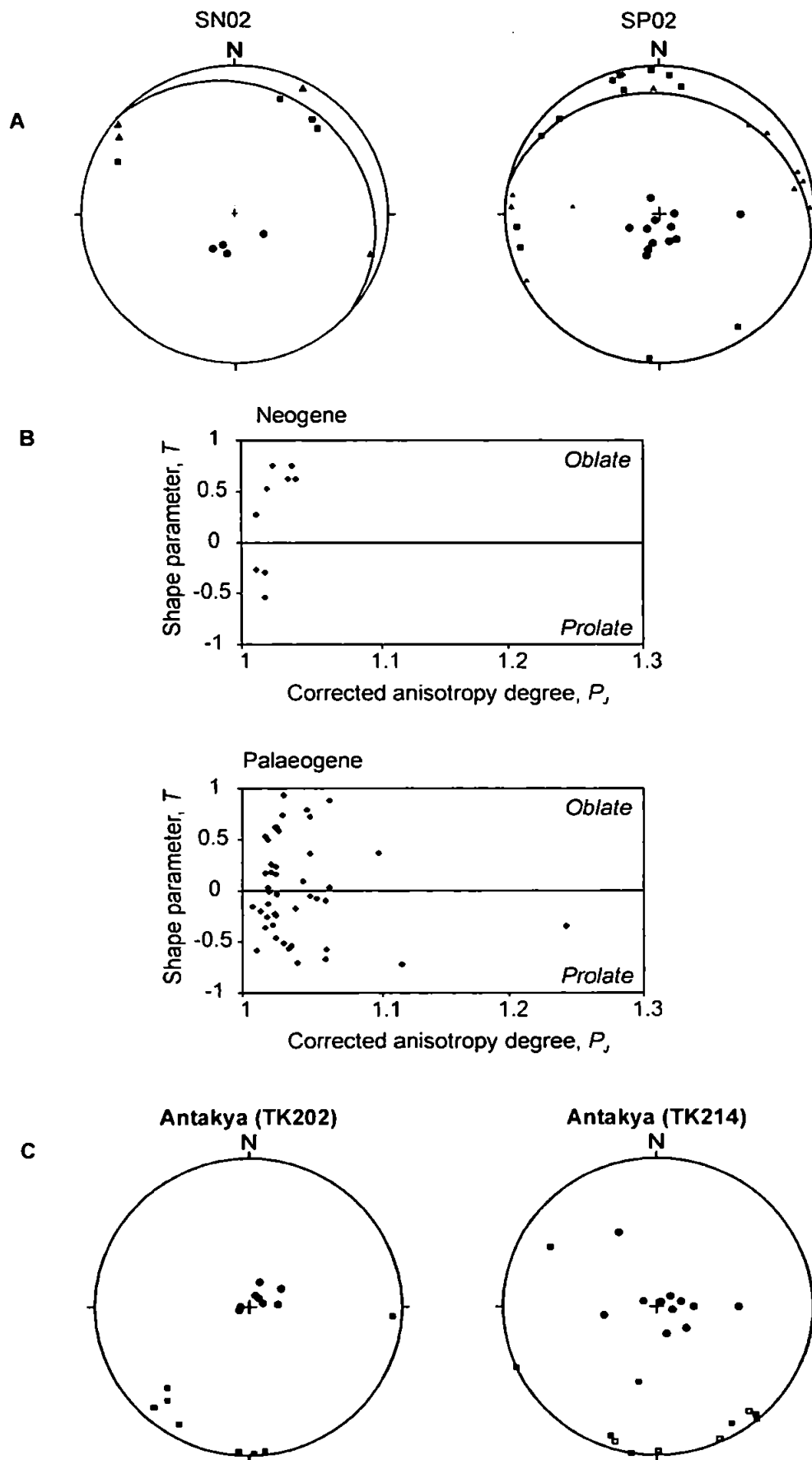


Figure 6.3: Anisotropy of magnetic susceptibility for the sedimentary cover of Hatay. A. Selected anisotropy data for sites measured for this thesis. B. Corrected shape parameter versus anisotropy degree for all sites measured for this thesis. C. Selected anisotropy data from sites within the sedimentary cover of the Hatay ophiolite as analysed by Kissel et al (2003; Fig. 7).

6.3.4 Palaeomagnetic results

NRM intensities are low for all samples from the sedimentary cover of the Hatay ophiolite. The average (geometric) NRM intensity for the older Palaeogene sites is 2.89×10^{-4} A/m and is 1.95×10^{-4} A/m for the Neogene samples, and these samples also have more variable NRM intensities. Five of the seven sites gave reliable palaeomagnetic results and include sites with both normal and reverse polarity. Figure 6.4 shows some representative demagnetisation plots from the interpretable sedimentary samples. The quality of the demagnetisation data varied from sample to sample, with some samples having large errors in the determination of the ChRM. However, as shown by Figure 6.4, enough samples yielded sufficiently high quality demagnetisation data to obtain reliable site mean directions for the majority, from both Neogene and Palaeogene sites. The average number of samples demagnetised per site is seven. The average number of samples included in the site ChRMs is reduced due to low NRM intensities, especially for the Neogene sites, resulting in analytical difficulties for certain samples. Combining the results from both Palaeocene and Neogene sites the average direction is: Dec = 343° , Inc = 49° prior to structural correction and Dec = 347° Inc = 36° following tilt correction, with an α_{95} of 16° .

Site SN03 has been excluded from this analysis due to the limited number of samples (difficulties due to drilling in soft sediments) and also the poor quality of the demagnetisation data. Table 6.1 shows the site-level palaeomagnetic results for the Hatay sedimentary cover.

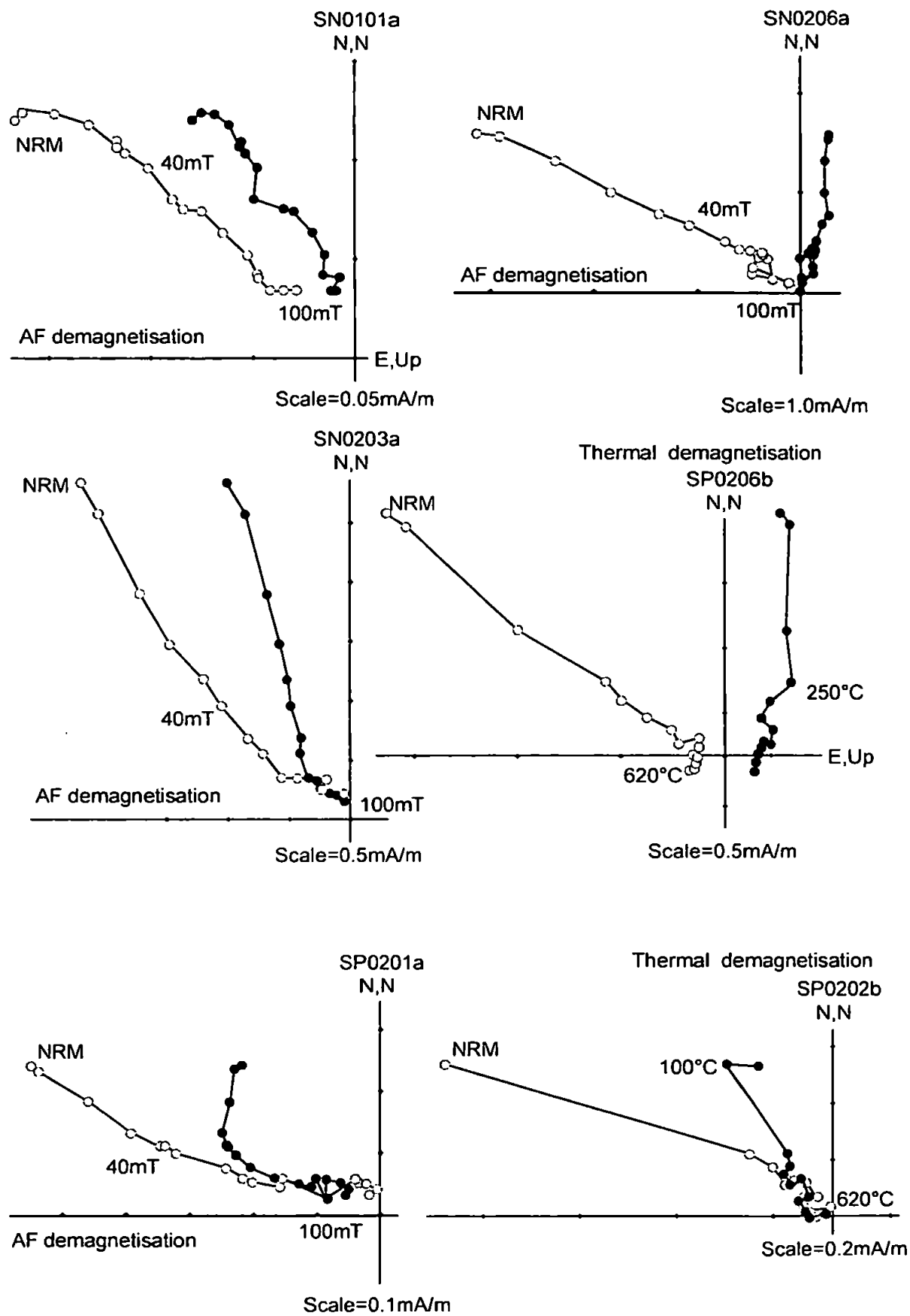


Figure 6.4: Sample demagnetisation plots for samples from the sedimentary cover of the Hatay ophiolite.

Site ^A	Lat.	Lon.	Str.	n	Dg	Ig	kg	α_{95g}	Ds	Is	ks	α_{95s}
SN01	36.16	36.01	155/18	/ ^B	/	/	/	/	/	/	/	/
SN02	36.15	36.07	040/15	1	317.1	46.5	44.4	8.4	331.5	42.8	44.4	8.4
SN03	36.31	36.18	140/28	/	/	/	/	/	/	/	/	/
SP01	36.41	36.13	295/23	4	348.8	50.1	15.1	25.9	340.5	36.9	39.6	15.7
SP02	36.37	36.18	012/20	7	176.5	-59.5	34.6	10.4	219.4	-61.1	34.7	10.4
SP03	36.48	36.25	109/20	5	337.3	59.2	15.1	20.4	349.1	41.5	15.1	20.4
SP04	36.48	36.24	050/16	6	162.3	-50.1	46.1	10.1	176.9	-42.1	46	10.2

Table 6.1: Site palaeomagnetic data for the sedimentary cover of the Hatay ophiolite, as measured for this thesis.

^AThe 1st letter of the site labels indicate that the site is a sediment (S) and the 2nd letter refers to the site age: N = Neogene; P = Palaeogene.

^B Diagonal lines indicate an inability to obtain data from that site due to magnetisation levels below the noise level of the 2G magnetometer.

Kissel et al. (2003) report extremely low magnetisation ($< 10^{-5}$ A/m) from many of the Antakya sedimentary samples, discarding 162 out of 414 samples for this reason. Of the 13 not discarded, nine sites have normal directions and four have reverse directions with some scatter in the data (Kissel et al. 2003). The average regional directions both before and after tectonic correction are slightly different to the direction of the present-day magnetic field, with a mean direction subsequent to correction having a declination of $348^{\circ} \pm 7^{\circ}$ and an inclination of 44° .

The reliable site means obtained from these 13 sites from the Hatay region can be combined with those obtained for the sedimentary cover of Hatay in this study, with a very good correlation between the two datasets. The results show that magnetisation direction is similar but slightly different to the present-day field direction. The average direction combining both datasets is: Dec = 344° , Inc = 47° in geographic coordinates and Dec = 349° , Inc = 45° in stratigraphic coordinates. The average using only the data from Kissel et al. (2003) is: Dec = 345° , Inc = 43° in geographic coordinates and Dec = 348° , Inc = 44° in stratigraphic coordinates.

Figure 6.5 summarises the directions from all reliable sites within the Hatay sedimentary cover from both Kissel et al. (2003) and the data from this study. Data include sites of

both normal and reverse polarity. These data, including those from the oldest (Palaeocene) sequences, indicate only minor anticlockwise rotation, with no differences in rotation magnitude or direction according the age of the sample. Large-scale rotations, such as those observed in the ophiolite are not observed in the sedimentary cover, with directions similar to those of the present-day magnetic field, although consistently rotated slightly anticlockwise.

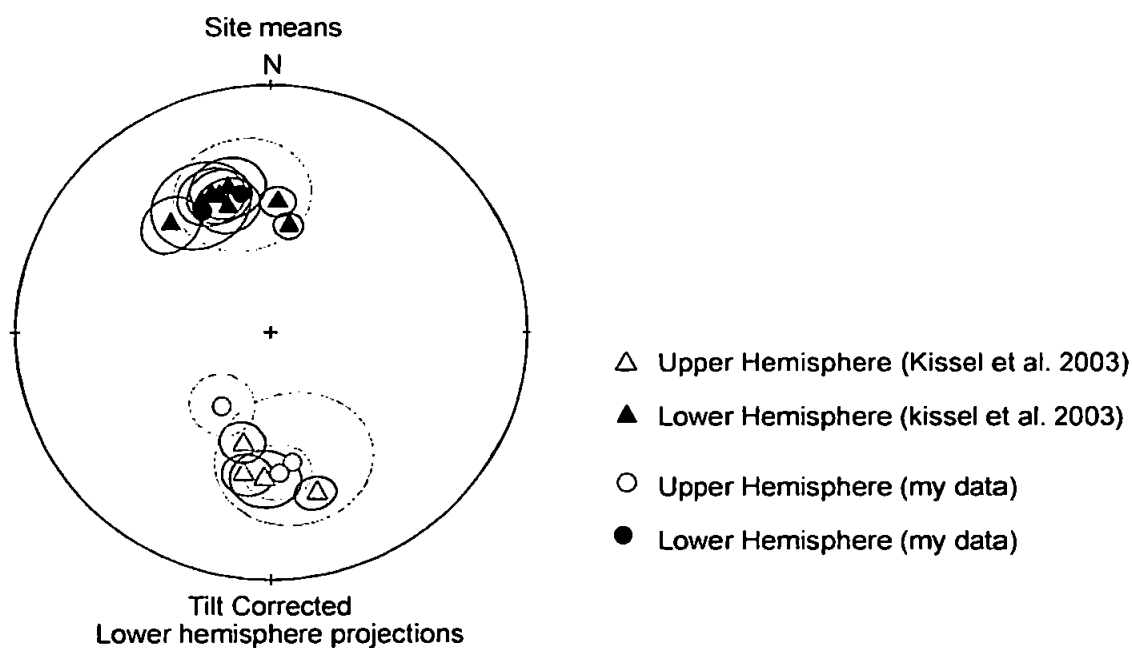


Figure 6.5: Stereonets displaying the site mean magnetic remanences for sites from the sedimentary cover of the Hatay ophiolite, including data from this thesis and also from Kissel et al. (2003). The confidence limits for the means of the normal and reversed antipodes overlap, suggesting that the two means cannot be distinguished at the 95% level of confidence and the data pass a reversal test.

6.3.5 Timing of magnetisation acquisition (tilt tests)

The data from the Hatay sedimentary cover sites include both normal and reversely magnetised samples that pass a reversal test: the means of the normal and reversed antipodes shown on Figure 6.5 have an angular separation of 9.6° and their $\alpha 95$ error circles overlap. A positive result is obtained from an inclination-only tilt test performed on the sedimentary cover sites (Table 6.2 and Figure 6.6). The 95% confidence limits, although more spread than for the ophiolite (section 5.8), straddle 100% of untilting. The precision parameter \hat{k} has a maximum of over 90 which is sufficiently high to be confident of the positive result (Enkin and Watson 1996) and implies the sediments acquired their remanence prior to deformation of the sampled sequences.

	<i>Number of sites included</i>	<i>Inclination \hat{I}^A</i>	<i>Precision parameter \hat{k}^B</i>	<i>95% confidence limits</i>
<i>In situ</i>	13	$43.1^\circ \pm 4.5^\circ$	32.6	
Tilt-corrected	13	$43.0^\circ \pm 3.2^\circ$	94.8	63.2-123.4%

Table 6.2: Results of the inclination-only tilt test formulation of Enkin and Watson (1996).

^A The maximum likelihood estimate of the true mean inclination in degrees.

^B The Fisher precision parameter.

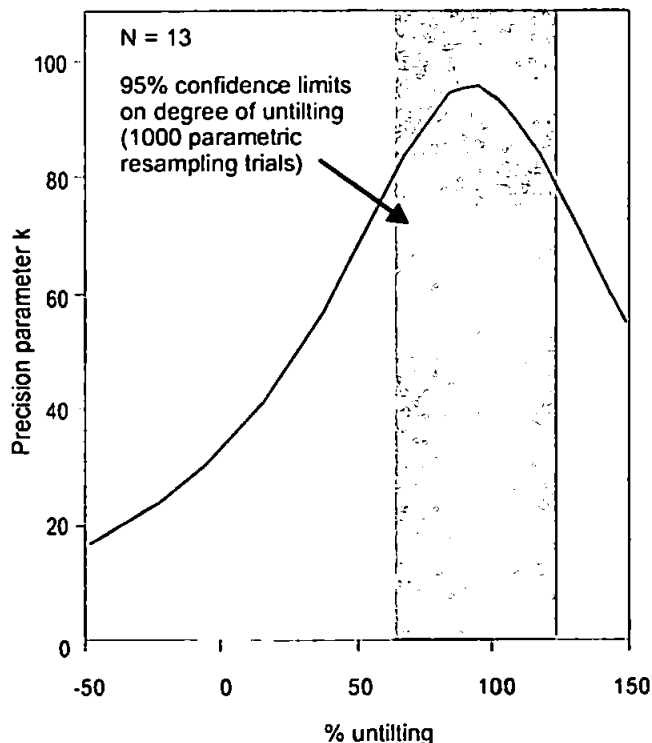


Figure 6.6: Results of an inclination-only tilt test performed on sites from the sedimentary cover of the Hatay ophiolite (after Enkin and Watson 1996).

6.4 Baër-Bassit sedimentary cover

6.4.1 Sampling localities

Palaeogene sequences are best exposed in the southwest of the study area, and eleven sites were sampled in this region within interbedded limestones and marls where clearly defined bedding could be observed (Figure 6.7). Sequences of limestones and marls of Neogene age are well developed in the east of the study area, but are generally poorly bedded and massive. Sampling was restricted here to eight sites where clear bedding could be observed, although samples were often collected from the less friable massive layers.

6.4.2 Rock magnetic summary

IRM acquisition curves reach saturation by applied fields of 200 mT, consistent with low coercivity magnetite as the remanence carrier in these rocks. Backfield IRM curves yield coercivities of remanence values of 30- 55 mT, consistent with magnetite grain sizes in the pseudo-single domain range (Figure 6.8). This is supported by median destructive fields during alternating field demagnetisation of natural remanent magnetisation (NRM) of 20-30 mT. Low field magnetic susceptibilities of the samples are weak with a mean value of 1.5×10^{-4} SI, indicating magnetite concentrations of less than 0.01% by volume.

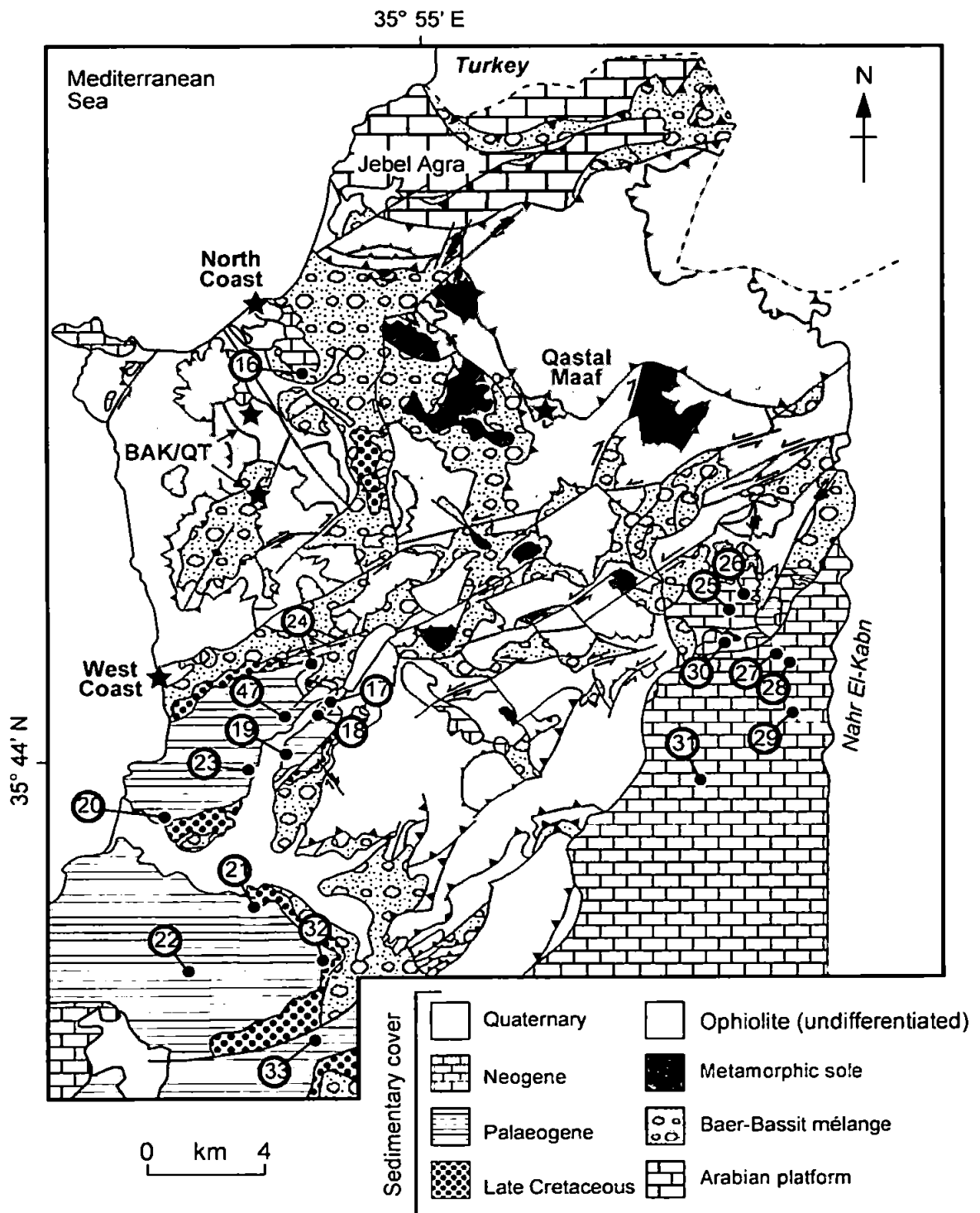


Figure 6.7: Geological map of the Baër-Bassit area, showing the distribution of Palaeogene and Neogene sequences of the neoautochthonous sedimentary cover and the location of palaeomagnetic sampling sites. Black stars indicate palaeomagnetic sampling localities within the Baër-Bassit ophiolite described by Morris et al. (2002). Map modified from Al-Riyami et al. (2000).

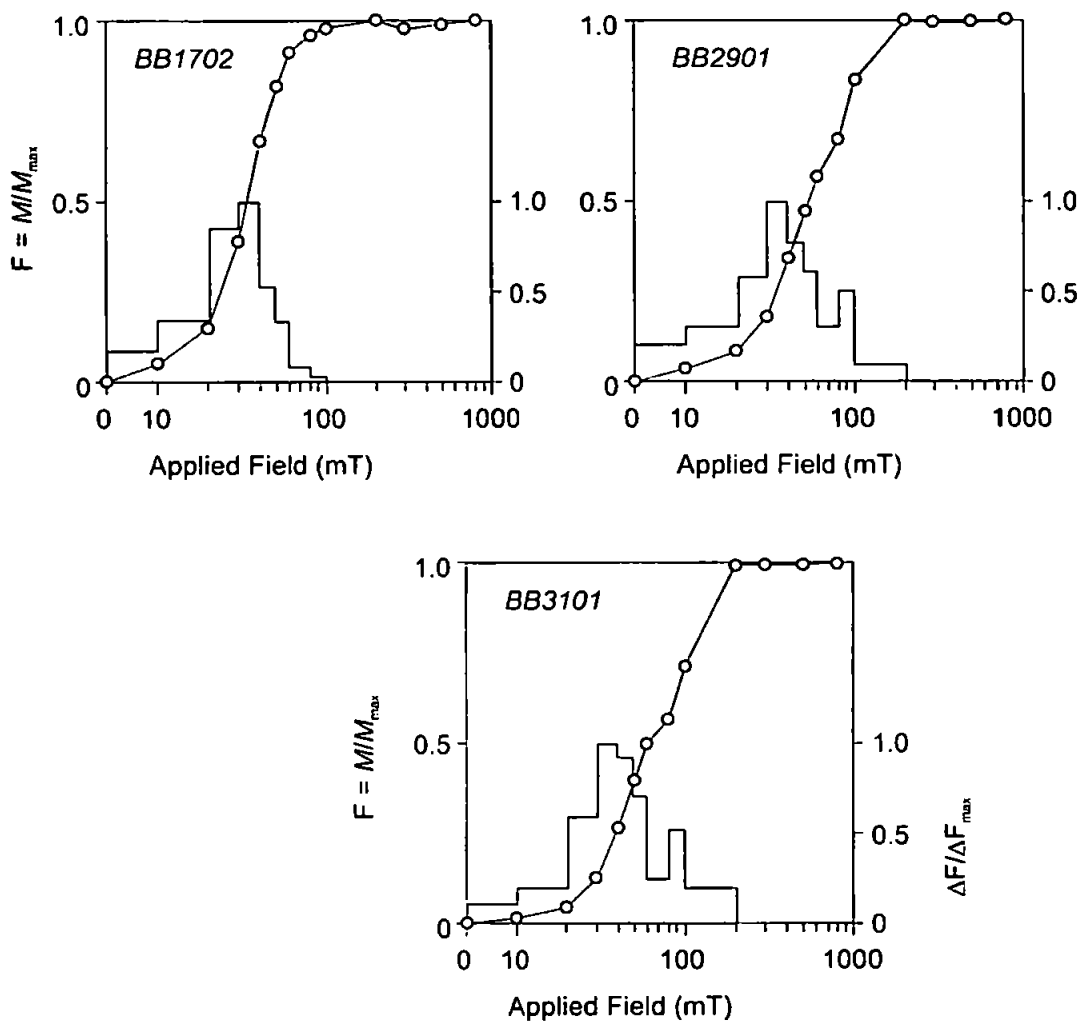


Figure 6.8: Rock magnetic results from the Baër-Bassit sedimentary cover (from Morris et al 2005).

6.4.3 Magnetic fabric analyses

The fabrics from 15 sites from the sedimentary cover were measured on the Agico KLY3 Kappabridge in the University of Plymouth laboratory. Both Palaeogene and Neogene sequences display a mixture of oblate and prolate fabrics at specimen-level, but 70% of Palaeogene specimens are oblate compared to 50% of the Neogene specimens (Figure 6.9).

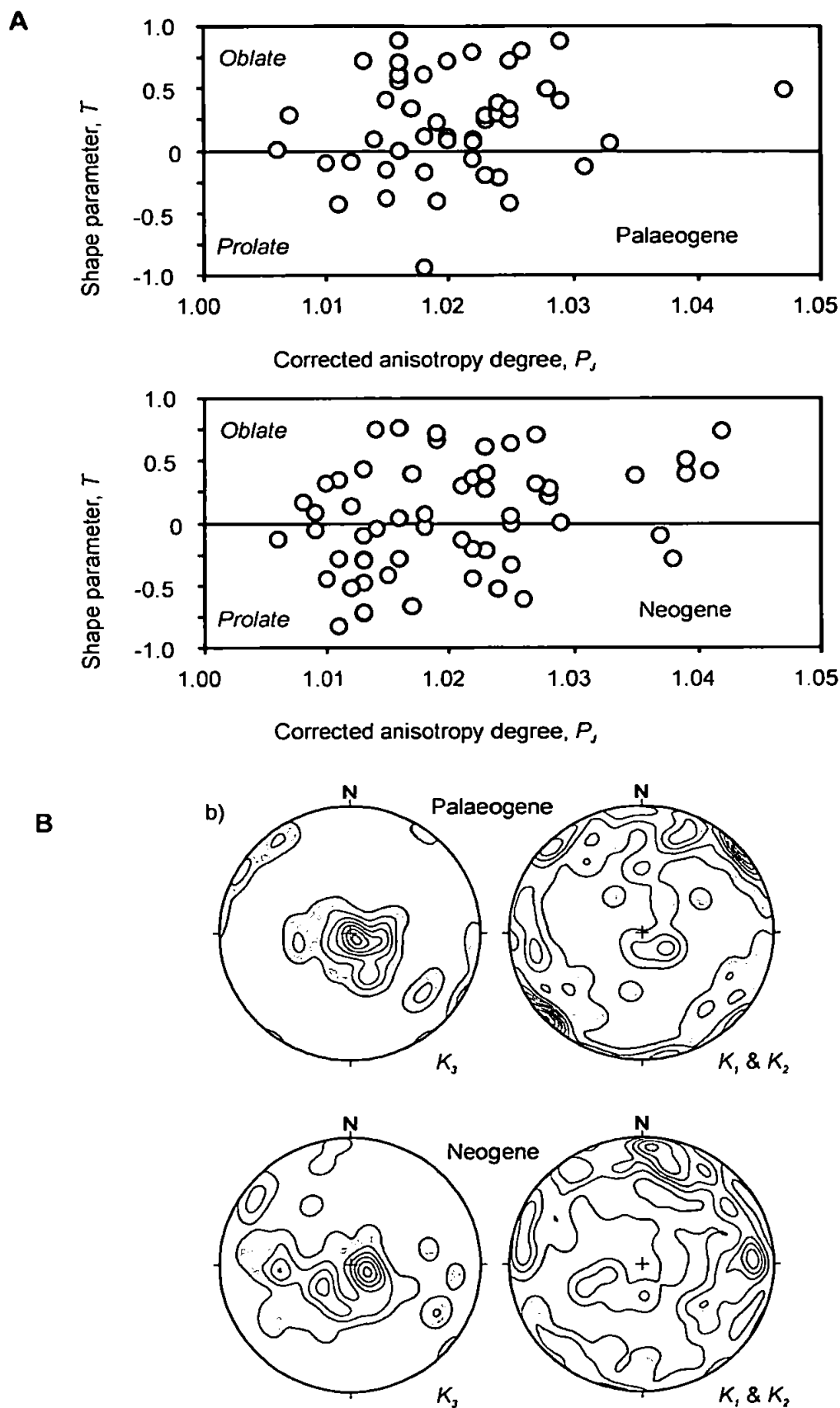


Figure 6.9: Summary of the magnetic fabrics (anisotropy of magnetic susceptibility) of the neoautochthonous sedimentary cover of the Baër-Bassit ophiolite.

A. Bi-plot of shape parameter, T , against corrected anisotropy degree, P_j . This indicates weak magnetic fabric development (mean anisotropy of 2% ($P_j = 1.02$)) with the presence of both oblate and prolate ellipsoids.

B. Summary of the fabrics for Neogene and Palaeogene sites displayed on stereographic projections.

This reflects the better development of bedding parallel laminations in the Palaeogene rocks, in contrast to the Neogene sequences where bedding is often poorly developed. Strength of anisotropy, P_j (Jelinek 1981; section 3.4.4), ranges from 1.005 to 1.05, with a mean value of 1.02 (i.e. 2% anisotropy). There is no preferred relationship between P_j and T , and no correlation between P_j and mean susceptibility, indicating that the degree of anisotropy is not dependent on ferrimagnetic concentration.

Following correction of the bedding tilt the orientation of AMS principal axes can be plotted on a stereonet. Fabrics are generally well-defined despite an element of analytical noise due to the low susceptibilities of the sampled rocks and the weakly developed fabrics. For instance, two thirds of sites had at least one axis of anisotropy clearly clustered, which in all except one case was K_{\min} , with K_{\max} and K_{int} either spread along the orthogonal plane or also tightly clustered. The one site (BB30) where K_{\min} axes were not the most tightly clustered displayed a girdle distribution of K_{\min} and K_{int} axes with K_{\max} orthogonal to this plane. K_{\min} axes form strong clusters close to the vertical in both Palaeogene and Neogene sequences, whereas K_{\max} and K_{int} axes form girdles around the primitive. This suggests that AMS fabrics in both sequences are primarily related to bedding parallel petrofabrics, and that inverse fabric effects due to SD magnetite are not significant. This distribution is less well defined in the Neogene sequences, as may be expected given the relatively poor definition of bedding fabrics in these rocks. Within the Palaeogene data, a minor girdle of sub-horizontal, NW directed K_{\min} axes relates to the fabric developed at site BB17, where indistinctly bedded limestones and marls are cut by numerous NE-SW trending minor strike slip faults. This is the only site where the magnetic fabric shows a demonstrable response to tectonism.

6.4.4 Palaeomagnetic results

NRM intensities are very low, with a mean value of 2.8×10^{-3} A/m. This value is raised, however, by significantly higher intensities at site BB16 (mean = 24.2×10^{-3} A/m). Remaining sites have a mean NRM intensity of 0.7×10^{-3} A/m. Despite the very weak intensities, stable components of magnetisation were isolated at 15 sites, following removal of minor secondary components during initial demagnetisation. The remaining four sites (in Palaeogene sequences; sites BB18 and 20-22) had NRM intensities too close to the noise level of the magnetometer to allow adequate demagnetisation. Figure 6.10 shows representative demagnetisation plots for the sedimentary sites from the Baër-Bassit sedimentary cover and Table 6.3 shows site-level palaeomagnetic data. Normal polarity remanences are observed at all sites. One site (BB24) exhibited antipodal low coercivity reverse and higher coercivity normal components. Magnetisation directions at sites in the Palaeogene sequence are unrelated to the present geocentric axial dipolar field direction in NW Syria (Dec = 000° ; Inc = 55°) and are divided into two groupings with NE and NW directed declinations. These large differences can only result from the effects of relative tectonic rotations of the sampled units subsequent to remanence acquisition (see below). Neogene sequences record magnetisation directions which cluster around north, displaying less variability than the Palaeogene sequences. Little or no between-site variability may be ascribed to the effects of secular variation, since this may be expected to be adequately averaged out at a site-level in these carbonate sediments.

Site	Age ^A	n	NRM	Str. ^B	Dg	Ig	k	α_{95}	Ds	Is	K	α_{95}
<i>Palaeogene sites:</i>												
BB17	Pal.	5	0.61	300/17	81.4	41.2	13.4	21.7	68.2	53.3	13.4	21.7
BB19	Pal.	6	4.30	075/34 & 031/40	44.9	66.7	20.5	15.1	46.3	31.6	35.8	11.4
BB24	Pal.	6	1.60	273/13	222	-59	26.8	14.7	200	-65	26.8	14.7
	Pal.	6		273/13	45.9	52.2	61.1	9.6	30	59.7	61.1	9.6
	<i>Mean:</i>				43.9	55.4	-	-	25.5	62.3	-	-
BB23	Pal.	4	0.19	190/11	341	32.7	30.2	17	336	42	30.2	17
BB32	Pal.	8	0.43	272/21	336	39.3	33.7	9.7	324	28	33.7	9.7
BB33	Pal.	8	0.47	193/10	329	34.8	112	5.3	323	41.7	112	5.3
BB47	P.-E.	6	0.17	246/20	333	37.5	138	5.8	319	33.9	138	5.8
<i>Neogene sites:</i>												
BB16	Plio.	8	24.00	217/22	352	45.3	27	10.9	329	57.7	27	10.9
BB25	Aquit.	6	0.21	258/49	43.8	52.7	31.9	12.9	309	64.2	31.9	12.9
BB26	Aquit.	6	0.16	336/15	346	59.6	35.4	11.4	343	44.7	35.4	11.4
BB30	Aquit.	5	0.28	310/12	17.9	59.7	33.4	13.8	2	53.6	33.4	13.8
BB27	Burd.	9	0.20	200/13	356	56.3	57.9	6.8	344	67.6	57.9	6.8
BB28	Burd.	9	0.23	200/14	358	52.7	35.6	8.8	348	65.3	35.6	8.8
BB31	Burd.	4	0.46	173/03	352	52.9	84.4	10.1	352	55.8	84.4	10.1
BB29	H-T.	3	0.25	218/16	359	52.9	71.5	14.7	340	63.7	71.5	14.7

Table 6.3: Site palaeomagnetic data for the neoautochthonous sedimentary cover of the Baër-Bassit ophiolite.

^A Pal = Palaeogene; P-E = Palaeocene-Eocene; Plio = Pliocene; Aquit = Aquitanian; Burd = Burdigalian; H-T. = Helvetian- Tortonian.

^B Structure as dip direction/dip.

Alternating field demagnetisation plots

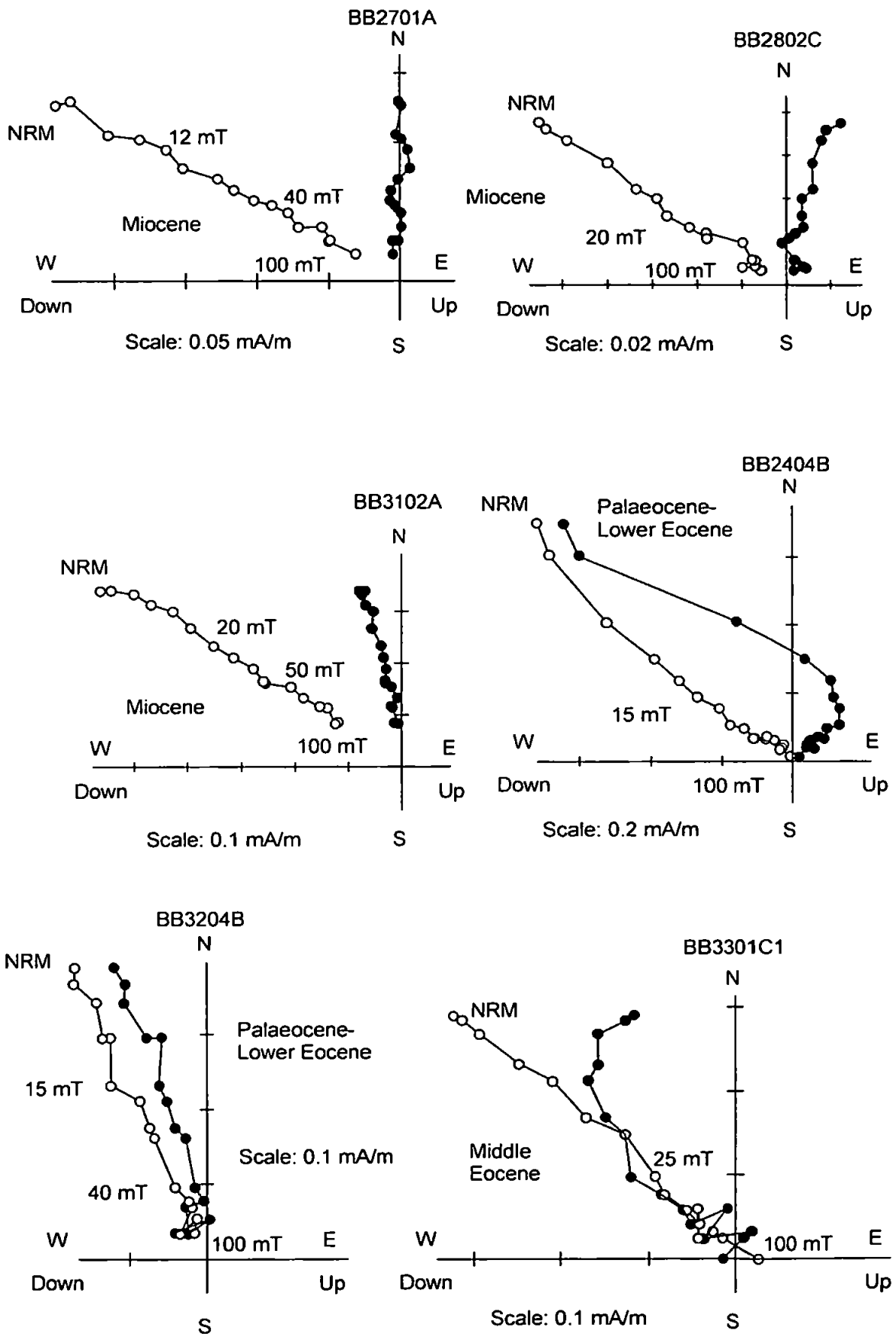


Figure 6.10: Examples of orthogonal demagnetisation plots from the sedimentary cover of the Baër-Bassit ophiolite, showing well-defined stable end point remanence directions isolated by alternating field treatment. Solid circles, horizontal plane; open symbols, vertical N-S plane. Note that the vertical projections are on the horizontal axes.

Tectonic rotations are specified by comparing site mean remanences with a reference vector derived from the APWP of Africa (section 3.6.2). An expected direction derived from the 40 Ma (Eocene) reference pole (Dec = 006°; Inc = 45°) is adopted for the Palaeogene sites, and a direction derived from the mean of the 10 and 20 Ma (Miocene) reference poles used for the Neogene sites (Dec = 006°; Inc = 50°). Confidence limits on rotation angles are calculated using the methodology of Butler (1992). Tilt tests indicate that magnetisation was acquired syn-deformation (section 6.4.5), with maximum likelihood of acquisition at 50% untilting. Comparison of mean magnetisation directions at 50% untilting for the Palaeogene sites with the reference direction indicates both anticlockwise and clockwise rotations have occurred post remagnetisation. Sites BB23/32//33/47 are rotated anticlockwise by statistically indistinguishable angles of $27^{\circ} \pm 17^{\circ}$, $37^{\circ} \pm 10^{\circ}$, $40^{\circ} \pm 6^{\circ}$ and $40^{\circ} \pm 7^{\circ}$ respectively. Sites BB17/19/24 have more variable clockwise rotations of $71^{\circ} \pm 25^{\circ}$, $40^{\circ} \pm 19^{\circ}$ and $33^{\circ} \pm 14^{\circ}$ respectively.

Geographic mean magnetisation directions for the Neogene sites cluster around north (Figure 6.11) and are indistinguishable from both the Miocene reference direction and the present day geomagnetic field. The only exception is site BB25, which has a mean geographic inclination comparable to the other Neogene sites but a NE declination. This may indicate a post-remagnetisation, clockwise rotation of $37^{\circ} \pm 17^{\circ}$. However, this seems geologically unlikely as site BB26 has a magnetisation in the main grouping and is within 0.6 km of site BB25. No major structures were observed in the field between the sites, although an inferred NE-SW trending fault is shown on the published 1:50 000 map (Kazmin and Kulakov 1968). Moreover, the BB25 remanence migrates towards more northerly declinations as moderate percentages of untilting are applied. It therefore seems more likely that the remagnetisation of this site occurred during the last stages of tilting, and does not require an explanation invoking significant rotation relative to the other Neogene sites.

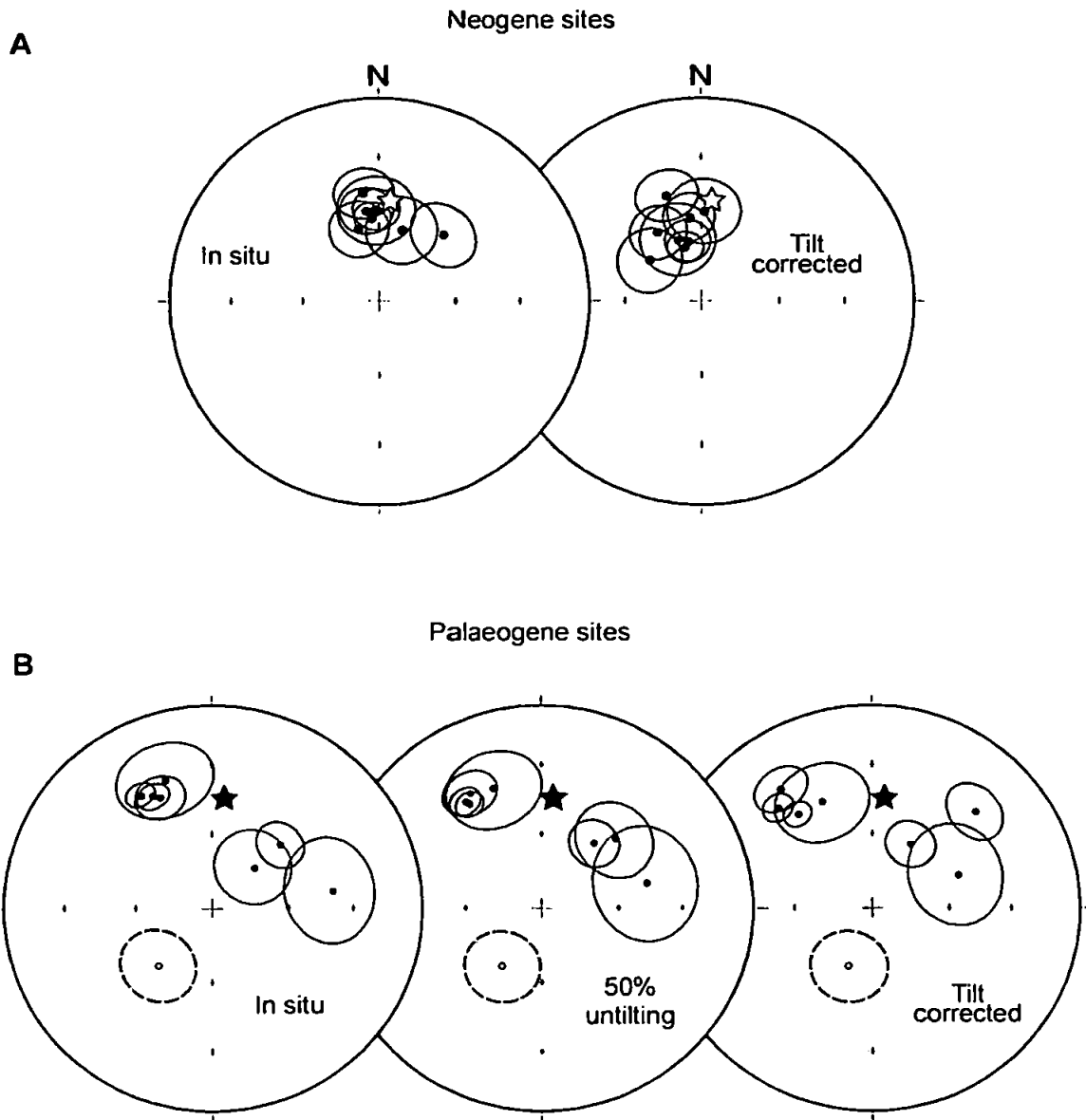


Figure 6.11: Stereographic projections showing the distribution of site mean directions of magnetisation within the sampled Neogene and Palaeogene sedimentary sequences of the Baër-Bassit ophiolite.

A. Data from Neogene sites are all of normal polarity and cannot be distinguished from the Miocene reference direction (white star) prior to tilt correction.

B. Palaeogene sites are dominantly of normal polarity, except site BB24 (grey shading) where samples display both polarities. Directions of all sites are distinctly different from the (Eocene) reference direction (black star) suggesting significant rotation after magnetisation. Sites display both anticlockwise (4 sites) and clockwise (3 sites) rotations. The magnitude of rotation of the sites rotated anticlockwise are statistically indistinguishable, whereas the clockwise rotations are more variable. Ellipses = projection of α_{95} cones of confidence around site mean remanences.

6.4.5 Timing of magnetisation acquisition (tilt tests)

An inclination-only tilt test was performed on the Neogene and Palaeogene samples from the Baër-Bassit sedimentary cover with results shown in Table 6.4 and Figure 6.12. Data from the Palaeogene sites (adopting the normal polarity component at site BB24) display a statistically insignificant increase in $\hat{\kappa}$ following tilt correction and the full tilt test is indeterminate. Stepwise untilting in 10% steps, however, gives a maximum $\hat{\kappa}$ value at 50% untilting, constituting a clear syn-tilting result (Enkin and Watson 1996) indicating acquisition of remanence during deformation of the sampled succession. Data from the Neogene sites display a decrease in $\hat{\kappa}$ following tilt correction suggesting that a post-tilting magnetisation is held by these rocks. Stepwise untilting in 10% steps gives a maximum $\hat{\kappa}$ value at 20% untilting. However, the inclination-only statistics at zero untilting are not sufficiently different from those at 20% untilting to conclusively support a syn-tilting age of magnetisation in these sequences and magnetisations are therefore interpreted as essentially post-deformational in origin. Remagnetisation of the Palaeogene carbonates is likely to have occurred during folding (regional folding occurred in the mid-Eocene; Al-Riyami et al. 2000). The data from the sub-horizontal Neogene sequences are inherently more difficult to interpret, since the distinction between northerly directed viscous overprints and unrotated Neogene magnetisations is impossible.

	<i>Number of sites included</i>	<i>Inclination \hat{I}^A</i>	<i>Precision parameter $\hat{\kappa}^B$</i>	<i>a_{95}</i>
<i>Neogene sediments</i>				
<i>In situ</i>	18	54.1° ^{+3.7°-5.9°}	119	5.1°
20% untilting	18		177.3	
Tilt-corrected	18	31.6° ^{±4.6°}	44.8	4.2°
<i>Palaeogene sediments</i>				
<i>In situ</i>	7	44.2° ^{+13.2°-10.4°}	17.7	
50% untilting	7		40.6	
Tilt-corrected	7	42.4° ^{+9.5°}	20.1	

Table 6.4: Results of the inclination-only tilt test formulation of Enkin and Watson (1996).

^A The maximum likelihood estimate of the true mean inclination in degrees.

^B The Fisher precision parameter.

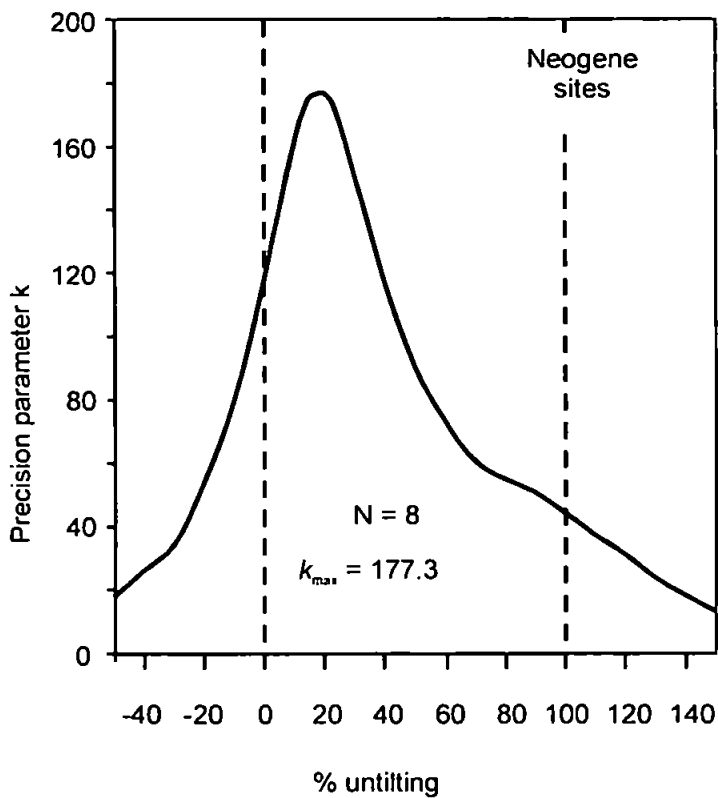
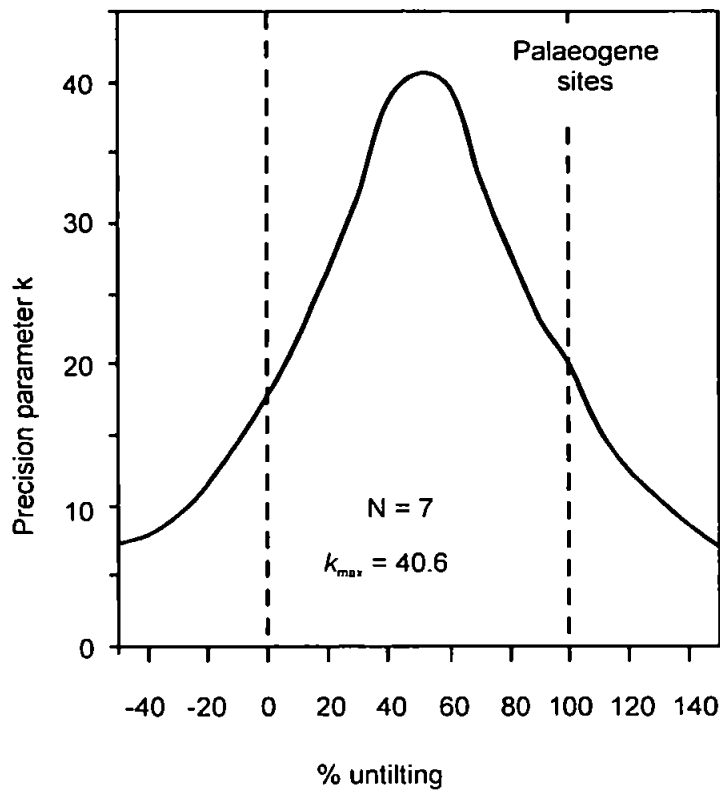


Figure 6.12: Results of inclination-only tilt tests (Enkin and Watson 1996) performed on site mean directions of magnetisation from the sedimentary cover of the Baër-Bassit ophiolite from: A. the sampled Palaeogene sequences, which indicates a syn-folding age of magnetisation with maximum clustering at 50% of total untilting; and B. the Neogene sequences, which indicates magnetisation acquisition during or after the latest phases of tilting.

6.5 Summary of results from Hatay and Baër-Bassit sedimentary covers

Inclination-only tilt tests indicate that the magnetisations in the sedimentary sequences of the Hatay ophiolite are pre-deformational in origin. The palaeomagnetic results from the sedimentary cover of the Hatay ophiolite from both Palaeogene and Neogene sediments indicate that only minor rotations have occurred and that the sediments have not experienced the larger rotations observed in the underlying ophiolitic units (Figure 6.5). Inclination-only tilt tests on the sedimentary cover of the Baër-Bassit ophiolite indicate that magnetisations are either syn- (Palaeogene sites) or post- (Neogene sites) deformational in origin. The palaeomagnetic results from rocks of Neogene age of the sedimentary cover of Baër-Bassit, similarly show that only minor rotations have occurred since these sediments were remagnetised (Figure 6.11). The rotations of the older Palaeogene sediments of the Baër-Bassit sedimentary cover may be attributed to the effect of Neotectonic strike-slip fault systems. The fact that the older sediments analysed from the Hatay sedimentary cover do not appear to have been remagnetised alongside the observation that this area is not significantly affected by strike-slip faulting lends support to this idea.

6.6 Discussion

The new palaeomagnetic data from the Tertiary sedimentary sequences which unconformably overlie the Hatay and Baër-Bassit ophiolites are important for understanding the timing of the large rotations in the underlying ophiolites (Figure 6.13). As these ophiolites are believed to comprise part of the same sheet they are expected to have similar pre-emplacement histories. These neoautochthonous rocks can only have been affected by tectonic rotations that post-date emplacement of the ophiolite. If sedimentary cover rocks are unrotated or have experienced only minor rotations, the large rotations in the underlying ophiolites must have occurred prior to their deposition.

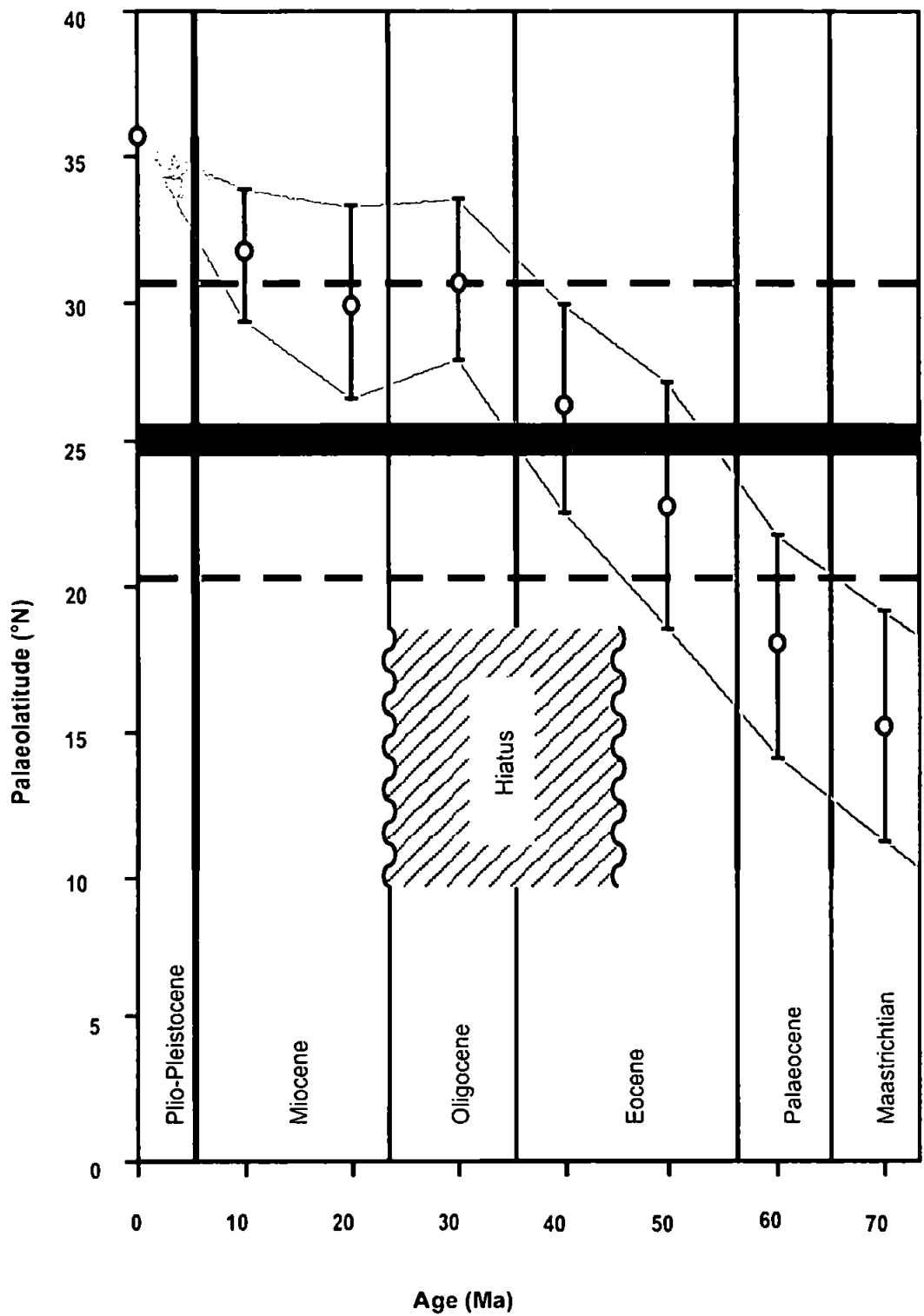


Figure 6.13: Tertiary palaeolatitudes for the Baër-Bassit area predicted from the African apparent polar wander path (of Besse and Courtillot 1991), following minor correction for the effects of opening of the Red Sea. Thick solid line indicates the palaeolatitude derived from the mean inclination of the Palaeogene sites at 50% untilting, together with the associated 95% confidence limits (dashed lines). The inferred mid Eocene timing of remagnetisation of these rocks is consistent with the timing of initiation of regional gentle folding in response to initial suturing between Arabia and Anatolia to the north. The hiatus refers to a hiatus in sedimentary deposition in the Baër-Bassit area.

Palaeomagnetic analyses of these sequences, therefore, provide the only means to assess the extent of Tertiary rotation(s) of the underlying ophiolitic units, and hence to compare the evolution of rotation of the Baër-Bassit and Hatay ophiolites with the well documented rotation of the Troodos microplate.

The data from the sedimentary cover sequences of the Hatay ophiolite, including those from the oldest (Palaeocene) sequences, indicate only minor anticlockwise rotation. This contrasts with the large anticlockwise rotations observed in the underlying ophiolite, and confirms that most (c. 60-70°) of the rotation of the ophiolite occurred either in an intra-oceanic setting and/or during tectonic emplacement in the Maastrichtian. The significant post-emplacement rotations of the Palaeogene sedimentary sites of the Baër-Bassit ophiolite are attributed to the affect of Neotectonic strike-slip fault systems. Rotations of the sedimentary cover of the Hatay ophiolite may be expected to be of smaller magnitude as this has been less affected by Neotectonic strike-slip faulting. The more varied and greater rotations observed in the southern part of the Baër-Bassit ophiolite (Morris et al. 2002) may also partially be explained by these major strike-slip fault systems.

6.7 Synthesis

Analysis of palaeomagnetic data from the sedimentary cover of the Hatay ophiolite and from results taken from a paper by Kissel et al. (2003) as well as analysis of the Baër-Bassit sedimentary cover show that the large rotations observed in the underlying ophiolite cannot be accounted for by Neotectonic rotations as the rotations experienced by the sedimentary covers of Hatay and Baër-Bassit are minor in comparison to those in the underlying ophiolites. The implication of this is that the majority of the large rotations of the ophiolites are pre-cover in origin. This supports the idea that at least a component of the large rotations occurred while the ophiolites comprised part of a coherent microplate.

7. ROCK MAGNETIC AND SCANNING ELECTRON MICROSCOPE ANALYSES FROM THE HATAY OPHIOLITE

7.1 Introduction to chapter

The demagnetisation analyses and tilt tests (Chapter Five) indicate that remanent magnetisations in the Hatay ophiolite are pre-tilting in origin and therefore have been stable throughout a complex tectonic history. To support this result as well as to gain further insight into the magnetic characteristics of oceanic crustal rocks, a series of rock magnetic experiments, thin section analyses and scanning electron microscope analyses were performed on a cross-section of samples. Initial rock magnetic experiments and thin section analyses were performed at the University of Plymouth laboratory and were followed by a measurement programme at the Institute for Rock Magnetism (IRM) at the University of Minneapolis, U.S.A. The primary magnetic minerals that form in oceanic crustal rocks are subsequently affected by seafloor hydrothermal activity and are potentially altered by obduction-related processes and by subsequent tectonic events. From the positive inclination-only tilt tests it was anticipated that the remanence-carrying magnetic minerals would be of pre-deformational origin. The magnetic minerals carrying the pre-deformational remanence in the ophiolite are anticipated to be either those observed within present day in situ oceanic crust, or an inversion that allows early magnetisation to be retained, with potential variations in magnetic mineralogy between the different lithologies sampled. In the Hatay ophiolite, the rocks being studied include most levels of the crustal pseudostratigraphy, from the ultramafic cumulates up through the gabbros and sheeted dykes to the extrusive rocks. Rock magnetic characteristics are often determined from studies of synthetic minerals and where research has been done on in situ present day oceanic crust it has tended to be concentrated on the more accessible upper

levels, i.e. pillowed and sheet lava flows and sheeted dykes. Prior to describing the rock magnetic results from the Hatay ophiolite, a brief description of the magnetic mineralogy of mafic igneous rocks and the processes by which magnetic minerals form within oceanic crust will be given in order for the terminology used in the description of experimental procedures and results to make sense to readers less familiar with rock magnetism. A basic description of the major rock magnetic parameters used in determining rock magnetic characteristics was given in Chapter Three and will not be repeated here.

7.2 Magnetic minerals in ocean floor rocks

7.2.1 Magnetic minerals

Most magnetic minerals are either iron oxides or iron titanium oxides and fall within the ternary system TiO_2 (rutile), FeO (wustite) and Fe_2O_3 (haematite) (O'Reilly 1984) (Figure 7.1A). Magnetite is the most abundant mineral carrying natural remanent magnetisation in rocks, and its properties and behaviour have been extensively studied. Magnetite forms a cubic spinel structure at temperatures above the Verwey transition (~ 120 K) and so will be a cubic spinel at geologically relevant temperatures. A titanomagnetite can be represented by the formula $\text{Fe}_{3-x}\text{Ti}_x\text{O}_4$ ($0 < x < 1$). For example, the idealised titanomagnetite to form in oceanic crust has the formula $\text{Fe}_{2.4}\text{Ti}_{0.6}\text{O}_4$ and is referred to as TM60, (O'Reilly 1984). In reality, oxidation and substitution of the Fe^{2+} and Fe^{3+} ions by Al^{3+} , Mg^{2+} and Mn^{2+} ions result in deviations from this idealised formula. No definitive boundary distinguishes between titanomaghemites and non-stoichiometric titanomagnetites. However, titanomagnetites that crystallise from the melt and cool from high temperature can only maintain a small degree of non-stoichiometry before separating into two end member phases of near-magnetite and near-ilmenite (O'Reilly 1984).

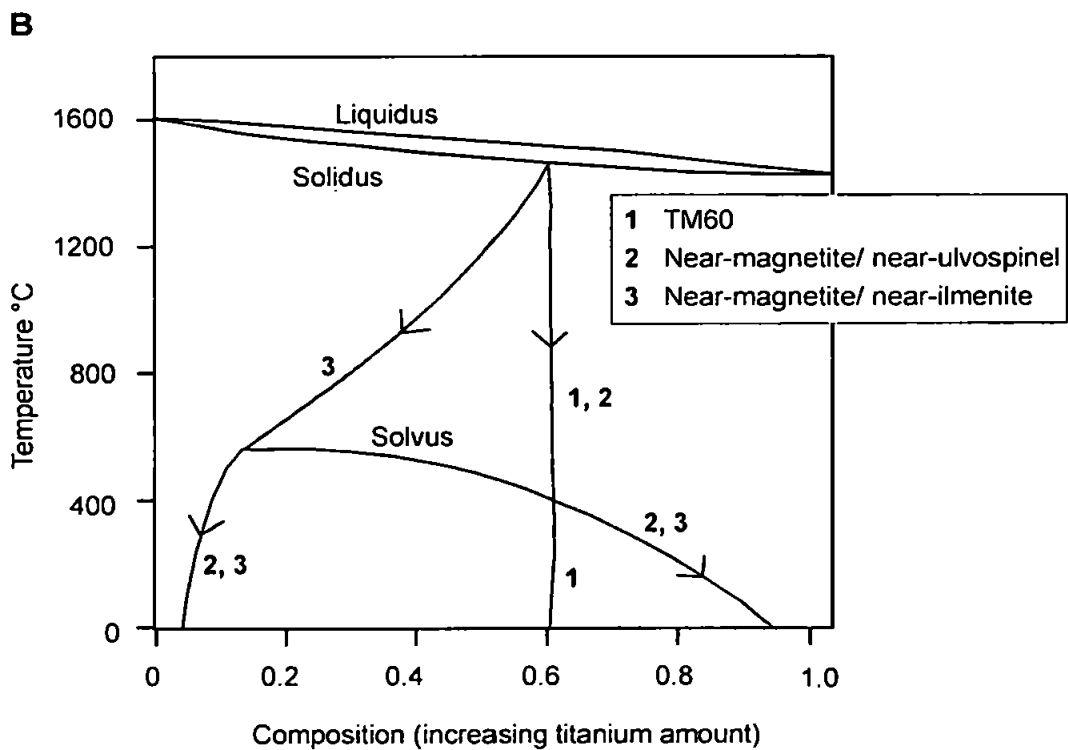
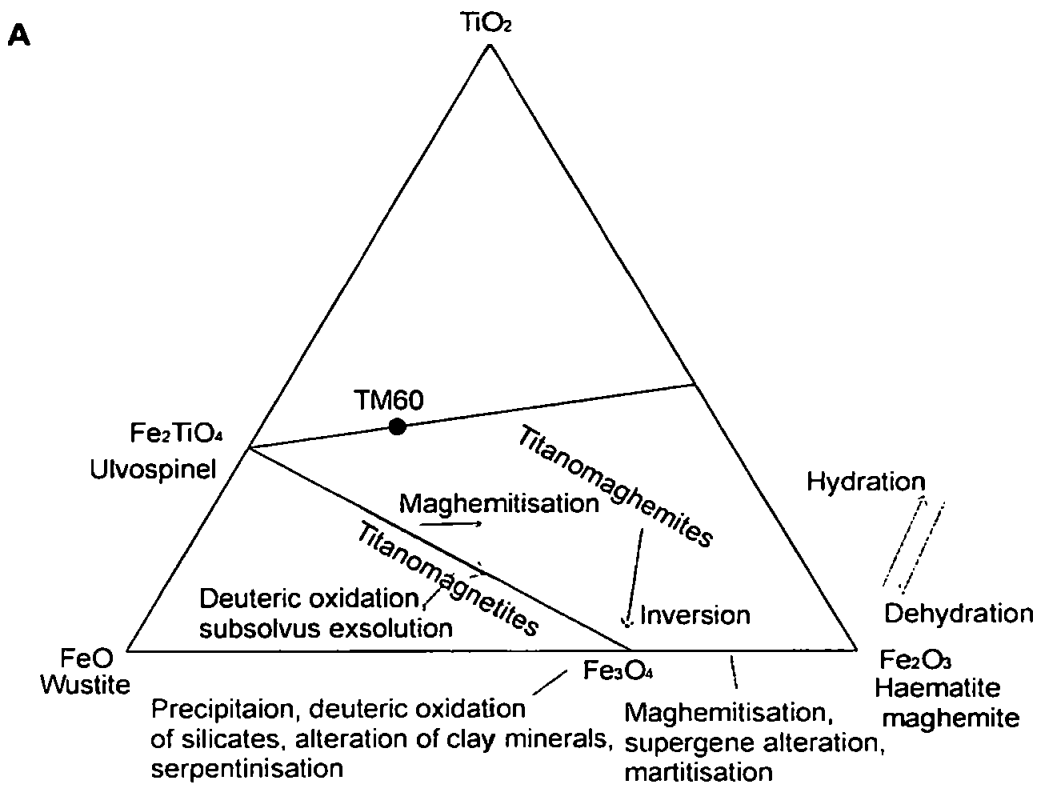


Figure 7.1: The composition of the magnetic minerals common in oceanic crust and their methods of formation (from O'Reilly 1984).

A. The location of common oceanic magnetic minerals on a ternary TiO_2 - Fe_2O_3 - FeO diagram.

B. Possible paths followed by a magnetite of composition $\text{Fe}_{3-x}\text{Ti}_x\text{O}_4$ ($0 < x < 1$) as magma cools in an oceanic environment. Firstly, rapid cooling (path 1) produces a titanomagnetite of composition TM60 whereas slow cooling with no oxidation (path 2) would preserve a near-magnetite and near-ulvospinel phase. Slow cooling with deuteric oxidation above T_c (path 3) preserves a near-magnetite and near-ilmenite phase.

Maghemitisation, occurring at low temperatures, is capable of producing very high levels of non-stoichiometry. Both titanomagnetites and titanomaghemites can be described by the formula $\text{Fe}_{(3-x)R}\text{Ti}_{xR}\square_{3(1-R)}\text{O}_4$, where x now has different limits compared to the formula for ideal stoichiometry, $8/(9+x) < R < 1$ (stoichiometry) and \square are vacancies occurring in the cation sites of the structure. Titanomaghemites are produced by oxidation of titanomagnetites, either by addition of oxygen or by removal of iron. The degree of stoichiometry is often described by the oxidation parameter, z , where z is the fraction of initial Fe^{2+} oxidised to Fe^{3+} ($0 < z < 1$) (O'Reilly 1984). When oxidation occurs by addition of oxygen, the addition of $(z/2)(1+x)\text{O}$ will have oxidised a fraction z of the initial Fe^{2+} , producing an additional $z(1+x)\text{Fe}^{3+}$ (O'Reilly 1984), although a detailed explanation of this will not be presented in this thesis.

7.2.2 Formation processes of the magnetic minerals in oceanic crust

The magnetic minerals in oceanic crust depend on variables such as the composition and cooling rate of the magma (Figure 7.1B). Both titanomagnetites and titanohematites crystallise at around 1300°C and are early in the crystallisation sequences of igneous rocks (Butler 1992). Rapidly cooled oceanic rocks (such as pillow basalts) often contain titanomagnetites with skeletal crystalline habits that are smaller than $1\ \mu\text{m}$, whereas grain sizes in more slowly cooled igneous rocks can exceed $100\ \mu\text{m}$ (Butler 1992). For a basaltic magma there are various theoretical paths that produce different magnetic minerals depending on variables such as magma composition and cooling rate. Total FeTi content of basalts is typically around 5% by volume, with approximately equal parts of titanomagnetite and titanohematite (Butler 1992). In a 'typical' basalt the titanomagnetite composition lies in the range $0.5 < x < 0.8$ (O'Reilly 1984). Primary titanohematite will generally have a composition in the range $0.8 < x < 0.95$ i.e. almost pure ilmenite and will

be paramagnetic under ambient surface conditions. Below, is an explanation of how possible rock magnetic carriers may form.

Magnetite or titanomagnetite are the primary magnetic minerals with any composition between magnetite and ulvospinel possible at high temperature. Below the solvus, intermediate compositions are unstable, but very rapid cooling of submarine basalts preserves titanomagnetite with intermediate titanium composition (TM60) and magnetic grains will generally be skeletal in texture. TM60 is therefore expected to be found in extrusive rocks such as basaltic pillow lavas.

Slower cooling with deuteric oxidation above the Curie temperature preserves an exsolution texture of near-ilmenite and near-magnetite lamellae (O'Reilly 1984) and is thought to occur at temperatures above around 750°C (Butler, 1992). Titanomagnetite has an irregular distribution of Fe^{3+} and Fe^{2+} on A sites and some B sites have Fe^{3+} and Fe^{2+} and others have Ti^{4+} . Exsolution is where at temperatures above the Curie temperature (T_c) the iron and titanium diffuse into regions of regular cationic arrangement and the cubic symmetry of the initial titanomagnetite is preserved. In nature, magnetite-ulvospinel intergrowths are uncommon, as usually titanomagnetite is oxidised in the melt by deuteric oxidation or oxyexsolution which results in an intergrowth of phases of near-magnetite and near-ilmenite. More of the magnetite phase is produced by oxyexsolution than by normal exsolution. Exsolution significantly reduces the effective magnetic grain size, with a large grain of homogenous composition transformed into fine-grained Ti-poor titanomagnetite in-between regions of Ti-rich paramagnetic titanomagnetite i.e. large unstable MD titanomagnetites are subdivided to produce stable SD magnetites.

Low temperature oxidation of (titano)magnetite forms (titano)maghemite with a cubic spinel structure like magnetite but the overall chemical formula of hematite.

Maghemitisation can also result from slow cooling below about 400°C or by mild reheating in an oxidising environment. Maghemite contains vacancies in the spinel lattice. In the submarine environment, maghemitisation usually proceeds by leaching of iron by seawater. At room temperature magnetite has an unusually high electrical conductivity for an oxide mineral which occurs because electrons are continuously hopping between the Fe^{3+} and Fe^{2+} cations in the octahedral sublattice giving an average valency of 2.5 to the B site cations. These electrons are therefore mobile and may contribute towards the process of maghemitisation (O'Reilly 1984). At a crystal surface, locally mobile electrons may momentarily accumulate in sufficient numbers on an Fe^{2+} or Fe^{3+} cation to make it momentarily neutral i.e. it attains the atomic form Fe. The atom is then no longer chemically bound and can be leached away by seawater or pore fluids. Electrons have been lost to the system and diffusion within the grain and change of valency of some electrons is required to bring about homogeneity. Numbers of Fe^{3+} cations therefore increase at the expense of Fe^{2+} cations to allow more free electrons to take part in bonding and so the loss of one electron requires the loss of 3 Fe^{2+} cations and the gain of 2 Fe^{3+} cations. Fe^{2+} cations diffuse to the surface which allows the process to continue, leaving vacancies or gaps in the lattice structure in their original position. The position of oxygen atoms within the structure is unchanged and the lattice retains the spinel structure. Oxidation of magnetite to maghemite reduces the size of a unit cell as Fe^{2+} cations are lost and so the crystal shrinks and cracks during maghemitisation. Remanence remains unchanged during this process as none of the Fe^{3+} cations in A sites have been affected and when B site Fe^{2+} cations change to Fe^{3+} their atomic dipoles are locked in through exchange interaction to the orientation of the primary A site Fe^{3+} . Pillow lavas and the upper portions of lava flows are more susceptible to maghemitisation due to their higher porosity and permeability compared to the interior of lava flows. Interstitial glass can protect titanomagnetite grains from the maghemitisation process.

Maghemite is metastable and inverts to hematite at temperatures of between 350 to 750°C, depending on grain size, oxidation and impurities. This phase transition involves no chemical change but a change in crystal structure from cubic spinel to rhombohedral with only a small displacement of atoms. This reorganisation removes a remanence preserved in the maghemite prior to its inversion to hematite. Maghemite can alter to magnetite during subsequent low-temperature inversion (O'Reilly 1984).

Other minerals can also undergo alteration during the cooling of an igneous body to produce magnetic minerals. Primary ilmenite will deuterically oxidise in the same manner as the ilmenite component of a deuterically oxidised titanomagnetite during the later stages (O'Reilly 1984), with haematite or a near-haematite member of the ilmenite-haematite series resulting alongside TiO_2 and maybe Fe_2TiO_5 . Iron-bearing silicates such as olivines and pyroxenes are susceptible to deuteric oxidation during the cooling of an igneous body (O'Reilly 1984). Iron oxides and oxyhydroxides can be produced during low-temperature alteration of silicates during the processes of serpentinisation and iddingitisation (O'Reilly 1984). These exsolved magnetic minerals generally comprise only a small proportion of the rock, although they tend to be fine grained and as such can be effective palaeomagnetic recorders (Butler 1992).

To summarise, major magnetic mineral sources that may carry the pre-deformational remanences preserved in the ophiolite are:

- Primary titanomagnetite (TM60)
- Titanomaghemite formed by low-temperature oxidation of TM60
- Magnetite formed during exsolution or by subsequent low-temperature inversion of titanomaghemite.
- Primary magnetite as inclusions in other minerals e.g. within silicates in gabbroic rocks.

7.3 Rock magnetic experiments

7.3.1 Overview of experiments

Rock magnetic analyses are an effective method for distinguishing between magnetic minerals, and include experiments such as hysteresis measurements, identifying low temperature inversions and Curie point determinations. Use of a combination of rock magnetic parameters is generally required due to non-uniqueness if only one parameter is known. Many experiments have been done on both synthetic and natural magnetic minerals and deciding on the detailed characteristics of the magnetic mineralogy of a sample can be a matter of comparing results to the established database of previous results. Theoretical predictions of results are not necessarily sufficiently constrained to use alone, without reference to experimental results. For instance, the temperature at which the Verwey transition occurs is well known for stoichiometric magnetite, but differences in the shape of field cooled and zero field cooled warming curves are generally compared to experimental results from synthetic samples with known compositions. Rock magnetic experiments can be non-destructive and low temperature experiments and hysteresis measurements have the advantage that these approaches also avoid permanent chemical changes, whereas heating specimens can introduce mineralogical changes. The aim of the rock magnetic experiments is to distinguish the magnetic composition and grain size distributions and any variations of these properties between lithologies in order to establish the stability of the magnetic signal and the timing of its acquisition.

The rock magnetic experiments that were carried out to find out the magnetic carriers of the rocks sampled for this thesis are described in Table 7.1:-

<i>Experiment</i>	<i>No. Samples measured</i>	<i>Equipment</i>	<i>Laboratory facility used</i>	<i>Description of Measurements</i>
Hysteresis loops	135 (2 per site)	Princeton Applied Research Vibrating Sample Magnetometer (VSM)	IRM	Loop; Saturation remanent magnetisation (Mrs); Coercivity of remanence (Hcr)
Acquisition of isothermal remanent magnetisation (IRM) analyses	63 (1 per site)	Molspin Pulse Magnetometer; Molspin fluxgate spinner magnetometer	University of Plymouth	IRM acquisition curve of remanent magnetisation against field
Curie point (T_c) determinations	(i) 51 powdered samples (ii) 5 samples	(i) Princeton Measurements Micro Vibrating Sample Magnetometer (MicroVSM) (ii) AGICO KLY3 Kappabridge with a furnace	(i) IRM (ii) University of Plymouth	(i) Magnetic moment against temperature (ii) Susceptibility against temperature to corroborate and add detail to a few of the measurements performed at the IRM
Low temperature experiments	(i) 54 powdered samples (ii) 5 selected samples	Quantum Design Magnetic Property Measurement System (MPMS)	IRM	Thermomagnetic curves (i) cooling room temperature (RT) SIRM acquired in 2.5T field from 300-10K, and warming a low temperature (LT) SIRM acquired in 2.5T field from 10-300K (ii) cooling and warming curves of RT SIRM and cooling curve both in field (FC) and in zero field (ZFC)
Alternating current (AC) susceptibility as a function of frequency	8 samples	MPMS and the Lakeshore AC Susceptometer	IRM	In-phase and out-of-phase susceptibility against frequency
Standard AF demagnetisation procedures	6-12 samples per site	AF tumbling demagnetiser; Molspin fluxgate spinner magnetometer	University of Plymouth	Information on median destructive fields (MDFs) gives indication of coercivity and corroborates results from hysteresis and IRM acquisition experiments
Standard thermal demagnetisation procedures	At least 1, usually 2 samples per site	Furnace; Molspin fluxgate spinner magnetometer	University of Plymouth	Information on unblocking characteristics of NRM

Table 7.1: The rock magnetic experiments carried out in the University of Plymouth and the Institute for Rock Magnetism (IRM).

7.3.2 Hysteresis of magnetic minerals

The path of magnetisation in a sample as a function of the applied magnetic field is referred to as a hysteresis loop. Hysteresis experiments measure the magnetisation of a sample in field, with diagnostic points being the saturation magnetisation (M_s), field at which saturation magnetisation is reached and coercivity (H_c) as well as the shape of the curve. The Princeton Applied Research VSM enables saturation of remanent magnetisation (M_{rs}) and coercivity of remanence (H_{cr}) to be measured in addition to the parameters measured in field.

Hysteresis parameters are commonly presented on a Day plot (Day et al. 1977), which plots the ratio of saturation remanence to saturation magnetisation, M_{rs}/M_s , against the ratio of remanent coercive force to coercive force, H_{cr}/H_c . The magnetisation ratio is generally accepted to have more discriminating power than the coercivity ratio (Dunlop and Özdemir, 1997). This plot is used to discriminate magnetic domain state and is divided up into regions of different magnetic domain sizes: single domain (SD); pseudo-single-domain (PSD); multidomain (MD). This plot is not definitive in terms of domain state, which can be affected by such variables as composition and internal stress introduced in sample preparation (Dunlop 2002). For example, the PSD trend for TM60 is narrower and occupies a different region in the Day plot from the PSD trend for magnetite (Dunlop 2002).

<i>Domain state</i>	<i>Hcr/Hc</i>	<i>Mrs/Ms</i>
MD	High Boundary $> 5.0^A$ or $\sim 4^B$	Low Boundary $< 0.02^A$ or 0.05^B
PSD	Medium (between SD and MD regions)	Medium (between SD and MD regions)
SD	Low Boundary $< 2.0^A$ or $\sim 1^B$	High Boundary $> 0.5^{A, B}$
SP (if present)	Higher than expected: measured coercive force is lowered by SP grains	Lower than expected: Ms is raised by SP grains

Table 7.2: The division of magnetic minerals into domain state using Hcr/Hc and Mrs/Ms ratios to aid diagnosis. The table indicates whether the ratios are high or low for each domain state and displays the values commonly assigned to the boundaries between fields on the Day plot. Due to the number of parameters that have been found to affect the value of these ratios they are used as a guide rather than a definitive boundary and thus boundaries between fields on a Day plot are not definitive and different values have been suggested by different authors.

^A Recent values for the field boundaries (Dunlop 2002).

^B Conventional values for the field boundaries (Day et al. 1977; Dunlop and Özdemir 1997).

One hundred and twenty three standard palaeomagnetic cores were measured on the Princeton Measurements VSM with the pole pieces set wide enough apart for the sample to fit between them. The absolute value of magnetisation is not entirely accurate due to the machine being designed to measure point dipoles rather than whole rock specimens. However, the measured value of M_s and M_{rs} will give a good indication of the correct value and the ratios M_{rs}/M_s will not be affected. The magnetic field of the VSM ranges from 0 T to 1.6 T with a sensitivity of $2 \times 10^{-8} \text{ Am}^2$. For 63 cores with higher intensities the range of the equipment was insufficient to measure the magnetisation. For these cores, a ‘Times Ten’ device (designed by Jim Marvin) was attached to the machine output in order for the magnetisation to be recorded. Six of the pillow lavas that were sampled using the ‘cork method’ were measured in the VSM, subsequent to being cut down to a cube of similar size to a standard palaeomagnetic core. Six sediment samples were also measured (results discussed in Chapter Six).

In rare cases, a sample did not contain a high enough quantity of ferromagnetic minerals to measure the hysteresis parameters and the magnetic fraction in the sample appeared to be composed primarily of paramagnetic minerals.

7.3.3 Acquisition of isothermal remanent magnetisation (IRM) analyses

Isothermal remanent magnetisation (IRM) experiments measure the remanent magnetisation (out of field) remaining in a sample following exposure to a magnetic field. The shape of the acquisition curve can indicate the magnetic mineralogy; for instance magnetite saturates by around 300 mT whereas haematite does not saturate until over 1 T. The return path can also be measured, enabling coercivity of remanence or backfield coercivity (H_{cr}) to be found. IRM demagnetisation data may not be representative of the original carriers of *natural* remanence because when the specimen is exposed to the direct field, all grains capable of being magnetised will become magnetised in this direction, even though some of these grains may not have contributed to the net remanence. IRM analyses therefore involve potential carriers of NRM rather than necessarily being limited to those grains that actually carry the remanence.

IRM experiments involve the use of a pulse magnetometer and a Molspin spinner magnetometer. The sample needs to be completely demagnetised initially and so IRM analyses are usually carried out subsequent to standard demagnetisation procedures. The sample is subjected to a unidirectional magnetic pulse, imparted along the z axis of the specimen, and this is increased in steps, with measurement of the remanent magnetisation (out of field) made subsequent to each step. Following the maximum applied field, which is 800 mT for the equipment in the University of Plymouth laboratory, the experiment may be repeated with fields applied in the opposite direction (sample turned upside down). This procedure results in forward and backfield IRM acquisition curves with the shape of the forward curve indicative of the magnetic mineralogy and the backfield curve defining the coercivity of remanence.

Some IRM acquisition curves were also measured on the MicroVSM at the University of Minneapolis in order to check consistency with the larger number of IRM curves obtained from earlier measurements at the University of Plymouth laboratory.

7.3.4 Curie point determinations

The Curie temperature (T_C) is indicative of mineralogy, although care must be taken due to non-uniqueness of T_C s (Table 7.3). Diagnostic features of high temperature experiments are temperatures at which changes in susceptibility/magnetisation are observed, for instance a sharp decrease corresponding to the Curie temperature, or mineralogical transformations during heating.

<i>Composition/ process</i>	T_C^A
Magnetite	~590°C
Haematite	680°C
Addition of titanium	Tc lowered
TM60	~140°C
Maghemite ^B	640°C
Maghemitisation ^B	Tc raised

Table 7.3: The Curie temperatures for the main magnetic minerals and the effect of the addition of titanium and of maghemitisation processes.

^A Published data for Curie points can be variable depending on factors such as measurement procedures as well as differences due to exact compositions.

^B Measurement of T_C can be difficult due to the conversion of maghemite to haematite below this temperature at around 300 to 400°C (estimates of different authors vary).

Single domain grains can be diagnosed if there is evidence of a ‘Hopkinson Peak’ where an increase in magnetisation/susceptibility is observed immediately prior to the Curie point due to unblocking of the magnetisation due to the SD grains reaching their narrow spectrum of unblocking temperatures (T_B) just prior to reaching T_C . The relationship between T_C and oxidation degree (z) and for different compositions of Ti content (x) can be plotted as calibration curves (Nishitani and Kono 1983). Alteration of the magnetic minerals shows up as a discrepancy between the heating and cooling curves. More than one component to the curve suggests either the existence of two minerals or different

compositions of the same mineral with different T_C s or the inversion of one mineral to another during heating. Curie points were determined by using the tangential intersection method i.e. a tangent was constructed either side of the area of the curve with the highest gradient with the intersection point of the two tangents giving the temperature of interest. Natural samples may show a range of Curie temperatures and so the effective Curie temperature has been taken to be the point at which the rate of decrease of magnetisation or susceptibility was maximum.

The MicroVSM with furnace attachment was used to measure samples with measurements taken every 1°C between 20°C and 700°C, measuring the induced moment versus temperature in a 250 mT field. The 250 mT field was expected to saturate all except the highest coercivity minerals. If haematite is present and not saturated, the resultant temperature of T_C could be affected slightly. The value for the appropriate field strength to use was obtained by analysis of hysteresis loops prior to measurement of T_C . Hysteresis loops were obtained both prior to and subsequent to the measurement of T_C in order for any mineralogical changes to be identified.

Analyses measuring the variation of either magnetisation or susceptibility with temperature should give identical results, although various authors have reported some discrepancies. It is possible for the thermocouple in the furnace of the Micro Vibrating Sample Magnetometer (VSM) to be easily nudged slightly out of position due to its high sensitivity. This produces results that will plot curves at slightly higher or lower temperatures than the real temperatures, out by a small consistent factor. This is easy to correct for by measurement of a standard sample in the MicroVSM or by a corroborating measurement carried out plotting susceptibility against temperature using a Kappabridge. A number of specimens measured for this thesis suffered from such a misalignment of the thermocouple in the VSM and were accurately corrected by repeating measurements of

selected samples using the University of Plymouth KLY3 Kappabridge system. For example, sample CD0605 had a T_C of 615°C measured using the MicroVSM and 595°C measured using the Kappabridge (similarly 350°C and 330°C respectively for the lower temperature component). This result, in conjunction with the other checks implies that the thermocouple misalignment of the VSM produced an overestimate of 20°C. One cumulate sample (KC0107) and one lava sample (ML0106) were dominated by paramagnetic minerals resulting in a noisy high temperature curve.

7.3.5 Low temperature experiments: the Verwey transition

Low temperature experiments enable any low temperature transitions occurring in the magnetic minerals to be observed. The transition that is particularly expected from oceanic crustal rocks is the Verwey transition, which is diagnostic of magnetite. The precise temperature and nature of the transition is affected by the amount of titanium in the sample as well as by oxidation and the degree of recovery of magnetisation through the transition is affected by the size of the magnetic grains. So, the transition is sensitive to the effects of non-stoichiometry, cation substitution and grain size (Muxworthy and McClelland, 2000). The Morin transition occurs at around 250 K due to the loss of spin canting in haematite on cooling below room temperature and magnetisation decreases across the transition.

The Verwey transition (T_V) occurs in magnetite (Verwey 1939) due to the transformation of magnetite from a cubic structure to a lower symmetry, probably monoclinic structure (e.g. Özdemir et al. 1993). Magnetite also has a magnetic isotropic point (T_i) at around 130 K (Kakol and Honig 1989). At the isotropic point, the first order magnetocrystalline anisotropy constant becomes zero as it changes sign and the easy directions of magnetisation change their orientation (Moskowitz et al. 1998). These transitions produce a distinctive magnetic signature in both remanence and magnetic susceptibility.

Remanence above or below T_V or T_i will be partially demagnetised on cycling through these transitions. Magnetic susceptibility is at a maximum at T_i , where the anisotropy energy is a minimum and susceptibility drops rapidly below T_V (Moskowitz et al. 1998). The exact controls on the transformation of remanence across the cubic-monoclinic phase transition remain unclear (Özdemir et al., 2002).

<i>Composition</i>	<i>Verwey transition</i>
Synthetic stoichiometric magnetite	120 K
Natural magnetite samples	Often ~110 to below 100 K
Small degrees of non-stoichiometry ($z < 0.05$)	Lowered to < 100 K (T_i not affected)
Higher degrees of non-stoichiometry ($z > 0.1$) e.g. produced by low-temperature magnetisation	Transition smeared out in submicron-sized particles (eventually suppressed at $z > 0.3$) (Özdemir et al. 1993)
Increasing titanium content	Transition becomes smeared out and is not observed for compositions $x > 0.4$ (Kakol et al. 1991)

Table 7.4: The temperature and nature of the Verwey transition for various magnetic mineral compositions.

The variation of remanence over the Verwey transition depends on the temperature at which the remanence was produced and the direction in which T_V is approached (Özdemir et al. 2002). Therefore, low temperature experiments ideally approach the transition from both directions. The behaviour of magnetite on crossing the transition is dependent on grain size. An SIRM acquired at room temperature (RT SIRM) shows a gradual decrease in magnetisation on cooling to T_V , by amounts that increase as grain size increases (Özdemir et al., 2002), but an SIRM acquired at low temperature (LT SIRM) scarcely changes with heating until T_V is reached and the curves are grain size independent. For both submicron and millimetric grains of magnetite, if SIRM is imparted into the monoclinic phase and T_V is approached from below, the shape of the curves is almost independent of grain size, except for the memories (recovery of remanence following re-cooling/warming), whereas if a room temperature SIRM is imparted to the cubic phase, the memories and shapes of the curves are strongly dependent on both domain state and grain size (Özdemir et al. 2002). For magnetite with a low temperature SIRM warmed through

T_V , demagnetisation at T_V is almost total and the isotropic point T_i is unimportant, whereas for magnetite with room temperature SIRM cooled through the transition, T_i and T_V both play a role in the demagnetisation mechanism (Özdemir et al. 2002). The reason for these differences is due to the different domain structures above and below T_V ; below T_V , spins lie along a single axis whereas above T_V , spins have a choice of six or eight easy directions (Özdemir et al. 2002). Spins during a change from cubic to monoclinic symmetry therefore have a possibility of realigning to only two directions whereas on warming through the transition from a monoclinic symmetry, spins may realign to any of eight easy directions, resulting in a greater destruction of remanence across the transition.

The Morin transition in haematite occurs at 260 K (-15°C) in pure haematite due to a change in orientation of the antiferromagnetic spin structure, with haematite displaying spin canting at room temperature. The temperature at which the transition takes place varies with both composition and grain size (O'Reilly 1984). The transition temperature falls as grain size is reduced and the introduction of other species of cations also usually lowers the transition (O'Reilly 1984). The Morin transition is more evident on cooling subsequent to imparting a RT SIRM than on warming subsequent to imparting a LT SIRM.

Samples cooled and warmed in zero fields can behave differently, with the nature of the differences influenced by grain size. Experiments measuring behaviour on warming following cooling of a RT SIRM in both zero field (ZFC) and in field (FC) can aid diagnosis of rock magnetic characteristics. For example, the percentage recovery of remanence during cooling and warming a RT SIRM in zero field is an indicator of grain size in magnetite; ranging from 86% for synthetic 0.037 μm magnetite crystals to 55% for 0.22 μm magnetite crystals (SD/SP at room temperature) (Özdemir et al. 2002). The loss of remanence cooling from room temperature to T_V is also a grain size indicator, ranging from 5% for 0.037 μm to 35% for 0.22 μm grains (Özdemir et al. 2002).

Standard low temperature experiments measure one cycle of a RT SIRM through T_v and one cycle of a LT SIRM through T_v so the magnetisation of the sample is measured approaching T_v from both directions following the imparting of a saturation magnetisation to the sample. This standard low temperature experiment was used in this thesis for most samples (described earlier) and is referred to as a RT-LT SIRM cooling-warming cycle or temperature sweep. Longer experiments were carried out on selected samples to allow more information to be gained regarding the magnetic characteristics of a sample crossing T_v . Longer experiments for this study measured warming curves of a sample in zero field following cooling both in (FC) and out of field (ZFC) followed by measurement of a RT SIRM cooled and re-warmed in a zero field. The resultant FC and ZFC curves were compared to those of synthetic magnetites of known composition, and the percentage recovery of remanence (magnetic memory) found from the cooling and warming curves of the RT SIRM was used as an indication of grain size.

Low temperature experiments were carried out using the Quantum Designs MPMS2 at the IRM which has a temperature range of 2.1 to 300 K and a magnetic field ranging from 0 to 5 T and a sensitivity of $1 \times 10^{-11} \text{ Am}^2$. The lowest temperature used for samples from this study was 10 K as, for temperatures below this, the machine requires a long time period to equilibrate and it was unnecessary to perform measurements at such low temperatures for the purposes of this study.

Figure 7.2 displays LT SIRM curves for synthetic titanomagnetites with varying titanium concentrations, showing the 'smearing out' of the transition with higher concentrations (e.g. TM60).

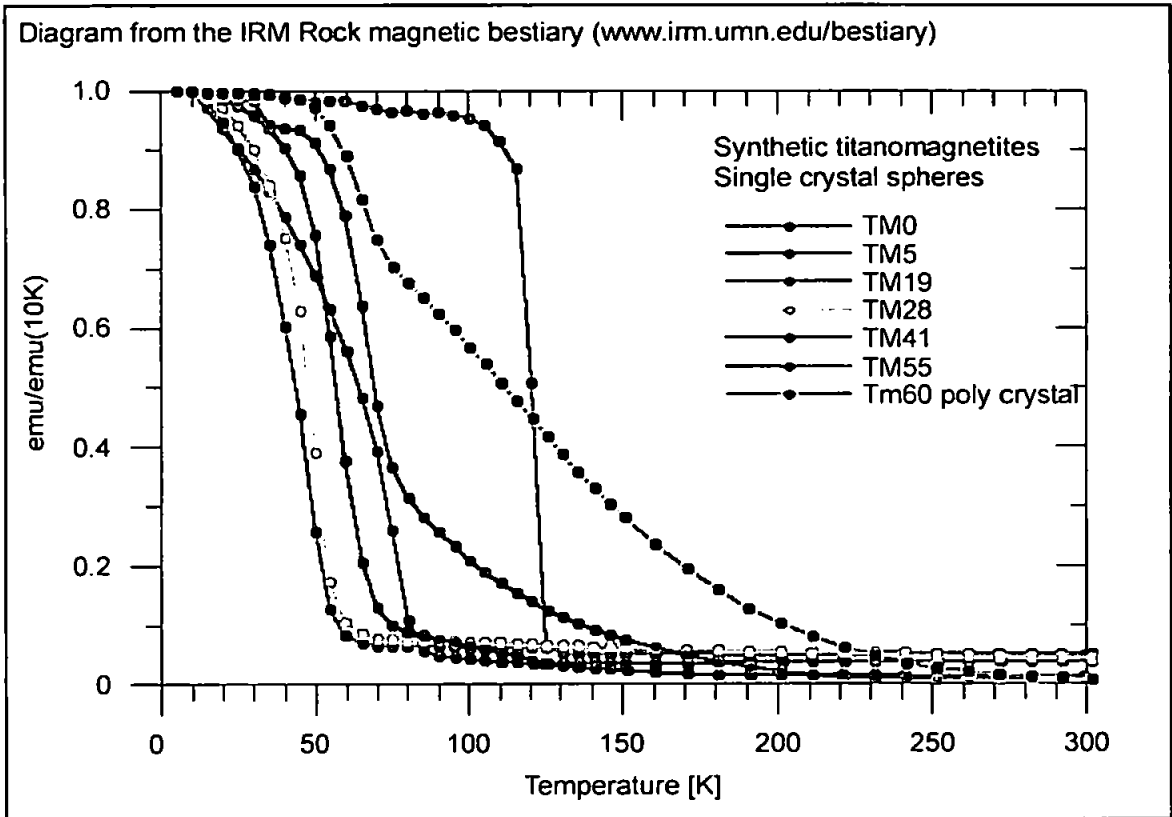


Figure 7.2: LT SIRM curves for synthetic titanomagnetites with varying titanium concentrations that can be used for comparison with the natural samples measured for this thesis.

7.3.6 Alternating current (AC) susceptibility measurements

Alternating current (AC) susceptibility measurements at either different frequencies or different field strengths can be useful in characterising magnetic minerals. AC susceptibility experiments involve superimposing a small AC field on a DC field and measurement of the resulting AC moment. The induced sample moment is time-dependent and so AC measurements can yield information about magnetisation dynamics that are not obtained by DC measurements. There is an in phase (k') and an out of phase or quadrature (k'') component of these measurements.

For this study, frequency dependent susceptibility curves were measured for selected samples with the field held constant. Differences between the susceptibility of a sample measured at different frequencies are produced by several methods, with two of particular significance for geological samples: viscous decay will result in a constant difference with the higher frequency generally lagging behind, and the effect of low temperature/weak field hysteresis loops will result in variable differences observed between frequencies. Viscous decay will produce frequency dependency in both in phase and out of phase components, whereas low temperature hysteresis will only introduce frequency dependency to the out of phase signal. The Verwey transition can be picked out in the in phase AC susceptibility measurements by a change in susceptibility. In stoichiometric magnetite, the out of phase susceptibility also shows a singularity across the transition (e.g. Skumryev et al. 1999) for millimetric size crystals, although temperature variation of k'' has not been reported for synthetic fine-grained magnetites or for the magnetites of natural samples (Kostervov 2001). The in phase graph in haematite is strongly dependent on grain size, with larger grains showing a higher increase in susceptibility around the Morin transition than smaller grains, with the increase disappearing for the finest grains.

The AC susceptibility measurements for this study were carried out at the IRM using the Quantum Designs MPMS at three different frequencies and the Lakeshore AC susceptometer at five different frequencies.

7.3.7 Sample preparation

The sample preparation for rock magnetic experiments depends on the exact experiment being carried out. The rock magnetic results from standard demagnetisation procedures as well as for the IRM analyses and the majority of the hysteresis measurements used standard 2.5 cm diameter whole rock cores. Some hysteresis measurements were carried out using the MicroVSM as part of the high temperature experiments and samples for these were prepared as for the high temperature experiments (see below).

For the Curie point determinations and the low temperature experiments, samples were measured in powder form. Powder was produced by using a pestle and mortar to crush a small rock chip into powder. The sample probe of the furnace of the MicroVSM can only take samples weighing a few tens of milligrams.

For high temperature experiments using the MicroVSM, cements were made from the powders and attached to a specially designed ceramic sample holder. The cement was made by mixing a small quantity of the powdered sample with a few drops of 'cement liquid' in roughly equal proportions before leaving to set on the sample holder overnight. Alternatively, the process can be hastened by heating the cement paste to 100°C in a furnace, although must be done with caution due to the potential for mineralogical changes to occur even during heating to this low temperature. Only two test samples for this thesis were heated to 100°C, and avoided for all subsequent samples to ascertain mineralogical changes did not occur, although in the test samples no difference in results was observed

between the heated samples and unheated samples that had been left to cool overnight. For high temperature experiments using the KLY3, a few centimetres of powder was added to a test tube which was then filled with argon gas to minimise the possibility of mineralogical changes due to oxidation, before being attached to the furnace of the KLY3.

The powders for the low temperature experiments were used to fill 2 cm glycerin medical/pill capsules which were then inserted into a straw in the correct position for the MPMS equipment to measure accurately.

7.4 Rock magnetic results and discussion

The rock magnetic characteristics of the ophiolite will be discussed in sections corresponding to crustal level as differences in magnetic mineralogy for the different lithologies are possible. These sections are most simply from deepest to shallowest: cumulate gabbros; sheeted dykes, and extrusives. The rock magnetic results from the gabbros samples that were taken from gabbro screens located at the base of the SDC have been included with the cumulate gabbro section. The initial results from the experiments carried out at the University of Plymouth will however be discussed first. Figures 7.3 to 7.6 show the results for representative samples for the rock magnetic experiments and will be referred to in the following sections.

7.4.1 Preliminary rock magnetic results from the University of Plymouth

The rock magnetic experiments and demagnetisation procedures carried out in the University of Plymouth laboratory prior to the more comprehensive measurements at the IRM enabled an initial diagnosis of the rock magnetic carriers to be made.

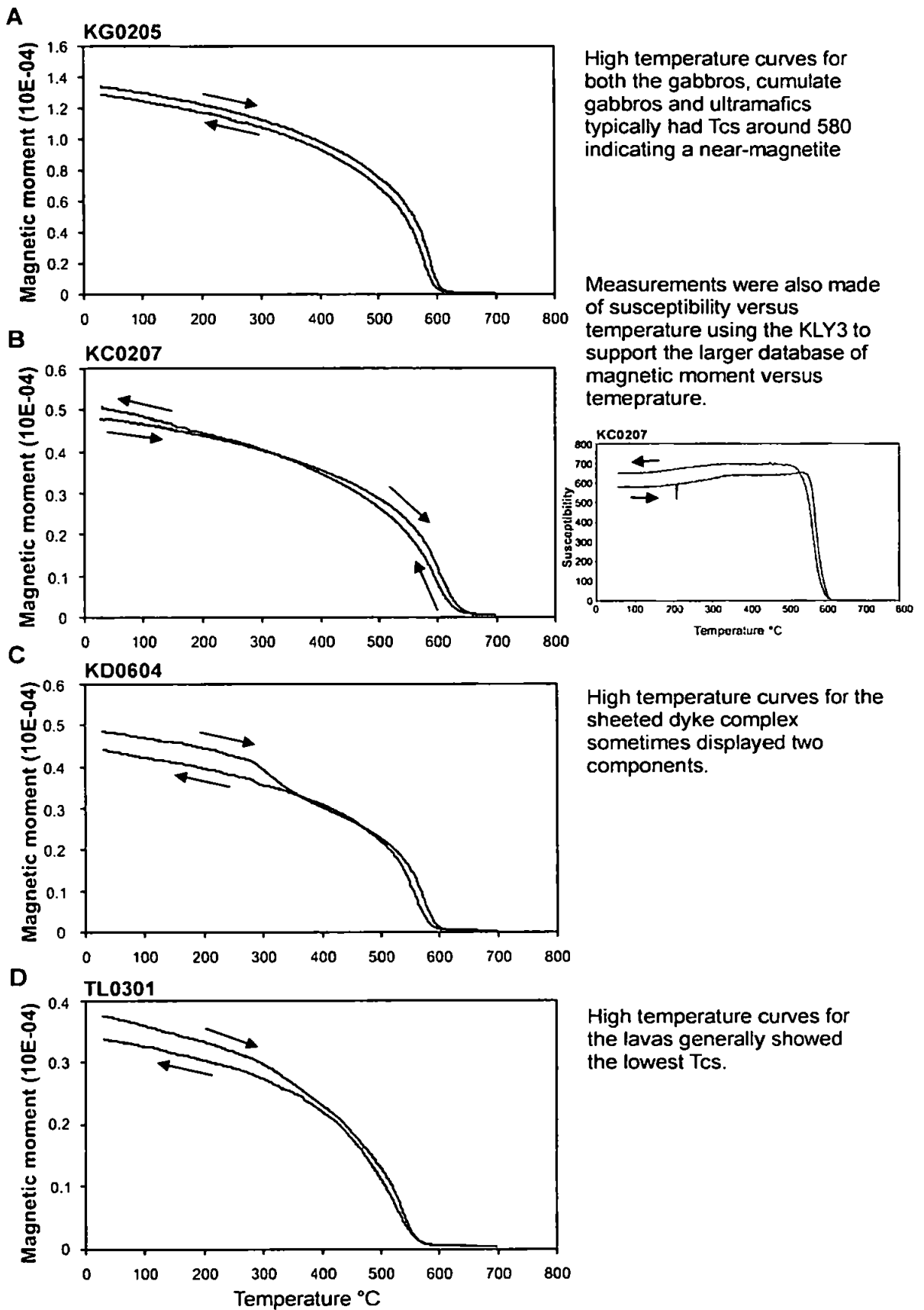
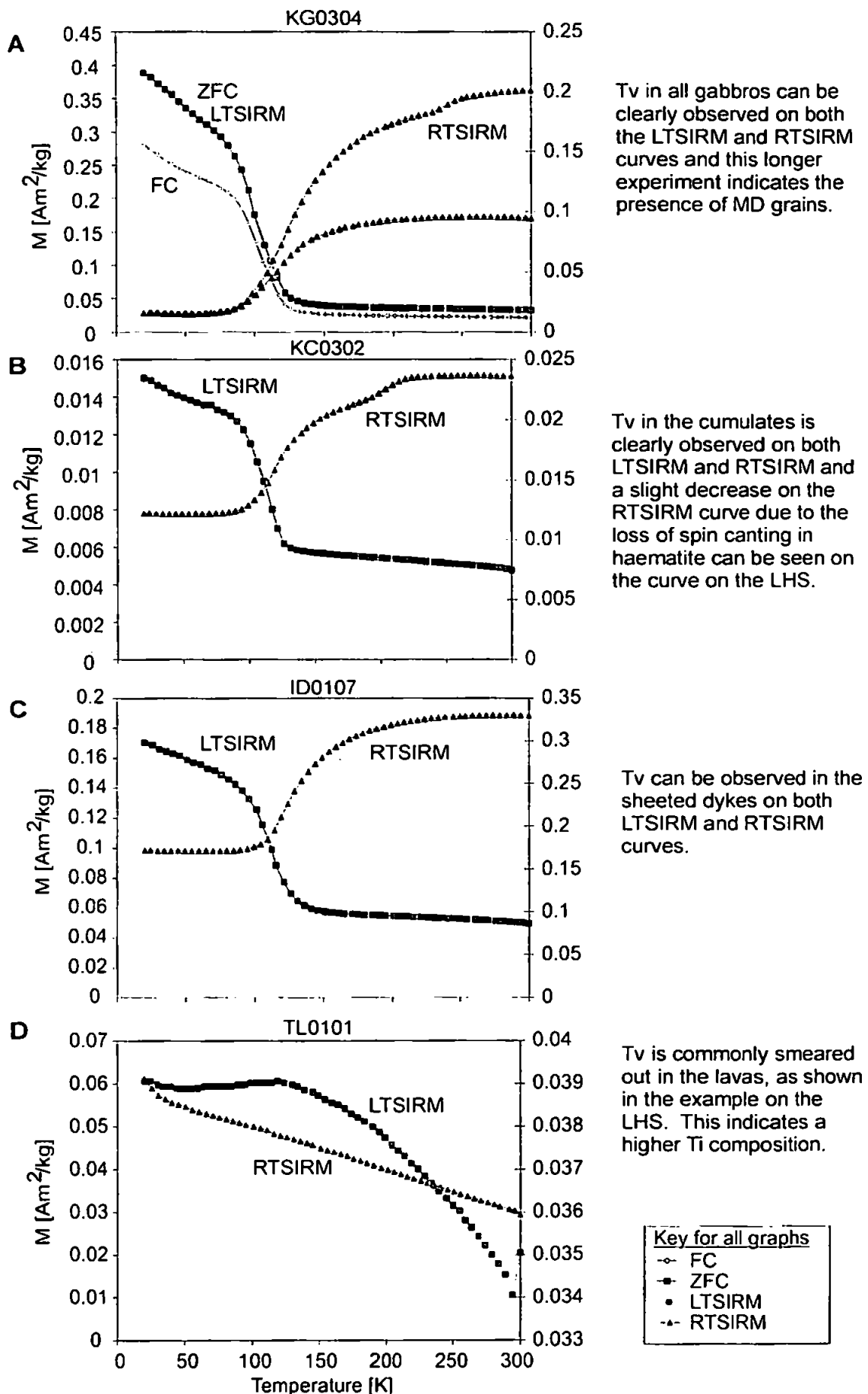


Figure 7.3: High temperature curves showing T_c points for a representative example of each ophiolitic lithology.



Tv in all gabbros can be clearly observed on both the LTSIRM and RTSIRM curves and this longer experiment indicates the presence of MD grains.

Tv in the cumulates is clearly observed on both LTSIRM and RTSIRM and a slight decrease on the RTSIRM curve due to the loss of spin canting in haematite can be seen on the curve on the LHS.

Tv can be observed in the sheeted dykes on both LTSIRM and RTSIRM curves.

Tv is commonly smeared out in the lavas, as shown in the example on the LHS. This indicates a higher Ti composition.

Figure 7.4: Representative low temperature curves for each lithology, showing the Verwey transition (where present).

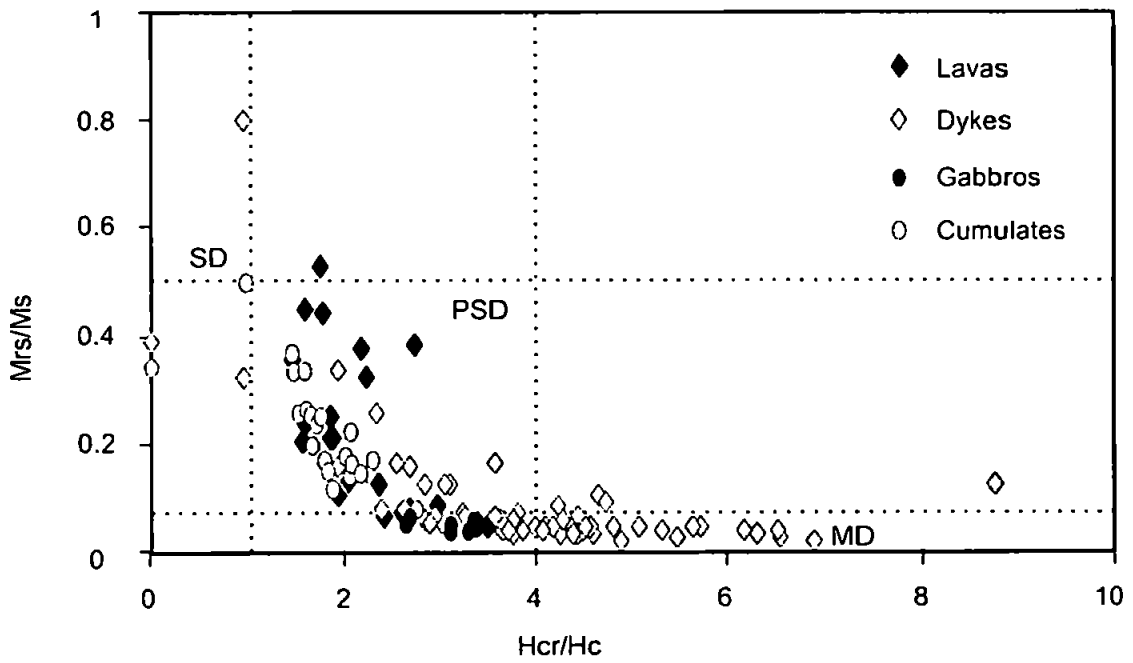


Figure 7.5: A Day plot of the samples measured from all lithologies of the Hatay ophiolite. The majority clearly lie in the PSD region on the plot, although samples from the SDC display more variability, with some lying within the MD region of the plot.

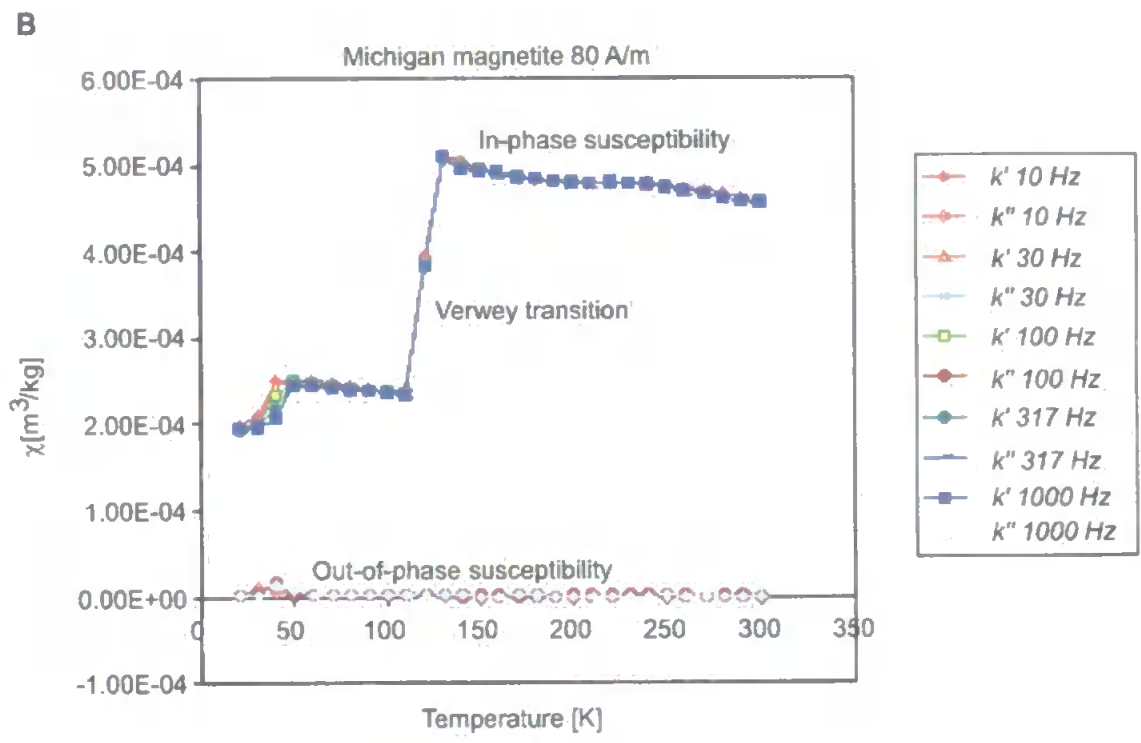
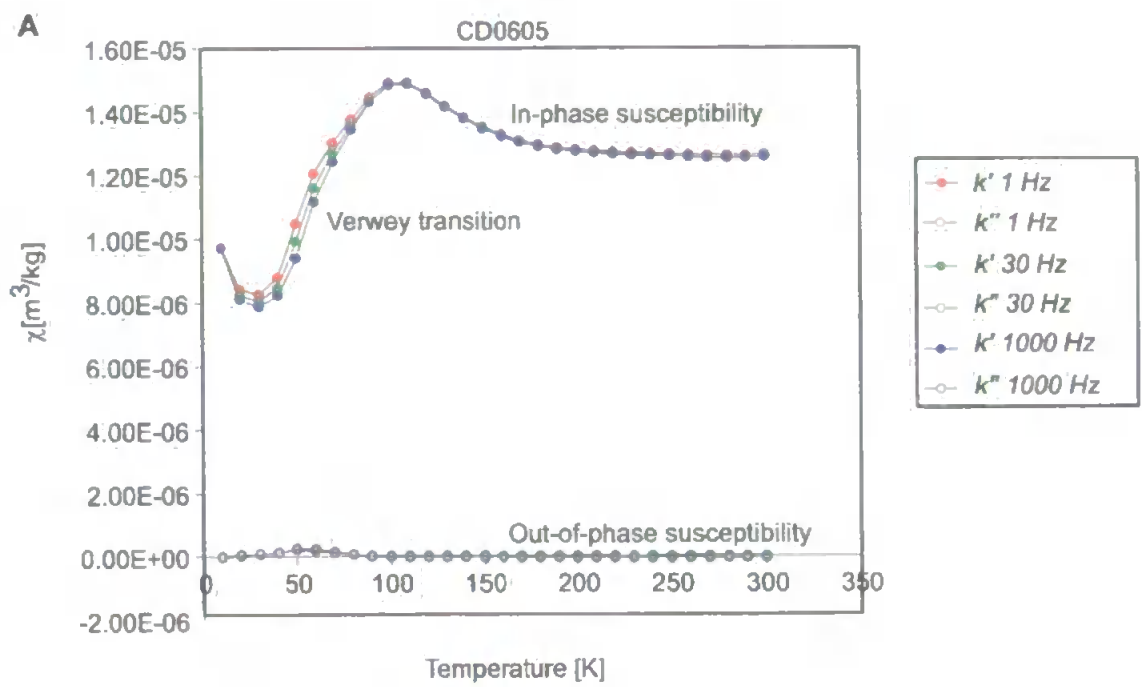


Figure 7.6: Alternating current (AC) susceptibility curves for a sample from the SDC and a reference curve.
 A. The AC susceptibility curve for sample CD0605 from the SDC.
 B. The AC susceptibility the curve for a sample of magnetite shown for comparison (from IRM bestiary www.irm).

Analyses of the acquisition of isothermal remanent magnetisation for at least one sample per site indicated a dominance of low coercivities for all samples. Saturation magnetisations were reached by around 200 mT, consistent with the presence of low coercivity magnetite. Stepwise thermal demagnetisation of natural remanences indicated differences in unblocking temperatures (T_B) between lithologies. The deeper levels (gabbros and cumulate gabbros) had unblocking temperatures near 580°C suggesting the presence of Ti-poor magnetite. Unblocking temperatures for the pillow lavas were generally lower, suggesting a higher titanium content. More variable T_B s were observed for the SDC with a maximum T_B of 560-580°C, but also in some samples a lower temperature component was observed to unblock at 350-400°C. Alternating field demagnetisation characteristics were consistent with the presence of both MD to SSD grains with median destructive fields ranging from 5 mT to >40 mT.

7.4.2 Cumulate gabbros and isotropic gabbros

Curie points in the cumulate gabbros and isotropic gabbros are generally higher than in the sheeted dykes and extrusives. T_C s in the isotropic gabbros are on average around 590°C which is consistent with the T_C of Ti-poor magnetite. Heating and cooling curves are generally reversible (Figure 7.3A-B); all curves in the isotropic gabbros are reversible and no curves display two components. However, two curves for the cumulate gabbros have a second component at temperatures 370°C and 390°C. The non-reversible curves in the cumulate gabbros show variation between those where the magnetisation of the cooling curve is greater than that of the warming curve and those where the opposite applies.

Low temperature experiments were carried out for four isotropic gabbro samples and 11 cumulate gabbro samples. The Verwey transition occurred at around 110 K in the majority of samples, and can be seen in both heating and cooling curves (Figure 7.4A-B). The step

was smeared out in some of the cumulate gabbro samples (e.g. KC0107) which suggests that the magnetite in these may have undergone some oxidation. The smearing will not be due to the addition of titanium in this case as the high temperature experiments show Curie points around 590°C which are too high for anything other than a Ti-poor magnetite/pure magnetite. Some of the cumulate gabbro samples (e.g. JC0103) display curves that are typical of magnetite and their curves are not smeared out. A few samples in the cumulate gabbros have cooling curves that display an initial gradual increase from 300 K downwards to less than 200K. This increase can be explained by the presence of titanomagnetites that lose ordering near room temperature, and as such do not contribute to the natural magnetic remanence. A similar feature is observed in a few samples from the extrusive sequences, but is not observed in any of the sheeted dyke or cumulate gabbro samples. FC and ZFC warming curves for the cumulate sample KC0107 display little difference and the recovery of remanence on rewarming through T_v is around 70%. AC susceptibility experiments show evidence for T_v in the cumulate gabbro samples; for example sample JC0103 shows T_v very clearly.

The gabbros have heating and cooling curves that are typical of magnetite, with no smearing out of the transition. The longer experiment carried out on gabbro sample KG0304 that determined both the heating and cooling curves of RT SIRM shows a low recovery of remanence following the second transition through T_v (second memory), which suggests the presence of MD grains. Remanence recovery for this sample is around 50%. The FC cooled warming curve plots above the ZFC warming curve which is a feature observed for synthetic MD magnetites. The AC susceptibility curve for gabbro sample KG0205 shows evidence for T_v around 110 K suggesting the presence of magnetite or Ti-poor titanomagnetite.

A slight decrease in magnetisation is observed on the cooling curves for three of the cumulate gabbro and isotropic gabbro samples, at temperatures between 200 to 250°, which corresponds to the loss of spin canting in haematite as the samples are cooled below room temperature.

Hysteresis parameters for the gabbroic samples plot in the PSD region on a Day plot (Figure 7.5). Points lie in a rough line with M_{rs}/M_s ratios inversely proportional to H_{cr}/H_c ratios. Average coercivity of remanence for the 30 cumulate gabbro and gabbro samples measured combined is 29.5 mT, consistent with PSD magnetite/Ti-poor titanomagnetite.

7.4.3 Sheeted dykes

T_C s are consistent with the presence of Ti-poor magnetite with a mean T_C value of 590°C and heating and cooling curves are reversible for the majority of samples. Several samples show evidence for two components (Figure 7.3C). Three curves show clear evidence for a lower temperature component and five curves show a slight decrease in magnetisation at a lower temperature: all of these components occur between 335 and 400° with an average of 365°C. For the three non-reversible samples (of the 19 samples measured in total), excluding those displaying two components, the cooling curves showed a slight increase in magnetisation, suggesting the possibility of a mineralogical change during heating.

Low temperature experiments were carried out on 27 dyke samples, with FC and ZFC curves measured for one sample. The Verwey transition occurred at around 100 to 110 K in most samples and could be observed on both warming and cooling curves (Figure 7.4C). Fourteen samples showed a very slight 'bump' on the cooling curve between 200 and 250°C due to the presence of a small amount of haematite causing magnetisation to decrease as spin canting is lost. The amount of haematite is likely to be small due to the

absence of this bump in the majority of samples and the fact that it is extremely slight in those samples where it is observed, although it should be noted that the Morin transition can be absent from finer grained haematite grains. In a very few samples, the warming curve showed a continuous decrease beginning at 10 K and continuing until temperatures just above the Verwey transition, rather than a sharper decrease over the transition. However, the cooling curves for these samples show the Verwey transition clearly and the warming curve trends are interpreted to be due to the effect of a small amount of superparamagnetic minerals causing an initial decrease in moment and so disguising the decrease due to the Verwey transition in the larger grain sizes of the titanomagnetites. Field cooled and zero field cooled warming curves for sample CD0605 are very similar. There is a loss of memory on rewarming through the Verwey transition, which indicates grain sizes larger than SD for the sample measured, although the recovery is better than for the cumulate gabbro and isotropic gabbro samples.

Certain components of the AC susceptibility measurements performed on sheeted dyke samples are not straightforward to interpret as they do not correspond simply to curves for known synthetic minerals. Their characteristics are probably due to a combination of paramagnetic decay, antiferromagnetic minerals and magnetite. An initial sharp decrease in susceptibility observed for sample CD0103 was linked to the magnetic minerals causing an initial decrease on the warming curve of the low temperature experiment, corroborated by the fact that the same features were also observed in sample CD0605 (Figure 7.6) although to a lesser extent. The initial sharp decrease may be explained by the presence of superparamagnetic minerals. The three samples for which AC susceptibility curves were measured all displayed an increase in susceptibility for the in phase component around 100 K, interpreted as the Verwey transition and the quadrature component peaked below 100 K which is similarly observed in synthetic titanomagnetites.

Hysteresis parameters show some variation with the majority of samples plotting within the PSD field, but a few samples lying within the MD region (Figure 7.5). The dyke samples consistently (with only a few exceptions) have low M_{rs}/M_s ratios. Average coercivity of remanence for the 64 samples measured is 32 mT, consistent with PSD magnetite/Ti-poor titanomagnetite.

7.4.4 Extrusive rocks

T_C s in the pillow lavas range from 475 to 560°C with a mean T_C value of 530°C (Figure 7.3D). These T_C s are lower than that for magnetite or a Ti-poor titanomagnetite and suggest the presence of a more Ti-rich titanomagnetite. These T_C s are still above that expected for TM60, which has T_C of around 140°C. One sample shows a lower temperature component at 340°C and three samples show a very slight decrease in magnetisation on the heating curve at temperatures between 310°C and 360°C. The cooling curves for several samples have a higher magnetisation than the warming curves, although the difference is only large for one sample.

Low temperature experiments were carried out on 11 lava samples. The Verwey transition is not present in all samples and where it is present, it shows more gradual decrease across the transition on warming: it is smeared out (Figure 7.4D). Two samples show evidence of a sharper decrease in magnetisation across the transition, although not as sharp as observed in the deeper levels of the ophiolite and also at temperatures below 100 K. In conjunction with the lower T_C s, this smearing or total absence of the transition suggest a more Ti-rich titanomagnetite than observed in the other lithologies. Some temperature sweeps have a significant initial decrease in magnetisation, with a corresponding decrease observed on the warming curve, which may be due to a superparamagnetic fraction. None of the samples show evidence for haematite as the cooling curves are smooth over the temperatures of the

Morin transition. A feature of several cooling curves in the lavas is an initial gradual increase in magnetisation observed on the cooling curves which is caused by the presence of titanomagnetites that lose ordering near room temperature (as previously discussed for cumulate gabbro sample JC0408). FC and ZFC warming curves are similar for both samples for which they were measured.

The single AC susceptibility curve shows evidence for titanomaghemite, although this is not necessarily a constituent of all lava samples and may not be a significant component of the magnetic minerals in the lava analysed as concentration cannot be accurately determined from the AC susceptibility experiments. The susceptibility peaks below 100°C on the out of phase component of the AC susceptibility plot for the lava sample measured (TL0407), which is comparable to synthetic Ti-rich titanomagnetites. There is a strong correlation between the shape of the in phase and out of phase curves for sample TL0407 which implies that the contribution from the superparamagnetic fraction is small. The Verwey transition is not observed on the in phase curve of the AC susceptibility measurement.

Hysteresis parameters plot within the PSD field on a Day plot. Points are fairly evenly distributed within the PSD field. Average coercivity of remanence for the 26 samples measured is 26.8 mT, consistent with PSD magnetite/low-Ti titanomagnetite.

7.4.5 Summary of rock magnetic results

The results obtained at the IRM are compatible with the presence of fine magnetic grain sizes capable of retaining a stable magnetisation throughout the complex history of the ophiolite, with PSD grains dominant in the majority of samples. There is a difference in magnetic mineralogy depending on the crustal level. The clear Verwey transitions and

high T_C s of the deeper levels of the crust indicate that Ti-poor titanomagnetite/magnetite is the major carrier of the magnetic signal, and the absence of the Verwey transition and lower T_C s of the higher crustal levels indicate the presence of a more Ti-rich titanomagnetite. These mineralogies are compatible with acquisition of stable remanences on the seafloor soon after genesis of the ophiolitic crust at an oceanic spreading centre.

A Day plot of the saturation magnetisation ratio against the coercivity ratio demonstrates that the majority of samples of all lithologies lie within the PSD field (Figure 7.5). The SDC shows more variation with some samples falling in the MD field. The average coercivity of remanence for all lithologies is around 30 mT, indicating a dominance of low coercivity minerals for all lithologies.

Curie point determinations (Figure 7.3) showed that the deeper levels of the ophiolite had Curie points near that of Ti-poor magnetite with a mean T_C value close to 590°C in both the gabbros and the SDC. Heating and cooling curves were reversible in the majority of samples. The pillow lavas had T_C s ranging from 475 to 560°C with a mean T_C of 530°C. These lower temperatures suggest the presence of a higher titanium phase than for the gabbros, although these T_C s are higher than that of TM60. Two components were observed in some samples at temperatures between 335 and 400°C, with all except two of these samples being from the SDC.

The dykes and lower crustal lithologies all displayed clear low temperature transitions in the vicinity of 110 K, indicating a Verwey transition temperature of low-Ti titanomagnetites. In some of the cumulate gabbros the step was 'smeared' out, probably due to the presence of more oxidised magnetite (Özdemir et al. 1993, 2002). In the pillow lavas, the Verwey transition was generally not clear, and a considerably more gradual change in magnetisation was seen on the warming curve. This, combined with the lower

Curie temperatures, implies that a higher degree of titanium substitution in the pillow lavas minimises the effect of the Verwey transition. Figure 7.4 shows representative plots for each level of the ophiolite.

7.4.6 Discussion of rock magnetic results

Most grain sizes from all lithologies fall within the PSD range on a Day plot and PSD grains are generally accepted as being capable of retaining stable magnetisations over geological time. PSD behaviour was first used to explain the transitional properties of magnetite over a broad grain size range between SD and truly MD by Stacey (1962). The origin of PSD grains is debated. Dunlop (2002) notes that on a Day plot, mixtures of MD and SD grains are capable of fitting the data from most well-sized PSD grains. Other theories for the microscopic origins of PSD behaviour include (Dunlop 1998 and references therein): permanent SD moments in MD grains; imbalance moments of irregularly shaped grains; surface moments which change with changes in body domain structure; and exotic micromagnetic structures unlike either classic SD or MD structures. However, the importance of PSD grain sizes in all lithologies of the Hatay ophiolite is that, whatever the origin, these grains behave magnetically similarly to SD grains and, as such, are capable of retaining stable magnetisations.

A good agreement was found between the IRM acquisition curves and remanent magnetisation and coercivity of remanence measured on the VSMs at the Institute for Rock Magnetism with the IRM acquisition curves and coercivities of remanence measured in the University of Plymouth laboratory. For instance, coercivity of remanence in many cases displays less than a one or two mT discrepancy between the two measurements and is less than twenty percent different in more than 75% of the 55 samples compared.

Fourteen T_C curves obtained from this study, mostly from the sheeted dykes, display two components in the heating curve. The magnetisation on the return cooling curve is greater for five samples (four of which are lavas), decreased for four samples and similar for five samples. The five samples where the magnetisation of the cooling curves is below that of the heating curves are similar to some identified by Kosterov (2001) in work on the low temperature properties of basalt samples and are interpreted in this case as resulting from an irreversible change in the domain structure of ferromagnetic grains rather than from chemical alteration, for the reason that no irreversible changes in saturation magnetisation occurred in this temperature range. Saturation magnetisation was measured for this study both before and after the T_C experiment. None of the samples where the magnetisation had decreased showed any irreversible change in M_S between hysteresis measurements before and after heating. Only one of the 14 samples with two components displayed any significant change in M_S between heating and cooling curves although H_c showed a significant change for six samples, although again not in any sample where the magnetisation had decreased. Ten samples with only one component showed a significant change in M_S subsequent to heating and two thirds of samples showed a significant change in coercivity. The samples where significant changes were observed were spread across all lithologies and there is no apparent simple correlation between the reversibility of the high temperature curves with the samples where there were significant irreversible changes in M_S or H_c .

7.5 Thin section analyses under the polarising microscope

Thin section analyses were carried out on 20 samples (at least three samples per lithology) using a polarising microscope. The gabbros, dykes and lavas are consistent with a tholeiitic composition. The dykes range from basaltic to doleritic and sphene is a common accessory mineral. There is no clear distinction in mineralogy between the grey suite of

dykes and the younger brown suite. The opaques observed are often skeletal or cubic, suggesting that they are primary in origin, and they are also generally quite abundant. Skeletal textures are formed when the mineral cannot grow to form cubes due to rapid rate of chilling. The opaques within the lavas varied from small opaques and opaques contained entirely within the groundmass to samples displaying larger skeletal opaques. In two cumulate samples from the Karaçay river section, the opaques are not abundant, although some contain skeletal and cubic opaques, again suggesting a primary origin. Certain of the cumulate gabbros from the Karaçay river and Kisecik valley sections show a degree of serpentinisation. A few opaques in one lava sample and two cumulate samples have a reddish colouration to the crystals suggesting the possibility of a different mineral to that of the generally black opaques, although distinguishing between opaque minerals is not possible without scanning electron microscope analyses. Several of the olivines observed in the cumulate gabbros show evidence of alteration to fine grained iron oxides along crystal boundaries.

7.6 Scanning electron microscope (SEM) analyses

In order to provide further constraints on the rock magnetic mineralogy of the Hatay ophiolite, a JSM6100 Scanning Electron Microscope with an Oxford INCA x-ray microanalyser was used at the University of Plymouth to study representative samples. A scanning electron microscope (SEM) is a useful aid in determining more precisely the magnetic minerals within a rock, with the magnetic minerals (heavier atomic weights) showing up on the image as lighter coloured areas. Backscattered electron (BSE) images were used to image specimens, with x-ray analysis of selected grains carried out to aid identification of the elements present and elemental mapping of selected regions also carried out. The resolution limit ranges from around 1 μm in x-ray images to 1 nm for secondary electron (SE) images under favourable circumstances. The maximum useful

magnification ranges from 1000 (for 1 μm resolution) to 100 000 (for 1 nm resolution) (Reed 1996).

The rocks being imaged for this study are basalts, gabbros and ultramafic cumulates. Therefore, pyroxenes, plagioclase and olivine will be expected to comprise the majority of the rock. A number of accessory magnetic phases could be present, as described earlier in this chapter. Certain distinctive elements are used to aid in mineral identification (Reed 1996):-

- Olivine by high magnesium
- Clinopyroxene by high calcium, low aluminium
- Plagioclase by high calcium and high aluminium
- Magnetite by high iron
- Ilmenite by high titanium

Most of the magnetic minerals that carry the remanent magnetisation are expected to be either magnetite, titanomagnetites or titanohematites. The SEM work can pick out whether any Ti is present in the high atomic number crystals observed.

In looking at the Fe oxides, it is not only important to assess the concentrations of the elements within them, but also to see how they are distributed. For instance, it is necessary to find out whether there are any exsolution textures within the crystals, as even if the x-ray count shows that there is a significant amount of titanium in the selected area, this could either all be confined to exsolution lamellae, or comprise part of the main structural make-up of the crystal.

If exsolution is observed, the crystal is expected to be separated into a near-ilmenite end member and a near-magnetite end member, with the ilmenite lamellae appearing darker

than the surrounding crystal. If the melt was not oxidised during the exsolution process, the intergrowths would be a near-magnetite phase and an ulvospinel phase. However, this is a less likely scenario than exsolution occurring with deuteric oxidation or oxyexsolution occurring in the melt. Exsolution may be more likely in the deeper levels due to slower cooling. In the lavas, exsolution is less likely to be observed due to faster cooling leading to higher possibility of primary titanomagnetite being preserved.

7.6.1 Sample preparation

The samples used for SEM analysis were polished thin sections that were then carbon coated in a vacuum chamber. Preparation is identical as for ordinary thin sections in the first stages apart from use of a stronger adhesive to attach the rock slice to the glass slide due to the stress of polishing. The thickness of the slides is around 30 μm . Carbon coating is necessary as the specimens are non-conductive so coating the specimen allows a path through for the electrical current of the beam. Studying the specimens under the SEM without the carbon coating resulted in charging effects interfering with the image. Carbon is commonly used due to its minimal effect on the x-ray spectrum with an optimum thickness of carbon of about 20 nm. The carbon coating can be easily removed to subsequently examine the sample using optical microscopy with a fine polishing medium. For both x-ray analysis and BSE imaging it is desirable to avoid topographic effects and so specimens should be flat and well polished as irregularities of less than 1 μm can have a significant effect on results.

7.7 Scanning electron microscope results and discussion

Grains capable of carrying the magnetic signal in the ophiolitic rocks are expected to be FeTi oxides and will be of higher atomic number than the surrounding minerals.

Therefore, under the SEM FeTi oxide crystals will appear brighter than the other minerals. Although information was gained during SEM analyses on all mineral compositions in the rock, these were previously described from analysis of thin sections under the polarising microscope and the following descriptions therefore concentrate on the crystals of higher atomic number: their size, texture and elemental concentrations.

7.7.1 Cumulate rocks and isotropic gabbros

SEM analyses confirm the presence in the gabbros of near-magnetite and near-ilmenite in very well-developed exsolution lamellae in large grains (≤ 1 mm), with skeletal and cubic crystals common (Figure 7.7). Isotropic gabbro samples displayed many large titanomagnetite crystals (≤ 2 mm), which generally showed little alteration and clear exsolution textures (Figure 7.7A). The lamellae were more Ti rich than the surrounding crystal. Some crystals also showed greyer areas around edges, or parts of the edge that were higher in Ti. Some of these were titanium silicates (sphene) and some lamellae had also altered to sphene. A general lack of iron oxides were observed in cumulate gabbro samples from the Karaçay valley, possibly due to large crystal size resulting in an unrepresentative section. Few titanomagnetites were observed. Many of the areas of higher atomic number were copper sulphates. All these crystals were small, whereas the magnetites expected in the cumulate gabbros would be large. The olivines in this slide had Fe growing in the cracks (Figure 7.7C). The x-ray profiles for the high atomic number minerals in a cumulate gabbro sample from the Kisecik valley show only Fe and O and no titanium, suggesting they are magnetite. The magnetite exists as patches of small rounded grains within larger patches of crystals that could have formerly been a single crystal (Figure 7.7H). The areas between these small rounded crystals are not Fe rich. Some of the larger and clearer looking crystals are a chromitite spinel (Fe, Cr, O).

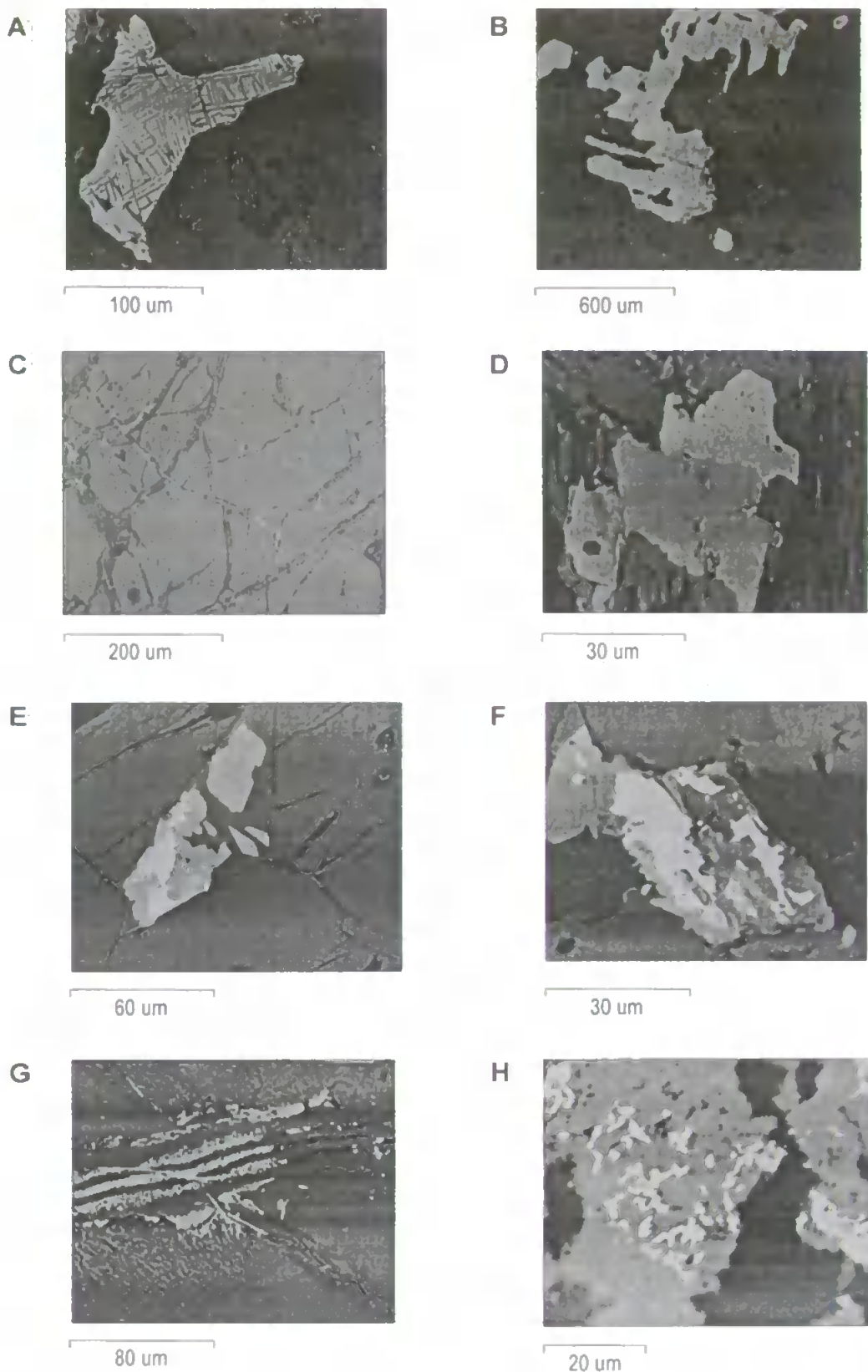


Figure 7.7: Examples of typical iron oxide grains in isotropic gabbros and cumulate gabbros and ultramafics as observed under the SEM.

A-D. Four examples of typical iron oxide grains from the Karacay valley. A-B. are examples of large skeletal crystals common within the gabros, which almost all display an exsolution texture.

C-D. show examples of the less common iron oxide crystals occurring in a different form, such as located in cracks in olivine crystals, as in C..

D. A titanomagnetite grain with the the top half Ti-poor and bottom half Ti-rich.

E-F. Iron oxide (white) and titanite (grey) observed in cumulates from the Karacay valley.

G-H. Examples of iron oxides forming later in the history of the grain (G) and displaying a large degree of alteration (H), both from the Kisecik valley.

7.7.2 Sheeted dykes

The dykes contained a mixture of near-magnetite grains, more titanium rich grains, as well as some grains displaying exsolution. Figure 7.8 shows some typical crystals observed under the SEM in the sheeted dykes.

Most crystals in a sample analysed from the SDC in the Karaçay valley are of similar size and are on average around 30 by 30 μm . Some crystals are larger than this and tend to have a more irregular shape, while the smaller crystals are more cubic (Figure 7.8A). No crystals display obvious exsolution, although some display hints of it, especially at higher magnifications where it is difficult to be certain. In the crystals where lamellae can be observed at lower magnifications, the lamellae do not contain Ti Fe oxides but instead are Mg, Al, Fe silicates.

The high atomic number minerals in a sample from the coastal SDC contain some titanium as well as the iron (Figure 7.8C). Both large and small crystals of magnetite and some crystals containing Ti are evident. The smaller crystals are around 10 μm and show no evidence of exsolution. Some of the larger crystals, however, show exsolution textures. All crystals are smaller than 200 μm .

7.7.3 Extrusive rocks

The pillow lavas were observed to contain grains with higher levels of titanium, as concluded from the rock magnetic results. Figure 7.9 shows some typical crystals observed under the SEM in the extrusive rocks.

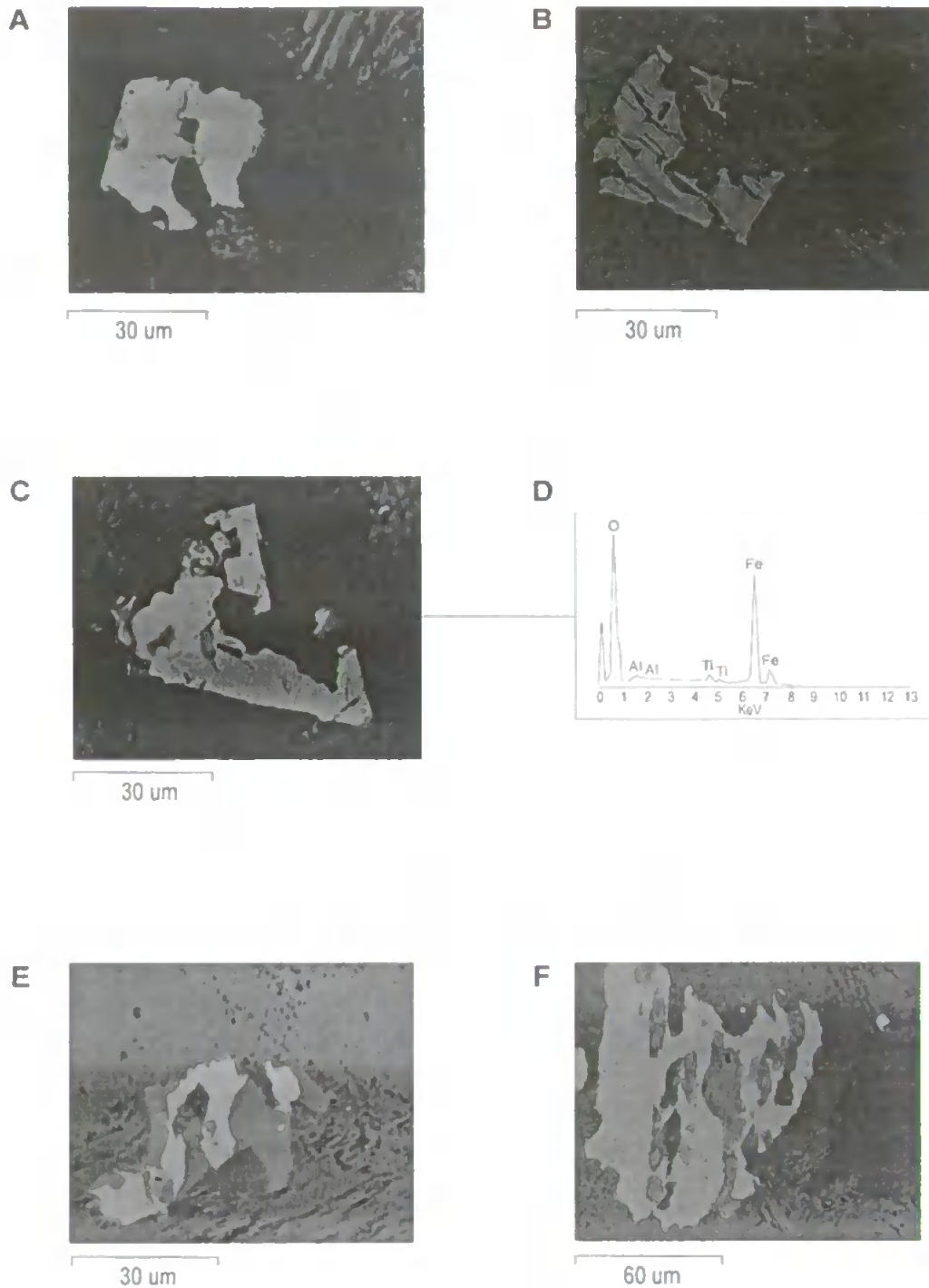


Figure 7.8: Examples of typical iron oxide grains in the sheeted dyke complex as observed under the SEM.

A-B. Examples of cubic crystals of magnetite in sheeted dykes from the Karacay valley. Cubic crystals were common in dykes from all locations and were also observed in other lithologies.

C. Example of a low-Ti iron oxide in a sheeted dyke sample from the Karacay valley.

D. The element concentration plot showing the existence of a small Ti concentration in sample C.

E-F. Examples of iron oxides (white) and titanite (grey) in the sheeted dyke complex from the coast and the Karacay valley.

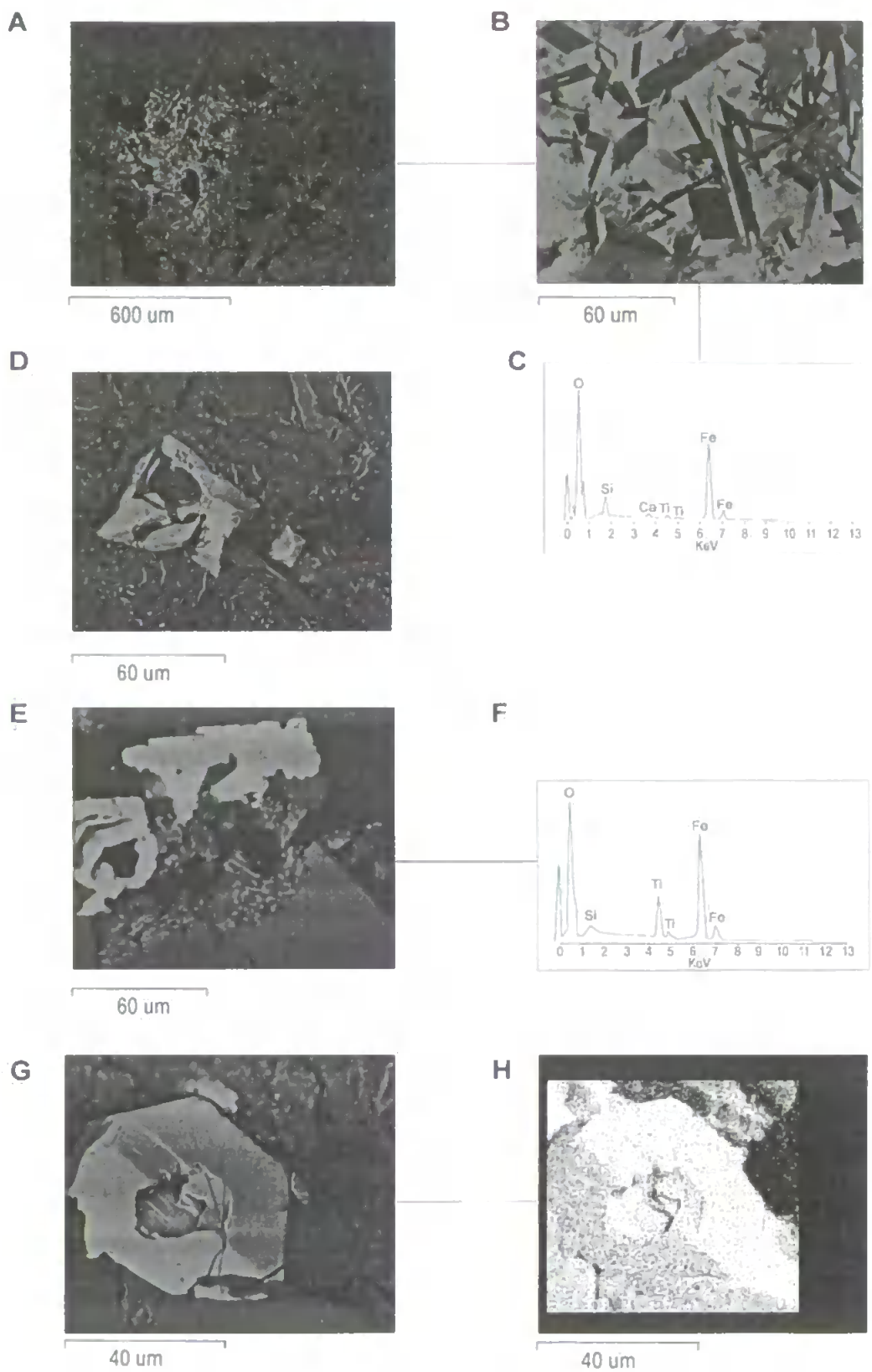


Figure 7.9: Examples of typical iron oxide grains in the pillowed lavas and lava flows as observed under the SEM.

A-B. Tahtakopru lava titanomagnetite with the a closer view of the same crystal shown in B.

C. The element x-ray spectra for the crystal in A-B.

D. A cubic titanomagnetite crustal from the Antakya locality.

E. Antakya lava titanomagnetite.

F. Representative x-ray spectra for iron oxides within the lavas, most of which contain some Ti and many crystals contain a significant proportion of Ti.

G-H. An Antakya lava titanomagnetite with an oxygen k alpha map for this same crystal illustrated in H.

A sample from the Tahtaköprü valley contains areas of large high atomic number crystals, which are shown by x-ray analysis to be iron oxides, generally containing some titanium (Figure 7.9A-C). There is no obvious exsolution, indicating that the titanium evident from the x-ray counts is forming titanomagnetites and is not limited to exsolution lamellae. A lava sample analysed from the Antakya locality contains scattered bright crystals that are uniform throughout the slide. Some crystals show exsolution with titanium rich lamellae and cubic crystals are also present (Figure 7.9D). Generally, these contain more titanium than the lava from Tahtaköprü. Many of the crystals in this slide display areas that are more titanium rich (Figure 7.9E), either titanium-iron oxides or titanium silicates (sphene).

7.7.4 Discussion of scanning electron microscope analyses

From the rock magnetic experiments it was expected that there would be a difference between the rock magnetic grains between the different lithologies. These results are supported by the SEM analyses, with additional information on the textural relationships also provided. SEM analyses show that both skeletal and cubic crystals are common in most samples and are observed in all lithologies (Figure 7.10).

From rock magnetic experiments, the cumulate gabbros were expected to contain Ti-poor titanomagnetites, some of which may have undergone a degree of oxidation. This conclusion is supported by SEM analyses which indicate that 20-60 μm sized grains of magnetite or Ti-poor titanomagnetites are present in the cumulate gabbros. It is not possible to tell how oxidised these crystals are from SEM work; however, the results do not contradict the inference from the IRM work that they are oxidised magnetites. Fe oxides appeared to be completely absent from one of the cumulate samples, a feature which is consistent with analysis under the polarising microscope.

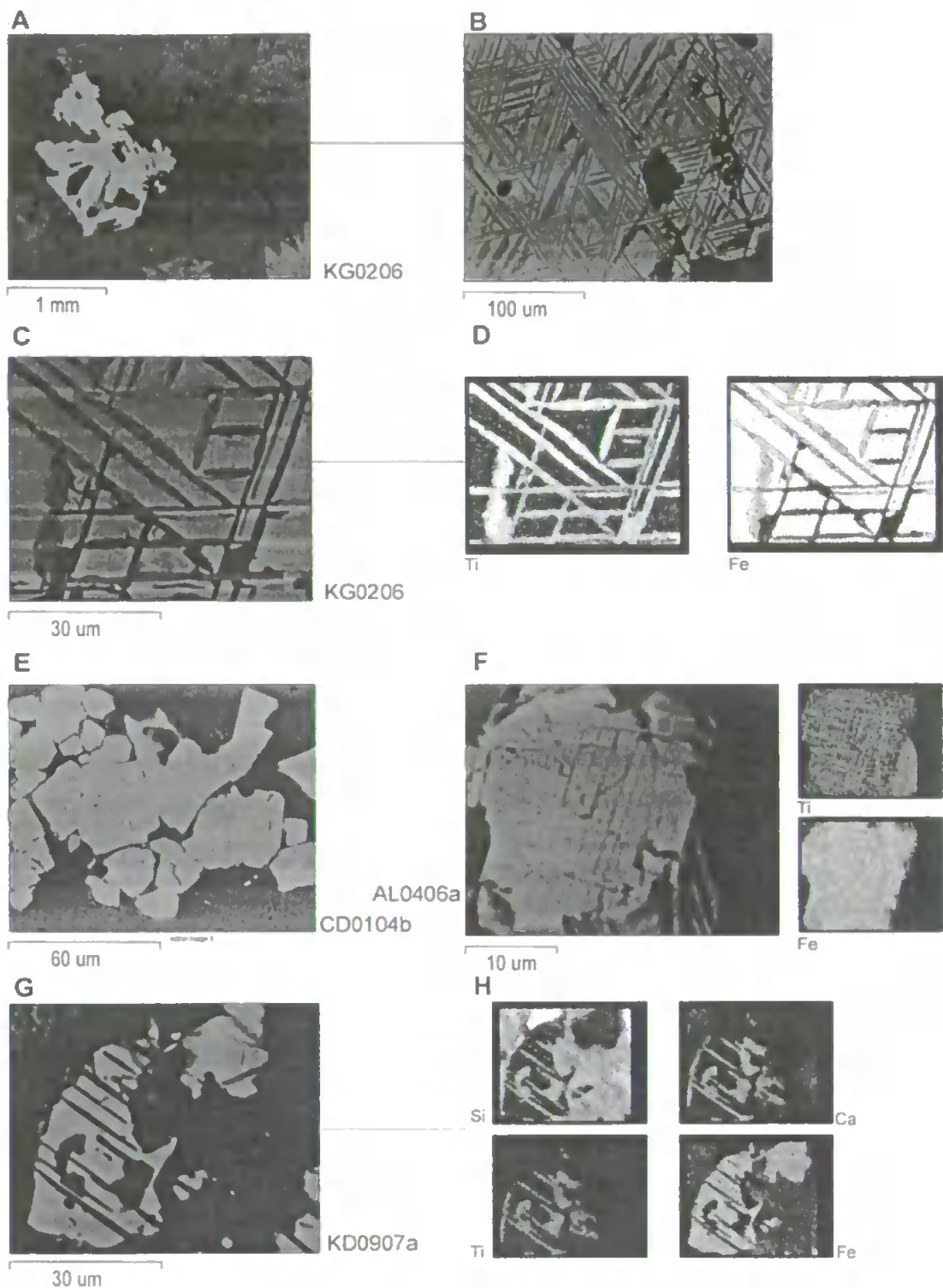


Figure 7.10: SEM images of exsolution textures, observed in all lithologies of the ophiolite, from the lavas to the ultramafics. They are most common and most well-developed in the isotropic gabbros and cumulate gabbros.

A-B. Exsolution is extremely clear in a large number of grains within the gabbros and is particularly well-developed in large skeletal iron oxide crystals, as in the example.

C. The exsolution lamellae comprise a near-magnetite and near-ilmenite phase, although this latter phase is commonly altered or part-altered to titanite.

D. The lamellae are picked out by Ti maps and also by Si and Ca maps if altered.

E-F. Exsolution textures are also observed in lava and dyke samples, although they are less common and sometimes not as well-developed, as shown by the examples.

G-H. Lamellae may have higher concentrations of Si and Ca as well as Ti implying alteration to titanite.

The gabbros had rock magnetic characteristics that were most typical of pure magnetite/Ti-poor magnetite crystals with recovery of remanence during low temperature experiments suggesting the presence of some MD grains. The existence of large (up to 200 μm) crystals of iron-titanium oxides and coarse exsolution lamellae, as observed under the SEM supports this. The exsolution displays end members of lamellae of a Ti-rich titanomagnetite (probably near-ilmenite) and lamellae of Ti-poor titanomagnetite (near-magnetite) and varies between very coarse in some crystals, to finer in other areas, with grains that are compatible with sizes in the PSD region.

SEM analysis of samples from the SDC indicate that a mixture of grain sizes and compositions are present which supports the inference from rock magnetic experiments that mixtures of several different magnetic compositions may be the cause of the more varied features observed, particularly in the frequency dependent AC susceptibility experiments and the two components observed in the T_C curves. Exsolution is not common, but is observed in a few crystals.

The rock magnetic results from the lavas indicated the presence of more Ti-rich titanomagnetites and SEM analysis corroborates this, demonstrating that the lavas contain more Ti-rich titanomagnetites than the deeper lithologies. The lavas contain generally smaller ($\sim 30 \mu\text{m}$) magnetite and titanomagnetite crystals and some crystals show exsolution textures.

Most of the minerals studied using the SEM were at least 10 μm in size. Due to the resolution limits of the SEM it is possible that other smaller grains existed that were not identified. Natural magnetic minerals have not been extensively studied using the SEM, partly due to their small grain size- often less than 5 μm (Xu et al. 1997). The average size of the magnetic grains in pillow lavas from four sites near the mid-Atlantic Ridge that can

be resolved by BSE imaging is 1 to 10 μm (Xu et al. 1997). The lavas may show a difference in grain size and texture between samples from the outsides of lava flows and pillows where cooling was fastest and those from the interior where cooling would have been slower; for instance Kostrov and Prevot (1998), found larger and more regularly shaped grains from the central parts of lava flows and Zhou et al. 2000 observed low-Ti magnetite intergrown with ilmenite lamellae ($\sim 50 \mu\text{m}$ long) in massive dolerites. Euhedral titanomagnetite/titanomaghemite grains are the dominant opaque mineral in ocean floor basalts with grains that usually have cruciform or dendritic quenched structures (Zhou et al. 2000; Wang and Van der Voo 2004), consistent with quenching from high temperatures (Somboonsuk and Trivedi 1985). Their size varies from less than 1 μm to a few tens of micrometres in fine grained basaltic lavas (Zhou et al. 2001) to $\sim 40\text{-}200\mu\text{m}$ in coarse-grained massive basalts (Zhou et al. 2000).

Following medium-grade deuteric oxidation during initial cooling (indicated by lattices of octahedrally oriented ilmenite lamellae), medium temperature (100 to 300°C) hydrothermal alteration will be expected to produce either areas of fine ($\sim 1 \mu\text{m}$) granules of anatase, rutile or titanite or the variable replacement of the ilmenite lamellae by titanite (Hall and Muzzatti 1999). The replacement of some ilmenite lamellae by titanite was observed in some of the exsolution textures in the Hatay ophiolite lithologies (Figure 7.10G-H).

SEM results for the cumulate gabbros failed to show the skeletal magnetite grains observed in the isotropic gabbros and also observed in the thin sections from the cumulate gabbros analysed under the polarising microscope. This is not interpreted to be representative of the lithology; instead the lack of magnetic grains is probably the result of their large size and dispersion in comparison to the area of the rock possible to examine under the SEM, resulting in difficulty in selection of a representative section for analysis.

7.8 Discussion of results from rock magnetic and supplementary analyses

The results from the rock magnetic experiments carried out in this study give much information on the magnetic composition and behaviour of the magnetic component of the ophiolitic lithologies, which has in all cases been supported by the SEM and thin section analyses. Important details regarding the location and formation of the magnetic grains were obtained from these complementary analyses; for example the observation of exsolution textures using the SEM and observation of fine grained iron oxides around olivine crystals from thin section analyses. Although differences were observed between ophiolitic lithologies, all results are consistent with magnetisation being acquired soon after formation at a spreading ridge, with magnetic grains capable of holding a magnetisation stable over geological time. Volcanic rocks are generally regarded as the most reliable recorders of the palaeomagnetic field, with rocks in which the titanomagnetite has undergone high temperature deuteric oxidation to form submicron sized magnetite-rich lamellae and ilmenite-rich lamellae being particularly reliable recorders (e.g. Haggerty 1978). Small SD or PSD grains are then capable of preserving their magnetisation over tens and hundreds of millions of years (Banerjee 1991; Dunlop and Özemir 1997). The formation of magnetite through the process of deuteric oxidation also ensures that the primary NRM of a rock is a thermoremanent magnetisation (TRM).

7.9 Comparison with the magnetisation of modern oceanic crust and ophiolites

Rocks broadly comparable to those of the upper levels of the Hatay ophiolite have been recovered during several ODP legs. The primary remanence carried by magnetic minerals in igneous rocks is a thermomagnetic remanence and this is accepted to be true for the uppermost 500 to 600 m of oceanic extrusives (Hall and Muzzatti 1999). However, there is considerably less agreement on the mechanisms and timings of magnetisation

acquisition in the remainder of the crust. Generally, the accepted constituents of modern oceanic crust are titanomaghemite or maghemite in pillow lavas (e.g. Xu et al. 1997), magnetite in the SDC (e.g. O'Donovan and O'Reilly 1983; Pariso and Johnson 1989, 1991) and SD magnetite formed by high temperature oxidation in the gabbros (e.g. Kent et al. 1978; Dunlop and Prevot 1982).

7.9.1 Comparison with oceanic crustal rocks of the modern day oceans

Table 7.5 describes the rock magnetic characteristics observed within modern day oceanic crust, as observed by various authors. The upper levels of the oceanic crust are most accessible and thus more information is available on magnetic minerals within these, especially for MORB. ODP Hole 504B is the only drill hole that extends continuously from the top of oceanic crust into the SDC and there are very few studies on the rock magnetic properties of gabbroic or deeper crustal rocks from the modern day oceanic crust.

For lavas in the modern oceanic crust, T_C s are generally lower than for the deeper levels and this is similarly observed in the Hatay ophiolite. However, values in modern day oceanic crust remain lower than observed in the Hatay extrusive rocks, suggesting these either contain a comparatively lower degree of titanium or alternatively have experienced a higher degree of maghemitisation. The Hatay extrusives display similarity with older crustal rocks i.e. higher but more variable degrees of maghemitisation. The observations of low-Ti magnetite in upper crustal rocks (Wang and Van der Voo 2004) is consistent with the magnetic properties observed in the Hatay extrusive rocks and also with previous studies on submarine massive doleritic basalts and intrusive rocks (Dunlop and Prevot 1982).

Depth	Characteristic	Reference	Description
Upper crust	Maghemitisation ^A	Bleil and Peterson 1983; Johnson and Pariso 1993	An important process in the upper crustal levels of modern oceanic crust and may account for the decrease in NRM observed with age of the crust. However, maghemitisation does not appear to be ubiquitous, neither do rocks of the same age display the same oxidation ratios.
Upper crust	Maghemitisation/ composition	Zhou et al. 2000	Gradual increase in oxidation observed with age of dredge and drill cores of MORB- no alteration in young lavas (< 20 ka) to $z < 0.35$ for Quaternary samples (< 2 Ma) to $z = 0.9$ for older samples (10s of Ma). Older samples display more variability.
Upper crust	Maghemitisation/ composition	Xu and Peacor 1997	Younger lavas (10 km from MAR) contain nearly unoxidised titanomagnetite; older samples contain near end-member titanomaghemite (900 km from MAR).
Upper crust	Maghemitisation/ composition	Shau et al. 2000	Younger rocks may display no maghemitisation e.g. TM0 observed in ODP Hole 504B, suggested to have formed by: (i) oxidation-exsolution and hydrothermal alteration (ii) oxidation-exsolution, a second stage of oxidation-exsolution and hydrothermal alteration. Primary TM60-70 thus evolved to end-member magnetite coexisting with e.g. titanite (sphene), ulvöspinel and ilmenite on a submicroscopic scale. NRM carried by exsolved TM10-20 subsequent to CRM acquisition.
Upper crust	Alteration	Zhao et al. 2002; Zhou et al. 1999	Samples with high z values often contain abundant clay minerals altered from silicates and glass. Alteration may occur at different rates (even within same sample) due to variations in the level of protection from surrounding matrix and in grain size/ permeability.
Upper crust	Tc	Xu and Peacor 1997	Tcs range from 180-350°C, increasing away from the spreading ridge. These are higher than values predicted assuming no oxidation (e.g. Readman and O'Reilly 1972; Nishitani and Kono 1983).
Upper crust	Composition/ Tc	Wang and Van der Voo 2004	Low-Ti magnetite is thought to have originated during early high-temperature (deuteric) oxidation and is intergrown with ilmenite lamellae. Tcs for these samples are typically > 500°C (530-585°C)- significantly higher than TM60, even if oxidised to titanomaghemite.
Upper crust	Grain size	Zhou et al. 2000; 2001	Two groups of grains identified: (i) grains that crystallise in equilibrium with the melt with grain sizes increasing from ~1 µm near pillow margins to 10s of µms towards interiors; (ii) grains embedded in interstitial glass with submicrometer SP/SD grains, again increasing in size towards the centre of pillows (to few 10s of µms). SEM observations support this revealing: (i) 100 µm sized titanomagnetite grains; (ii) micrometer to submicrometer sized grains.
Upper crust	Grain Size	Shau et al. 2000	Ocean ridge basalts of Hole 504B contain TM0 of extremely fine grain size (30-100 nm), primarily in the PSD range.
SDC	Composition	Hall and Muzatti 1999	Magnetite forms by two main processes with the resulting grains difficult to distinguish between. The second type is recognised by swelling/ pinching of ilmenite lamellae, protusion of ilmenite into the surrounding silicates, and the presence of more small dark inclusions than in the first type. The second type becomes more common at depth, as also observed in the Troodos ophiolite.
Gabbros	T _{UBS}	Worm 2001	ODP Hole 735B gabbros have TUBS slightly below the Tc of magnetite, with NRMs that are suggested to be extremely stable over geological time.
Gabbros	MDFs	Kikawa et al. 1996	Mean MDFs of 28.6 mT are found in ODP Hole 894G gabbros.

Table 7.5: Magnetic properties of modern oceanic crust for comparison with those of the Hatay ophiolite.

^A Synthetic experiments have simulated the maghemitisation process, both by the addition of oxygen (e.g. Özdemir and Dunlop 1985) and, more rarely (although how maghemitisation proceeds on the seafloor) by the removal of iron (e.g. Worm and Banerjee 1984; Kelso et al. 1991). Low and medium degrees of oxidation ($z < 0.7$) of SD titanomagnetites should not affect the original NRM directions of submarine basalts (Özdemir and Dunlop 1985).

Exsolution in the Hatay dykes is generally not well-developed and it is hard to be certain which type of exsolution (as described by Hall and Muzatti 1999) is observed. However, ilmenite lamellae display alteration to titanite in places indicating that the process of altering to the second type has begun. T_{UB} and MDF values measured in the deeper levels of the modern oceanic crust (Kikawa et al. 1996; Worm 2001) are similar to those of the Hatay gabbros and cumulate gabbros. These are consistent with magnetite formed by high temperature oxidation, as generally expected for the deeper levels of the crust (e.g. Kent et al. 1978; Dunlop and Prevot 1982).

7.9.2 Comparison with other ophiolites

Following the work of Moores and Vine (1971) in the Troodos ophiolite, the magnetic properties of ophiolites have been of interest for researchers investigating the source of the marine magnetic anomalies. Original magnetisations may be irregularly preserved within an individual ophiolitic massif (Gnos and Perrin 1996; Hagstrum and Jones 1998). Alteration of the primary magnetic minerals may occur both as a result of seafloor hydrothermal processes and during obduction and subsequent events, with the former more significant in the upper crustal rocks and obduction processes more likely to affect the magnetisation of the lower crustal rocks.

Originally, it was thought that the sheeted dykes in the Troodos ophiolite would be unsuitable for palaeomagnetic study due to the destruction of titanomagnetite by hydrothermal processes (Moores and Vine 1971). Stable components of magnetisation have been identified in both zeolite and greenschist facies dykes and from extrusive samples, with hydrothermal alteration appearing to have little effect on primary TRM (Morris 1996). Reverse components of magnetisation have been found in the Troodos

ophiolite and suggest acquisition of a CRM some time subsequent to original formation of the rocks (Gee et al. 1993).

Feinberg et al. (1999) investigated remagnetisation during seafloor and obduction processes affecting the Semail ophiolite. Earlier studies (e.g. Thomas et al. 1988; Perrin et al. 1994) lead to the conclusion that successive episodes of remagnetisation occurred at the base of the nappe whilst on the seafloor, although some results are ambiguous (Luyendyk and Day 1982; Thomas et al. 1988). The gabbros and peridotites of the Semail ophiolite are dominated by PSD magnetite with occasional alteration to secondary haematite (Feinberg et al. 1999). Curie temperatures range from 548° to 578°C suggesting magnetite or Ti-poor titanomagnetite, with a mean MDF value near 50 mT and 90% of the remanence destroyed at 560°C consistent with a magnetite-dominated mineralogy (Feinberg et al. 1999). Primary magnetite is found mainly in the high-level gabbro (Luyendyk and Day 1982) but most of the magnetite is of secondary origin and reaches the highest concentrations in the ultramafics. The lower levels (mantle section) of the Semail ophiolite in the southeast are found by Feinberg et al. (1999) to be remagnetised from the base up to the layered gabbros, with remagnetisation inferred to have occurred as a consequence of hydrothermal alteration during emplacement of the ophiolitic nappe onto the continental platform. The deepest crustal rocks analysed for this thesis were cumulate gabbros and the implication of the results regarding remagnetisation in the Semail ophiolite is that these would not have been affected by remagnetisation during obduction processes.

7.9.3 Timing of magnetisation acquisition

The importance of characterising the magnetic carriers in a rock, irrespective what they are is to understand whether these are capable of carrying a remanence stable over geological time and how long after crustal genesis this was acquired. Some studies suggest that

magnetisation can be acquired in the deeper levels at considerable time after initial crustal genesis (e.g. Hall and Muzzatti 1999; Hole 504B; Gee et al. 1993; Troodos), although the timing of alteration to secondary magnetite is poorly constrained. Hall and Muzzatti (1999) concluded that it may either occur early at the spreading axis, or up to around 2.5 Ma subsequent to genesis. From the 88-92 Ma age of formation indicated for the Troodos ophiolite, falling within the Cretaceous LNP chron, the fact that reverse components of magnetisation are observed indicates acquisition of magnetisation 5-9 Ma after genesis.

7.10 Synthesis

The rock magnetic data from the Hatay ophiolite are consistent with the magnetic minerals forming on the ocean floor. Exsolution textures have been observed in all lithologies in the Hatay ophiolite and have also been observed in all structural levels of modern oceanic crust. The lower crustal levels, the sheeted dykes and gabbros are less affected by hydrothermal alteration whilst on the seafloor. The rock magnetic properties of lavas from the seafloor often show hydrothermal alteration and many lavas have titanomaghemite as a major constituent, whereas the titanomaghemite concentration of lavas in this study did not appear to be significant. However, higher concentrations of titanium were observed in the magnetic minerals within the upper crustal rocks (extrusives) of the Hatay ophiolite, consistent with observations in the modern oceans.

CHAPTER EIGHT

8. STRUCTURAL ANALYSES AND SYNTHESIS OF STRUCTURAL AND PALAEOMAGNETIC DATA

8.1 Introduction to chapter

The key aims of this chapter are to investigate the structural development of the Hatay ophiolite and relate this to the rotations identified by the palaeomagnetic work (see Chapters Five and Six) in relation to the different phases in the evolution of the ophiolite. To this aim, a comprehensive series of structural measurements were obtained from key localities from all levels of the ophiolite and the sedimentary cover (Figure 8.1). No previous studies have concentrated on fault analysis within the ophiolitic basement of the Hatay ophiolite in relation to rotations. It is therefore important for an independent study of the structures within both the ophiolite and sedimentary cover to be carried out in order to constrain both the pre- and post-emplacement structural history. The ophiolite has a complex history and is expected to have experienced deformation as a consequence of seafloor spreading, initial detachment of the ophiolite, emplacement onto the Arabian margin and post-emplacement deformation associated with the development of the current plate configurations in the eastern Mediterranean. The legacy of this is a complicated pattern of structures within the Hatay region, and in order to link these structures with the successive deformation phases experienced, the regional structure of the ophiolite is discussed in the context of both pre-existing and new observations. Fuller details on the structural evolution are provided by a palaeostress analysis performed on the new structural data acquired. Finally, the concluding section of the chapter aims to synthesise the results from all aspects of the structural and palaeomagnetic research and discuss their implications for the evolution of the eastern Mediterranean.

Komurcukuru
Faults measured within the ultramafics of the basal shear zone. 4 drill sites in pillowed lavas and lava flows.

Belen Road
Faults measured in the sediments along the Belen-Antakya road in a roughly 5 km section SE of Belen. 2 drill sites in same sediments.

Belen turn-off to Komurcukuru (H04)
Faults measured in muddy sandstones and siltstones.

Kisecik Valley
Faults measured in the ultramafics. 4 drill sites in ultramafics and 4 in the SDC.

Ucedik
Faults measured in the SE of the valley within sediments within a small quarry.

Isikli
Faults measured in gabbros and SDC along a river section to the NE and the gabbro/ultramafic transition to the SW. 4 drill sites in the SDC.

Coast Road
Faults measured in the SDC, gabbros and ultramafic cumulates. 15 drill sites (13 within the SDC).

Karacay Valley
Faults measured along river valley in cumulate gabbros and ultramafics and also measured in the sedimentary cover in the south of the valley. 15 drill sites in cumulate gabbros and SDC.

Samandag-Antakya Road
Faults measured within the sediments of the Hatay graben, mostly on the NW margin. 2 drill sites within the sedimentary cover.

Antakya (and Dursunlu)
Faults measured in the hills behind Antakya in the sedimentary cover. 4 drill sites in pillowed lavas and lava flows.

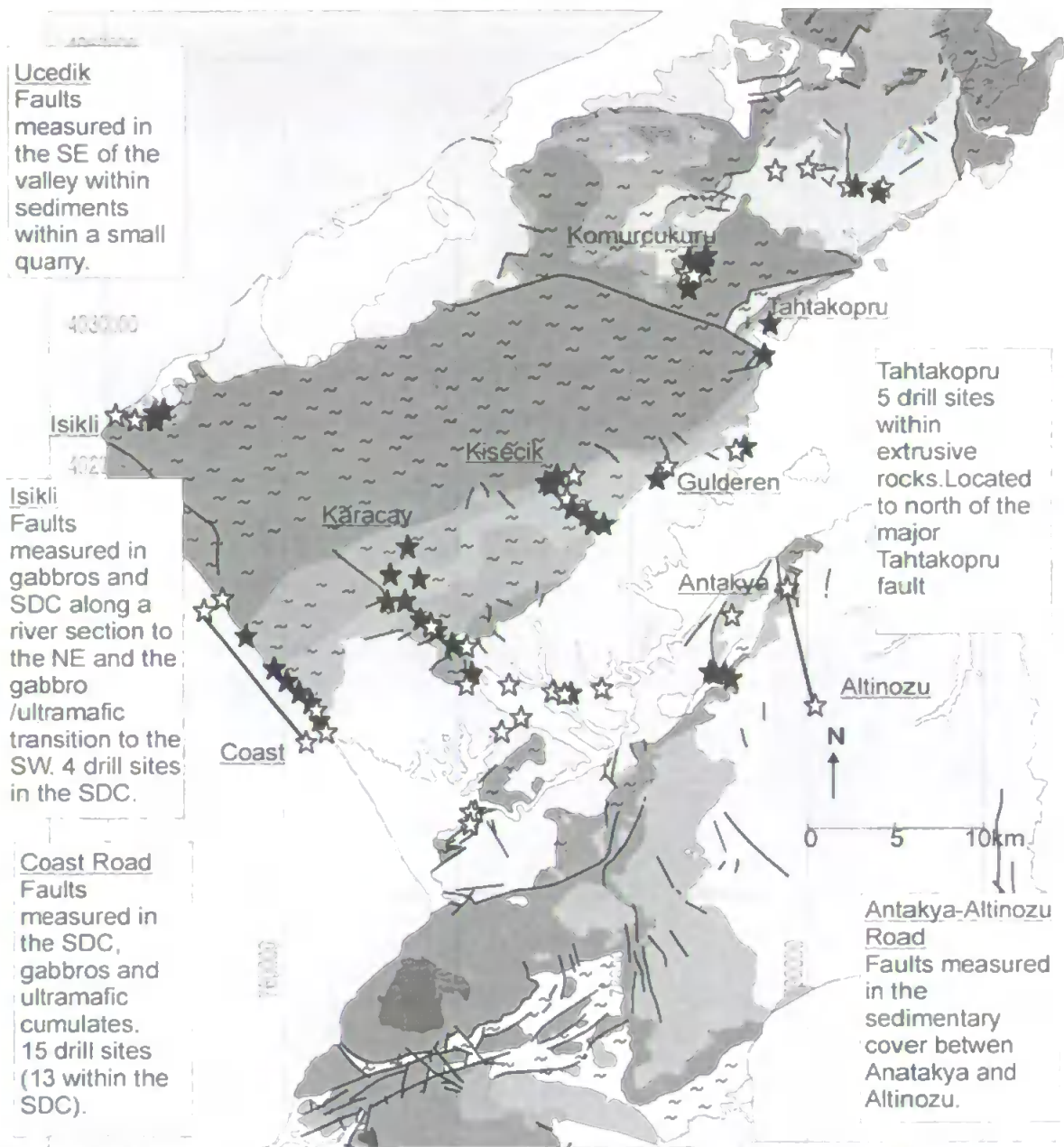


Figure 8.1: Distribution of structural sampling localities (white stars) and palaeomagnetic sampling sites (black stars). The key is as for Figures 2.12/5.1/6.1. A brief description of each locality including the nature of both structural and palaeomagnetic measurements within it is included. Much of the structural sampling was carried out along road section transects, with the major ones shown by two stars linked by a line.

8.2 Structural sampling localities and nature of data

Much of the structural sampling was carried out in similar areas to the palaeomagnetic sampling localities, both due to the quality of outcrops in these areas and the importance of being able to correlate the structural data with the palaeomagnetic data, but measurements were also obtained from new localities, particularly within the sedimentary cover framework. The three main settings for structural sampling were:

- (i) the basal shear zone of the ophiolite
- (ii) the main body of the ophiolite
- (iii) the sedimentary cover framework

The basal shear zone and limestones of the Arabian platform of the ophiolite are exposed in an erosional window near Kömürçukuru (section 2.7.5). As such this area represents an important locality for interpreting the structures relating to emplacement of the ophiolite, particularly as the lack of a metamorphic sole prevents mineral lineations and fold vergence directions being used to identify the emplacement direction (c.f. Baër-Bassit; Al-Riyami et al. 2002). Faults within the main body of the ophiolite record the signature of all phases of the deformation experienced; thus analysis of the structural development of the ophiolite is incomplete without knowledge of these structures. Investigation of faults affecting the cover framework provides constraints on post-emplacement deformations, important both for the determination of sequential structural events and to allow back-stripping of these younger structural events in the ophiolitic basement prior to the recognition of earlier pre-cover phases of deformation. Structural measurements included the measurement of 617 faults, with 452 of these from the ophiolitic basement and shear zone, 165 from the cover framework and three from the ophiolite-sedimentary cover boundary. Measurements included wherever possible the orientation of the shear planes

and their associated slip vector and movement direction, referred to as 'fault slip data', in order to use these to provide kinematic constraints on the deformation in the Hatay region.

8.3 Regional structure

8.3.1 Outcrop patterns and topographic expression

The Hatay ophiolite massif forms a broad NE-SW trending antiformal structure with the deepest structural levels of the ophiolite outcropping in the centre of the massif and the extrusive sequences of the ophiolite tectonically separated from the main massif and outcropping in small areas in the north (see section 2.7 for a detailed discussion). The major faults of the ophiolite are illustrated on the published map (Pişkin et al. 1985), on which the geology and faults of Figure 8.1 are based. The ophiolite consists of two structurally distinct massifs that are separated by the NW-SE striking steeply dipping Tahtaköprü fault with the main massif lying to the west of this fault. The timing and nature of the fault are not constrained, although Dilek and Thy (1998) propose that it represents a fossil transform structure (section 2.8).

The boundaries between the deeper levels of the ophiolite (tectonites, gabbros and SDC) run NE-SW and have been variously interpreted (section 2.7.1). The three main possibilities are shown on Figure 8.2. Many of the major contacts between the deeper lithologies are characterised by large gullies, as observed along the coast, trending roughly NE-SW at a high angle to the coastline (Figure 8.3A-B). Smaller faults adjacent to major contacts also pick out this direction; for example faults oriented NE-SW are observed north of the gully separating the SDC from gabbros [0759022; 4007029]. Dilek and Thy (1998) suggest that many of the contacts between lithologies can be explained by primary seafloor spreading tectonics e.g. detachment faults (cross-section 8.2A).

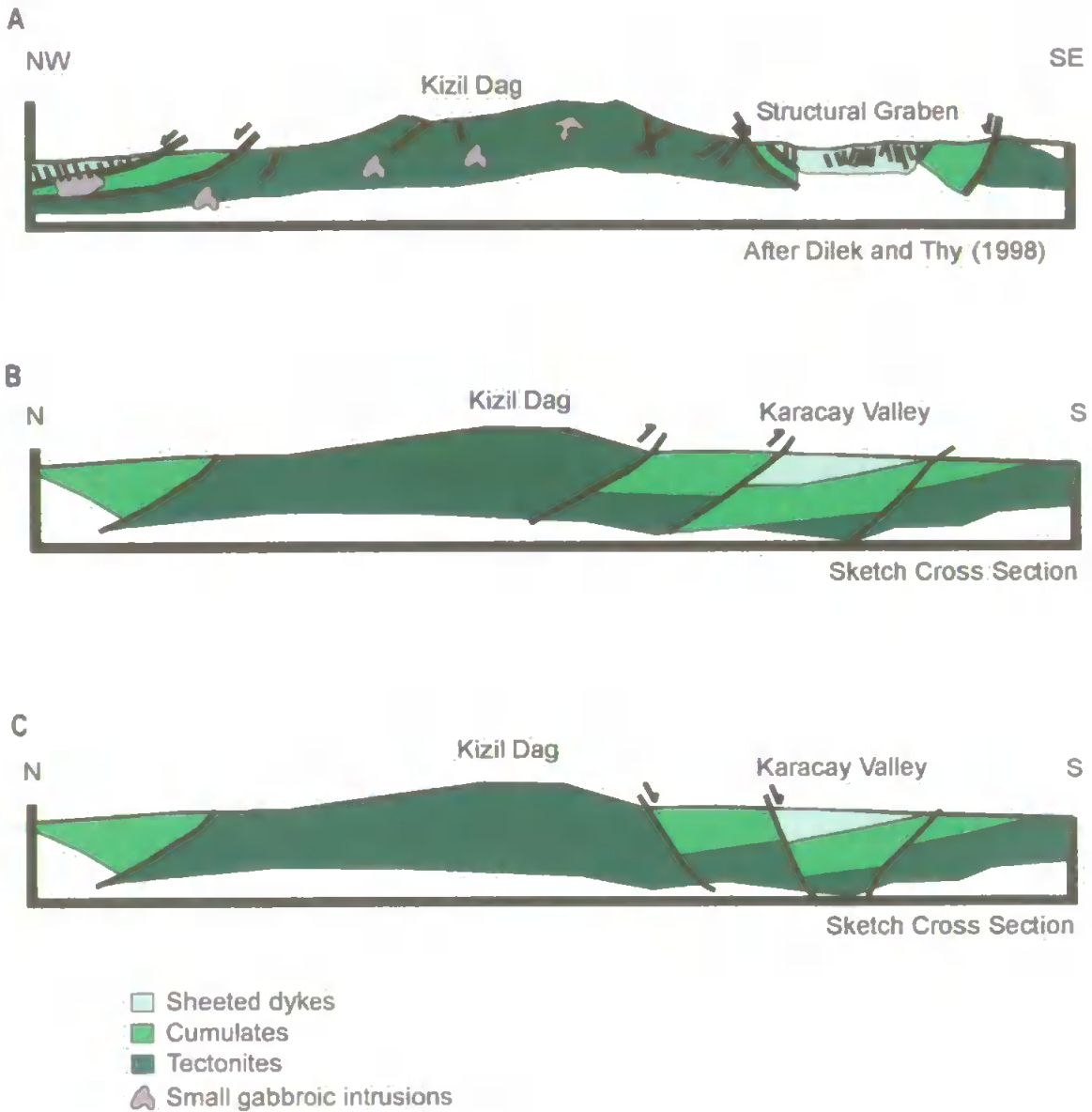


Figure 8.2: Various possible models for the outcrop patterns observed within the Hatay ophiolite. Boundaries between major ophiolitic units trend NE-SW and have been variously interpreted by different authors.

A. The interpretation of Dilek and Thy (1998) that the structures within the Hatay ophiolite represent seafloor spreading tectonics.

B. Boundaries interpreted as normal faults formed during Neotectonic faulting, rather than on the seafloor prior to emplacement.

C. Boundaries interpreted as reverse faults, most-likely linked to thrusting during emplacement of the ophiolite.

Cross-sections A and B both explain the outcrop pattern using normal faulting, but with differing interpretations of the origins of the faulting. Normal faulted boundaries would better explain the steep dip of the cumulate layering whereas reverse faulting would more easily explain the apparent lack of tilt about a horizontal axis suggested by the steep dip of the SDC. An additional possibility is that folding alone may explain the outcrop pattern. However, this appears unlikely due to the number of faults observed running parallel to the boundaries (section 8.3.2). Some previous research has suggested that at least some contacts are primary magmatic contacts, although this cannot explain all due to the lower levels of the ophiolite (e.g. Ultramafic complex) outcropping at higher topographic levels than the higher levels (e.g. SDC) to both sides of the ultramafic core.

Another possibility is that many of the contacts are marked by reverse faults (cross-section 8.2B). Reverse faults may cause minimal rotation of footwall rocks which would account for the apparent lack of rotation about a horizontal axis suggested by the consistently steep dip of the SDC. However, normal faulting under a Neotectonic phase of deformation (cross-section 8.2C) is favoured by the work of this thesis due to the parallelism of the strike of the cumulate layering and the strike of Neotectonic faults identified from this study (section 8.5), with the moderate-steep dip of the layering also favouring normal rather than reverse faulting.

The sedimentary cover is transgressive over the ophiolite (section 2.7.4) and the NE-SW trending Hatay graben discussed in section 2.2.3, stretching from Antakya in the NE to the Mediterranean coast in the SW, can be clearly seen on Figure 8.1 (SE of the main ophiolite outcrop) from boundary-parallel faults marking its extent. The contact between the ophiolite and the sedimentary cover can be observed in several places, including localities along the Antakya-Altınözü road and to the south of the Antakya graben (Figure 8.3C).

8.3.2 Inherited structure of the ophiolitic basement

The Hatay ophiolite has a well-developed (generally sub-vertical) SDC oriented on average E-W in present-day coordinates (Figure 8.4), and as such is oblique to the general NE-SW trend of the outcrop pattern. Dykes around Isikli in the NW are shallower and have more variable strikes (Figure 8.4). Along the coast dykes generally dip northwards in the north and southwards in the south. Most previous workers (e.g. Tinkler et al. 1981; Pişkin et al. 1990) reach similar conclusions regarding the structure of the SDC. Dilek and Thy (1998), however, suggest that a first generation of diabasic dykes observed along the coast strike NE-SW and a second population of grey basaltic dykes strike NNW-SSE. This orientation is parallel to the NE-SW trending seafloor graben these authors propose to

explain the structures observed within the SDC, but the average E-W orientation of the SDC measured for this thesis does not tie in so nicely with their model.

Along the coast, measurements of discrete rodingitised dykes within the gabbros and ultramafic complex taken during this project showed that the consistency in strike is poor, although a broadly NE-SW orientation is apparent. It is possible that these discrete dykes are linked to an episode of deformation, although the lack of consistency of strike lessens the likelihood of this.

The layering in cumulate gabbros was measured in all areas where palaeomagnetic drill sites are located, with additional measurements taken during structural sampling (Figure 8.5). All measurements of cumulate layering were taken from the SE limb of the antiform due to the quality of exposures and easier access (although there is mention in the literature of minor outcrops of cumulates in the Isikli area in the north). On average, the cumulate layering dips towards the NW at 57° (e.g. Karaçay valley). However, there is a degree of variation, even within the same area; for example layers in the cumulate rocks along the coast vary from dipping towards the NW through to layers dipping southwards, although the average remains a moderate NW dip.

8.3.3 Structural indicators of tectonic rotation

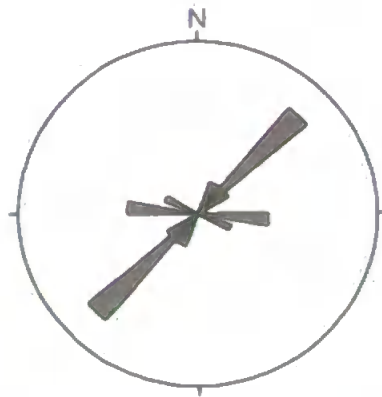
The dip of sedimentary sequences within the Hatay region may be used as an indication of the amount by which the Neotectonic faults have tilted the successions. During the structural sampling programme, the orientations of over one hundred beds (121) were measured to provide a gauge on the degree of rotation resulting from the faulting. The dip of the sedimentary sequences is generally low with over a third of beds dipping between 20° and 30° , and an average dip of 25.4° (Figure 8.6).

A



B

Orientation of gullies along the coast



C

Boundary between ophiolitic basement and sedimentary cover



Figure 8.3: The nature and orientation of major contacts within the Hatay ophiolite.

A. Photo showing the contact between the isotropic gabbros (to the NW) and the SDC (to the SE) exposed along the coastal road between Cevlik and Isikli [0759022; 4007029] with a NE-SW striking gully forming a topographic low along the contact. The sedimentary cover can be seen transgressing the ultramafic hills in the background.

B. Rose diagram of the trend of gullies assumed to mark major fault planes, as observed along the coastal road.

C. Photos illustrating the nature of the contact between the ophiolitic basement and sedimentary cover. Antakya-Altinozu road (photo 0917_204513) showing the contact with conglomerate containing ophiolitic detritus above.

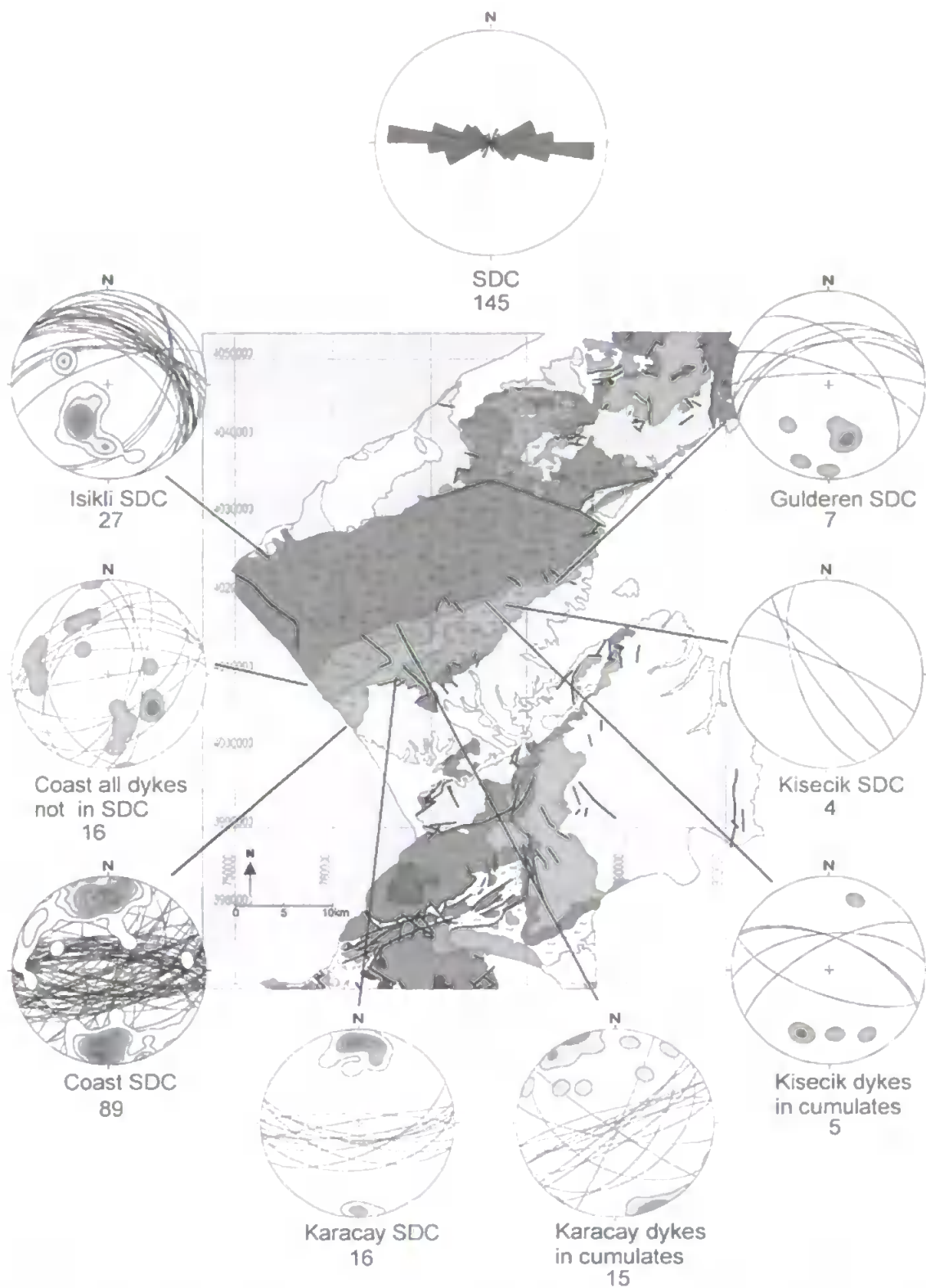


Figure 8.4: Geology map and stereonet projections showing the orientation of dykes within the SDC and discrete dykes within gabbros and ultramafic cumulates by locality in order to recognise any spatial variation. Structural data are displayed by locality in order to recognise any spatial variations in orientation, with poles to the dyke margins contoured. Key to map and place names is as shown on Figure 2.12. The average orientation of the SDC is E-W in present-day coordinates. This consistent E-W orientation is illustrated by the coastal and Karacay valley SDC. Dykes in Isikli are shallower with more variable orientations, on average NW-SE and broadly parallel to those in Kisecik and Gulderen valleys (although only limited data are available for these latter localities). The coastal, Karacay and Kisecik dykes are steep and dip to both N and S whereas dykes towards the north (e.g. Isikli, Gulderen) have a higher proportion of dykes dipping N. Dykes within the deeper levels of the ophiolite (gabbros and ultramafic complex) display more variable orientations. Dykes within the cumulate gabbros and ultramafics in the Karacay valley have similar orientations to the average trend of the SDC, although strike ENE-WSW rather than E-W.

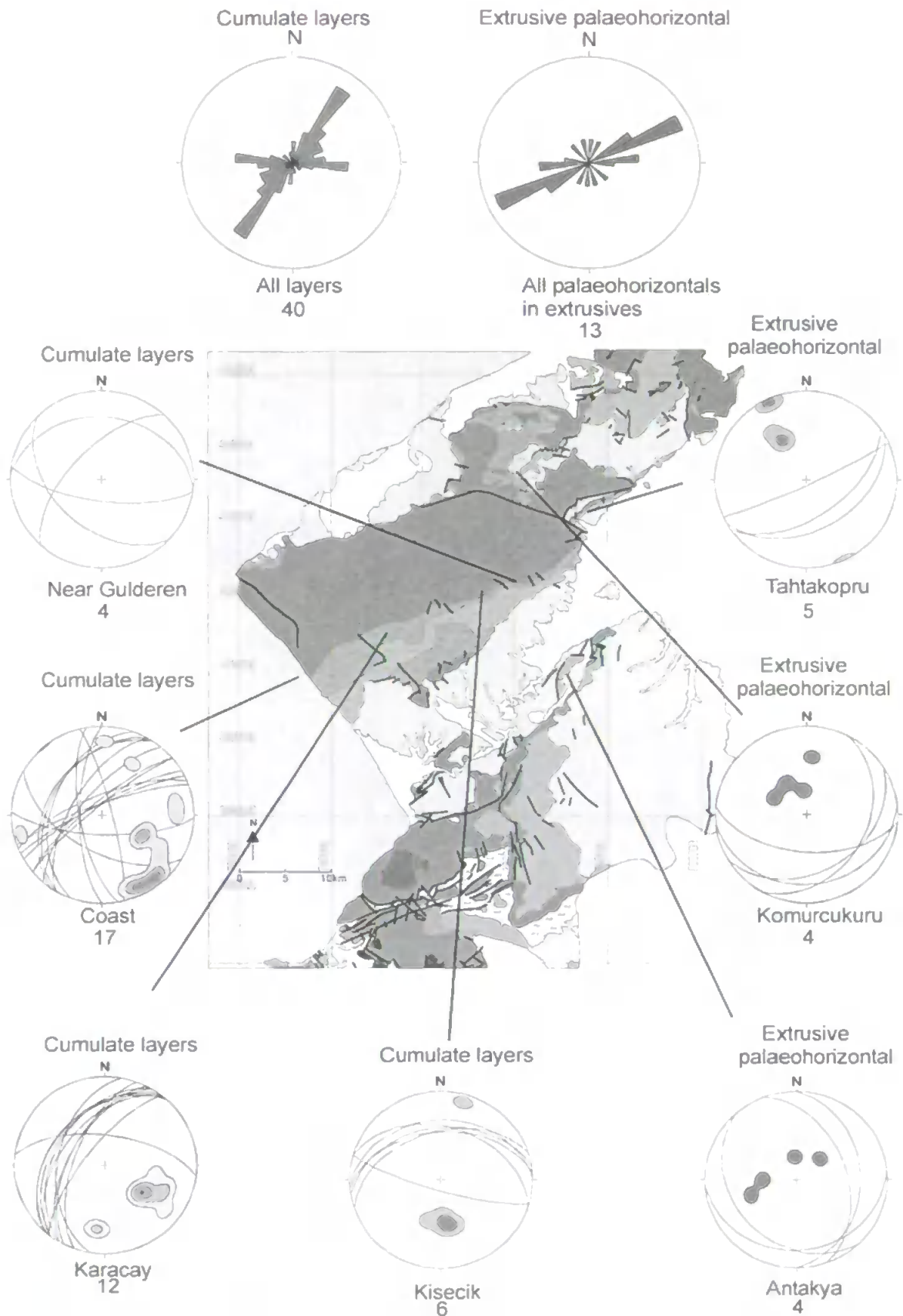


Figure 8.5: Geology map and stereonets showing the orientation of cumulate layering and pillowed and sheet lava flows (extrusive palaeohorizontals) by locality in order to recognise any spatial variation. The summary rose diagrams at the top illustrate that cumulate layering striking NE-SW dominates (e.g. in the Karaçay valley), with layering striking E-W (e.g. in the Kiseçik valley) also a significant trend. From the measurements taken of pillow lavas and sheet lava flow orientations, an ENE-WSW trend appears dominant, although a more limited number of measurements were taken. Key to map and place names as shown on Figure 2.12.

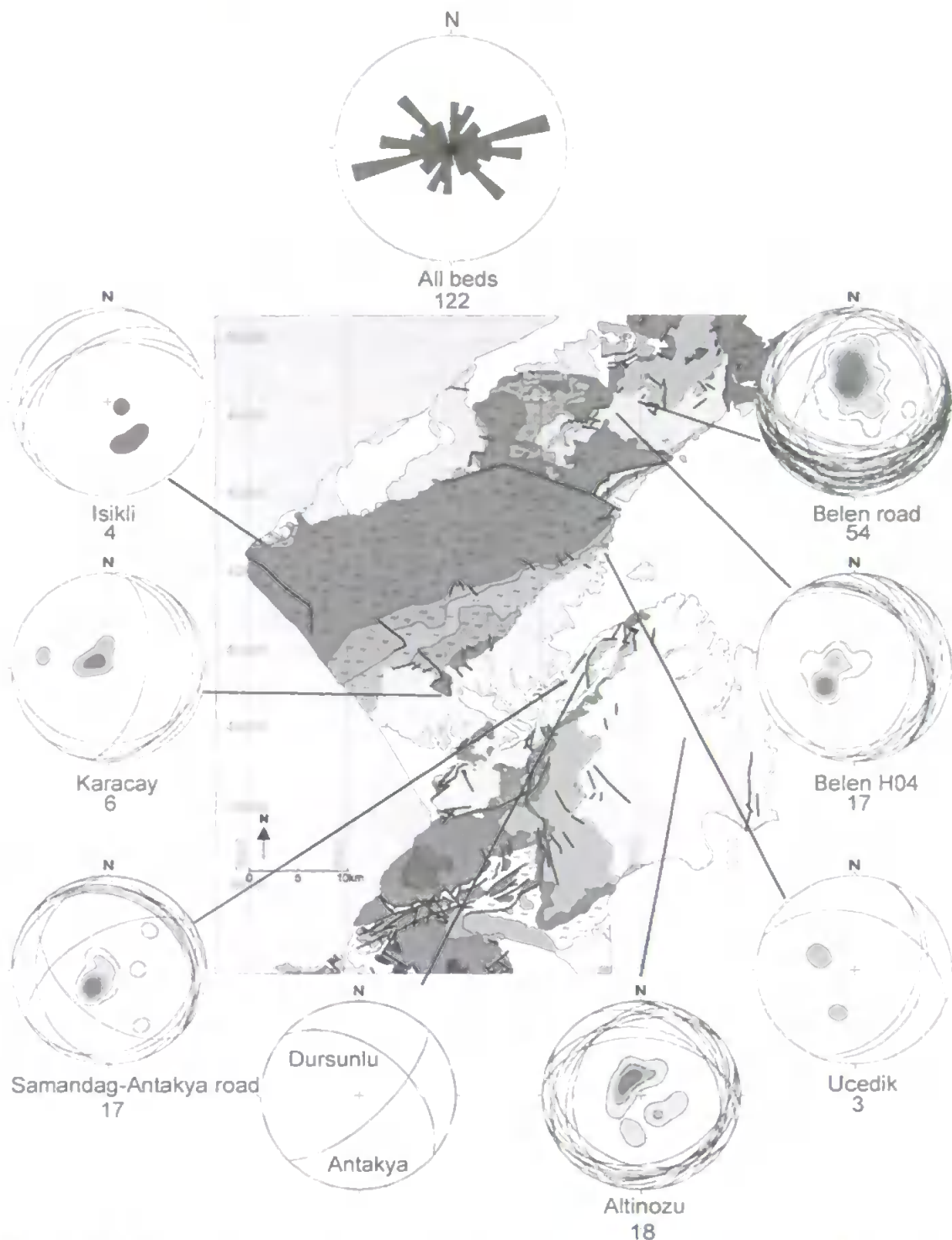


Figure 8.6: Geology map and stereonet showing the orientation of bedding planes by locality in order to recognise any spatial variation (with the number of planes measured indicated below each plot). Measurements within the Hatay graben were taken from along the Samandag-Antakya road, along the Antakya-Altinozu road (E end of graben), from the southern limit of the Karacay valley and from a quarry near Ucedik (NE end of graben). The beds along the Samandag-Antakya road are located on the NW axis of the graben near the centre and predominantly dip NE, whereas beds along the Altinozu-Antakya road, in the Karacay valley and near Ucedik predominantly dip SE. Outside the graben, sedimentary sequences in the north (SE of Belen) predominantly dip S, although display considerable dispersion with a small cluster of NE dips; substantial steepening in the immediate vicinity of a fault is common. South of Belen (locality H04) beds dip consistently eastwards and in Isikli beds dip NW. Using the method outlined by Woodcock and Naylor (1983), only the datasets for all beds and for the Belen area show significance regarding whether the data forms a cluster or girdle distribution. A weak girdle distribution is indicated for all beds and a stronger girdle and cluster respectively indicated for Belen H04 and Belen road localities. A general shallow dip of bedding is apparent in all localities. From the summary rose diagram (top) a significant dispersion in bedding orientations is apparent, although ENE-WSW, E-W and NW-SE trends are observed. Key to map and place names as shown on Figure 2.12.

The Hatay graben is a major Neotectonic graben that has resulted in significant vertical displacements, thought to be in the order of several kilometres (Tinkler et al. 1981; Lyberis et al. 1992). The major graben-bounding faults are expected to produce horizontal axis rotations in the blocks adjacent to the faults; the orientation of bedding within the graben may be used to indicate the degree of rotation (although syn-tectonic deposition may be a factor). Movement on the graben-bounding fault between Harbiye and Antakya is thought to induce a general E/SE dip in Miocene sediments within the graben (Lyberis et al. 1992). Bedding measurements within the Hatay graben were taken for this thesis from various localities (Figure 8.6) with dips rarely above 25°, although locally beds up to vertical are observed in some instances immediately adjacent to a fault. The key conclusion from these measurements is that the degree of variability in orientation and dip makes an assumption of a simple coherent tilt towards the main graben-bounding fault in the SE inaccurate.

For sedimentary sequences not restricted to those within the Hatay graben, Tinkler et al. (1981) refer to a general regional eastwards dip of sedimentary layers. However, measurements for this study found considerable variability. For instance, sedimentary sequences in the north (SE of Belen) predominantly dip southwards, on the turn-off to Kömürçukuru (locality H04) beds dip consistently eastwards and in Isikli beds dip towards the NW (Figure 8.6). A 40° dip for beds 7 km south of Belen for the Maastrichtian sediments and 20° for the Miocene conglomerate and limestones is referred to by Tinkler et al. (1981). Within the wider region, to the east of the study area, Lyberis et al. (1992) describe a change in dip within Neogene sediments across the Amik basin (north of Antakya) from E/SE in the south to a W/NW dip closer to the Amanos range to the north and west (Lyberis et al. 1992), again indicating significant variability within restricted areas.

The degree of variability observed in the dip of sedimentary sequences prevents simple backstripping of younger tilts from the earlier structural data. This lack of consistency in the orientation suggests that local smaller-scale faults are influencing the horizontal axis rotations to at least an equivalent degree to the more major faults within the region.

The orientation of palaeovertical and palaeohorizontal indicators within the ophiolite can be used to indicate the degree of rotation, as was discussed in relation to the palaeomagnetic data (section 5.8). For example, the on-average near-vertical dykes of the SDC indicate potentially limited tilting of the complex, whereas the on-average moderate-steep NW dip of the cumulate layering and the variable (generally SE) dip of palaeohizontals measured in extrusive rocks within the Tahtaköprü and Kömürçukuru areas (Figure 8.4) suggest more significant tilting. The relationship between these palaeohorizontal and palaeovertical indicators can be insightful. For instance, the average strikes of dykes in the SDC and the strike of cumulate layering within adjacent areas are not parallel and the angle between these palaeohorizontal/vertical indicators is not orthogonal. This implies that a simple rotation to simultaneously restore layers to horizontal and dykes to vertical is not possible and more complex rotations varying spatially are likely. The order of tilting is important in analysing the influence of originally palaeovertical/palaeohorizontal layers on subsequent faulting. For instance, faults occurring prior to the main tilting of originally horizontal units will not be influenced by the structure.

8.3.4 Faults and shear zones

The structures within the ophiolite are dominated by brittle faults. Major faults are characterised by considerable erosion and landslip, and streams and rivers often follow these major structures, particularly within the ophiolitic basement. The nature of the fault

zones varies, some being marked by continuous, linear planes and some by undulose surfaces. The majority of faults are marked by clear planes, with deformation mostly confined to the narrow region of the plane. However, some faults, particularly within the gabbros and ultramafic rocks in the Isikli area, and within areas of the sediments south of Belen, are characterised by wider areas of deformation and the development of breccia within the zone. Slickenlines observed on fault planes are sometimes mineralised and sometimes marked by steps indicating the sense and direction of movement, particularly in the sedimentary cover. The movement direction could be distinguished for 42% of the faults measured and from this it is clear that the majority of faults, both in the ophiolitic basement (55 %) and particularly within the sedimentary cover (88 %), are normal faults and that strike-slip faults are slightly more numerous than reverse faults. Spatially, the different fault types are not confined to any one area but are ubiquitous, with the occasional absence of either a strike-slip or reverse fault from a locality explained by their small number rather than a difference in structural history.

The basal shear zone is characterised by sheared serpentinites containing large allochthonous limestone blocks. A limestone gully, deeply incised by a river is observed at the topographically lowest point accessible within the valley from the K m r ukuru direction, and interpreted as the limestone of the Arabian platform (e.g. Aslaner 1973). The shear zone is marked by the development of s-c fabrics associated with brittle structures (Figure 8.7). Lineations are defined by serpentinite mineralisation in the serpentinites and carbonate mineralisation in the limestones.

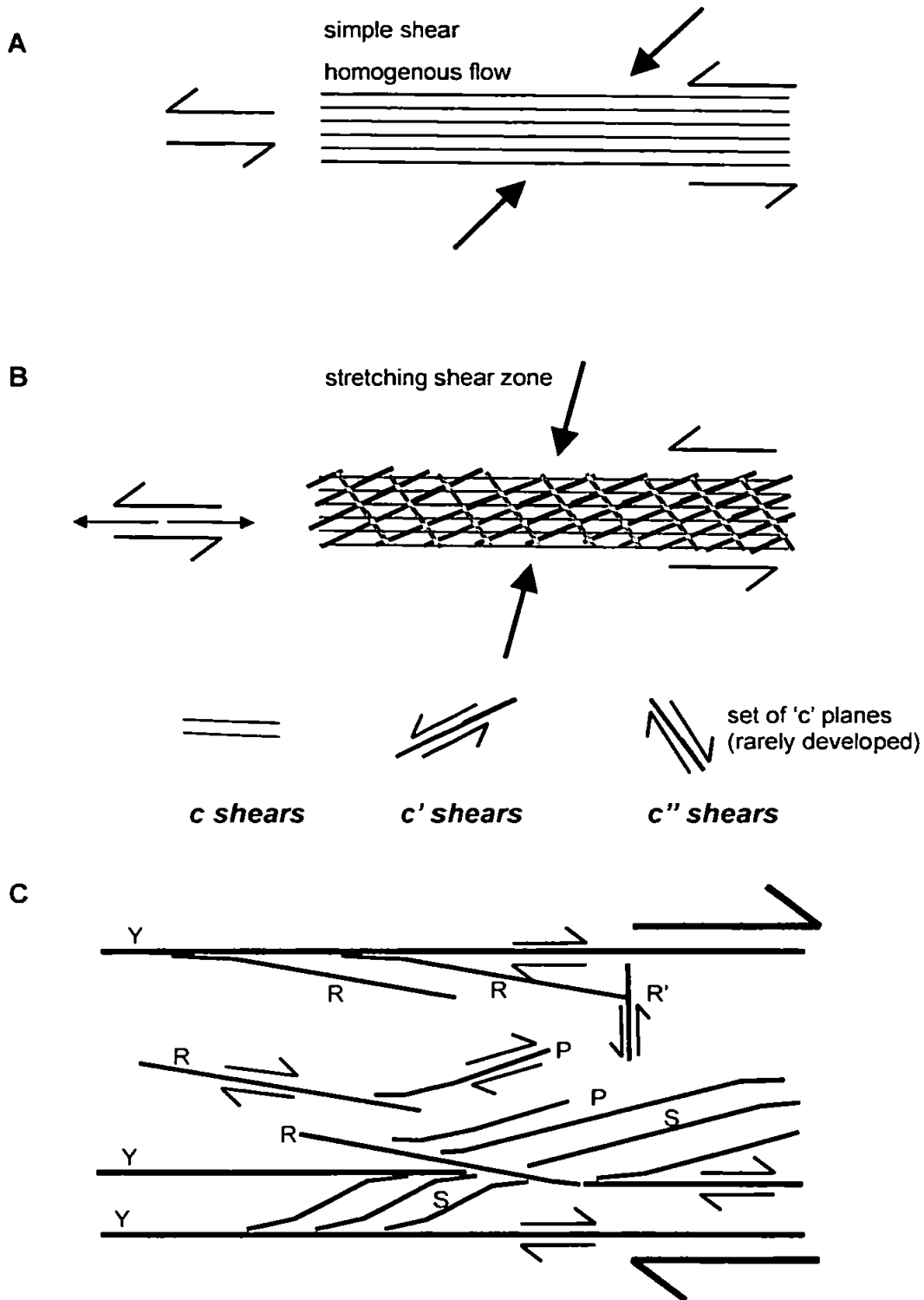


Figure 8.7: Synoptic diagram of structures expected to form within a shear zone, and as were measured within the basal shear zone of the Hatay ophiolite.

A. Plan view of a simple shear zone with homogenous flow.

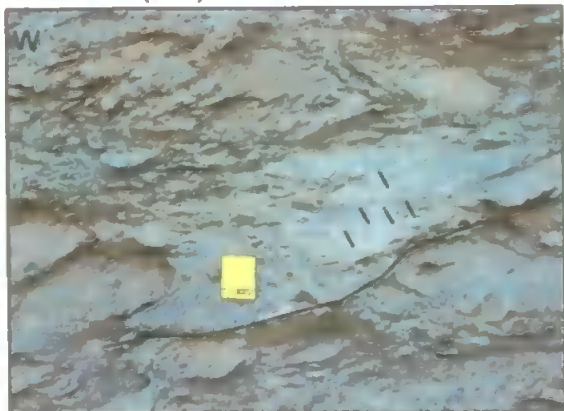
B. Plan view of a shear zone where stretching also occurs. The development of more than one '*c*' plane is illustrated.

C. Cross-section view of the features identified in the field that aid interpretation of the movement direction within the shear zone include the development of '*s*' fabric. R = Riedel shears; R' = Reverse riedel shears; Y = shear-zone bounding parallel surfaces; P = '*P*' shears; S = *s* fabric with shape of the '*s*' an indication of movement direction.

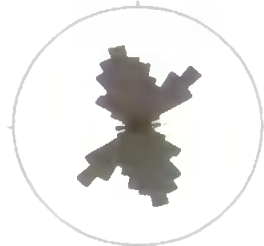
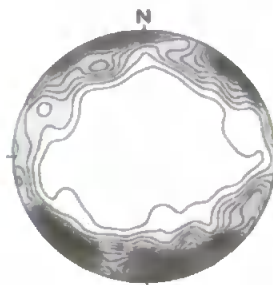
The majority of the measured lineations in the basal shear zone are either SE or SW plunging, although there is considerable dispersion (Figure 8.8). The SE lineations are slightly dominant and associated with top-to-the SE indicators in the fabric (Figure 8.8) and brittle SE and NW dipping faults, whereas the SW lineations were not obviously associated with any larger scale fault structures. In a few localities N-S lineations and top-to-the N fabrics dominate, and these seem to be in the areas nearest to the tectonically overlying extrusive sequence (Figure 8.9). These lineations appear to be earlier and are more strongly associated with the fabric development. The basal shear zone is overlain by the extrusive sequence along tectonic contacts. Where observed, these contacts dip shallowly to the NW and may be associated with the brittle SE and NW dipping faults.

The traces of faults illustrated on the published map of the Hatay region (Pişkin 1985) can be seen in Figure 8.1. Generally, trends observed from the published map are corroborated by the results obtained independently from measured structures for this thesis. Minor variations in direction between the two datasets are explained by the published map compilers using valleys to map major faults rather than actual measurements of fault surfaces. From the published map the exact strike of over one hundred (146) faults was measured with the size, nature and units displaced noted. There are comparatively few faults marked on the published map that are confined to the basement and trends observed should thus be interpreted with caution. Both the number and the total length of faults in each orientation were analysed with potential differences providing an indication of the degree to which movement is taken up on a fewer number of large faults or, alternatively by numerous smaller faults (Figure 8.10). A generally clear correlation between the prominence of faults in a certain orientation when regarding either the number or total length of faults in that orientation indicates that no particular trend is different in terms of fault size. The faults measured for this study are also split according to the location where they are found in order to recognise spatial variations in fault trends (Figure 8.11).

Lineations (271)



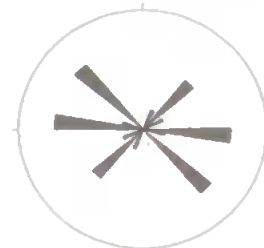
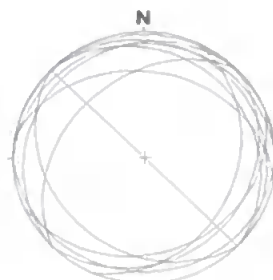
Komurcukuru (photo 1011_030040). SE lineations in basal shear zone are shown by short black lines on the c plane on which they were measured, with the edge of this plane picked out by the longer black line.



C planes (14)



Komurcukuru (photo 1014_235000). Top to SW fabric and NE dipping c planes in basal shear zone.



Fault planes (47)



Komurcukuru (photo 1010_225759). SE dipping brittle fault displacing large coherent blocks.

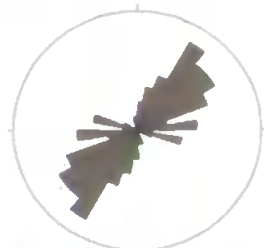
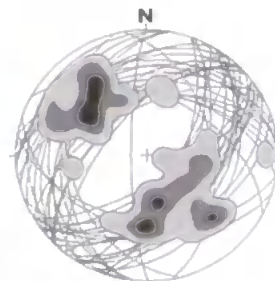
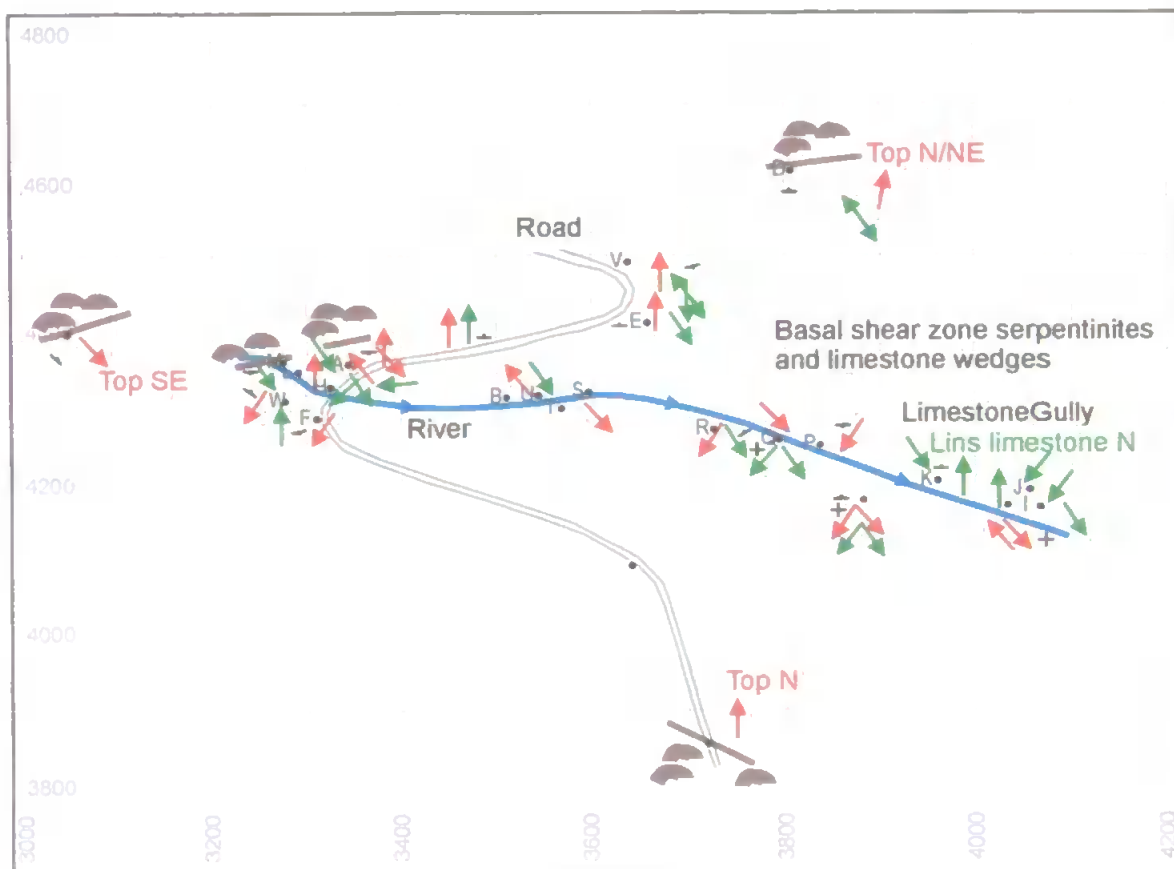


Figure 8.8: Photos (LHS) of the kinematic indicators measured within the basal shear zone of the Hatay ophiolite, with the stereonet and rose plots (RHS) illustrating the orientation of these structures. These structural measurements can provide insight into the emplacement history of the ophiolite. A dominance of lineations in a SE-NW direction, with a subsidiary set oriented NE-SW is apparent. C planes display more variability, although these same trends can also be picked out. Brittle fault planes display a dominant NE-SW trend.



Key






-  Direction of movement along lineations as indicated by fabric
-  Plunge and strike of lineations measured on c planes
-  Pillowed lava flows
-  Dip of c planes/dominant surfaces
-  Locality description in notebook

Figure 8.9: Kinematic indicators and their spatial distribution within the basal shear zone (Komürçukuru) area. The majority of the measured lineations are either SE or SW plunging, with a spread from SE through S to SW directions (and a smaller number of lineations plunging in the opposite direction i.e. NW through N to NE). Although a large degree of variability is observed, the dominance of lineations towards the SE can clearly be seen. Lineations are associated with either top-to-the SW or top-to-the SE indicators in the fabric. The top-to-the SE lineations are associated with brittle SE and NW dipping faults, whereas the top-to-the SW lineations are not obviously associated with any larger scale fault structures. Both normal and reverse SE dipping faults were observed. Lineations trending N-S and a few localities where top-to-the N fabrics are observed appear to become more dominant towards the contact with the overlying pillow lavas. These N-S lineations appear to be earlier and are more strongly associated with the fabric development.

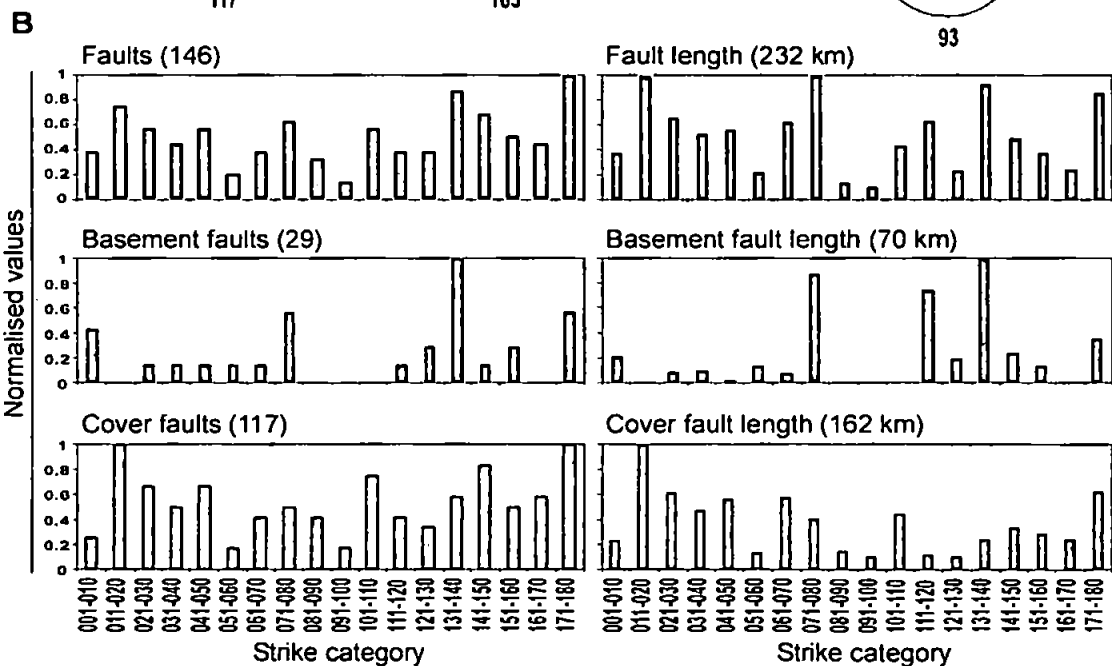
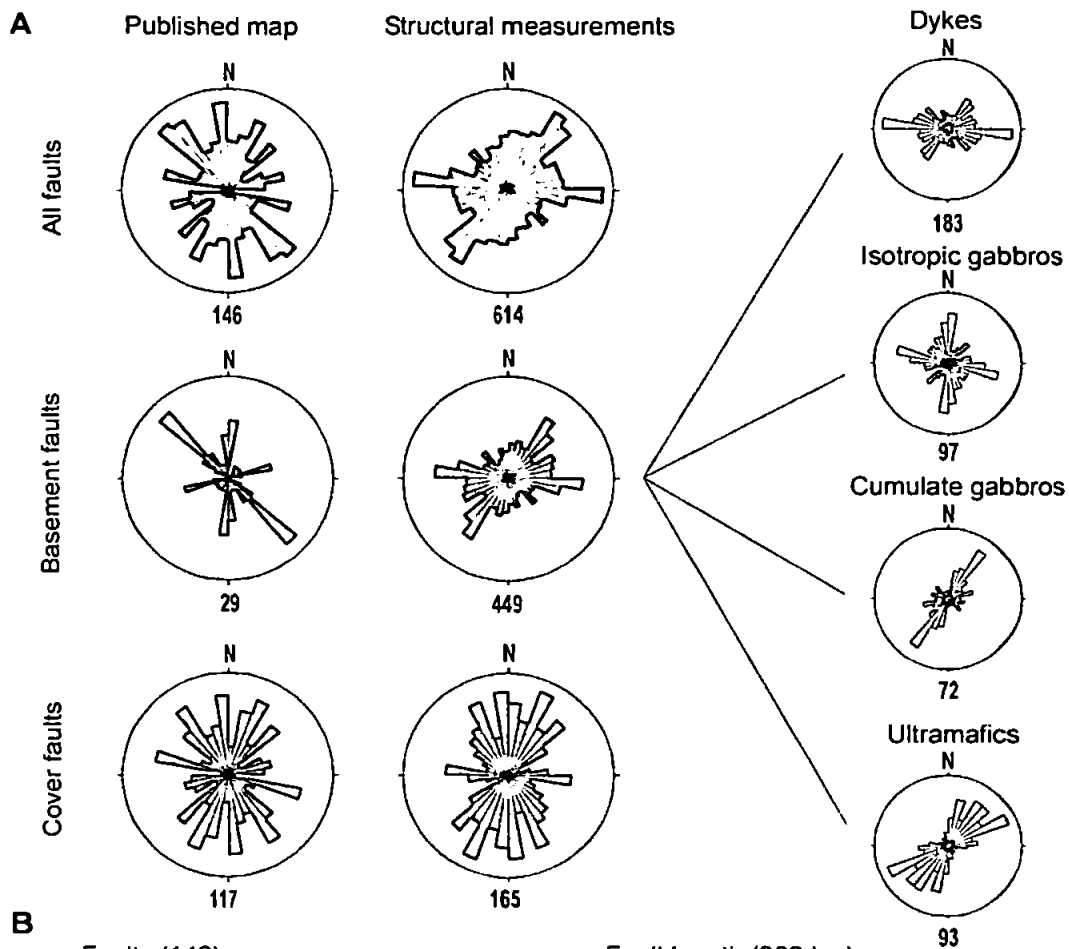


Figure 8.10: Comparison between published map fault strikes and those measured during structural sampling for this thesis. Many of the discrepancies are explicable by fault traces of major faults being used to compile the published map rather than the smaller faults used by this thesis. Note should also be taken of the limited basement fault dataset obtained from the published map.

A. Stereonets comparing the strike of faults. E-W trending faults are a more significant trend in the faults measured for this study whereas the NW-SE trend is picked up more clearly by the published map faults. In the ophiolitic basement, the influence of the E-W trending SDC and the NW-SE trending layering in the cumulate rocks is clear. The cover displays a wider dispersion of fault orientation.

B. Histograms illustrating the dominant trends in fault strikes from the published map (Piskin 1986) when analysing either the number of faults in a category (LHS) or the total length of faults in that category (RHS). A general correlation is apparent, although some trends differ, for instance E-W trending faults are more significant when fault length is considered.

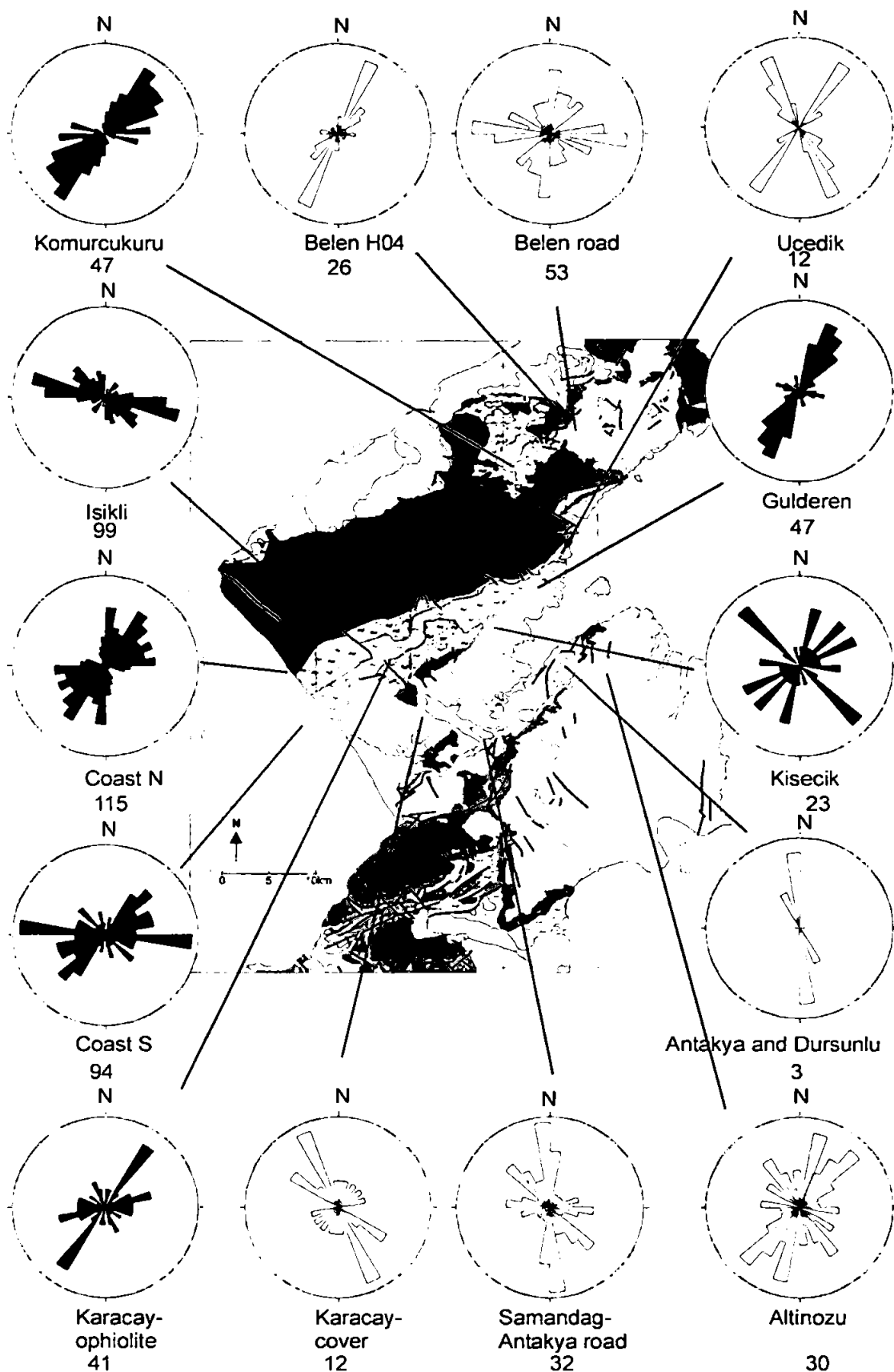


Figure 8.11: Geology map and rose diagrams illustrating fault strikes separated into localities in order to recognise any spatial variations in orientation. Key to map and place names as shown on Figure 2.12.

The darker grey shows faults measured within the ophiolitic basement and the lighter grey indicates faults measured within the sedimentary cover, with the number of faults included in the rose diagram plot listed below each plot. Although, there is some variability in fault strike between localities, most identified trends (see text) are picked up across the ophiolite and cover indicating that the faults are not spatially discrete.

From consideration of the 617 faults measured for this thesis and the fault traces illustrated on the published map, it is apparent that although fault strikes display considerable dispersion in orientation, four main trends can be identified:

- (i) E-W striking
- (ii) NE-SW striking
- (iii) NW-SE striking
- (iv) N-S striking

(i) E-W striking faults

E-W trending faults are a clear trend when considering those faults measured for this study (Figure 8.10). The structures are less significant from analysis of the published map, although become more dominant when fault length is considered, implying that for this category larger faults dominate. Lineament analysis in the Hatay region (Over et al. 2004b) identifies a similar trend, with identification of a major ~75 km ENE-WSW lineament branching into three main segments trending 60°, 90° and 70°. Regarding the faults measured for this thesis, E-W striking faults are slightly more dominant within the basement than the cover. These faults are especially dominant within the SDC (Figure 8.10A) indicating the influence of the steep present-day E-W striking dykes on fault development. Dyke margins commonly display evidence for utilisation as a fault surface. Spatial analysis shows that the E-W striking trend is picked out by a small number of E-W striking faults in most areas of the ophiolitic basement, but is most significant in the southern coastal exposures. Immediately to the north within the deeper structural levels of the ophiolite (gabbros and ultramafic rocks), the E-W fault trend dies out, again suggesting the strong influence of the SDC on fault orientation. In the cover sequences, E-W striking faults are a significant trend in the sandstones and limestones along the road to the SE of Belen

(ii) NE-SW striking faults

NE-SW striking faults are a trend that is clearly picked up by the faults measured for this study, particularly within the basal shear zone (Kömürçukuru area) and within the Gulderen valley, but less so for the more evenly distributed published map faults where the NW-SE and N-S categories are equally as significant (Figure 8.10A). Lineament analysis (Over et al. 2004b) also recognises this trend, with NE-SW trending lineaments between 30-40° and 50-60° most numerous, although with a smaller total length than the lineaments observed between 70-90°. The dominant strike of faults within the cumulate gabbros and ultramafic rocks is NE-SW, parallel to the average layering observed in the cumulate rocks. If many of these faults are post-tilting the cumulate layering may have influenced the development of the faults in a similar way to that observed within the SDC. Within the cover framework, this trend is clear within the Uçedik valley, although slightly more NNW-SSE in orientation, and dominates in the muddy siltstones measured on the turn-off from Belen to Kömürçukuru (locality H04). From analysis of the published map it appears that NNW-SSE striking faults are spatially ubiquitous.

(iii) NW-SE striking faults

NW-SE trending structures are clearly identified from analysis of the published map but less significant when considering the complete dataset of faults measured for this study (Figure 8.10). They become clearer when analysis is restricted to the cover framework alone and when the faults are separated into the areas where they were measured. For instance this trend is very clear within the Uçedik valley and in the sandstones and limestones along the road to the SE of Belen, although slightly more NNE-SSW in orientation. From the published map it appears that NNE-SSW trending faults become less significant towards the west of the study area.

(iv) N-S striking faults

N-S faults are clearly identified from analysis of the published map but less significant when considering the faults measured for this study (Figure 8.10). When separated into cover and basement, this N-S trend becomes clearer. Spatial analysis highlights faults in this orientation as in some areas the faults measured within the cover framework are almost N-S (e.g. to the SE of Belen), although it cannot be known from initial analyses whether these faults comprise a real N-S trend or part of the NW-SE or NE-SW trends observed in adjacent areas of the cover. From study of the published map, it can be seen that N-S striking faults are more prevalent towards the north, around Belen, and to the east of the Hatay area. The N-S faults become increasingly prevalent eastwards, which suggests a link with movements along the Dead Sea Fault (DSF) zone to the east of the area and implies that the DSF zone has limited influence within the study area.

8.3.5 Summary and discussion of regional structure

From the above analysis of regional structures, several important patterns become apparent. There is a clear NE-SW orientation of both outcrop boundaries and comprising a dominant fault trend. The strikes of the different terrains within the Amanos range, of which the Hatay ophiolite forms part, similarly trend NE-SW (Pişkin et al. 1986). The present-day average E-W strike of the SDC in Hatay is thus oblique to this trend. As a general rule, sedimentary sequences have shallow-moderate ($< 30^\circ$) dips towards the east, although the degree of variability results in backstripping younger rotations using bedding orientations being inaccurate. A large dispersion of fault orientations exists, as expected due to the complex tectonic history of the region. However, it is possible to identify four main trends, with faults trending E-W and NE-SW recognised as significant in both ophiolite and cover, NW-SE trending faults more significant within the cover framework

and N-S trending faults clearest from analysis of the published map. The dominant NE-SW and NW-SE trends identified appear to have a slightly different orientation in the cover, being more NNE-SSW and NNW-SSE respectively, with either one of these trends, or both (e.g. in the Uçedik valley), dominating each cover locality. Generally, in each area there is a spread of orientations, although one or two directions usually dominate. There is no spatial pattern in fault orientation; for instance, fault trends in the south of the area are not consistently similar and distinct from fault trends in the north of the region, although spatially adjacent localities may show different trends. However, the N-S faults are more prevalent to the east and as such may be linked with the roughly N-S trending DSF. The dominance of normal faults within both the ophiolite and cover framework ties in with the observation from the review of literature on the region (section 2.2.4) that the Neotectonic history has been dominated by extension/transtension. To analyse these structures further requires more detailed structural analysis using the fault slip data measured in the field.

8.4 Palaeostress analysis

The general patterns from the 617 faults measured within the ophiolitic basement and cover framework discussed in the preceding section gives a good indication of the structural patterns, but palaeostress analysis provides a more in-depth and subtle analytical technique and can provide significant insights into the structural phases affecting the ophiolite and cover. For example, from analysis of fault strikes alone it is difficult to determine whether faults in the same orientation or within a selected area formed under a single event whereas this is possible using palaeostress analysis techniques. The outcome of palaeostress analysis in a region known to have had a complex structural history is expected to be the recognition of a series of distinct structural events with associated palaeostress axes.

8.4.1 Methodology of palaeostress analysis

There are many different ways of reconstructing palaeostresses from field data, many of which are based on faults and their associated slip vectors- 'fault-slip' methods (see Angelier 1994 for a review). These methods use the observed direction of slip to indicate the direction of the resolved shear stress vector that acted on the plane of the fault with the required field data input into these methods consisting of the orientations of the fault planes and their associated slip directions. Palaeostress analysis of all but the smallest datasets makes use of various computer programs; the program used to analyse the Hatay data is TectonicsFP version 1.6 by Franz Reiter and Peter Acs, based on TectonicsVB, by Hugo Ortner for Apple Mackintosh. This program is a standard palaeostress analysis package following those principles outlined above, with the required input parameters being the orientations of the fault and fault-slip vector. The output of the analysis gives the directions on the principal stress axes [σ_1 (P), σ_2 (B) and σ_3 (T)], as well as the stress ratio: [$\Phi = (\sigma_2 - \sigma_3) / (\sigma_1 - \sigma_3)$] and confidence limits on the solutions.

The inclusion of a large number of faults in palaeostress analysis from an area with a complex structural history (as for Hatay) is expected to result in a large array of faults that do not have palaeostress orientations that conform precisely to those for the main structural events. Principal stresses for these faults are expected to be dispersed and overlap with principal stresses from the main structural events, potentially obscuring them. This necessitates clear limits to be set on the confidence limits acceptable for any palaeostress event identified with clear determinations of criteria for the inclusion or exclusion of faults from the final datasets. The lower limit of confidence for any group of faults identified as acting together under a single structural event is set at 80% (where 100% would be complete agreement between palaeostress axes), irrespective of which stress axis is being considered. The inclusion of a greater number of faults may lower the confidence levels;

conversely datasets with fewer faults may give misleadingly high confidence limits. The optimum result is clearly a sufficiently large dataset to be confident of the stress determination with high confidence limits, as illustrated extremely well for the post-emplacement events recognised within the cover framework (section 8.5.5).

8.4.2 Assumptions and limitations

Assumptions of the palaeostress method are that the stress field is homogenous, that there is parallelism between shear and the slip vectors on a fault plane, and that fault sets forming under a discrete event are independent from pre-existing faults, as first proposed by Wallace (1951). It is assumed that the faulting obeys the Coulomb criterion that: $\tau = C + \mu\sigma_n$, where τ is the shear stress, σ_n the normal stress, C the cohesion and μ the coefficient of internal friction. The palaeostress method cannot determine the complete stress tensor (six variables), but determines the reduced stress tensor, consisting of three variables specifying the orientation of the principal stresses and their ratio. No information is gained on the magnitude of the stresses and friction of the fault surfaces is not considered to be important (Angelier 1994). A stress-system will preferentially develop two sets of faults in a conjugate arrangement (due to the symmetry of the stress tensor) with σ_1 as the bisector of the acute angle between the two fault planes implying plane strain with zero deformation along the intermediate stress axes (Angelier 1994). Palaeostress analysis assumes that faulting can be treated as a stress phenomenon, which leads to different predictions of fault patterns than if faulting is treated as a strain phenomenon (Twiss and Unruh 1998). If faulting is controlled by strain, multiple fault patterns are predicted (e.g. Reches 1983, 1987; Marrett and Allmendinger 1990; Twiss et al. 1991, 1993). The palaeostress analysis assumes that multiple fault patterns are produced by two or more events of faulting with the principal palaeostress changing orientation in each event. However, this simple scenario may be complicated by potential reactivation of earlier

structures in each successive event (Bott 1959) or in a single three dimensional strain producing an orthorhombic four-fault pattern with two slickenline sets on pairs of conjugate faults (e.g. Reches 1978, 1983; Krantz 1988). Alternatively, complex interaction between pre-existing planes of weakness and blocks forming under one or more events under either two or three dimensional strain (Nieto-Samaniego and Alaniz-Alvarez 1997) may result in non-plane strain.

The orientation of slip vectors may display variation even within the same fault plane due to fault-slip directions close to fault segment boundaries recording local strain patterns at fault tips (Roberts 1996; Roberts and Ganas 2000). Thus, the assumption in palaeostress analysis that a measured slip vector is representative of the mean movement on a particular fault should be used with caution.

Rotation of earlier structures in subsequent events and interaction between faults adds greater complexity and ambiguity into a simple analysis procedure. Ideally, the rotations associated with successive events should be identified, allowing backstripping of these rotations prior to a palaeostress determination being performed on older faults. If rocks are folded, for instance if a dome structure is present, structures around this may be rotated back to the appropriate pre-tilting orientation prior to analysis. In reality incremental rotations and the relative timing of structural events are difficult to constrain and the assumption is often made that the errors resulting from using the uncorrected/partially corrected dataset are sufficiently minor for palaeostress orientations to be distinguished. Ideally, coeval fault sets should be identified, usually on the basis of their orientation in cases where detailed chronological information is absent. The sub-division of measured faults into meaningful categories by the analyser may introduce bias. Even numerical methods designed for heterogeneous fault data (e.g. Yamaji 2000) cannot separate out fault

populations without some decision by the inputting geologist regarding the most appropriate parameters to use.

It is a requirement of palaeostress analysis to only incorporate faults where all 'fault slip' parameters are constrained and it may be impossible to constrain all of these accurately in the field. For instance, in the Hatay area, larger faults in particular are often picked out by topographic lows due to erosion of the scarp; the fault plane is commonly obscured. The assumption is therefore made that measuring faults on a smaller-scale will produce results that are representative of all faults. A power-law scaling relationship between smaller and larger faults is hypothesised to exist, with greater numbers of smaller faults in the same orientations as larger ones (e.g. Walsh and Watterson 1992). There may be a reason why there is difficulty in measuring a certain parameter for a population of faults. For example, the movement history on an earlier generation of faults may be difficult to measure due to degradation of the fault plane over time.

8.5 Description of data and results of palaeostress analysis

8.5.1 Overview of data

Just over a third of the 617 faults in the complete dataset have been included in the palaeostress analysis, with 148 basement faults and 71 cover faults suitable for palaeostress analysis: the 'palaeostress subset'. A significant number of the measured faults (398 of 617; 65%) from the Hatay area have been excluded from the palaeostress analysis due to the inability to measure one of the required parameters. The degree to which the palaeostress subset is representative of the complete dataset may be indicated by comparing parameters such as fault strikes. The correlation between dominant trends in the fault strikes using the complete dataset compared and fault strikes restricted to the

palaeostress subset (Figure 8.12A-C) indicates that it is a reasonable assumption that the faults suitable for palaeostress analysis are representative of all faults measured.

The four trends identified previously (section 8.3.4) are similarly observed in the palaeostress subset and become slightly clearer when regarding only the cover faults in the subset (i.e. the data are less dispersed). The trends of basement fault strikes in the palaeostress subset are almost identical to the complete dataset, with a very slight increase in the dominance of the NW-SE trend being the only difference; this trend also increases in comparative significance for the cover faults in the subset. Comparison of the complete and palaeostress subsets of faults in different localities also indicates that the subset is representative (Figure 8.12D). The percentage of faults included in the palaeostress analysis from the basement and cover units differs slightly with 33% (148 of 452) of basement faults included and 43% (71 of 165) of cover faults included. The greater percentage of faults in the cover framework suitable for palaeostress analysis is anticipated due to their younger age with the likelihood of being affected by fewer structural events.

The large number of faults necessitates division of these faults into categories prior to performing a comprehensive palaeostress analysis. If the entire dataset of faults used in the palaeostress analysis is plotted on a stereonet (Figure 8.13), there is a large dispersion in fault strikes and lineations with no particular patterns distinguishable. Palaeostress analysis produces extremely low confidence levels on principal palaeostress axes and the directions identified have no geological relevance (Table 8.1). These faults can be broken down according to a variety of parameters e.g. fault type, strike of the fault plane, orientation of the slip vector or dip of the fault.

Initially faults were separated into ophiolitic basement and cover framework as the faults confined to the cover units are only affected by post-emplacement events and should be

more straightforward to interpret. Figure 8.13 shows that it remains difficult to identify patterns, especially within the ophiolitic basement where a greater number of structures were measured and overprinting of pre-emplacment events by post-emplacment events is expected. Faults were also separated into normal, reverse and strike-slip faults prior to in-depth analysis as the nature of the palaeostress analysis and the dependence of the vertical principal axis (σ_1 , σ_2 or σ_3) on fault type make it easier to analyse these separately.

<i>Unit</i>	<i>Faults</i>	<i>Level^A</i>	σ_1 (R%)	σ_2 (R%)	σ_3 (R%)	<i>No. Faults</i>
All	All	1	63/162 (017)	04/065 (04)	19/288 (07)	219
Basement	All	2	48/165 (06)	05/075 (13)	32/300 (01)	148
Basement	Normal	3	88/268 (64)	00/259 (26)	04/352 (27)	82
Basement	Reverse	3	02/155 (46)	04/061 (38)	79/295 (57)	32
Basement	Dextral strike-slip	3	04/338 (49)	84/167 (83)	03/061 (46)	19
Basement	Sinistral strike-slip	3	04/356 (54)	77/097 (81)	15/272 (50)	15
Cover	All	2	85/080 (61)	04/003 (31)	01/079 (48)	71
Cover	Normal	3	87/024 (80)	03/187 (48)	03/084 (47)	59
Cover	Reverse	3	47/077 (70)	03/342 (60)	32/253 (91)	2
Cover	Dextral strike-slip	3	15/123 (52)	69/005 (87)	26/217 (52)	5
Cover	Sinistral strike-slip	3	04/320 (62)	80/000 (80)	09/072 (64)	5

Table 8.1: Orientations of palaeostress axes for all faults and for the initial breakdown of data into basement and cover and fault types.

^A. The level of division of data (as shown on Figure 8.13).

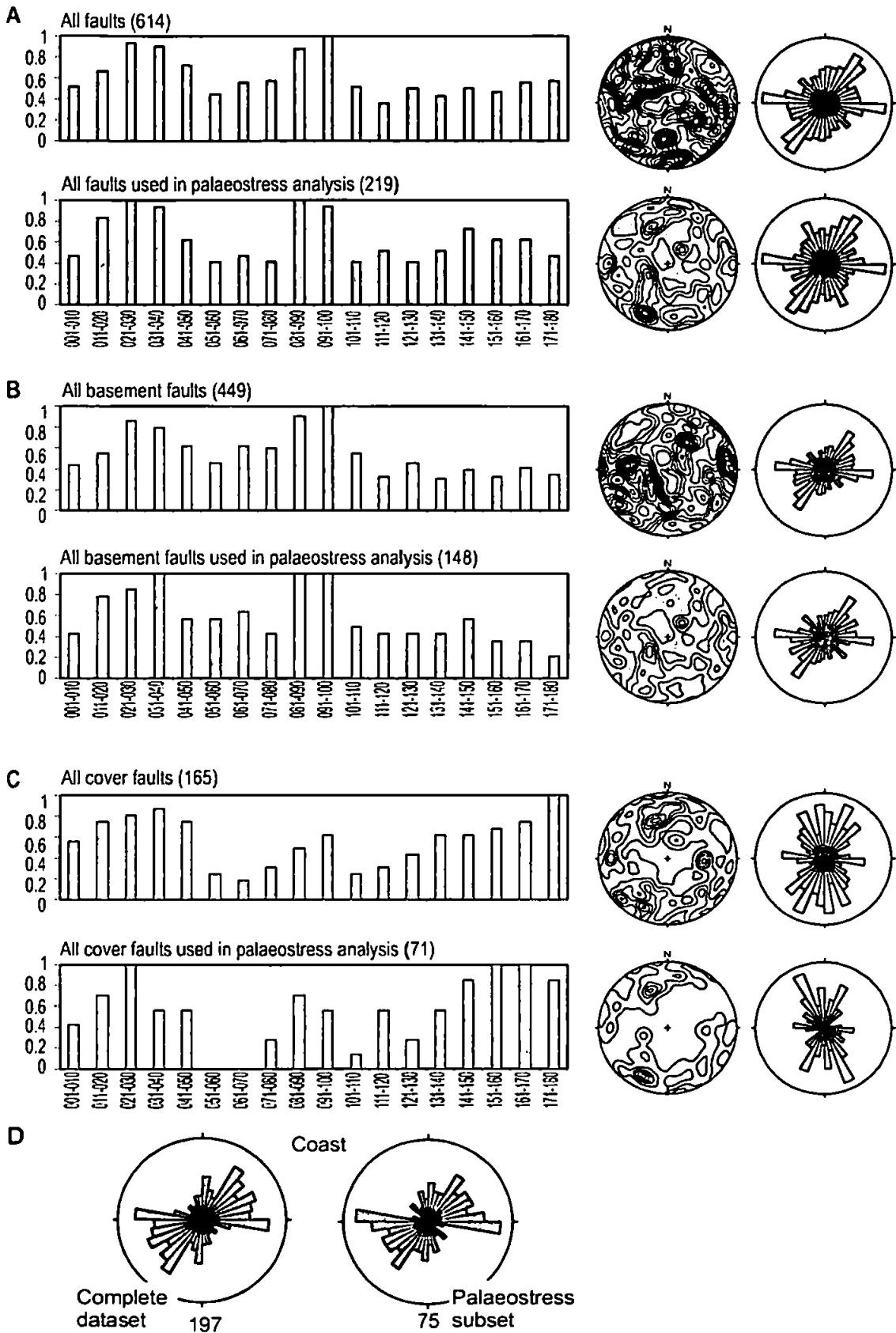


Figure 8.12: Comparison between the fault strikes of all faults measured compared to the strikes of faults limited to those used in the palaeostress analysis.

A-C. Separated into all faults, basement faults and cover faults respectively. The data is shown as histograms (LHS) and rose diagrams (RHS) of strike of faults for easy comparison between datasets and as contoured stereonet (middle) for the presentation of both fault dip and strike. An extremely good comparison between the complete dataset with faults restricted to those used in palaeostress analysis indicates the validity of results from using a smaller subset.

D. Comparison between the complete dataset (LHS) and palaeostress subset (RHS) for the coastal locality, illustrating the representability of the subset.

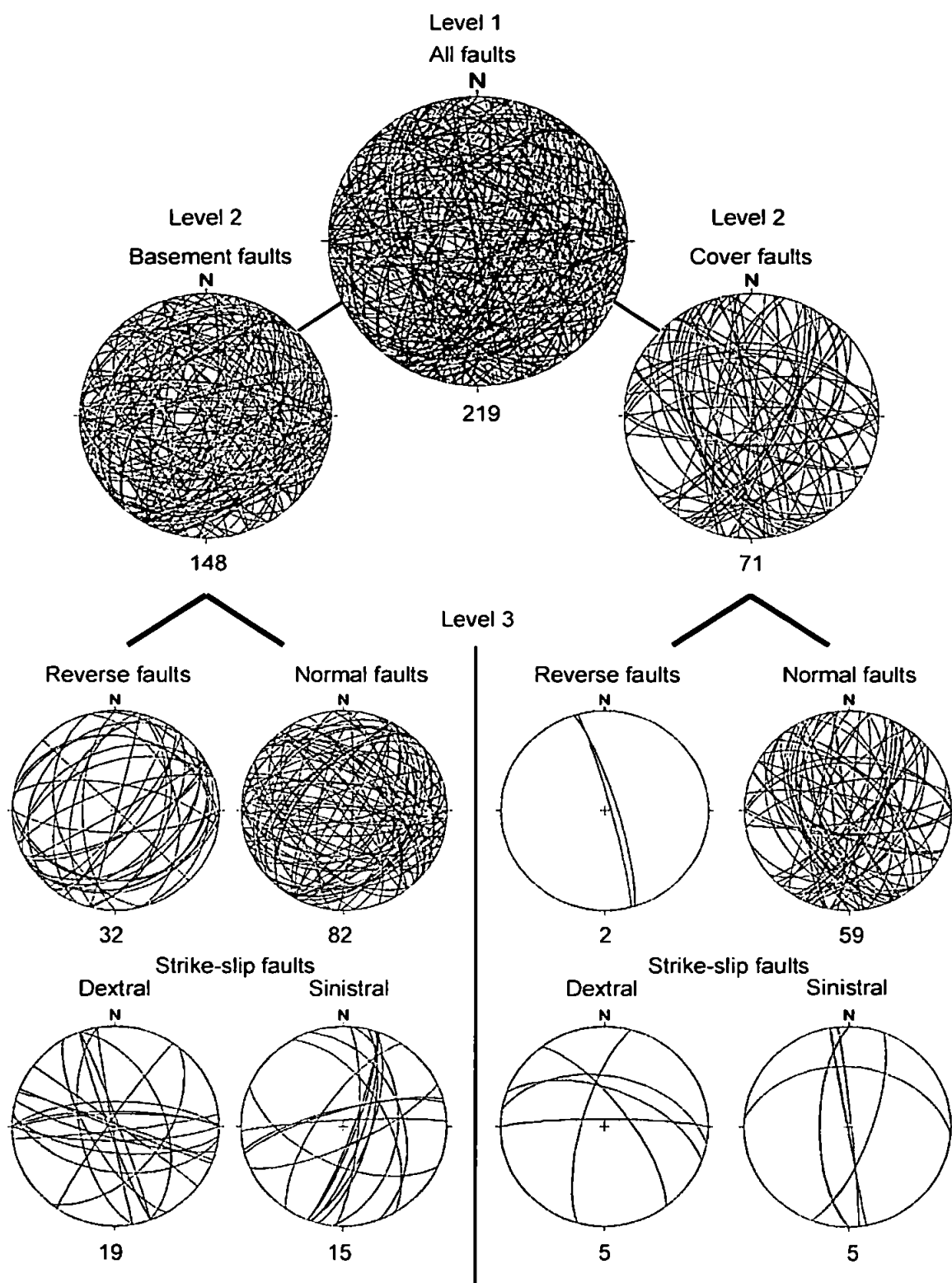


Figure 8.13: Stereonetic projections illustrating the necessity of categorising data prior to a palaeostress analysis. The stereonet on the top level shows all faults used in the palaeostress analysis prior to any breakdown of the data. Separating them into ophiolitic basement and cover categories indicates that further division is necessary. For palaeostress analysis, the faults are analysed separately in relation to their movement direction. The lower eight stereonets illustrate the dominance of normal faults throughout the ophiolite and cover sequences, but particularly for the sedimentary cover. If all faults where the sense of movement is constrained are considered, the percentages of these included in the palaeostress analysis of the basement is: 80% of normal faults; 96% of strike-slip faults and 80% of reverse faults, and for the cover these statistics are: 84% of normal faults; 66% reverse faults and 100% of strike-slip faults. These percentages are similar for all fault types (with the higher inclusion of basement strike-slip faults and higher exclusion of cover reverse faults likely due to low numbers of faults in these categories) which is another indication that the palaeostress subset of faults is representative of all faults.

Figure 8.13 and the low confidences apparent from Table 8.1 indicate that even following the two initial separations of the data, further breakdown is necessary to prevent clouding of the dataset by successive faulting events resulting in large errors and a geologically irrelevant palaeostress result. Although, in all but the simplest scenario, each stress system is expected to produce faults in more than one orientation, a preferred strike is expected to dominate and the development of conjugate fault sets can be invaluable for identifying palaeostress events.

Therefore, it seems valid as an early categorisation of faults into subsets to break them down into faults of similar strikes. This analysis of dominant strikes, especially if conjugate sets can be identified, is a good first step towards finding the stresses that have resulted in the measured faults and is particularly valid for the cover where the breakdown into fault types immediately allows trends in strike to become apparent. A feature of a significant number of basement faults is the fact that none of the three principle palaeostress axes is vertical, whereas a common assumption in palaeostress analysis is that one stress axis will be vertical. Analysis of these faults is discussed in section 8.5.8.

8.5.2 Palaeostress maps

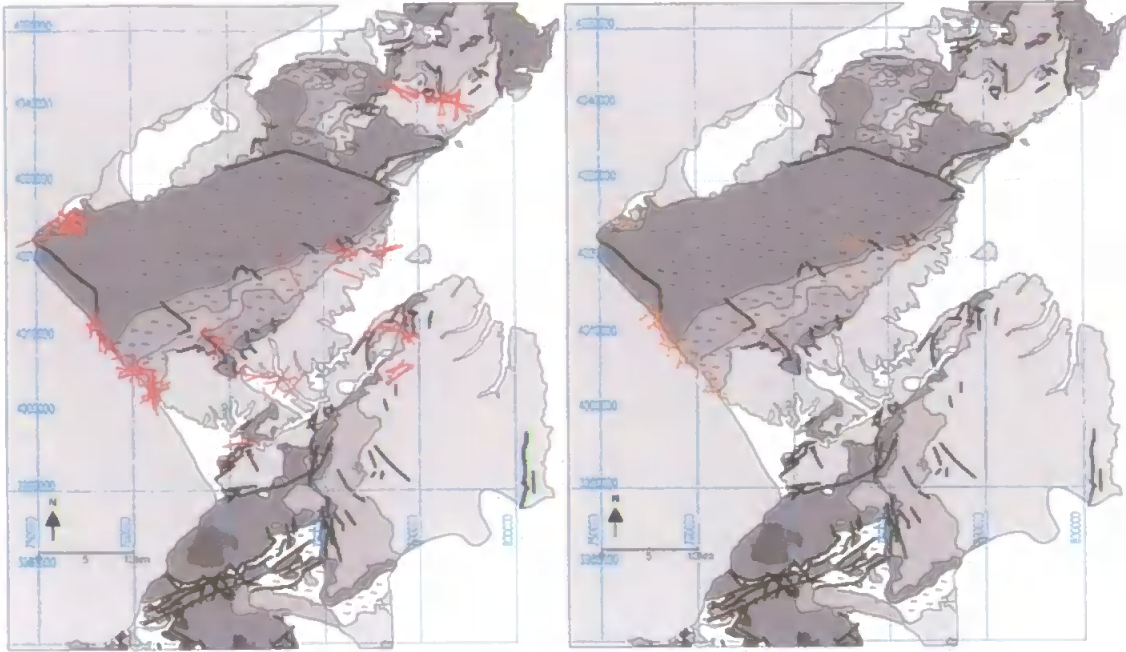
The palaeostress results subsequent to the separation of faults into normal, reverse and strike-slip faults can be illustrated on a geological map of Hatay to provide a clear picture of both the spatial distribution of these faults and the variability of palaeostress orientations and plunges. The principal horizontal palaeostress for each individual fault analysed is plotted on the map (Figure 8.14) with each fault type shown on a separate map for clarity. The palaeostress maps enable all faults used in the analysis to be observed.

Palaeostress axes for the normal faults display a wide range in orientation as would be expected from their greater number. However, NW-SE and NE-SW striking orientations of σ_3 axes are both evident as significant trends in both the ophiolitic basement and cover framework, although there is some variation in exact direction. A N-S orientation of σ_3 axes is also apparent, picked out most clearly along the coast within all lithologies from the SDC in the south to the ultramafics further north. This northerly trend is mirrored by a number of faults within the Belen area within the cover framework. In the Gulderen valley area within the ophiolitic basement, the faults measured are spatially close to the sedimentary cover, located on the southern edge of the ophiolitic massif. In this area, the palaeostress orientations on the map closely resemble the trends observed in the cover and major gullies cutting the valley also have similar trends.

The reverse faults display a wide distribution around a mean southerly direction: from the map it can be seen that almost all of the reverse faults swing between SE to SW directions. In a few localities, reverse faults with near-orthogonal palaeostress axes occur spatially adjacent to each other (e.g. along the coast). This is generally a strong indication of two separate compressional events, although exceptions to this arise from such events as emplacement of ophiolitic nappe sheets over a continental platform where considerable variability in thrusting direction might be expected, along with complicated inclined axes of rotation (Macdonald 1980; Allerton 1998).

(i) normal faults (sigma 3 axis)

(ii) reverse faults (sigma 1 axis)



Normal	00-09
Reverse	10-19
Dextral	20-29
Sinistral	30-39
	40-49

(iii) strike-slip faults (sigma 3 axis)

(iv) Strike-slip faults (sigma 1 axis)

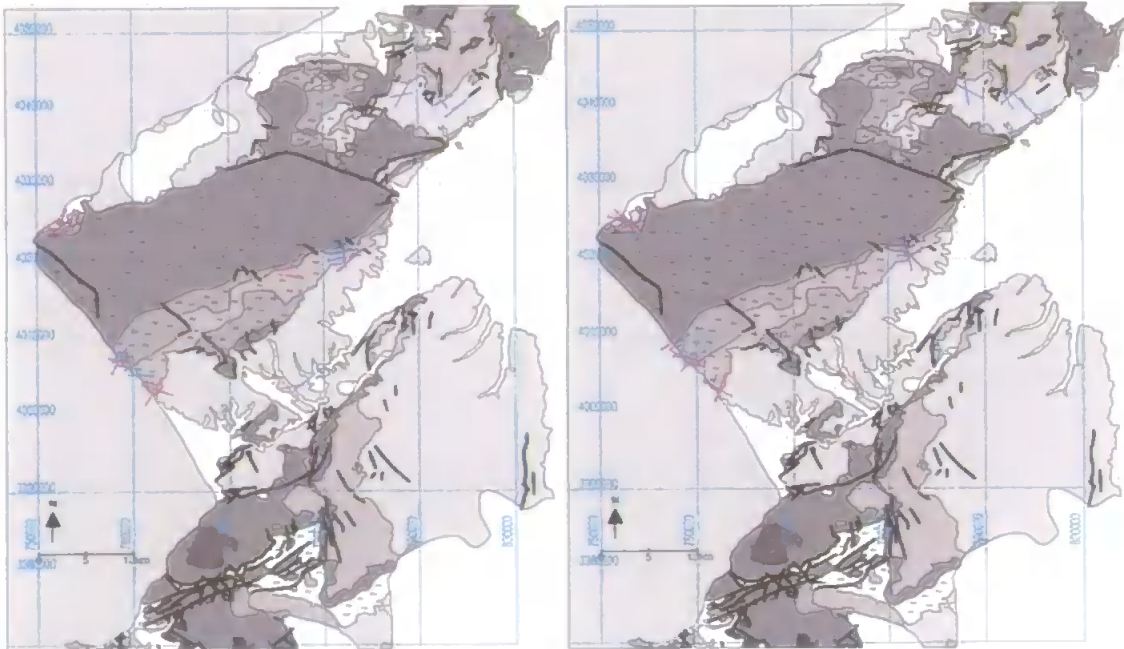


Figure 8.14: The orientation of the horizontal palaeostress axis identified from the palaeostress analysis for each individual fault analysed. Maps (i) to (ii) show normal and reverse faults respectively, with maps (iii) to (iv) showing sigma 3 and sigma 1 axes respectively for easy comparison with both normal and reverse faults. The key to the maps and the localities and place labels have been omitted for clarity; these were displayed on Figure 2.12.

Strike-slip faults are not numerous and, although these may represent separate events, they may have formed under the same extensional and compressive events that produced the normal and reverse faults. Strike-slip faults within the cover generally appear to have σ_3 axes oriented either roughly NE-SW or NW-SE (or σ_1 oriented NW-SE or NE-SW). These orientations of σ_3 axes resemble the trends observed for σ_3 axes of the normal faults within the sedimentary cover and similar orientations are also observed for the strike-slip faults within the basement. The similarity between many of the σ_3 axes of the normal and strike-slip faults suggests that these faults may result from the same stress systems. However, comparison of σ_1 axes of strike-slip faults with those of reverse faults also indicates that certain strike-slip faults may have formed under the same events. Strike-slip faults within the basement have less consistent trends than faults within the cover with σ_3 axes also oriented E-W and N-S (or σ_1 oriented N-S and E-W). Either of these has the potential to be a distinct event, that might be determined by subsequent detailed palaeostress analysis of the faults.

8.5.3 Separation into categories: cover framework

From the general trends observed in strike from all faults measured within the sedimentary cover (section 8.3.4), four different directions appeared dominant, with clusters of strikes oriented roughly N-S, NE-SW, NW-SE and E-W. In places in the cover, the NE-SW and NW-SE trends display a slight variation in strike to more NNE-SSW and NNW-SSE. Following separation into fault type, the initial separation of the 71 cover faults suitable for the palaeostress analysis was done using these categories in order to determine if there is a simple division of palaeostress according to faults with similar strikes acting under a single event.

It was found that division into NNE-SSW oriented faults and NNW-SSE oriented faults immediately results in the determined stress axes having a much higher confidence, with many of the roughly N-S faults also falling within these groups. However, the E-W striking faults have no coherent pattern in orientation of the stress axes and also display disparate directions of slip vectors.

8.5.4 Separation into categories: ophiolitic basement

From the general analysis of the structural patterns, significant groups of dominant strikes recognised within the basement were faults striking NE-SW, E-W and a slight peak of faults striking NW-SE. Due to the more protracted (and therefore more complicated) history of the basement units, with each successive event potentially causing older faults to be reactivated, rotations to occur and faults to interact, it would be expected for patterns to be less readily identified than in the cover rocks. From the large number and variation in strikes of basement faults (Figure 8.13), it is apparent that an important step in performing a robust analysis is to recognise faults forming under post-cover events within the basement and to backstrip these from the basement dataset.

Subsequent to separation into fault type, basement faults were further split using the dominant orientations recognised previously (section 8.3.4), as in the cover framework. However, in the case of the basement faults, as a result of the higher number of faults and more complicated history, the division into these categories did not yield confident palaeostress determinations. Faults in the cover almost invariably have one near-vertical palaeostress axis, but a significant number of those in the basement do not. Therefore, a further division was made into those faults with a near-vertical palaeostress axis and those without (with one palaeostress axis $> 60^\circ$ arbitrarily used as the deciding factor). This resulted in the identification of two clear events with high confidence levels for a NW-SE

trending group of faults and a NE-SW trending group of faults, interpreted to relate to the two well-constrained post-emplacment events recognised from analysis of the cover. Although there is a slight variation in orientation of the stress axes, the basic similarity between both fault strikes and axes of minimum principal stresses between these basement and cover groupings clearly suggests formation under the same events.

In order to analyse earlier events, these NW-SE striking and NE-SW striking normal faults were subtracted from the dataset before carrying out more detailed analysis of those remaining faults. The exclusion of faults where all three palaeostress axes are intermediate between horizontal and vertical may not be so valid for earlier events. However, the justification for leaving these faults out of the analysis (initially) is the theory that, at least for the youngest basement events (as for the cover events), the stress axes should not have been rotated significantly from vertical. Therefore major palaeostress events can still be recognised even if certain faults forming under them may have been excluded. Section 8.5.9 presents further discussion and analyses of these excluded faults and reinforces the validity of this assumption.

Following this categorisation using stress axes, and then repeating the breakdown of data using the main trends identified from earlier analysis, three main pre-emplacment groups are clearly identified: an E-W striking normal fault group, a conjugate strike-slip group and a group of reverse faults striking NE-SW. The peak in NE-SW striking faults identified from pre-palaeostress analysis of the basement thus comprises NE-SW striking faults from a post-emplacment NW-SE extension event augmented by faults from the NE-SW trending reverse fault group.

8.5.5 Identified structural events

As a result of the palaeostress analysis, it was possible to identify five clear structural events to have affected the Hatay ophiolite, with two of these post-dating the emplacement of the cover (Figure 8.15). These five groups within the ophiolitic basement with the orientation of their principal stress axes and confidences from earliest to latest are shown in Table 8.2. Figures 8.16 and 8.17 display photos of faults from pre-cover and post-cover events respectively, illustrating characteristic examples of faults from each of identified event.

There is a slight change in orientation of the faults and palaeostress axes observed between the two post-emplacement structural events observed in the cover compared with the same events within the ophiolitic basement, particularly for Event 5, which may be due to either a slight spatial variation in palaeostress between the sampling localities within the basement and cover or to differences in the inherited structure of the basement and cover resulting in the same stress being taken up slightly differently, or potentially merely an artificial difference due to the particular faults sampled. This last possibility is lent support by a group of NE-SW trending faults observed within the cover rocks with orientations displaying more similarity with those observed in the basement. These may be added to the clearly defined cover event resulting in greater similarity in the orientations of the principal stress axes accompanied by a slight decrease in confidence level. If faults from both basement and cover for the two events recognised in both units are analysed in conjunction confidence in the determination remains high.

<i>Unit</i>	<i>Identified Event</i>	<i>Evt</i>	σ_1 (R%)	σ_2 (R%)	σ_3 (R%)	<i>Con. Angle</i>	<i>Stress Ratio</i>	<i>No. Faults</i>
Basement	N-S Extension	1	82/13 4 (87)	07/272 (88)	03/002 (85)	57	0.33	11
Basement	NW-SE Contraction	2	00/33 3 (96)	02/242 (93)	052/88 (92)	58	0.08	6
Basement	N-S Compression	3	06/00 2 (81)	86/159 (87)	04/272 (80)	55	0.02	11
Basement	NW-SE Extension	4	86/06 9 (87)	03/217 (88)	04/307 (89)	75	0.60	14
Basement	NE-SW Extension	5	83/32 1 (92)	06/133 (87)	01/042 (87)	65	0.03	12
Cover	NW-SE Extension	4	81/00 5 (91)	08/205 (91)	02/115 (90)	53	0.80	18
Cover	NE-SW Extension	5	85/29 6 (83)	03/162 (87)	04/071 (87)	62	0.66	19
Cover ^A	NE-SW Extension	5a	89/34 9 (81)	01/330 (70)	04/060 (80)	/ ^D	/	26
Comb ^B	NW-SE Extension	4b	84/02 0 (89)	06/210 (88)	00/300 (88)	/	/	32
Comb ^C	NE-SW Extension	5b	84/30 7 (86)	04/151 (79)	03/060 (84)	/	/	31

Table 8.2: Orientations of palaeostress axes and other parameters for the five identified groups.

^A. The identified group within the cover incorporating a group of additional faults in a slightly different orientation.

^B. The faults from both cover and basement for Event 4 combined.

^C. The faults from both cover and basement for Event 5 combined.

^D. The conjugate angles and stress ratios have not been calculated for groups where these values are not used in further analysis.

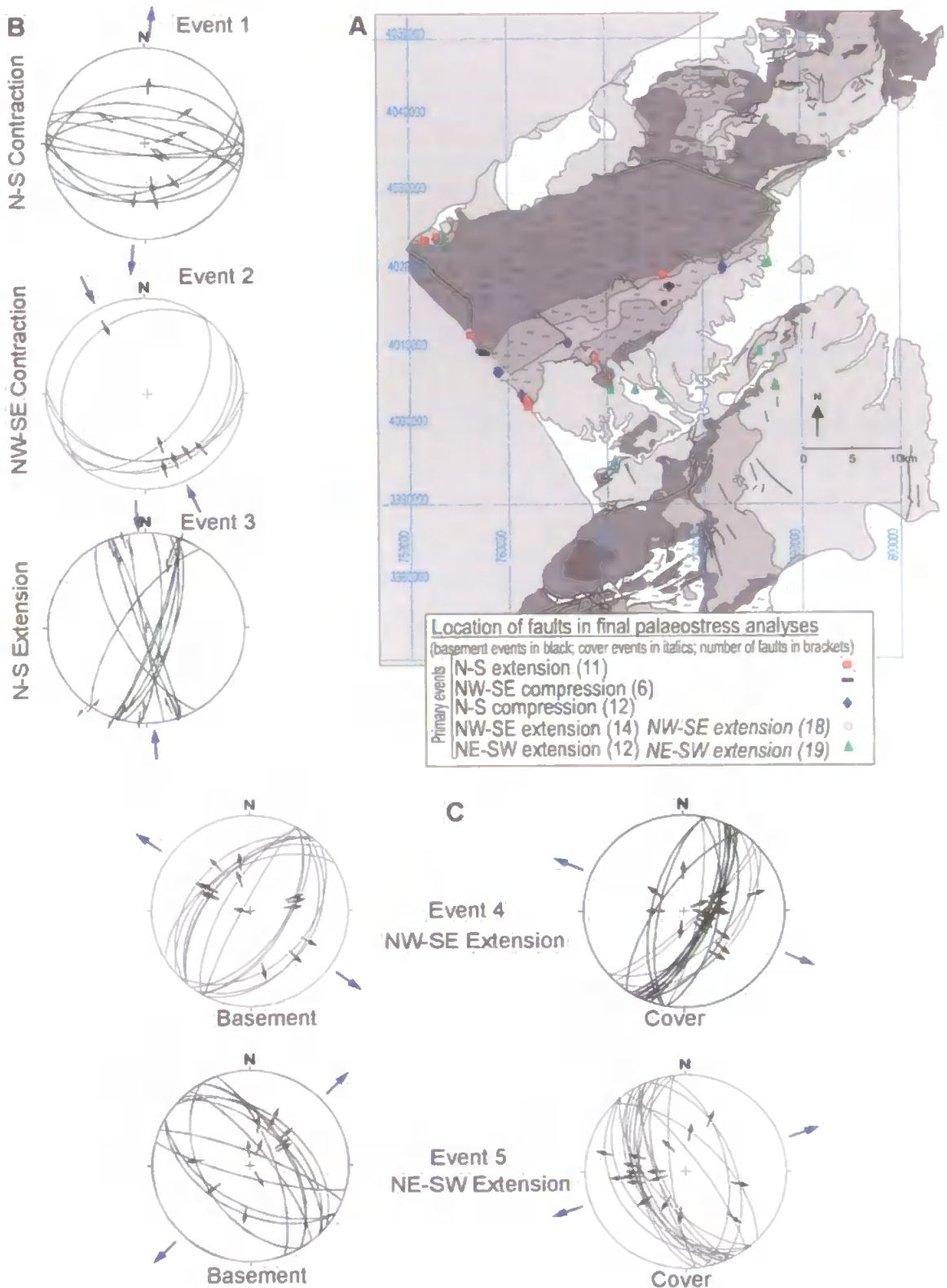


Figure 8.15: The five final events identified within the ophiolitic basement and cover framework of the Hatay ophiolite.

A. The geology map shows the location of the faults included in the final groups identified by the palaeostress analysis (same symbol shape = same fault orientation; same colour = same event). Key and locations on map are as on Figure 2.12/8.1.

B-C. The stereonets illustrate the five events identified from the palaeostress analysis, three only affecting the ophiolitic basement (upper LHS) and two younger post-emplacement events observed within both the ophiolitic basement (lower LHS) and cover framework (lower RHS).

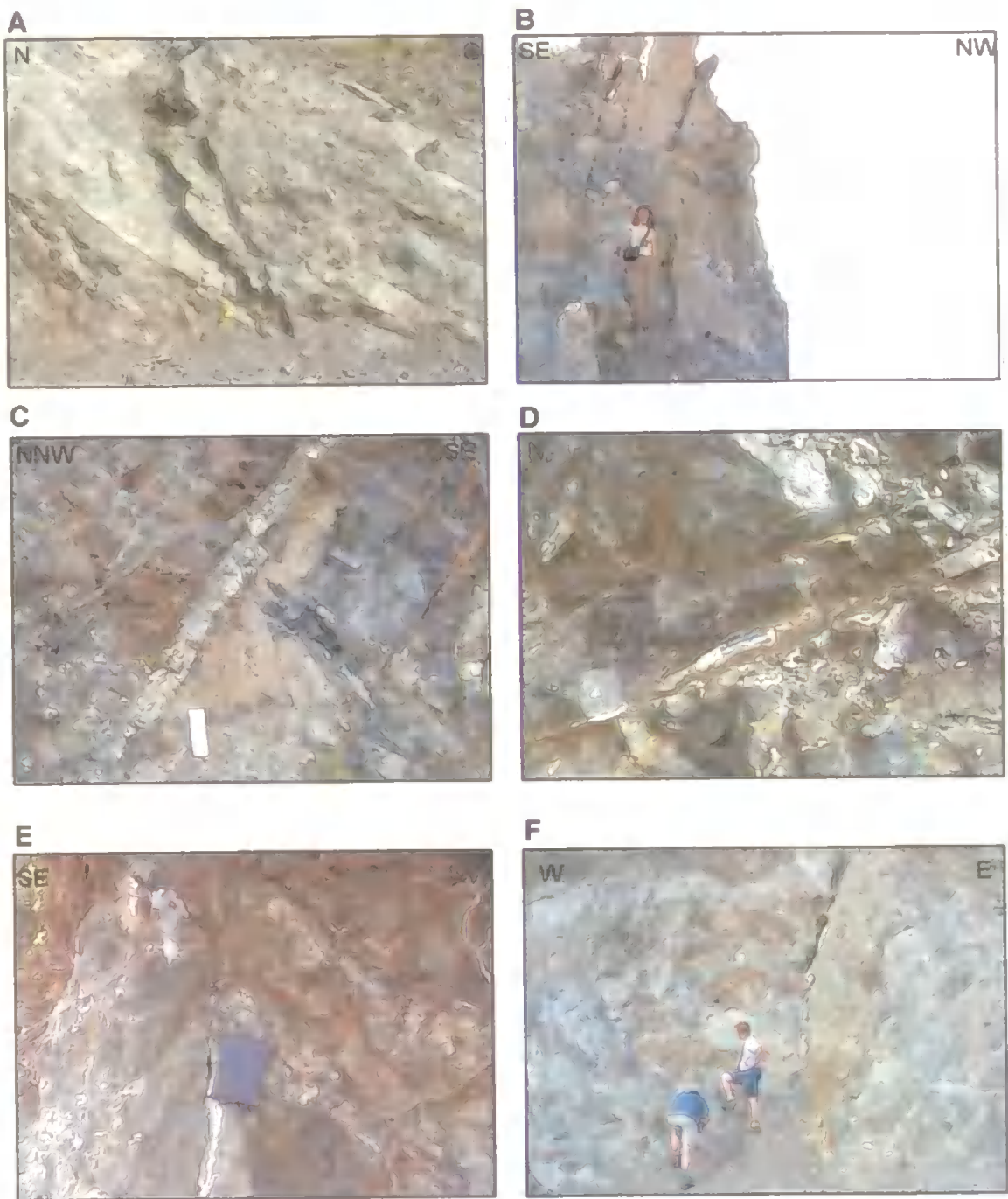


Figure 8.16: Examples of faults from each pre-cover structural event identified within the ophiolitic basement.

A. Event 1: N-S extension, coast (photo 1001_003642), GPS [0761786 ; 4003659]. An E-W striking fault parallel to the SDC is observed cutting through an exposure of moderately dipping dykes, marked in this instance by a clear planar fault trace.

B. Event 1: N-S extension, coast (photo 1012_223010). E-W striking faults are particularly dominant in the SDC.

C. Event 2: NW-SE compression, coast (photo 1003_014530) GPS [0757702 ; 4009120]. SE dipping reverse fault of event 2 within gabbros oriented 150/44 displaces a NW dipping dyke oriented 346/52 with a reverse sense of displacement.

D. Event 2: NW-SE compression, Komurcukuru (photo 1018_203948). NW dipping fault with indication of reverse movement, possibly acting as a riedel shear. Not included in palaeostress analysis due to lack of constraints on slickenside orientation.

E. Event 3: N-S compression, near Gulderen (photo 1017_212618). Sinistral strike-slip fault striking NNE-SSW and included in final analysis.

F. Event 3: N-S compression, Karacay Valley E side (photo 0916_020210). Steep NNW-SSE trending strike-slip faults (no movement direction obtained).

Neotectonic faults: ophiolitic basement

Neotectonic faults: cover framework

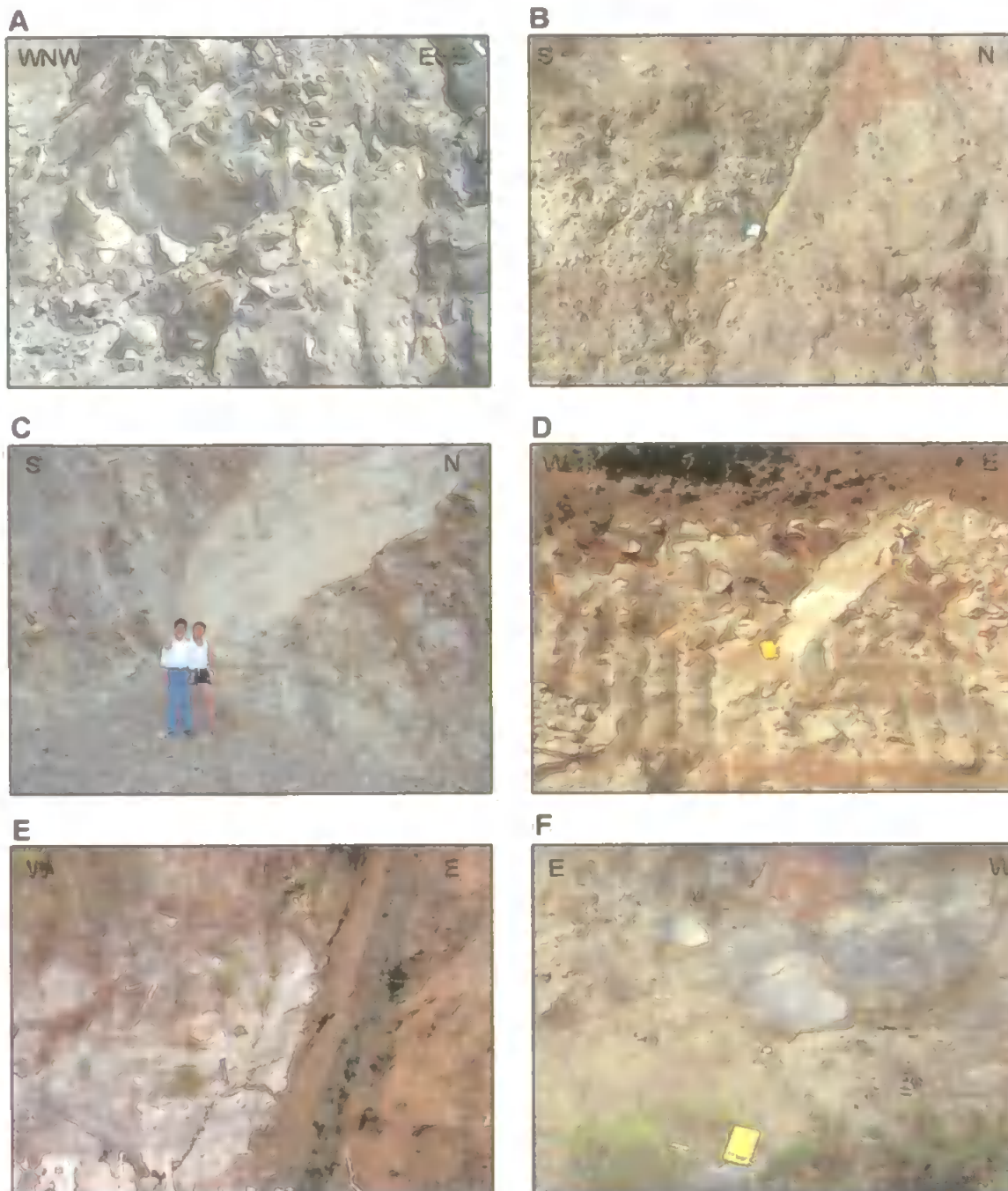


Figure 8.17: Photos of faults of the Neotectonic events identified within the ophiolitic basement and cover framework.

A. Event 4: Neotectonic NW-SE extension, coast (photo 0930_230340). NW dipping fault cuts SDC.

B. Event 4: Neotectonic NW-SE extension, Altinozu (photo 0923_194707). SE dipping fault in muddy sediments.

C. Event 4: Neotectonic NW-SE extension; near Gulderen (photo 1018_013350). SE dipping fault cuts SDC.

D. Event 5: Neotectonic NE-SW extension, Ucedik (photo 0928_021820). SW dipping normal fault in sandy clays and marls.

E. Event 5: Neotectonic NE-SW extension, near Gulderen (photo 1018_023815). Incorporates reactivated E-W striking faults as strike-slip faults, here characterised by breccia development. NE-SW faults dominant within river valley, itself potentially caused by a Neotectonic fault.

F. Event 5: Neotectonic NE-SW extension, Karacay River (photo 0927_221922). SW dipping small normal fault in sandstones in same orientation as larger similarly dipping faults within the mainly shallowly-dipping sediments located at the southern end of the Karacay river valley.

8.5.6 Description of identified structural events: cover framework

Both structural events recognised within the cover are characterised by normal faults, often in conjugate arrangement. Events 4 and 5 are characterised by NNE-SSW and NNW-SSE striking faults respectively, with well-constrained stress directions with σ_3 axes oriented respectively ESE and ENE. These represent two discrete structural events affecting the cover rocks, which appear to be temporally rather than spatially discrete, although it is not possible to determine the relative age of these two events unequivocally from the structural analyses because cross-cutting relationships between two clearly consistent planes from each event were not found (Figure 8.18). Generally the NNW-SSE striking faults appear to be younger. This is suggested from several localities where both orientations of faults can be observed in the near-vicinity of each other but the NNW-SSE striking faults are more consistent in orientation than the NNE-SSW striking faults.

There are a few localities, notably along the Antakya-Altinözü road where the NNW-SSE striking faults are observed to cross-cut faults in other orientations whereas the NNE-SSW faults do not appear to cross-cut other faults. Analysis of the spatial distribution of faults identified in the two well-constrained structural groups of cover faults can aid determination of whether the identified events are spatially discrete. Faults from both groups are observed over the entire area studied which indicates that the two fault groups are not spatially discrete and so, by implication, must be temporally discrete. This conclusion is supported by palaeostress analysis of the cover faults separated into localities as resultant palaeostress axes lack any coherency and have extremely low confidences.

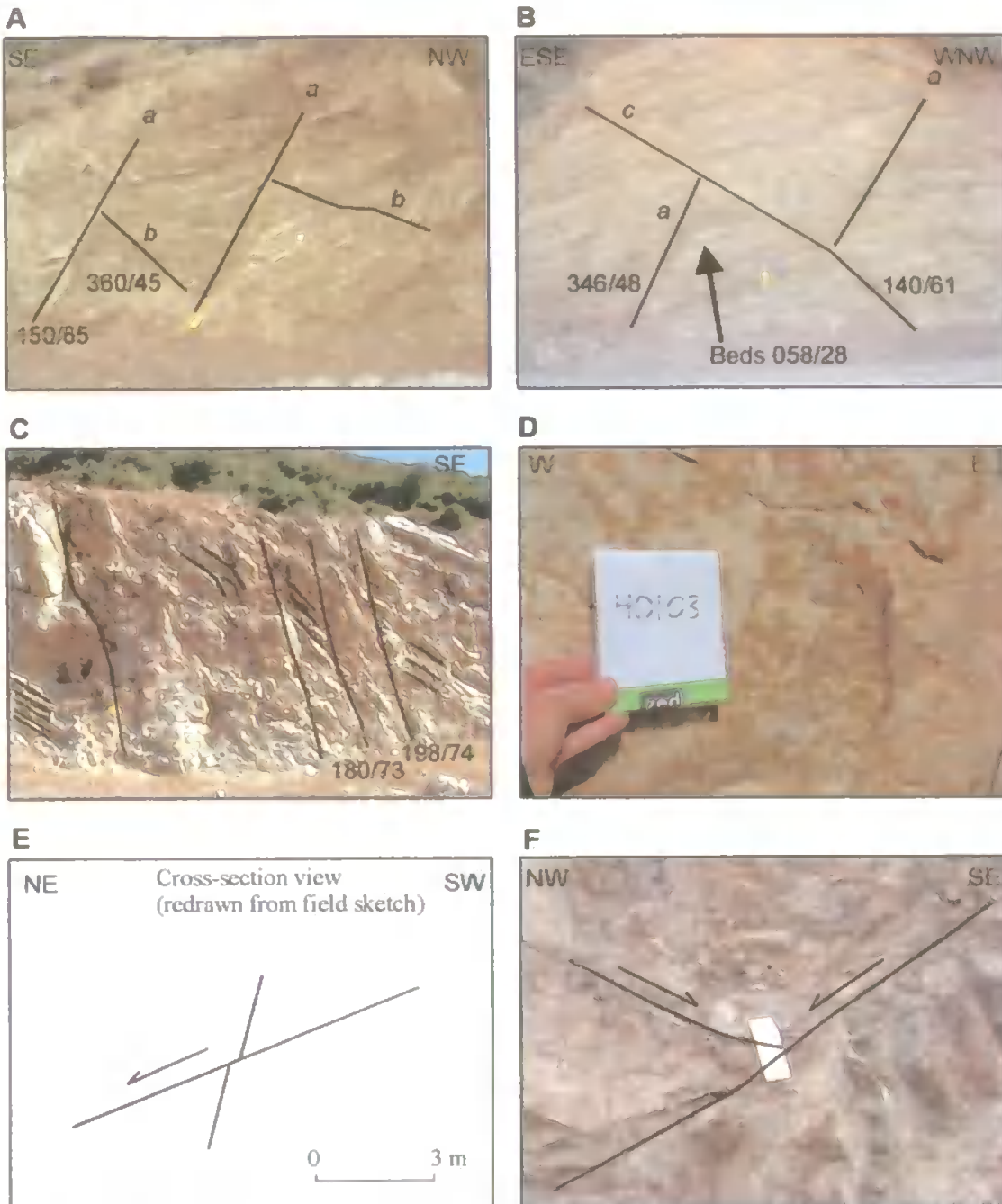


Figure 8.18: Faults of Neotectonic post-emplacement events and cross-cutting relationships within the cover framework (top four photos) and ophiolitic basement (bottom two photos). A-B. Locality H04 (photos 0925_010035 and 0925_021403). A. Dominant fault set *a* cross-cutting set *b*; B. Fault set *a* cross-cut by set *c*. Faults are in muddy sandstones, siltstones and mudstones with fault planes often calcified and standing out in relief from the softer sediments. Bedding planes in this locality are NE dipping with NE-SW striking fault planes predominant. C. Belen (photo 0928_203821). A significant number of faults along the road SE of Belen trend ~E-W with steep dips and curvature of beds into the fault plane. These comprise part of Event 5, which is not characterised by NW-SE striking fault planes here. A number of NNE-SSW striking faults comprise part of Event 4. D. Altinozu (photo 0923_204234). Most lineations on cover faults are steeply plunging, as illustrated above. Occasional faults display evidence of two lineations, particularly on E-W striking faults, which may be reactivated by both NW-SE and NE-SW extension events. E. Coast, GPS [0757776 ; 4008890]. A clear fault dipping NE oriented 030/60, continuous through the cliff (>5m) clearly cross-cuts a fault plane oriented 156/72 with a normal sense of displacement. Neither of these faults could be included in the palaeostress analysis due to incomplete fault slip data but a SE dipping fault ~4 ms N comprises part of Event 4. F. Coast (photo 1008_011124). Clear instances of cross-cutting faults of events 4 and 5 were not observed within the ophiolitic basement. Cross-cutting relationships between faults with opposing dips of either Event 4 or Event 5 were mutually cross-cutting, as shown in the above photo where a NW dipping fault of Event 4 cuts off a SE dipping fault of the same event.

(i) NW-SE/NNW-SSE extension (Event 4)

This event is characterised by NNE-SSW trending normal faults, often in a conjugate relationship. The NNE-SSW category of faults dominate in locality H04 [0248232; 4041979], located on the turn-off to Kömürçukuru to the south of Belen (Figure 8.18A-B). In this locality, three sets of normal faults were identified with the NNE-SSW striking faults comprising the dominant set generally cross-cutting other sets that are characterised by smaller faults with less consistent strikes. Palaeostress analysis in this locality indicates that the smaller faults could be acting under the same palaeostress system as the NNE-SSW striking faults and the orientation of the principal palaeostress axes from this locality are only a few degrees different from the results incorporating all NNE-SSW striking cover faults. The bedding in this locality consistently dips towards the NE (Figure 8.18B), which is not easily accounted for by the NNE-SSW striking faults, indicating that the faults in this orientation are not singly responsible for rotating the sediments and suggesting the influence of another orientation of faults on the prevailing dip in this area.

(ii) NE-SW/NNE-SSW extension (Event 5)

This event is characterised by NNW-SSE trending faults, often in a conjugate relationship. The faults measured along the Antakya-Altınözü road are characterised by beds steepening towards the fault planes indicating the direction of movement of the fault with several good examples of conjugate relationships. Two faults from the NNW-SSE striking event that illustrate this are found within two metres of each other along the Antakya-Altınözü road [0247441; 4005677]. These strike within a few degrees of each other with identical dips and a 60° angle between the planes.

(iii) E-W trending faults

The E-W striking faults are unlikely to comprise formation of a fault group resulting from a discrete palaeostress event due to the considerably lower confidences in the principal palaeostress axis determinations (< 80%). Analysis of these E-W striking structures, taking confidence limits into consideration, shows that certain of these faults could have been activated under either of the two identified stress systems. Subsequent analysis of the ophiolitic basement suggests that these faults may be inherited basement structures propagating into the cover framework (section 8.6.2). However, it is also possible that this group of faults formed under an older event and were later rotated or reactivated by the two better-defined cover events, accounting for the dispersion in the slickenlines measured.

8.5.7 Description of identified structural events: ophiolitic basement

The relative timing of the basement events can be constrained from observation of cross-cutting relationships (Figure 8.19). Faults from these events appear to be temporally discrete rather than representing spatially discrete coeval events.

(i) N-S extension (Event 1)

The oldest structural event identified is a N-S extensional event (Event 1), characterised by numerous E-W striking normal faults, in cases showing the development of mixed populations of slickenside lineations. This event is interpreted as the oldest event due to the observation of faults in several other orientations cutting through the E-W striking faults, for example a location within the Karaçay valley (Figure 8.19A). The existence of two slickenside lineations observed in several instances on these fault planes also suggests that these faults are older and have been subsequently reactivated by younger events.

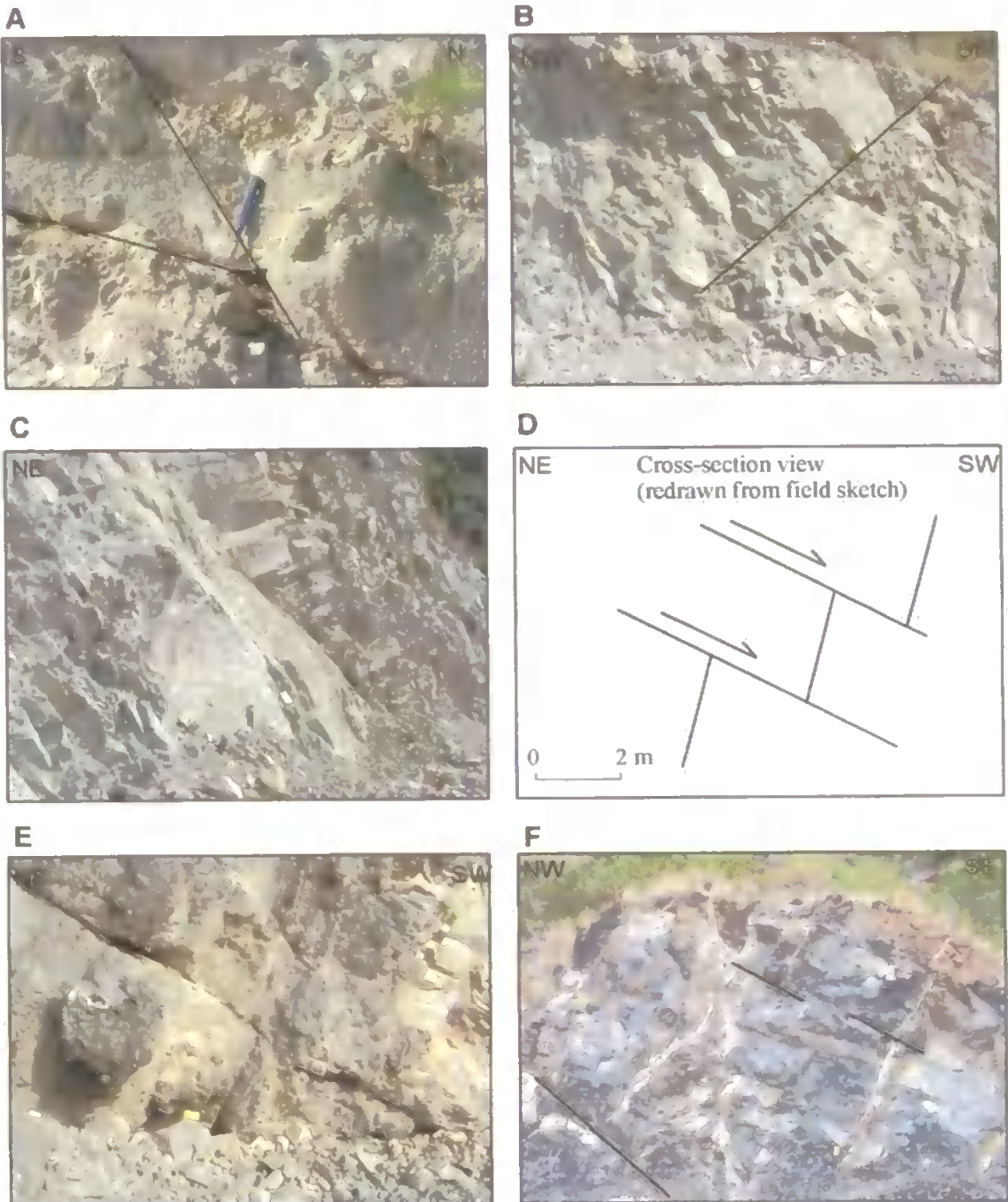


Figure 8.19: Cross-cutting relationships and faults of pre-cover events within the basement.

A. Karacay Valley (photo 1013_231006). A steep fault in layered gabbros oriented NW-SE of Event 3 cuts E-W striking faults.

B. Coast (photo 0930_230340). Shallow faults oriented NE-SW, either of Event 2 or Event 4 dipping NW cut earlier E-W striking faults.

C. Karacay Valley (photo 0930_231514). Faults in later events utilise dyke margins. In this photo, the upper part of the fault lies along the plane between two dykes and in the lower part cuts through the dykes. The dyke margins in this locality dip southwards, oriented 170/67.

D. Coast GPS [0761863 ; 4003554]. Moderately dipping normal faults oriented NW-SE are observed to consistently cross-cut steeper E-W striking faults with a normal sense of displacement.

E. Coast (photo 1001_024255) GPS [0760211 ; 4005840]. Moderately-dipping fault planes oriented NE-SW (here within the SDC) sometimes show signs of reverse movement, as in the above case where dyke margins are displaced up and NE. Some of these shallow shears appear to have been later reactivated as normal faults and several display development of multiple populations of slickenlines.

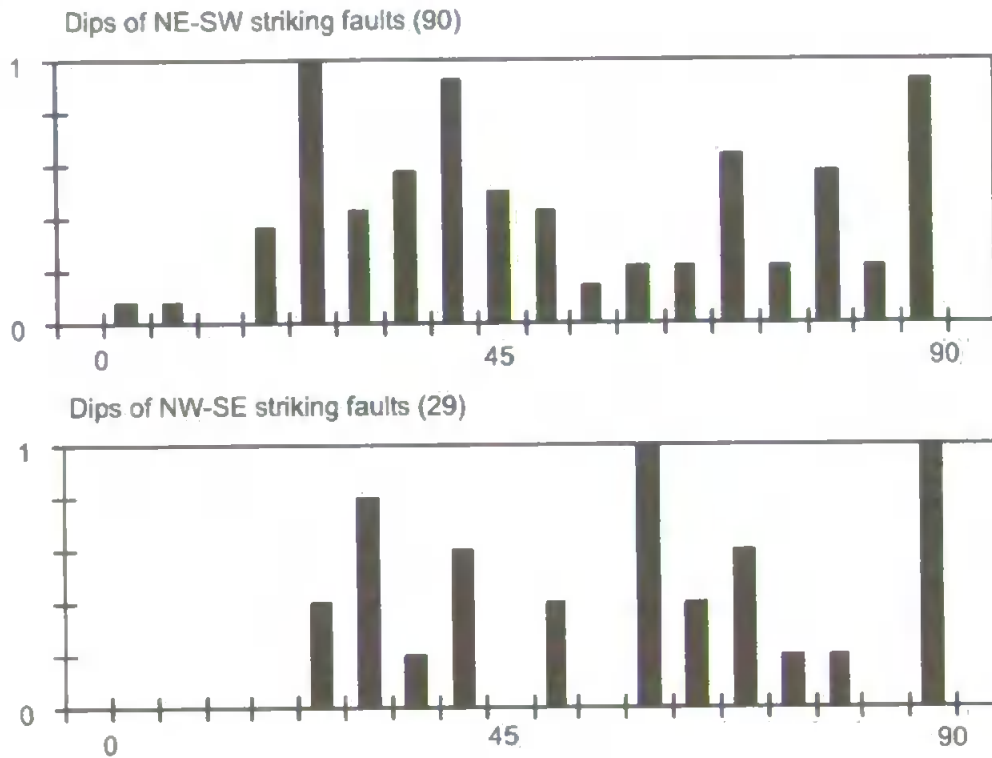
F. Coast (photo 1003_013355) GPS [0757702 ; 4009120]. A clear shear zone (lower left) within gabbros characterised by development of dark serpentinitised fabric within zone, oriented 140/38. Interpreted as an earlier reverse fault of Event 2 reactivated as strike-slip fault under Event 3. Faults in the same orientation show apparent reverse movement. Shear zone cuts E-W striking fault (357/85), interpreted as a fault from event 1 subsequently reactivated under Event 4.

Although the confidences on this event meet the required cut-off limit, they are lower than the confidences for the post-emplacement events identified, which would be explained by these faults being earlier and subsequently experiencing some rotation under later events, dispersing the lineation directions. The E-W striking faults are parallel with the average present-day E-W strike of the SDC.

(ii) NW-SE contraction (Event 2)

A NW-SE contraction is characterised by NE-SW striking thrust faults. Faults oriented NE-SW consistently cut the E-W striking faults along the coastal road. Within the gabbros these faults are characterised by serpentinite minerals forming the slickensides and the shear zone is often marked by a narrow shear zone accompanied by fabric development rather than a planar surface. Some of these faults are observed to have two senses of movement- normal and reverse. For example, along the coast a shear zone within the gabbros at GPS [0758985; 4007065] with development of serpentinite fabric within the zone shows evidence of both reverse and normal movement. Many of these faults are shallower than would be expected for normal faults, although many are clearly normal in their latest movement. This can be explained by the theory that these were originally shallow NE-SW striking thrust faults later reactivated as NE-SW striking normal faults under Neotectonic NW-SE extension (Figure 8.20A). Faults in this orientation are observed within the Kömürçukuru area, some of which are reverse, but lack of lineation data does not allow their inclusion in the palaeostress analysis.

A



B



Figure 8.20: Nature of fault dip amounts along the coast and of the ophiolite-sedimentary cover boundary.

A. Histograms showing dip amounts of the NE-SW striking and NW-SE striking fault groups along the coast. The larger number of shallower NE-SW, which occur both as reverse faults and as normal faults, suggests the influence of the earlier NE-SW reverse faults during the younger Neotectonic extensional event, being reactivated as NE-SW trending normal faults.

B. Utilisation of the ophiolite-sedimentary cover boundary during the faulting of Event 5. South of Antakya-Samandag road showing limestone above contact and later utilisation as a fault surface during NE-SW extension.

(iii) N-S contraction (Event 3)

A N-S contraction is characterised by conjugate strike-slip faulting, with dextral NNW-SSE striking strike-slip faults and sinistral NNE-SSW striking strike-slip faults resulting from N-S compression. Some NW-SE thrust faults appear to have been reactivated by this later event. Large strike-slip faults in these orientations are observed to cut E-W striking faults in several localities. For example, along the coast at GPS [0757347; 4009664] a steep SE-dipping fault oriented 156/86 with very clear strike-slip lineations in the centre of the fault plane, is observed to cross-cut shallower faults dipping to the SE with indication of reverse movement (interpreted as Event 2 faults). This steep fault is continuous throughout the cliff (> 8m) and normal slickensides are observed to overprint the strike-slip slickensides suggesting subsequent reactivation under a Neotectonic event (see below). Another example is within the SDC at Isikli GPS [0752817; 4024390] where a steep dextral strike-slip fault oriented 022/79 cuts an E-W trending fault oriented 180/84.

(iv) Post-cover events (Events 4 and 5)

The youngest events within the ophiolitic basement correspond to the two post-cover Neotectonic extensional events initially identified from analysis restricted to the cover framework. These NE-SW and NW-SE striking faults are observed to cross-cut faults in all other orientations, particularly apparent along the coastal road. Some of the faults interpreted to be activated under these events are observed to have an older lineation on the fault plane that is overprinted by the lineation resulting from the younger Neotectonic event. For example, in Isikli location H26 GPS [0753; 4024642] a NE dipping fault oriented 052/75 has normal lineations with a rake of 82°NW on the fault plane that overprint lineations with a rake of 18°NE. Faults of Event 5 are often characterised by the

development of breccia along the zones, in particular along the stream sections measured in Isikli and near Gulderen.

8.5.8 Stress ratios and conjugate angles

The stress ratio is defined by Angelier (1994) as $\Phi = (\sigma_2 - \sigma_3) / (\sigma_1 - \sigma_3)$, and this definition is also used by the TectonicsFP program. If the vertical axis is roughly equivalent to the intermediate axis, it allows easy flipping between the two stress axes (and so flipping between for example a strike-slip and extensional regime) whereas if the two horizontal principal stress axes are roughly equivalent the faults resulting from that system will display little preferred orientation. Stress ratios for older events are less likely to be geologically relevant due to the effect of subsequent tectonic events on the original strikes of the older faults. Stress ratios in areas where the structural history is especially complex should not be over interpreted due to the influence and interaction of pre-existing structures reactivated during younger faulting regimes.

The stress ratios for each structural event identified can be seen in Table 8.2. For both post-emplacement events observed in the cover, the stress ratio is anticipated to be most accurate due to the comparatively simpler structural history. The ratio for both of these events is between 0.5 and 1.0 which is tending towards the end-case of uniaxial confined extension where $\Phi = 1.0$ and there is a strong preferred extension direction (Angelier 1994). The stress ratio for the NW-SE compression event characterised by reverse faults and the N-S compression event characterised by strike-slip faults tend towards zero i.e. uniaxial confined compression (Angelier 1994), indicating both a strong preferred direction of contraction and also easy flipping between σ_2 and σ_3 axes with the associated change between a reverse faulting regime and a strike-slip faulting regime. The stress ratio for one of the post-emplacement events within the ophiolitic basement is considerably

lower than that for the corresponding event within the cover framework, which may indicate the unreliability of determining stress ratios within regions known to be affected by numerous earlier events.

The conjugate angle between the sets of faults dipping in opposing directions for each structural event gives an indication of the nature of the material that contains the faulting. The conjugate angle for all events except the post-cover NW-SE extension (Event 4) is within 5° of 60° (Table 8.2). Event 4 has a larger conjugate angle in the basement which may be explained by reutilisation by this event of the shallow NE-SW striking fault planes of the earlier NW-SE compression event.

In both Neotectonic events within the cover, there is some apparent bias towards faults dipping towards one orientation. In the NW-SE extension event most fault planes dip SE and in the NE-SW event more fault planes dip SW, indicating a general displacement down towards the south. The NW-SE contraction event in the basement shows significant bias in fault dip directions. However, these apparent biases may result from the relatively small sizes of the datasets, which is supported by a more even bimodal distribution of fault plane dips when a greater number of NE-SW trending reverse faults are considered, incorporating those with non-vertical palaeostresses.

8.5.9 Analysis of faults with non-vertical palaeostress axes

The Hatay ophiolite has experienced at least five structural events in its tectonic evolution and each successive event has the potential to rotate earlier structures, affecting the orientation of their principal stress axes. This is clearly illustrated by the fact that almost all of the cover faults had one palaeostress axis near-vertical, whereas palaeostress axes for the older faults in the basement units were considerably more variable. Although in the

analysis of the basement it was assumed that these rotations would be sufficiently minor for the exclusion of these faults not to result in the identification of misrepresentative trends (but rather identification of trends to be made more efficiently), these faults are part of the dataset and their orientations must also be discussed to be confident of the trends recognised.

Analysis of these faults can be aided by constructing a contoured plot of all palaeostress axes to identify areas of high density. Only one high density area (oriented around 70° to the NE) is picked out by this analysis and faults comprising this fail to produce a coherent palaeostress orientation implying that they were not acting together. Visual analysis of these faults with non-vertical palaeostresses by presenting the orientation and plunge of the principal palaeostress for each fault on a map (Figure 8.14) has the advantage of also allowing observation of their spatial location. The implication is that if the orientations of these excluded faults are consistent with those of the major, clearly identified, structural events then they are not likely to result from separate events and the differences in their plunges may be explained by the complicating effects of reactivation or fault interaction (resulting in non-theoretical orientations of palaeostress axes). Alternatively, if faults where no palaeostress axis is near-vertical form clusters of faults with similar plunges, the implication is that these faults are acting together within localised areas. The non-verticality of the palaeostress axes in this case would be caused by a coherent rotation under an event (or events) younger than that in which the faults formed. It is apparent from the palaeostress maps (Figure 8.14) that faults with no near-vertical principal palaeostress axes are found in the same areas as those included in the primary analysis and do not form clusters with similar palaeostress orientations and plunge; conversely these faults are evenly distributed over the region. The dominant trends of faults with no near-vertical palaeostress axis appear identical to the trends of faults with a near-vertical palaeostress axis and the implication is that faults forming during a single event are

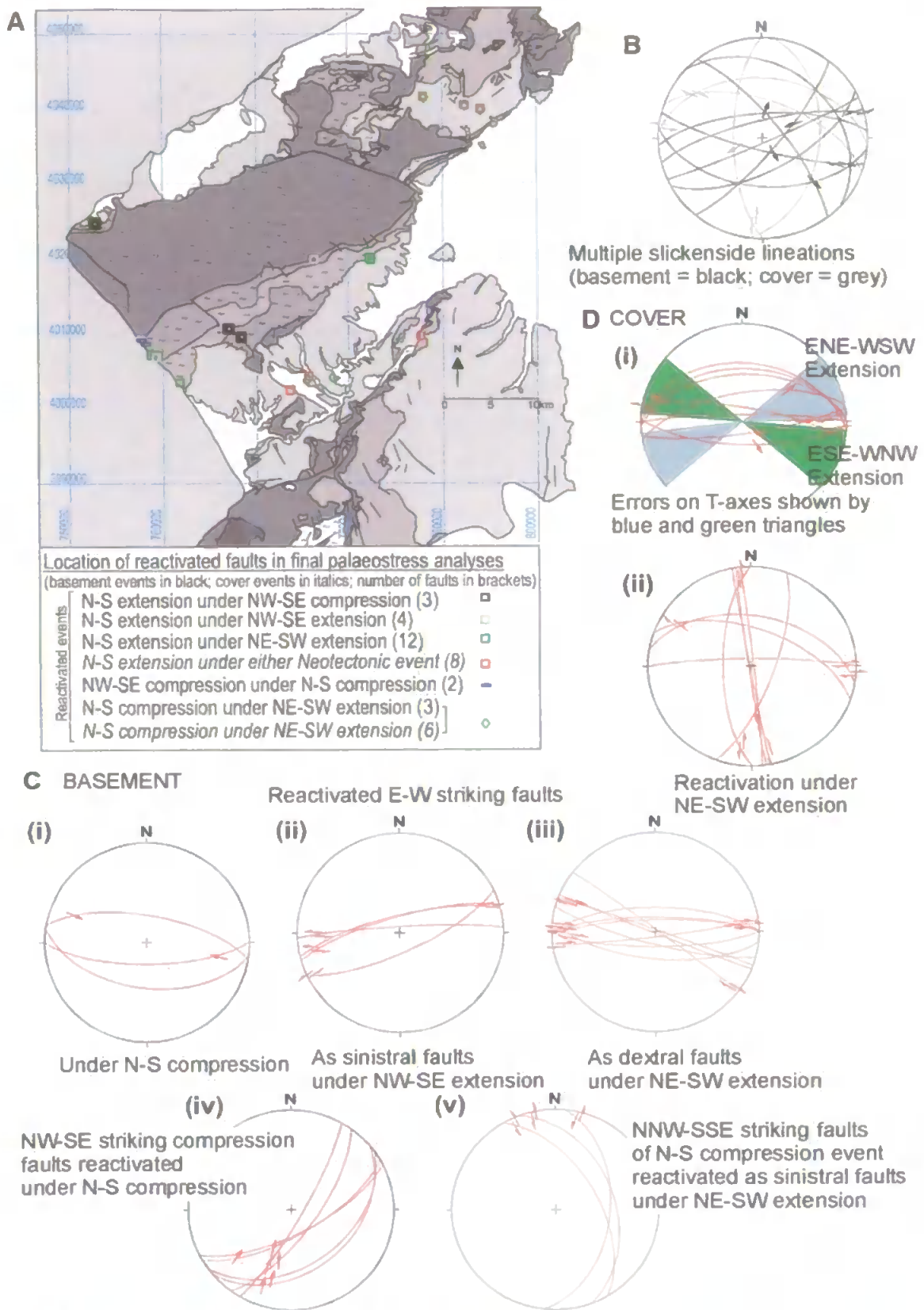
displaying a spread of plunges rather than forming under discrete events. It is possible that these individual faults have experienced rotation, but the mechanism which allows some faults within an area to rotate whilst others do not is unresolved. The proportionally large numbers of reverse faults that have no near-vertical palaeostress axis may be explained by formation during emplacement of the ophiolite, with significant variation in thrust directions and complex rotations expected (Macdonald 1980; Allerton 1998).

8.6 Reactivation

In an area such as Hatay that has experienced a protracted tectonic history, faults from older stress systems will be reactivated under subsequent systems (Figure 8.21A). Evidence for two or more slip lineations on a fault surface is a clear indication of reactivation and a number of faults measured in both the ophiolite and the cover display evidence of two lineations (Figure 8.21B). Over et al. (2002) note the general existence of more than one slickenside set on fault planes within the study area, although this is not supported by this thesis where only one slickenside set was observed on the majority of fault planes. Rojay et al. (2001) note a lack of overprinting of fault striations on faults between Antakya and Kirikhan (to the north of the study area). Coskun and Coskun (2000) suggest that the splaying of the DSF in the Miocene caused widespread reactivation of older structures.

8.6.1 Reactivation in the ophiolitic basement

In each successive structural event identified within the ophiolitic basement, earlier structures are observed to be reactivated, with E-W trending faults appearing to be most prone to reactivation (Figure 8.21C(i)-(iii)).



Location of reactivated faults in final palaeostress analyses
(basement events in black; cover events in italics; number of faults in brackets)

Reactivated events	N-S extension under NW-SE compression (3)	□
	N-S extension under NW-SE extension (4)	□
	N-S extension under NE-SW extension (12)	□
	N-S extension under either Neotectonic event (8)	□
	NW-SE compression under N-S compression (2)	-
	N-S compression under NE-SW extension (3)	-
	N-S compression under NE-SW extension (6)	○

Figure 8.21: Reactivation in the Hatay ophiolite.

A. Geology map showing the location of the faults reactivated by the final groups identified by the palaeostress analysis (same shape = same fault orientation; same colour = same event). Key and places as on Figure 2.12/8.1.

B. The orientation of faults with two lineations in both basement (black) and cover (grey). Basement faults with two lineations are dominated by E-W striking faults.

C. Reactivated basement faults: (i)-(iii) show reactivation of E-W striking faults with the only event which does not reactivate these faults the N-S compression event; and (iv)-(v) illustrate reactivation of faults in other orientations.

D. Inherited faults in the cover. (i) showing E-W striking faults potentially reactivated under either extension event; (ii) illustrating faults potentially reactivated under NW-SE extension.

E-W trending faults are most commonly reactivated as either dextral or sinistral strike-slip faults in the younger post-emplacment extensional regimes but are not as prone to reactivation under either Event 2 or Event 3 where they would be expected to be reactivated as thrust faults. This is a likely consequence of their originally steep orientations. However, the possibility that more E-W striking faults were reactivated under these events (although not observed for this study) should not be excluded as the general scarcity of thrust faults included in palaeostress analysis should be taken into consideration. An example of the susceptibility of E-W trending faults to reactivation was observed in Altinözü where one fault had a NE-plunging lineation interpreted to have formed under Event 4 as well as a sinistral strike-slip lineation that could have formed under Event 5.

The event that incorporates more reactivated faults than any other event is the youngest NE-SW extension event (Figure C(iii), C(v), D(ii)). This reactivates, in particular, a significant number of E-W striking faults, especially in the ophiolitic basement. The contact between the ophiolite and the overlying sedimentary cover in places appears to have been utilised by this tectonic event as a fault plane (Figure 8.20B). There is no evidence for reactivation of Event 4 faults during this event. Since the faults of the postulated earlier event strike almost parallel to the extension direction of the later event, this would not be expected.

Unless there are a greater number of structural events than have been identified, many of the faults that do not fall simply into one of the constrained palaeostress directions should be explained by potential reactivation of earlier structures. This would produce faults in later regimes with different orientations to the predicted theoretical orientation (where the assumption is made that no interaction occurs with pre-existing structures). Many of these faults can be accounted for by reactivation under one of the later systems.

8.6.2 Propagation of reactivated basement structures into the cover

Earlier basement structures can be reactivated and propagated into the cover framework during a younger event, producing faults that are in different orientations to those predicted. In the cover, roughly half of the faults that display two lineations (Figure 8.21B) are E-W striking and half are N-S/NNE-SSW striking. E-W trending faults are not identified as forming under a separate event in the cover and may display two lineations due to propagation of basement structures into the cover with potential activation under both cover events. The N-S striking faults potentially formed under either cover event. If formed under Event 4 they could potentially have been reactivated by Event 5. Analogue models have demonstrated the possibility of propagation of inherited basement structures into overlying units during subsequent deformation: modelling of fault reactivation by Dubois et al. (2002) submitted brittle and viscous layers to extension, followed by oblique or parallel extension or contraction, both with and without a 'sedimentary cover'. These authors find that where the secondary deformation is oblique, all newly formed faults are parallel to the older grabens and oblique to the directions of the principal stress, rather than in the preferred direction for the new regime. In cases without sedimentation, all older faults were reactivated, whereas in cases with sedimentation (analogous to the Hatay area), only certain faults from the older regime were reactivated (Dubois 2002).

In Hatay, the significant number of E-W striking faults observed in the cover framework that display a lack of consistency in slickenside lineations are interpreted to be inherited basement structures. Certain NNW-SSE trending faults may also be the result of propagation into the cover framework of the faults of this orientation that formed in the strike-slip event identified within the basement.

8.7 Structural synthesis

From the general structural framework recognised in the Hatay region in conjunction with the events identified from the palaeostress analysis, it is possible to produce a synthesis of the structural history of the region. Five structural events affecting the Hatay area have been constrained (Figure 8.15). The two youngest events are well-constrained, especially within the cover, but are also identified in the ophiolitic basement. The three earliest events are confined to the basement units without affecting the cover, and so occurred prior to deposition of the cover framework. These events are listed below and can be linked into the regional structural history of the Hatay ophiolite.

(i) Event 1: N-S extension characterised by E-W striking normal faults

The parallelism of the early (present-day) E-W striking faults with the (present-day) E-W striking SDC, along with the cross-cutting relationships and multiple slickenside lineation development observed, indicates that these faults comprise the earliest structural event within the ophiolite. This suggests that this N-S extension event is linked with the development of the SDC early in the seafloor history of ophiolite formation.

(ii) Event 2: NW-SE contraction characterised by NE-SW striking thrust faults

The NE-SW compression event is interpreted to be the structural event to follow the N-S extension event and the SE oriented lineations (Figure 8.8) and the NE-SW striking brittle faults associated with these lineations may be linked with this event. The similarity between structures observed within the basal shear zone where they are likely to be linked to emplacement of the ophiolite and the reverse faults observed elsewhere within the ophiolite suggest that these may also be linked to emplacement of the ophiolite onto the

Arabian platform. If this is the case, the spread observed of thrust faults with σ_1 axes and lineation orientations distributed from the SW to SE can be easily explained by variations in the direction of thrusting during emplacement over the Arabian platform.

(iii) Event 3: N-S contraction characterised by conjugate strike-slip faults

The NNW-SSE and NNE-SSW trending strike-slip faults appear to be the youngest pre-cover event and could be linked to the final stages of the emplacement of the ophiolite or to the continued N-S movement of the African and Eurasian plates. If the near-zero stress ratios for the NW-SE compression event and the N-S compression event can be assumed to be real values and unaffected by the complexity of fault interaction within the basement, the compressional regime characterised by thrust faulting could have easily switched to a compressional regime characterised by strike-slip faulting in the later stages, with the concomitant change in orientation due to variation in the exact emplacement direction of the ophiolite onto the continental platform.

(iv)- (v) Events 4 and 5: NW-SE and NE-SW extensions characterised by NNE-SSW and NNW-SSE striking normal faults respectively

The post-emplacement Neotectonic extension events are likely to be linked to the development of the present-day plate configuration. Most previous workers agree that the Neotectonic history of the Hatay region has been characterised by extension, although within the general framework of the N-S compressional movements of the African and Eurasian plates. A NE-SW extension direction was found to dominate the recent history of the Hatay region by Over et al (2002, 2004a); the direction which was inferred by the work of this thesis to be youngest.

8.8 Discussion

8.8.1 Faults not accounted for by the palaeostress analysis

It was not possible to assign all faults in the palaeostress subset to one of the main structural events or account for them by reactivation. This outcome is not unexpected for faults from a region with such a protracted and complex structural history. In the ophiolitic basement, half of the faults can be assigned to one of the identified structural events. Most of the faults not accounted for are those where no palaeostress axis is near-vertical, the analysis of which has previously been both described and justified (section 8.5.9). Within the cover, few faults are not accounted for by one of the identified extensional events or by reactivation or by the propagation of pre-existing basement structures. Two thirds of cover faults are interpreted as forming under one of the two extensions recognised. Almost all cover faults have a near-vertical palaeostress axis and including faults without in the palaeostress analysis does not greatly affect the confidence limits. As an illustration, if the few faults with non-vertical palaeostress axes were to be excluded from the youngest cover event, the confidence levels would improve by less than three percent and palaeostress orientations would change by only a few degrees. Occasionally, the inclusion of a certain fault would dramatically reduce confidence limits for an identified event, even though it appears to match the criteria used to recognise faults from that event. This refers to a very small number of steep, near vertical faults within the cover that would be expected to be strike-slip faults but instead have anomalous steeply plunging lineations. Although a couple of these faults strike in the same orientation as the identified post-emplacment events they have instead been added to the small quantity of faults not accounted for.

8.8.2 Relative timing of the identified events

The five events identified from the palaeostress analysis have been timed relative to each other based on cross-cutting relationships, supported by comparison with other structural features of the ophiolite (e.g. the basal thrust sheet). The two cover events are least well constrained in timing, and due to the lack of unequivocal cross-cutting relationships the possibility that these are coeval cannot be ruled out. However, they are not spatially discrete and so if they are coeval, formation under a non-plane strain event is likely, such as a three-dimensional strain event or a transtensive system. It is possible for four sets of conjugate faults to develop under a single stress regime (Reches 1978, 1983) in which case the two events identified may be coeval. If developing under a transtensive system, it is difficult to explain how both ENE and ESE oriented minimum principal stress axes operate under the same regional stress system. The assumption that the two post-cover events are temporally discrete relies on the assumption that the palaeostress analysis is valid. From the results of this study there is nothing to contradict the conclusion that these events are temporally discrete plane strain events.

The present-day E-W striking faults have been interpreted to be the earliest structures in the ophiolite and that this is true for a large number can be stated with a high degree of confidence. The consistency of the N-S orientation of σ_3 axes, mainly observed along the coast (as apparent from the palaeostress map of Figure 8.14) is interesting as these axes would be expected to have experienced a degree of differential rotation. One interpretation is that there is a later N-S extensional event that was not picked up by the palaeostress analysis. However, the orientation of the SDC is equally consistent and so these faults may not have been significantly rotated under later events. E-W striking faults to the south of the coastal SDC cross-cut the dykes in places suggesting that they are younger, although the dykes here have more variable strikes.

8.9 Comparison with previous tectonic interpretations and regional structural history

8.9.1 Critical appraisal of previous tectonic interpretations for the Hatay ophiolite

The main pre-existing interpretation of the Hatay ophiolite that must be critically appraised in light of the structural data obtained for this thesis is the Dilek and Thy (1998) model suggesting that formation of almost all major structural features within the Hatay ophiolite occurred whilst on the seafloor.

The mean dyke strike of the coastal SDC trends consistently E-W which differs from the average NE-SW trend stated by Dilek and Thy (1998). A major hypothesis of these authors is that the SDC represents an extensional NE-SW oriented graben of seafloor origin, with dykes to the west (south of the coastal SDC) dipping NW and dykes to the east dipping SE (at İkizköprü). Thus, a NE-SW strike of dykes would lie parallel to the graben whereas the actual E-W strike observed is oblique. However, the major discrepancies between the results of this thesis and the hypotheses of Dilek and Thy (1998) concern the interpretations of the structures observed. For instance, two fault trends are described within the coastal SDC by Dilek and Thy (1998): a NE-SW trend and a second almost perpendicular set striking roughly NW-SE. Both of these trends are picked up by this study. Also, the orientation of σ_3 of 325° (Dilek and Thy 1998) and 307° (this thesis) calculated from the NE-SW trending faults is similar. However, Dilek and Thy (1998) suggest that these faults formed due to extensional tectonics on the seafloor, whereas the observation that not only do these faults match the orientations of the Neotectonic events observed in the cover framework, but also cross-cut faults in all other orientations indicates that these are the youngest basement faults and post-cover rather than seafloor in origin. The Neotectonic faulting events were spatially ubiquitous and therefore for these events to

leave no expression in the underlying basement would be difficult to explain. Dilek and Thy (1998) suggest that the NE-SW dyke-parallel faults and the NW-SE trending tear faults are not observed in the deeper lithologies and that the tear faults are overlain by undeformed Maastrichtian sediments. However, as previously stated, both of these trends are observed in the cover framework and, even if certain faults in this orientation are earlier, the majority are clearly post-emplacment in age. The tear faults observed by Dilek and Thy (1998) are said to have oblique to strike-slip lineations and as such may represent the NNW-SSE trending strike-slip faults of Event 3 which are pre-cover. Dilek and Thy (1998) interpret the basal shear zone near Komürçukuru as a ductile zone of seafloor origin. However, this was observed to be dominated by brittle fabrics more likely to have formed during emplacement, supported by the location of this zone immediately above the Arabian platform limestones and by the consistency of kinematic indicators within this zone and the inferred SE direction of emplacement.

Generally, the prevalence of ductile, intrusive and cross-cutting magmatic relationships described by Dilek and Thy (1998) were not observed and there is a lack of convincing evidence for either a structural graben of seafloor origin or primary seafloor relationships preserved along contacts between units; most of these features are more convincingly interpreted as either emplacement or post-emplacment structures.

The data from this thesis tie in more closely with the tectonic interpretation by Tinkler et al. (1981) who recognise several episodes of post-emplacment normal faulting (section 2.8) and suggest that the boundaries between units are either controlled by emplacement (e.g. between the mantle rocks and gabbros) or post-emplacment (e.g. between the gabbros and SDC) structures. Tinkler et al. (1981) suggest that the post-emplacment history of the ophiolite was dominated by movement along the DSF. Although fewer events are recognised by this thesis, Tinkler et al. (1981) recognise that several of their

events are not constrained sufficiently in timing to determine whether all of these represent separate events. As such, the NE-SW trending normal faulting events recognised by these authors could easily be the same as the post-emplacement event identified by this study. Tinkler et al. (1981) base their observations on field and sedimentological evidence and do not carry out a palaeostress analysis.

8.9.2 Comparison with regional structural history

The dominant movement on the major faults within the wider region (i.e. EAF and DSF) is strike-slip. However, within the region constrained to the Hatay ophiolite and its sedimentary cover, normal faults dominate, with reverse and strike-slip faults forming only a small percentage of the total. A general change from transpression to transtension is recognised (e.g. Over et al. 2004a; section 2.2), both within Hatay and the wider region. The transtensional regime produces NE-SW extension with a strike-slip component that correlates to the direction obtained from this thesis for the fault set inferred to represent the youngest structural event. Over et al. (2002; 2004a) also recognise an E-W extension within the Hatay area which they interpret to be local. This direction is not supported by data from this study. However, a NW-SE extension direction does appear to be consistent across the Hatay region and has not been picked up by previous studies on the region.

E-W striking faults measured for this thesis were more dominant than ENE-WSW striking faults identified from lineament analysis (Over et al. 2004b) and appear to be both early (parallel with the SDC and linked to seafloor spreading tectonics) and reactivated under later events rather than comprising a separate group of faults acting in conjunction with the similarly oriented CAT, as suggested by Over et al. (2004b) (section 2.2).

8.10 Combining palaeomagnetic and structural results

The aim of combining the results of the structural analyses discussed above and the palaeomagnetic results from the Hatay and Baër-Bassit ophiolites and their sedimentary covers (Chapters Five to Seven; Figure 8.22) is to identify the timing and mechanisms of the rotations experienced in order to produce a tectonic synthesis of the evolution of the Hatay ophiolite.

8.10.1 Main results and timing of rotations

A main result of the palaeomagnetic work is that large rotations have occurred about vertical axes with dispersion in the data an indication that additional differential rotations have occurred about either vertical, horizontal or inclined axes. Part of the large rotation of the Hatay and Baër-Bassit ophiolites is likely to represent a pre-emplacement coherent vertical axis rotation linked to the rotation of the Troodos ophiolite. The minor rotations observed for the sedimentary sequences indicate that the post-cover structures cannot account for either the consistent westerly directed remanences nor for the dispersion observed in the magnetic declinations of the ophiolite. Differential vertical axis rotations are perhaps the most likely source of the dispersion and would have been most significant in the strike-slip faulting event (Event 3) which only affected the basement. Thrusting during emplacement (Event 2) may also have caused a degree of vertical axis rotation (Allerton 1998). It is also known from the analyses carried out on the SDC (section 5.11) that a simple rotation is not sufficient to explain the entire rotation history and that rotations about non-vertical axes (dyke-normal axes) must have occurred.

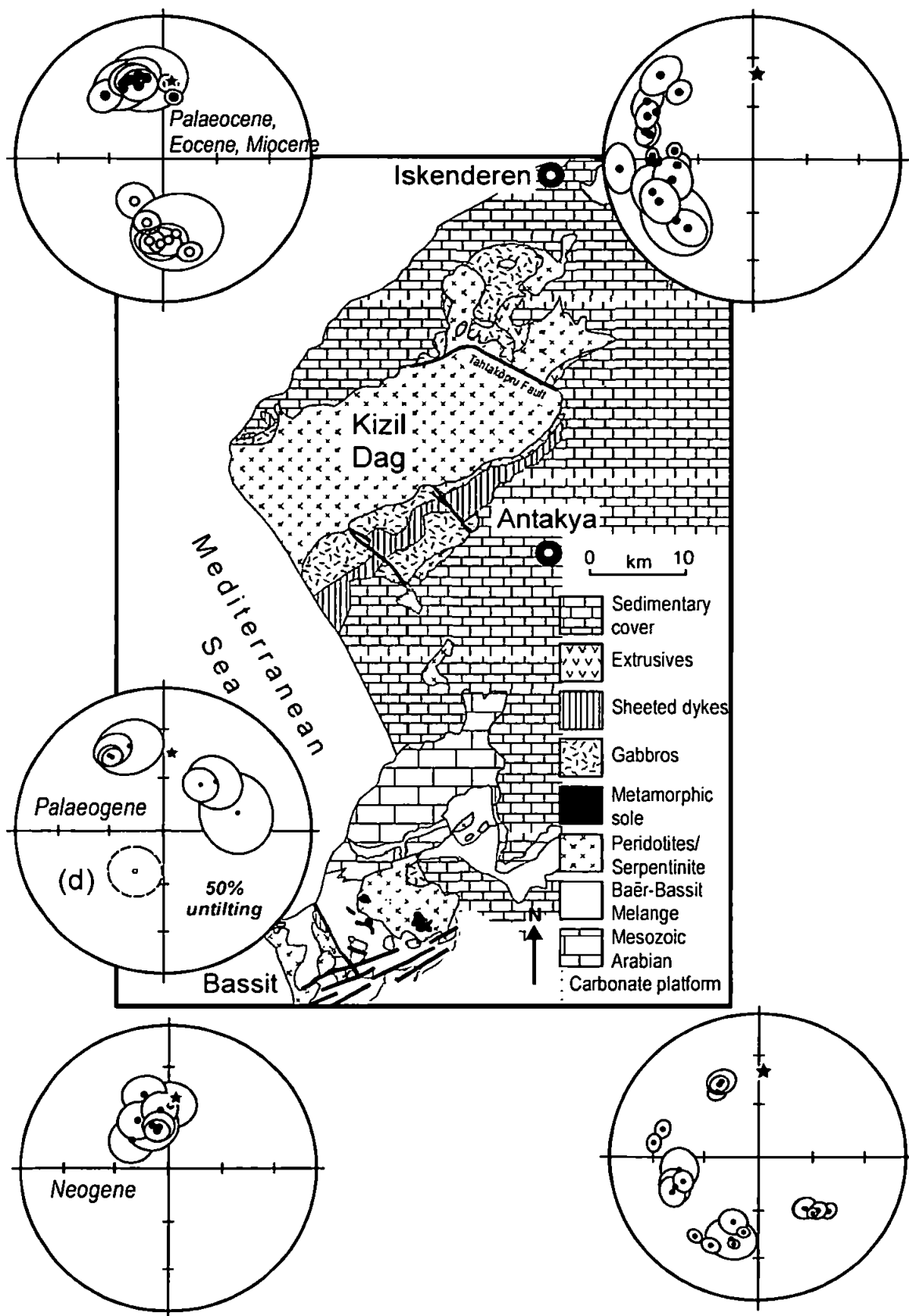


Figure 8.22: Lower hemisphere stereographic projections of tilt-corrected site-level palaeomagnetic data summarising palaeomagnetic data obtained from the Hatay and Baër-Bassit ophiolites and their sedimentary covers. Outline geological map of the Hatay and Baër-Bassit ophiolites, showing the distribution of lithologies and major structures is also shown. The data from the sedimentary covers is shown on the LHS and data from the underlying ophiolites on the RHS, with Hatay above the map and Baër-Bassit below. Data sources are the results of this thesis apart from the data from the Baër-Bassit ophiolite, obtained from Morris et al. (2003) and from the sedimentary cover of the Hatay ophiolite where data from this thesis has been supplemented by data from Kissel et al. (2003). Reverse polarity sites have been antipoded to allow easy comparisons.

The coastal section may provide an important key to understanding the tectonic evolution of the region due to the excellent, easily accessible and continuous exposure down through all levels of the ophiolite, with the palaeomagnetic and structural results for the coastal area summarised on Figure 8.23. The three coastal groups display a spread of magnetic declinations almost equivalent to those observed throughout the ophiolite, and therefore it can be inferred that the rotations of other areas of the ophiolite can be accounted for by similar rotation sequences. The steep structurally-corrected magnetic inclinations observed in the SDC are most easily accounted for by rotations about dyke-normal axes.

The near-vertical slightly NE dipping rotation poles identified from net tectonic rotation analysis (Figure 8.23B) may imply a dyke-normal component of rotation about a NE-SW trending axis (if rotation can be divided simply into a vertical axis and a horizontal axis component of rotation with the orientation of the horizontal axis given by the direction of deviation of the rotation pole from vertical). From the structural events identified, rotation about a NE-SW horizontal axis would be expected during emplacement (Event 2) or during the Neotectonic extension of Event 4. However, this axis is not normal to the present-day strike of the dykes, and is actually near-parallel to some of the dykes at the southern end of the coastal SDC (Figure 8.23D). The present-day E-W trending SDC restores to an original N-S average orientation (section 5.13.3). If the intraoceanic coherent axis rotation only partially accounts for the total magnitude of the vertical axis rotation, it is possible that during emplacement the dykes were oriented NW-SE and thus rotations about a dyke-normal axis may have occurred during emplacement. This would require a further small degree of anticlockwise (near-coherent) vertical axis rotation either during a later stage of emplacement or during the strike-slip faulting of Event 3 to produce the present-day average E-W orientation of the SDC.

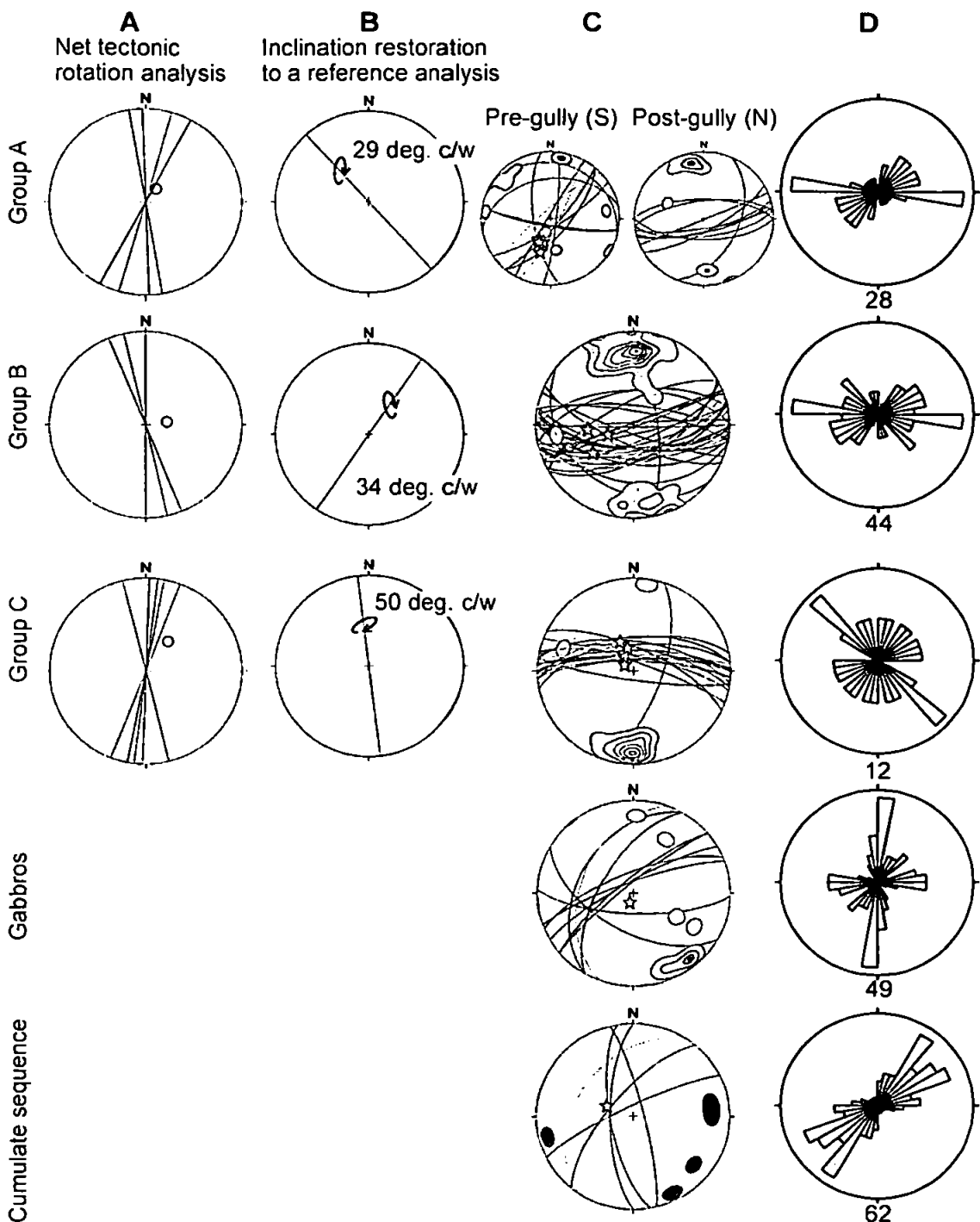


Figure 8.23: Synthesis of palaeomagnetic and structural data along the coast including rotations identified from analysis of the SDC (section 5.11). The coastal section is an area with extremely good and continuous exposure and provides an excellent locality in which to determine the relationship between the rotations identified from the palaeomagnetic analyses and the structures measured. The coastal SDC is divided into three main groups (as described in section 5.8); the gabbros and ultramafic cumulate sites are not grouped.

A. Original dyke strikes and rotation poles calculated from net tectonic rotation analysis for the three coastal groups within the SDC. Steep inclined rotation axes dipping NE are identified for all three groups, indicating a large coherent vertical axis rotation, with the slight deviation from a vertical rotation pole due to inclined/dyke-normal axis rotations.

B. The results of the 'Inclination restoration to a reference method' with clockwise rotation about either a roughly NE-SW axis (Group B) or a roughly NW-SE axis (Groups A and C).

C. All palaeohorizontal/vertical structural indicators with those measured during palaeomagnetic sampling shown in grey; these were the structures used to restore the in situ remanence directions (stars) to their pre-tilting orientations. Note the steepness of the in situ remanences, which remain steep when structurally-corrected indicating that rotations about dyke-normal axes have occurred that are indistinguishable using standard analytical procedures.

D. Rose diagrams illustrating fault strikes along the coast. There is a clear correlation between the E-W striking SDC and NE-SW striking cumulate layering with fault orientation.

However, it seems more likely that the inclined axis identified from the net tectonic rotation axis represents a combination of rotations and thus the 'inclination restoration to a reference' method is more insightful. This results in a 29°-50° clockwise rotation (Figure 8.23B) inferred about either a roughly NE-SW or NW-SE axis. Rotation about a NW-SE axis would be expected to have occurred during Event 5 whereas rotation about a NE-SW axis may have occurred in either Event 2 or 4 (or a combination of both). These magnitudes of rotation are larger than expected for a single event (< 25° from dip of sedimentary sequences) and again strongly imply that composite events account for the rotations. A combination of rotations under various structural events identified can easily account for the rotation experienced by all coastal SDC groups.

8.10.2 Spatial distribution of rotations

The dispersion in the magnetic declinations and the above discussion of the rotations experienced by the coastal SDC illustrate the prevalence of differential rotations between areas. Again, the coastal section can provide a key to determining the spatial distribution of rotations throughout the ophiolite. Plots of longitude along the coast against palaeomagnetic declinations, inclinations, dyke margins and fault types can be constructed (Figure 8.24 illustrates a selection). From these plots, the three blocks the coastal SDC has been divided up into are evident from the change in dyke orientations and the palaeomagnetic data, supported by the inference of large-scale structures between the groups. However, no consistent patterns can be recognised over the length of the coastal SDC between any other fault strike or lineation trends. This implies, that although these blocks are clearly identified to have acted in some respects as discrete blocks, the majority of structures observed are ubiquitous over these areas and so the differential rotations are occurring either due to variously oriented structures between the blocks or as a result of varying magnitudes of rotation on similarly oriented structures.

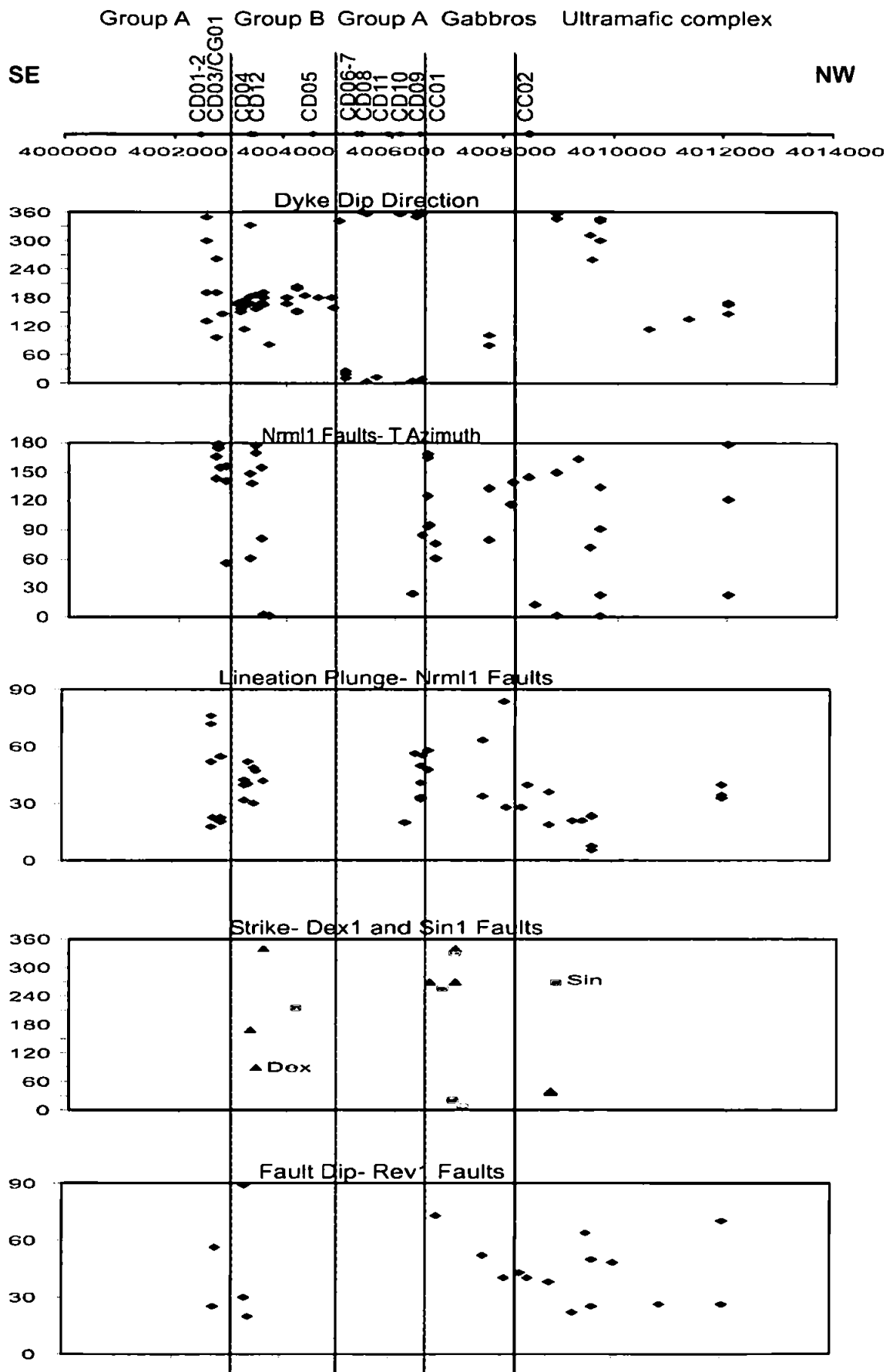


Figure 8.24: Transects along the coast (from SE to NW from left to right along the x-axis of the transect plots) illustrating the orientations (y axes of plots) of various features of the faults and lithologies. The groups identified along the coast are shown at the top (separated by vertical lines on the underneath plots). The construction of these transects aids the recognition of any spatial patterns in the orientations and dips of faults, dykes and palaeostress axes.

According to the 'inclination restoration to a reference' technique, coastal Groups A and C (Figure 8.23B) have experienced rotation about similar axes but by varying amounts which tends to support the latter hypothesis, as does the observation that the topographic lows between these areas have similar trends.

Generally, over the entire study area, faults from the five structural events occur over the whole extent of the area, sedimentary sequences display a wide variation in orientation and tilt and a large dispersion in magnetic declinations is observed. These observations indicate that rotations of varying magnitudes are occurring about structures rather than that rotations are occurring in spatially discrete localised blocks.

8.10.3 Successive rotations and implications for microplate rotation

Each of the five structural events identified not only has the potential to rotate palaeostress axes of earlier events, but to also affect the orientation of all structures (e.g. the SDC) as well as palaeomagnetic directions. The effect of these successive rotations can be modelled. The method and the basis for the assumptions made are illustrated in Figure 8.25.

The effect of each rotation depends on the orientation of previous structures as well as the magnitude of the tilt and will also affect the orientation of the fault axes of earlier events. If a moderate tilt of 15° is assumed about the most recent fault-strike-parallel NW-SE trending axis of Event 5, the resultant change in strike on the strike of all previous fault axes is insignificant. For instance, tilt about this axis affects the orientation of the present-day E-W trending axis of Event 1 most, but the magnitude of change is less than 1° . Similarly, tilt about a fault-parallel axis during Event 4 produces very little change in the

strike of fault-axes from previous events. The largest potential change in strike results from the strike-slip faulting system (Event 3), as rotation is expected to be about a vertical axis. As this event is believed to be the youngest pre-cover event, any rotations about a vertical axis will have affected structures formed during the earlier NW-SE compression (Event 2) and the earliest extensional event (Event 1). One assumption made is that the effect of each event is ubiquitous over the area. In reality, all areas may not be affected by all events.

The effect of successive rotations on initially vertical and horizontal structures is illustrated in Figure 8.26. Figure 8.27 illustrates the potential effect of incorporating a large coherent pre-emplacement microplate rotation. The end results of all of these models are summarised in Figure 8.28 with the dispersion of magnetisation directions of sites with horizontal control on the structure shown for comparison. From Figure 8.26, it can be seen that the present-day tilt of initially horizontal structures such as cumulate layering and the sedimentary sequences can easily be accounted for by a combination of rotations under the five events identified. As can be seen from Figure 8.28, the consistent westwards direction of magnetic remanences is difficult to explain by the structural events alone. This lends support to the hypothesis that a larger coherent rotation must account of a large component of the rotations identified. A 60° magnitude was assumed for this rotation in the modelling process, and this seems to be the minimum likely, as a larger magnitude would account for the magnetisation directions more easily.

The 15° of rotation assumed for each event can be demonstrated to be reasonable, at least in the case of the Neotectonic events, by the fact that an originally horizontal structure experiencing 15° of rotation under these two events (Figure 8.28C) can accumulatively experience a 22-26° magnitude of rotation, which is the average observed for the cover sequences.

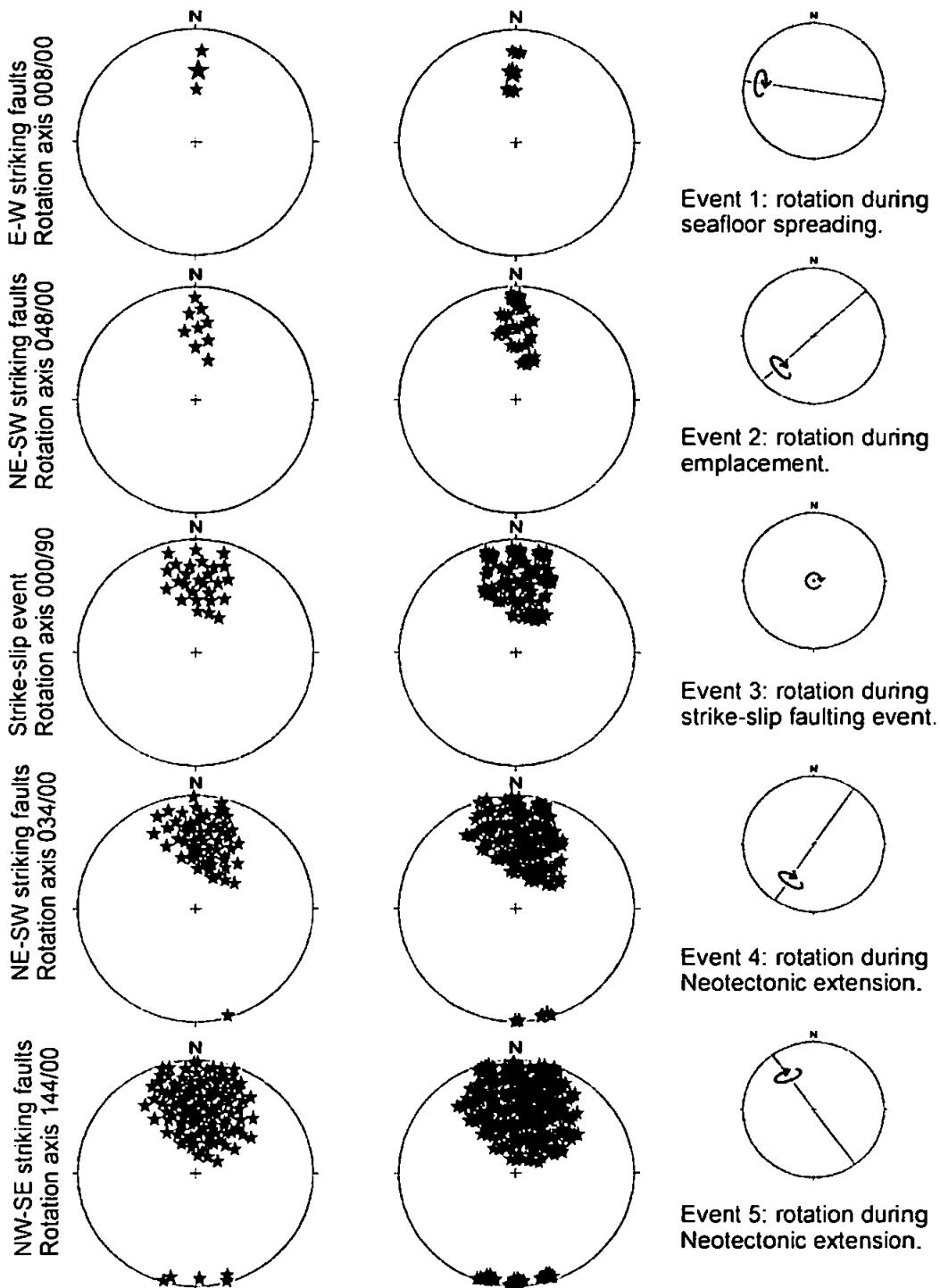


Figure 8.25: The method of modelling the effect of successive rotations illustrating the effect of these successive rotations on the magnetisation. The starting magnetisation is taken to be 002/36 i.e. that predicted from Late Cretaceous sites of this latitude by Westphal et al. (1986). Rotations caused by extensional and compressional events are expected to be about an axis parallel to the average strike of the conjugate fault sets that characterise the event. The degree of rotation would be expected to be not greater than the magnitude of the dip of the sedimentary cover, as this can only have been tilted during Neotectonic events. Bedding tilts are generally $<25^\circ$ (except in the immediate vicinity of faults), produced during two events and so a figure of 15° seems reasonable as an estimate of the magnitude of rotation, although the real magnitude may vary spatially. This tilt may be either clockwise or anticlockwise about a fault-parallel axis, particularly in systems with an equal distribution between the two fault sets forming a conjugate relationship. In systems where there is an unequal distribution, preference for tilting by the dominant fault set is anticipated. For the structural events identified in Hatay, all events have faults dipping in both directions, with events where the distribution is unequal likely to be an artefact of the smaller number of faults within those groups (e.g. Event 2). For the strike-slip faulting event (Event 3) rotations are expected to be about a vertical axis (section 4.8). An allowance for the effect of this vertical axis rotation on the earlier events is also introduced into the middle diagrams. The rotation axes and interpretation of the origin of the faults are shown on the RHS.

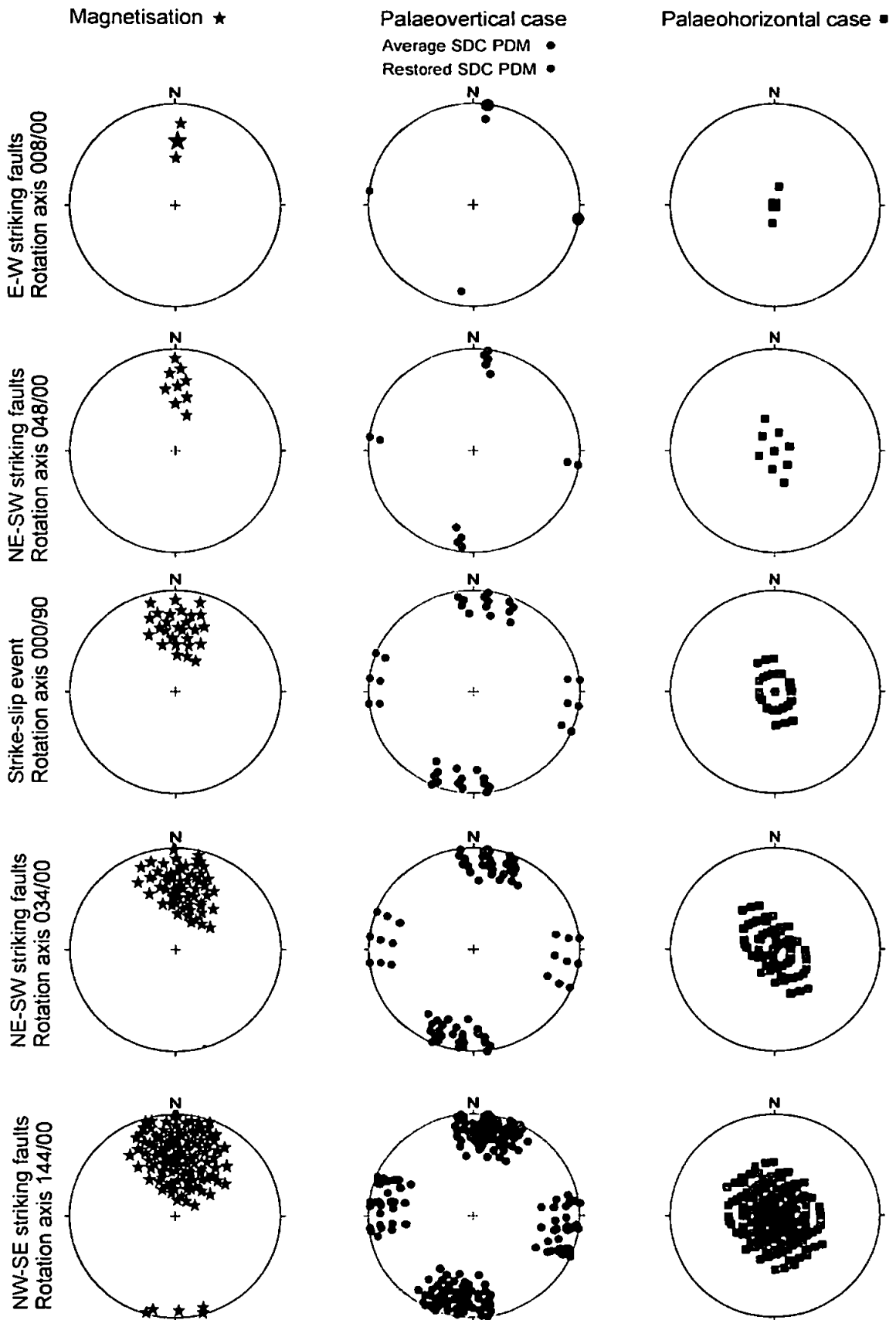


Figure 8.26: An illustration of the effect of successive rotations (using the same error and rotation axes as in the previous diagram), firstly on a palaeovertical case, for both a pole to the strike of dykes margins (PDM) of the average present-day strike in the sheeted dyke complex and dykes restored using net tectonic rotation analysis (middle diagrams), and secondly for a palaeohorizontal case (RHS). The magnetisation is repeated from the previous diagram for the purpose of comparison. No allowance is made for potential rotation of earlier fault axes under the strike-slip faulting event i.e. a 'minimum' possible error sequence.

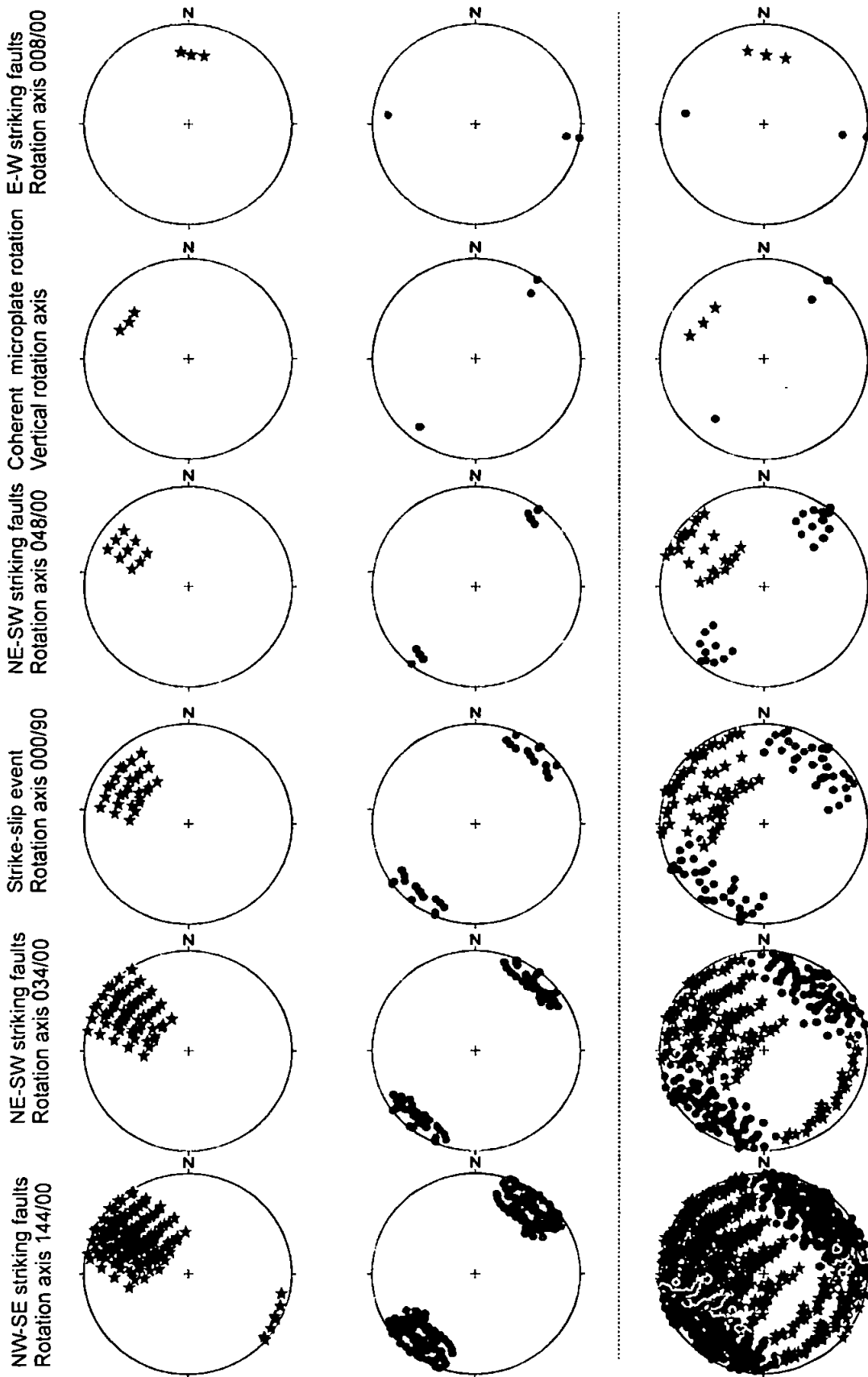


Figure 8.27: Incorporating a coherent vertical axis rotation in its postulated place in the sequence of tectonic events to have affected the ophiolite. The diagrams on the RHS show the increase in potential directions if a 25° rotation about each axis occurs as well as allowing for a 25° rotation of earlier fault axes under the strike-slip faulting event i.e. a 'maximum error sequence'.

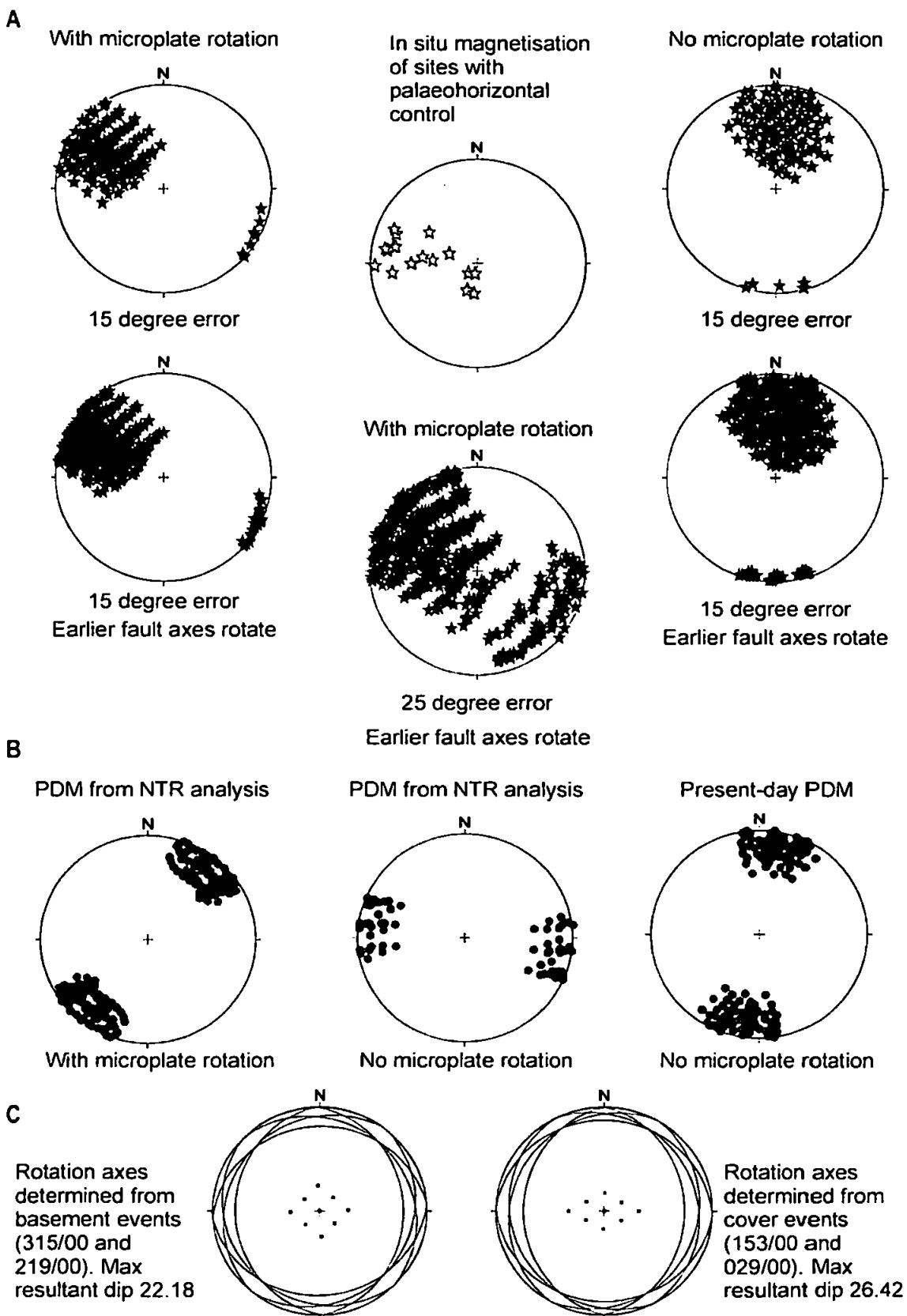


Figure 8.28: Summary of effect of successive rotations illustrating the possible end scenarios obtained from preceding three diagrams, both with and without a coherent microplate rotation. A. The in situ magnetisation of all palaeohorizontal sites is displayed next to the magnetisation directions resulting from successive rotations. It is clear that these magnetisations are difficult to explain under the structural events identified without a coherent anticlockwise rotation. B. The poles to the dyke margins (PDMs) worked out both with and without a rotation of a microplate (symbols as in preceding diagrams) using net tectonic rotation (NTR) analysis. C. The same method is performed on the pole to originally horizontal bedding, but successive rotations can only have occurred under the two post-emplacement events identified.

Figure 8.27 illustrates the extra dispersion in data if 25° of rotation is allowed about fault axes, with the dispersion in magnetic remanences easily explained by the accumulation of rotations. The method illustrated here necessitates several assumptions and cannot be an exact replication of the rotations occurring under each successive event. However, it clearly supports the idea that a large coherent rotation must have occurred in order to produce the magnetic remanences observed.

8.11 Synthesis

Five structural events are identified to have affected the Hatay ophiolite. Their relative timings have been constrained and the events linked into the regional structural history. None of these events can easily account for the consistent westerly directed remanences of the ophiolitic units, thus lending support to the hypothesis of a coherent oceanic microplate rotation linked to that of the Troodos ophiolite. The sequence of tectonic events identified are (from earliest to latest): dyke-parallel normal faulting whilst on the seafloor; a large anticlockwise rotation as part of a coherent microplate; emplacement-related thrust faulting; a strike-slip faulting event related to the N-S convergence of the African and Eurasian plates; Neotectonic extensional deformation, probably during two discrete events. Rotations during these events occur with different magnitudes in different areas resulting in the dispersion in declinations observed from the palaeomagnetic results and also the lack of consistency in orientation of sedimentary sequences. Successive rotations under the identified structural events can account for the present-day tilts observed in both originally horizontal and originally vertical structures. The rotations that have caused the steepening of inclinations in certain areas of the SDC can be explained largely by rotations during the Neotectonic events, or by a combination of smaller successive rotations throughout the structural history of the ophiolite.

9. DISCUSSION AND MODEL FOR TECTONIC EVOLUTION OF THE HATAY OPHIOLITE

9.1 Introduction to chapter

An important implication of the new palaeomagnetic and structural data obtained is the need to re-evaluate existing models for the rotation of the Troodos microplate. The Neotethyan setting in the eastern Mediterranean of SSZ formation in a slow-spreading system has no precise modern analogue (section 2.4.1), and this is particularly true when rotation of a microplate is considered. The fact that both Hatay and Troodos are believed to have formed at slow-spreading ridges and yet preserve continuous and complete sheeted dyke complexes is unusual and the implication that a primary variation in dyke orientation existed within the southern Neotethyan ocean indicates formation within a complex spreading system. Characteristic elements of the Neotethyan system, however, display similarity with fast-spreading systems in the modern oceans and with the increased complexity observed in marginal basins. Thus, in order to produce a revised model, comparison with potential analogues for microplate rotations within the modern oceans and a discussion of complex spreading systems is valuable. In light of the need for re-evaluation of the nature of the rotating area, it is also important to further discuss rotations observed within the Semail ophiolite, alongside a consideration of the effect of major changes in plate motions. A new model for the evolution of the ophiolites within the southern Neotethyan basin in relation to the rotation, its cause and the nature of the spreading system will be presented here.

9.2 Can existing models for the rotation of the 'Troodos' microplate account for the rotations observed in the Hatay and Baër-Bassit ophiolites?

The large-scale anticlockwise rotations observed in the Troodos, Baër-Bassit and Hatay ophiolites suggest the likelihood of a common origin for at least some of the rotation, and for a significant element of this to be occurring as part of a coherent microplate prior to emplacement of the Hatay/Baër-Bassit sheet onto the Arabian platform. The implication is that the microplate comprises a more extensive area than previously thought and existing models where the microplate is spatially constrained to a localised area around the Troodos massif (roughly confined to the present-day margins of Cyprus) must now be modified. Alternatively, the previously 'small' inferred size of the Troodos microplate may be accurate, with rotations occurring within separate smaller areas over a larger area. As Hatay and Baër-Bassit were previously assumed to have been unrotated, the rotation of a larger area within the Neotethyan ocean has not been considered in the development of existing models: the revised model using this data is presented here.

The magnitude and timing of the large anticlockwise rotation of the Troodos microplate are well-documented from palaeomagnetic studies of the ophiolite and in-situ sedimentary cover (section 4.4). The most popular mechanism invokes impingement of the subduction zone to the south of Cyprus with the Arabian continental margin to the east producing an anticlockwise torque that results in a segment of oceanic crust becoming detached and free to rotate in response to the torque (Robertson 1998; Figure 9.1A-B). Previous models have suggested that emplacement of the Hatay/Baër-Bassit sheet onto the Arabian margin was coincident with the initiation of rotation of the Troodos microplate (Clube and Robertson 1986). However, the most recent resolution of the timing of this rotation from the available dataset suggests that it may have been occurring for potentially ~20 Ma prior to the emplacement (Morris et al. 2005; section 4.4.2).

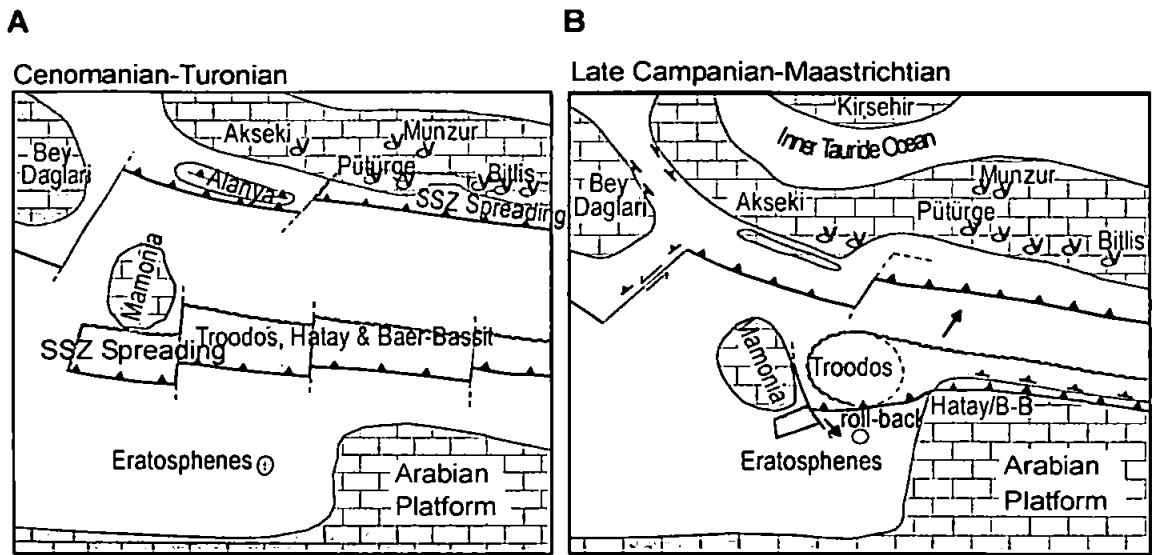


Figure 9.1: Existing models for the palaeorotation of Troodos.

A-B. The Robertson (1998) model for Neotethyan evolution and the rotation of the Troodos microplate.

C. A simple modification of the Robertson (1998) model illustrating how the size of the Troodos microplate may be increased to encompass the Hatay and Baer-Bassit ophiolites in order to account for the rotations observed in these ophiolites.

The difference in mean dyke strike between Troodos and Hatay and Baër-Bassit was a major line of evidence used to infer that the ophiolites to the east were unrotated. The new results from Hatay and Baër-Bassit show not only that these areas are rotated by similar magnitudes to Troodos but also that the differences in dyke trends are likely to be a primary feature of the spreading system within which the ophiolites formed. Therefore, it was misleading to rely on dyke trends to distinguish between rotated and unrotated areas.

A revised model can be drawn from the existing model by simply enlarging the extent of the microplate to encompass the Hatay and Baër-Bassit ophiolites (Figure 9.1C). However, this model remains too simplistic a representation that cannot fully account for the rotation in Hatay and Baër-Bassit, or for the difference in dyke strike through the spreading system. For instance, impingement of a subduction zone on the Arabian platform with simultaneous emplacement of the Hatay and Baër-Bassit ophiolites cannot be coincident with initiation of the rotation because the Hatay and Baër-Bassit ophiolites are inferred to have been rotating for some period prior to emplacement. Analogues in the modern oceans for a torque resulting from the impingement of a subduction zone on a continental platform and causing rotation of a microplate are unknown. However, precise modern analogues are lacking for several aspects of the tectonic situation inferred to have existed in the Neotethyan ocean.

9.3 Modern analogues of microplate rotation

The Hatay ophiolite is believed to represent slow-spreading oceanic crust but modern analogues concerning the rotation of microplates are only known from fast-spreading oceanic systems. These may still provide insight into the nature and mechanisms of the rotation. Table 9.1 illustrates the characteristics of examples of modern microplates, with those postulated for the microplates of the Neotethyan ocean shown for comparison.

<i>Microplate: Modern/ Neotethyan</i>	<i>Spreading system</i>	<i>Location</i>	<i>Size: width (km)</i>	<i>Rate of Rotation (° Ma⁻¹)</i>	<i>Durati on (Ma)</i>	<i>Magnitude (°) and sense</i>	<i>Ref.</i>
Juan- Fernandez: Modern	Fast, mid- ocean	EPR	< 180 ^C	< 29	~6	90 c/w ^E	Bird et al. 1998
Easter: Modern	Fast, mid- ocean	EPR	100s	23.5 ± 11	2.5 ± 0.5	48.5 ± 11 c/w	Cogne et al. 1995
Manus Basin: Modern	Fast, backarc	Eastern Bismarck Sea	100	51	Since < 0.78	ac/w ^E	Martinez and Taylor 1996
Semail: Neotethyan	Fast	Middle East	400 ^D	20	~6	~120 c/w	Weiler 2000
Troodos: Neotethyan ^A	Slow	Eastern Mediterranean	~100	2	~40	90 ac/w	Morris 1996 (review)
H/T/BB ^B : Neotethyan	Slow	Eastern Mediterranean	>250 ^D	2	<40	~80 ac/w	This thesis

Table 9.1: Comparison of microplate rotation in the modern oceans and those inferred to have occurred within Neotethys in the eastern Mediterranean.

^A Although, the 'Troodos' microplate is now inferred to be of increased size, the remaining information regarding the microplate rotation will be accurate.

^B H/T/BB refers to the three western Neotethyan ophiolites known to have rotated anticlockwise. The data combine the new results from this thesis with the previous results from the Troodos microplate. The duration of rotation may be shorter than for the Troodos microplate as rotation stopped with emplacement of Hatay and Baër-Bassit onto the Arabian platform.

^C The size varies according to different authors; for instance 300 km is quoted by Weiler (2000).

^D The sizes of the palaeomicroplates are not well constrained. The 400 km suggested by Weiler (2000) represents the maximum likely. The H/T/BB microplate is inferred to have been a minimum of 250 km in width as this is the current distance between the Hatay and Troodos ophiolites.

^E c/w = clockwise; a/cw = anticlockwise

Two examples of rotating microplates occurring along a mid-ocean system are the Easter and Juan-Fernandez microplates of the East Pacific Rise, located along the very fast spreading Pacific-Nazca boundary and both rotating rapidly clockwise. Geophysical studies show that the Easter microplate exists as a small rigid plate that is trapped and rapidly rotating between the diverging Pacific and Nazca plates (Cogne et al. 1995). The Juan Fernandez microplate is located to the south of the Easter microplate and believed to comprise a central component in the reorganisation of the East Pacific Rise and the northward migration of the Pacific-Antarctic-Nazca (P-A-N) triple junction (Bird et al. 1998). The rotation rate of the Juan-Fernandez microplate is variable and thought to be

inversely proportional to its size (Bird et al. 1998). The Manus Basin microplate is an example of a rotating microplate within a complex backarc system, with rotation occurring as a consequence of an anticlockwise torque exerted by left-lateral shear between the Pacific and Bismarck plates (Martinez and Taylor 1996).

In fast-spreading systems, the boundaries to the rotating microplates comprise a combination of spreading ridges and complex transform-like faults, with complex zones of strike-slip deformation often forming part of but not the entire boundary. For instance, the east and west boundaries of the Easter microplate are two N-S trending, simultaneously active spreading boundaries whereas the north and south boundaries are complex transform-like fault zones with components of extension, compression and shear (Cogne et al. 1995). The 150 km long Manus Basin spreading system is complex, with three major transform zones bounding four extensional zones, with the microplate boundaries comprising fast-slipping transform faults and two overlapping rift grabens (Martinez and Taylor 1996).

There are various kinematic models for the mechanisms by which mid-ocean ridge microplates at fast-spreading ridges rotate. These range from edge-driven models where rotation is about a vertical axis driven at the edges by drag imposed by coupling with the major plates, to models suggesting processes of dual rift propagation and microplate rotation about Euler poles located proximal to propagating rift tips (Bird et al. 1994). Neves et al. (2004) model patterns of stress at mid-ocean ridges, concluding that their results are consistent with the possibility that at overlapping spreading segments, the curvature of the rift tips at high angles to the ridge trend could result in partially unlocked offsets. They suggest that this could create the conditions for microplate rotation with the large overlaps due to lithospheric thickening at the rift tips increasing the ridge strength and unlocking of part of the offset causing initiation of a microplate. An alternative model

for microplate rotation is proposed by McKenzie and Jackson (1986) and requires coupling of a shear flow of the mantle beneath the microplate (floating block model). This model predicts rotation rates half that predicted by the edge-driven model. The rotation of the Easter microplate has been approximated as a circular plate rotating between two major plates with a torque exerted about a vertical axis from the interaction of overlapping spreading centres. The Juan-Fernandez microplate originated from an intra-transform setting, likely the fastest-slipping transform on earth at that time, with a transformation in deformation from internal shear to rigid rotation (Bird et al. 1998), whereas the Manus Basin microplate rotation is a clear example of an edge-driven rotation.

9.4 Complex spreading systems

The differences in the average present-day trend of dykes in the consistent and continuous SDCs of Hatay (E-W) and Troodos (N-S) and the trend of dykes in Baër-Bassit, are significant and remain so following correction to their initial orientations, implying that this variation is a primary feature of the spreading system. The regional palaeo-spreading direction is believed to have been ~NW-SE, fitting in with the palaeogeography and rifting of continental fragments from the E-W trending African margin and also with the restored trend of the Troodos dykes. The slightly oblique restored trend of the Baër-Bassit dykes and more oblique mean strike of the Hatay dykes to this roughly N-S spreading direction implies the effect of a more complicated spreading system, either spatially or temporally. Existing models for the Neotethyan spreading system do not account for this primary variation in dyke orientation; occasional schematic diagrams do illustrate a difference in the orientation of spreading axis (Figure 9.2), but this appears to be coincidental rather than based on restored dyke strikes.

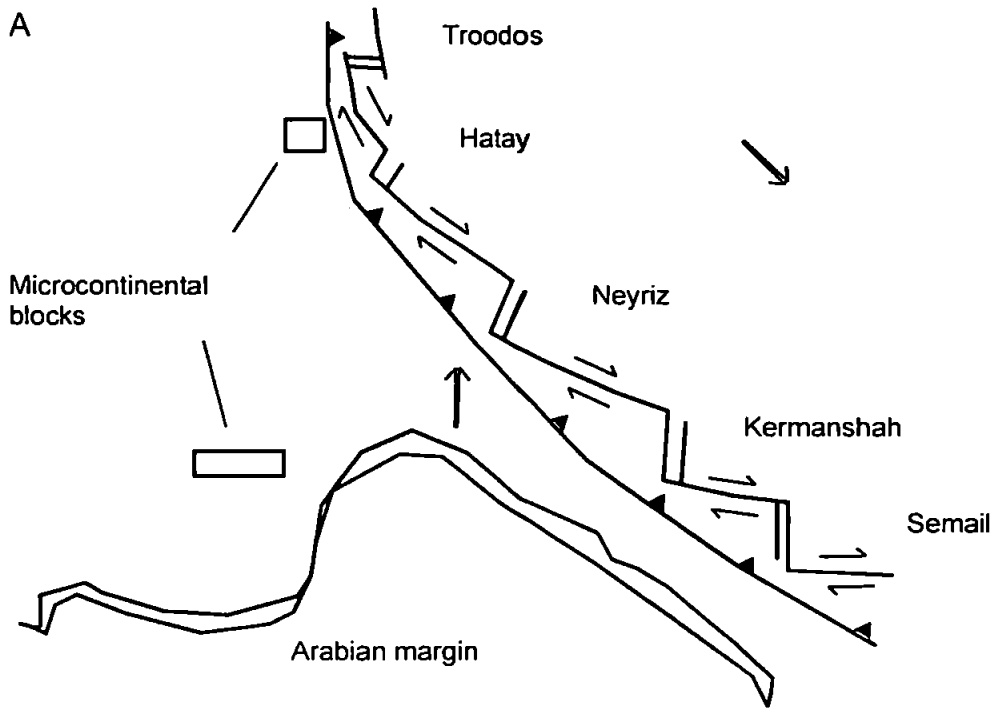
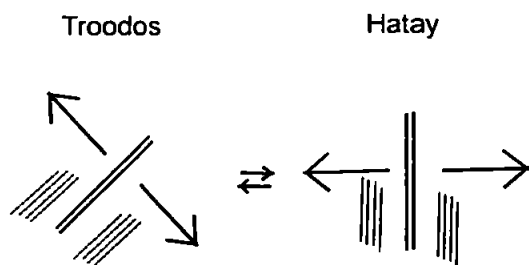


Figure 9.2: An example of an existing model for the framework of the Neotethyan ocean. The suggested framework for the southerly ophiolite belt from Troodos to Semail is illustrated (after Moores et al. 1984), displaying a variation in spreading axis orientation. However, this diagram is merely schematic and no basis for these orientations is discussed by these authors. Existing models do not account for the observed variation in mean dyke trend between the Hatay and Troodos ophiolites. Previously palaeomagnetic data with which to restore the orientation of the SDCs to their original strike only existed for the Troodos ophiolite.

Spreading systems displaying extreme complexity are found in the marginal oceans of the present-day, influenced by subduction processes, regional plate reorganisation and characterised by propagating rifts and spreading axes with complex relationships between system segments (e.g. Tanahashi 1994; Ruellan 1994; Schellart 2002). Modern analogues for variations in spreading-related fabrics within the same spreading system include complications from temporal changes in spreading direction (Figure 9.3A-B) in response to regional or major plate reorganisations or motion changes, and from spatial changes in structural orientation resulting from oblique spreading or a spatial variation in stress fields.

A Temporal change in spreading orientation



B (i) Reorientation by rotation

(ii) Reorientation by propagation

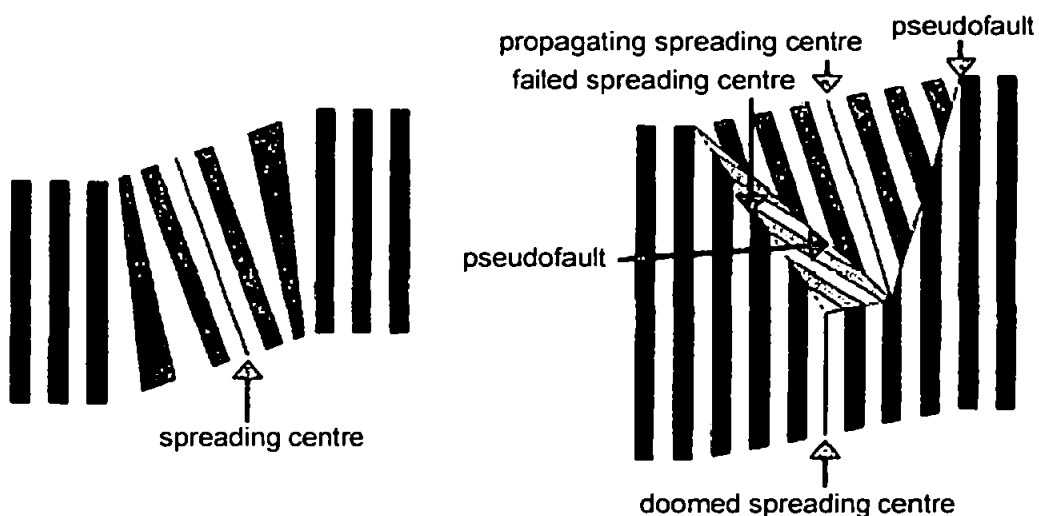


Figure 9.3: Models illustrating causes and mechanisms by which dyke orientation may change within a spreading system.

A. A temporal change may account for the variation between the inferred ~NE-SW oriented Troodos spreading ridge and ~N-S oriented Hatay spreading ridge. A temporal variation in spreading orientation may result from a regional plate reorganisation in a complex spreading system or could be induced by a large-scale plate movement change. Rollback of the subduction zone may also influence the orientation of the dykes over time. Spatial changes may also be introduced by the effects of rollback of the subduction zone or from a torque introduced by the movement of major plates.

B. Mechanisms by which the orientation of dykes may adapt to a new spreading orientation (after Goodliffe et al. 1997) and which may account for the difference in dyke strike between Hatay and Troodos.

A temporal change in spreading orientation occurred in the Philippine Sea plate when two propagating rifts joined together as an R-R-R triple junction to accommodate the difference in spreading direction between the Parece Vela (E-W) and Shikoku (ENE-WSW) basins, followed by a larger temporal orientation change to NE-SW spreading at ~20 Ma (Sdrolias et al. 2004). This was interpreted to relate to initiation of the rotation of the Philippine Sea plate with the catalyst for the rotation suggested to be the ~20-22 Ma change in plate boundary configuration between the Australian and Philippine Sea plate (Sdrolias et al. 2004). A reconfiguration of ridge geometry was also observed in the Lau-Havre-Taupo system with a newly created ridge propagating into older crust in response to changes in opening orientation (Parson and Wright 1996). In the North Fiji marginal basin, ridge axes are characterised by highly variable trends, with present-day trends 20°NW, 20°NE and 5°NNE (Ruellan et al. 1994), representing a 40° variation in spreading direction, analogous to that suggested between Hatay and Troodos.

Dykes may reorient to adapt to a change in spreading direction by rotating or by ridge propagation (Figure 9.3B), with synchronous reorganisation of ridge boundaries over a larger area another possibility, as observed in the Woodlark basin (Goodliffe et al. 1997). A large and rapid change in direction of plate motion due to complex movements of smaller plates buffering the oblique convergence of the Pacific and Australian plates is believed to be the catalyst for synchronous reorganisation of the Woodlark basin spreading centre (Goodliffe et al. 1997).

The fast-spreading Semail ophiolite preserves examples of complex spreading systems with along-strike variations in the SDC suggesting that the spreading axis was segmented by first and/or second order discontinuities, most probably propagating rifts and overlapping spreading centres, representing the terminations of axial magma chambers (MacLeod and Rothery 1992). At least four and potentially seven discontinuities are

identified along a ~500 km ridge-parallel length, suggesting segmentation on the scale of 50-100 km (comparable with the EPR), although unequivocal transform structures are not evident (MacLeod and Rothery 1992). In the southern part of the ophiolite a younger SE-NW ridge segment is observed cross-cutting a NW-SE trending segment, interpreted to represent a ridge-propagator analogous to an EPR-type rapidly spreading microplate system (Boudier et al. 1997).

Morphological and structural patterns mapped within the median valley floors of orthogonally-spreading slow-spreading ridges suggest that these structures will be parallel/sub-parallel to the ridge (McAllister et al. 1995) and in many ophiolites, dykes, faults and other features that are expected to form parallel to a spreading centre during the spreading process have consistent, parallel trends over tens to hundreds of kilometres (Casey et al. 1981; Varga and Moores 1985; MacLeod and Rothery 1992; Rivvizigno and Karson 2004). However, in areas where spreading is not orthogonal, the expected trends may be more complicated. Examples of obliquely spreading ridges are documented along many parts of the mid-ocean ridge system (Bird and Philips 1975; Bicknell et al. 1986; Dauteuil and Brun 1996; Grindlay et al. 1998) and commonly include spreading segments and discontinuities that are oblique to the regional spreading direction. For instance, considerable variations in fault strike from the Reykjanes ridge (McAllister et al. 1995) and obliquely oriented structures in the Macquarie Island ophiolite (Rivvizigno and Karson 2004) are attributed to the complications of oblique spreading. Offsets in the discontinuities are generally less than 10 km and separate intervening spreading segments a few tens of kilometres in length (Rivvizigno and Karson 2004) and thus, although variations in orientation are documented from slow-spreading systems these appear to occur on a smaller scale than observed between the Late Cretaceous Neotethyan ophiolites.

9.5 Synthesis of rotations in Neotethyan ophiolite belt

The implications of the new results are that large rotations in this southerly belt of Neotethyan ophiolites are more extensive than previously thought, and that it may be more appropriate to consider the rotations of all the ophiolites in this chain in conjunction rather than individually.

No palaeomagnetic information is available for the ophiolites of the central part of the belt, but the Semail ophiolite experienced large, differential internal rotations (section 4.6). Clockwise rotation of the northern part of the massif may be attributed to rapid, active microplate rotation of a portion of the ophiolite resulting from spreading at an EPR-type propagating ridge at a high angle to the previous spreading direction (Weiler 2000). This rapidly rotating microplate is suggested to be similar to the Juan Fernandez microplate of the modern oceans (Boudier et al. 1997; Weiler 2000). Similarities between this model and the large rotations observed in the ophiolites at the western end of the ophiolite belt are that both systems appear to represent complex spreading systems. However, the ophiolites to the west formed in slow-spreading systems where no examples of microplate rotation or significant changes in dyke orientation are documented from the modern oceans. These ophiolites rotated considerably slower and with a significantly smaller total magnitude of rotation than the Semail ophiolite to the east. The key observation regarding the rotations is their occurrence in opposite senses at each end of the ophiolite belt, with clockwise rotations experienced by the Semail ophiolite at the eastern end and anticlockwise rotations experienced by Troodos, Hatay and Baër-Bassit to the west. An implication of the opposite sense of these rotations is that the impingement of the Arabian platform northwards is likely to have strongly influenced the rotation, potentially by inducing vorticity in the mantle wedge underlying the Neotethyan crust as a result of plate-scale processes.

9.6 Regional and major plate movements

A distinctive feature of both spreading ridge orientation changes and microplate rotation in the modern oceans is their common coincidence in timing with regional plate reorganisations or changes in plate motion. The southern Neotethyan ocean is believed to have comprised a series of small oceanic basins separated by microcontinental fragments between the major African and Eurasian plates. As such, this tectonic scenario suggests a regime where changes in major plate motions may produce large local changes in spreading direction due to the accommodation of the changes by reorganisation of local spreading systems, with the Woodlark basin as a modern analogue. The summary of the relative movement of the African and Eurasian plates given in sections 3.6 and 4.3 highlighted a change in motion from a sinistral shear to north-south convergence, occurring around 90 Ma. The timing and sharpness of this change cannot be constrained entirely due to the limits of the resolution of the data with some reconstructions indicating a smoother transition (e.g. Livermore and Smith 1984) accommodating the change in motion and some suggesting a sharper change (e.g. Savostin et al. 1986). In the Woodlark Basin, a rapid change of plate movement is believed to have resulted in synchronous reorientation of dykes (Goodliffe et al. 1997).

Major and regional plate movements appear to be extremely significant in both reorientation of spreading centres and initiation of microplate rotation. The conditions for SSZ spreading may be restricted to rare episodes of major plate reorganisation (Robertson 2002, 2004) and thus these same unusual conditions may be expected to produce the necessary setting for the microplate rotation and increased complexity inferred for the Neotethyan ocean. The ~90 Ma change in the motion of the major plates must have been a significant influence in the complex tectonic evolution of the eastern Mediterranean collisional orogen (Figure 9.4).

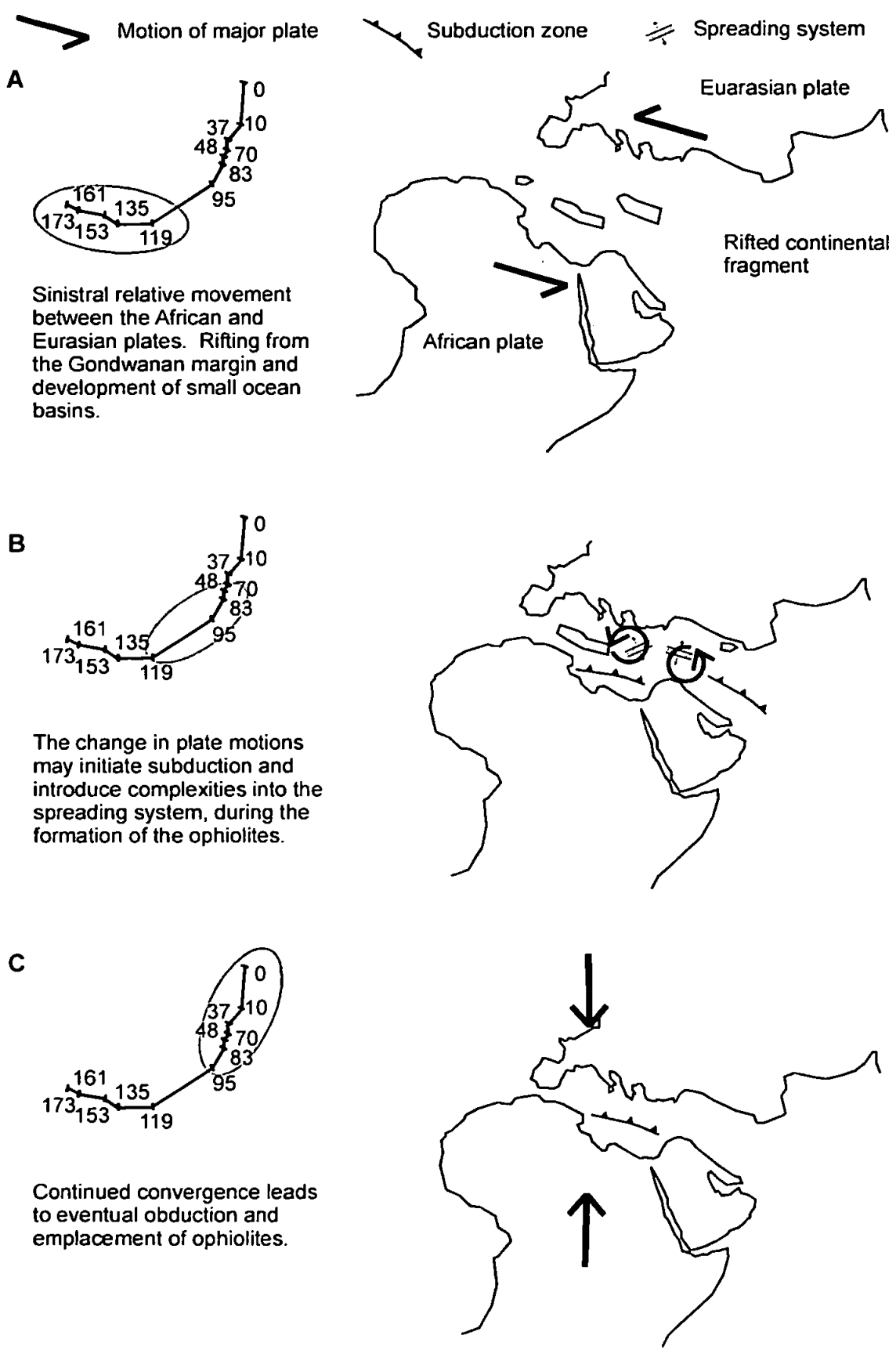


Figure 9.4: Model for the potential affect of large-scale plate movements on Neotethyan ophiolites. The relative positions of Europe relative to Africa (Livermore and Smith 1984) through time at the most relevant geographical point to the ophiolites are shown on the LHS with their interpreted effect on the evolution of the eastern Mediterranean in relation to the ophiolites, concentrating on the change in motion at ~90 Ma. The schematic diagrams on the RHS illustrate the changes. These large-scale plate motions involve lithospheric motion and may be intimately linked to the rotations and complex spreading systems inferred to have existed within the southern Neotethyan ocean at the time of formation of the ophiolites and microplate rotation.

9.7 Model for the tectonic evolution of the Hatay ophiolite

Figure 9.5A illustrates the revised model for the rotation of the Troodos, Hatay and Baër-Bassit ophiolites. In this model, impingement of the Arabian platform on the trench occurs long enough prior to emplacement of the Hatay and Baër-Bassit ophiolites to allow them to rotate anticlockwise prior to emplacement. The torque causing the microplate rotation is the impingement of the Arabian platform on the subduction zone. The mechanism for the rotation is likely to have more similarity with the floating block model of McKenzie and Jackson (1986), where the vorticity of the underlying mantle exerts a torque on the overlying lithosphere. Part of the complexity of backarc basin systems in the modern oceans may be attributed to complexities of flow of the mantle around the subduction zones (e.g. Martinez and Taylor 2002; Schellart 2002) and so the impingement of a continental platform onto a subduction zone would be expected to introduce similar complexities into the system. An anticlockwise torque may also have been introduced into the system by left-lateral shear between the major African and Eurasian plates, similarly to that proposed between strike-slip faults in continental crust (section 4.7). Both the large size of the microplate and the low rate of rotation are more comparable with those suggested for a floating block model than an edge-driven or propagating-ridge influenced model. For instance, the Troodos and Hatay ophiolites are currently located ~250 km distant whereas the maximum width of the Juan-Fernandez microplate was ~180 km, at which time it was rotating at its slowest rate (Bird et al. 1998), which was still faster than the $\sim 2^\circ \text{Ma}^{-1}$ inferred for the western Neotethyan microplate. The influence of the Arabian platform on the rotation is supported by the opposing clockwise sense of rotation observed for the Semail ophiolite at the eastern end of the Neotethyan ophiolite belt (Figure 9.5B).

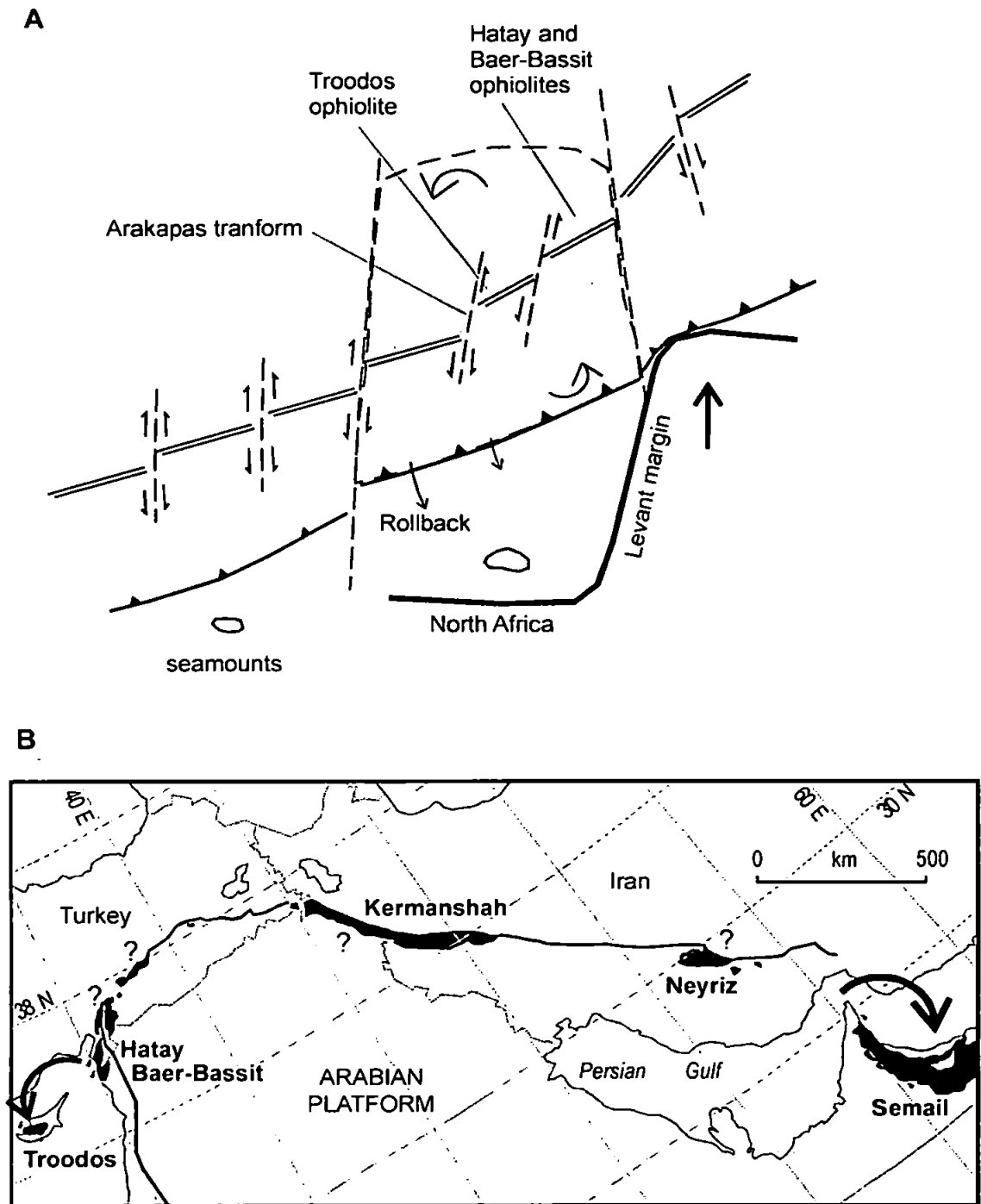


Figure 9.5: Revised model for the evolution of the Neotethyan ophiolites.

A. A large area rotates anticlockwise due to the torque exerted by the impingement the Arabian platform on the subduction zone. Arabia could impinge upon the subduction zone for an extended period of time prior to emplacement of the ophiolites which is likely to be the key that allows it to provide the driving force for sometime before emplacement. The boundaries of the rotating area are transform faults, but on a larger scale than the Arakapas transform which is known not to comprise a microplate-bounding fault. Emplacement of the ophiolites may not be instantaneous geologically with the initial impingement of the subduction zone, allowing a significant component of anticlockwise rotation to occur prior to emplacement of the Hatay and Baër-Bassit ophiolites.

B. A large area to the west (incorporating the Hatay, Troodos and Baër-Bassit ophiolites) within a slow-spreading system rotated slowly anticlockwise whereas a large area to the east (part of the Semail ophiolite) located within a fast-spreading system rotated clockwise, thus indicating the important influence of the Arabian margin on the rotation, producing rotation in opposite senses on either side. The rotations of the ophiolites between either end of the chain are unknown.

The Arakapas transform fault zone was initially suggested as the logical place for the boundary of the Troodos microplate but the discovery that the crust on both side of the transform had experienced similar rotations made this unlikely. With the knowledge that a larger area has experienced rotation, transform faults located some distance from Troodos are likely to comprise a significant component of the microplate boundaries. The Arakapas transform may have been a comparatively minor transform explaining why it was not utilised as a microplate boundary (Figure 9.5A). The transform zone was however partially disrupted by extensional faulting during the initial phases of the rotation (MacLeod 1990). The variation in mean orientation of dykes between the ophiolites may be explained by a temporal change in spreading orientation due to a regional reorganisation of plate boundaries in a complex marginal basin spreading system, with the Woodlark basin as a modern analogue. This indicates that there is an age difference between the Hatay and Baër-Bassit ophiolites and Troodos. The Troodos ophiolite may be older, as the ~90 Ma age of formation is well-constrained, whereas radiometric ages for Baër-Bassit span a larger range and the existence of reverse polarities in Baër-Bassit (and to a lesser extent in Hatay) are more likely to have been acquired during the later Chron 33R rather than the previous reverse polarity chron 30 Ma prior to formation of Troodos.

The rotation of a microplate and change in dyke orientation within the Neotethyan ocean are consistent with characteristics of the modern oceans, particularly those of modern marginal basins, and the implication is that such features would be expected from the Neotethyan ocean due to the known complexity of its tectonic evolution and marginal basin setting. The lack of a precise modern analogue for the setting of the Neotethyan ophiolites supports formation and emplacement during a rare episode of major and regional plate reorganisation.

CHAPTER TEN

10. SUGGESTIONS FOR FUTURE WORK AND CONCLUSIONS

The major conclusions of this thesis link into various areas of interest, especially oceanic tectonics, the structural development of ophiolites, and the tectonic evolution of the eastern Mediterranean orogenic belt and have significant implications in particular for the evolution of the southern Neotethyan ocean and show that the revision of existing models are required.

10.1 Rotations and timing constraints

The large coherent anticlockwise rotation of the Troodos microplate was a key event in the tectonic evolution of the eastern Mediterranean region. The new results from this thesis demonstrating consistent westerly-directed remanences in all lithologies of the Hatay ophiolite indicate that this ophiolite also underwent a large coherent anticlockwise rotation. The magnitude and sense of this rotation are equivalent both to that of the most northerly locality in the Baër-Bassit ophiolite and are also directly comparable to that observed in the Troodos ophiolite between the Campanian and Maastrichtian. A large component of this rotation is thus likely to have been of common cause and to have occurred prior to emplacement of the Hatay/Baër-Bassit ophiolite sheet as part of a coherent microplate.

Timing constraints on the large anticlockwise rotations experienced by the Hatay and Baër-Bassit ophiolites have been provided by palaeomagnetic analyses of their neoautochthonous sedimentary covers, statistical tests for the timing of magnetisation acquisition, and by comprehensive rock magnetic testing.

The new palaeomagnetic analyses performed on the neoautochthonous sedimentary cover sequences of the Hatay and Baër-Bassit ophiolites indicate that a large component of the anticlockwise rotations occurred prior to the deposition of the cover units. For instance, the minor rotations documented by the sedimentary cover of the Hatay ophiolite demonstrate that post-cover rotations cannot explain the larger rotations in the underlying ophiolite. The older Palaeogene sediments of the Baër-Bassit ophiolite document larger rotations than the Neogene sedimentary sequences, attributed to the effect of large-scale Neotectonic strike-slip faulting. The larger and more varied rotations of the southern part of the Baër-Bassit ophiolite would thus be partially explained by the effect of this same fault system.

The magnetisation of both the Hatay ophiolite and its sedimentary cover are pre-deformational in origin, as inferred from positive inclination-only tilt tests. In contrast, inclination-only tilt tests performed on the sedimentary sequences of the Baër-Bassit ophiolite indicate that the magnetisation of Palaeogene sequences is syn-deformational and that of Neogene sequences is post-deformational. These may be explained by remagnetisation during Tertiary folding and strike-slip faulting, tying in with both the lack of remagnetisation in the Hatay sedimentary cover sequences which are little affected by strike-slip faulting, and the larger and more varied rotations experienced by the southern part of the Baër-Bassit ophiolite where these fault systems are most significant.

The inference of stable pre-deformational magnetisations are supported by comprehensive rock magnetic testing within all lithologies of the Hatay ophiolite. Results are consistent with acquisition of the magnetisation soon after genesis at a spreading ridge, carried predominantly by (varying Ti) titanomagnetites of pseudo-single domain grain size and thus capable of carrying a remanence stable over geological time. Rock magnetic results

display similarities with those observed from both modern oceanic crust and other ophiolites.

The Hatay ophiolite is predominantly of normal polarity, as is the Troodos ophiolite, although a small number of sites are of reverse polarity, and may be compared with the widespread observation of reverse polarities within the Baër-Bassit ophiolite. From this it may be inferred that the Hatay and Baër-Bassit ophiolites might be younger allowing magnetisation acquisition during or soon after formation in the first reverse polarity chron subsequent to the Cretaceous LNP. A possibility for future work would be to more tightly constrain the age of the Hatay ophiolite by, for instance accurate radiometric dating techniques to establish the timing of acquisition of the reverse polarity magnetisations.

10.2 Synthesis of structural and palaeomagnetic observations

Five structural events have been identified and linked into phases in the tectonic evolution of the Hatay ophiolite; three occurring prior to the deposition of the cover framework and two observed in both the ophiolitic basement and overlying sediments:

Event 1: Dyke-parallel normal faulting during seafloor deformation;

Event 2: Emplacement-related faulting;

Event 3: Strike-slip faulting linked to the expression of continued convergence of the African and Eurasian plates within continental crust;

Events 4 and 5: Post-cover Neotectonic extensional faulting linked to the development of the current plate boundary configuration.

The orientations of the faults and principal palaeostress axes observed within the ophiolite and sedimentary cover are generally consistent with previous observations, although certain interpretations differ. Most significantly, the interpretation of Dilek and Thy

(1998) that the majority of structures observed within the Hatay ophiolite can be attributed to seafloor deformation is unconvincing, as most of these structures appear to be of Neotectonic or emplacement origin rather than forming as a result of seafloor deformation. The identified structural events cannot either singly or in conjunction account for the consistent westerly directed remanences observed in the Hatay ophiolite, supporting the hypothesis of a coherent microplate rotation. The spread of magnetic declinations observed in the ophiolitic lithologies must be pre-cover in origin as an equivalent dispersion is not observed in declinations from the sedimentary cover. This ties in with the structural analyses as the structural event(s) most likely to account for the spread of declinations are the pre-cover vertical axis rotations during either emplacement-related thrusting or subsequent strike-slip faulting. The dyke-normal rotations that affect the SDC and the orientation of cumulate layering and bedding are easily explained by a combination of rotations during several events. However, the fact that these rotations do not affect all areas of the ophiolite equivalently indicates that, although structural events are not spatially discrete, the degree of rotation experienced about faults of a certain event varies between areas.

10.3 Implications for the evolution of the eastern Mediterranean Neotethys

An important implication of the new palaeomagnetic and structural data obtained is the need to re-evaluate existing models for the rotation of the Troodos microplate. The size of the microplate inferred previously must be considerably increased to account for the rotations of Hatay and Baër-Bassit. The boundaries of the microplate are likely to utilise transform faults of a more significant scale than the Arakapas transform preserved in the Troodos ophiolite. The torque responsible for rotation may be the impingement of the Arabian margin on the subduction zone with rotation occurring for an extended period prior to emplacement of the Hatay/Baër-Bassit sheet. The influence of the Arabian margin

is supported by the observation of rotation in opposite senses occurring at the western and eastern ends of the ophiolite belt. This raises questions concerning the sense and magnitude of potential rotations that have occurred in the mid-chain ophiolites (e.g. the Iranian ophiolites) where no palaeomagnetic work has been carried out. Research on these could provide greater insight into the mechanism(s) responsible for the rotations. For instance, if impingement of the Arabian platform on the subduction zone provides a significant influence, a change in sense from anticlockwise to clockwise at some point between the western and eastern extent of the chain would be anticipated. If the rotations are due to more localised mechanisms and the large opposite-sense rotations observed at either end of the chain of ophiolites are coincidental, the mid-chain ophiolites may have experienced only small rotations, disparate rotations or no rotation.

The restoration of sheeted dykes in the Hatay ophiolite to their original orientation indicates that a primary variation in dyke strike existed within the Neotethyan spreading system, with the mean restored trend of dykes roughly NE-SW and N-S for Troodos and Hatay respectively. Both the microplate rotation and the inferred primary variation in dyke strike imply formation of the ophiolites within a complex spreading system analogous to certain modern day marginal basins where microplate rotation and temporal reorientation of dykes are observed.

LIST OF REFERENCES

- Abrahamsen, N. and G. Schonharting (1987). "Palaeomagnetic timing of the rotation and translation of Cyprus." *Earth and Planetary Science Letters* 81: 409-418.
- Aktas, G. and A. H. F. Robertson (1984). "The Maden Complex, SE Turkey: evolution of a Neotethyan continental margin. In: Dixon, J. E. & Robertson, A. H. F. (Eds.), *The geological evolution of the eastern Mediterranean.*" *Special Publication of the Society of London* 17: 375-402.
- Al-Riyami, K., A. H. F. Robertson, J. Dixon and C. Xenophontos (2002). "Origin and emplacement of the Late Cretaceous Baer-Bassit ophiolite and its metamorphic sole in NW Syria." *Lithos* 65(1-2): 225-260.
- Al-Riyami, K., A. H. F. Robertson, C. Xenophontos, T. Danelian and J. E. Dixon (2000). "Mesozoic tectonic and sedimentary evolution of the Arabian continental margin in Baer-Bassit (NW Syria). In: Malpas, J., Xenophontos, C. & Panayides, A. (Eds.)." *Proceedings of the 3rd International Conference on the Geology of the Eastern Mediterranean, Nicosia, Cyprus*: 61-81.
- Alexander, R. J. and G. D. Harper (1992). "The Josephine ophiolite: an ancient analogue for slow-intermediate-spreading oceanic ridges." *Special Publication of the Society of London* 60: 3-38.
- Allen, M., J. Jackson and R. Walker (2004). "Late Cenozoic reorganisation of the Arabia-Eurasia collision and the comparison of short-term and long-term deformation rates." *Tectonics* 23: TC2008 1-16.
- Allerton, S. (1989). "Fault block rotations in ophiolites: results of palaeomagnetic studies in the Troodos Complex, Cyprus. In: Kissel, C. & Laj, C. (Eds.), *Palaeomagnetic rotations and continental deformation.*" *NATO ASI Series C* 254: 393-410.
- Allerton, S. (1998). "Geometry and kinematics of vertical-axis rotation in fold and thrust belts." *Tectonophysics* 299: 15-30.

- Allerton, S. and F. J. Vine (1987). "Spreading structure of the Troodos ophiolite, Cyprus: some palaeomagnetic constraints." *Geology* 15: 593-597.
- Alt, J. C., H. Kinoshita, L. B. Stokking and P. J. Michael (1996). "(Eds.)." *Proceedings of the Ocean Drilling Program, Scientific Results* 148.
- Angelier, J. (1994). "Fault slip analysis and palaeostress reconstruction." In: *Continental Deformation*: edited by P. L. Hancock. Chapter 4: 53-99.
- Angelier, J., J. F. Dumont, H. Karamenderesi, A. Poisson, S. Simsek and S. Uysal (1981). "Analyses of fault mechanism and expansion of southwestern Anatolia since the Late Miocene." *Tectonophysics* 75: 1-9.
- Anonymous (1972). "Penrose field conference on ophiolites." *Geotimes* 17: 24-25.
- Arpat, E. and F. Saroglu (1972). "The East Anatolian fault system: thoughts on its development." *Mineral Research Exploration Institute Turkey Bulletin* 78: 33-39.
- Aslaner, M. (1973). "Iskendereun-Kirikhan bolgesindeki ofiyolitlerin jeoloji ve petrografisi." *Bulletin M. T. A. Ankara*.
- Bagci, U., O. Parlak and V. Hock (2005). "Whole-rock and mineral chemistry of cumulates from the Kizildag (Hatay) ophiolite (Turkey): clues for multiple magma generation during crustal accretion in the southern Neotethyan ocean." *Mineralogical Magazine* 69: 53-76.
- Banerjee, S. K. (1991). "Magnetic properties of Fe-Ti oxides." *Mineralogical Society of America Reviews in Mineralogy* 25: 107-128.
- Barka, A., S. H. Akyuz, H. A. Cohen and F. Watchorn (2000). "Tectonic evolution of the Niksar and Tasova-Erbaa pull-apart basins, North Anatolian fault zone: their significance for the motion of the Anatolian block." *Tectonophysics* 322: 243-264.

- Barka, A. and P. L. Hancock (1984). "Neotectonic deformation patterns in the convex-northwards arc of the North Anatolian fault zone. In: Dixon, J. E. & Robertson, A. H. F. (Eds.), *The geological evolution of the Eastern Mediterranean.*" Special Publication of the Society of London 17: 763-774.
- Barka, A. and R. Reilinger (1997). "Active tectonics of the Mediterranean region, deduced from GPS, neotectonic and seismicity data." *Annales Geofisika* 11(3): 587-610.
- Beck, M. E. (1976). "Discordant paleomagnetic pole positions as evidence of regional shear in the Western Cordillera of North America." *American Journal of Science* 276: 694-712.
- Bellier, O., S. Over, A. Poisson and J. Andrieux (1997). "Recent temporal change in the stress state and modern stress field along the North Anatolian fault zone (Turkey)." *Geophysical Journal International* 131: 61-86.
- Ben-Avraham, Z., G. Tibor, A. F. Limonov and M. B. Leybov (1995). "Structure and tectonics of the eastern Cyprian Arc." *Marine and Petroleum Geology* 12(3): 263-271.
- Besse, J. and V. Courtillot (1991). "Revised and synthetic apparent polar wander paths of the African, Eurasian and Indian plates, and true polar wander since 200 Ma." *Journal of Geophysical Research* 96(B3): 4029-4050.
- Besse, J. and V. Courtillot (2002). "Apparent and true polar wander and the geometry of the geomagnetic field over the last 200 Myr." *Journal of Geophysical Research* 107(B11): doi: 10.1029/2000JB000050.
- Bicknell, J. D., K. C. Macdonald, S. P. Miller, P. F. Lonsdale and K. Becker (1986). "Tectonics of the Nereus Deep, Red Sea: A deep-tow investigation of a site of initial rifting." *Marine Geophysical Researches* 8: 131-148.
- Bird, P. and J. D. Phillips (1975). "Oblique spreading near the Oceanographer Fracture." *Journal of Geophysical Research* 80: 4021-4027.

- Bird, R. T., D. F. Naar, R. L. Larson, R. C. Searle and C. R. Scotese (1998). "Plate tectonic reconstructions of the Juan Fernandez microplate: Transformation from internal shear to rigid rotation." *Journal of Geophysical Research* 103(B4): 7049-7067.
- Bleil, U. and N. Peterson (1983). "Variations in magnetization intensity and low-temperature titanomagnetite oxidation of ocean floor basalts." *Nature* 301: 384-388.
- Blome, C. D. and W. P. Irwin (1985). "Equivalent radiolarian ages from ophiolitic terranes of Cyprus and Oman." *Geology* 13: 401-404.
- Bonhommet, N., P. Roperch and F. Calza (1988). "Paleomagnetic arguments for block rotations along the Arakapas Fault (Cyprus)." *Geology* 16: 422-425.
- Borradaile, G. J. (2001). "Paleomagnetic vectors and tilted dikes." *Tectonophysics* 333: 417-426.
- Borradaile, G. J. and K. Lucas (2003). "Tectonics of the Akamas and Mamonia ophiolites, Western Cyprus: magnetic petrofabrics and paleomagnetism." *Journal of Structural Geology* 25(12): 2053-2076.
- Borradaile, G. J. and K. Lucas (2005). "Correspondence." *Journal of Structural Geology* 27: 175-178.
- Bott, M. H. P. (1959). "The mechanics of oblique slip faulting." *Geological Magazine* 96(2): 109-117.
- Boudier, F., J. F. Chouchz, A. Nicolas, M. Cannat, G. Ceuleneer, M. Misseri and R. Monthy (1985). "Kinematics of oceanic thrusting in the Oman ophiolite: model for plate convergence." *Earth and Planetary Science Letters* 75: 215-222.
- Boudier, F., A. Nicolas and J. L. Bouchez (1982). "Kinematics of oceanic thrusting and subduction from basal sections of ophiolites." *Nature* 296: 825-828.
- Boudier, F., A. Nicolas, B. Ildefonse and D. Jousset (1997). "EPR microplates: a model for the Oman ophiolite." *Terra Nova* 9: 79-82.

- .Boulton, S. (2005 (in press)). "Hatay graben." Special Publication of the Society of London.
- .Bozkurt, E. (2001). "Neotectonics of Turkey- a synthesis." *Geodinamica Acta* 14: 3-30.
- .Butler, R. F. (1992). "Paleomagnetism: Magnetic domains to geologic terranes." Blackwell Scientific Publications: 319.
- .Cameron, W. E. (1985). "Petrology and origin of primitive lavas from the Troodos ophiolite, Cyprus." *Contributions to Mineralogy and Petrology* 89: 239-255.
- .Cande, S. C. and D. V. Kent (1992). "A new geomagnetic polarity timescale for the Late Cretaceous and Cenozoic." *Journal of Geophysical Research* 97: 13917-13951.
- .Cann, J., H. M. Prichard, J. Malpas and C. Xenophontos (2001). "Oceanic inside corner detachments of the Limassol Forest area, Troodos ophiolite, Cyprus." *Journal of the Geological Society of London* 158(5): 757-768.
- .Cannat, M., C. Mevel, J.-M. Aczende, J. Dubois, Y. Fouquet, P. Gente and J. A. Karson (1988). "Serpentinized upper mantle on the median valley walls of the MARK area: geology and geophysics from NAUTILE." *Earth and Ocean Science Transactions* 69: 1431.
- .Capan, U. Z., P. Vidal and J. M. Cantagrel (1987). "K-Ar, Nd, Sr and Pb isotopic study of the Quaternary volcanism in Karasu Rift (Hatay), N-end of Dead sea rift zone in SE Turkey." *Hacateppe University Earth Science* 14: 165-178.
- .Casey, J. F. and J. F. Dewey (1984). "Initiation of subduction zones along transforms and accreting plate boundaries, triple junction evolution, and fore-arc spreading centres- implications for ophiolitic geology and obduction." *Special Publication of the Society of London* 13: 269-290.
- .Casey, J. F., J. F. Dewey, P. J. Fox, J. A. Karson and E. Rosencrantz (1981). "Heterogenous nature of the oceanic crust and upper mantle: A perspective from the Bay of Islands ophiolite. In: Emilani, C. (Ed.)." *The Oceanic Lithosphere, Volume III The Sea: New York, Wiley: 305-338.*

- Channell, J. E. T., O. Tuysuz, O. Bektas and A. M. C. Sengor (1996). "Jurassic-Cretaceous palaeomagnetism and paleogeography of the Pontides (Turkey)." *Tectonics* 15: 201-212.
- Chorowicz, J., P. Luxey, N. Lyberis, J. Carvalho, J.-F. Parrot, N. Yurur and N. Gundogdu (1994). "The Maras triple junction (southern Turkey) based on digital elevation model and satellite imagery interpretation." *Journal of Geophysical Research* 99: 20225-20242.
- Christensen, N. I. and M. H. Salisbury (1975). "Structure and constitution of the lower oceanic crust." *Reviews of Geophysics and Space Physics* 13: 57-86.
- Cita, M. B. and A. Camerlenghi (1990). "The Mediterranean ridge as an accretionary prism in a collisional context." *Geological Society of Italy Memoirs* 45.
- Cladouhos, T. T. (1999). "A kinematic model for deformation within brittle shear zones." *Journal of Structural Geology* 21: 437-448.
- Clube, T. M. M., K. M. Creer and A. H. F. Robertson (1985). "The palaeorotation of the Troodos microplate." *Nature* 317: 522-525.
- Clube, T. M. M. and A. H. F. Robertson (1986). "The palaeorotation of the Troodos microplate, Cyprus, in the Late Mesozoic-Early Cenozoic plate tectonic framework of the Eastern Mediterranean." *Surveys in Geophysics* 8: 375-437.
- Cochran, J. R. (1981). "The Gulf of Aden structure and evolution of a young ocean basin and continental margin." *Journal of Geophysical Research* 86: 863-888.
- Cogne, J. P., J. Francheteau and V. Courtillot (1995). "Large rotation of the Eastern microplate as evidenced by oriented paleomagnetic samples from the ocean floor." *Earth and Planetary Science Letters* 136(3/4): 213-222.
- Cogulu, E., M. Delaloye, M. Vuagnat and J. J. Wagner (1975). "Some geochemical, geochronological and petrophysical data on the ophiolitic massif from the Kizil Dag, Hatay, Turkey." *C. R. Seances Soc. Phys. Hist. nat. Geneve* 10: 141-150.

- Coleman, R. G. (1981). "Tectonic setting for ophiolite obduction in Oman." *Journal of Geophysical Research* 86: 2497-2508.
- Collinson, D. W. (1983). "Methods in Palaeomagnetism and Rock Magnetism-Techniques and Instrumentation." Chapman and Hall, London: 500pp.
- Coskun, B. and B. Coskun (2000). "The Dead Sea Fault and related subsurface structures, Gaziantep Basin, southeast Turkey." *Geological Magazine* 137(2): 175-192.
- Dauteuil, O. and J. P. Brun (1996). "Deformation partitioning in a slow spreading ridge undergoing oblique extension, Mohns Ridge, Norwegian Sea." *Tectonics* 15: 870-884.
- Day, R., M. Fuller and V. A. Schmidt (1977). "Hysteresis properties of titanomagnetites: Grain size and composition dependence." *Physics of the Earth and Planetary Interiors* 13: 260-267.
- Delaloye, M., H. De Souza, J. J. Wagner and I. Hedley (1980b). "Isotopic ages on ophiolites from the eastern Mediterranean. In: Panayiotou (Ed.)." *International Symposium on Ophiolites, Lefkose*: 292-295.
- Delaloye, M., O. Piskin, H. Selcuk, M. Vuagnat and J. J. Wagner (1980a). "Geological section through the Hatay ophiolite along the Mediterranean coast, southern Turkey." *Ophioliti* 5(2/3): 205-216.
- Delaloye, M. and J. J. Wagner (1984). "Ophiolites and volcanic activity near the western edge of the Arabian plate. In: Dixon, J. E. & Robertson, A. H. F. (Eds.), *The geological evolution of the eastern Mediterranean.*" *Special Publication of the Society of London* 17: 225-234.
- Delaune-Mayere, M., J. Marcoux, J. Parrot and A. Poisson (1976). "Modele d'evolution mesozoi que de la paleo-marge tethysienne au niveau des nappes radiolarites et ophiolitiques du Taurus Lycien d'Antalya et du Ber-Bassit. In: Biju-Duval, B. & Montadert, L. (Eds.)." *The Structural History of the Mediterranean Basins*: 79-94.

- .Dercourt, J., M. Gaetani, B. Vrielynck, E. Barrier, B. Biju-Duval, M. F. Brunet, J. P. Cadet, S. Crasquin and M. E. Sandulescu (2000). "Peri-Tethys Palaeogeographical atlas." Commission for the Geological Map of the World, Paris.
- .Dercourt, J., M. Gaetani, B. Vrielynck, E. Barrier, B. Biju-Duval, M. F. Brunet, J. P. Cadet, S. Crasquin and M. E. Sandulescu (2000). "Peri-Tethys Palaeogeographical atlas." Commission for the Geological Map of the World, Paris.
- .Dercourt, J., L. E. Ricou, B. Vrielynck and (Eds.) (1993). "Atlas Tethys Palaeoenvironmental Maps." Beicip-Franlab.
- .Dercourt, J., L. P. Zonenshain, L. E. Ricou, V. G. Kazmin, X. Le Pichon, A. L. Knipper, C. Grandjacquet, I. M. Sbotshikov, J. Geysant, C. Lepvrier, D. H. Pechersky, J. Boulin, J. C. Sibuet, L. A. Savostin, O. Sorokhtin, M. Westphal, M. L. Bazhenov, J. P. Lauer and B. Biju-Duval (1986). "Geological evolution of the Tethys belt from the Atlantic to the Pamirs since the Lias." *Tectonophysics* 123: 241-315.
- .Dewey, J. F. (1976). "Ophiolite obduction." *Tectonophysics* 31: 93-120.
- .Dewey, J. F., M. R. Hempton, W. S. Kidd, F. Saroglu and A. M. C. Sengor (1986). "Shortening of continental lithosphere: the neotectonics of eastern Anatolia- a young collision zone. In: Coward, M. P. and Reis, A. C. (Eds.), *Collision Tectonics*." Special Publication of the Society of London 19: 2-36.
- .Dewey, J. F., R. E. Holdsworth and R. A. Strachan (1998). "Transpression and transtension zones." Special Publication of the Society of London 135: 1-14.
- .Diabat, A. A., M. Atallah and M. R. Salih (2004). "Paleostress analysis of the Cretaceous rocks in the eastern margin of the Dead Sea transform, Jordan." *Journal of African Earth Sciences* 38: 449-460.
- .Dick, H. J. B., J. Lin and H. Schouten (2003). "An ultraslow-spreading class of ocean ridge." *Nature* 426: 405-412.

- .Dietrich, D. and S. Spencer (1993). "Spreading-induced faulting and fracturing of oceanic crust: examples from the sheeted dyke complex of the Troodos ophiolite, Cyprus. In: Prichard, H. M. Alabaster, T., Harris, N. B., Neary, C. R. (Eds), Magmatic processes and plate tectonics." Special Publication of the Society of London 76: 121-139.
- .Dietrich, V. J., R. Emmerman, R. Oberhansli and H. Puchelt (1978). "Geochemistry of basaltic and gabbroic rocks from the West Mariana Basin and the Mariana." *Earth and Planetary Science Letters* 39: 127-144.
- .Dilek, Y. and M. Delaloye (1992). "Structure of the Kizildag ophiolite, a slow-spread Cretaceous ridge segment north of the Arabian promontory." *Geology* 20: 19-22.
- .Dilek, Y. and E. M. Moores (1990). "Regional tectonics of the eastern Mediterranean ophiolites. In: Malpas, J., Moores, E. M., Panayiotu, A. & Xenophontos, C." *Ophiolites, Oceanic Crustal Analogues, Nicosia, Cyprus, Geological Survey Department: 295-309.*
- .Dilek, Y. and P. Thy (1998). "Structure, petrology and seafloor spreading tectonics of the Kizildag Ophiolite, Turkey." *Special Publication of the Society of London* 148: 43-70.
- .Dilek, Y., P. Thy, B. Hacker and S. Grundvig (1999). "Structure and petrology of Tauride ophiolites and mafic dike intrusions (Turkey): Implications for the Neotethyan ocean." *Geological Society of America Bulletin* 111(8): 1192-1216.
- .Dubertret, L. (1955). "Geologie des roches verts du nord-ouest de la Syrie et du Hatay (Turquie)." *Notes et Mem. Moyen-Orient* 6: 2-179.
- .Dubois, A., F. Odonne, G. Massonnat, T. Lebourg and R. Fabre (2002). "Analogue modelling of fault reactivation: tectonic inversion and oblique remobilisation of grabens." *Journal of Structural Geology* 24(11): 1741-1752.
- .Dunlop, D. (1998). "Thermoremanent magnetization of nonuniformly magnetized grains." *Journal of Geophysical Research* 103: 30561-30574.

- Dunlop, D. (2002). "Theory and application of the Day plot (Mrs/Ms versus Hcr/Hc) 1. Theoretical curves and tests using titanomagnetite data." *Journal of Geophysical Research* 107(B3).
- Dunlop, D. and O. Ozdemir (1997). "Rock magnetism: Fundamentals and frontiers." Cambridge University Press, New York: 573 pp.
- Dunlop, D. and M. Prevot (1982). "Magnetic properties and opaque mineralogy of drilled submarine intrusive rocks." *Geophysical Journal of the Royal Astronomical Society* 69: 763-802.
- Enkin, R. J. and G. S. Watson (1996). "Statistical analysis of palaeomagnetic inclination data." *Geophysical Journal International* 126: 495-504.
- Erendil, M. (1984). "Petrology and structure of the upper crustal units of the Kizil Dag ophiolite In: Tekeli, O. & Concuoglu, C. M. (Eds)." *Geology of the Taurus Belt, Proceedings*: 269-284.
- Feinberg, H., H. Horen, A. Michard and O. Saddiqi (1999). "Obduction-related remagnetization at the base of an ophiolite: Paleomagnetism of the Samail nappe lower sequence and of its continental substratum, southeast Oman Mountains." *Journal of Geophysical Research* 104(B8): 17703-17714.
- Fisher, R. A. (1953). "Dispersion on a sphere." *Proceedings of the Royal Society of London, Series A* 217: 295-305.
- Freund, R. (1970). "Rotation of strike slip faults in Sistan, Southeast Iran." *Journal of Geology* 78: 188-200.
- Freund, R., Z. Garfunkel, I. Zak, M. Goldberg, T. Weissbrod and B. Berrin (1970a). "The shear along the Dead Sea rift." *Philosophical transactions of the Royal Society of London* 267: 107-130.
- Gahagan, L. M., C. R. Scotese, J.-Y. Royer, D. T. Sandwell, J. K. Winn, R. L. Tomlins, M. I. Ross and e. al. (1988). "Tectonic fabric of the ocean basins from satellite altimetry data." *Tectonophysics* 155: 1-26.

- Garfunkel, Z. (1981a). "Internal structure of the Dead Sea leaky transform (rift) and its relations to plate kinematics." *Tectonophysics* 80: 81-108.
- Garfunkel, Z. (1981b). "Dead Sea Rift- Introduction." *Tectonophysics* 141: 1-4.
- Garfunkel, Z. (1998). "Constraints on the origin and history of the Eastern Mediterranean basin." *Tectonophysics* 298(1-3): 5-35.
- Garfunkel, Z. and Z. Ben-Avraham (1996). "The structure of the Dead Sea basin." *Tectonophysics* 255: 155-176.
- Gass, I. G. (1968). "Is the Troodos massif of Cyprus a fragment of Mesozoic ocean floor?" *Nature* 220: 39-42.
- Gass, I. G. and J. D. Smewing (1973). "Intrusion and metamorphism at constructive margins: evidence from the Troodos massif, Cyprus." *Nature* 242: 26-29.
- Gee, J., R. Varga, Y. Gallet and H. Staudigel (1993). "Reversed-polarity overprint in dikes from the Troodos ophiolite: Implications for the timing of alteration and extension." *Geology* 21(9): 849.
- Gnos, E. and M. Perrin (1996). "Formation and evolution of the Masirah ophiolite constrained by paleomagnetic study of volcanic rocks." *Tectonophysics* 253: 53-64.
- Goodliffe, A. M., B. Taylor, F. Martinez, R. Hey, K. Maeda and K. Ohno (1997). "Synchronous reorientation of the Woodlark Basin spreading center." *Earth and Planetary Science Letters* 146: 233-242.
- Gradstein, F., J. Ogg and A. Smith (2004). "A geological timescale 2004." Cambridge University Press: 589pp.
- Grindlay, N. R., J. A. Madsen, C. Rommevaux-Jestin and J. Sclater (1998). "A different pattern of ridge segmentation and mantle Bouguer gravity anomalies along the ultra-slow spreading Southwest Indian Ridge (15°30'E to 25°E)." *Earth and Planetary Science Letters* 161: 243-253.

- Gubbins, D. (1999). "The distinction between geomagnetic excursions and reversals." *Geophysical Journal International* 137(1): F1.
- Gursoy, H., J. D. A. Piper and O. Tatar (2003a). "Neotectonic deformation in the western sector of tectonic escape in Anatolia: palaeomagnetic study of the Afyon region, central Turkey." *Tectonophysics* 374(1-2): 57-79.
- Gursoy, H., O. Tatar, J. D. A. Piper, A. Heimann and L. Mesci (2003b). "Neotectonic deformation linking the east Anatolian and Karatas-Osmaniye intracontinental transform fault zones in the Gulf of Iskenderun, southern Turkey, deduced from palaeomagnetic study of the Ceyhan-Osmaniye volcanics." *Tectonics* 22(6): 1067-1079.
- Haggerty, S. E. (1978). "Mineralogical constraints on Curie isotherms in deep crustal magnetic anomalies." *Geophysical Research Letters* 5: 105-108.
- Hagstrum, J. T. and D. L. Jones (1998). "Paleomagnetism, paleogeographic origins and uplift history of the Coast Range ophiolite at Mount Diablo, California." *Journal of Geophysical Research* 103: 597-603.
- Hailwood, E. A. (1989). "Magneostratigraphy." *Special Report- Geological Society of London* 19: 84 pp.
- Hall, A. (1996). "Igneous Petrology." Longman Group Limited Second Edition: 551p.
- Hall, J. M. and A. Muzzatti (1999). "Delayed magnetisation of the deeper kilometer of oceanic crust at Ocean Drilling Project Site 504." *Journal of Geophysical Research* 1999: 12843-12851.
- Hall, J. M. and A. Muzzatti (1999). "Delayed magnetization of the deeper kilometer of oceanic crust at Ocean Drilling Project Site 504." *Journal of Geophysical Research* 104(B6): 12853-12851.
- Hamilton, W. B. (1995). "Subduction systems and magmatism in Volcanism associated with extension at consuming plate margins." *Special Publication of the Society of London* 81: 3-28.

- Hancock, P. L. and A. A. Barka (1987). "Kinematic indicators on active normal faults in western Turkey." *Journal of Structural Geology* 9: 573-584.
- Hatzor, Y. and Z. Reches (1990). "Structure and paleostresses in the Gilboa' region, western margins of the central Dead Sea rift." *Tectonophysics* 180(1): 87-100.
- Hawkins, J. W., S. H. Bloomer, C. A. Evans and J. T. Melchior (1984). "Evolution of intra-oceanic arc-trench systems." *Tectonophysics* 102: 175-205.
- Hempton, M. R. (1987). "Constraints on Arabian plate motion and extensional history of the Red Sea." *Tectonics* 6(6): 687-705.
- Hurst, S. D., K. L. Verosub and E. M. Moores (1992). "Paleomagnetic constraints on the formation of the Solea Graben, Troodos Ophiolite, Cyprus." *Tectonophysics* 208: 431-445.
- Irving, E. (1977). "Drift of the major continental blocks since the Devonian." *Nature* 270: 304-309.
- Irving, E. and G. A. Irving (1982). "Apparent polar wander paths: Carboniferous through Cenozoic and the assembly of Gondwana." *Geophysical Survey* 5: 141-188.
- Jackson, J. (1994). "Active tectonics of the Aegean region." *Annual Reviews Earth Planet Science* 22: 239-271.
- Jelinek, V. (1981). "Characterization of the magnetic fabric of rocks." *Tectonophysics* 79: 63-67.
- Johnson, H. P. and J. E. Pariso (1993). "Variations in Oceanic Crustal Magnetization: Systematic Changes in the Last 160 Million Years (Paper 92JB01322)." *Journal of Geophysical Research* 98(B/1): 435.
- Kakol, Z. and J. M. Honig (1989). "Influence of deviations from ideal stoichiometry on the anisotropy parameters of magnetite $Fe_{3-x}O_4$." *Phys. Rev.* 40: 9090-9097.
- Kakol, Z., J. Sabol and J. M. Honig (1991). "Magnetic anisotropy of titanomagnetites $Fe_{3-x}Ti_xO_4$ $0 < x < 0.55$." *Phys. Rev.* 44: 2198-2204.

- Karamata, S. (1980). "Metamorphism beneath obducted ophiolite slabs. In: Panayiotu, A. (Ed.)." *Ophiolites: Proceedings of the International Symposium, Cyprus, 1979*, Cyprus Geological Survey Department: 219-227.
- Karig, D. E. and H. Kozlu (1990). "Late Paleogene-Neogene evolution of the triple junction near Maras, south-central Turkey." *Journal of the Geological Society of London* 147: 19-32.
- Karson, J. A. (1990). "Seafloor spreading on the Mid-Atlantic ridge: implications for the structure of ophiolites and oceanic lithosphere produced in slow-spreading environments. In: Malpas, J., Moores, E. M., Panayiotu, A. & Xenophontos, C." *Ophiolites, Oceanic Crustal Analogues, Nicosia, Cyprus, Geological Survey Department: 547-555*.
- Karson, J. A., M. Cannat, D. J. Miller and D. Elthon (1997). "Eds." *Proceedings of the Ocean Drilling Program, Scientific Results* 153.
- Karson, J. A. and P. A. Rona (1990). "Block tilting, transfer faults and structural control of magmatic and hydrothermal processes in the TAG area, Mid-Atlantic ridge, 26°N." *Geological Society of America Bulletin* 102: 1635-1645.
- Kazmin, V. G. and V. V. Kulakov (1968). "The geological map of Syria. Scale 1: 50 000 (Sheet Al-Latheqiyeh). Explanatory note." *Technoexport, Nedra, Moscow: 124 pp.*
- Kelso, P. R., N. R. Banerjee and H. U. Worm (1991). "The effect of low-temperature hydrothermal alteration on the remanent magnetization of synthetic titanomagnetites: A case for acquisition of chemical remanent magnetization." *Journal of Geophysical Research* 96: 19545-19553.
- Kempler, D. and Z. Garfunkel (1994). "Structures and kinematics in the northeastern Mediterranean: a study of an irregular plate boundary." *Tectonophysics* 234: 19-32.

- .Kent, D. V., B. M. Honnorez, N. D. Opdyke and P. J. Fox (1978). "Magnetic properties of dredged oceanic gabbros and the source of marine magnetic anomalies." *Geophysical journal of the Royal Astronomical Society* 55: 513-517.
- .Kikawa, E., P. R. Kelso, J. E. Pariso and C. Richter (1996). "Paleomagnetism of gabbroic rocks and peridotites from sites 894 and 895, leg 147, Hess Deep: results of half-core and whole-core measurements." *Proceedings of the Ocean Drilling Program, Scientific Results* 147: 383-391.
- .King, G., D. Oppenheimer and F. Amelung (1994). "Block versus continuum deformation in the western United States." *Earth and Planetary Science Letters* 128: 55-64.
- .Kirschvink, J. L. (1980). "The least-squares line and plane and the analysis of paleomagnetic data." *Geophysical journal of the Royal Astronomical Society* 62: 699-718.
- .Kissel, C., O. Averbuch, D. Frizon de Lamotte, O. Monod and S. Allerton (1993). "Preliminary paleomagnetic evidence of a post-Eocene clockwise rotation of the Western Taurides thrust belt, east of the Isparta reentrant (southern Turkey)." *Earth and Planetary Science Letters* 117: 1-14.
- .Kissel, C., C. Laj, A. Poisson and N. Gorur (2003). "Paleomagnetic reconstruction of the Cenozoic evolution of the Eastern Mediterranean." *Tectonophysics* 362(1-4): 199-217.
- .Kosterov, A. (2001). "Magnetic properties of subaerial basalts at low temperatures." *Earth Planets Space* 53: 883-892.
- .Kosterov, A. and M. Prevot (1998). "Possible mechanisms causing failure of Thellier palaeointensity experiments in some basalts." *Geophysical Journal International* 124: 554-572.
- .Krantz, R. W. (1988). "Multiple fault sets and three-dimensional strain: Theory and application." *Journal of Structural Geology* 10(3): 225-237.

- .Krasheninnikov, V. A. (1994). "Stratigraphy of the Maastrichtian and Cainozoic deposits of the coastal part of Northwestern Syria (Neoautochton of the Bassit ophiolite massif). In: Krasheninnikov, V. A. & Hall, J. M. (Eds.)." Geological Structure of the Northeastern Mediterranean (Cruise 5 of the Research Vessel Akademik Nikolaj Strakhov) Historical Productions Hall Jerusalem: 265-276.
- .Le Pichon, X. and J. Angelier (1979). "The Hellenic arc and trench system: a key to the Neotectonic evolution of the eastern Mediterranean area." *Tectonophysics* 60: 1-42.
- .Le Pichon, X. and J. Francheteau (1978). "A plate tectonic analysis of the Red Sea- Gulf of Aden area." *Tectonophysics* 46: 369-406.
- .Leitch, E. C. (1984). "Island arc elements and arc-related ophiolites." *Tectonophysics* 106: 177-203.
- .Livermore, R. A. and A. G. Smith (1984). "Some boundary conditions for the evolution of the Mediterranean region." In: *Proceedings NATO A.R.I.*
- .Lowrie, W. (1990). "Identification of ferromagnetic minerals in a rock by coercivity and unblocking temperature properties." *Geophysical Research Letters* 17(2): 159-162.
- .Luyendyk, B. P. and R. Day (1982). "Paleomagnetism of the Semail ophiolite, Oman, 2, The Wadi Kabir gabbro section." *Journal of Geophysical Research* 87: 10903-10917.
- .Luyendyk, B. P., B. R. Laws, R. Day and T. B. Collinson (1982). "Paleomagnetism of the Semail ophiolite, Oman, 1, The Sheeted Dyke Complex at Ibra." *Journal of Geophysical Research* 87: 10883-10902.
- .Lyberis, N., T. Yurur, J. Chorowicz, E. Kasapoglu and N. Cundogdu (1992). "The east Anatolian fault: an oblique collisional belt." *Tectonophysics* 204: 1-15.

- Lytwyn, J. N. and J. F. Casey (1993). "The geochemistry and petrogenesis of volcanics and sheeted dikes in the Hatay (Kizildag) ophiolite, southern Turkey: Possible formation within the Troodos ophiolite, Cyprus, along fore-arc spreading centers." *Tectonophysics* 223: 237-272.
- MacDonald, W. D. (1980). "Net tectonic rotation, apparant rotation, and the strcutural tilt correction in palaeomagnetic studies." *Journal of Geophysical Research* 85: 3659-3669.
- MacLeod, C. J. (1990). "Role of the Southern Troodos Transform Fault in the rotation of the Troodos microplate: evidence from the Eastern Limassol Forest. In: Malpas, J., Moores, E. M., Panayiotu, A. & Xenophontos, C. (Eds.)." *Ophiolites, Oceanic Crustal Analogues, Nicosia, Cyprus, Geological Survey Department: 75-85.*
- MacLeod, C. J., B. Celerier, G. L. Fruh-Green and C. E. Manning (1996). "The tectonics of Hess Deep: a synthesis of drilling results from Leg 147. In: Mevel, C. Gillis, K. M. and Meyer, P." *Proceedings of the Ocean Drilling Progam, Scientific Results, College Station, TX: 461-474.*
- MacLeod, C. J. and B. J. Murton (1993). "Structure and tectonic evolution of the Southern Troodos Transform Fault Zone, Cyprus. In: Prichard, H. M., Alabaster, T. Harris, N. B. W. & Neary, C. R. (Eds), *Magmatic processes and plate tectonics.*" *Special Publication of the Society of London* 76: 141-176.
- MacLeod, C. J. and D. A. Rothery (1992). "Ridge axial segmentation in the Oman ophiolite: Evidence from along-strike variations in the sheeted dyke complex. In: Browning, P. (Ed.), *Ophiolites and their modern oceanic analogues.*" *Special Publication of the Society of London* 60: 39-63.
- Makris, J., Z. Ben-Avraham, A. Behle, A. Ginzburg, P. Giese, A. Steinmetz, S. Eleftherion and B. Whitmarsh (1983). "Deep seismic soundings between Cyprus and Israel and their interpretation." *Geophysical Journal of the Royal Astronomical Society* 75: 575-591.

- Malpas, J., T. Calon and G. Squires (1993). "The development of a Late Cretaceous microplate suture zone in SW Cyprus. In: Pritchard, H. M., Alabaster, T. Harris, N. B. W. & Neary, C. R. (Eds.), Magmatic processes and plate tectonics." Special Publication of the Society of London 76: 177-195.
- Malpas, J., C. Xenophontos and D. Williams (1992). "The Ayia Varvara Formation of SW Cyprus: a product of complex collisional tectonics." *Tectonophysics* 212: 193-241.
- Mantis, M. (1970). "Upper Cretaceous-Tertiary foraminiferal zones in Cyprus." *Epetiris* 3: 227-241.
- Marrett, R. and R. W. Allmendinger (1990). "Kinematic analysis of fault-slip data." *Journal of Structural Geology* 12(8): 973-986.
- Mart, Y. and P. D. Rabinowitz (1986). "The northern Red Sea and the Dead Sea rift." *Tectonophysics* 124: 85-113.
- Martinez, F. and B. Taylor (1996). "Backarc Spreading, Rifting, and Microplate Rotation, Between Transform Faults in the Manus Basin." *Marine Geophysical Researches* 18(2/4): 203-224.
- McAllister, E. and J. Cann (1995). "The evolution of crustal deformation in an oceanic extensional environment." *Journal of Structural Geology* 17(2): 183-199.
- McClusky, S., S. Balassanian, A. Barka, C. Demir, S. Ergintav, I. Georgiev, O. Gurkan, M. Hamburger, K. Hurst, H. G. Kahle, K. Kastens, G. Keklelidze, R. King, V. Kotzev, O. Lenk, S. Mahmoud, A. Mishin, M. Nadariya, A. Ouzounis, D. Paradissis, Y. Peter, M. Prilepin, R. Reilinger, I. Sanli, H. Seeger, A. Tealeb, M. N. Toksoz and G. Veis (2000). "Global positioning system constraints on plate kinematics and dynamics in the eastern Mediterranean and Caucasus." *Journal of Geophysical Research* 105(B3): 5695-5719.
- McElhinny, M. W. (1964). "Statistical significance of the fold test in palaeomagnetism." *Geophysical Journal of the Royal Astronomical Society* 8: 338-340.

- McFadden, P. L. and D. L. Jones (1981). "The fold test in palaeomagnetism." *Geophysical Journal of the Royal Astronomical Society* 67: 53-58.
- McFadden, P. L. and M. W. McElhinny (1990). "Classification of the reversal test in palaeomagnetism." *Geophysical Journal International* 103: 725-729.
- McKenzie, D. (1972). "Active tectonics of the Mediterranean region." *Geophysical Journal of the Royal Astronomical Society* 30: 109-185.
- McKenzie, D. (1978). "Active tectonism in the Alpine-Himalayan belt: the Aegean Sea and the surrounding regions (tectonics of the Aegean region)." *Geophysical journal of the Royal Astronomical Society* 55: 217-254.
- McKenzie, D., D. Davies and P. Molnar (1970). "Plate tectonics of the Red Sea and east Africa." *Nature* 226: 243-248.
- McKenzie, D. and J. Jackson (1983). "The relationship between strain rates, crustal thickening, palaeomagnetism, finite strain and fault movements within a deforming zone." *Earth and Planetary Science Letters* 65: 182-202.
- McKenzie, D. and J. Jackson (1986). "A block model of distributed deformation by faulting." *Journal of the Geological Society of London* 143: 349-353.
- McKenzie, D. and J. Jackson (1988). "The kinematics and dynamics of distributed deformation. In: Kissel, C., Laj, C. (Eds.), *Palaeomagnetic rotations and continental deformation.*" *NATO ASI Series C* 254: 17-31.
- McKenzie, D. P. and W. J. Morgan (1969). "Evolution of triple junctions." *Nature* 224: 125-133.
- Merrill, R. T. and M. W. McElhinny (1983). "The Earth's magnetic field: Its history, origin and planetary perspective." *Academic Press*: 401.
- Merrill, R. T. and M. W. McElhinny (1983). "The Earth's magnetic field: Its history, origin and planetary perspective." *Academic Press*: 401pp.

- .Moores, E. M., P. T. Robinson, J. Malpas and C. Xenophontos (1984). "Model for the origin of the Troodos Massif, Cyprus and other mideast ophiolites." *Geology* 12: 500-503.
- .Moores, E. M. and F. J. Vine (1971). "Troodos Massif, Cyprus and other ophiolites as oceanic crust: Evaluations and implications." *Philosophical Transactions of the Royal Society of London Series A* 268: 443-466.
- .Morris, A. (1990). "Palaeomagnetic studies of the Mesozoic-Tertiary tectonic evolution of Turkey, Cyprus and Greece." PhD Thesis, University of Edinburgh.
- .Morris, A. (1996). "A review of palaeomagnetic research in the Troodos ophiolite, Cyprus." *Special Publication of the Society of London* 105: 311-324.
- .Morris, A. (2003). "The Late Cretaceous palaeolatitude of the Neotethyan spreading axis in the eastern Mediterranean region." *Tectonophysics* 377: 157-178.
- .Morris, A. and M. W. Anderson (2002). "Palaeomagnetic results from the Baer-Bassit ophiolite of northern Syria and their implication for fold tests in sheeted dyke terrains." *Physics and Chemistry of the Earth Parts a B C* 27(25-31): 1215-1222.
- .Morris, A., M. W. Anderson, J. Inwood and A. H. F. Robertson (2005 (in press)). "Palaeomagnetic insights into the evolution of Neotethyan oceanic crust in the eastern Mediterranean." *Special Publication of the Society of London*.
- .Morris, A., M. W. Anderson, A. H. Robertson and K. Al-Riyami (2002). "Extreme tectonic rotations within an eastern Mediterranean ophiolite (Baer-Bassit, Syria)." *Earth and Planetary Science Letters* 202(2): 247-261.
- .Morris, A., M. W. Anderson and A. H. F. Robertson (1998). "Multiple tectonic rotations and transform tectonism in an intra-oceanic suture zone, SW Cyprus." *Tectonophysics* 299: 229-253.

- .Morris, A., M. W. Anderson and A. H. F. Robertson (2005). "Comment on: "Tectonics of the Akamas and Mamonia ophiolites, Western Cyprus: magnetic petrofabrics and paleomagnetism" by G.J. Borradaile and K. Lucas." *Journal of Structural Geology* 27: 171-174.
- .Morris, A., K. M. Creer and A. H. F. Robertson (1990). "Palaeomagnetic evidence for clockwise rotations related to dextral shear along the Southern Troodos Transform Fault, Cyprus." *Earth and Planetary Science Letters* 99: 250-262.
- .Morris, A. and A. H. F. Robertson (1993). "Miocene remagnetisation of carbonate platform and Antalya Complex units within the Isparta angle, south west Turkey." *Tectonophysics* 220: 243-266.
- .Morris, A. and D. H. Tarling (1996). "Introduction. In: Morris, A. & Tarling, D. H. (Eds.), *Palaeomagnetism and Tectonics of the Mediterranean Region.*" Special Publication of the Society of London 105: 1-18.
- .Moskowitz, B. M. (1987). "Towards resolving the inconsistencies in characteristic properties of synthetic titanomagnetites." *Physics of the Earth and Planetary Interiors* 46: 173-183.
- .Moskowitz, B. M., M. Jackson and C. Kissel (1998). "Low-temperature magnetic behaviour of titanomagnetites." *Earth and Planetary Science Letters* 157: 141-149.
- .Mukasa, S. and J. N. Ludden (1987). "Uranium-lead isotopic ages of plagiogranites from the Troodos ophiolite, Cyprus, and their tectonic significance." *Geology* 15: 825-828.
- .Murton, B. J. (1986). "Anomalous oceanic lithosphere formed in a leaky transform fault: evidence from the western Limassol Forest Complex, Cyprus." *Journal of the Geological Society of London* 143: 845-854.

- Murton, B. J. (1990). "Was the Southern Troodos Transform Fault a victim of microplate rotations? In: Malpas, J., Moores, E. M., Panayiotu, A. & Xenophontos, C. (Eds.)." *Ophiolites, Oceanic Crustal Analogues*, Nicosia, Cyprus, Geological Survey Department: 87-98.
- Mutter, J. C. and J. A. Karson (1992). "Structural processes at slow-spreading ridges." *Science* 257: 627-634.
- Muxworthy, A. R. and E. McClelland (2000). "Review of the low-temperature magnetic properties of magnetite from a rock magnetic perspective." *Geophysical Journal International* 140: 101-114.
- Nelson, M. R. and C. H. Jones (1987). "Palaeomagnetism and crustal rotations along a shear zone, Las Vegas range, Southern Nevada." *Tectonics* 6: 13-33.
- Neves, M. C., M. H. P. Bott and R. C. Searle (2004). "Patterns of stress at midocean ridges and their offsets due to seafloor subsidence." *Tectonophysics* 386: 223-242.
- Nicolas, A. (1989). "Structures of ophiolites and dynamics of oceanic lithosphere." *Series in Petrology and Structural Geology* 4: 367pp.
- Nicolas, A. and F. Boudier (1999). "Slow spread accretion and mantle denudation in the Mirdita ophiolite (Albania)." *Journal of Geophysical Research*: 15155-15167.
- Nicolas, A., F. Boudier, K. Michibayasi and L. Gebert-Gaillard (2000). "Aswad massif (United Arab Emirates): Archetype of the Oman-UAE ophiolite belt In: Dilek, Y., Moores, E. Elthon, D. and Nicolas, A. (Eds.). *Ophiolites and Oceanic Crust: New Insights from Field Studies and Ocean Drilling Program.* Geological Society of America Special Paper 349.
- Nieto-Samaniego, A. F. and S. A. Alaniz-Alvarez (1997). "Origin and tectonic interpretation of multiple fault patterns." *Tectonophysics* 270(3-4): 197-206.

- Nishitani, T. and M. Kono (1983). "Curie temperature and lattice constant of oxidised titanomagnetite." *Geophysical Journal of the Royal Astronomical Society* 74: 585-600.
- Nur, A. and Z. Ben-Avraham (1978). "The eastern Mediterranean and the Levant: tectonics of continental collision." *Tectonophysics* 46: 297-311.
- O'Donovan, J. B. and W. O'Reilly (1983). "Magnetic properties of basalt from Hole 504B, Deep Sea Drilling Project Leg 69. In: Cann, J. R. & Langseth, M. G. (Eds.)." *Initial Reports of the Deep Sea Drilling Project*: 721-726.
- O'Reilly, W. (1984). "Rock and Mineral Magnetism." Blackie: 230pp.
- Okay, A. I. and O. Tuysuz (1999). "Tethyan sutures of northern Turkey. In: Durand, B., Jolivet, L., Horvath, F. and Sranne, M. (Eds.), *The Mediterranean Basins: Tertiary Extension within the Alpine Orogen*." *Special Publication of the Society of London* 156: 475-515.
- Oral, M. B., R. Reilinger, M. N. Toksoz, R. W. Kong, A. Barka, I. Kinik and O. Lenk (1995). "Global positioning system offers evidence of plate motions in eastern Mediterranean." *Earth and Ocean Science Transactions* 76(9).
- Over, S., K. S. Kavak, O. Bellier and S. Ozden (2004b). "Is the Amik basin (SE turkey) a triple-junction area? Analyses of SPOT XS imagery and seismicity." *International Journal of Remote Sensing* 25(19): 3857-3872.
- Over, S., S. Ozden and U. C. Unlugenc (2004d). "Late Cenozoic stress distribution along the Misis range in the Anatolian, Arabian and African plate intersection region, SE Turkey." *Tectonics* 23(TC2008).
- Over, S., S. Ozden, U. C. Unlugenc and H. Yilmaz (2004a). "A synthesis: Late Cenozoic stress field distribution at northeastern corner of the Eastern Mediterranean, SE Turkey." *Comptes Rendus Geosciences* 336(1): 93-103.
- Over, S., S. Ozden and H. Yilmaz (2004c). "Late Cenozoic stress evolution along the Karasu Valley, SE Turkey." *Tectonophysics* 380: 43-68.

- Over, S., C. C. Unlugenc and O. Bellier (2002). "Quaternary stress regime change in the Hatay region (SE Turkey)." *Geophysical Journal International* 148(3): 649-662.
- Ozdemir, O. and D. Dunlop (1985). "An experimental study of chemical remanent magnetizations of synthetic monodomain titanomagnhemitites with initial thermoremanent magnetizations." *Journal of Geophysical Research* 90(B13): 11513-11523.
- Ozdemir, O. and D. Dunlop (1993). "The effect of oxidation on the Verwey transition in magnetite." *Geophysical Research Letters* 20: 1671-1674.
- Ozdemir, O., D. Dunlop and B. M. Moskowitz (2002). "Changes in remanence, coercivity and domain state at low temperature in magnetite." *Earth and Planetary Science Letters* 194: 343-358.
- Papazachos, B. C. and C. A. Papaioannou (1999). "Lithospheric boundaries and plate motions in the Cyprus area." *Tectonophysics* 308: 193-204.
- Pariso, J. E. and A. M. Johnson (1989). "Magnetic properties and oxide petrography of the sheeted dike complex in Hole 504B." *Proceedings of the Ocean Drilling Program, Scientific Results* 111: 159-167.
- Pariso, J. E. and A. M. Johnson (1991). "Alteration products at Deep Sea Drilling Project/Ocean Drilling Program Hole 504B at the Costa Rica Rift: Implications for magnetization of oceanic crust." *Journal of Geophysical Research* 96: 11703-11722.
- Parlak, O., A. Kop, U. Unlugenc and C. Demirkol (1998). "Geochemistry and geochronology of basaltic rocks in the Karasu graben near Kirikhan (Hatay), Southern Turkey." *Turkish Journal of Earth Science* 7: 53-61.
- Parrot, J. (1973). "Petrologie de la coupe du Djebel Moussa massif basique-ultrabasique du Kizil Dag (Hatay, Turquie)." *Sciences de la Terre* 18(2): 143-172.

- Parrot, J. (1974). "L'assemblage ophiolitique du Baer-Bassit (Nord ouest de la Syrie): Etude petrographique et geochemique du complex filonien des lavas en coussins qui lui sont associees, et de une partie des formations effusives du volcanosedimentaire." Cahiers ORSTROM: Serie Geologie 6(2): 94-126.
- Parrot, J. (1977). "Assemblage ophiolitique du Baer-Bassit et termes effusifs du volcano-sedimentaire: petrologie de un fragment de la croute oceanique Tethysienne charree sur la plate-forme Syrienne." Travaux et Documents ORSTROM 72: 333pp.
- Parson, L. M. and I. C. Wright (1996). "The Lau-Havre-Taupo back-arc basin: a southward-propagating, multi-stage evolution from rifting to spreading." Tectonophysics 263(1/4): 1-22.
- Party, E. S. (2005). "Oceanic core complex formation, Atlantis Massif—oceanic core complex formation, Atlantis Massif, Mid-Atlantic Ridge: drilling into the footwall and hanging wall of a tectonic exposure of deep, young oceanic lithosphere to study deformation, alteration, and melt generation." IODP Preliminary Report 305.
- Pearce, J. A. (2003). "Supra-subduction zone ophiolites: The search for modern analogues." Special Papers- Geological Society of America(373): 269-294.
- Pearce, J. A., T. Alabaster, A. W. Shelton and M. P. Searle (1981). "The Oman ophiolite as a Cretaceous arc-basin complex: evidence and implications." Philosophical Transactions of the Royal Society of London Series A A300: 299-317.
- Pearce, J. A., S. J. Lippard and S. Roberts (1984). "Characteristics and tectonic significance of supra-subduction zone ophiolites." Special Publication of the Society of London 16: 77-94.

- Perfit, M. R., C. H. Langmuir, M. Baekisapa, B. Chappell, R. W. Johnson, H. Staudigel and S. R. Taylor (1987). "Geochemistry and petrology of volcanic rocks from the Woodlark Basin: addressing questions of ridge subduction. IN: Taylor, B. & Exxon, N. F. (Eds.)." *Marine Geology, Geophysics and Geochemistry of the Woodlark Basin- Solomon Islands*: 113-154.
- Perincek, D. and I. Cemen (1990). "The structural relationship between the East Anatolian and Dead Sea fault zones in southeastern Turkey." *Tectonophysics* 172(3-4): 331-340.
- Perrin, M., G. Plenier, J. M. Dautria, E. Cocuaud and M. Prevot (2000). "Rotation of the Semail ophiolite (Oman): Additional Paleomagnetic data from the volcanic sequence." *Marine Geophysical Researches* 21(3/4): 181-194.
- Perrin, M., M. Prevot and F. Bruere (1994). "Rotation of the Oman ophiolite and initial location of the ridge in hotspot reference frame." *Philosophical Transactions of the Royal Society of London Series A* 300: 299-317.
- Piper, J. D. A., J. M. Moore, O. Tatar, H. Gursoy and R. G. Park (1996). "Palaeomagnetic study of crustal deformation across an intracontinental transform: the North Anatolian fault zone in northern turkey. In: Morris, A. and Tarling, D. H. (Eds.), *Palaeomagnetism and Tectonics in the Mediterranean Region*." Special Publication of the Society of London 105: 299-310.
- Piper, J. D. A., O. Tatar and H. Gursoy (1997). "Deformational behaviour of continental lithosphere deduced from block rotations across the North Anatolian fault zone in Turkey." *Earth and Planetary Science Letters* 150: 191-203.
- Piskin, O., M. Delaloye and J. J. Wagner (1986). "Guide to the Hatay geology." *Ofioliti* 11: 87-104.
- Platzman, E. S., J. P. Platt, C. Tapirdamaz, M. Sanver and C. C. Rundle (1994). "Why is there no clockwise rotation along the North Anatolian fault zone?" *Journal of Geophysical Research* 99: 21705-21715.

- Platzman, E. S., C. Tapirdamaz and M. Sanver (1998). "Neogene anticlockwise rotation of Central Anatolia (Turkey): preliminary palaeomagnetic and geochronological results." *Tectonophysics* 299: 175-189.
- Poole, A. J. and A. H. F. Robertson (1992). "Quaternary uplift and sea-level change at an active plate boundary, Cyprus." *Journal of the Geological Society of London* 148: 909-921.
- Rautenschlein, M., G. A. Jenner, J. Hertogen, A. W. Hofmann, R. Kerrich, H.-U. Schmincke and W. M. White (1985). "Isotopic and trace element composition of volcanic glasses from Akaki Canyon, Cyprus: implications for the origin of Troodos ophiolite." *Earth and Planetary Science Letters* 75: 369-383.
- Readman, P. W. and W. O'Reilly (1972). "Magnetic properties of oxidised (cation-deficient) titanomagnetites (Fe, Ti)₃O₄." *Journal of Geomagnetism and Geoelectricity* 24: 69-90.
- Reches, Z. (1978). "Analysis of faulting in three-dimensional strain field." *Tectonophysics* 47(1-2): 109-129.
- Reches, Z. (1983). "Faulting of rocks in three-dimensional strain fields II. Theoretical analysis." *Tectonophysics* 95(1-2): 133-156.
- Reches, Z. (1987). "Determination of the tectonic stress tensor from slip along faults that obey the coulomb yield condition." *Tectonics* 6(6): 849-861.
- Reches, Z. and G. Schubert (1987). "Models of post-Miocene deformation of the Arabian plate." *Tectonics* 6(6): 707-725.
- Reed, S. J. B. (1996). "Electron Microprobe Analysis and Scanning Electron Microscopy in Geology." Cambridge University Press Book (University of Cambridge).
- Reeves, C. and M. de Wit (2000). "Making ends meet in Gondwana: retracing the transforms of the Indian ocean and reconnecting continental shear zones." *Terra Nova* 12: 272-282.

- Reilinger, R. E., S. C. McClusky, M. B. Oral, R. W. King, M. N. Toksoz, A. A. Barka, I. Kinik, O. Lenk and I. Sanli (1997). "Global Positioning System measurements of present-day crustal movements in the Arabia-Africa-Eurasia plate collision zone." *Journal of Geophysical Research* 102(B /5): 9983-9999.
- Ricou, L. E. (1971). "Le croissant ophiolitique peri-arabe, une ceinture de nappes mises en place au Cretace superieur." *Revue Geographie Physique Geologie Dynamique* 13: 327-349.
- Ricou, L. E. (1995). "The plate tectonic history of the past Tethys ocean. In: Nairn, A. E. M. et al. (Eds.). *The Ocean basins and Margins.*" Plenum, New York: 3-70.
- Ricou, L. E., J. Marcoux and H. Whitechurch (1984). "The Mesozoic organisation of the Taurides: one or several ocean basins. In: Dixon, J. E. & Robertson, A. H. F. (Eds.), *The geological evolution of the Eastern Mediterranean.*" *Special Publication of the Society of London* 17: 349-360.
- Rivizzigno, P. A. and J. A. Karson (2004). "Structural expression of oblique seafloor spreading in the Macquarie Island ophiolite, Southern Ocean." *Geology* 32(2): 125-128.
- Roberts, G. P. (1996). "Variation in fault-slip directions along active and segmented normal fault systems." *Journal of Structural Geology* 18(6): 835-845.
- Roberts, G. P. and A. Ganas (2000). "Fault-slip directions in central and southern Greece measured from striated and corrugated fault planes: Comparison with focal mechanisms and geodetic data." *Journal of Geophysical Research* 105(B10): 23443-23462.
- Robertson, A. (2004). "Development of concepts concerning the genesis and emplacement of Tethyan ophiolites in the Eastern Mediterranean and Oman regions." *Earth Science Reviews* 66: 331-387.

- Robertson, A. and C. Xenophontos (1993). "Development of concepts concerning the Troodos ophiolite and adjacent units in Cyprus." Special Publication of the Society of London 76: 85.
- Robertson, A. H. (2002). "Overview of the genesis and emplacement of Mesozoic ophiolites in the Eastern Mediterranean Tethyan region." *Lithos* 65(1-2): 1-67.
- Robertson, A. H. F. (1975). "Cyprus umbers: basalt-sediment relationships on a Mesozoic ocean ridge." *Journal of the Geological Society of London* 131: 511-531.
- Robertson, A. H. F. (1986). "The Hatay ophiolite (southern Turkey) in its eastern Mediterranean tectonic context: a report on some aspects of the field excursion." *Ophioliti* 11: 105-119.
- Robertson, A. H. F. (1990). "Tectonic evolution of Cyprus. In: Malpas, J., Moores, E. M., Panayiotou, A. & Xenophontus, C. (Eds.)." *Ophiolites, Oceanic Crustal Analogues, Nicosia, Cyprus, Geological Survey Department*: 235-252.
- Robertson, A. H. F. (1991). "Origin and emplacement of an inferred Late Jurassic subduction-accretion complex, Eurobea, eastern Greece." *Geological Magazine* 128: 27-41.
- Robertson, A. H. F. (1993). "Mesozoic-Tertiary sedimentary and tectonic evolution of Neotethyan carbonate platforms, margins and small ocean basins in the Antalya complex, SW Turkey. In: Frostick, L. E. and Steel, R. (Eds.). *Sedimentation, Tectonics and Eustasy: sea-level changes at active margins*." Special publication of the International Association of Sedimentologists 20: 415-465.
- Robertson, A. H. F. (1998a). "Mesozoic-Tertiary tectonic evolution of the easternmost mediterranean area: integration of marine and land evidence." *Proceedings of the Ocean Drilling Program, Scientific Results* 160: 723-782.

- Robertson, A. H. F. (1998b). "Tectonic significance of the Eratosthenes Seamount: a continental fragment in the process of collision with a subduction zone in the eastern Mediterranean (Ocean Drilling Program Leg 160)." *Tectonophysics* 298: 63-82.
- Robertson, A. H. F. (2000). "Mesozoic-Tertiary tectonic-sedimentary evolution of a south Tethyan oceanic basin and its margins in southern Turkey." *Special Publication of the Society of London* 173: 97-138.
- Robertson, A. H. F. and M. Comas (1998). "Collision-related processes in the Mediterranean region- introduction." *Tectonophysics* 298: 1-4.
- Robertson, A. H. F. and J. E. Dixon (1984). "Introduction: aspects of the geological evolution of the Eastern Mediterranean. In: Dixon, J. E. & Robertson, A. H. F. (Eds.), *The geological evolution of the Eastern Mediterranean.*" *Special Publication of the Society of London* 17: 1-74.
- Robertson, A. H. F., J. E. Dixon, S. Brown, A. Collins, A. Morris, E. A. Pickett, I. Sharp and T. Ustaömer (1996). "Alternative tectonic models for the Late Palaeozoic-Early Tertiary development of Tethys in the Eastern Mediterranean region." *Special Publication of the Society of London* 105: 239-264.
- Robertson, A. H. F., S. Eaton, E. J. Follows and J. E. McCallum (1991). "The role of local tectonics versus global sea-level change in the Neogene evolution of the Cyprus active margin." *International Association of Sedimentologists, Special Publication* 12: 331-369.
- Robertson, A. H. F., K.-C. Emeis and C.-c. scientists) (1995). "Evidence of collisional processes associated with ophiolite obduction in the eastern Mediterranean: results from the Ocean Drilling Program Leg 160." *GSA Today* 5(11): 213-221.
- Robertson, A. H. F. and M. Grasso (1995). "Overview of the Late Tertiary-Recent tectonic and palaeo-environmental development of the Mediterranean region." *Terra Nova* 7: 114-127.

- Robertson, A. H. F. and J. D. Hudson (1974). "Pelagic sediments in the Cretaceous and Tertiary history of the Troodos massif, Cyprus. In: Hsu, K. J., Jenkyns, H. C. (Eds.), Pelagic sediments on land and under the sea." International Association of Sedimentologists, Special Publication 1: 403-436.
- Robertson, A. H. F., E. A. Pickett and T. Ustaömer (1999). "Inter-relationships between Palaeotethys and Neotethys in the eastern Mediterranean region: possible role of changing subduction polarity." Journal of Conference Abstracts EUG 10(4): 315.
- Robertson, A. H. F. and N. H. Woodcock (1979). "The Mamonia Complex, southwest Cyprus: the evolution and emplacement of a Mesozoic continental margin." Geological Society of America Bulletin 90: 651-665.
- Robertson, A. H. F. and N. H. Woodcock (1980). "Tectonic setting of the Troodos massif in the east Mediterranean. In: Panayiotou, A. (Ed.)." Ophiolites: Proceedings of the International Symposium, 1979, Cyprus Geological Survey Department: 261-272.
- Robertson, A. H. F. and N. H. Woodcock (1982). "Sedimentary history of the southwestern segment of the Mesozoic-Tertiary Antalya continental margin, southwestern Turkey." *Eclogae Geol. Helv.* 75: 517-562.
- Robinson, P. T. and J. Malpas (1990). "The Troodos ophiolite of Cyprus: new perspectives on its origin and emplacement. In: Malpas, J., Moores, E. M., Panayiotou, A. & Xenophontus, C. (Eds.)." Ophiolites: Oceanic Crustal Analogues. Cyprus Geological Survey Department: 13-26.
- Robinson, P. T., W. G. Melson, T. O'Hearn and H.-U. Schmincke (1983). "Volcanic glass compositions of the Troodos ophiolite, Cyprus." *Geology* 11: 400-404.
- Rochette, P. (1988). "Inverse magnetic fabric in carbonate-bearing rocks." *Earth and Planetary Science Letters* 90: 229-237.

- Rojay, B., A. Heimann and V. Toprak (2001). "Neotectonic and volcanic characteristics of the Karasu fault zone (Anatolia, Turkey): The transition zone between the Dead Sea transform and the East Anatolian fault zone." *Geodinamica Acta* 14: 197-212.
- Ron, H., R. Freund, Z. Garfunkel and A. Nur (1984). "Block rotation by strike-slip faulting: structural and palaeomagnetic evidence." *Journal of Geophysical Research* 89: 6256-6270.
- Rotstein, Y. and A. L. Kafka (1982). "Seismotectonics of the southern boundary of Anatolia, eastern mediterranean region, subduction, collision and arc-jumping." *Journal of Geophysical Research* 87(7694-7706).
- Ruellan, E., J. Delteil, I. C. Wright and T. Matsumoto (2003). "From rifting to active spreading in the Lau Basin- Havre Trough backarc system (SW Pacific): locking/unlocking induced by seamount chain subduction." *Geochemistry, Geophysics, Geosystems* 4: art. no. 8909.
- Saroglu, F., O. Emre and I. Kuscu (1992). "The East Anatolian fault zone of Turkey." *Annales Tectonicae* 6: 99-125.
- Saunders, A. D. and J. Tarney (1979). "The geochemistry of basalts from a back-arc spreading center in the East Scotia Sea." *Geochimica et Cosmochimica Acta* 43: 555-572.
- Savostin, L. A., J. C. Sibuet, L. P. Zonenshain, X. Le Pichon and M. J. Roulet (1986). "Kinematic evolution of the Tethys Belt from the Atlantic Ocean to the Pamirs since the Triassic." *Tectonophysics* 123: 1-35.
- Schellart, W. P. (2004). "Kinematics of subduction and subduction-induced flow in the upper mantle (DOI 10.1029/2004JB002970)." *Journal of Geophysical Research* 109(SECT 2): B07401.

- .Schellart, W. P., G. S. Lister and M. W. Jessell (2002). "Analogue modelling of asymmetrical back-arc basin extension. In: Schellart, W. P. and Passchier, C. Analogue Modelling of Large Scale Tectonic Processes." *Journal of the Virtual Explorer* 7: 25-42.
- .Schettino, A. and C. R. Scotese (2001). "New internet software aids for palaeomagnetic analysis and plate tectonic reconstructions." *Transactions of the American Geophysical Union- EOS* 82(45): 7p.
- .Schmincke, H.-U. and M. Rautenschlein (1987). "Troodos extrusive series (Akaki River Canyon) and the sheeted diabase. In: Xenophontos, C. & Malpas, J. G. (Eds)." *Field Excursion Guidebook to accompany the Troodos 87 Ophiolites and Oceanic Lithosphere Symposium, Geological SURvey Department, Nicosia*: 36-91.
- .Schmincke, H.-U., M. Rautenschlein, P. T. Robinson and J. M. Megehan (1983). "Troodos extrusive series of Cyprus: A comparison with oceanic crust." *Geology* 11: 405-409.
- .Searle, M. P. and J. Cox (1999). "Tectonic setting, origin and obduction of the Oman ophiolite." *Geological Society of America Bulletin* 111: 104-122.
- .Searle, R. C. and J. Cox (2002). "Subduction zone metamorphism during formation and emplacement of the Semail ophiolite in the Oman mountains." *Geological Magazine* 139(3): 242-255.
- .Selcuk, H. (1981). "Etude geologique de la partie meridionale du Hatay (Turquie)." Ph.D. Dissertation (unpublished), Univ. de Geneve: 116pp.
- .Sengor, A. M. C. (1979). "The North Anatolian transform fault: its age, offset and tectonic significance." *Journal of the Geological Society of London* 136: 269-282.
- .Sengor, A. M. C., N. Gorur and F. Saroglu (1985). "Strike-slip faulting and related basin formation in zones of tectonic escape: Turkey as a case study." *Special Papers-The Society of Economic Paleontologists and Mineralogists* 37: 227-264.

- Sengor, A. M. C., H. Yilmaz and O. Sungurlu (1984). "Tectonics of the Mediterranean Cimmerides: nature and evolution of the western termination of Palaeo-tethys. In: Dixon, J. E. and Robertson, A. H. F. (Eds.). *The Geological Evolution of the Eastern Mediterranean.*" Special Publication of the Society of London 17: 77-111.
- Sengor, A. M. C. and Y. Yilmaz (1981). "Tethyan evolution of Turkey: a plate tectonic approach." *Tectonophysics* 75: 181-241.
- Shau, Y. H., M. Torii, C. S. Horng and D. R. Peacor (2000). "Subsolidus evolution and alteration of titanomagnetite in ocean ridge basalts from Deep Sea Drilling Project/Ocean Drilling Program Hole 504B, Leg 83: Implications for the timing of magnetization (Paper 2000JB900191)." *Journal of Geophysical Research* 105(B10): 23,635-23,650.
- Shelton, A. W. and I. G. Gass (1980). "Rotation of the Troodos microplate. In: Panayiotou, A. (Ed.)." *Ophiolites: Proceedings of the International Symposium, Cyprus, 1979, Cyprus Geological Survey Department: 61-65.*
- Shervais, J. W. (2000). "Birth, death and resurrection: the life cycle of suprasubduction zone ophiolites." *Geochemistry, Geophysics, Geosystems* 2: Paper No 2000GC000080.
- Simonian, K. O. and I. G. Gass (1978). "Arakapas fault belt, Cyprus: a fossil transform belt." *Geological Society of America Bulletin* 89: 1220-1230.
- Skumryev, V., H. J. Blythe, J. Cullen and J. M. D. Coey (1999). "AC susceptibility of a magnetite crystal." *Journal of Magnetism and Magnetic Material* 196-197: 515-517.
- Somboonsuk, K. and R. Trivedi (1985). "Dynamical studies of dendritic growth." *Acta Metallurgica* 33: 1051-1060.

- Sonder, L. J., P. C. England and G. A. Houseman (1986). "Continuum calculations of continental deformation in transcurrent environments." *Journal of Geophysical Research* 91: 4797-4810.
- Stacey, F. D. (1962). "A generalised theory of thermoremanence, covering the transition from single-domain to multi-domain grains." *Philosophical Magazine* 7: 1887-1900.
- Stampfli, G. and G. D. Borel (2002). "A plate tectonic model for the Palaeozoic and Mesozoic constrained by dynamic plate boundaries and restored synthetic oceanic isochrons." *Earth and Planetary Science Letters* 196: 17-33.
- Stampfli, G., J. Marcoux and A. Baud (1991). "Tethyan margins in space and time." *Palaeogeography, Palaeoclimatology, Palaeoecology* 87(1-4): 373-409.
- Stampfli, G., J. Mosar, P. Faure, A. Pillevuit and J.-C. Vanney (2001). "Permo-Triassic evolution of the western Tethys real: the Neotethys east Mediterranean basin connection. In: Ziegler, P., Cavazza, W., Robertson, A. H. F. and Crasquin-Soleau, S. (Eds.). *Peri-Tethys Memoir no. 5: Peri Tethyan Rift/Wrench Basins and Passive Margins.*" *Memoirs du Museum Nationale D'Histoire Naturelle*: 51-108.
- Stephenson, A., S. Sadikun and D. K. Potter (1986). "A theoretical and experimental comparison of the anisotropies of magnetic susceptibility and remanence in rocks and minerals." *Geophysical journal of the Royal Astronomical Society* 84: 185-200.
- Stem, R. J. and S. H. Bloomer (1992). "Subduction zone infancy; examples from the Eocene Izu-Bonin-Mariana and Jurassic California arcs." *Geological Society of America Bulletin* 104: 1621-1636.
- Swarbrick, R. E. (1993). "Sinistral strike-slip and transpressional tectonics in an ancient oceanic setting: the Mamonia Complex, southwest Cyprus." *Journal of the Geological Society of London* 150: 381-392.

- .Tanahashi, M., K. Kisimoto, M. Joshima and P. Jarvis (1994). "800-km-long N-S spreading system of the North Fiji Basin." *Marine Geology* 116(1/2): 5.
- .Tarling, D. H. and F. Hrouda (1993). "The magnetic anisotropy of rocks." Published by Chapman and Hall: 217pp.
- .Tatar, O., J. D. A. Piper, H. Gursoy, A. Heimann and F. Kocbulut (2004). "Neotectonic deformation in the transition zone between the Dead Sea Transform and the East Anatolian fault zone, southern Turkey: a palaeomagnetic study of the Karasu Rift volcanism." *Tectonophysics* 385: 17-43.
- .Tauxe, L. (1998). "Paleomagnetic principles and practise." 299pp.
- .Taylor, R. N. and R. W. Nesbitt (1988). "Light rare-earth enrichment of a supra subduction-zone mantle: Evidence from the Troodos ophiolite, Cyprus." *Geology* 16: 448-451.
- .Taymaz, T., J. Jackson and D. McKenzie (1991). "Active tectonics of the north and central Aegean Sea." *Geophysical Journal International* 106: 433-490.
- .Tekeli, O. and M. Erendil (1985). "The Kizildag ophiolite: An additional field guide to aspects of the crustal sequence of the Kizildag ophiolite, Hatay, Turkey." Field meeting: "Ophiolites and Lithosphere of Marginal Seas" project of IGCP, lead by Delaloye, M.: 20 pp.
- .Thomas, V., J. P. Pozzi and A. Nicolas (1988). "Paleomagnetic results from Oman ophiolites related to their emplacement." *Tectonophysics* 151: 297-321.
- .Thuziat, R., H. Whitechurch, R. Montigny and T. Juteau (1981). "K-Ar dating of some intra-ophiolite metamorphic soles from the East Mediterranean: new evidence for oceanic thrusting before obduction." *Earth and Planetary Science Letters* 52: 302-310.
- .Thy, P. and C. Xenophontos (1991). "Crystallization orders and phase chemistry of glassy lavas from the pillow sequences, Troodos ophiolite, Cyprus." *Journal of Petrology* 32: 403-428.

- Tinkler, C., J. J. Wagner, M. Delaloye and H. Selcuk (1981). "Tectonic history of the Hatay ophiolites (south Turkey) and their relation with the Dead sea rift." *Tectonophysics* 72: 23-41.
- Twiss, R. J., G. M. Protzman and S. D. Hurst (1991). "Theory of slickenline patterns based on the velocity gradient tensor and microrotation." *Tectonophysics* 186: 215-239.
- Twiss, R. J., B. J. Souter and J. R. Unruh (1993). "The Effect of Block Rotations on the Global Seismic Moment Tensor and the Patterns of Seismic P and T Axes (Paper 92JB01678)." *Journal of Geophysical Research* 98(B/1): 645.
- Twiss, R. J. and J. R. Unruh (1998). "Analysis of fault slip inversions: Do they constrain stress or strain rate?" *Journal of Geophysical Research* 103(B6): 12,205-12,222.
- Umino, S., S. Yanai, A. R. Jaman, Y. Nakamura and J. T. Iiyama (1990). "Regional tectonics of the eastern Mediterranean ophiolites. In: Malpas, J., Moores, E. M., Panayiotu, A. & Xenophontos, C." *Ophiolites, Oceanic Crustal Analogues, Nicosia, Cyprus, Geological Survey Department: 375-383.*
- Ustaomer, T. and A. H. F. Robertson (1993). "A Late Palaeozoic-Early Mesozoic marginal basin along the active southern continental margin of Eurasia: evidence from the Central Pontides (Turkey) and adjacent regions." *Geological Journal* 28: 219-238.
- Ustaomer, T. and A. H. F. Robertson (1994). "Late Palaeozoic marginal basin and subduction-accretion: the Palaeotethyan Kure Complex, Central Pontides, northern Turkey." *Journal of the Geological Society of London* 151: 291-305.
- Van der Voo, R. (1993). "Paleomagnetism of the Atlantic, Tethys and Iapetus Oceans." 411pp.
- Van der Voo, R. and R. B. French (1974). "Apparant polar wandering for the Atlantic-bordering continents: Late Carbiniferous to Eocene." *Earth Science Reviews* 10: 99-119.

- Vandenberg, J. and H. Zijdeveld (1982). "Palaeomagnetism in the Mediterranean area. In: Alpine Mediterranean geodynamics series." American Geophysical Union 7: 83-112.
- Varga, R. J. and E. M. Moores (1985). "Spreading structure of the Troodos ophiolite." *Geology* 13: 846-850.
- Verosub, K. L. and N. R. Banerjee (1977). "Geomagnetic excursions and their paleomagnetic record." *Reviews of Geophysics and Space Physics* 15: 145-155.
- Verosub, K. L. and E. M. Moores (1981). "Tectonic rotations in extensional regimes and their paleomagnetic consequences for oceanic basalts." *Journal of Geophysical Research* 86: 6335-6349.
- Verwey, E. J. W. (1939). "Electronic conduction of magnetite (Fe_3O_4) and its transition point at low-temperature." *Nature* 44: 327-328.
- Vine, F. J. and E. M. Moores (1969). "Palaeomagnetic results from the Troodos Igneous Massif, Cyprus." *Transactions of the American Geophysical Union* 50: 131.
- Vuagnat, M. and E. Cogulu (1967). "Quelques reflexions sur le massif basique-ultrabasique du Kizil Dag, Turquie." *C. R. Seances Soc. Phys. Hist. nat. Geneve* 2: 210-216.
- Wallace, R. (1951). "Geometry of shearing stress and relation to faulting." *Journal of Geology* 59: 118-130.
- Walley, C. D. (1988). "A braided strike-slip model for the northern continuation of the Dead Sea fault and its implications for Levantine tectonics." *Tectonophysics* 145: 63-72.
- Walsh, J. J. and J. Watterson (1992). "Populations of faults and fault displacements and their effects on estimates of fault-related regional extension." *Journal of Structural Geology* 14(6): 701-712.

- Wang, D. and R. Van der Voo (2004). "The hysteresis properties of multidomain magnetite and titanomagnetite/titanomaghemite in mid-ocean ridge basalts." *Earth and Planetary Science Letters* 220(1-2): 175-184.
- Weiler, P. D. (2000). "Differential rotations in the Oman ophiolite: paleomagnetic evidence from the southern massifs." *Marine Geophysical Researches* 21: 195-210.
- Wernicke, B. (1985). "Uniform sense normal simple shear of the continental lithosphere." *Canadian Journal of Earth Sciences* 22: 108-122.
- Westaway, R. (1994). "Present day kinematics of the Middle East and eastern Mediterranean." *Journal of Geophysical Research* 99: 12071-12090.
- Westaway, R. and J. Arger (1996). "The Golbasi basin, southeastern Turkey: a complex discontinuity in a major strike-slip zone." *Journal- Geological Society London* 153.
- Westphal, M., M. L. Bazhenov, J. P. Lauer, D. H. Pechersky and J. C. Sibuet (1986). "Palaeomagnetic implications on the evolution of the Tethys Belt from the Atlantic Ocean to the Pamirs since the Triassic." *Tectonophysics* 123: 37-82.
- Whitechurch, H. (1977). "Les roches metamorphiques infraperidotiques du Ber-Bassit (NW Syrien), temoin de l'ecailage intraoceanique tethysien. Etude petrologique et structurale." PhD Thesis, Universite de Nancy, France: 194 pp.
- Wilson, D. S., D. A. H. Teagle, G. D. Acton and e. al (2003). *Proceedings of the Ocean Drilling Program, Initial Reports* 206.
- Wood, D. A., N. G. Marsh, J. Tarney, J.-L. Joron, P. Fryer and M. Treuil (1981). "Geochemistry of igneous rocks recovered from a transect across the Mariana Trough, arc, fore-arc and trench, Sites 453 through 461, Deep Sea Drilling Project Leg 60. In: Hussong, D. M. et al. (Eds.)." *Initial Reports of the Deep Sea Drilling Project* 60: 611-630.

- .Woodcock, N. H. and M. A. Naylor (1983). "Randomness testing in three-dimensional orientation data." *Journal of Structural Geology* 5: 539-548.
- .Worm, H. U. (2001). "Magnetic stability of oceanic gabbros from ODP Hole 735B." *Earth and Planetary Science Letters* 193(3-4): 287-302.
- .Worm, H. U. and N. R. Banerjee (1984). "Aqueous low-temperature oxidation of titanomagnetite." *Geophysical Research Letters* 11: 169-172.
- .Xenophontos, C. and J. Malpas (1987). "Field excursion guidebook. Troodos 87-Ophiolites and Oceanic Lithosphere." Cyprus Geological Survey Department.
- .Xu, W., D. R. Peacor, W. A. Dollase, R. Van der Voo and R. Beaubouef (1997). "Transformation of titanomagnetite to titanomaghemite: a slow, two-step, oxidation-ordering process in MORB." *American Mineralogist* 82: 1101-1110.
- .Yamaji, A. (2000). "The multiple inverse method: a new technique to separate stresses from heterogeneous fault-slip data." *Journal of Structural Geology* 22: 441-452.
- .Yazgan, E. and R. Chessex (1991). "Geology and tectonic evolution of Southeastern Taurus in the region of Malatya." *Turkish Association of Petroleum Geologists Bulletin* 3: 1-42.
- .Yilmaz, H., O. Tuysuz, S. Yigitbas, C. Genc and A. M. C. Sengor (1997). "Geology and tectonic evolution of the Pontides. In: Robinson, A. C. (Ed.). *Regional and Petroleum Geology of the Black Sea and Surrounding Region.*" *American Association of Petroleum Geologists Memoir* 68: 183-226.
- .Yilmaz, Y. (1993). "New evidence and model on the evolution of the southeast Anatolian orogen." *Geological Society of America Bulletin* 105: 251-271.
- .Yurtmen, S., H. Guillou, R. W. C. Westaway, G. Rowbotham and O. Tatar (2002). "Rate of strike-slip motion on the Amanos Fault (Karasu Valley, southern Turkey) constrained by K-Ar dating and geochemical analysis of Quaternary basalts." *Tectonophysics* 344: 207-246.

- .Yurtmen, S., G. Rowbotham, F. Isler and P. A. Floyd (2000). "Petrogenesis of basalts from southern Turkey: the Plio-Quaternary volcanism to the north of Iskenderun. In: Bozkurt, E. Winchester, J. A. and Piper, J. D. A. (Eds.). Tectonics and magmatism in Turkey and the surrounding area." Special Publication of the Society of London 173: 489-512.
- .Yurur, M. T. and J. Chorowicz (1998). "Recent volcanism, tectonics and plate kinematics near the junction of the African, Arabian and Anatolian plates in the eastern Mediterranean." *Tectonophysics* 85: 1-15.
- .Zack, I. and R. Freund (1981). "Asymmetry and basin migration in the Dead Sea rift." *Tectonophysics* 80: 27-38.
- .Zanchi, A. and J. Angelier (1993). "Seismotectonics of western Anatolia: regional stress orientation from geophysical and geological data." *Tectonophysics* 222: 259-274.
- .Zanchi, A., G. B. Crosta and A. N. Darkal (2002). "Paleostress analyses in NW Syria: constraints on the Cenozoic evolution of the northwestern margin of the Arabian plate." *Tectonophysics* 357: 255-278.
- .Zhao, X., M. Antretter, P. Solheid and H. Inokuchi (2002). "Identifying magnetic carriers from rock magnetic characterization of Leg 183 basement cores." *Proceedings of the Ocean Drilling Program, Scientific Results* 183: 1-28.
- .Zhou, W., R. Van der Voo and D. R. Peacor (1997). "Single-domain and superparamagnetic titanomagnetite in young ocean-floor basalts with variable Ti-content." *Earth and Planetary Science Letters* 150: 353-362.
- .Zhou, W., R. Van der Voo and D. R. Peacor (1999). "Preservation of pristine titanomagnetite in older ocean-floor basalts and its significance for paleointensity studies." *Geology* 27: 1043-1046.

- Zhou, W., R. Van der Voo, D. R. Peacor, D. Wang and Y. Zhang (2001). "Low-temperature oxidation in MORB of titanomagnetite to titanomaghemite: A gradual process with implications for marine magnetic anomaly amplitudes." *Journal of Geophysical Research* 106: 6409-6421.
- Zhou, W., R. Van der Voo, D. R. Peacor and Y. Zhang (2000). "Variable Ti-content and grain size of titanomagnetite as a function of cooling rate in very young MORB." *Earth and Planetary Science Letters* 179: 9-20.
- Ziegler, P., W. Cavazza, A. H. F. Robertson and S. E. Crasquin-Soleau (2001). "Per-Tethys Memoir 5 Peri-Tethyan rift/wrench basins and passive margins." *Memoirs du Musee National D'Histoire Naturelle*: 752.
- Zijderveld, J. D. A. (1967). "A.C. demagnetization of rocks: analysis of results." *Methods in Palaeomagnetism*, Elsevier, Amsterdam, New York edited by K. M. Creer, S. K. Runcorn: 254-286.

PUBLISHED PAPERS AND CONFERENCE ABSTRACTS

- A. Inwood, J., Morris, A., Anderson, M. W., Robertson, A. H. F., Unlugenc, U. 2003. First Palaeomagnetic Results from the Hatay (Kizil Dağ) Ophiolite of Turkey and their Implication for the Tectonic Evolution of the Eastern Mediterranean Neotethys. Geophysical Research Abstracts, 5, EGS-AGU-EUG Joint Assembly.
- B. Inwood, J. 2004. Rock Magnetic Evidence for a Sea-floor Origin for Magnetic Remanences in a Late Cretaceous Tethyan Ophiolite. The IRM Quarterly, Volume 14, No 2, p3-4.

FIRST PALAEOMAGNETIC RESULTS FROM THE HATAY (KIZIL DAĞ) OPHIOLITE OF TURKEY AND THEIR IMPLICATION FOR THE TECTONIC EVOLUTION OF THE EASTERN MEDITERRANEAN NEOTETHYS

J. Inwood (1), A. Morris (1), M. W. Anderson (1), A. H. F. Robertson (2), U. Ünlügenç (3)
(1) Dept. of Geology, University of Plymouth, UK, (2) School of Geosciences, University of Edinburgh, UK, (3) Geological Engineering Department, Çukurova University, Turkey
jinwood@plymouth.ac.uk/Fax: +44-1752-233117

Late Cretaceous ophiolitic rocks are found throughout the eastern Mediterranean and represent remnants of small Tethyan ocean basins destroyed during collision of the African and Eurasian plates. A prominent Neotethyan ophiolitic belt stretches eastwards from Cyprus (Troodos ophiolite) through Syria (Baer-Bassit), Turkey (Kizil Dağ) and Iran (Kermanshah) to Oman (Semail ophiolite) and represents formation in a southern basin of Neotethys.

Palaeomagnetic results can be invaluable in elucidating the tectonic evolution of these units. In particular, data from the Troodos ophiolite in Cyprus identified a regionally significant 90° anticlockwise rotation of the Troodos 'microplate' between the Late Cretaceous to Eocene (Clube and Robertson 1986). More recently, palaeomagnetic results have been obtained from the tectonically emplaced Baer-Bassit ophiolite to the east (Morris et al. 2002) which indicate extreme anticlockwise rotations of ophiolitic thrust sheets varying on a kilometric scale. Here we present the first palaeomagnetic results from the Hatay (Kizil Dağ) ophiolite to the north. This is closely related spatially to the Baer-Bassit ophiolite and represents the less deformed main body of a large ophiolite sheet emplaced onto the Arabian platform in the Maastrichtian.

New palaeomagnetic results have been obtained from various levels of the ophiolite. Stable components of magnetization are recorded by all lithologies, with directions of magnetization unrelated to the present day field. Application of an inclination-only tilt test to data from sites with palaeohorizontal control indicates minimum dispersion at 100% of untilting, demonstrating that the magnetization of the ophiolite pre-dates deformation. Minor variability in tilt-corrected declinations from these sites may result from relative tectonic rotation of sampled units. However, the overall mean direction for the ophiolite indicates a significant bulk anticlockwise rotation of c. 80°. This is equivalent to the rotation of the most northerly part of the Baer-Bassit ophiolite to the south of Hatay. The rotation history of the Troodos ophiolite to the west is well constrained, with 60° of the 90° of anticlockwise 'microplate' rotation being completed by the Maastrichtian (Clube and Robertson 1986), i.e. by the time of emplacement of the Hatay/Baer-Bassit ophiolite. This suggests a common intraoceanic origin for a significant component of the observed rotation in Hatay, and the more variable rotations observed in Baer-Bassit. The combined datasets from all three ophiolites are consistent with a model involving: (i) intraoceanic rotation of a coherent region of oceanic crust within the southern Neotethyan basin; (ii) emplacement of part of the rotated unit onto the Arabian platform; and (iii) subsequent localised post-emplacement modification.

Understanding Multidomain Remanence: Viscous Magnetization of Multidomain Magnetite

During my visit to the IRM, I made a series of key experiments which are integral to a bigger project currently being undertaken in Edinburgh. This project is examining the viscous behaviour of multidomain (MD) magnetite in attempt to not only understand viscous magnetisation in itself but also to try and unravel remanence acquisition in MD magnetite. We are doing this using a series of complementary techniques; direct measurement of viscous magnetisation and viscous remanent magnetisation acquisition and demagnetisation, and observation of viscous behaviour through the Bitter pattern method as function of time and temperature.

All previous viscous magnetisation measurements we have made have been in relatively low fields of about 0.2 mT. It was of interest to understand the behaviour in higher fields which is possible with the Princeton high-temperature VSM. I examined the possibility of disaccommodation contributing to viscosity by comparing the viscosity of the virgin samples with the viscosity after high-temperature thermal stabilization. The viscosity acquisition constant (the rate of viscosity acquisition) was significantly reduced

Rock Magnetic Evidence for a Sea-floor Origin for Magnetic Remanences in a Late Cretaceous Tethyan Ophiolite

The project carried out on my visit to the IRM was to identify and characterize the NRM carriers in rocks from the Hatay Ophiolite of southeastern Turkey. This forms part of my doctoral research which aims to constrain the tectonic history of the Hatay ophiolite, using a combination of palaeomagnetic and structural techniques.

The Hatay ophiolite forms part of a prominent ophiolite chain in the eastern Mediterranean and Middle East which stretches from the Troodos ophiolite of Cyprus eastwards to the Semail ophiolite of Oman. These ophiolites represent fragments of the oceanic lithosphere generated in the Late Cretaceous by supra-subduction zone spreading within a small "Neotethyan" ocean basin. Subsequent closure of Tethys during convergence of the African and Eurasian plates resulted in the emplacement of ophiolitic thrust sheets onto the Arabian continental margin in the Maastriachian.

The Hatay ophiolite was sampled for palaeomagnetic analysis at various

after thermal stabilization in samples thought to have medium levels of stress (Figure 1). This suggests a disaccommodation contribution to the viscosity in the virgin samples. During viscosity experiments it is normal to measure both viscous acquisition and demagnetisation. Due to the instrument software it was only possible to make acquisition experiments, however, the inability to accurately control the zero field state with the high-temperature VSM meant that this was no great loss

To tie in with the Bitter pattern domain observations, I made some magnetic force microscopy (MFM)

images of the same grains to investigate how well the domain structures seen with the Bitter pattern image represent the higher-resolution MFM structures. As expected the MFM revealed much finer detail than that observed by the Bitter pattern image, however, generally the main features were the same, which is encouraging.

I also took the opportunity to measure some Mössbauer spectra on some natural samples involved in another study. Much thanks go to Mike, Thelma and Jim the rest of the IRM'ers for their time, help and patience.

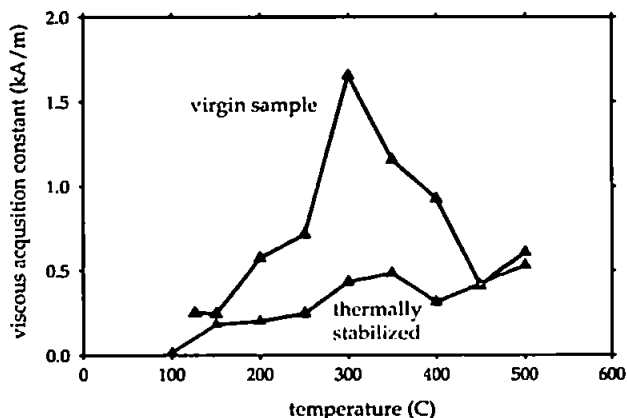


Figure 1. Viscous acquisition constant versus temperature for a commercial synthetic magnetite sample with a mean grain size of $\sim 11 \mu\text{m}$. The sample was AF demagnetized at room temperature before each measurement

crustal levels, from the cumulate gabbros up to the extrusives, excluding only the serpentinised ultramafics. Specimens from 63 sites were demagnetized in the University of Plymouth laboratory. Demagnetization diagrams show mostly simple rectilinear decay to the origin. Westerly-directed remanences indicate that the ophiolite has experienced large anticlockwise rotations during its history, similar to those previously documented in the coeval Troodos and Baer-Bassit ophiolites. An inclination-only tilt test demonstrates that magnetizations are pre-deformational in origin, despite a complex history of low temperature seafloor alteration, intra-oceanic detachment, thrust emplacement and subsequent neotectonic faulting. Determining precisely what is carrying the stable magnetizations is therefore critical to understanding the magnetic history of the ophiolite.

The magnetic minerals in oceanic crust depend on variables such as the composition and cooling rate of the magma. Research on in situ day oceanic crust has concentrated on the more accessible upper levels, i.e. pillowed and sheet lava flows and sheeted dykes. For a basaltic magma, rapid cooling

preserves titanomagnetite with intermediate titanium composition (TM60), whereas slower cooling with deuteric oxidation above the Curie temperature preserves an exsolution texture of near-ilmenite and near-magnetite lamellae (O'Reilly, 1984). Low temperature oxidation at ambient temperatures on the seafloor oxidises (titano)magnetite to (titano)magnetite due to leaching of the iron by seawater. This can alter to magnetite during subsequent low-temperature inversion (O'Reilly, 1984). The magnetic minerals carrying the pre-deformational remanence in the ophiolite were anticipated to be either those observed within in situ oceanic crust, or an inversion that allows an early magnetization to be retained, with potential variations between the different lithologies sampled.

Preliminary Rock Magnetic Results from the University of Plymouth

1. Analyses of IRM acquisition for at least one sample per site indicated a dominance of low coercivities for all samples.

Stepwise thermal demagnetization of natural remanences indicated differences in unblocking temperatures (T_b) between lithologies. The deeper levels (gabbros and cumulate gabbros) had T_b s near 580°C suggesting the presence of Ti-poor magnetite. For the pillow lavas T_b s were generally lower, suggesting a higher titanium content. More variable T_b s were observed for the sheeted dyke complex with a maximum T_b of 560-580°C, but also in some samples a lower temperature component was observed to unblock at 350-400°C. Alternating field demagnetization characteristics were consistent with the presence of both MD to SSD grains with median destructive fields ranging from 5 mT to >40 mT.

EXPERIMENTS PERFORMED AT THE IRM

Hysteresis loops were determined for 135 cores using the Princeton Applied Research VSM, with coercivity of remanence (H_{cr}) also measured. Curie point (T_c) determinations were carried out using the Princeton Measurements MicroMag VSM on 51 powdered samples. Low temperature experiments using the Quantum Design Magnetic Property Measurement System (MPMS) were carried out on 54 powdered samples. Thermomagnetic curves were obtained by cooling a room temperature (RT) SIRM acquired in a 2.5 T field from 300 to 10K, and by imparting a low temperature (LT) SIRM in a 2.5 T field and warming the sample from 10 to 300K. For selected samples, both cooling and warming curves of RT SIRM were plotted, as was the curve following cooling of the sample both in field (FC) and in zero field (ZFC). Alternating current (AC) susceptibility measurements as a function of frequency were taken for eight samples using the MPMS and the Lakeshore AC Susceptometer.

RESULTS

The majority of samples of all lithologies lie within the PSD field of a Day plot (Figure 1). The sheeted dyke complex showed more variation with some samples falling in the MD field.

Deeper levels of the ophiolite had Curie points near that of Ti-poor magnetite with a mean T_c value close to 590°C in both the gabbros and sheeted dyke complex. Heating and cooling curves were reversible in the majority of samples. The pillow lavas had T_c s ranging from 475 to 560°C with a mean of 530°C. These lower temperatures suggest the presence of a higher titanium phase than for the gabbros, although these T_c s are higher than that of TM60. Two components were observed in some samples at temperatures between 335 and 400°C, with all except two of these samples being from the sheeted dyke complex.

Low temperature runs allow easy recognition of the Verwey transition in magnetite on both the warming and cooling curves if it is present. The

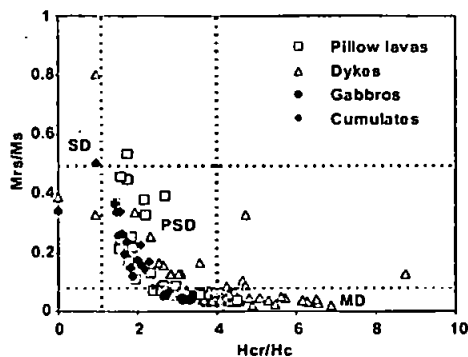


Figure 1: A Day plot of the 135 samples measured on the VSM.

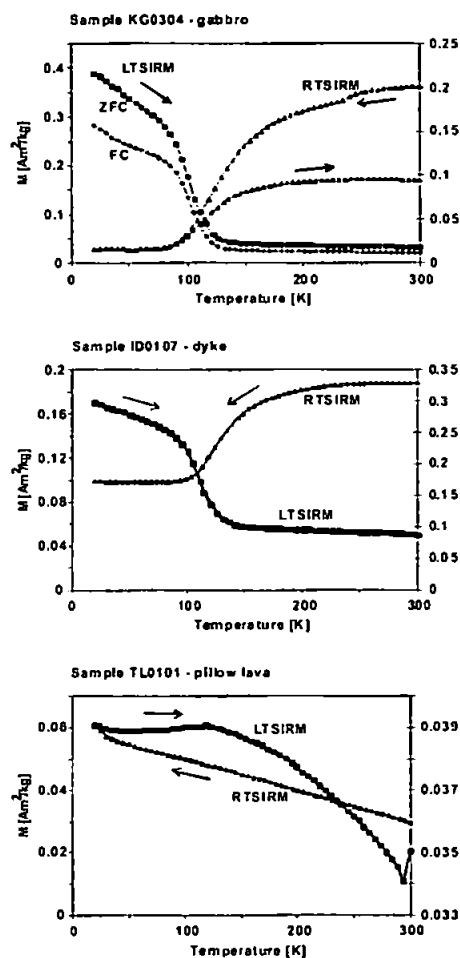


Figure 2: Low temperature thermomagnetic curves of saturation remanence for a representative sample from each main lithology: (i) gabbro sample, clearly showing the Verwey transition; (ii) sample from the sheeted dyke complex showing the Verwey transition; (iii) basaltic lava sample showing a 'smeared out' curve suggesting presence of a higher degree of titanium than in the other samples.

transition occurs at 120K in stoichiometric magnetite, but is decreased by oxidation or the presence of impurities such as titanium (Muxworthy and McClelland, 2000). The dykes and lower crustal lithologies all displayed clear low temperature transitions in the vicinity of

110K. In some of the cumulate gabbros the step was 'smeared' out, probably due to the presence of more oxidised magnetite (Figure 2(i), 2(ii)) (Özdemir et al. 1993, 2002). In the pillow lavas, the Verwey transition was generally not clear, and a considerably more gradual change in magnetization was seen on the warming curve (Figure 2(iii)). This, combined with the lower Curie temperatures, implies that a higher degree of titanium substitution in the pillow lavas minimises the effect of the Verwey transition.

SUMMARY

The results obtained at the IRM are compatible with the presence of fine magnetic grain sizes capable of retaining a stable magnetization throughout the complex history of the ophiolite, with PSD grains dominant in the majority of samples. There is a difference in magnetic mineralogy depending on the crustal level. The clear Verwey transitions and high T_c s of the deeper levels of the crust indicate that Ti-poor titanomagnetite/magnetite is the major carrier of the magnetic signal, and the absence of the Verwey transition and lower T_c s of the higher crustal levels indicate the presence of a more Ti-rich titanomagnetite. These mineralogies are compatible with acquisition of stable remanences on the seafloor soon after genesis of the ophiolitic crust at an oceanic spreading centre.

COMPLEMENTARY ANALYSES

In order to support the rock magnetic results obtained at the IRM, I have used a JSM6100 SEM with an Oxford INCA x-ray microanalyser at the University of Plymouth to study representative samples. This confirms the presence in the gabbros of near-magnetite and near-ilmenite in very well-developed exsolution lamellae in large grains (up to 1mm). The pillow lavas were observed to contain grains with higher levels of titanium, as concluded from the rock magnetic results. The dykes contained a mixture of near magnetite grains, more titanium rich grains, as well as the presence of some grains displaying exsolution. Skeletal and cubic crystals were common, supporting the existence of a primary remanence.

I would like to thank everyone I met at the IRM for being so helpful, for showing me how to use the instruments and for helping with the interpretation of results.

REFERENCES

Muxworthy, A.R. and E. McClelland, 2000. Review of the low-temperature magnetic properties of magnetite from a rock magnetic perspective. *Geophys. J. Int.*, 104: 101-114.
 O'Reilly, W., 1984. *Rock and mineral magnetism*. Blackie.
 Özdemir, Ö., D.J. Dunlop and B. M. Moskowitz, 1993. The effect of oxidation on the Verwey transition in magnetite. *Geophys. Res. Letters.*, 20: 1671-1674.
 Özdemir, Ö., D.J. Dunlop and B.M. Moskowitz, 2002. Changes in remanence, coercivity and domain state at low temperature in magnetite, *Earth and Planetary Science Letters*, 194: 343-358.